The Development of Empirical Chloride-induced Corrosion Rate Prediction Models for Cracked and Uncracked Steel Reinforced Concrete Structures in the Marine Tidal Zone

Mike Benjamin Otieno

Thesis presented in fulfilment of the requirements for the Degree of

DOCTOR OF PHILOSOPHY

Faculty of Engineering and the Built Environment

Department of Civil Engineering

UNIVERSITY OF CAPE TOWN

February, 2014

Cape Town

DECLARATION

I, Mike Benjamin Otieno, hereby declare that this Thesis is my own, unaided work. All the work in this document, save for that which is properly acknowledged, is my own. It is being submitted for the degree of DOCTOR OF PHILOSOPHY at the University of Cape Town. It has not been submitted before for any degree or examination in any other University.

Signed by candidate

Mike Benjamin Otieno

February, 2014

Abstract

Empirical chloride-induced corrosion rate prediction models for cracked and uncracked reinforced concrete (RC) structures in the marine tidal exposure zone are proposed in this study. The data used to develop the models were obtained from parallel corrosion experiments carried out by exposing half of 210 beam specimens to accelerated laboratory corrosion (cyclic 3 days wetting with 5% NaCl solution followed by 4 days air-drying) while the other half were left to undergo natural corrosion in a marine tidal zone in Cape Town (Table Bay). The main experimental variables were pre-corrosion flexural cover cracking, cover depth and concrete quality (binder type and w/b ratio). Corrosion rate, half-cell potential and concrete resistivity were monitored bi-weekly throughout the experimental period. The experimental results show that even though each of the variables investigated affects corrosion rate in a certain manner, their combined influence is complex. In general, regardless of the exposure environment (laboratory or marine tidal zone), for a given concrete quality and cover depth, pre-corrosion cover cracking was found to result in higher corrosion rates than in uncracked concrete, but with the field corrosion rates being much lower than the corresponding laboratory ones. Even though corrosion rates in both the field and laboratory specimens increased with an increase in crack width, the influence of concrete quality and cover depth was still evident. However, the effect of cover cracking on corrosion rate diminished with increasing concrete quality. In the blended cement concretes, the effect of concrete quality is further diminished by the inherent high resistivities of these concretes. The increase in corrosion rate due to increase in crack width, regardless of w/b ratio and cover depth, was generally higher in the 100% CEM I 42.5N concrete specimens than in the blended ones.

A framework is proposed that can be used to objectively compare predicted corrosion rates for specimens with similar concrete quality (influenced by binder type and w/b ratio) but different cover depths and crack widths. The framework, which incorporates the combined influence of cover depth, crack width and concrete quality (quantified using chloride diffusion coefficient) on corrosion rate, is the basis of the proposed corrosion rate prediction models for cracked concrete. Sensitivity analyses on the proposed models show that if any two of the three input parameters (cover depth, crack width and concrete quality) are simultaneously varied, their effect on corrosion rate is dependent on the value of the third (unchanged) parameter. Furthermore, (i) the initial cover depth was found to have no effect on the extent to which a change in cover depth affects corrosion rate; a similar trend was found in the case of sensitivity of corrosion rate to change in crack width, and (ii) the extent to which a change in either crack width or cover depth affects corrosion rate is dependent mainly on the concrete quality. In general, the sensitivity analyses showed that corrosion rate is more sensitive to change in concrete quality than crack width and cover depth. The proposed models can be used to (i) quantify the propagation phase with respect to a given performance limit using relevant corrosion-induced damage prediction models, and (ii) select suitable design combinations of cover depth, concrete quality and crack width to meet the desired durability performance of a given RC structure in the marine environment.

Summary

The main objective of this study was to develop empirical chloride-induced corrosion rate prediction models for cracked and uncracked steel reinforced concrete (RC) structures in the marine tidal exposure zone. To achieve this, parallel laboratory and field experiments were carried out. The experimental programme was designed to assess the influence of pre-corrosion flexural cover cracking, cover depth, and concrete quality (influenced by binder type and w/b ratio) on corrosion rate. A total of 210 beams (120 x 130 x 375 mm long) were cast using five different concretes. The concretes were made using two w/b ratios (0.40 and 0.55) and three binders (100% CEM I 42.5N plain Portland cement (PC), 50/50 PC/GGBS and 70/30 PC/FA). The 0.55 w/b ratio was not used to make PC specimens. Other experimental variables included cover depth (20 and 40 mm) and crack width (0, 0.4 and 0.7 mm). Incipient-cracked specimens were also made but only for specimens with 20 mm cover - these were made by flexurally cracking the beams and unloading just after visually sighting a crack on the concrete surface. A high yield strength 10 mm diameter steel bar was embedded in each beam. To facilitate the formation of a transverse (flexural) crack at approximately the longitudinal centre of the beam specimens during machine loading, a 1.0 mm thick x 4 mm deep PVC sheet was placed at the centre of each beam (transversely) during casting; the PVC sheet was embedded in the beam mould, and did not remain in the beam at de-moulding (after 24 hours). After 28-days of water-curing (at 23 ± 2 °C) and 10 days air-drying (temperature: 25 ± 2 °C, relative humidity: 50 ± 5%) in the laboratory, anodic impressed current was used with the objective to eliminate the corrosion initiation phase in all the specimens after which they were pre-cracked under 3-point flexural machine loading. The 0.4 and 0.7 mm cracked specimens were then placed in specially designed individual loading rigs where they remained for the entire experimental duration. This was done to ensure the crack widths remained at roughly the required width during the experiment duration. The specimens were then placed in their respective exposure environments (laboratory or field). Prior to exposure of the field specimens to natural marine tidal zone, all their faces (except the face with the specified cover depth) were epoxy-coated. Throughout the experimental duration, the laboratory-based specimens were subjected to accelerated corrosion by cyclic 3 days wetting with 5% NaCl solution (contained in a reservoir on the face of the beam with the specified cover depth) followed by 4 days air-drying while the field specimens were left to undergo natural corrosion. Corrosion rate, half-cell potential and concrete resistivity were measured bi-weekly in both the laboratory-based and field-based specimens.

The results show that even though each of the variables investigated affects corrosion rate in a certain manner, their combined influence is complex. In general, regardless of the exposure environment, for a given concrete quality and cover depth, pre-corrosion cover cracking was found to result in higher corrosion rates in comparison to those in uncracked concrete, but with the field corrosion rates being much lower than the corresponding laboratory ones. Even though corrosion rates in both the field and laboratory specimens increased with an increase in crack width, the influence of concrete quality (binder type and w/b ratio) and cover depth was still evident, the effect of cover cracking diminishing with increasing concrete quality. In the blended cement concretes, the effect is further diminished by the inherent high resistivities of these concretes. The increase in corrosion rate due to increase in crack width, regardless of the binder type, w/b ratio and cover depth, was generally higher in the PC concrete specimens than in the blended ones - up to approximately 50% in both field-based and laboratory-based specimens due to an increase in crack width from uncracked to incipient-cracked. However, considering the field-based specimens with 40 mm cover, the results show that the effect of

increasing crack width was higher in the blended cement concrete specimens than in the PC specimens. In the PC specimens, the relatively high penetrability of the concrete even in the absence of cracks diminishes the effect of increased crack width. On the contrary, in blended cement concretes, their relatively low penetrability in an uncracked state is significantly increased in the presence of cracks, and even further due to an increase in crack width. Even though it could not be confirmed from the results due to a limited number of crack widths investigated and the relatively short-term (2¼ years) of the field corrosion rates, the field-based results suggest that as the crack width increases, its influence on corrosion rate diminishes. This trend was not observed in the laboratory-based specimens, and clearly highlights, to some extent, the limitations of relying on laboratory accelerated corrosion results to predict in-situ performance of RC structures. The results of this study also corroborated those of previous studies that adopting 0.4 mm as a universal corrosion threshold crack width for all concretes regardless of quality and cover depth is, inasmuch as being conservative, prescriptive and not valid. This study proposes the adoption of performance-based crack width limits that take into account the combined influence of relevant factors affecting corrosion rate, in this case, cover depth, crack width and concrete quality. It is on this understanding that the proposed prediction model was developed.

The impact of increasing cover depth on corrosion rate was relatively lesser in the field-based specimens than in the laboratory-based specimens, with the highest reductions being recorded in the laboratory-based blended cement specimens - up to 43% in uncracked specimens made with 70/30 PC/FA (0.55 w/b) and up to 45% in 0.7 mm cracked specimens made with 50/50 PC/GGBS (0.40 w/b). These results contradict those of some previous studies where the highest reductions in corrosion rate as a result of increased cover depth were recorded in PC concretes. It is not clear why this trend was reversed in this study, and further work is needed to ascertain this. Furthermore, the trend was not observed in the field-based specimens where no specific trend was evident, and again, highlights the limitations of relying solely on laboratory-based accelerated corrosion experiments to predict the performance of in-service RC structures. Although the impact of increased cover depth was expected to have a significant impact on corrosion rate in uncracked specimens, this was not the case, and underscored the fact that corrosion rate is not only controlled by cover depth but by a complex interaction of other influencing factors.

The results also show that regardless of the exposure environment, for a given set of crack width and cover depth, corrosion rate increased with decreasing concrete quality (or increase in penetrability). The quality of the concretes, quantified using the diffusion coefficient determined empirically from the chloride conductivity index test, which measures chloride ion penetrability of concrete, decreased in the order PC/GGBS (0.40 w/b) → PC/FA (0.40 w/b) → PC/GGBS (0.55 w/b) → PC/FA (0.55 w/b) → PC (0.40 w/b). However, the change in concrete quality due to change in binder type had a relatively lower effect on corrosion rate in the field-based specimens than in the laboratory-based specimens. The results also show that the blended cement concretes respond to changes in w/b ratio in a similar manner but are not as sensitive to the change in w/b ratio (0.40 to 0.55 or vice versa) as PC concrete. In general, for a given blended cement concrete, even though reducing the w/b ratio further decreases the concrete's penetrability and hence corrosion rate, the effect is less (up to 60% decrease in uncracked field-based PC/FA specimens with 40 mm cover due to increase in w/b ratio from 0.55 to 0.40) in comparison to that due to the presence of the supplementary cementitious material itself (up to 74% decrease in incipient-cracked laboratory-based specimens with 20 mm cover due to 30% replacement of PC with FA at a w/b ratio from 0.40).

Based on the experimental results, a framework was proposed that can be used to objectively compare predicted corrosion rates for specimens with similar concrete qualities (binder type and w/b ratio) but different cover depths and crack widths. The framework, which incorporates the combined influence of cover depth, crack width and concrete quality on corrosion rate, is the basis of the proposed corrosion rate prediction models for cracked concrete. In the proposed models, the cover-to-crack width ratio is used in conjunction with concrete quality. The models can be used to (i) quantify the propagation phase with respect to a given performance limit (e.g. loss of steel cross-section area) using relevant corrosion-induced damage prediction models, and (ii) select suitable design combinations of cover depth, concrete quality and crack width to meet the desired durability performance (with respect to steel corrosion) of a given RC structure in the marine environment. In addition, the models can aid in the development of pro-active maintenance and repair strategies for corrosion-affected RC structures.

The sensitivity analyses performed using the field-based corrosion rate prediction model for cracked concrete due to its output being natural corrosion rate show that if any two of the three input parameters (cover depth, crack width and concrete quality/penetrability) are simultaneously varied, their effect on corrosion rate is dependent on the value of the third (unchanged) parameter. For example, the extent to which a combined change in both cover depth and crack width affects corrosion rate is dependent on the value for concrete quality; the higher the concrete penetrability, the greater the change in corrosion rate due to a combined change in cover depth and crack width. Further, the extent to which a change in either crack width or cover depth affects corrosion rate is dependent mainly on the concrete quality. For example, the higher the concrete quality, the higher the extent to which a change in crack width affects corrosion rate. The initial cover depth was found to have no effect on the extent to which a change in cover depth affects corrosion rate; a similar trend was found in the case of sensitivity of corrosion rate to change in crack width. In general, the findings of this study are in agreement with those of some previous studies where corrosion rate is reported to be more sensitive to change in concrete quality than crack width (and cover depth). This work has shown that the change in corrosion rate is greater whenever concrete quality is varied than when either crack width or cover depth are varied. The practical implication of the findings of this study is that even though cover cracking increases corrosion rate, and that it should be objectively minimized, corrosion protection cannot be achieved solely by limitation of crack width; a holistic approach, in this case, considering cover depth, concrete quality and crack width should be adopted. The proposed empirical model, which will need to be updated and calibrated using long-term natural corrosion rate data and extended to incorporate more input parameters, is a step towards achieving this goal.

This study and previous ones have shown that cover cracking affects corrosion rate of steel in RC structures. Therefore, it is essential to quantify its effect on corrosion initiation and its propagation, and more importantly, develop a design framework to incorporate this effect in performance-based design codes. Consequently, the development of (a) accurate models to quantify transport properties in cracked concrete, and (b) practical and reliable corrosion rate prediction models. This study was an effort towards achieving the latter challenge but further work is inevitably still needed.

Acknowledgements

I would like to express my sincere gratitude to my supervisors Associate Professor Hans-Dieter Beushausen and Professor Mark Gavin Alexander for their guidance, encouragement and technical support during this study. It was a great privilege to work under your supervision.

I would also like to extend my sincere gratitude to the following persons for their valuable support:

- Professor Michael Raupach - Institute of building materials research (ibac), RWTH Aachen University, Germany.
- Associate Professor Manu Santhanam - Building Technology and Construction Management Division, IIT Madras, India.
- My fellow postgraduate colleagues in the in the Concrete Materials and Structural Integrity Research Unit (CoMSIRU), Department of Civil Engineering, University of Cape Town.
- Ms Elly Yelverton - Research Administrative Officer in CoMSIRU
- Personnel in the Civil Engineering Concrete Laboratory and the Workshop under the leadership of, respectively, Mr Nooredien Hassen and Mr Charles Nicholas.

I also thank the following organizations for their valuable support in one way or another:

- The Concrete Institute (TCI) - erstwhile Cement and Concrete Institute (C&CI), South Africa
- Pretoria Portland Cement Ltd (PPC)
- Afrisam South Africa (Pty) Ltd
- Ash Resources (Pty) Ltd
- Sika South Africa (Pty) Ltd

TABLE OF CONTENTS

APPENDICES

List of Figures

List of Tables

Lists of abbreviations and symbols

Abbreviations

CCI: Chloride conductivity index
DI: Durability index
FA: Fly ash
GGBS: Ground granulated blastfurnace slag
PC: Plain Portland cement
RC: Reinforced concrete
SCM: Supplementary cementitious material

Symbols

c: Concrete cover depth (mm)
CCI_{90}: 90-day chloride conductivity index (mS/cm)
D_{90}: Chloride diffusion coefficient (cm^2/s) obtained from CCI_{90}
i_{corr}: Corrosion current density (corrosion rate)
***i_{corr}* (*t_i* + 2¼ yrs)**: Corrosion rate corresponding to approximately 2¼ years after corrosion initiation
t_i: Corrosion initiation phase
t_p: Corrosion propagation phase
w_{cr}: Surface crack width (mm)
ρ: Concrete resistivity (kΩ-cm)

Chapter 1

Introduction

1.1 *Background*

Corrosion of steel reinforcement is one of the main deterioration mechanisms for reinforced concrete (RC) structures in temperate, marine, and industrial environments. It has therefore become a major durability concern for both asset owners and engineers. If left unabated, it accelerates the ageing of RC structures and may lead to several inter-related negative consequences including, but not limited to, cracking and spalling of concrete cover, loss of steel cross-section area, degradation of steel-concrete interface bond, and ultimately reduction in service life of the RC structure. In addition, it requires high expenditures for maintenance, repair or replacement, and compromises public safety. Even though corrosion of steel in RC structures can be caused mainly by either ingress of carbon dioxide (carbonation-induced) or chlorides (chloride-induced) as will be seen in Chapter 2, the latter is the chief cause of steel corrosion in RC structures (in most countries). Notably, chloride-induced corrosion causes widespread damage of the RC structure and may ultimately result in failure (depending on the pre-defined limit state) within a relatively short period of time (before the structure meets its target service life). Much research has focused on the first phase of chloride-induced corrosion (i.e. corrosion initiation, t_i, characterised by negligible corrosion-induced damage, Figure 1.1) and a good understanding exists on this topic although more research is still required to fully comprehend some issues such as chloride binding mechanisms, and hence facilitate its accurate mathematical (numerical and analytical) modelling. However, the second phase (i.e. corrosion propagation, t_p, characterised by increased corrosion-induced damage, Figure 1.1) is still not well understood both in terms of process and prediction. Maintenance and repair of corrosion-damaged RC structures has therefore for a long time been based largely on reactive strategies and past experience. An accurate prediction of the corrosion propagation process is therefore vital from both economic and structural performance viewpoints.

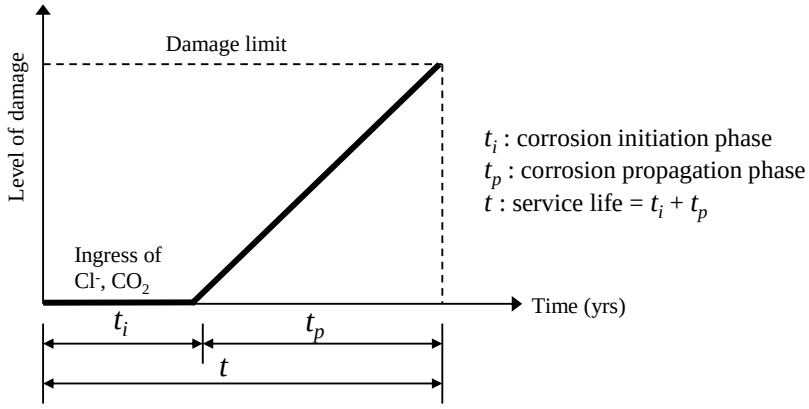

Figure 1.1: Tuutti's corrosion damage model - corrosion initiation and propagation phases [1]

In the past, the service life of corrosion-affected RC structures has been quantified only by the initiation phase, t_i, [2]; prediction models that have been used to describe this phase satisfactorily are available e.g. LIFE 365 [3], DuraCrete [4], Clinconc [5] and the South African chloride penetration model [6]. However, as the number of deteriorated RC structures continues to increase rapidly, and in an effort to meet both durability and sustainability requirements of corrosion-affected RC structures, service life prediction and life-cycle management beyond the initiation phase is now receiving more attention than in the past [7]. As a result, there is currently a move towards extending the service life definition of RC structures prone to steel corrosion. In addition to the initiation phase, there are attempts to quantitatively incorporate the corrosion propagation phase. The impetus of this move to include corrosion propagation in the design service life of RC structures can be assigned to a combination of the following premises:

(i) The rapid increase in the number of deteriorated RC structures due to corrosion and the resulting urgent need to develop pro-active maintenance and repair strategies for RC structures.
(ii) At the end of the initiation phase, the RC structure may still have adequate residual serviceability and strength with or without remedial measures [8].
(iii) The propagation phase may in some circumstances be sufficiently long to merit quantification and hence be part of the structure's service life, t, e.g. in the presence of service load-induced concrete cracking where active corrosion initiation may be almost instantaneous in the presence of corrosion-inducing species i.e. $t_i = 0$ or $t = t_p$ [9].
(iv) For new RC structures exposed to corrosion-aggressive environments, the propagation phase may extend for a relatively long period of time after corrosion initiation depending on the performance limit state indicator adopted (e.g. corrosion-induced cover cracking) and the effectiveness of the maintenance and repair actions undertaken.
(v) For existing RC structures, there is always a need to predict the propagation state of the structure (during the corrosion process), for maintenance, repair and/or protection evaluation purposes.

Coupled with this paradigm shift is a strong interest to understand, predict and hence design for the corrosion propagation phase of the service life of RC structures. In short, it is appropriate to state that the determination of steel depassivation in concrete (i.e. corrosion initiation) is now beginning to be seen as a step towards the determination of either a serviceability or ultimate limit state within the propagation phase. Consequently, a demand exists for both reliable prediction models for the corrosion propagation phase (i.e. durability performance forecasting) and non-destructive in-situ corrosion propagation assessment techniques to meet the aforementioned goals.

Despite considerable research on the corrosion propagation phase reported in the literature, it is seldom taken into consideration when defining the service life of new or existing RC structures. It is generally perceived that the corrosion initiation phase will be much longer than the corrosion propagation phase ($t_i >> t_p$) although this may not be valid in the case of cracked concrete as will be seen in Chapter 2. Some reasons why the corrosion propagation phase is not included in service life prediction models include the following:

(i) Corrosion rate is a function of many variables, some of which are still not well understood; and present a considerable degree of variability and uncertainty. These variables are inter-related in such a complex way that the mutual influence may be additive, synergistic, or opposing [4].

Although this is also the case with corrosion initiation, the focus of this study is on the propagation phase. To allow for the fact that there are still considerable degrees of variability and uncertainty in data and in some of the models, probabilistic methods should be applied [10]. However, although effort is being made towards developing and applying probabilistic methods, the main hindrance is usually lack of adequate data.

(ii) There are no "standard" corrosion assessment techniques. The available techniques have their inherent advantages and disadvantages that are either not known or if known, are seldom taken into consideration during the interpretation of the results. Furthermore, different corrosion assessment techniques have been reported to give varied results for the same subject parameter under the same measurement conditions e.g. corrosion rate [11].

(iii) Lack of a clear definition of the corrosion-induced damage indicators (i.e. for serviceability and ultimate limit states).

1.2 *Definition of service life for RC structures prone to corrosion*

The service life (t) of RC structures, with respect to reinforcement corrosion, is usually modelled as comprising distinct phases following pre-defined limit states with distinct corrosion-induced damage indicators. A *limit state* refers to a state beyond which the structure or part of it no longer satisfies the relevant performance criteria [12]. The approach of modelling service life into distinct phases was first used by Tuutti [1] who proposed a conceptual model dividing the service life (t) of a corrosion-affected RC structure into two phases viz the initiation phase, t_i, (or time to active corrosion initiation) and propagation phase, t_p, i.e. $t = t_i + t_p$ (see Figure 1.1). Tuutti's model is generalised with respect to t_p; it does not depict the different stages of corrosion-induced damage in the propagation phase. To account for this, the propagation phase, which is the focus of this study, can further be sub-divided into sub-phases as shown in Figure 1.2. In this approach, the boundaries between these sub-phases can be defined by different limit states (i.e. corrosion-induced damages on the RC structure) such as loss of concrete-steel interface bond [13], appearance of surface corrosion-induced cracks [14, 15], longitudinal deflections of flexural members [16], loss of flexural stiffness [17, 18] and reduction of a member's ultimate load capacity [13, 19].

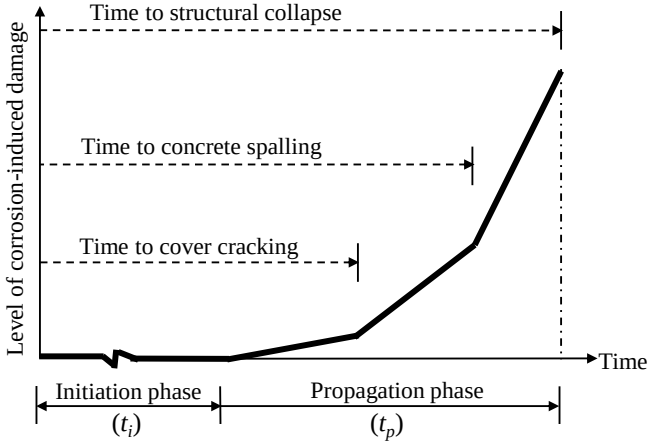

Figure 1.2: Service life of corrosion affected RC structures incorporating sub-phases [20]

The approach presented in Figure 1.2 is preferable to Tuutti's model because in most cases, although the degree of corrosion is closely related to structural deterioration, the relationship between the degree of corrosion to cracking, deflection and strength is not straightforward [17, 21]. Furthermore, such an approach makes it possible to compare and evaluate alternative solutions more objectively, plan for maintenance and repairs and optimize the cost with respect to the life cycle of structures.

1.2.1 *Classification of marine exposure environments*

Chloride-induced corrosion (which will be discussed in detail in Chapter 2) is one of the main causes of deterioration in RC structures located in chloride laden environments. Such environments are found mostly in coastal (marine) regions in South Africa. With respect to steel corrosion in concrete, marine environments are usually classified depending on the severity of chloride-induced corrosion damage over a given time. The classification adopted in this study is that of EN 206-1 [22] given in Table 1.1. Notice that, in Table 1.1, some Classes have been modified for South African conditions [23].

Table 1.1: South African marine environmental classes for chloride-induced corrosion [22]

EN206-1 Class	Description of the environment
XS1	Exposed to airborne salt but not in direct contact with seawater
XS2a	Permanently submerged
XS2b*	XS2a + exposed to abrasion
XS3a	Tidal, splash and spray zones
XS3b*	XS3a + exposed to abrasion

* These sub-classes have been added for South African coastal conditions

This study focuses on exposure Class XS3a (tidal zone) mainly because (i) it is considered the most common aggressive marine environment in terms of steel corrosion in RC structures [24, 25] and, (ii) the economic and social consequences of failure of the vast infrastructure (e.g. bridges, jetties) in this exposure environment are high.

1.3 *Research motivation and significance*

In order to incorporate the propagation phase in the service life of corrosion-affected RC structures, it must be reasonably accurately quantified, similar to the initiation phase. The quantification must be carried out based on corrosion-induced damage indicators that can be directly or indirectly related to the in-service structural response. Some of these damage indicators, as mentioned in the previous sections, include loss of concrete-steel interface bond, loss of a member's ultimate load capacity, loss of flexural stiffness, appearance of surface corrosion-induced cracks and increased longitudinal deflections of flexural members. Prediction models have been developed by various researchers to predict the time to occurrence of some of these damage indicators. Among other input parameters in these prediction models, corrosion rate, which is one of the most important input parameters in corrosion-induced damage prediction models [26], is seldom well defined with respect to its prediction and measurement (or quantification). There have been attempts to predict corrosion rate in the past by some researchers such as Alonso *et al*. [27], Katwan *et al*. [28], Yalcyn and Ergun [29], DuraCrete [4], Vu and Stewart [30], Scott [31], Bastidas-Arteaga *et al*. [32] and Martinez and Andrade [33]. These will be covered in detail in Chapter 2. A critical examination of the available corrosion rate prediction

models indicates that their applicability may be limited, and more importantly, that they do not directly or indirectly take into account the effect of service load-induced cover cracking on corrosion rate. The fact that most in-service RC structures are often in cracked state is often ignored [34, 35].

In determining a corrosion rate value to input in the corrosion-induced damage prediction models, it is important that relevant quantifiable parameters are taken into consideration. This study focuses on the quantification of the effect of cover depth, concrete quality (binder type and w/b ratio), concrete resistivity (or its inverse, conductivity) and crack width on chloride-induced corrosion rate. The goal is to develop an empirical chloride-induced corrosion rate prediction model expressed as a function of a combination of these parameters. This is main contribution of this study.

With respect to maintenance and repair of corrosion-affected RC structures, it is acknowledged that remedial measures on RC structures are usually more economical and viable prior to the end of the corrosion initiation phase than during the propagation phase. Nevertheless, this study focuses on the propagation phase and will assume that the RC structure is in this phase of deterioration, because practically, this period is of importance to maximize the life of corrosion-affected RC structures, and because a large stock of existing RC structures are in this phase and require proper management. With this in mind, a good understanding and prediction of performance of the RC structure during the corrosion propagation phase will assist both asset owners and engineers to plan and implement cost-effective and durable maintenance and repair strategies for RC structures. In general, the prediction of corrosion rate can be used to plan and prioritize inspection, testing, preventative maintenance and repair activities. The improved knowledge will enable designers not only to properly rehabilitate and maintain the current stock of corrosion-affected RC structures, but will also improve the durability of new ones by giving, in the design stage, proper consideration to (i) the selection of suitable combinations of corrosion rate-influencing parameters such as cover depth, crack width and concrete quality, and (ii) the exposure environment and conditions within which they operate [36].

Finally, this study also contributes towards sustainable concrete construction directly and/or indirectly by ensuring that the service life of corrosion-affected RC structures is maximised.

1.4 *Why an empirical corrosion rate prediction model?*

Despite the challenges faced when developing mathematical (numerical and analytical) corrosion rate prediction models, such as simulating complicated geometries (e.g. reinforcement details), non-homogeneous material (concrete and steel) properties, and the influence of cover cracking on corrosion, a number of researchers have developed and validated such models using data from well-controlled laboratory experiments [37-43]. However, even though these models are usually very comprehensive with respect to describing the corrosion process of steel in concrete and can theoretically be applied to RC structures in a wide range of exposure conditions, their practical application has been limited mainly because the selection and quantification of the input parameters poses a major challenge (e.g. distribution of anodic and cathodic sites on steel surface, potential distribution on the steel surface, pH of concrete pore solution and Tafel slopes). Even amongst researchers, there is uncertainty associated with the selection of the parameters, and different researchers have used different parameters (and even different values for the same parameter) to

model the corrosion process. Furthermore, even though mathematical models are based on fundamental governing equations for steel corrosion, they may not have a direct correlation to the actual corrosion process in concrete and the related corrosion-induced damage in in-service RC structures, and must be validated using experimental data. Finally, the implementation of the complex mathematical corrosion rate prediction models is sometimes computationally expensive.

These challenges have prompted the preference of empirical corrosion rate prediction models to mathematical ones despite the limitations associated with the former, such as being (to a large extent) limited to the experimental set-up conditions used to obtain data for its development. However, it is important to note that empirical models can be improved using numerical methods, and can form a strong foundation on which mathematical models can be developed. This study therefore opted for the development of empirical models mainly because, in comparison to mathematical models, they are simple in form and hence relatively simpler to apply in practice than the latter. This is in addition to the limitations faced during the study (see Section 1.6). More details on mathematical and empirical models will be presented in Chapter 2.

1.5 *Objectives and aims of the study*

The main objectives of this study are:

1. to develop empirical corrosion rate prediction models for chloride-induced corrosion in cracked and uncracked RC structures in the tidal marine environment i.e. exposure class XS3a according to the modified EN 206-1 [22] exposure classes (see Table 1.1), and
2. to demonstrate that the models are practical and easy-to-use for engineers, especially with respect to obtaining the model input parameters.

In addition to the objectives mentioned above, this study aims to achieve the following:

(i) to carry out a sensitivity analysis on the model input parameters to establish which parameter or combination of parameters corrosion rate is most sensitive to. The experimental model input parameters considered are cover depth, concrete quality (binder type and w/b ratio) and crack width.

(ii) to illustrate how the corrosion rate prediction models can be used in the design of new RC structures prone to chloride-induced corrosion deterioration i.e. selection of a suitable combination of performance-based design parameters such as concrete quality, cover depth and limiting crack width.

(iii) to illustrate how the corrosion rate prediction models can be used to extend the life of existing chloride-induced corrosion-affected RC structures beyond the initiation phase by aiding in the quantification of the propagation phase.

(iv) to establish a correlation between laboratory accelerated (cyclic 4-days wetting with 5% NaCl and 3-days air-drying) and natural (marine tidal zone) corrosion rates of steel in concrete.

1.6 *Scope and limitations*

Chloride-induced corrosion in RC structures is influenced by a complex inter-relationship of factors such as concrete quality, cover depth, cover cracking, concrete resistivity (or its inverse, conductivity) and severity of the exposure environment with respect to corrosion-sustaining species such as

chlorides and moisture. It is now well appreciated that for an accurate service life prediction of RC structures prone to corrosion, the inter-relationship between these factors should be considered to obtain suitable performance-based combinations of the relevant parameters and exposure environment. However, before this can be conclusively achieved, it is important to understand the relationship between the individual factors and corrosion rate. In addition, as will be seen in Chapter 2, several methods are available for the assessment of corrosion, each with its inherent advantages and disadvantages. It would be ideal to simultaneously consider these issues in order to fully describe the corrosion propagation process and hence quantify the propagation phase of service life in corrosion-affected RC structures. However this is not experimentally possible - only a limited combination of parameters can be investigated at a time and their relationship with corrosion rate evaluated. Therefore, the scope of this study was limited to the following aspects:

1. Only chloride-induced corrosion propagation of steel was studied. Even though carbonation-induced corrosion of steel also occurs in RC structures, it is not usually a major concern for RC structures in marine environments where chloride-induced steel corrosion is the main cause of deterioration.
2. As already mentioned, marine environments are classified according to the severity of chloride-induced steel corrosion in RC structures. This study was limited to marine exposure in the tidal zone (i.e. Class XS3a, see Table 1.1). This is considered the most severe marine exposure in Cape Town (Table Bay) in the Western Cape Province, South Africa (Figure 1.3), where this study's field-based specimens were exposed.

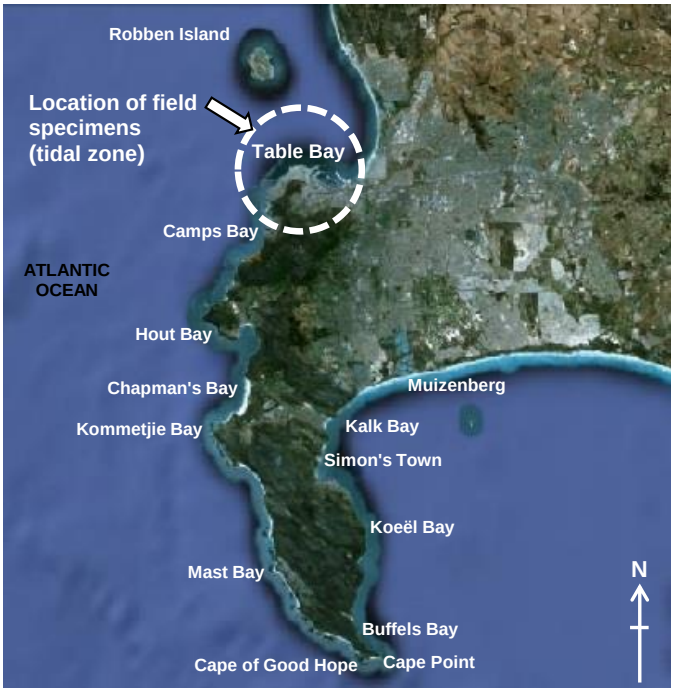

Figure 1.3: Geographical location of the marine exposure environment for the field-based specimens

3. In an experimental programme such as the one used in this study, only a limited number of the parameters affecting corrosion rate can be investigated at a time. In this study, the experiments were carried out in the laboratory (accelerated corrosion) and in the marine tidal exposure (natural

corrosion) in parallel. The experimental parameters were limited to the list given below. Details on the selection criteria of these parameters, specimen geometry, sample size and exposure environments are given in Chapter 3.

(i) Concrete quality: this was differentiated by varying the binder type and w/b ratio. Three binder types (CEM I 42.5N (PC), 50/50 PC/GGBS and 70/30 PC/FA) and two w/b ratios (0.40 and 0.55) were used.

(i) Cover depth: two cover depths, 20 and 40 mm, were used.

(ii) Crack widths were limited to: uncracked, incipient-cracked, 0.4 mm and 0.7 mm. However, incipient-cracked specimens were made using only specimens with 20 mm cover depth.

(iii) Two exposure environments were selected: (a) laboratory environment where accelerated chloride-induced corrosion occurred by cyclic 3 days wetting (with 5% NaCl solution) and 4 days air-drying (at controlled temperature and relative humidity of 25 ± 2 ^{o}C and 50 ± 5% respectively), and (b) field environment where natural chloride-induced corrosion occurred in the tidal marine zone.

(iv) The sample size was limited to a total of 210 corrosion beam specimens of dimensions 120 x 130 x 375 mm long. Each of the exposure environments (laboratory and field) had an equal number of specimens i.e. 105 beams each.

4. Only a single flexural macro-crack (visible on the concrete surface) was induced in each cracked beam specimen. Even though this may not be representative of crack patterns in most in-service RC structures, it greatly simplifies the experimental set-up, and more importantly, the understanding of the influence of one crack characteristic, crack width, which is the focus of this study. Further studies will be required to extend this understanding, and the model developed using the results of this study to incorporate not only multiple cracks but other crack characteristics such as crack healing, crack density/frequency and so on.
5. The study focused on the corrosion propagation phase, where most corrosion-induced damage occurs. The experimental programme was therefore designed to intentionally eliminate the initiation phase which, as mentioned before, is relatively well understood in process and prediction compared to the propagation phase. Furthermore, the initiation phase was eliminated due to the experimental time constraint for this study i.e. 2¼ years.
6. There are a variety of techniques that can be used to assess corrosion of steel in concrete. These are discussed in detail in Chapters 2 and 3. In this study, corrosion was assessed by taking the following measurements: (a) corrosion rate (using coulostatic linear polarization resistance method), (b) half-cell potential (with reference to Silver/Silver chloride, Ag/AgCl, electrode), and (c) concrete resistivity (using the 4-point Wenner probe).
7. Concrete quality with respect to ingress of corrosion-sustaining agents (oxygen and moisture) was assessed using the diffusion coefficients determined from the chloride conductivity test (details in Appendix D). Even though other (similar) test methods such as the Bulk Diffusion Test (also called NordTest NT BUILD) [44] and the Rapid Chloride Permeability Test [45] are available, the chloride conductivity test is the most commonly used test in South Africa for performance-based durability design and quality control.
8. Long-term data is necessary for the development of a reliable corrosion rate prediction model. In this study, both the field (natural corrosion) and laboratory (accelerated corrosion) corrosion rate

data were limited to 2¼ years due to time constraint. It is however important to note that long-term data will be required to verify and/or modify the proposed model.

9. The determination of gravimetric mass loss of steel due to corrosion and characterization of the surface morphology of corroded steel are important aspects of corrosion, and can be used to validate electrochemical measurement techniques. Previous studies have shown that in cracked concrete large corrosion pits are formed in the crack region where the anode is dominantly located. However, these aspects were not included in this study mainly because they are destructive assessment processes. They will be carried out in the future after sufficiently long-term results have been collected.
10. This study did not investigate the response of RC members/structures to steel corrosion. Aspects such as damage of steel-concrete interface and reduction of member flexural strength due to steel corrosion were not investigated.
11. Quantification of variability of the factors influencing corrosion rate is essential for an accurate prediction of corrosion rate. However, this was not comprehensively carried out in this study. Only the variability of the predicted corrosion rate was quantified using statistical distributions of the input parameters (crack width, cover depth and concrete quality) adopted from previous studies.
12. Finally, it is important to note that even though temporal (time-related) and spatial (location-related) variability of corrosion rate are important aspects in the quantification of corrosion rate, they were not considered in this study due to experimental constraints (i.e. design and equipment) with respect to measurement and quantification of the relevant parameters.

1.7 *Thesis outline*

This thesis has six chapters.

Chapter 2 presents a review of literature and is divided into two parts. Part I presents the fundamental principles of steel corrosion in concrete; emphasis is placed on chloride-induced corrosion and on cracked concrete which are the foci of this study. The thermodynamic and kinematic principles are covered in detail in this part. Part II presents a critical review of existing corrosion rate prediction models. Both empirical and numerical models are reviewed but focus is placed on chloride-induced corrosion and on empirical prediction models.

Chapter 3 presents a detailed description of the experimental work carried out in this study. This includes the laboratory (accelerated) and field (natural) corrosion experiments. Details on experimental variables and constants, materials, exposure environments, specimen geometry, number of specimens and corrosion assessment techniques are given. This chapter also presents a summary of other tests carried out in conjunction with the corrosion assessments.

Chapter 4 presents the results, analyses thereof and discussion of the experimental work (as described in Chapter 3). Both corrosion and concrete quality-related results are discussed. In this Chapter, empirical correlations are established between corrosion rate and other experimental variables such as cover depth, crack width, concrete quality and concrete resistivity. The results are synthesized to obtain a holistic view of the inter-relationships between corrosion rate and other experimental variables.

Chapter 5 presents the empirical chloride-induced corrosion rate prediction models based on the experimental results presented in Chapter 4. An attempt is made to establish an empirical relationship between laboratory (accelerated) and field (natural) corrosion rates. A sensitivity analysis of the proposed model input parameters (concrete quality, cover depth and surface crack width) is carried out to establish which parameter or a combination of parameters corrosion rate is most sensitive to. Examples illustrating the application of the proposed prediction models are also presented. Further, a simulation of the proposed models is carried out to quantify the variability in the predicted corrosion rate based on the variability of the input parameters. The variability is expressed as a statistical distribution. Finally, the model limitations are discussed.

Chapter 6 presents the conclusions and recommendations of this work.

1.8 *References*

[1] Tuutti, K. (1982) Corrosion of steel in concrete. *Swedish Cement and Concrete Research Institute, S-100 44 Stockholm*. Report No. CBI Research 4:82, ISSN 0346-6906, Stockholm, pp. 468.

[2] Sirivivantnanon, V. (2001) Effect of cracking on service life of concrete. *Proceedings of the international conference by the Concrete Institute of Australia*. 11th-14th September, Perth, Western Australia. pp. 273-279.

[3] LIFE-365 (2005) Computer program for predicting the service life and life-cycle costs of reinforced concrete exposed to chlorides. *ACI Committee 365*.

[4] DuraCrete (1998) Probabilistic performance-based durability design: modelling of degradation. Document No. BE95-1347/R4-5**,** The Netherlands.

[5] Tang, L. (2008) Engineering expression of the ClinConc model for prediction of free and total ingress in submerged marine concrete. *Cement and Concrete Research,* Vol. 38(8-9)**,** pp. 1092-1097.

[6] Mackechnie, J. R. (1996) Predictions of reinforced concrete durability in the marine environment. *PhD Thesis*, Department of civil engineering, University of Cape Town.

[7] Stewart, M. G., Wang, X.. & Nguyen, M. N. (2012) Climate change adaptation for corrosion control of concrete infrastructure *Structural Safety,* Vol. 35(3)**,** pp. 29-39.

[8] Jung, W. Y., Yoon, Y. S. & Sohn, Y. M. (2003) Predicting the remaining service life of land concrete by steel corrosion. *Cement and Concrete Research,* Vol. 33(5)**,** pp. 663-677.

[9] Otieno, M. B., Alexander, M. G. & Beushausen, H.-D. (2010) Corrosion in cracked and uncracked concrete - influence of crack width, concrete quality and crack re-opening. *Magazine of Concrete Research,* Vol. 62(6)**,** pp. 393-404.

[10] Li, C. Q., Yang, Y. & Melchers, R. E. (2008) Prediction of reinforcement corrosion in concrete and its effects on concrete cracking and strength reduction. *ACI Materials Journal,* Vol. 105(1)**,** pp. 3-10.

[11] Breysse, D., Klysz, G., Derobert, X., Sirieix, C. & Lataste, J. F. (2008) How to combine several non-destructive techniques for a better assessment of concrete structures. *Cement and Concrete Research,* Vol. 38(6)**,** pp. 783-793.

[12] ISO-2394 (1998) General principles on reliability for structures. *International Organization for Standardization, Geneva*.

[13] Zhang, R., Castel, A. & Francois, R. (2009) Serviceability limit state criteria based on steel-concrete bond loss for corroded reinforced concrete in chloride environment. *Materials and Structures,* Vol. 42(10)**,** pp. 1407-1421.

[14] Liu, Y. & Weyers, R. E. (1998) Modelling the time-to-corrosion cracking in chloride contaminated reinforced concrete structures. *ACI Materials Journal,* Vol. 95(6)**,** pp. 675-681.

[15] El Maaddawy, T. & Soudki, K. (2007) A model for prediction of time from corrosion initiation to corrosion cracking. *Cement & Concrete Composites,* Vol. 29(3)**,** pp. 168-175.

[16] Ballim, Y. & Reid, J. C. (2003) Reinforcement corrosion and the deflection of RC beams - an experimental critique of current test methods. *Cement and Concrete Composites,* Vol. 25(6)**,** pp. 625-632.

[17] Malumbela, G., Moyo, P. & Alexander, M. (2009) Behaviour of reinforced concrete beams under sustained service loads. *Construction and Building Materials,* Vol. 23(11)**,** pp. 3346-3351.

[18] Torres-Acosta, A. A., Fabela-Gallegos, M. J., Munoz-Noval, A., Vazques-Vega, D. & Hernandez-Jimenez, J. R. (2004) Influence of corrosion on the structural stiffness of reinforced concrete beams. *Corrosion,* Vol. 60(9)**,** pp. 862-872.

[19] Torres-Acosta, A. A., Navarro-Guitierrez, S. & Teran-Guillen, J. (2007) Residual flexure capacity of corroded reinforced concrete beams. *Engineering Structures,* Vol. 29(6)**,** pp. 1145-1152.
[20] Li, C. Q. (2004) Reliability based service life prediction of corrosion affected concrete structures. *ASCE Journal of Structural Engineering,* Vol. 130(10)**,** pp. 1570-1577.
[21] Yoon, S., Wang, K., Weis, W. J. & Shah, S. P. (2000) Interaction between loading, corrosion, and serviceability of reinforced concrete. *ACI Materials Journal,* Vol. 97(6)**,** pp. 637-644.
[22] BS-EN-206-1 (2000) *Concrete - Part 1: Specification, performance, production and conformity*, European Standard.
[23] Alexander, M. G. & Beushausen, H. (2007) Performance-based durability design and specification in South Africa. *Proceedings of the International Concrete Conference and Exhibition (ICCX - Concrete Awareness),* 14-16 February, 2007, Cape Town, South Africa.
[24] Broomfield, J. P. (2007) *Corrosion of steel in concrete - understanding, investigation and repair (2nd Edition),* Taylor & Francis, Oxford, United Kingdom.
[25] Melchers, R. E. & Jeffrey, R. (2012) Corrosion of long vertical steel strips in the marine tidal zone and implications for accelerated low water corrosion. *Corrosion Science,* Vol. 65(12)**,** pp. 26-36.
[26] Li, C. Q., Melchers, R. E. & Zheng, J. J. (2006) An analytical model for corrosion-induced crack width in reinforced concrete structures. *ACI Structural Journal,* Vol. 103(4)**,** pp. 479-487.
[27] Alonso, C., Andrade, C. & Gonzalez, J. A. (1988) Relation between resistivity and corrosion rate of reinforcements in carbonated mortar made with several cement types. *Cement and Concrete Research,* Vol. 18(5)**,** pp. 687-698.
[28] Katwan, M. J., Hodgkiess, T. & Arthur, P. D. (1996) Electrochemical noise technique for the prediction of corrosion rate of steel in concrete. *Materials and Structures,* Vol. 29(5)**,** pp. 286-294.
[29] Yalcyn, H. & Ergun, M. (1996) The prediction of corrosion rates of reinforcing steels in concrete. *Cement and Concrete Research,* Vol. 26(10)**,** pp. 1593-1599.
[30] Vu, K. & Stewart, M. G. (2000) Structural reliability of concrete bridges including improved chloride-induced corrosion models. *Structural Safety,* Vol. 22(4)**,** pp. 313-333.
[31] Scott, A. N. (2004) The influence of binder type and cracking on reinforcing steel corrosion in concrete. *PhD Thesis*, Department of civil engineering, University of Cape Town.
[32] Bastidas-Arteaga, E., Bressolette, P., Chateauneuf, A. & Sánchez-Silva, M. (2009) Probabilistic lifetime assessment of RC structures under coupled corrosion - fatigue deterioration processes. *Structural Safety,* Vol. 31(1)**,** pp. 84-96.
[33] Martínez, I. & Andrade, C. (2009) Examples of reinforcement corrosion monitoring by embedded sensors in concrete structures. *Cement & Concrete Composites,* Vol. 31(8)**,** pp. 545-554.
[34] Pettersson, K. & Sandberg, P. (1997) Chloride threshold levels, corrosion rates, and service life for cracked high-performance concrete. *Proceedings of the 4th CANMET/ACI International Conference on Durability of Concrete,* SP-170, V. M. Malhotra, Ed., Sydney, Australia**,** pp. 451-472.
[35] Coleman, J. W. (2013) Cracking... Defect of Normal? - Part 1: When is concrete cracking a construction defect? *Concrete International,* Vol. 35(9)**,** pp. 35-38.
[36] Isgor, O. B. & Razaqpur, A. G. (2004) Finite element modeling of coupled heat transfer, moisture transport and carbonation processes in concrete structures. *Cement & Concrete Composites,* Vol. 26(1)**,** pp. 55-73.
[37] Bažant, Z. (1979) Physical model for steel corrosion in concrete sea structures - Theory and application. *Journal of The Structural Division,* Vol. 105. ST6**,** pp. 1137–1166.
[38] Balabanic, G., Bicanic, N. & Durekovic, A. (1995) Numerical analysis of corrosion cell in concrete. *International Journal of Engineering Modelling,* Vol. 8(1-2)**,** pp. 1-5.
[39] Kranc, S. C & Sagues, A. A. (1997) Modelling the time-dependent response to external polarization of a corrosion macrocell on steel in concrete. *Journal of The Electrochemical Society,* Vol. 144(8)**,** pp. 2643-2652.
[40] Raupach, M. & Gulikers, J. (1999) A simplified method to estimate corrosion rates - a new approach based on investigations of macrocells. *Proceedings of the 8th International conference on durability of building materials and components*. May 30th - June 3rd, Vancouver, Canada.
[41] Isgor, O. B. (2001) A durability model for chloride and carbonation induced steel corrosion in reinforced concrete members, *PhD Thesis*, Cartelon University, Ottawa, Ontario, Canada.
[42] Song, H. W., Kim, H. J., Kwon, S. J., Lee, C. H., Byun, K. J. & Park, C. K. (2005) Prediction of service life in cracked reinforced concrete structures subjected to chloride attack and carbonation. *Proceedings of the International conference on cement combinations for durable concrete*. Dundee, Scotland, U.K.
[43] Huet, B., L'hostis, V., Santarini, G., Feron, D. & Idrissi, H. (2007) Steel corrosion in concrete: Determinist modelling of cathodic reaction as a function of water saturation degree. *Corrosion Science,* Vol. 49(4)**,** pp. 1918-1932.

[44] NT-Build-443 (1995) Nordtest Method: Concrete hardened; accelerated chloride penetration. Published by Nordtest, ISSN 0283-7153.
[45] ASTM-C1202-12 (2012) Standard test method for electrical indication of concrete's ability to resist chloride ion penetration. ASTM International, 100 Barr Harbour Drive, West Conshohocken, PA 19428-2959, USA.

Chapter 2

Literature review

2.1 *Overview*

This chapter is a review of corrosion of steel in RC structures with the aim to present (i) a fundamental understanding of the corrosion process in RC structures based on electrochemical and kinetic principles of corrosion, and (ii) a critical state-of-the-art review of previous studies on the prediction of corrosion rate. The chapter is divided into two parts. Part I, *Fundamentals of steel corrosion in concrete*, presents detailed electrochemical (both thermodynamic and kinetic) principles of corrosion in general followed by a focus on corrosion of steel in concrete and the factors that affect it. Part II, *Review of corrosion rate prediction models*, presents a critical review of the available/published corrosion rate prediction models for steel in RC structures. Specifically, the review identifies the strengths and weaknesses of the available models, and general and specific proposals to improve on them with respect to being representative of the actual corrosion process in RC structures.

Before proceeding, it is important to note that selected critical reviews relating to the experimental work (presented in Chapter 3) is carried out in this chapter in line with the focus of the study. Further, even though the review presented in this chapter covers, in general, corrosion of steel in concrete, focus will, from time to time, be placed on: (i) chloride-induced corrosion, (ii) empirical chloride-induced corrosion rate prediction models, and (iii) the influence of cracking on chloride ingress in concrete and corrosion rate of steel which are the foci of this study.

Chapter 2 PART I

Fundamentals of steel corrosion in concrete

2.2 *Introduction*

Corrosion may be defined as a dissolution process that occurs when metals are exposed to corrosive environments. It is an electrochemical process in which iron (Fe) enters into solution at the anode and oxygen (O_2) is reduced at the cathode [1]. It results in the flow of electrons (e^-) between anodic and cathodic sites (defined later) on the steel surface. The fundamental cause of corrosion is the inherent instability of metals in the refined metallic form. The tendency is for metals to revert to more stable forms, such as oxides, hydroxides or sulphides [2]. It is important to understand both the thermodynamics and kinetics of corrosion. These will be covered first to gain a general understanding of the corrosion process before focusing on steel corrosion in concrete later in the chapter.

2.3 *Thermodynamics of corrosion*

The tendency for any chemical reaction to proceed, including the reaction of a metal with its environment, is measured by the change in Gibbs free-energy (ΔG). Gibbs free energy is a thermodynamic potential that measures the maximum amount of non-expansive process-initiating work in an isothermal, isobaric thermodynamic system i.e. closed system. It can only be attained in a completely reversible process [3]. The more negative the value of ΔG, the greater the tendency for the reaction to proceed [4]. It is expressed as follows:

$$\Delta G = -zF\phi \tag{2.1}$$

where z is the number of electrons (or chemical equivalents) taking part in the reaction, F is Faraday's constant (96,500 C/mole) and ϕ is the electromotive force, *emf*, or half-cell potential, HCP, (V). The *emf* can be calculated from Nernst equation as follows:

$$\phi = \phi^o - \frac{RT}{zF}\ln K \tag{2.2}$$

Hence;

$$\Delta G = -zF\phi^o + RT\ln K \tag{2.3}$$

where ϕ^o is the *emf* when all reactants and products are in their standard states[1] [5] (activities equal to unity or, the electrode potential when the concentration in the adjacent solution is 1 mol/dm^3, temperature is 298.15 K and pressure is 1 bar = 101.325 kPa), R is the universal gas constant

[1] This is a reference point used to calculate its properties under different conditions. In principle, it can be arbitrarily chosen; but IUPAC (International Union of Pure and Applied Chemistry) recommends a conventional set of standard states for general use i.e. temperature of 298.15 K and pressure of 1 bar.

(8.314 J/deg.mole), *T* is the absolute temperature (also called thermodynamic temperature, 298.15 K) and *K* is the equilibrium constant of the reaction given by:

$$K = \frac{a_Q^q \times a_R^r}{a_L^l \times a_M^m} \quad \begin{matrix} \text{… Reactants in the forward reaction} \\ \text{… Products in the forward reaction} \end{matrix} \tag{2.4}$$

where a_Q^q, a_R^r, a_L^l and a_M^m are the activities of substances *Q* of quantity *q*, *R* of quantity *r*, *L* of quantity *l*, and *M* of quantity *m* respectively ('activity' is a dimensionless measure of the effective concentration of a species in a mixture i.e. its tendency to react). The activity of a substance a_i is given by:

$$a_i = e^{\left(\frac{\phi - \phi^o}{RT}\right)} \tag{2.5}$$

From Eqn. (2.2), the non-standard equilibrium potentials of the anodic and cathodic reactions, ϕ_{Fe} and ϕ_{O_2} (in the case of steel corrosion in concrete), can respectively be represented by the Nernst equation as follows [4]:

$$\phi_{Fe} = \phi_{Fe}^o - \frac{RT}{zF} \ln\left[Fe^{2+}\right] \tag{2.6}$$

$$\phi_{O_2} = \phi_{O_2}^o - \frac{RT}{zF} \ln\left[\frac{[OH^-]}{C_{O_2}^{0.25}}\right] \tag{2.7}$$

where ϕ_{Fe}^o and $\phi_{O_2}^o$ are the standard half-cell potentials of Fe and O_2 respectively and C_{O_2} is the concentration of O_2 at the steel-concrete interface. A system is said to be in thermodynamic equilibrium when its properties (e.g. temperature, pressure, potential) have defined values, and which do not tend to change with time [3]. Typical equilibrium electrode reaction potentials are given in Table 2.1.

Table 2.1: Standard anodic and cathodic electrode half-cell potentials [6]

Reaction		Electrode potential (mV vs. SHE[a]) at 25 °C
Cathodic	$2H^+ + e^- \rightarrow H_2$	0
	$O_2 + 2H_2O + 4e^- \rightarrow 4OH^-$	401
Anodic	$Fe^{2+} + 2e^- \rightarrow Fe$	-440

[a] Standard hydrogen electrode

The standard hydrogen electrode (SHE) is a redox electrode which forms the basis of the thermodynamic scale of oxidation-reduction potentials. Its absolute electrode potential is estimated to be 444 ± 20 mV at 25 °C, but to form a basis for comparison with all other electrode reactions,

hydrogen's standard electrode potential (E°) is taken to be zero at all temperatures. Potentials of any other electrodes are compared with that of the SHE at the same temperature.

2.3.1 *Graphical representation of thermodynamic equilibrium (Pourbaix diagram)*

The thermodynamic equilibrium of a metal in aqueous solution can be represented graphically in a plot of equilibrium half-cell potential ($ø_o$) vs. pH. Such a graphical representation, known as Pourbaix diagram (or potential (E)-pH equilibrium diagram), is essentially a phase diagram from which the conditions for thermodynamic stability of a single aqueous phase, or equilibrium of this phase with one or more solid phases, may be determined [7]. It is a map of thermodynamic possibilities. In this section, considering the scope of this study, a simplified form, which is commonly used, of the Pourbaix diagram of iron in water is presented as an example (Figure 2.1).

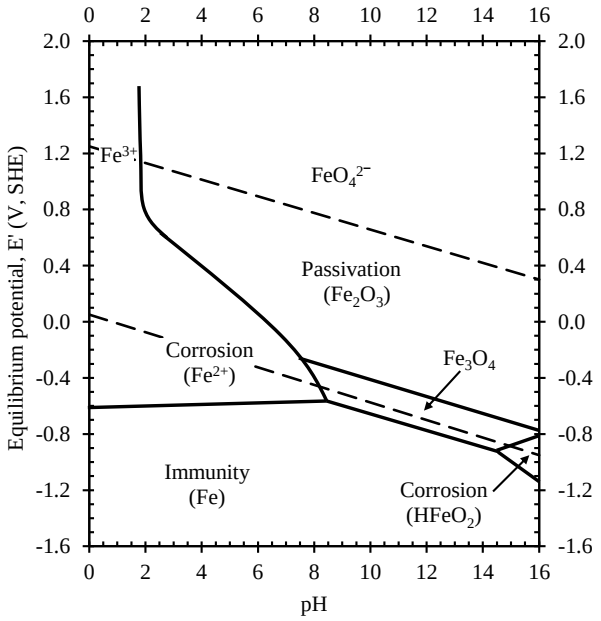

Figure 2.1: Simplified Pourbaix diagram for the iron/water system at 25 °C [8]

In concrete where chlorides are present, a fourth region is introduced in the Pourbaix diagram (Figure 2.2) denoting the range of potentials and pH over which pitting corrosion is possible [8]. This introduces a rupture potential (E_r) on the anodic polarization curve at which passivity breaks down and localized corrosion can initiate on the steel bar surface. At low concentrations of chlorides, E_r may exist at high potential values; thus, corrosion of depassivated areas may occur concurrently with oxygen evolution where passivity is intact.

The regions in Figure 2.1 and Figure 2.2 are interpreted as follows [7]; (i) immunity: if the potential and pH are in this region, the iron is thermodynamically immune from corrosion, (ii) corrosion: in these regions of potential and pH, the iron should ultimately become virtually all ions in solution, and therefore, iron exposed at these conditions should corrode, (iii) passivation: in this region, the equilibrium state is one of oxide plus solution. If iron is placed in potential-pH environments along one of these boundaries, oxide will form on the surface. If this oxide is adequately adherent, non-porous, and has high resistance to ion and/or electron transport, it will significantly decrease the rate of

corrosion. Under these conditions, the iron is said to have undergone passivation. Thus the stability of the passive film depends on two parameters, the electrode potential and the pH value [1].

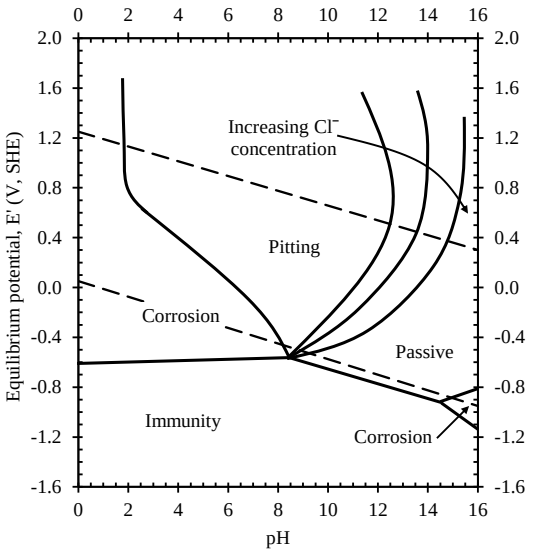

Figure 2.2: Potential-pH diagram for iron and water in the presence of chlorides [8]

Although Pourbaix diagrams are useful in making preliminary or very general predictions (i.e. as a quick reference) of the corrosion of metals as a function of electrode potential and pH, the following should be taken into consideration [7]:

(i) Interpretation of the Pourbaix diagram requires discussion of the experimental conditions under which, at least in principle, it would be determined.

(ii) In most cases, unavailability of data does not always permit construction of the diagram with acceptable accuracy for some purposes. For example, there may be uncertainties as to exactly which metal phase is stable at a given combination of pH and potential. Also, different phases may appear depending on the immediate past sequence of pH and potential changes, and although such phases are not truly equilibrium phases, they may persist and for practical purposes represent the steady state of the system.

(iii) The diagram has been criticized for leading to incorrect conclusions because reference only to the diagram does not recognize the generally controlling factors of rate and non-equilibrium.

In conclusion, the Pourbaix diagram is a useful resource for making predictions about the thermodynamic equilibrium of a metal in a given aqueous solution at a given potential, pH and temperature but should only be used as a quick reference.

2.4 *Kinetics of corrosion*

The concept of the tendency of corrosion to occur is based on thermodynamics presented in the previous section. In practice, however, also of primary concern is the rate of corrosion i.e. kinetics of corrosion. During corrosion process, current (in the form of electrons) flows between the anode and the cathode because of a potential difference between the two sites; the anode potential is more negative than the cathode potential, and the difference is the driving force for the corrosion current. The complete system of anode, cathode, electrolyte and metallic connection between anode and

cathode is termed a *corrosion cell* [9]. A metal may have a pronounced tendency to react but nevertheless react at a very slow rate, and may also be more resistant in some media than other metals that have inherently less tendency to react [4]. Electrode kinetics (i.e. the study of reaction rates at the interface between an electrode and a liquid (electrolyte)) makes it possible to understand corrosion and hence make practical measurement of corrosion rates. However, experiments by Scott [10] on corrosion of steel in various simulated pore solutions showed that the results are not similar to corrosion of steel embedded in actual concrete.

Important concepts of corrosion kinetics are polarization, corrosion potential (also called the mixed potential and the rest potential), corrosion current density, exchange current density and Tafel slope.

2.4.1 *Polarization*

An electrode is not at equilibrium when a net current flows to or from its surface. Depending on the magnitude of an external current and its direction, the potential of an electrode at equilibrium can be altered. In order to restore equilibrium in the system, the direction of potential change always opposes the shift from equilibrium and hence, opposes the flow of current whether the current is impressed externally or is of galvanic origin. The potential change caused by the net current to or from an electrode, measured in volts (V), is called polarisation, η [4]. Polarisation can be caused by one or a combination of different factors that are covered in the next sections.

2.4.1.1 *Concentration polarization*

Concentration polarisation, η_{conc}, (also called diffusion over-potential) occurs when the reaction rate or the applied external current is so large that the species being oxidized or reduced cannot reach the metal surface at a sufficiently rapid rate [11] i.e. it is caused by a slow supply of ions/molecules to the electrode (e.g. the lack of oxygen on the cathodic surfaces of steel in concrete). It mainly contributes to polarisation of the cathodic reaction, and is calculated based on the Nernst equation [4]:

$$\eta_{conc} = \frac{RT}{zF} \ln\left(\frac{i_L}{i_L - i}\right) \tag{2.8}$$

where i is the external (or applied) current density (A/m^2) and i_L (A/m^2) is the limiting current density of the cathodic reaction i.e. the corresponding current density that results when the activity, a, of the resulting metal ions approaches zero at the electrode surface. i_L is given by [4]:

$$i_L = D\frac{zF}{\delta t} \times C \times 10^{-3} \tag{2.9}$$

where D is the diffusion coefficient of the ion being reduced (O_2 in the case of steel corrosion in concrete) (m^2/s), δ is the thickness of the stagnant layer of electrolyte next to the electrode surface (about 0.005 mm in an unstirred solution e.g. concrete pore solution), t is the transference number (also called transport or Hittorf number) of all ions in solution except the ion being reduced (equal to

unity if many other ions are present) and C is the concentration of the diffusing ion (O_2 in the case of steel corrosion in concrete) in moles/litre. Transference number refers to the fraction of the total current carried in a solution by a given ion, or the contribution of an ionic species to the total current. The transference numbers of the anion and the cation adds up to unity. i_L can also be calculated by considering the concrete cover as a diffusion layer (the Nernst diffusion layer) through which steady-state diffusion of O_2 takes place. With this approach, the limiting current density, i_L, can be calculated as a closed-form equation as a function of concrete cover thickness, d (m), in the following form [12]:

$$i_L = D\frac{zF}{d} \times C \tag{2.10}$$

2.4.1.2 *Activation polarisation*

This is caused by a slow electrode reaction which requires activation energy in order to proceed [4]. The activation energy can either be an over-potential or over-voltage. *Over-potential* (η_a) is defined as the polarisation of an equilibrium electrode that results from current flow across the electrode-electrolyte interface. It is the difference between the measured potential ($\phi_{measured}$) and the thermodynamic or reversible potential ($\phi_{reversible}$):

$$\eta_a = \phi_{measured} - \phi_{reversible} \tag{2.11}$$

Over-voltage (ε) is the polarisation of a corroding electrode caused by flow of an applied current (e.g. in accelerated corrosion using impressed current). It is the difference between the measured potential and the corrosion (or mixed) potential (ϕ_{corr}):

$$\varepsilon = \phi_{measured} - \phi_{corr} \tag{2.12}$$

Corrosion (or mixed) potential (ϕ_{corr}) refers to the measured mixed potential of both polarized anode and cathode of a corroding metal. Activation polarisation increases with current density (i) according to the Tafel equation (which relates the rate of an electrochemical reaction to the over-potential) as follows [4]:

$$\eta_a = \beta \ln\left(\frac{i}{i_o}\right) \tag{2.13}$$

where β (Tafel slope) and i are constants for a given metal and environment and are both temperature-dependent, i_o is the exchange current density defined as follows: For a single half-cell reaction at equilibrium, a dynamic state exists in which charges move in equal numbers in each direction across the interface (see Figure 2.3). The kinetic activity of this dynamic equilibrium may be expressed as the number of ions moving in either direction per unit area per unit time. Since ions are transferred, the movement may also be expressed as charges transferred per unit area per unit time, or equivalently, as the current density, i (milliCoulombs/(s.m^2) or mA/m^2). Positive ions passing into solution constitute

an oxidation component of the current density, $i_{ox,M}$; positive ions passing from the solution account for the reduction component of the current density, $i_{red,M}$. At equilibrium: $i_{ox,M} = i_{red,M} = i_{o,M}$ where $i_{o,M}$ is the exchange current density; it is a measure of the kinetic activity of the half-cell reaction at equilibrium. Values of i_o vary from the order of 10^{-7} to 10^{+5} mA/m^2 [7].

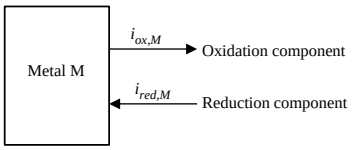

Figure 2.3: Schematic illustration of exchange current density [7]

The larger the value of i_o and the smaller the value of β, the smaller the corresponding over-potential. The i_o can be calculated as follows [13]:

$$i_o = nFk_o[Ox_s][Rx_s]^{\alpha-1} \tag{2.14}$$

where k_o [m/s] is the rate constant, [Ox_s] and [Rx_s] are, respectively, the activities of the oxidised and reduced species at the electrode surface at equilibrium. The Tafel equation (Eqn. (2.13)) is applied to each of the two (corrosion) half electrode reactions (i.e. anode and cathode) separately using appropriate constants for the anodic reaction (β_a and i_a), cathodic reaction (β_c and i_c) and exchange current densities ($i_{a,o}$ and $i_{c,o}$). The equation assumes that the reverse reaction rate is negligible compared to the forward reaction rate, and is applicable to regions where polarisation is high. At low values of polarisation, the dependence of current on polarisation is usually linear. The slope of the linear region (AB in Figure 2.4, for uniform corrosion, which is not common in RC structures as will be seen in Section 2.5) given by Eqn. (2.15) is called polarisation resistance, R_p [4].

$$i = \eta_a\left(\frac{zF}{RT}\right)i_o \text{ or } \eta_a = \frac{zF}{RT}\left(\frac{i}{i_o}\right) \tag{2.15}$$

Equation (2.15) gives a good approximation of current density if $\eta_a\left(\frac{zF}{RT}\right) < 0.5$ [13].

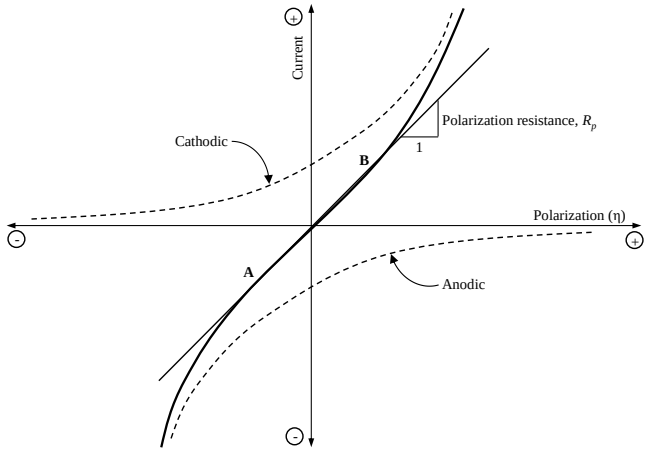

Figure 2.4: Schematic illustration of the linear part of a polarisation curve [11]

2.4.1.3 *Ohmic potential (iR) drop*

Ohmic potential drop occurs during polarisation measurements at (*a*) a portion of the electrolyte surrounding the electrode, (*b*) a metal-reaction product film on the metal surface, or both. It mostly occurs between the working electrode (reinforcing steel) and the capillary tip of the reference electrode (usually on the concrete surface), and is equal to *iR* (V/cm), where *i* is the current density and $R = l/k$, represents the value (in Ω) of the resistance path of length *l* cm and specific conductivity *k* ($\Omega^{-1}cm^{-1}$ i.e. S/cm) [4]. The *iR* contribution to polarisation can therefore be calculated as:

$$\text{Ohmic potential drop}\,(iR) = i \times \left(\frac{l}{k}\right) \text{V/cm} \tag{2.16}$$

iR decays instantaneously with shutting off of the current, whereas concentration polarisation and activation polarisation usually decays at measurable rates.

2.4.2 *Polarisation of steel in concrete*

Polarisation of steel in concrete can be caused by concentration, activation, *iR* drop or a combination thereof. *iR* drop is generally small except in cases where the anodic and cathodic sites are well separated and the conductivity of the pore solution is low, e.g. in 'dry' or high resistivity concrete [14] in which case the value of *R* in Eqn. (2.16) is taken as the Ohmic resistance of the concrete pore solution. Activation causes the anodic and cathodic polarisation while concentration controls cathodic polarisation in cases of insufficient O_2. The cathodic portions of the steel surface are therefore predominantly polarized by concentration polarisation [14]. This is covered in the next sections. Some researchers [e.g. 15] have assumed that during a cathodic-controlled corrosion process in concrete (i.e. where mainly concentration polarisation occurs), the anodes on the steel surface do not polarize. However, Isgor and Razaqpur [14] have noted that this is an over-simplification and that they are polarized by activation. In low resistivity concretes (e.g. PC concretes), where corrosion rate is cathodic-controlled [16], it is mainly concentration polarisation that is hindered by low O_2 concentration.

2.4.2.1 *Polarisation of anodic reaction*

Anodic polarisation is an activation polarisation process and can therefore be defined based on Eqn. (2.13) (also called *Anodic Tafel equation*) as follows:

$$\eta_a = \beta_a \ln \frac{i_a}{i_{a,o}} \tag{2.17}$$

where β_a is the Tafel slope of the anodic reaction (V/decade), i_a is the anodic current density (A/m^2) and $i_{a,o}$ is the exchange current density of the anodic reaction. Therefore the polarized potential (ϕ_a, V) of the anodic reaction can be represented as:

$$\phi_a = \phi_{a,o} + \eta_a = \phi_{a,o} + \beta_a \ln \frac{i_a}{i_{a,o}} \tag{2.18}$$

where $\phi_{a,o}$ is the equilibrium potential of the anode (V) under the prevailing conditions. The Tafel slope β_a is equal to [7]:

$$\beta_a = \ln\left(\frac{RT}{\alpha_a (z_a F)}\right) \tag{2.19}$$

where α_a is the anodic transfer coefficient ($\alpha_a < 1$ according to Pour-Ghaz *et al*. [17]) and z_a is the number of electrons exchanged at the anode.

2.4.2.2 ***Polarisation of cathodic reaction***

Both activation and concentration can contribute to polarisation of the cathodic reaction. Concentration polarisation can be determined based on Eqn. (2.8) (also called *cathodic Tafel equation*) as follows [4]:

$$\eta_{cc} = -\frac{RT}{z_c F}\ln\left(\frac{i_L}{i_L - i_c}\right) \tag{2.20}$$

where i_c is the cathodic current density (A/m^2), z_c is the number of electrons exchanged at the cathode ($z = 4$), and i_L (A/m^2) is the limiting current density of the cathodic reaction, and is defined based on Eqn. (2.9) as follows:

$$i_L = D_{O_2}\frac{z_c F}{\delta.t} C_{O_2} \times 10^{-3} \tag{2.21}$$

where D_{O_2} (m^2/s) is the effective O_2 diffusion coefficient in (unsaturated) concrete, C_{O_2} is the concentration of dissolved O_2 at the steel-concrete interface (mol/l) and z_c is the number of electrons transferred (for oxygen reduction, $z = 4$). The other terms are as defined in Eqn. (2.9), with $t = 1$ and $\delta \approx 0.005$ mm is the thickness of the layer or film of electrolyte around the steel surface [18]. The limiting cathodic current density takes into account the influence of oxygen diffusion through the concrete cover on the cathodic reaction [19]. It can also be calculated based on Eqn. (2.10).

Based on Eqn. (2.13), the contribution of activation polarisation to the cathodic polarisation can be determined as follows:

$$\eta_{ca} = -\beta_c \ln\frac{i_c}{i_{c,o}} \tag{2.22}$$

where β_c is the Tafel slope of the cathodic reaction (V/decade), i_c is the cathodic current density (A/m^2) and $i_{c,o}$ is the exchange current density of the cathodic reaction. The Tafel slope β_c is equal to [7]:

$$\beta_c = \ln\left(\frac{RT}{(1-\alpha_c)z_c F}\right) \tag{2.23}$$

where α_c is a constant (symmetry factor [17]). Therefore the total polarized potential (ϕ_c, V) of the cathodic reaction due to both concentration and activation can be represented as:

$$\phi_c = \phi_{c,o} + \eta_{cc} + \eta_{ca} = \phi_{c,o} - \left(\frac{RT}{z_c F}\ln\left(\frac{i_L}{i_L - i_c}\right)\right) - \left(\ln\left(\frac{RT}{(1-\alpha_c)(z_c F)}\right)\ln\frac{i_c}{i_{c,o}}\right) \tag{2.24}$$

where $\phi_{c,o}$ is the equilibrium potential of the cathode (V) under the prevailing conditions. Figure 2.5 summarises the anodic and cathodic polarisation processes. Note that the anodic and cathodic polarization curves do not intersect. This is due to resistance of the electrolyte between the anode and the cathode, which cannot be zero for concrete. When this resistance is significantly large, the amount of current (and hence the amount of polarization) is dependent on the resistance of the electrolyte; in these circumstances the corrosion is said to be under resistance control. The corresponding values of the current (or the current density) and equilibrium (open-circuit) potentials of the anode and the cathode are called anodic and cathodic exchange current density, i_{oa} and i_{oc} respectively.

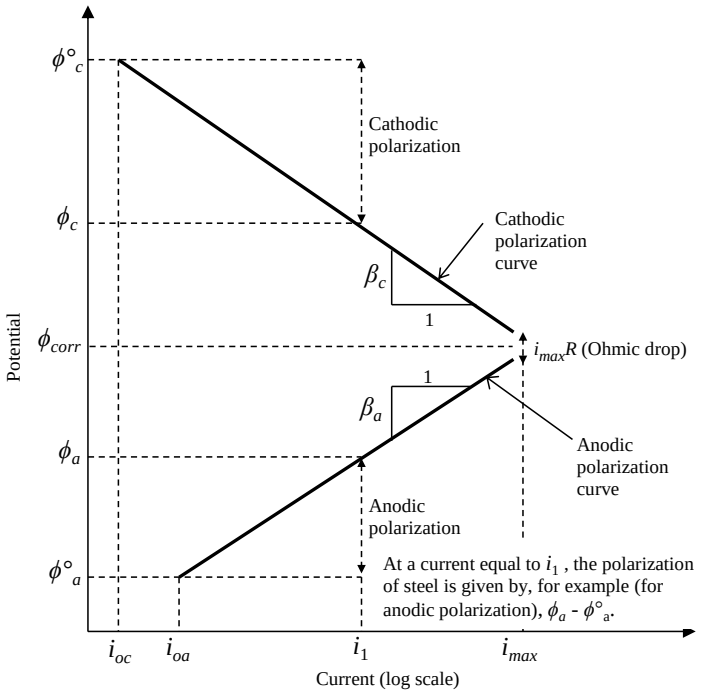

Figure 2.5: Combined polarisation curves on anodic and cathodic reactions [4]

2.4.3 *Influence of polarisation on corrosion rate (types of corrosion control)*

Both the resistance of the electrolyte and polarisation of the electrodes influence the magnitude of corrosion current. Depending on the dominant type and/or combination of polarisation, the following types of corrosion are possible [4]:

(i) when polarisation occurs mostly at the cathode, the corrosion reaction is said to be *cathodic-controlled*.

(ii) when polarisation occurs mostly at the anodes, the corrosion reaction is said to be *anodic-controlled*.
(iii) *resistance control* occurs when the electrolyte resistance is very high that the resultant current is not sufficient to appreciably polarize anodes and cathodes.
(iv) when polarisation occurs in some degree at both anodes and cathodes, the situation is referred to as *mixed control*.

Even though 'mixed control' type of corrosion is the case for all types of corrosion of steel in concrete, 'cathodic-control' dominates in blended cement concretes, with high resistivities, while 'anodic-control' dominates in PC concretes, with low resistivity [16].

2.4.4 ***Butler-Volmer equations***

If the potential deviates from the equilibrium potential, either the anodic or the cathodic reaction dominates (see Section 2.4.3). The electrochemical behaviour of active and passive steel areas is described using the Butler-Volmer equations (polarisation curves). The polarisation curves describe the relationship between the electrical current in an electrode and the electrode potential, considering that both cathodic and anodic reactions (or sites) occur on the same electrode (e.g. steel surface). If the rate-determining step in the electrode reaction is controlled only by the activation energy (without diffusion control) for the electron transfer for both the anodic and cathodic reactions, then the net current density can be described by the Butler-Volmer equation (see Eqns. (2.25) and (2.26), assuming uniform corrosion) [20].

$$i_a = i_{a,o}\left[\exp\left(\frac{\eta_a}{\beta_a}\right)\right] \text{ for the active steel area} \tag{2.25}$$

$$i_c = i_{c,o}\left[\exp\left(\frac{\eta_c}{\beta_c}\right)\right] \text{ for the passive steel area} \tag{2.26}$$

where β_a and β_c are, respectively, the anodic and cathodic Tafel slopes, α_a and α_c are, respectively, the anodic and cathodic charge transfer coefficients, z_a = 2 and z_c = 1 are, respectively, the number of electrons involved in the anodic and cathodic reactions, and $\eta_a = \phi_a - \phi_{a,o}$ and $\eta_c = \phi_c - \phi_{c,o}$ are, respectively, the anodic and cathodic activation over-potentials. In a combined form;

$$i = i_{a,o}\left[\exp\left(\frac{\eta_a}{\beta_a}\right)\right] + i_{c,o}\left[\exp\left(-\frac{\eta_c}{\beta_c}\right)\right] \tag{2.27}$$

Note that the sign convention for current is positive for i_a (anodic current) and negative for i_c (cathodic current). In summary, the Butler-Volmer equations describe the relationship between the electrical current on an electrode and the electrode potential, considering that both the anodic and cathodic reactions occur on the same electrode.

2.5 *Corrosion of steel in concrete*

Steel is an alloy made by combining iron (Fe) and other elements, the most common of these being carbon; other alloying elements such as manganese, chromium, vanadium and tungsten are sometimes used. When carbon is used, its content is between 0.2 and 2.1% by weight, depending on the grade of steel required i.e. hardness, ductility and tensile strength.

The conventional carbon steel grades commonly used as reinforcing steel in concrete are susceptible to corrosion when exposed to the atmosphere. However, steel embedded in concrete is naturally protected by the high alkalinity of the cement matrix (pH > 12.5) and by the barrier effect of the concrete cover. The concrete cover limits the amount of oxygen (O_2), moisture, carbon dioxide (CO_2) and chlorides (Cl^-), which are required to initiate and sustain corrosion. The high alkalinity results from the presence of sodium hydroxide (NaOH) and potassium hydroxide (KOH), due to the dominant alkalis in the cement i.e. sodium oxide (Na_2O) and potassium oxide (K_2O), in a saturated calcium hydroxide solution ($Ca(OH)_2$). Without ingress of species such as CO_2 and Cl^- into concrete during its service life, reinforcing steel remains protected due to the alkaline concrete pore solution, resulting in negligible corrosion rates. The high pH suppresses steel corrosion by encouraging the formation of a very thin (approximately 1-10 nm) passive and dense oxide film on the steel surface, a process called passivation [2, 4, 21, 22]. The passive and dense oxide film is made up of either gamma ferric oxide, γ-Fe_2O_3, [23] or a mixture of γ-Fe_2O_3 and magnetite (Fe_3O_4) [24]. The properties of the passive film (e.g. porosity, thickness and density) depends on factors such as chemistry and pH of the concrete pore solution, presence of chlorides, variation in temperature and chemistry and microstructure of steel reinforcement [25, 26].

The basic anodic and cathodic reactions in a steel corrosion process are as follows [27], Figure 2.6:

$$\text{Anodic reaction: } Fe \rightarrow Fe^{2+} + 2e^- \tag{2.28}$$

$$\text{Cathodic reaction: } 2H_2O + O_2 + 4e^- \rightarrow 4OH^- \tag{2.29}$$

Electrons released at the anode (oxidation) are consumed at the cathode (reduction). There are a variety of possible cathodic reactions depending on the availability of O_2 and the pH in the vicinity of the steel surface. In addition to the anode (where corrosion occurs and from which current flows) and cathode (where no corrosion occurs and to which current flows), the following are also essential to sustain the corrosion process (Figure 2.6):

- *Electrolyte*: a medium capable of conducting electric current by ionic current flow. In the case of concrete, the (alkaline) pore solution constitutes the electrolyte and,
- *Metallic path*: connection between the anode and cathode, which allows current return and completes the circuit. Steel serves this purpose in reinforced concrete.

Corrosion of steel in concrete results in the formation of rust, which can be oxides, hydroxides, oxide-hydroxides, sulphides of iron or complex mixtures of these depending on the O_2 availability, pH, potential and pressure [7]. For example Fe_2O_3 (red/brown rust), with a volume approximately twice the dissolving iron (but with same mass) is formed in presence of adequate O_2 while ‘black’ or ‘green’ rust is formed in O_2-deficient cases [28]. In the case of chloride-induced corrosion, the iron can also

complex with the chloride ions. Table 2.2 presents some of the possible products for corrosion of steel in concrete [29]. Table 2.2 also shows that the corrosion products have a higher volume (and lower density) compared to that of steel.

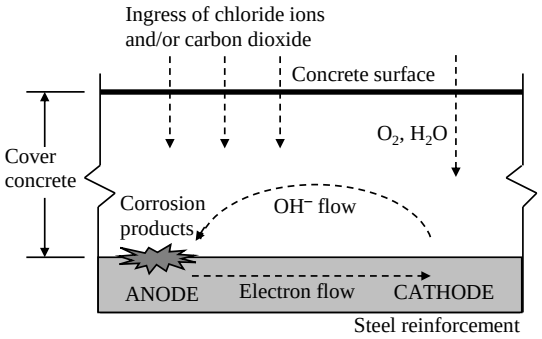

Figure 2.6: A schematic illustration of the corrosion process in concrete [30]

Table 2.2: Corrosion products [29, 31, 32]

Corrosion product	Density (g/cm^3)	Molar mass*	Volume ratio*
Iron (Fe)	7.87	1.000	1.00
Wustite FeO	5.74	0.778	1.70
Haematite α-Fe_2O_3	5.17	0.350	2.00
Magnetite Fe_3O_4 - Black	5.24	0.241	2.10
Goethite α-FeOOH	4.26	0.629	2.91
Lepidocrocite γ-FeOOH - Red-brown	4.09	0.629	3.03
$Fe(OH)_2$ - Dirty-green (Initial product)	3.40	0.622	3.60
Bernalite $Fe(OH)_3$ - Ferric hydroxide	3.90	0.523	4.00
Hydrated ferric hydroxide $Fe(OH)_3.3H_2O$	–	0.348	6.15
Other corrosion products			
β-Fe_2O_3			
ε-Fe_2O_3			
δ-FeOOH			
Maghemite γ-Fe_2O_3			
Akagenite β-FeOOH			
Feroxyhyte δ-FeOOH			
Ferrihydrite $Fe_5HO_8 \cdot 4H_2O$			
Schwertmannite, $Fe_{16}O_{16}(OH)_y(SO_4)_z \cdot nH_2O$			

* Molar mass and volume ratio relative to that of Fe

2.5.1 *Microcell vs. macrocell corrosion*

In concrete, the main causes of corrosion of the embedded steel are ingress of Cl^- and/or CO_2. Corrosion is characterised by spatial distribution of anodes and cathodes on the steel surface [19]. Macrocell (non-uniform or local) corrosion is characterised by a small anode and a large cathode i.e. the anode and cathode are clearly separated in different areas. This frequently occurs in chloride-induced corrosion and/or in concrete with a low resistivity (high conductivity) and is characterised by high local or pitting corrosion and hence localised steel cross-section reduction. In microcell (uniform

or general) corrosion the anodic and cathodic sites are adjacent to each other. It is common in carbonation-induced corrosion and/or in concrete with high resistivity e.g. carbonated concrete [1, 27].

This study focuses on chloride-induced corrosion and will therefore proceed with the latter in this Chapter unless explicitly mentioned otherwise.

2.5.2 *Chloride-induced steel corrosion initiation in concrete*

The time required for chlorides to penetrate through the cover concrete and reach the steel is dependent mainly on the penetrability of the cover concrete, and whether it is cracked or uncracked [33, 34]. For uncracked concrete, chloride ingress is usually assumed to occur predominantly by diffusion although other transport mechanisms such as convection and permeation, or a combination thereof, are possible. These are covered in Section 2.6.1. In the case of diffusion process, Crank's error function solution (also called *Gauss error function*) of Fick's 2nd law is commonly used to model the ingress of chlorides through concrete [35]:

$$C_{x,t} = C_s\left[1 - erf\left(\frac{x}{2\sqrt{Dt^{1-m}}}\right)\right] \tag{2.30}$$

where $C_{x,t}$ is the chloride concentration at the depth x after a given time t of exposure to chlorides, C_s is the surface chloride concentration, *erf* is the error function (a numerical function available in mathematical tables) and D is the diffusion coefficient and m is the ageing factor which takes into account the decrease in chloride diffusivity with time due to concrete densification as a result of continued cement hydration process and chloride binding [36].

However, in cracked concrete, the transport mechanisms involved in the transport of chlorides are still not well understood. Mohammed *et al*. [37] suggest that transport of different species in cracked concrete is a coupled phenomenon between the matrix and the crack. Parameters such as crack width, depth and shape, crack density/frequency and degree of connectivity, as well as crack origin, govern the transport of species in cracked concrete [38]. Therefore, no predictions on the behaviour of cracked concrete can be made based on data for uncracked concrete.

However, regardless of whether the concrete cover is cracked or not, for chloride-induced depassivation to occur, a given concentration of chlorides (chloride threshold) is required at the steel surface to disrupt the protective passive layer and initiate corrosion [28]. The chloride threshold is not a single value for all concretes but is affected by, among other factors, cover quality, exposure environment and chemistry of the binder [39, 40]. The chlorides (Cl^-) act as a catalyst to corrosion and are not consumed in the process of breaking down the passive layer. This allows the corrosion process to proceed faster [26, 28, 41], Figure 2.7. Chloride ions act as a catalyst for the oxidation of iron through the formation of the $FeCl_3^-$ complex which is unstable and can be drawn into solution where it reacts with the available hydroxyl ions (OH^-) to form $Fe(OH)_2$. This results in the release of Cl^- back into the solution and consumption of hydroxyl ions, as shown in the following equations:

$$2Fe + 6Cl^- \leftrightarrow 2FeCl_3^- + 4e^- \quad (2.31)$$

followed by:

$$2FeCl_3^- + 4OH^- \leftrightarrow 2Fe(OH)_2 + 6Cl^- \quad (2.32)$$

The electrons released in the oxidation reaction, Eqn. (2.31), flow through the steel to the cathode. Consequently, the concentration of chloride ions increases and pH at the points of corrosion initiation decreases, probably accounting for the process of pitting corrosion. The lowered pH (i.e. acidification) at these sites contributes to the continual breakdown of the passive oxide film [42]. The decrease in the ferrous ion concentration, due to its reaction with chlorides, leads to a change in half-cell potential, which can be measured following the procedures in ASTM C 876-91 [43]. Thus, lower half-cell potential does not indicate that 'more rust is present' but, actually, demonstrates dynamically that a corrosion process is almost certain to occur. This is the reason that, according to ASTM C 876-91, the half-cell potential measurements being more negative than –350 mV vs. $Cu/CuSO_4$ electrode demonstrates 90% certainty of possible corrosion.

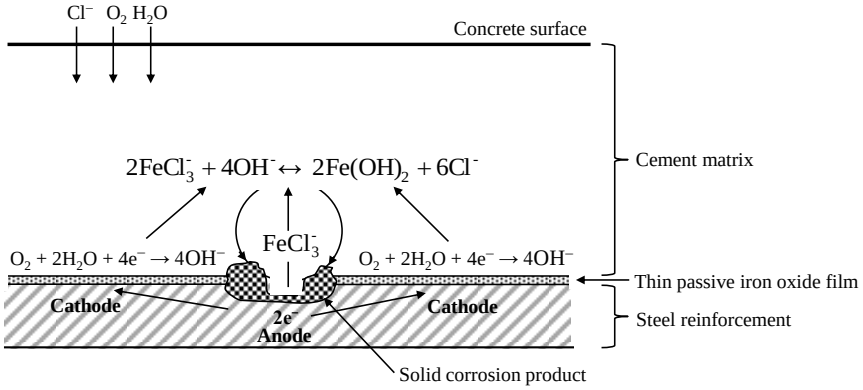

Figure 2.7: Corrosion of steel in concrete exposed to chloride ions [28, 41]

The exact manner in which chlorides break down the passive layer on the steel surface (under otherwise stable conditions) is still not clearly understood, with a number of different suggestions from various researchers [44-46]. However, it is important to note that the passive layer is normally in a continual state of breakdown and repair under normal conditions and that the presence of Cl^- will contribute towards its breakdown while other anions such as OH^- have inhibiting properties and are responsible for its stability. Therefore, at a point where the concentration of Cl^- (aggressive ions) overcomes the OH^- (inhibiting ions), active corrosion is initiated. This point is known as the *pitting potential* (also called *transpassive* or *breakdown potential*), below which passivity is maintained - see Figure 2.8 [7, 27]. Figure 2.8 is a schematic representation of the polarization curve of an active-passive alloy such as stainless steel in de-aerated 1N H_2SO_4 in the absence of chloride ions. In the figure, potential increases from the cathodic potential range, passes through the corrosion potential, E_{corr}, then through the active peak into the passive region. Transition to the transpassive region occurs at approximately 1200 mV (SHE). In the presence of chloride ions, the passive film breaks down at a specific potential identified, E_{pit}, (i.e. the breakdown potential for pitting corrosion) at which there is a rapid increase in current density (curve AB). However, if the chloride concentration is sufficiently

high to completely prevent passivation, the polarization curve follows the curve CD, and very high current densities are observed with increasing potential. The interpretation of the increase in current density at E_{pit} is that of a composite surface consisting of passive film with a low current density and pits, essentially free of protective film, corroding at the high current density given by the curve CD at the pitting potential. With time, the current density increases as a larger fraction of the surface becomes pitted. For a given metal, the potential at which pitting occurs is lower for a higher chloride ion concentration. Progressive local breakdown of the passive film will result in the entire surface approaching a condition of rapid active dissolution [7].

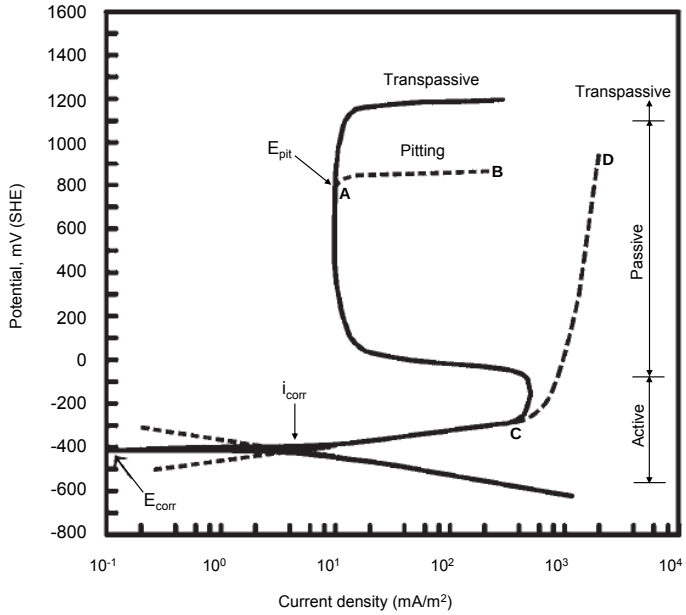

Figure 2.8: Schematic polarization curve [28]
(Note: Polarization curve for an active-passive alloy having susceptibility to pitting due to chloride ions)

Apart from chloride threshold, corrosion initiation is also conventionally taken to have occurred when an active corrosion rate of 0.1 μA/cm^2 is attained [7, 47]; this corrosion rate (also referred to as active corrosion rate threshold) marks the beginning of the corrosion propagation phase. After depassivation, corrosion may propagate at a rate depending on a variety of inter-related factors such as concrete resistivity (or its inverse, conductivity), cover depth, concrete quality, crack width, temperature, relative humidity and oxygen availability as summarised in the following sections.

2.6 *Mechanism of steel corrosion in cracked concrete*

Even though the exact mechanism of corrosion in cracked concrete is still not well understood, Schieβl and Raupach [48] have proposed two different corrosion mechanisms that are theoretically possible in the region of cracks. In the first case, both the anodic and cathodic processes take place in the zone of the crack, and is characterised by microcell corrosion (see Section 2.5.1). The oxygen required for the cathodic reaction is supplied through the crack. In the second case, the reinforcement in the crack zone acts as an anode, and the passive steel surface between the cracks forms the cathode, and is characterised by macrocell corrosion (see Section 2.5.1). The oxygen penetrates mainly through the uncracked area of the concrete. The steel surface involved in this corrosion process is larger than that in the first mechanism, hence, higher corrosion rates can be expected.

However, it is not clear under what conditions each of the proposed corrosion mechanisms will prevail; furthermore, it may be possible for both corrosion mechanisms to prevail depending on the cover depth, concrete quality and resistivity. Further studies are required to ascertain these hypotheses.

2.6.1 *Transport properties of cracked concrete*

The presence of cracks in concrete can greatly modify its transport properties and significantly decrease the durability of RC structures. In cracked porous media such as concrete, penetration of most of the aggressive species takes place through water contained in the porous structure of the matrix and in the cracks by two main mechanisms namely diffusion and advection [49, 50], but capillary suction has also been reported to be an important transport mechanism [51]. Diffusion occurs under a concentration gradient [21, 52] whereas advection is related to transport of substances by bulk movement of water under a pressure gradient. The latter case includes water movement in saturated conditions and water suction under unsaturated conditions. In most cases, chlorides penetrate concrete by both mechanisms. Due to the relatively low penetrability of uncracked concrete, diffusion tends to be the dominant mechanism for chloride ingress in uncracked concrete. This is not the case for cracked concrete, especially when subjected to wetting and drying cycles. In such exposure conditions, there can be deep penetration of chlorides under high negative pressures through the matrix (unsaturated case) and through the cracks. Because both diffusion and advection mechanisms require the presence of moisture and depend on the degree of concrete saturation, accurate prediction of chloride ingress in cracked concrete requires an accurate prediction of water movement over time under the existing environmental conditions [49].

There have been limited studies in the past, some with conflicting results, relating to the effect of cracking on the penetrability of concrete [53, 54]. Even for numerical simulations, not many studies have been dedicated to quantifying chloride penetration in cracked concrete [55]. From these studies, the general consensus is that the presence of cracks in concrete increases its penetrability. Therefore, studying the transport mechanisms of concrete without taking into account its heterogeneities like cracking deviates from the reality [56]. Based on experimental results, Gerard *et al*. [57] state that the penetrability of cracked concrete cannot be correlated with that measured in uncracked concrete because different transport mechanisms are involved. Further, results by Boulfiza *et al*. [49] and Rodriguez and Hooton [58] also confirm that Fick's second law of diffusion does not give satisfactory results in cracked concrete and is therefore not adequate to describe the transport property of chlorides in cracked concrete.

When investigating the transport properties of cracked concrete, it is important to note that in addition to the presence of cracks, crack properties such as activity or dormancy, density, width, tortuosity, crack network (and its continuity) and self-healing potential (see Section 2.7.8.4) play an important role in modifying the transport properties. Some of these crack properties are discussed in the sections following. First, cracks in concrete can range from very fine internal micro-cracks, to large macro-cracks caused by undesired interactions with the environment and external loading. Micro-cracks always exist in concrete at a microscopic level but are conventionally assumed to be part of the porous concrete structure [49]. Load-induced cracks appear mostly at the paste-aggregate interface (in normal

strength concrete, compressive strength > 50 MPa [59]) and extend into the cement paste as the load is increased [54]. This study focuses on load-induced macro-cracks.

Secondly, either loaded or unloaded cracked concrete specimens can be used to study transport properties of cracked concrete [60]. Previous studies show that the characteristics of cracks after unloading of concrete are quite different from those while under load because the former can, for example undergo self-healing. In short, the transport properties of cracked concrete can be influenced by the test condition i.e. whether the test is performed under load or after load removal [61]. Most previous studies have been performed on unloaded specimens, and do not simulate real conditions [62]. In this study, as will be seen in Chapter 3, some of the cracked specimens were corroded under load.

Thirdly, cracks used (in the laboratory) to simulate and study transport properties in concrete (and corrosion of steel) can be divided into three groups depending on the method of production:

(i) Natural (or load-induced) cracks produced from loading tests including:
   (a) uniaxial compressive test [54, 61]
   (b) splitting test [63]
   (c) ring-shaped test set-ups with an expansive core [64] and
   (d) flexural (3- or 4-point loading) tests [65-67]

(ii) Artificial cracks which are produced by (i) using cast-in shims by placing thin sheets of plastic or metal in the fresh concrete and later removing to leave a crack, or (ii) saw-cutting [58].

(iii) Cracks produced by a combination of cast-in shims as in (ii) and later extended by loading [67]. In this case, the cast-in shims are used to ensure the load-induced cracks form at or around pre-determined locations.

Natural cracks or those produced by a combination of cast-in shims and loading are usually preferred to artificial cracks because they represent the reality but are difficult to model and the different techniques used to produce them make it difficult to compare results. Artificial cracks are easy to produce and model, and in most cases, have parallel surfaces but their main disadvantage is that they do not represent reality e.g. they are not tortuous and have a higher cement content on their walls compared to real cracks [55]. The pre-corrosion cracks used in this study were produced using technique (iii).

2.6.1.1 *Quantification of chloride ingress in cracked concrete*

Although there is a general consensus that cracks can significantly modify the transport properties of concrete, the limited research in this area has hindered accurate quantification of such effects. With respect to chloride ingress, even though previous researchers have shown that the presence of cracks increases concrete penetrability and hence chloride ingress, the actual characteristics of chloride ion transport in cracked concrete are still not clear. In most studies, it has been explained only by diffusion even though advection and capillary suction have also been found to be major transport mechanisms in cracked concrete [49, 50, 55, 56, 58, 62, 64, 65, 68-73]. Only some of these studies (closely related to this study) are reviewed here.

Gowripalan *et al*. [65] studied chloride ingress in cracked RC beams (90 x 100 x 650 mm long) made using PC (similar to ASTM Type I and complying with AS 3972) and a w/b ratio of 0.60. A uniform cover of 30 mm was used in all the beams. At 28 days, the beams were pre-cracked using a 3-point loading arrangement (back-to-back loading, see Figure 2.9) and the mid-span crack opened and maintained at 0.3 mm (measured on the concrete surface). All the faces of the beams were epoxy-coated leaving only two faces (90 x 650 mm) uncoated. The beams were then immersed in 3% NaCl solution for 300 days in a controlled room at a temperature of 23 ± 2 °C and relative humidity of 50 ± 5%. The experimental results showed that the chloride penetration in the tension zone was greater than that in the compression zone of the specimens, a phenomenon that can be attributed to the presence of 'open' cracks in the tensile zones of the beams as opposed to 'closed' ones in the compression zones. They also found that there was no significant difference in the chloride diffusion coefficients at 30 and 100 mm away from the crack.

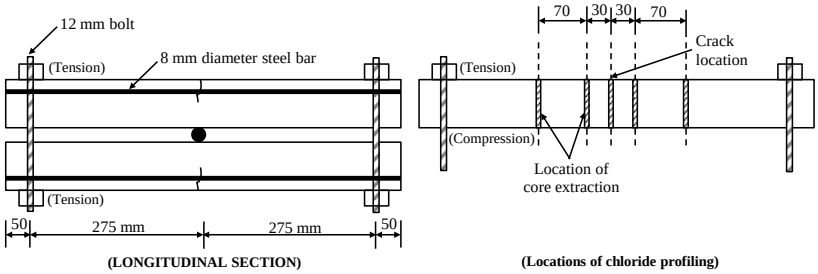

Figure 2.9: Location of core extraction for chloride content measurement [65]

Rodriguez and Hooton [58] investigated the influence of parallel-wall cracks and the crack wall roughness on chloride diffusion in concrete. Cracked and uncracked concrete specimens (100 diameter x 200 mm cylinders) were made using PC and 75/25 PC/GGBS at a w/b ratio of 0.40 and cured in lime-saturated water for 5 months before testing. Smooth-surfaced (crack widths 0.09 - 0.67 mm) and rough-surfaced (crack widths 0.09 - 0.47 mm) cracks were formed by, respectively, saw-cutting and splitting. After epoxy-coating the surfaces, the specimens were exposed to a 40-day chloride bulk diffusion test and the lateral movement of chlorides from the crack wall into the bulk of the concrete measured (see Figure 2.10). Contrary to other researchers, their results showed that the depth of chloride penetration (or chloride diffusion coefficient) is independent of either the crack width (0.08 to 0.68 mm) or the crack surface roughness. The diffusion coefficients for these crack widths were similar to those of uncracked concrete. This is also in contrast to previous results and may be attributed to experimental set-up amongst other factors such as crack self-healing.

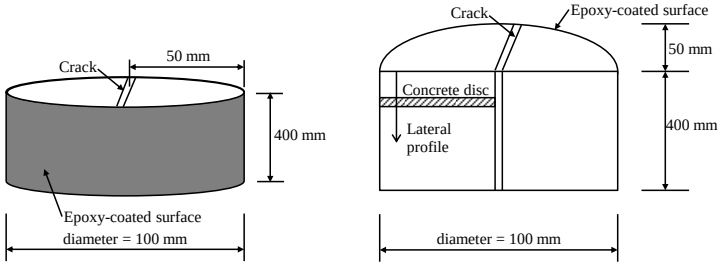

Figure 2.10: Location of concrete discs for chloride profiling [58]

In a study by Scott [10] on cracked steel RC beam specimens (120 x 120 x 375 mm long) made with a constant w/b ratio of 0.58 but using different binder types, chloride concentrations were determined at two locations along the steel: 30 and 90 mm on either side of the crack (see Figure 2.11). The results are presented in Table 2.3. It can be noted that generally, the chloride content increased not only with proximity of the sampling location to the crack but also with increasing crack width. The differences in chloride concentration in the vicinity of the crack between those concretes made with 100% CEM I 42.5N and those made using blended cements, regardless of the crack width, is attributable to differences in penetrability; blended cement concretes have been shown to have denser microstructure and better chloride binding. However, their results for chloride content with respect to distance from the crack contradict those of Gowripalan *et al*. [65] who found no influence of sampling location on diffusion coefficient.

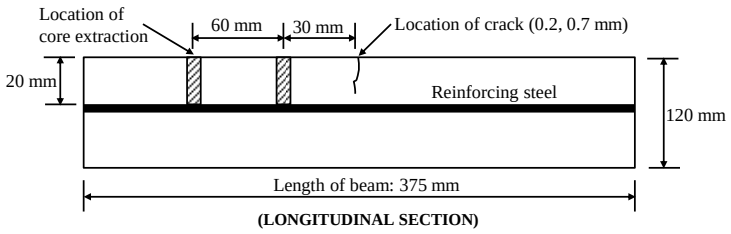

Figure 2.11: Location of core extraction for chloride content measurement [10]

Table 2.3: Chloride penetration in cracked concrete [10]

Binder type	Crack width (mm)	Chloride concentration (% by mass of cement)	
		At 30 mm from crack	At 90 mm from crack
100 % CEM I 42.5N (PC)	0.2	4.36	1.78
	0.7	4.15	1.73
50/50 PC/GGBS	0.2	1.86	0.22
	0.7	2.25	0.28
70/30 PC/Fly ash	0.2	1.91	0.25
	0.7	2.05	0.21
50/43/7 PC/GGBS/Silica fume	0.2	2.47	0.92
	0.7	2.92	0.39

(Specimen age: 86 weeks, cover depth: 20 mm)

Djerbi *et al*. [68] conducted tests to investigate chloride penetration in traversing cracks in concrete. Cylindrical concrete specimens (110 mm diameter x 220 mm) were made from three concrete mixes using PC (w/b, 0.50 and 0.32) and 94/6 PC/silica fume (w/b, 0.38), stored at 20 °C and approximately 95% relative humidity for 24 hours after casting followed by curing under water at 20 °C for 3 months after which they were stored in an air-conditioned room (20 °C and relative humidity 50 ± 5%) until testing. Cracks were induced in 110 mm diameter x 50 mm discs (obtained from the cylindrical concrete specimens) using a splitting tensile test (see Figure 2.12); average crack widths ranged from 30 to 250 μm. After unloading the chloride diffusion coefficient was evaluated by steady state migration test (no pre-conditioning of the specimens was reported). Their results showed that chloride diffusion coefficient of cracked specimens (D_{cr}) increased with increasing crack width. Their results showed that D_{cr} increased linearly with increasing crack width from 30 to 80 μm and remained almost constant when the crack width was approximately ≥ 80 μm, Eqn. (2.33). Their results conformed to

those of Rodriguez and Hooton [58] that showed that D_{cr} is independent of material effects, even if the tortuosity and roughness are different. Even though Rodriguez and Hooton's [58] concluded that chloride diffusion coefficient was independent of crack width, they dealt with large crack widths (0.08 to 0.68 mm) which were much larger that the limiting value of 80 μm found by Djerbi *et al*. [68].

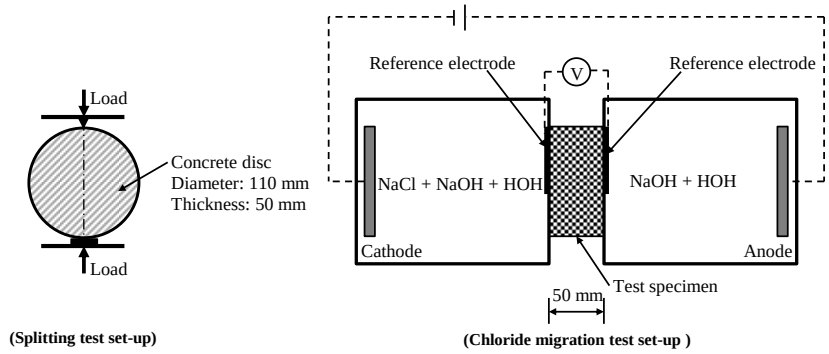

Figure 2.12: Specimen splitting and chloride migration test set-up [68]

$$\begin{cases} D_{cr}, \mathrm{m^2/s} = 2\times10^{-11}w - 4\times10^{-10} & 30\mu\mathrm{m} \le w \le 80\mu\mathrm{m} \\ D_{cr}, \mathrm{m^2/s} \approx 14\times10^{-10} & w \ge 80\mu\mathrm{m} \end{cases} \quad (2.33)$$

where w is the crack width (μm).

Marsavina *et al*. [55] experimentally and numerically investigated the influence of artificial cracks on chloride ion penetration in concrete using carbonated and non-carbonated concrete specimens made using GGBS and PC (52.5N) at a 0.5 w/b ratio. Notched 150 mm cube specimens were cast and cured by storing in a climate room at 20 ± 2 ^{o}C and > 90% relative humidity. The notches were made by means of positioning and removal after a few hours of thin copper shims in the fresh concrete (thickness 0.2, 0.3 and 0.5 mm; placed at depths of 5, 10, 15 and 20 mm). Cylindrical cores (100 mm diameter x 50 mm thick) were then taken from the notched cubes (see Figure 2.13) and subjected to a non-steady-state migration test (NT BUILD 492 test method) to determine chloride penetration. The results showed that a higher penetration of chlorides is obtained at the notch tip in comparison to the uncracked parts of the specimens and that the penetration depth increases with increasing notch depth. However, the results did not show a clear influence of the notch width on chloride penetration. These results show that crack depth (and indirectly, cover depth) is important when considering the effect of cracking on steel corrosion in RC structures.

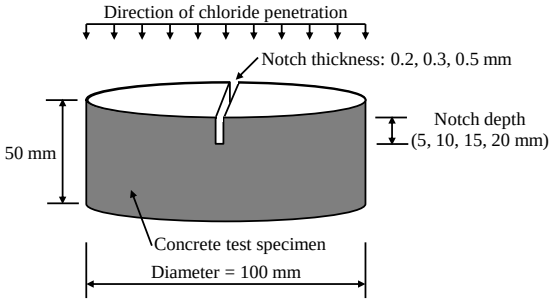

Figure 2.13: Specimen geometry for chloride penetration set-up [55]

2.6.1.2 *Summary and critique of chloride ingress in cracked concrete*

From the reviews presented here regarding transport in cracked concrete, the following general conclusions relating to chloride ingress can be drawn:

1. The characteristics of chloride ion transport in cracked concrete are still not well understood and hence its accurate quantification is still not possible. Further studies are still required in this area.
2. The presence of cracks in concrete increases moisture and chloride ingress in concrete.
3. Crack width, shape and depth appear to be important parameters controlling the local ingress of chloride ions in cracked concrete. Chloride penetration depth increases with increasing crack depth. This shows that crack depth (and indirectly, cover depth) is important when considering the effect of cracking on steel corrosion in RC structures. Further work is required in this area.
4. The effect of cover cracking is relatively more important for dense concrete for which the initial (uncracked) transport coefficient is reduced than in normal concrete. The more dense or less penetrable the concrete, the more sensitive it is to the effect of cracking.
5. Fick's second law of diffusion, which describes only the case of one-dimensional diffusion process does not give satisfactory results in cracked concrete and should be cautiously applied when dealing with cracked concrete.
6. Crack self-healing can lead to a significant reduction of diffusion coefficient of chloride ingress with time in cracked concrete. However, its quantification is still a challenge.

However, even though the above general conclusions are made, it is important to take note of some critical issues regarding experimental programmes that have been used in the past to study transport properties in cracked concrete. One common disadvantage of a majority of studies is the use of single artificial cracks made by positioning of shims (thin metal or plastic sheets) in the concrete during casting of the specimens, and removal at a later age. These types of cracks, as mentioned earlier, do not simulate real cracks. Further, even though, to some extent, the results from experiments using specimens with single cracks can be extrapolated to multiple cracks which are most common in in-service RC structures, it is necessary to carry out more studies using multiple cracks [58].

It is also important to critique the use of mortar specimens as opposed to concrete specimens e.g. Ismail *et al*. [64]. The applicability and/or extension of results from such studies to RC may not be valid, and should be carefully used. In addition to these discrepancies, the use of loaded vis-à-vis unloaded cracked specimens should be taken into account. Previous research has shown that even in cracked specimens, the stress level influences the rate of both chloride ingress and active corrosion (corrosion propagation) of the steel in RC structures.

2.6.2 *Pitting factor and residual cross sectional area*

Even though the characterization of surface morphology of corroded steel is not a focus of this study, it is important to mention pitting when dealing with chloride-induced corrosion especially in cracked concrete. In the development and application of corrosion-induced damage prediction models, average corrosion rate is usually assumed to be uniform over the steel surface to simplify the analysis [e.g. 31]. This approach is conservative and may be valid for carbonation-induced corrosion but for chloride-induced corrosion, especially in cracked concrete, where local pitting occurs, this approach results in

determination of an average depth of attack (or loss of steel bar radius), $P_{avg.}$, (see Figure 2.14) considering uniform corrosion, Eqn. (2.34), and can lead to unprecedented failures [74].

$$P_{avg.}(t) = \frac{\text{Mass loss}, g}{\text{Surface area}, \text{cm}^2 \times \text{Density}, \text{g/cm}^3} = \frac{\left(\frac{MIt}{zF}\right)}{A \times \rho} \tag{2.34}$$

where M is the molar mass of steel (56 g), I is the corrosion current, t is the duration of the corrosion process (seconds), z is the valency of steel (equal to 2), ρ is the density of steel (7.85 g/cm^3) and F is Faraday's constant (96,500 C/mol). The numerator of Equation (2.34) is the mass loss based on Faraday's law [7]. Equation (2.34) is sometimes simplified to $0.0116 i_{corr} t$ where i_{corr} is the corrosion current density (μA/cm^2) and 0.0116 is a conversion factor for $P_{avg.}(t)$ in mm/yr i.e. penetration depth.

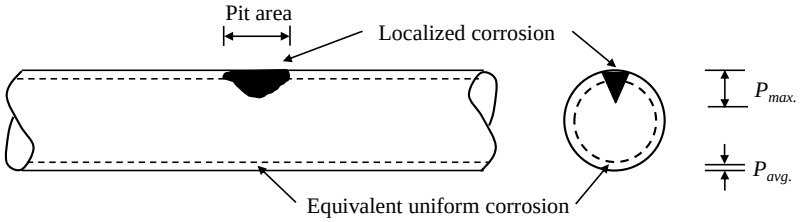

Figure 2.14: Schematic representation of pitting and average corrosion [75]

To account for pitting, a correction factor α_{pit} (called *pitting factor* or *pit concentration factor*) is introduced to estimate the maximum pit depth P_{max}, Equation (2.35) [74]:

$$P_{\max}(t) = \alpha_{\text{pit}}\left(P_{avg.}(t)\right) \tag{2.35}$$

where P_{max} is the maximum penetration depth of corrosion in the steel. In the case of carbonation-induced corrosion, α_{pit} is close to 1 while for chloride-induced corrosion, it is larger than one. The pitting factor can be determined experimentally by carrying out a morphology assessment of the corroded steel surface to establish the maximum pit depth, size and distribution.

A range of values for the pitting factor have been proposed in previous experimental studies but most of these studies have dealt with steel corrosion in uncracked concretes, with some using impressed current to accelerate the corrosion process [e.g. 74]. Tuutti [76] proposed values of α_{pit} between 4 and 10 based on accelerated (application of external voltage) chloride-induced corrosion tests while experiments by Gonzalez *et al*. [74] showed pitting factors ranging from about 4 to 8 for natural chloride-induced corrosion, and from about 5 to 13 for accelerated (application of impressed anodic current) chloride-induced corrosion. In the work of Gonzalez *et al*. [74], it is important to point out that a pitting factor of 4.5 was reported for a naturally corroding cracked specimen but it is not possible to make a conclusion based on this single result. Furthermore, the cracks in their work were longitudinal corrosion-induced cover cracks (as opposed to transverse flexural cracks used in this study) and no information was given regarding the crack width, density, length and concrete quality. DuraCrete [77] takes a stochastic approach by characterizing the pitting factor for chloride-induced

corrosion using a normal distribution (mean = 9.28, std. dev. = 4.04) based on a statistical analysis of experimental data. In a recent study, Harnisch and Raupach [78] investigated the time-dependency of the morphology of corroding steel in concrete using both accelerated (cyclic wetting and drying) and natural (outdoor) chloride-induced corrosion. They reported pitting factors as high as 18. However their results showed that pitting factors are not only time-dependent but also decrease with time i.e. the pit depth increases with time but at a decreasing rate. They reported that the growth of the pit depth is dependent on a complex interaction of several factors including the transport of chloride ions to the pit, corrosion products out of the pit and the extent of self-corrosion i.e. additional mass loss due to the hydrolysis at the anode [79, 80]. However, even though their results were short-term (up to 2 years), it can be expected that with time, the pitting factor will remain more or less constant and an average value can be adopted for practical application purposes.

From the review presented here, it is evident that there is still no clear guidance on values of pitting factor to use for chloride-induced corrosion. More studies on cracked and uncracked concrete are still required in this area. Andrade *et al*. [81] propose a conservative approach by recommending pitting factors ranging between 4 and 10 for both natural and accelerated corrosion in cracked and uncracked concrete, with the upper limit being more appropriate for cracked concrete than uncracked concrete.

In addition to the maximum pitting depth, and taking into consideration that steel is a ductile material, the residual cross sectional area ($A_{s,min}$) is of great importance for determining the load bearing capacity of a RC member (Figure 2.15).

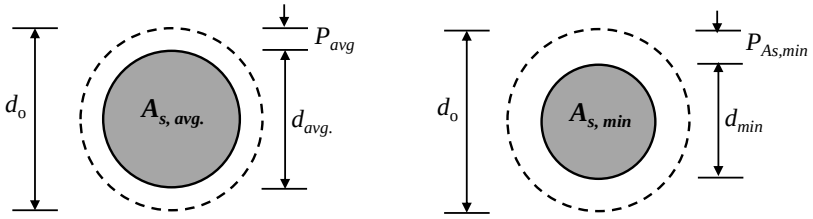

Figure 2.15: Illustration of average and minimum residual cross section after corrosion

In order to determine the residual cross-sectional area, an experimental study by Harnisch [82] reported time-dependent residual cross-section factors $\alpha_{As}(t)$ relating the average to the minimum cross-sectional areas i.e.:

$$\alpha_{As}(t) = \frac{P_{As,\min}(t)}{P_{avg}(t)} = P_{As,\min}\left(\frac{P_{\max}(t)}{\alpha_{pit}(t)}\right) = \frac{(0.5d_o) - \sqrt{\frac{A_{s,\min}(t)}{\pi}}}{(0.5d_o) - \sqrt{\frac{A_{s,avg}(t)}{\pi}}} \tag{2.36}$$

and

$$A_{s(avg)}(t) = \pi\left((0.5d_o)^2 - \frac{V_{corr}(t)}{\pi l}\right) \tag{2.37}$$

where $P_{As,min}$ is the average corrosion depth at the location of maximum cross-section loss, P_{avg} is the corrosion depth assuming uniform corrosion, d_o is the initial diameter of the steel, $A_{s,min}$ is the minimum residual cross-section area, $A_{s,avg}$ is the average cross-section area considering uniform

corrosion, V_{corr} is the mass loss due to corrosion (calculated using Faraday's law) and l is the length of the polarized area of the steel (or macrocell anode). Similar to the pitting factors (α_{pit}) discussed earlier, the residual cross section area factors (α_{As}) decrease with time at a decreasing rate. The pitting factors (α_{pit}) are also much higher than the residual cross section area factors (α_{As}) e.g. up to 4.8 and 3.4 times higher for, respectively, PC and GGBS concretes at 8 months (cover depth: 20 mm, w/b ratio: 0.50). The residual cross section area factor is important to structural engineers in the calculation of residual load bearing capacity of structural members. Furthermore, the pitting factor is a critical parameter for assessing change in ductility of a corroded RC member.

2.7 *Review of selected factors affecting corrosion rate of steel in concrete*

Once the chloride threshold is attained at the steel level and the passive protective layer on the steel surface is destroyed, active corrosion is initiated. However, the propagation of corrosion depends on, among other factors, the adequate supply of corrosion-sustaining species (H_2O and O_2) and concrete properties. These factors are in most cases inter-related. In the following sub-sections, selected factors affecting (chloride-induced) corrosion of steel in concrete are discussed.

2.7.1 *Effect of cover depth*

If other factors (e.g. w/b ratio, binder type, degree of water saturation) are kept constant, concrete cover depth is an important determinant of corrosion rate of steel in concrete. During corrosion propagation, cover thickness affects corrosion rate by governing the travel path of oxygen to the embedded steel. Fundamentally, it affects corrosion rate by governing the cathodic reaction (O_2 availability). It is the main factor that influences the limiting cathodic current that was discussed in Section 2.4.2.2. In general, a small concrete cover may be used for a high quality (less penetrable) concrete while the same cover thickness may not apply for a lower quality concrete cover. However, cover thickness can only be increased to a certain limit in order to limit surface crack widths which have an accelerating effect on corrosion rate. Therefore, a careful trade-off between cover depth and quality should be sought.

In short, cover thickness, quality (with respect to its penetrability) and condition (with respect to cracking - covered later) influences the ease of ingress of chlorides, moisture and oxygen into concrete, and hence the corrosion rate [16, 33, 83]. The effect of cover on the diffusion of O_2 is illustrated in Figure 2.16 using the results from Bentur *et al*. [83]. It can be seen that an increase in cover depth from 20 to 50 mm (at 60% relative humidity, RH) resulted in a reduction in the availability of O_2. The coupled effect of an increasing cover depth and a shift in RH from 60 to 80% resulted in approximately twice the decrease in the availability of O_2. The increased cover depth is also likely to minimize the influence of the external drying thus sustaining a fairly high moisture content at the steel level which might promote corrosion rate if sufficient O_2 is available.

Therefore, similar to w/b ratio (covered in the next section), concrete cover may be used to inhibit corrosion in RC structures. In fact, when cover, w/b ratio, binder type and binder content are carefully selected, corrosion may be greatly inhibited during the service life of a RC structure. A significant portion of the service life of a structure may be compromised if the actual cover thickness is less than required, is of a lower quality or is cracked.

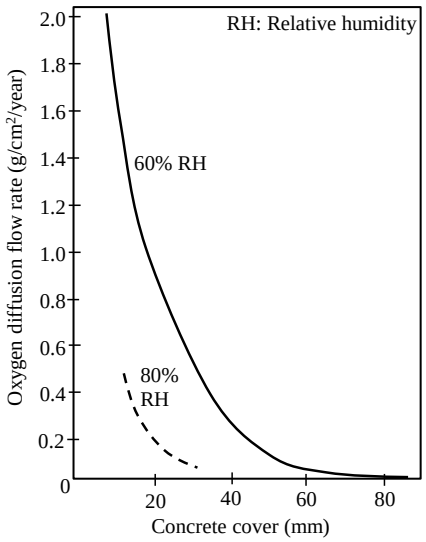

Figure 2.16: Effect of concrete cover on the diffusion of O_2 [83]

2.7.2 *Effect of concrete quality (binder type and w/b ratio)*

The use of supplementary cementitious materials, SCMs, (also referred to as mineral additives) such as fly ash (FA), slag and silica fume (SF) to replace partially Portland cement (PC) in marine concretes is now well established due to their durability and life cycle cost benefits [84-86]. The most widely used mineral additives in South Africa are fly ash (FA) and slag (ground granulated blastfurnace slag (GGBS) and Corex slag (GGCS) [87]) which are industrial by-products [84, 88]. Apart from having an influence on corrosion initiation, SCMs such as slag, FA and SF also have a profound effect on the rate at which corrosion progresses [16, 89, 90]. Extensive research has been done on the use of cement extenders and as a result, a better understanding on the influence of cement extenders on the corrosion rate has been developed. A brief review for FA and GGBS, which were used in this study, is presented here.

Partial replacement of PC with GGBS may decrease the early-age strength, but increase the later strength and improve microstructure and durability of concrete very significantly [91]. Previous studies have shown also that the presence of sulphides in the pore solution of GGBS concretes may be incorporated into the passive layer thus reducing its ability to protect the steel [10, 92]. However, this is only noticeable in the early stages of passive corrosion state [33]. For example Valentini *et al*. [93], using steel embedded in GGBS mortars, showed that immediately after curing the corrosion rate in the GGBS-containing specimens was 10 times higher than that of the PC concrete. However, with time the difference in corrosion rate decreased but the GGBS-containing samples generally maintained a passive state of corrosion. Apart from this, incorporation of GGBS improves the durability of concrete by creating a denser, less penetrable matrix and thereby enhancing the service life of RC structures. The denser microstructure or lower porosity is due to more capillary pores being filled with low density calcium silicate hydrate (C-S-H) gel than Portland cement paste [94, 95]. Also, due to the refined pore structure, the resistivity of the concrete is increased hence contributing significantly to reduction of corrosion rate due to a reduction in the mobility of chloride and hydroxyl ions [96, 97].

Similar to GGBS, the pore size distribution in concrete made with FA is substantially finer than of plain PC concrete; the percentage of gel pores is higher while that of capillary pores lower but the total porosity is not influenced substantially [85]. In general, addition of FA in concrete is considered an effective measure to mitigate chloride-induced corrosion in RC structures. For example, using FA blended cement is known to reduce chloride permeability of concrete [98]. Dhir *et al*. [99] also reported that the chloride-binding capacity of cement paste increased with the increase in FA replacement level up to 50% and then declined at 67%. The increase in chloride binding capacity of FA concrete may be attributed to (i) the high alumina (Al_2O_3) content in FA [100], which results in the formation of more Friedel's salt [101], and (ii) the production of more gel during hydration, which results in better physical adsorption of chlorides [102].

Water-to-binder ratio (w/b) affects the corrosion characteristics of steel primarily by governing the pore structure of the concrete. High w/b ratio has a negative effect on steel corrosion due to increased penetrability and reduced resistivity of concrete [103]. For concrete in a moist environment, the cathodic reaction rate depends on the availability of oxygen and hence the corrosion rate may be limited by stifling the cathodic reaction. With a decrease in w/b ratio, the quantity of oxygen at the steel level decreases due to decreased concrete penetrability. This suppresses the cathodic reaction and subsequently decreases the corrosion rate. In addition, concrete resistivity increases with a decrease in w/b ratio; if sufficient oxygen is available to support higher corrosion rate, concrete resistivity may be the controlling factor that determines the maximum possible corrosion rate [16, 89]. As an illustrative example, test results by Mangat *et al*. [89] are presented here (Table 2.4). In their tests, corrosion rates for 12 mm deformed steel in concrete prisms (100 x 100 x 370 mm) exposed to 1200 wetting and drying cycles in a sea-water spray chamber after 14 days air-curing, with a cover of 10 mm and three different w/b ratios and cement contents were examined.

From the results, it is evident that w/b ratio had a significant impact on the corrosion rate of steel in concrete. The highest corrosion rate was observed in the 0.76 w/b ratio with the accompanying highest chloride concentration while the lowest corrosion rate of 0.13 $\mu A/cm^2$ was found to occur in the w/b 0.45 sample. The influence of w/b ratio on corrosion rate is therefore significant and should be taken into account at the concrete mix design stage if the RC structure will be exposed to aggressive environments.

Table 2.4: Influence of w/b ratio on corrosion rates [89]

w/b ratio	Cement (kg/m^3)	i_{corr} ($\mu A/cm^2$)	Acid soluble Cl^- at steel level (10 mm) (% by mass of cement)
0.45	430	0.13	1.4
0.58	430	0.65	2.0
0.76	430	2.16	2.3

2.7.3 *Effect of concrete resistivity*

RILEM TC 154-EMC [104] defines electrical resistivity of concrete as a physico-chemical and geometry-independent material property which describes its electrical resistance. It is fundamentally related to the penetrability of fluids and diffusivity of ions through porous materials such as concrete

[105]. The electrical resistivity of concrete may vary over a wide range, from 1 to 10^4 kΩ-cm. It is influenced by many factors including the binder type and content, w/b ratio, degree of pore saturation, type of aggregate, presence of salts such as chlorides, temperature and age of the concrete [106]. However, the degree of saturation of the pore structure has been identified as the most important factor influencing concrete resistivity [107]. For example, experimental results by Gjörv *et al*. [106] show that the resistivity of concrete increased three orders of magnitude when the degree of saturation was reduced from 100 to 40 % (w/b ratio = 0.42). The influence of temperature on concrete resistivity can be modelled using Arrhenius equation [108]:

$$\rho_c(T_2) = \rho_{c,o} \mathrm{e}^{\frac{E}{R}\left(\frac{1}{T_2}-\frac{1}{T_1}\right)} \tag{2.38}$$

where $\rho_c(T_2)$ is the expected resistivity at temperature T_2, $\rho_{c,o}$ is the initial resistivity at temperature T_1, E is the activation energy (12 - 37 kJ/mol [104, 109] dependent on e.g. the moisture content and the w/b ratio) and R is the universal gas constant (8.314 $JK^{-1}mol^{-1}$).

Concrete resistivity is affected only moderately by the w/b ratio or cover depth e.g. Tuutti [76] found that a reduction in w/b from 0.7 to 0.4 (75% decrease) results in only a doubling of the resistivity while a reduction in relative humidity from 100 to 50% resulted in a change in the resistivity by several orders of magnitude. Concrete resistivity affects corrosion rate of steel through resistivity control (see Section 2.4.3). The non-destructive nature, speed, and ease of conducting resistivity measurements make it a potential option that can be performed to characterize concrete.

Corrosion current density (or corrosion rate) is inversely proportional to the resistivity of concrete (or directly proportional to its conductivity i.e. the inverse of resistivity) [110]:

$$i_{corr} \propto \frac{1}{\rho_c} \approx \sigma_c \tag{2.39}$$

where i_{corr} is the corrosion current density (μA/cm^2), ρ_c is the concrete resistivity and σ_c is the concrete conductivity. The interpretation of measured concrete resistivity measurements as proposed by Rodriguez *et al*. [111] is given in Table 2.5.

Table 2.5: Relationship between resistivity and corrosion risk [104]

Resistivity (kΩ-cm)	Risk level
> 100	Very low corrosion rate
> 50 - 100	Low to moderate corrosion rate
10 - 50	Moderate to high corrosion rate
< 10	Resistivity is not the controlling parameter

However, even if the resistivity values given in Table 2.5 are measured on a RC structure, the presence and/or level of corrosion can only be ascertained by actual corrosion rate measurement using, for example, linear polarization resistance technique. Furthermore, from past studies [e.g. 112], and as

will be seen in Chapter 4 where the results of this study are discussed, the presence of cracking can greatly affect the resulting corrosion rate even in the case of high concrete resistivities. Therefore, precaution should be taken in the interpretation of resistivity results using such guidelines.

2.7.4 *Effect of temperature*

Corrosion rate of steel in concrete is increased by high temperature. Generally, corrosion rate increases up to a temperature of about 40 °C followed by an inhibiting effect above this temperature, caused by the decreasing oxygen solubility in the pore solution at higher temperatures, and by the concrete progressively drying out if moisture is not readily available [113]. Similar to concrete resistivity, Arrhenius equation can be used to estimate the influence of temperature on corrosion rate [31]:

$$i_{corr}(T_2) = i_o \mathrm{e}^{\frac{E}{R}\left(\frac{1}{T_2}-\frac{1}{T_1}\right)} \tag{2.40}$$

where $i_{corr}(T_2)$ is the expected corrosion rate at temperature T_2, i_o is the initial corrosion rate at temperature T_1, E is the activation energy and R is the universal gas constant (8.314 $JK^{-1}mol^{-1}$). However, it is important to note that such an approach should be carefully applied mainly because it does not take into account the opposing effects of temperature mentioned here.

2.7.5 *Effect of relative humidity*

Moisture is an important factor for both corrosion initiation and propagation. In the propagation phase the corrosion rate is slow in dry or fully saturated concretes; intermediate moisture contents allow the concrete to act as an electrolyte while also permitting the ingress of oxygen needed for the corrosion process. Active corrosion can therefore not occur if the concrete is too dry such that the pore solution does not serve as an electrolyte, or too wet (saturated) to allow ingress of oxygen. Corrosion activity is most vigorous at relative humidity (RH) values above about 80% [21]. Concerning the rate of ingress of oxygen to the cathodic areas, this depends on its diffusion coefficient, the depth of the steel, and the condition of the cover concrete. The diffusion coefficient is affected by the w/b ratio and the moisture content of the concrete. The oxygen diffusion coefficients for two w/b ratios of cement paste at various RH are shown in Figure 2.17.

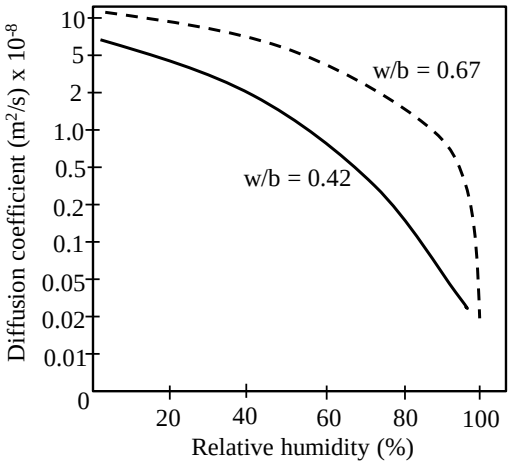

Figure 2.17: Influence of relative humidity and w/b ratio on oxygen diffusion coefficient [83]

2.7.6 *Effect of oxygen availability on corrosion*

Oxygen reduction (see Eqn. (2.29)) is generally considered to be the sole cathodic reaction during steel corrosion in concrete [114], even though this has been disputed by some researchers [115]. In simplified form, the equation for the electrode reaction in oxygen reduction is usually presented as was given in Eqn. (2.29) i.e. $O_2 + 2H_2O + 4e^- \rightarrow 4OH^-$. However, in a review by Raupach [115], according to Febjan *et al*. (1980), Hamann *et al*. (1981), Schwabe (1986), Rechberger (1987) and Forker (1989), Kaesche (1990), this reaction actually takes place in a series of steps. In alkaline media such as concrete, it is separated into at least two stages, in which hydrogen peroxide (H_2O_2) is first formed as an intermediate product, and is then reduced:

$$O_2 + 2H_2O + 2e^- \rightarrow H_2O_2 + 2OH^- \quad (2.41)$$

$$H_2O_2 + 2e^- \rightarrow 2OH^- \quad (2.42)$$

The formation of hydrogen peroxide, Eqn. (2.41), is also suspected to take place in a series of reaction steps. The stage determining its (H_2O_2) formation rate is probably the ionization of the oxygen molecule (i.e. $O_2 + 2e^- \rightarrow O_{2^-}$), while a number of different variants are possible for the subsequent reaction stages. The dominant reaction mechanism is important in assessing the role played by oxygen in the corrosion process, as the reduction of the hydrogen peroxide adsorbed at the steel surface may cause cathodic currents without any diffusion of oxygen to the cathode from the concrete surface.

The dependence of the cathodic reaction on oxygen availability means that the rate of steel corrosion in concrete should be primarily controlled by the oxygen concentration at the steel level [76, 116]. In both uncracked and cracked concrete, the dissolved oxygen penetrates the cover concrete by diffusion [117]; in cracked concrete, the cathodes are dominantly located in the uncracked concrete regions as already discussed in Section 2.6.

Oxygen availability at the steel level, and hence corrosion rate of steel in concrete, is affected by a variety of factors such as moisture content of concrete, its salt concentration, cover depth and concrete quality. However, a study by Andrade *et al*. [118] showed that (i) oxygen availability to support corrosion rate is most affected by the relative humidity of concrete, and that (ii) concrete quality and cover depth also affect oxygen availability but to a lesser extent. The influence of salt concentration in concrete on oxygen ingress is discussed in the next section.

Andrade *et al*. [118] carried out corrosion tests on specimens made using cement paste, mortar, and concrete to investigate the influence of cover depth, w/b ratio and degree of pore saturation on oxygen flow and steel corrosion rate. The cement paste and mortar specimens (20 x 55 x 80 mm) were made using two w/b ratios of 0.40 and 0.50 respectively. A cement-to-sand ratio of 1/3 for mortar was used. The cement paste specimens were made using plain PC while the mortar specimens were made using blast furnace slag cement. Two bars of diameter 6 mm and length 80 mm were embedded in each specimen as duplicate testing electrodes. The exposed embedded steel surface area was 6 cm^2. A graphite bar was also embedded to act as a counter electrode for corrosion rate measurements. A cover of 5 mm was used. The concrete specimens (150 mm diameter x 300 mm long) were made using plain PC with two binder contents of 375 and 200 kg/m^3, and two w/b ratios of 0.5 and 1.0 respectively.

Two bars of 12 mm were embedded in each specimen. The exposed embedded steel area was 7.5 cm^2. Two concrete covers of l5 and 70 mm were used. The mortar and paste specimens were cured in a chamber at a 100% RH and 20 ± 2 °C for 28 days while the concrete specimens were cured for 15 days under water. The latter were then exposed to wet and dry periods as follows: 30 days at 100% RH, 30 days at 50% RH, 30 days under water, 365 days at 50% RH and 150 days under water. The paste and mortar specimens were held for 150 days at 100% RH.150 days at 50% RH and 150 days in under water. Corrosion rate was measured using linear polarization technique.

The main conclusions from the work of Andrade *et al*. [118], as already mentioned, were that (i) oxygen availability to support corrosion rate is most affected by the relative humidity of concrete, and that (ii) concrete quality and cover depth also affect oxygen availability but to a lesser extent. As will be seen in Section 2.7.7, the salt concentration of the concrete also affects the oxygen availability.

2.7.6.1 *Corrosion phenomena during progressive water-saturation of concrete*

The corrosion process at the cathode during progressive saturation of concrete exhibits two overlapping effects, (i) an initial increase in corrosion current due to increased cathodic polarization, caused by decreased electrolytic resistance, and (ii) a decrease in corrosion current with time due to the growing oxygen deprivation at the steel [115]. At low saturation levels, corrosion is influenced more strongly by the change in electrolytic resistance, but as the saturation level of the concrete increases, the influence of oxygen deprivation becomes dominant. However, in a few studies, even when concrete is fully saturated, the embedded steel has been observed to continue to corrode for a given time [114, 115, 119]. Some of these studies are briefly summarized here.

In the study by Wilkins and Lawrence [119], a review by Raupach [115] shows that after several months of full immersion in water, they observed that steel bars embedded in concrete reacted cathodically when anodes were connected, although the concrete was fully saturated with water. This behaviour may be attributable to hydrogen peroxide reduction (discussed earlier in Section 2.7.6) or to a similar reaction with oxygen adsorbed on the steel surface.

Raupach [115] investigated the possible role of oxygen remaining in concrete i.e. the residual oxygen inside the concrete where oxygen can no longer penetrate to the steel from the concrete surface. In his experiments, concrete was made with different binders, w/b ratios and cover depths. The following combinations of binder type, w/b ratio and cover depths were used: PC 35N (300 kg/m^3, w/b ratio 0.60, 25 mm cover), 65/35 PC/GGBS-sulphate resistant (300 kg/m^3, w/b ratio 0.60, 25 mm cover) and 65/35 PC/GGBS-sulphate resistant (450 kg/m^3, w/b ratio 0.40, 40 mm cover). The specimens were cured in a water vapour chamber for between 0 and 7 days. The ratio of the cathode-to-anode area was 400:20 cm^2. The amount of admixed chlorides in the chloride-containing concrete (50 mm thick layer, Figure 2.18) was not reported.

Throughout the experiment, the steel embedded in the chloride-free concrete was exclusively cathodic - final examination of the steel after completion of the experiment showed no signs of corrosion activity. The influence of oxygen diffusion on cathodic reaction rate was investigated using potentiostatic tests and determination of current density/potential curves. The concrete surface was

covered with 50 mm thick layer of water and stored for one year. During storage duration, the cathode (upper electrode) potential was slowly lowered using a potentiostat (an instrument that controls the potential difference between a working electrode and a reference electrode) to a constant value after which the rate of oxygen reduction was determined by measuring the current flowing between the cathode and anode (lower electrode). The current flowing with the potential adjusted to the reduced level was measured and evaluated as the current output of the potentiostat. As long as the potentials set at the cathode do not exceed the limiting potential for hydrogen production, current may be converted directly into a rate of oxygen consumption at the cathode using the equation 1 Ah = 597 mg O_2 [115].

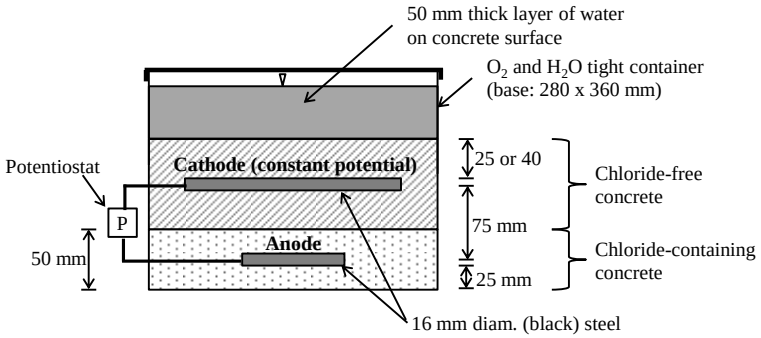

Figure 2.18: Schematic representation of the concrete corrosion cell [115]

At a potential of -700 mV MnO_2, large corrosion currents of about 2.5 μA/cm^2 were initially measured. It was observed that this current decreased with time, a phenomenon that was interpreted as consumption of the residual oxygen still present in the vicinity of the cathode which diminished after 1 year. After about 10 days, a limiting current determined by oxygen diffusion through the water-saturated concrete cover was reached. The limiting oxygen diffusion current density under the test conditions were about 0.05 μA/cm^2. In order to confirm if this was the limiting diffusion current, the potential was reduced further by 100 mV, without reaching the water decomposition range of -1100 to -1200 mV [120]. Since a limiting diffusion current will, by definition, remain constant irrespective of the potential, no change was expected. There was however a significant increase in current by a power of 10, but lasted only for 10 days. The previous limiting current of 0.05 μA/cm^2 was then re-established. Raupach asserts that the results indicate that the cathodic oxygen reduction takes place in a number of intermediate steps (as shown previously). Given a multi-stage reaction mechanism, the increase in current was attributed to possible decomposition of oxygen adsorbed at the steel surface, for example as hydrogen peroxide, requiring a very low potential for cathodic reaction [115].

In another study, Garcia *et al*. [114], carried out experiments to investigate the influence of oxygen availability on chloride-induced corrosion rate. They used two binder contents (375 and 200 kg/m^3) of plain Portland cement, two w/b ratios (0.5 and 1.0), and the concrete was admixed with 3.0% $CaCl_2$ by weight of cement. Cylindrical corrosion specimens of 150 mm diameter by 300 mm length were made. Each specimen was embedded with two steel bars of 12 mm diameter x 290 mm long. The steel bars were located at two different locations to achieve two cover depths of 15 and 70 mm. After 15 days curing under water, the specimens were exposed to wet and dry periods as follows: 30 days in a 100% relative humidity (RH) chamber → 30 days in a 50% RH chamber → 30 days under water → 485 days in a 50% RH chamber → 695 and 1595 days (for concrete made with, respectively, 200 and

375 kg/m^3 binder content) under water. Corrosion rate was measured using a linear polarization technique. Their results showed that even under long periods in saturated conditions, oxygen deficiency was not found to be an inhibiting factor on corrosion rate. They attributed the continued corrosion process even in saturated conditions to the following possible reasons (i) presence of other cathodic processes other than that of oxygen reduction such as the reduction of corrosion products (oxides), (ii) acidification occurring at the bottom of the corrosion pits [121], and/or (iii) the reduction of hydrogen. However, no further studies have been carried out to confirm these hypotheses.

In summary, if the steel in concrete is initially actively corroding, the few studies that are available relating to the influence of oxygen on corrosion propose the following hypotheses to explain the continued corrosion for a given period of time after full saturation when oxygen ingress from the concrete surface through the cover is inhibited:

(i) Presence of cathodic processes other than that of oxygen reduction such as the reduction of corrosion products [114, 115].
(ii) Decomposition of oxygen adsorbed at the steel surface, for example as hydrogen peroxide [115].
(iii) Reduction of hydrogen [114, 120].
(iv) Local acidification occurring at the bottom of the corrosion pits [121].

The results also show that even though in the short-term, high cathodic reaction rates may occur even where oxygen contents in the concrete are low, for long-term oxygen deprivation, the corrosion rate will progressively decrease since the total quantity of residual oxygen is small. Once the residual oxygen is depleted (i.e. anaerobic conditions), it would be expected, based on the general knowledge of corrosion-dependence on oxygen availability, that the corrosion of steel would be stifled due to lack of oxygen to sustain the cathodic reaction. However, contrary to these expectations, corrosion has been observed to proceed e.g. where a RC member is submerged for long periods [114, 115].

2.7.6.2 *Anaerobic corrosion of steel in concrete*

Once the residual oxygen has been depleted and full saturation conditions exist at the steel level, the environment around the steel is described as being anaerobic. Anaerobic conditions also arise at the steel-corrosion products interface as the volume of corrosion products increases with time hindering access of oxygen to the steel. In such anaerobic conditions, corrosion mechanisms are different, and several theories have been proposed to explain the corrosion process. These include cathodic depolarisation theory [122], formation of iron/iron sulphide galvanic cells [123], corrosive and volatile phosphorous compounds, stimulated anodic dissolution by sulphide [124], and binding of metal ions by exopolymers[2] [125]. In concrete, two theories, both relating to the existence of sulphate-reducing bacteria[3] (SRB), have been proposed to explain the corrosion of steel i.e. cathodic depolarization theory and iron sulphide theory. Even though these are discussed in the following sections, it is important to note that the underlying mechanisms of SRB-induced corrosion are apparently complex and still not well understood.

[2] An exopolymer is a biopolymer that is secreted by an organism into the environment (i.e. external to the organism). Exopolymers include the biofilms produced by bacteria to anchor them and protect them from environmental conditions.

[3] SRB are strict anaerobes that gain their biochemical energy for growth by oxidising certain organic compounds or hydrogen (H_2) with sulphate (or other sulphur compounds such as sulphite and thiosulphate) as terminal electron acceptors, and reducing these compounds to sulphides (H_2S and HS^-) [122].

2.1.1 *Cathodic depolarization theory*

This theory was first proposed by Kuhr in 1923 [126]. In saturated conditions, or with the increasing difficulty of oxygen diffusion through the thickening rust layer on the steel surface, anaerobic conditions are produced at the steel-corrosion products interface [127, 128]. Such conditions may permit the activity of SRB which are present in natural soils and seawater [129]. These organisms reduce sulphates to insoluble sulphides in their metabolism, Eqn. (2.43). In such anaerobic conditions, hydrogen gas is the cathodic product during steel corrosion (as opposed to the conventional cathodic reaction i.e. $2H_2O + O_2 + 4e^- \rightarrow 4OH^-$):

$$SO_4^{2-} + 9H^+ + 8e^- \rightarrow HS^- + 4H_2O \quad (2.43)$$

$$2H_2O + 2e^- \rightarrow H_2 + 2OH^- \text{ (absence of oxygen)} \quad (2.44)$$

The SRB can in turn accelerate steel corrosion by consuming this cathodic hydrogen gas [130] and inducing the formation of ferrous sulphides [131]. Severe corrosion cells (pits) develop when sulphides, produced by the microbial reduction of sulphates, combine with ferrous ions, released by the corrosion process, to produce insoluble black iron sulphides [132]:

$$4Fe + SO_4^{2-} + 8H^+ \rightarrow FeS + 3Fe^{2+} + 4H_2O \quad (2.45)$$

The main problem with this theory is the difficulty in quantification of corrosion due to cathodic depolarization by the SRB. It has been criticized for not being able to account for the levels of corrosion seen in experiments as determined by mass loss [133]. As noted by Melchers and Jeffrey [134], simply acknowledging that SRB are present and that corrosion may have been influenced by microbial action is not helpful from a practical point of view.

2.1.2 *Iron sulphide theory*

Later in 1971, it was shown by Miller and King [135] that corrosion could be caused by the presence of iron sulphide itself. They proposed that iron sulphide (produced in the presence of SRB) could act as the cathode and that the role of the bacteria would therefore be (i) to regenerate (or depolarize) iron sulphide, (ii) to produce more iron sulphide by their growth reaction(s), or even (iii) to bring fresh iron sulphide surfaces constantly into contact with the steel by their movement [135]. This theory, to some extent, disputes the cathodic depolarization theory.

In this case, that the primary cause appears to be the production of a volatile phosphorous compound by SRB which reacts with iron to form a black precipitate, iron phosphide, as a corrosion product [136]. The highly reactive phosphorous compound is produced from an organic compound, inositol hexaphosphate ($C_6H_6O_{24}P_6$), the major source of phosphorous in plants. H_2S gas produced by the SRB normally produces a film of iron sulphide on iron at pH near neutrality under anaerobic conditions. When the pH is >7, HS^- is formed [133]; SRB can regulate the pH of their environments by changing their metabolism [137]. These differences in pH have been cited to account for the initiation of an anode at a site of low pH and a cathode at areas of higher pH. Corrosion can occur when the film of

iron sulphide is disrupted, allowing the phosphorus-containing compound to come into contact with the iron surface.

2.7.7 *Effect of chloride ion concentration on corrosion process*

As was mentioned in Section 2.5.2, for a given metal, the potential at which pitting occurs is lower for a higher chloride ion concentration. This trend is evident from the anodic polarization curves which show progressive lowering of the transpassive (pitting) potential with increasing chloride content (Figure 2.19). Alvarez and Galvele [138] studied the effects of chloride ion concentration on the pitting potential, E_{pit}, of pure iron-alkali solutions and showed that it follows the relationship:

$$E_{pit} = -0.364 - 0.064\log C_{Cl^-} \quad \begin{array}{l}\text{for } 0.01\text{M} \le \text{NaCl} \le 1.0\text{M, pH of 10 and} \\ \text{potential measured against normal hydrogen electrode}\end{array} \tag{2.46}$$

Even though Figure 2.19 shows the anodic curve for stainless steel in a neutral solution, a similar trend can be expected for conventional carbon steel in concretes with different chloride concentrations [7].

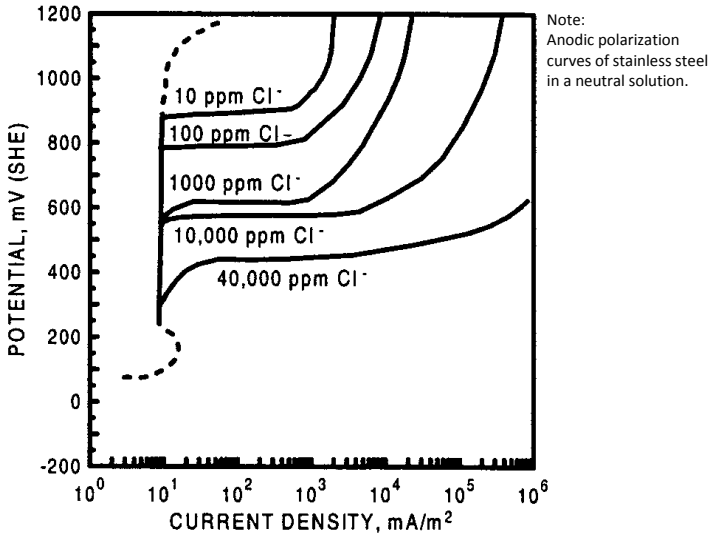

Figure 2.19: Effect of chloride ion concentration on anodic polarization curve [7]

For a given cathodic polarization curve the progressive lowering of the transpassive portion of the curve (see Figure 2.19) can result in an increase in corrosion current density with increasing chloride concentration. However, while this is true to some extent, the effects of chloride concentration on the solubility of oxygen and thus cathodic processes must also be considered. The solubility of oxygen in various concentrations of salts is shown in Figure 2.20 where it is evident that oxygen solubility decreases with increase in chloride concentration. Further, Foley [44] showed that there is an optimum chloride concentration where the decrease in the cathodic reaction due to oxygen depletion is countered by the increase in anodic dissolution. From Figure 2.21, it is evident that the greatest corrosion rate (as mass loss) occurs at a NaCl concentration of approximately 0.5N. In Figure 2.21, the initial increase in corrosion rate can be attributed to increased conductivity of the electrolyte. Similar results of increased corrosion rate, but for steel in concrete, with increased chloride concentration have also been reported by Bamforth [139].

In conclusion, the effect of chloride ion concentration on corrosion rate can be summarised as follows: as the chloride ion concentration is increased, the corrosion rate increases due to decreased pitting (transpassive) potential and increased electrolyte conductivity. At the same time, the oxygen solubility progressively decreases and hence stifles the cathodic reaction. However, an optimum chloride ion concentration is reached where the decrease in the cathodic reaction due to oxygen depletion is countered by the increase in anodic dissolution, and corrosion rate can still remain high. Beyond the optimum chloride concentration, the further reduced oxygen solubility due to increased chloride ion concentration results in decreased corrosion rates mainly due to lack of oxygen to sustain the cathodic reaction.

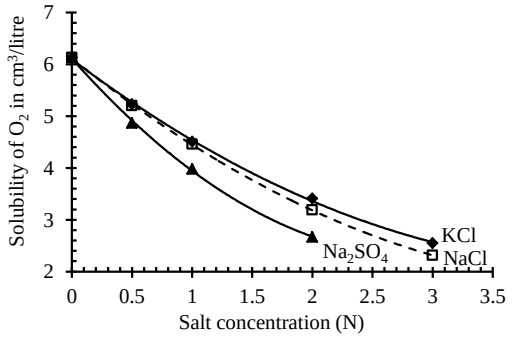

Figure 2.20: Effect of salt concentration on oxygen solubility [44]

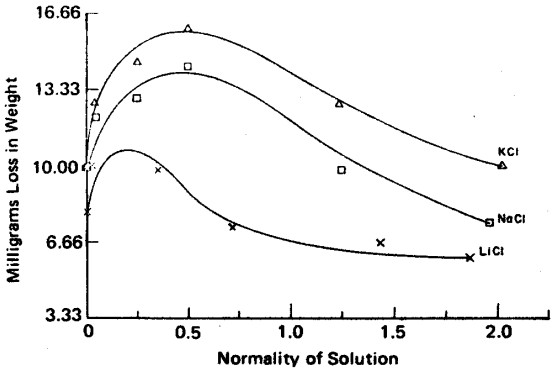

Figure 2.21: Effect of chloride content on corrosion rate [44]

2.7.8 *Effect of pre-corrosion cover cracking*

Cracks impair the durability of RC structures by creating preferential paths for the penetration of corrosion-inducing species (H_2O, O_2, CO_2, Cl^-) leading to relatively faster initiation and propagation of steel corrosion and consequently a reduction in service life. If no cracks are present, both the initiation and propagation phases (See Figure 1.2, Chapter 1) are usually a function of the penetrability of the concrete cover, the cover thickness, and the corrosion resistance of the steel bars. However, in the presence of cracks, the corrosion resistance of the bars may be the main factor that has practical influence on the initiation and propagation phases even though other factors such as concrete quality and resistivity also play important roles. The effects of cracks vary not only with their width, but also with depth, frequency, orientation (relative to the steel reinforcement), self-healing and activity or dormancy; these are discussed in detail in this section. Two schools of thought exist with regard to the influence of cracks on corrosion.

On the one hand, some researchers state that there is no direct relationship between crack width and corrosion rate [48, 83, 140, 141]. They state that cracks may accelerate corrosion initiation but not its propagation. They consider important factors to include crack properties (e.g. whether the crack is active or dormant) and exposure conditions (i.e. service environment). For example, results obtained by Beeby [141] after 10 years of testing carried out on outdoor-exposed (offshore) specimens with surface crack widths ranging from 0.13 to 1.27 mm showed that there were negligible increases in corrosion rate (measured in terms of average mass loss) with increasing crack width. For crack widths of 0.13, 0.25, 0.51 and 1.27 mm, the average depths of corrosion on the steel bar surface were, respectively, 0.16, 0.16, 0.18 and 0.21 mm. It is important to note that this may be a function of exposure environment, e.g. presence of moisture, crack self-healing potential, activity of crack, etc.

On the other hand, other researchers have shown that cracks accelerate both corrosion initiation and propagation, but these are dependent on the concrete quality (w/b ratio and binder type) and cover depth [16, 33, 142-145]. For example, Pettersson and Jorgensen [142] investigated the influence of crack width on the corrosion process using PC and silica fume concrete with w/b ratio of 0.30 and found that for crack widths <0.4 mm, a change in cover (from 15 to 30 mm) affected corrosion rates; however, for crack widths >0.4 mm, change in cover had negligible effect on corrosion. These observations were attributed to oxygen availability at the steel level and/or area of steel exposed. However, this may not be true for all types of binders.

In another study, Raupach [144], carried out accelerated chloride-induced corrosion in cracked beam specimens of 100 x 150 x 700 mm long made using 65/35 PC/fly ash concrete with two w/b ratios (0.50 and 0.60) and two cover depths (15 and 35 mm). The beams were cracked using a 3-point loading rig to produce a single centrally-placed flexural crack. The surface crack widths ranged from 0 to 0.5 mm. The potentially cathodic reinforcement (14 mm diameter) between the cracks was simulated by adding reinforcing steel sections on each side of the crack, allowing cathodic action to be determined as a function of distance from the crack. The specimens were exposed to 12 (wetting and drying) cycles comprising of wetting once a week with 1% chloride solution in a reservoir on the cracked face for 24 hours and drying for the rest of the week, followed by 2 wetting and drying cycles using tap water with no chlorides added. The side faces and underside of the beams were epoxy-coated to prevent rapid drying. The specimens were then stored without further wetting at 80% relative humidity in a climate chamber. After one year the cycle of wetting periods was repeated. The current between the reinforcing steel electrodes was measured to determine whether they were anodes or cathodes. The results showed that regions of the reinforcement outside the crack behaved cathodically up to a crack distance of more than 200 mm. The current density of the cathodes was found to decrease with increasing distance from the crack, and was attributed to the increase in electrolytic resistance increase in distance from the crack. The results also showed that increasing concrete cover from 15 to 35 mm decreased the corrosion rates while a reduction in the w/b ratio from 0.60 to 0.50 resulted in a further reduction in corrosion rate in the crack zone (see Figure 2.22). However, the influence of w/b ratio (or concrete quality) was found to be more pronounced after 24 weeks, than after one year. Based on the results, it was concluded that the quality of the concrete cover was the dominant influencing variable for the corrosion rate in the crack zone. This was, however, only true for crack widths up to about 0.4 mm beyond which crack width was also of decisive importance. In

summary, even though this study shows the influence of crack width on corrosion rate, it also shows the importance of taking other parameters such as cover depth and concrete quality into account in addition to crack width.

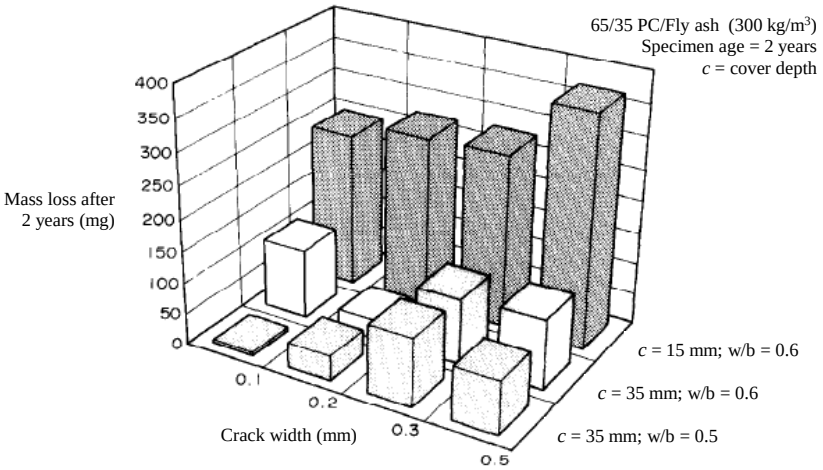

Figure 2.22: Influence of crack width, cover depth and w/b ratio on corrosion rate [144]

Similar results were obtained by Scott and Alexander [16], and Otieno *et al*. [33]. Scott and Alexander [16], in a study using different binder types, surface crack widths of 0.2 and 0.7 mm, constant w/b ratio of 0.58, and cover of 20 and 40 mm, showed that change in cover was only influential for PC concretes where corrosion rate is governed mainly by oxygen availability, as opposed to blended cements where high concrete resistivity is a governing factor. They showed that, at a given crack width, decrease in cover results in a significant increase in corrosion rate for a PC concrete compared to blended cement concretes (Figure 2.23). They used 120 x 120 x 375 mm long RC beams with a single 16 mm mild steel bar.

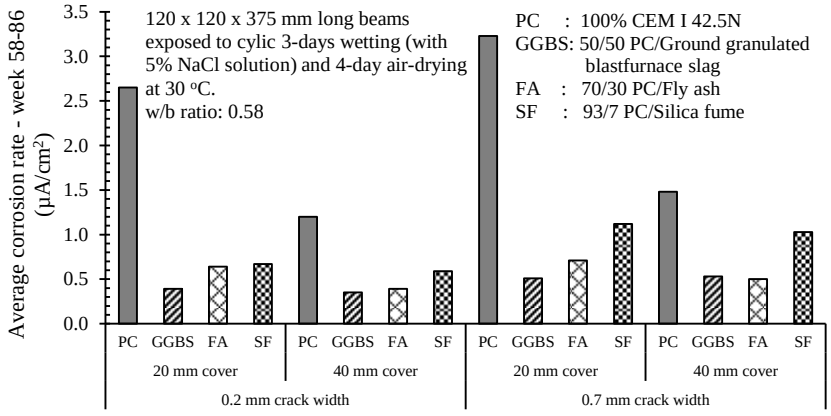

Figure 2.23: Influence of crack width and cover depth on corrosion rate [16]

Otieno *et al*.'s [33] study investigated the effect of load-induced surface crack width, concrete quality (binder type and w/b ratio) and concrete resistivity on corrosion rate (Figure 2.24). The study used 100 x 100 x 500 mm long beam specimens from four concrete mixes made using two w/b ratios (0.40 and 0.55) and two binder types (100% CEM I 42.5N (PC) and 50/50 PC/Corex slag (GGCS) blend [146]). A constant concrete cover to the steel reinforcement of 40 mm was used. The beam specimens were pre-cracked (including incipient cracks, being cracks that effectively had zero crack width) and

then subjected to a cycle of 3-day wetting (with 5% NaCl) and 4-day air drying under laboratory conditions (16-24 °C and 60-75% relative humidity) for a period of 32 weeks.

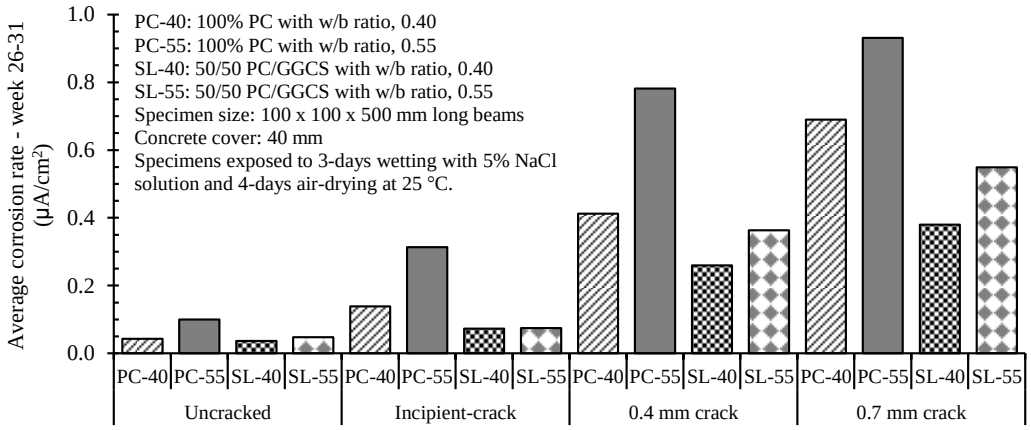

Figure 2.24: Effect of crack width and concrete quality on chloride-induced corrosion rate [33]

After 32 weeks, all the uncracked and incipient-cracked specimens and the uncracked PC specimens had not attained active corrosion rates (i_{corr} > 0.1 µA/cm^2). In the cracked specimens, active corrosion rates were recorded after only one cycle of wetting and drying except for the incipient cracked specimens where active corrosion rates were recorded after 6 and 21 weeks for, respectively, PC-55 and PC-40 specimens. Therefore, the presence of cracks significantly affected the initiation phase and in some cases, eliminated it. The following conclusions were drawn from the study:

(i) The initiation phase may be either substantially shortened or completely eliminated depending on the combination of surface crack width, concrete quality and resistivity.

(ii) Cracking affects corrosion rate during the propagation period but the extent of its effect depends on the interaction between surface crack width, concrete quality and concrete resistivity.

Therefore, despite the previous conflicting viewpoints on the influence of cracking on corrosion of steel in concrete, recent studies [e.g. by 16, 33] have shown that cracks accelerate both corrosion initiation and propagation, but these are dependent on the concrete quality (w/b ratio and binder type) and cover depth. However, other crack characteristics should also be taken into consideration. These are briefly discussed in the following sub-sections.

2.7.8.1 *Influence of crack density*

Crack density (or frequency) refers to the number of transverse (i.e. transverse with respect to the orientation of the steel bars) surface cracks per unit length. Previous studies such as the one by Arya and Ofori-Darko [147] have shown that corrosion rate increases with increasing crack frequency (Figure 2.25). This can be attributed to the increase in the penetrability of the concrete, and hence ease of chlorides and oxygen ingress into the concrete. It must be noted that in the results by Arya and Ofori-Darko (Figure 2.25), the specimens with the highest crack frequency of 20 did not correspond to the highest corrosion rate, which seems to be an anomalous result.

It is important to note that the concept of increasing corrosion rate with increasing crack frequencies should also be viewed in conjunction with the crack width. In the case Arya and Ofori-Darko [147],

the crack width was kept constant (using cast-in plastic shims) as the crack frequency was increased. However, in in-service structures, increase in crack frequency is usually associated with both increased loads and increased crack widths. In this case, the increase in corrosion rate should be expected to be much higher.

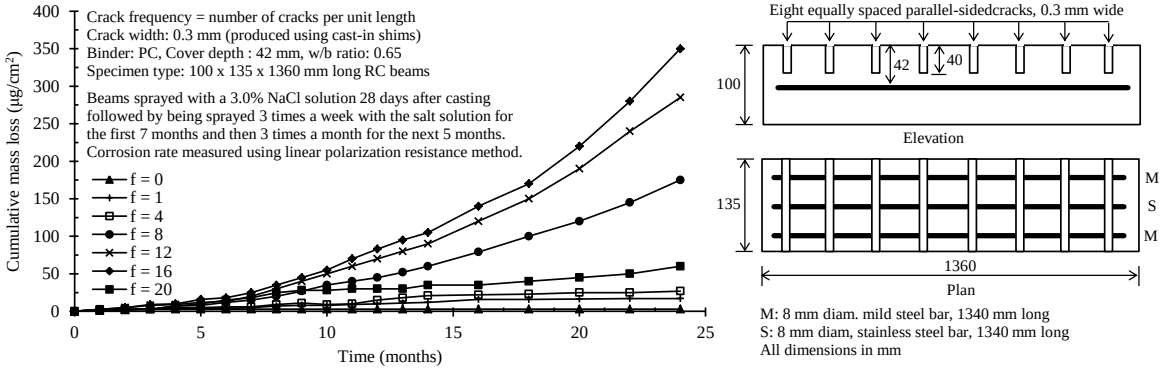

Figure 2.25: Effect of crack frequency on cumulative mass loss due to corrosion [147]

2.7.8.2 *Influence of crack activity or dormancy*

Cracks in RC structures can be either active or dormant depending on whether they frequently open and close (i.e. active) or not (i.e. dormant). The opening and closing of cracks can be due to application and removal of cyclic or occasional loads, for example in roads and bridges. It is very important to consider these phenomena because they can determine whether a crack can undergo self-healing (also called autogenous healing, covered later in Section 2.7.8.4), a process which decreases the severity of cracks by decreasing concrete penetrability (at the crack) and hence improving the protection of the embedded steel from corrosion [148, 149].

The terms '*crack re-opening*' and '*crack re-activation*' are commonly used when referring to crack activity, and refer to either widening of existing (dormant) cracks or re-activating self-healed ones by either cyclic or occasional mechanical loading of the member. In either case, the process makes the crack active. In the study by Otieno [67] that was described in Section 2.7.8, crack re-opening actions were carried out (after 18 weeks of chloride-induced corrosion) by reloading the incipient, 0.4 mm and 0.7 mm cracked 100 x 100 x 500 mm beam specimens. The incipient, 0.4 mm and 0.7 mm crack widths were widened to, respectively, 0.6 mm, 1.0 mm and 0.2 mm. The crack widths at reloading were maintained for about 24 hours before being relaxed to their original respective widths. The results (see Table 2.6) showed that:

(i) crack re-opening increases corrosion rate but only if the RC structure was actively corroding prior to crack re-opening (i.e. $i_{corr} > 0.1$ µA/cm^2).
(ii) for passively corroding RC members, the effect of crack re-opening may allow chlorides to reach the embedded steel and start (or accelerate) the destruction of the passive protective layer.
(iii) if cracks are subsequently allowed to remain dormant, corrosion rates reduce again, which infers some form of crack-healing.
(iv) for an actively corroding RC structure, crack re-opening may accelerate the corrosion process by one or a combination of the following mechanisms: a) widening the existing cracks,

b) re-activating (re-opening) any self-healed cracks, c) increasing the loading level (i.e. stressing the steel), and d) damaging the concrete-steel and/or aggregate-paste interfaces.

Table 2.6: Percentage increases in corrosion rates after crack re-opening [67]

	Percentage increase in i_{corr} after crack re-opening (%)			
Specimen condition	PC-40	PC-55	SL-40	SL- 55
Incipient-cracked	3	16	8	9
0.4 mm cracked	13	7	10	30
0.7 mm cracked	11	2	28	12

In general, incipient-cracked specimens (except PC-55 ones) experienced the lowest percentage increases in corrosion rate due to crack re-opening, while the 0.4 mm and 0.7 mm cracked specimens showed a higher increase. The results by Otieno [67] should be interpreted taking into consideration that (i) the 0.4 mm cracked specimens were actively corroding before the crack re-opening process, and (ii) for all binder types (except PC-55), the incipient-cracked specimens were passive (corrosion rate below 0.1 µA/cm^2) before and after the crack re-opening, a condition which did not favour corrosion rate increasing substantially. Crack self-healing probably occurred in these specimens although this was not measured in the study. The minimal 2% increase in corrosion rate for the 0.7 mm cracked PC-55 specimens (which were actively corroding before the reloading process) means that even before reloading, corrosion agents could easily penetrate to the steel and promote corrosion. Crack re-opening therefore did not affect the concrete penetrability to a great extent, with respect to corrosion rate, in these specimens.

In summary, while crack activity or dormancy affects corrosion rate, it should be interpreted taking into account aspects such as preceding corrosion state (active or passive) before re-activation and crack width.

2.7.8.3 *Influence of crack orientation*

Cracks in concrete can be either longitudinal (coincident) or transverse (intersecting). Longitudinal cracking is extremely detrimental, since chlorides, moisture, and oxygen can easily penetrate to the embedded steel and attack large areas of steel in the corrosion process. For transverse cracks, the cathodic areas mostly occur in the uncracked regions [144]. Therefore, moisture and oxygen that enter through the cracks may be expected not to greatly affect the rate of corrosion. However, results of an experimental study by Otieno *et al.* [33] show that this is dependent on concrete quality (binder type and w/b ratio), as discussed previously. For concrete in service, transverse cracks are more likely in tensile-stressed areas of a RC structure. Longitudinal cracks are more associated with corrosion cracking along the longitudinal reinforcement due to the expansive nature of corrosion products. Restrained deformations in concrete such as thermal deformations and shrinkage may result in both transverse and longitudinally cracked sections, however often with relatively low crack widths.

2.7.8.4 *Influence of crack self-healing*

Finally, the occurrence and benefits of crack self-healing is significant in the reduction in concrete penetrability and hence improving the protection of the embedded steel from corrosion by limiting the

diffusion of chlorides into concrete [149, 150]. However, its practical quantification is challenging. The most significant factor which influences self-healing is the precipitation of calcium carbonate crystals in the cracks, as a result of $Ca(OH)_2$ leaching [151]. Other causes of crack self-healing include swelling and hydration of cement paste, ettringite formation, and blocking of the crack by impurities in water and concrete particles (debris) broken from the crack surface [152].

Other important crack characteristics, not covered in this review, but which have been shown to affect transport properties of fluids through concrete include crack tortuosity, length, depth, profile and surface roughness [153-155].

2.8 *Acceleration of corrosion in concrete*

The subject of acceleration of corrosion is reviewed here because it will be applied in the development of this study's experimental programme in Chapter 3. Due to the slow nature of natural corrosion process coupled with the urgent need to provide working solutions to the day to day corrosion problems in RC structures, the use of accelerated corrosion to simulate the corrosion process and predict the associated corrosion-induced damage (e.g. cover cracking, spalling, loss of steel cross-section, loss of stiffness) has become common; these techniques are inexpensive and fast but have inherent drawbacks, some of which will be discussed here in detail.

In general, the term *accelerated corrosion* of steel is conventionally used to refer to a steel corrosion process that is faster than a corresponding natural one. Contrary to natural corrosion, the effects of accelerated corrosion can be realised within a relatively short period of time. Miyagawa [145] outlined four basic principal requirements for accelerated corrosion tests as follows:

(i) The corrosion mechanism of the technique should simulate the actual corrosion mechanism of steel in concrete.
(ii) The effect of the acceleration should be relatively high compared to natural corrosion.
(iii) The applicability should be wide e.g. simulate both the corrosion process and corrosion-induced damage.
(iv) The test should be relatively easy to conduct.

Though it is difficult to satisfy all of these requirements, several techniques, have been developed. This study focuses on chloride-induced corrosion and hence only accelerated chloride-induced corrosion techniques are discussed. Before proceeding, it is important to clarify that regardless of whether the corrosion of steel in concrete is natural or accelerated, both anodic and cathodic reactions still occur. However, depending on the O_2 concentration (relative to the rate of anodic reaction) and the pH, different corrosion products (in terms of composition, density, expansion volume and stability) may be formed [22, 156, 157]. These factors (pH and O_2 concentration) are extremely variable and difficult to quantify in an in-service RC structure. When there is adequate supply of O_2, more stable corrosion products such as haematite and magnetite (see Table 2.2) are formed; when there is limited supply of O_2 (e.g. in fully submerged elements or when the corrosion rate is high as in accelerated conditions), less stable/soluble products such as ferrous hydroxide are expected.

Despite the several critiques and test results from previous studies showing that accelerated corrosion is not representative of the natural corrosion process [e.g. 158, 159], the slow rate of the latter has made it inevitable to continue using accelerated corrosion processes to study both the corrosion process and the associated damage on the RC structure. Accelerated chloride-induced corrosion can be achieved in different ways including (i) application of a constant (impressed) direct anodic current (galvanostatic) or potential (potentiostatic) between the reinforcement and a counter electrode (e.g. stainless steel or copper), (ii) use of admixed chlorides, (iii) use of cyclic wetting and drying with a chloride-based salt solution (e.g. NaCl, $CaCl_2$) or (iv) a combination thereof [160].

2.8.1 *Use of impressed current (IC)*

Acceleration of corrosion using IC is a common technique used to study corrosion-induced damage such as cover cracking in RC structures. It involves application of direct anodic IC (galvanostatically) or potential (potentiostatically) between the steel reinforcement (anode) and a separate (internal or external) cathode (e.g. stainless steel, copper). Typical experimental set-ups are shown in Figure 2.26.

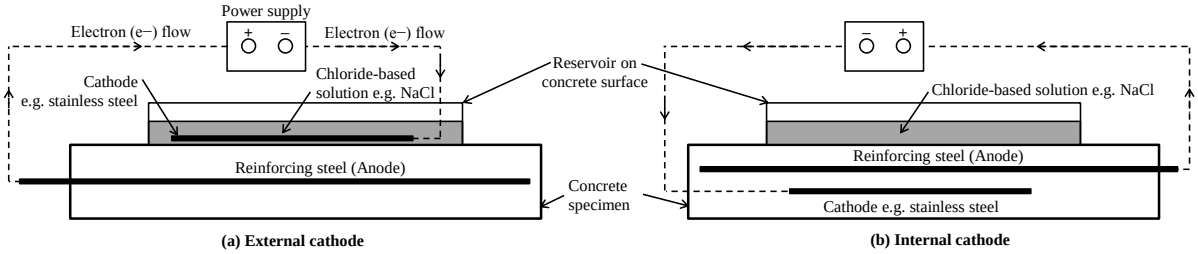

Figure 2.26: Typical experimental set-ups for accelerated corrosion of steel in concrete [33, 156]

The main electrochemical difference between this technique and naturally corroding systems is the raising of the potential to a value greater than the transpassive/pitting potential where corrosion rate does not correspond to an equilibrium corrosion potential or a potential obtainable under natural conditions [161]. Such a potential results in the steel bar being in an artificially polarized state [162]. Corrosion rate is increased by an electric field on the steel surface [161]. Contrary to the ingress of chlorides by a diffusion-dominated process in in-service RC, the penetration of chloride ions (Cl^-) in concrete when impressed current or voltage is used creates a chloride ion front (flux) in the concrete and can be modelled using the Nernst-Planck equation, which governs the movement of ions in a solution under an electrical field, i.e. migration/electro-diffusion [52, 163], Eqn. (2.47):

$$J = -\left(\frac{zF}{RT}\right)DC\left(\frac{\partial E}{\partial x}\right) \tag{2.47}$$

where J is the flux of the ionic species, in this case Cl^-, (mol/m^2.s), D is the diffusion coefficient of the ionic species (m^2/s), C is the concentration of the ionic species (mol/m^3), z is the valence of the ionic species (-1 for Cl^-), F is Faraday's constant (96,500 A.s), R is the universal gas constant (8.314 J/mol.K), T is the absolute temperature (298 K) and E is the applied electrical potential (V).

It is also important to note that in the use of anodic IC, steel de-passivation exhibits different characteristics compared to that produced by chlorides. In the former case, the entire exposed surface

area of the steel is anodic and hence results in general corrosion; in the latter case, the chlorides, having reached a threshold value, cause localized breakdown of the passive film at discrete locations on the steel surface while the remaining steel area becomes cathodic. This results in a larger cathode-to-anode area ratio and hence higher corrosion rates in the anodic areas. Moreover, the applied anodic IC alters the ionic distribution in the concrete pore solution around the steel, attracting the anions while repelling the cations, and thus, changing the local chemistry of the pore solution near the steel.

As already mentioned, accelerated corrosion using IC is mainly used to assess corrosion-induced damage in RC structures; El Maaddawy and Soudki [156] recommend limiting the IC density to 200 $\mu A/cm^2$ if the corrosion characteristics and structural response are to be similar to those for natural corrosion. Even though the use of impressed current or voltage has the advantage of allowing corrosion rates (and hence the degree of damage) to be varied, it has been criticised because of the following reasons:

(i) Previous studies [e.g. 156, 158, 160] have shown that the use of Faraday's law to obtain corrosion rates (in terms of steel mass loss) from such tests is not valid, and can lead to over-estimation or under-estimation of steel mass loss. El Maaddawy and Soudki [156] state that the degree of variation between predicted mass loss (based on Faraday's law) and actual mass loss is also dependent on the IC density applied.

(ii) In most studies, 100% current efficiency is assumed, i.e. all the applied or resulting/effective current is assumed to be consumed in dissolution of the steel [158], even though this may not be the case. For example, results by Ballim and Reid [160] in an accelerated corrosion study to investigate the effect of corrosion on beam deflection, showed that Faraday's law over-estimated mass loss and that the current efficiency was less than 100%, typically 70%.

(iii) The IC density used to accelerate corrosion has been a subject of debate; a summary by El Maadawy and Soudki [156] of previous studies where IC has been used to accelerate corrosion showed that IC densities ranging from 45 to 10,400 $\mu A/cm^2$ are 3-100 times greater than the maximum current densities reported from field studies involving natural corrosion. As indicated above, they recommend limiting the IC density to 200 $\mu A/cm^2$.

2.8.2 *Use of admixed chlorides*

The use of admixed chlorides in concrete, ranging from 1% [164] to 5% [156] by weight of cement, is another way of accelerating corrosion of steel in concrete. This technique results in uniform distribution of chlorides around the steel leading to formation of very small microcells, which is contrary to that under natural conditions (except in submerged conditions) where spatial distribution of chlorides is usually the case. It also poses the disadvantage that the steel will not have the opportunity to develop a passive protective film on its surface before the chloride threshold is reached (to depassivate the steel). This is the main disadvantage of this technique. Furthermore, it does not allow for chloride binding effects which occur in natural conditions, and is very likely to affect the alkalinity of the concrete pore solution.

2.8.3 *Cyclic wetting and drying with a chloride-solution*

Corrosion can also be accelerated by cyclic wetting and drying with a chloride-solution. The wetting phase can be achieved in various ways including:

(i) Application of a salt spray or fog in a closed chamber with controlled temperature [e.g. 165, 166]. In most cases, the salt spray is uniformly distributed around the concrete specimen.
(ii) Immersion in chloride-solutions with concentrations ranging from 3% [167] to 5% [168] by weight of the solution. This involves full or partial immersion of the specimen in a salt solution bath and removal after a predetermined time for drying [e.g. 169, 170].
(iii) Ponding on one face (usually the top face) with a chloride-solution, typically using a small reservoir. It is one of the most commonly used wetting and drying techniques and simulates natural exposure conditions (e.g. marine tidal zone) where spatial distribution of chlorides is expected. It has been adopted in the ASTM G-109 [171] standard to assess the resistance of concretes to chloride-induced corrosion of reinforcement in concrete.

The third wetting technique has been experimentally shown to simulate natural corrosion processes better than the use of impressed current/voltage or admixed chlorides [172]. The drying phase can be achieved by removing the chloride-solution, e.g. by a vacuum device, and allowing the specimens to dry (e.g. in ASTM G109) [171], exposing the specimens to ambient (temperature and relative humidity may be controlled) or elevated temperatures, e.g. 70 °C. The latter approach can be criticized for leading to microstructural damage in the concrete, and hence influencing the transport mechanisms [173].

Cyclic wetting and drying with a chloride-solution accelerates corrosion by (i) allowing the chloride solution to penetrate the concrete rapidly by capillary suction rather that by diffusion, and (ii) allowing for the replenishment of dissolved oxygen at the steel surface to sustain the cathodic reaction process. These two processes occur during the drying phase. Previous studies have shown that in this technique, the longer the drying phase, the higher the corrosion rate. For example Malumbela [174] found that corrosion rate in RC beam specimens (153 x 254 x 3000 mm long) increased by up to 55% when the air-drying period was increased from 2 to 4 days while keeping the wetting period (5% NaCl solution) constant at 2 days. This trend is attributed to sufficient drying time to allow for the penetration of oxygen through the cover concrete to the steel; the availability of dissolved oxygen also allows the formation of less voluminous and stable corrosion products, and hence more space for corrosion species to access the steel from the concrete surface. Even though Malumbela contends that longer drying phases simulate in-service structures more realistically than shorter ones, this conclusion should be applied selectively to RC structures depending on the exposure conditions. Logically, the choice of either short or long drying phases should be based on a balance between accelerating the corrosion rate, and simulating in-service exposure conditions.

2.8.4 *Use of simulated pore solutions*

Finally, it is also worth mentioning the use of simulated pore solutions (SPSs) which is sometimes used to study the corrosion kinetics of steel in concrete [175, 176]. SPSs have also been used to study chloride thresholds for steel in concrete, with results indicating that SPSs give lower values than those determined using concrete or mortar [10, 177]. This may be attributable to chloride binding in cementitious materials and the interface conditions existing between steel and mortar or concrete, in which a lime-rich layer not only acts as a physical barrier but also buffers the action of chloride

activity; homogenous SPSs cannot provide this inhibition function. The main draw-backs with the use of SPSs include the following:

(i) Simulated pore solutions do not accurately reflect the true mechanisms of steel corrosion in concrete as there is no bonding of hydrates to the steel or variability in pore solution chemistry which may exist within localized regions of the concrete.
(ii) Previous investigations on the electrochemical behaviour of iron immersed in alkaline solutions have highlighted very low oxidation kinetics [176].
(iii) It is difficult to determine the actual concrete pore solution chemistry to be simulated. There is no standard pore solution chemical composition, and hence no standard procedure can be adopted to make one. The use of cement extenders (e.g. fly ash, silica fume and ground granulated blastfurnace slag) and the introduction of new cements makes pore solution chemistry vary from one binder to another.

2.9 *Closure (fundamentals of steel corrosion in concrete)*

This part of the literature review presented an overview of the electrochemical principles (both thermodynamic and kinetic) of corrosion and the fundamentals of steel corrosion in concrete. In addition, factors affecting corrosion rate of steel in concrete, with a focus on chloride-induced corrosion, were discussed. Specifically, the influence of cover cracking was critically reviewed. These were covered to provide a holistic understanding of the underlying corrosion processes and the factors affecting it. This understanding will help in the, (i) development of the experimental programme in Chapter 3 i.e. selection of variables, (ii) understanding the principles underlying the measurement techniques used, and (iii) interpretation of experimental data collected in Chapter 4. It is important to note that, in general, the electrochemical and kinetic processes of corrosion of metals (e.g. steel) in ideal or standard conditions (such as in air, water or at a specific pH and temperature) are well understood. However, because these governing principles are derived for ideal or standard conditions, most of them are not directly applicable to other corrosion regimes. In such cases, the existing governing principles are modified to suit the corrosion regime. In the case of steel corrosion in concrete, much research has been carried out in the past and the governing principles are now relatively well understood.

The review covered mainly chloride-induced steel corrosion in concrete which is the focus of this study. Phenomena relating to chloride-induced corrosion such as corrosion initiation (chloride threshold), macrocell corrosion, pitting and residual cross-section area, effect of cover cracking, concrete quality and cover depth on chloride ingress and/or corrosion rate were reviewed, and the effect of chloride ion concentration on corrosion process as well as artificial chloride-induced corrosion acceleration were discussed.

The next part of this chapter presents a critical review of the available corrosion rate prediction models.

Chapter 2 PART II

Critical review of corrosion rate prediction models

2.10 *Background*

Corrosion rate, i_{corr}, is one of the most important input parameters in corrosion-induced damage prediction models for reinforced RC structures. Its accurate assessment and/or prediction is therefore required if the damage prediction models are to be reliably used to predict both the rate and severity of damage and to plan for maintenance of these structures. However, it has not been assigned the level of importance it deserves especially with respect to its prediction. In most cases, instantaneous measurements or conservative values are used in damage prediction models. In other cases, salient factors that affect corrosion rate such as cover cracking and concrete quality are not taken into consideration during the model development. The consequence of this may be under-estimation or over-estimation of the severity and the time to corrosion-induced damage such as for example cover cracking, and hence incorrect estimation of the service life of the structure. This second part of Chapter 2 presents a critical review of some of the available corrosion rate prediction models focusing mainly on chloride-induced corrosion. In addition, general proposals, some of which may be outside the actual scope of this study, for the improvement of these models are made.

2.11 *Introduction*

In the light of the paradigm shift to incorporate the corrosion propagation phase (t_p) in the service life of corrosion-affected RC structures [178-180], several models have been developed to predict times to different corrosion-induced damages (i.e. limit states - defined in Chapter 1) such as cover cracking, loss of steel cross-section area, loss of stiffness, etc. Even though these prediction models usually have several input parameters, it is clear that the rate of corrosion governs their outcome either in terms of the time to attainment of a pre-defined limit state or the level of damage at a given time. A sensitivity analysis by Li *et al*. [181] showed that corrosion rate is one of the most important input parameters in corrosion-induced damage models.

The success in incorporating t_p in the service life of RC structures will therefore depend on how accurately and realistically i_{corr} can be predicted. As already mentioned, its current treatment with respect to prediction does not match the level of importance it deserves. Instead, more focus has been placed on the prediction of corrosion-induced damage, with little attention to the assessment and prediction of i_{corr}. The result of this has been the development of several corrosion-induced damage prediction models for a given limit state (e.g. time to corrosion-induced cover cracking). This makes the task of selecting appropriate models difficult for practical application.

The number of available or published i_{corr} prediction models is relatively small in comparison to that for damage prediction models; this shows where the focus has been placed, as mentioned above. This part of Chapter 2 reviews the literature on the available or published i_{corr} prediction models. It is sub-

divided into two main sub-parts; the first sub-part presents a review of individual models while the second one presents a summarising critique of the models.

Before proceeding, it is important to note the following:

(i) i_{corr} is affected by many inter-related factors and can be expressed, using a factorial approach [182], as follows:

$$i_{corr} = f(k_1, k_2, ..., k_n) \tag{2.48}$$

where k_1, k_2, …, k_n represent the factors affecting corrosion rate e.g. use of supplementary cementitious materials, moisture content, cyclic wetting and drying, sustained loading, loading history, concrete resistivity, concrete quality, cover depth, cover cracking, temperature, dissolved oxygen concentration, chloride concentration and exposure conditions; these were covered in Part I of Chapter 2. However, it is important to note that it may be impractical to incorporate each of these factors explicitly in a model. Some can be incorporated indirectly in a prediction model e.g. concrete resistivity can be indirectly used to account for temperature, concrete quality and moisture content of the concrete.

(ii) i_{corr} prediction models can be developed based on one or a combination of the following approaches (a) electrochemical principles of corrosion of steel in concrete [e.g. 14], (b) statistical analysis of experimental test results [e.g. 183], and (c) electrochemical principles of corrosion and experimental testing [e.g. 184]. This study uses the second method to develop an empirical corrosion rate prediction model, discussed later in Chapter 5.

(iii) The following factors should be considered in the development of i_{corr} prediction models:
- It should be (as far as possible) representative of the actual i_{corr} characteristics in the RC structure in its service environment.
- It should account for variability in both i_{corr} and the model input parameters such as cover depth and concrete quality. Furthermore, this variability should be taken into account using probabilistic approaches.
- If developed based solely on either electrochemical principles of corrosion or accelerated corrosion test results, its validation using natural corrosion data is important.
- It should be capable of being adjusted to suit the prevailing concrete and exposure conditions of the RC structure.

The next section will present a general overview of the types of corrosion rate models and model development techniques.

2.12 *Types of corrosion models*

Corrosion rate models can be grouped as either mathematical (numerical and analytical) or empirical depending on the criterion used in their development. The following sections give an overview of the different types of corrosion rate models, but without mention of specific available models; this will be done in later sections.

2.12.1 *Empirical models*

Empirical models are based on assumed direct relationships between corrosion and basic concrete parameters such as w/b ratio, binder type, and also environmental conditions [185]. Such models are usually developed using data from laboratory experiments that, by design, isolate other corrosion-influencing parameters. Empirical models are sub-divided into three types namely [178]:

(i) *Delphic oracle models*: This is a systematic, interactive prediction method where corrosion rate (and hence corrosion-induced damage) is estimated based on *experts' knowledge*, usually based on the practical experience gained from past years. However, it has not been used for chloride-induced corrosion due to its complexity, both in terms of the process, its effects on the RC structure and variability.

(ii) *Fuzzy logic models*: In these models, sets of assumed relationships (e.g. between corrosion rate and polarisation resistance) are defined hence allowing the calculation of corrosion rate using fuzzy set theory which incorporates a simple rule-based '*if x and y then z*' approach (i.e. subjective uncertainty) to solving a problem rather than modelling the system mathematically [186, 187]. It has been used to assess corrosion-induced deterioration and to estimate the reduction in steel cross-sectional area [185]. Fuzzy set theory has been criticised in the past for its inability to reflect different kinds of fuzzy phenomena in the natural world (e.g. corrosion process) correctly but this has since been modified and it can therefore be applied to corrosion in RC structures [188].

(iii) *Models based on electrical resistivity and/or oxygen diffusion of concrete*: These assume that electrical resistivity and/or oxygen diffusion of concrete can, among other influencing factors, be used to predict corrosion processes and hence corrosion-induced damage in corroding structures, and hence RC structural performance. They indirectly take into account other corrosion-influencing factors including exposure conditions, w/b ratio and binder type. Examples of empirical models based on this approach include those by Scott and Alexander [16], Rodriguez *et al*. [111] and Andrade *et al*. [189]. The model developed in this study follows this approach.

One of the main disadvantages of empirical models is that the selected variables under consideration (for both concrete (*material*) and corrosion (*process*)) are commonly investigated in isolation from other influencing parameters and/or the interaction thereof. Consequently such models may be limited to the set of conditions under which they are developed. However, the limitations associated with the models are commonly neglected. A common procedure is to carefully select and apply the most convenient model, usually, based on the available or easily quantifiable input parameters. The consequence could be a gross under- or over-estimation of the service life of the RC structure.

2.12.2 *Numerical and analytical models*

These models (also called mathematical models) comprise a set of mathematical equations which when solved, gives approximate solutions of the subject parameter(s) over time [180]. Numerical simulations can be used to estimate corrosion rates, the effects of changes in electrochemical conditions, and structural response to corrosion-induced damage. One important aspect of mathematical models is they need to be calibrated against experimental (laboratory and/or field) test results before they can be applied. Three different approaches can be used to develop mathematical

models namely: (i) finite element method, (ii) boundary element method and (iii) resistor networks and transmission line method [190]. These are covered in the following sections.

2.12.2.1 *Finite element method*

The finite element method (FEM) is a process of approximation to continuum problems such that (i) the continuum is sub-divided into a finite number of individual parts (referred to as *elements*), the behaviour of which is specified by a finite number of parameters whose behaviour can be readily understood, and (ii) the solution and/or understanding of the complete system is an assembly of its individual elements i.e. the sum of sub-models [191].

With respect to RC structures, the concrete, steel and the concrete-steel interface can all be modelled using FEM. Therefore, in FEM models, all the three aspects of interfacial properties, changes in transport properties of the concrete with time, and the geometrical properties can be taken into account. In FEM models, the objective is to satisfy the boundary conditions set for the problem, which in the case of steel corrosion in concrete may include temperature, relative humidity, chloride ion concentration (in the case of chloride-induced corrosion), concrete resistivity and the electrochemical behaviour of both active and passive steel areas [14].

FEM models also provide the ability to easily vary the bulk concrete properties e.g. porosity. However, the main drawback of these models is that for practical situations, the numerical size of the model can be impractically large and hence expensive and time consuming [179, 192].

2.12.2.2 *Boundary element method*

Boundary element method (BEM) modelling technique requires that mesh elements, similar to those in FEM, be created, but only on the boundary (or surfaces) of the element's geometry. When the approach is applied to corrosion, only the concrete-steel interfaces are modelled as opposed to FEM models where the corrosion process is comprehensively described [179] with the objective to satisfy the differential equations used to describe the corrosion system. Boundary conditions that can be applied to the surface elements of the corrosion model include: (i) constant corrosion potential, (ii) constant current density and (iii) linear or non-linear relation between current density and potential. The BEM approach is commonly used in analyses where galvanic steel corrosion is expected to occur (e.g. where steel corrodes preferentially when in electrical contact with a different type of metal) because of the advantage that only the surface and interface areas of the electrolyte, and not the whole system, need to be subdivided into elements [180].

In comparison with FEM, BEM has the advantage that much fewer elements are required and that two dimensional elements can be used to simulate a three dimensional problem. A further advantage of BEM is the reduction of the problem dimension and hence the cost of pre-processing and mesh generation is also greatly reduced. The main disadvantages of BEM are the requirements that the electrolyte conductivity has to be constant and that within the electrolyte, results can only be calculated at discrete points [180].

2.12.2.3 ***Resistor networks and transmission line approach***

In this approach, the relationship between the driving voltage (corrosion potential), the resistances of the corroding system, and the electrical macrocell current, which is proportional to the corrosion rate, can be calculated based on simplified electrical circuits (also referred to as *Randle's circuit*); however, the validity of the simple Randle's circuit to adequately represent the steel-concrete interface is still uncertain. Models developed using this approach consist of the driving voltage (U_e), the resistances of steel (R_{steel}), anode (R_{anode}), cathode ($R_{cathode}$) and electrolyte ($R_{electrolyte}$), and the electrical current (I_e) flowing between the anode and the cathode (Figure 2.27).

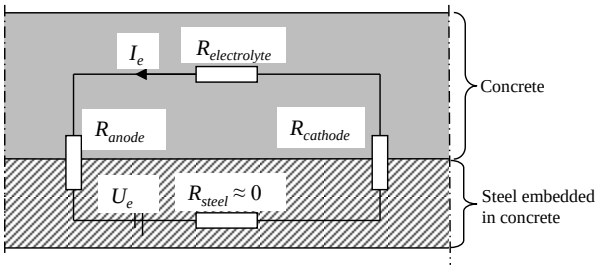

Figure 2.27: Simplified schematic electrical circuit model for corrosion of steel in concrete [144]

The galvanic current can be calculated using the following equation [144]:

$$I_e = \frac{U_{R,c} - U_{R,a}}{\frac{r_a}{A_a} + \frac{r_c}{A_c} + \frac{\rho_{el}}{k}} \tag{2.49}$$

where I_e is the corrosion current i.e. electrical current between the anode and cathode, $U_{R,c}$, $U_{R,a}$ are, respectively, the equilibrium potentials at the cathode and anode, r_a, r_c are, respectively, the specific anodic and cathodic polarisation resistances, A_a, A_c are, respectively, the anodic and cathodic steel surface areas, ρ_{el} is the specific resistance of the electrolyte (concrete) and k is a cell geometry constant. The resistance of the steel with respect to the transport of the electrons is usually ignored because it is negligibly small compared to other active resistances.

A number of alternative electrical circuits have also been proposed incorporating additional components such as concrete-steel interfacial capacitance in order to improve on the simulation or to improve on the fit of the model to experimental data. The shortcoming of this approach is that a number of influencing parameters are not taken into account e.g. the geometry of the corrosion cells, i.e. the anode-to-cathode surface area ratio and the distance between the anode and cathode [193]. The galvanic cell geometry determines the galvanic current and thus significantly influences the corrosion behaviour. Although equivalent circuit model considers activation and resistance control mechanisms of corrosion, its application to real corrosion situations in RC structures is very limited since the exact distribution of the anodic and cathodic sites on the steel surface should be known in advance [194]

The next sections will now present a review of the available empirical corrosion rate prediction models. Only empirical prediction models are reviewed because this study focuses on developing such a model.

2.13 *Existing empirical corrosion rate prediction models*

2.13.1 *Alonso et al.'s model (1988)*

The prediction model by Alonso *et al*. [195] is based on a statistical analysis of resistivity and accelerated carbonation-induced i_{corr} results. Even though the focus of this study is chloride-induced corrosion, this model is reviewed mainly because it incorporates concrete resistivity as the main input parameter; concrete resistivity, as will be seen in Chapters 3 and 4, was one of the main parameters measured in the experiments carried out in this study. Therefore, useful insights can be drawn from Alonso *et al*.'s model. The experiments by Alonso *et al*. were carried out using 20 x 55 x 80 mm mortar specimens made with various binders (plain Portland cement (PC), Sulphate resistant PC, slag cement, Pozzolanic cement, and 70/30 PC/FA cement) with a w/b ratio of 0.50. Accelerated carbonation was achieved by keeping the specimens in a 100% CO_2-filled chamber at 50-70% relative humidity. i_{corr} was assessed by linear polarisation resistance technique and later ascertained using the gravimetric mass loss method. The experimental results are presented in Figure 2.28. The mathematical expression for the trend-line in Figure 2.28 was adopted as the prediction model, with concrete resistivity as the main input parameter, Eqn. (2.50):

$$i_{corr} = \frac{k_{corr}}{\rho_{ef}} \tag{2.50}$$

where k_{corr} is a constant with a value of 3 x 10^4 μA/cm^2/kΩ-cm (slope of graph in Figure 2.28) and ρ_{ef} is the resistivity of the concrete at its actual degree of saturation. Alonso *et al*.'s [195] experimental results show a clear relationship between i_{corr} and concrete resistivity.

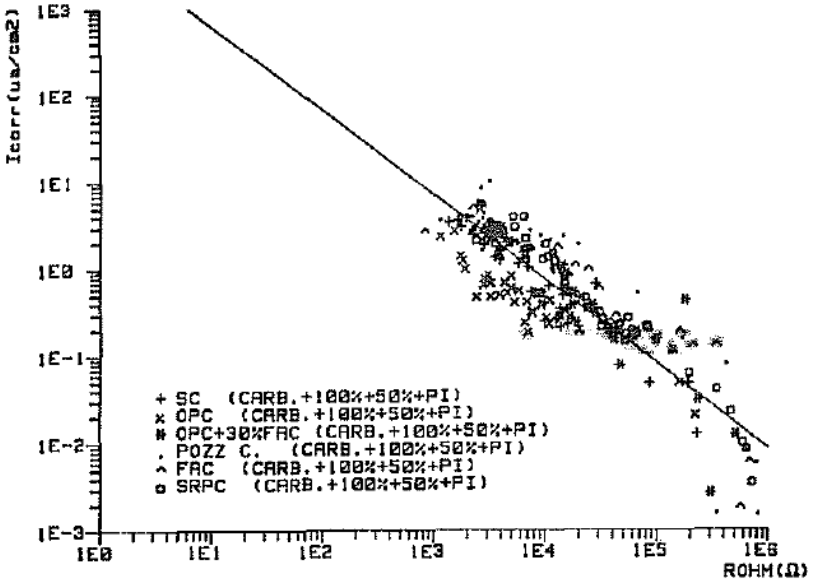

Figure 2.28: Corrosion rate vs. resistivity (for steel in carbonated mortars) [195]

The following can be noted with respect to this model:

- Even though accelerated tests were used without validation using natural corrosion test results, recent studies [107] have shown a similar trend i.e. inverse relationship between corrosion rate and resistivity.

- The use of small (mortar) specimens (20 x 55 x 80 mm) may have a size-effect on the experimental results [196].
- The nature of corrosion products at 100% CO_2 concentration may be significantly different from that in natural exposure conditions.
- In addition to concrete resistivity, i_{corr} in concrete can be affected by, among other factors, the presence of cracks, concrete cover depth and concrete quality [197].
- Variability of factors influencing corrosion rate was not taken into accounted.
- It is not clear whether the i_{corr} predicted by the model is a long-term/stable i_{corr} or not.

However, even though shortcomings of this model can be cited, it provides a clear indication of the possibility of using concrete resistivity as a potential corrosion indicator. The electrical resistivity of concrete provides indications on the pore connectivity and therefore, on the concrete resistance to penetration of fluids; it can therefore be related to reinforcement corrosion [198].

2.13.2 *Morinaga's model (1990)*

Two empirical models, each for carbonation-induced and chloride-induced i_{corr}, were developed by Morinaga [199]. Only the chloride-induced prediction model is presented here. Chloride-contaminated specimens were exposed to outdoor environment for a 10-year period. The experimental variables included cement (PC), w/b ratio (0.40, 0.55 and 0.70), admixed chloride content (0, 0.1, 0.5, 1.0, 1.5 and 3.0% as NaCl by mass of mixing water) and cover (4, 5, 6, 8, 9, 12, 13, 16, 20, 22, 27, 29 and 37 mm). Corrosion rate was determined by gravimetric mass loss method. Equation (2.51) represents the model developed after a regression analysis ($R^2 = 0.95$) on the experimental results:

$$i_{corr} = \frac{d_{st}}{d^2}\left(-0.51 - 7.60C_{Cl} + 44.97(w/b)^2 + 67.95C_{Cl}(w/b)^2\right) \tag{2.51}$$

where i_{corr} is the corrosion rate (x 10^{-4} g/cm^2/year), C_{Cl} is the chloride content in the form of NaCl (% by mass of mixing water), d_{st} is the diameter of reinforcing steel (mm) and d in the cover thickness (mm). It is important to note that the model does not incorporate environmental parameters such as temperature and relative humidity. In order to develop a more comprehensive model, the effect of environmental parameters on the chloride-induced corrosion rate was investigated by exposing grout-coated reinforcing steel to different environmental conditions of temperature (20 and 40 °C), relative humidity (0, 51, 62, 100% and submerged) and O_2 concentration of air (0, 10 and 20%) for 8 years. The improved model ($R^2 = 0.85$) was expressed as:

$$\begin{aligned} i_{corr} = {} & 2.59 - 0.05T - 6.89(h-0.45) - 22.87C_{O_2}^{air} - 0.99C_{Cl} + 0.14(h-0.45) \\ & + 0.51TC_{O_2}^{air} + 0.01TC_{Cl} + 60.81(h-0.45)_{O_2}^{air} + 3.36(h-0.45)C_{Cl} + 7.32_{O_2}^{air}C_{Cl} \end{aligned} \tag{2.52}$$

where T is the temperature (°C), h is the relative humidity (%) and $C_{O_2}^{air}$ is the concentration of oxygen in the air (%). However, in the 'improved' model (Eqn. (2.52)), there are still no parameters relating to concrete quality (e.g. binder type and w/b ratio), yet they can significantly affect the resulting corrosion rate, as was seen in Part I this chapter.

Even though Morinaga's models can be considered to be quite comprehensive since they are built on long-term data covering a large number of test variables, the parameters were considered independently, and no guideline was provided for merging them. Under natural exposure conditions, these parameters cannot be considered independently. It should also be noted that because grout-coated reinforcing bars were used instead of steel embedded in concrete, extrapolating the results to concrete may not be valid since many properties (e.g. porosity, water content, diffusivity) of grout may be substantially different from those of concrete.

Finally, it should be noted that Morinaga's models show that factors such as cover depth, concrete quality (w/b ratio), chloride content, dissolved oxygen content, relative humidity and temperature affect corrosion rate and should be taken into account depending on the exposure conditions.

2.13.3 *Morinaga's model (1996)*

Morinaga [200] proposed a further model for predicting i_{corr} of steel in cracked concrete based on the assumption that in cracked concrete, i_{corr} increases due to the abundant supply of oxygen and moisture. Hence, it was assumed that steel in cracked concrete will corrode at the same rate as that exposed to the atmosphere. An experiment was therefore carried out in which bare reinforcing steel specimens were exposed to six different environmental conditions of temperature and relative humidity, and the steel mass loss measured over a 3-year period. The relationship between the mass loss (m_{corr} x 10^{-4} g/cm^2), environmental parameters and exposure time was presented as:

$$m_{corr} = B_{corr} t \tag{2.53}$$

where t is the exposure duration (years) and B_{corr} is a corrosion rate coefficient and is a function of exposure temperature and relative humidity (Figure 2.29). Although the presence of cracks on the concrete cover has been found to affect i_{corr} in RC structures [16, 33, 83, 142, 147], the hypothesis used in the study by Morinaga (i.e. assuming that the i_{corr} in cracked concrete would be the same as that in freely corroding steel) is subject to debate. For example the exposed steel surface areas and exposure conditions in the two cases are significantly different. Further, the formation of anodes and cathodes on the steel surface as well as the kinetics of corrosion can also be expected to be different. Finally, it must also be mentioned that the data used to determine the corrosion rate coefficient, B_{corr}, in Figure 2.29 was scanty.

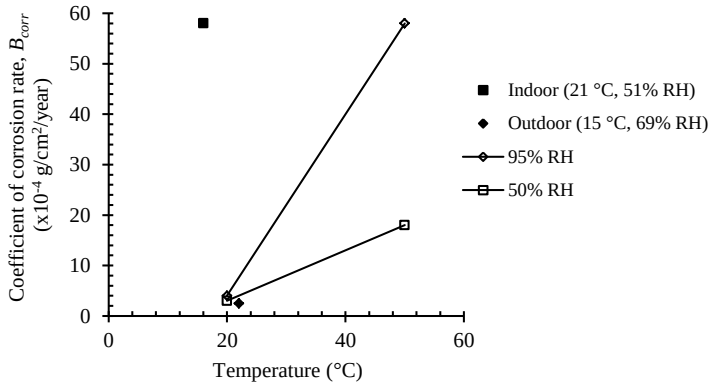

Figure 2.29: Relationship between coefficient of i_{corr} in Eqn. (2.53) and temperature [200]

2.13.4 *Katwan et al.'s model (1996)*

Katwan *et al*. [201] proposed an empirical model using corrosion rate data obtained using the electrochemical noise (ECN) technique. Measurements were made on full-scale RC beams (150 x 250 x 3000 mm) under dynamic (0.17 Hz) and static loading, and exposed to a corrosive environment (3.5% NaCl solution). Results from short and long-term tests suggested that for a given test condition, the i_{corr} can be predicted from the standard deviation (SD) of the half-cell potential (HCP) readings obtained using the ECN method. Although Katwan *et al*. [201] did not provide a mathematical expression for the relationship between corrosion current (I, μA) and SD of the HCP from the ECN technique, it is similar to that obtained by Page and Lambert [202] as shown in Eqn. (2.54):

$$\mathrm{Log}\, I = 0.171 + 0.823\mathrm{Log}\left(\mathrm{SD}_{\mathrm{HCP}}\right) \tag{2.54}$$

The following can be noted with respect to this model:

- The use of HCP to assess corrosion has been criticised in the past for its instability depending on the prevailing measurement conditions; there is no general correlation between i_{corr} and HCP [28]. In most cases, for practical applications, HCP measurements need to be complemented with other corrosion assessment techniques e.g. corrosion rate measurement.
- The use of ECN technique in the field of RC is not common (or well established) and therefore limits its practical applicability.
- In their work [201], Katwan *et al*. reported that the SD was sensitive to changes in the rate of sampling by the ECN technique but no guidance was provided on how to account for this.
- It is not clear whether the i_{corr} predicted by the model is a long-term/stable i_{corr} or not.

2.13.5 *Liu and Weyers' model (1998)*

Liu and Weyers [183] developed an empirical model based on statistical analyses of experimental results obtained from a 5 year accelerated corrosion testing programme on 44 uncracked bridge deck slabs (1180 x 1180 x 216 mm) with cover depths of 25, 51 and 76 mm, w/b ratios of 0.41, 0.42, 0.43 and 0.45 and binder contents ranging from 337 to 382 kg/m^3. Different levels of accelerated corrosion rates were achieved by varying the amount of admixed NaCl from 0 to 7.2 kg/m^3. The specimens were exposed to outdoor conditions during the test period. Corrosion rate was measured using the LPR technique (3LP and Gecor devices were used). Liu and Weyers found that the dynamic corrosion process of steel in in-service concrete is a function of the chloride content, temperature, resistivity of the concrete and active corrosion time. The outcome of statistical analyses of the results was a non-linear regression i_{corr} prediction model presented in Eqn. (2.55):

$$i_{corr} = 102.47 + 10.09\ln(1.69Cl) - 0.0015\rho - \frac{3903.896}{T} + \frac{290.91}{t^{-0.215}} \tag{2.55}$$

where i_{corr} is the 3LP corrosion rate (μA/cm^2), Cl is the total chloride content at the steel level (kg/m^3), T is the temperature at the steel surface (K), $\rho = e^{8.03-0.549\ln(1+1.69Cl)}$ is the resistivity of the cover concrete (Ohm) and t is the corrosion time (years). The following can be noted with respect to Liu and Weyers's model:

– Although concrete cover was a variable in the experimental set-up, it is not an input parameter in the model. This was based on their statistical analysis of the results, but may also be partly due to the use of admixed chlorides. The absence of cover as an input parameter in the proposed model suggests that it has no influence on i_{corr}; this stands in contrast to results reported by various researchers indicating that concrete cover affects both corrosion initiation and its propagation [e.g. 16, 83].
– Similar to previous models discussed, it is not clear whether the i_{corr} predicted by the model is a long-term/stable i_{corr} or not.
– Similar to Morinaga's models [199], Liu and Weyers' model shows that factors such as chloride content, concrete resistivity and temperature affect corrosion rate and should be taken into account depending on the exposure conditions.

2.13.6 *DuraCrete model (1998)*

The DuraCrete model [203] is an attempt to improve on Alonso *et al.*'s model [195] and proposes the incorporation of other i_{corr}-influencing factors by the introduction of coefficients or correction factors in the model as shown in Eqn. (2.56):

$$\left.\begin{aligned} i_{corr} &= \frac{k_{corr}}{\rho(t)} F_{Cl}\, F_{galv} F_{oxide} F_{oxy} \\ \rho(t) &= \rho_o\, f_e\, f_t \left(\frac{t}{t_o}\right)^n \end{aligned}\right\} \qquad (2.56)$$

where k_{corr} is a constant regression parameter (10^4), F_{Cl}, F_{galv}, F_{oxide} and F_{oxy} are factors to take into account the influence of, respectively, chloride content, galvanic effects, continuous formation and ageing of oxides and availability of oxygen on i_{corr}, $\rho(t)$ is the resistivity of concrete (Ω-m) at time t, ρ_o is the resistivity of concrete (Ω-m) at time t_o, n is a factor which takes into account the influence of ageing on ρ_o, f_e is a factor which modifies ρ_o to take into account the influence of the exposure environment and f_t is a factor which takes into account the influence of the resistivity test method. The following can be noted with respect to the DuraCrete model:

– Even though the DuraCrete model [203] attempted to improve on Alonso *et al.*'s model [195], it is still inherently susceptible to criticisms similar to those for Alonso *et al.*'s model as they are based on the same background. Furthermore, Alonso *et al.*'s model was based on carbonation-induced corrosion and hence its extension to chloride-induced corrosion is questionable.
– Although a number of factors influencing i_{corr} are suggested, no mention is made with respect to their quantification i.e. no guidelines are given on how to obtain or predict the values.
– It is not clear whether the i_{corr} predicted by the model is a long-term/stable i_{corr} or not.
– The DuraCrete model shows that factors such as chloride content, concrete resistivity, concrete quality and oxygen availability affect corrosion rate and can be used in its prediction. However, this should depend on other factors such as exposure conditions and concrete quality (binder type and w/b ratio) which influences concrete resistivity and penetrability.

2.13.7 *Vu and Stewart's model (2000)*

Vu and Stewart [204] developed an i_{corr} prediction model based on the assumption that O_2 availability at the steel surface (which depends on, among other factors, concrete quality, cover depth and environmental conditions such as temperature and relative humidity) is the governing factor. This was due to the consideration that for many locations in Australia, US, Europe and Asia, the average relative humidity (RH) is > 70%. For an ambient RH of 75% and a temperature of 20 °C, the influence of w/b ratio and cover depth (c, in cm) on corrosion rate up to 1 year ($i_{corr(1)}$, μA/cm^2) after the end of the corrosion initiation phase was expressed empirically as shown in Eqn. (2.57):

$$i_{corr(1)} = \frac{37.8(1-w/b)^{-1.64}}{c} \tag{2.57}$$

During the propagation phase i_{corr} is expressed as follows (Eqn. (2.58)):

$$i_{corr} = i_{corr(1)}\, 0.85 t_p^{-0.29} = \left(\frac{32.13(1-w/b)^{-1.64}}{c}\right) t_p^{-0.29} \tag{2.58}$$

where $t_p = t - t_i$, t is the time to which i_{corr} is to be predicted and t_i is the time to corrosion initiation. Plotting Eqn. (2.58) for a selected set of input parameters, as shown in Figure 2.30, indicates that the model results in a decreasing i_{corr} with time; this is contrary to the expected variability in i_{corr} depending on the prevailing concrete and exposure conditions, which vary from time to time. In addition, the initial i_{corr} is at the start of corrosion propagation is unexpectedly high. This trend is the reverse of what should be expected i.e. corrosion rate in the propagation phase should initially increase gradually with time but at a rate depending on the existing exposure conditions. It is unlikely that such a trend and high initial corrosion rates are obtained in in-service RC structures. Furthermore, it is necessary to note that the model does not take into account the variation in concrete quality with change in binder type, at a constant w/b ratio.

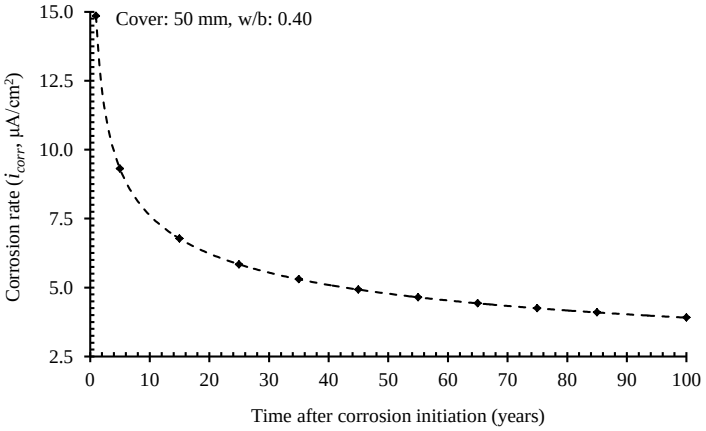

Figure 2.30: Variation of predicted i_{corr} with time as per Vu and Stewart's model [204]

Later in 2005, Vu *et al*. [205] attempted to improve Vu and Stewart's model [204] to account for the time-variant nature of i_{corr} by replacing the constants '0.85' and '-0.29', respectively, with α and β (Eqn. (2.59)) whose values depend on whether the i_{corr} is time-variant or not. For time-variant i_{corr}, α

and β are, respectively, 0.85 and -0.29 [204], while for time-invariant i_{corr}, α and β, respectively, are 1.0 and 0 [205]. The issue of time-variant nature of corrosion rate will be discussed in detail later in section 2.14.1.

$$i_{corr} = \left(\frac{37.8(1-w/b)^{-1.64}}{c} \right) \alpha \, t_p^{\beta} \tag{2.59}$$

Finally, it must be noted that the models by Vu and Stewart show that concrete quality (w/b ratio) and cover depth are important parameters that should be taken into account in the prediction of corrosion rate.

2.13.8 *Scott's model (2004)*

Scott's model [10] was developed using results from an experimental set-up comprising cracked beam specimens (120 x 120 x 375 mm) with 0.2 and 0.7 mm crack widths, concrete cover depths of 20 and 40 mm, a constant w/b ratio of 0.58 and a variety of binder types: 25/75 PC/GGBS, 50/43/7 PC/GGBS/Silica fume (SF), 50/50 PC/GGBS, 70/30 PC/FA, 75/25 PC/GGBS and 93/7 PC/SF. The proposed i_{corr} prediction model was expressed as shown in Eqn. (2.60):

$$i_{corr} = \left(1.43 \frac{CCI_{90}}{f} + 0.02 \right) \exp\left[\left(\frac{40-c}{20} \right) \times 1.2 \left(\frac{CCI_{90}}{f} \right)^3 \right] \tag{2.60}$$

where f is a slag correction factor, $f = 10^{(|0.5-S|-0.5+S)}$ (where S is the slag concentration expressed as a decimal e.g. 0.25 for 25%), CCI_{90} is the 90-day chloride conductivity index value (mS/cm, see Appendix D for test procedure) [206] and c is the concrete cover depth (mm). A plot of Eqn. (2.60) for a selected set of input parameters is presented in Figure 2.31.

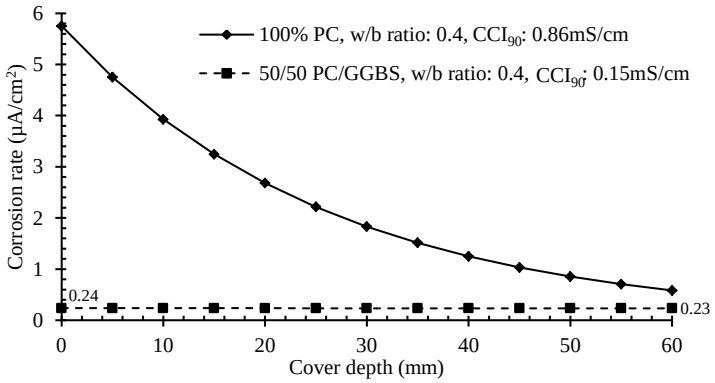

Figure 2.31: Plot of Scott's prediction model (values from [33])

The following can be noted with respect to Scott's model:

- Even though corrosion rate in blended cement concretes are usually relatively low (and virtually constant with change in cover depth) compared to that in PC concretes, the predicted corrosion rates for the GGBS concrete are unrealistically low.
- Although the model was developed using data from cracked specimens, it does not explicitly incorporate crack width as an input parameter. The applicability of this model to different scenarios

other than those used during its development has not been conclusively ascertained in subsequent similar studies e.g. in Otieno *et al.*'s [33] study.

- Similar to other models already discussed, it is not clear whether the i_{corr} predicted by the model is a long-term/stable i_{corr} or not.
- Scott's model, similar to Alonso *et al.*'s [195], also underscores the possibility of using concrete resistivity (or its inverse conductivity) as a potential corrosion indicator and hence a service life prediction model input parameter.
- Even though concretes made using different supplementary cementitious materials (e.g. FA, GGBS) can exhibit the same chloride conductivity index value but different diffusion coefficients mainly due to differences in chloride binding capacities [30, 100], this does not seem to be incorporated in the model.

2.14 *Summarising critique of existing corrosion rate prediction models*

A number of empirical corrosion rate prediction models have been presented, discussed and critiqued in the previous sections. The following sections present a summary of the salient issues relating to these models.

2.14.1 *Temporal variability of corrosion rate*

Corrosion rate in RC structures is affected by several factors that vary with time and with continued ageing of the structure e.g. moisture content (relative humidity), temperature, O_2 concentration, Cl^- concentration, OH^- concentration, concrete resistivity, concrete penetrability and pH. Consequently, corrosion rate is also expected to show a similar variability and should be treated as such. This phenomenon has been appreciated by some researchers [e.g. 183, 207, 208] but is yet to be successfully incorporated in prediction models mainly because it requires prior knowledge of the temporal and spatial distribution of the factors affecting corrosion rate at every time-step during the propagation stage [14]. This is the main challenge towards incorporating the time-variant nature of corrosion rate in prediction models, and more experimental and numerical studies are still needed. Currently, the available empirical and mathematical (numerical and analytical) models are valid for predicting corrosion rate only up to a time equivalent to the age of the experimental data used to either, respectively, develop or validate them.

Temporal variability of corrosion rate can be accounted for by taking into account the variation of the factors that affect it directly or indirectly (see Section 2.7 on factors affecting corrosion propagation). The main challenge with this is that it requires accurate forecasting and quantifying the factors affecting corrosion rate, a task which is currently not possible due to the heterogeneous nature of concrete properties and variations in environmental exposure conditions. Some numerical-based studies [e.g. 13] have attempted to overcome these challenges but the practical application is still limited.

2.14.2 *Influence of cover cracking on corrosion rate*

Pre-corrosion load-induced cracking and crack characteristics can significantly influence both corrosion initiation and its propagation; its influence should certainly be taken into account when dealing with corrosion in RC structures. The effect of crack width and concrete quality (binder type

and w/b ratio) on i_{corr}, obtained from experimental studies by Scott [10] and Otieno *et al*. [33] were summarised in Figure 2.23 and Figure 2.24. To demonstrate the significance of the effect of crack width, concrete quality and resistivity on i_{corr}, Alonso *et al*.'s model [195], Eqn. (2.50), is compared with results obtained by Otieno *et al*. [112] (Figure 2.32).

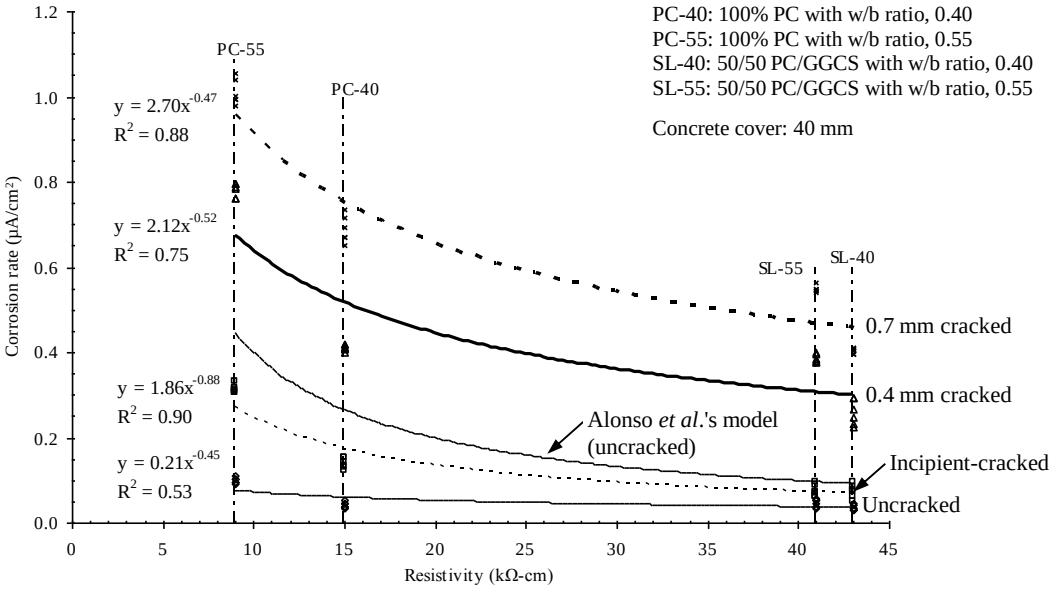

Figure 2.32: Effect of cracking, concrete quality and resistivity on i_{corr} (comparison of Alonso *et al*.'s model [195] and Otieno's results [67])

Even though the corrosion mechanisms (chloride-induced corrosion for Otieno *et al*. and carbonation-induced corrosion for Alonso *et al*.) in the two studies are different, this comparison shows that crack width, concrete quality and resistivity are important factors when predicting i_{corr}. Concluding from the data presented in Figure 2.32, a general relationship between i_{corr} and concrete resistivity (ρ) may be expressed as (Eqn. (2.61)):

$$i_{corr} = k\rho^{-m} \tag{2.61}$$

where k and m are coefficients depending on crack width, concrete quality and/or resistivity. It is therefore important that, among other factors that affect corrosion rate, cracking is incorporated in i_{corr} prediction models. However, it is important to note that both Alonso *et al*.'s and Otieno *et al*.'s data were obtained from accelerated tests and should be verified with natural corrosion results.

Based on the discussion here, and on the review presented earlier in Section 2.7.8 (i.e. effect of cracking on corrosion), it is therefore important to appreciate the influence of load-induced cracking on corrosion rate when developing prediction models so that they can be representative of real structures [33]. The following should also be noted:

(i) The effect of cracking and concrete quality should be directly or indirectly accounted for in corrosion rate prediction models.

(ii) Inasmuch as corrosion rate prediction models for uncracked RC concrete structures cannot be applied to cracked ones, the reverse is also not applicable.

2.14.3 *Corrosion rate measurement techniques*

Different assessment techniques and instruments can be used to quantify i_{corr} both in the laboratory and in the field. However, significant differences have been reported between different instruments when used to measure i_{corr} under the same conditions [183, 209]. For example, Liu and Weyers' [183, 210] reported that the difference among three i_{corr} assessment techniques (gravimetric mass loss, three electrode linear polarisation device (3LP) and Gecor 6) was more than an order of magnitude; up to a factor of 17 with the 3LP being highest. Furthermore, in addition to the i_{corr} values differing from one measurement technique to another, they also differed from the actual (gravimetric) values. The Gecor and 3LP i_{corr} values were, respectively, conspicuously higher (up to 261%) and lower (up to 84%) than the gravimetric results (which are usually used in the laboratory to depict actual i_{corr}). It is therefore important that the assessment technique to obtain the i_{corr} data used during the model development stage is reported. In this way, adjustments can be made to obtain relevant i_{corr} values for use in the model.

In addition to different assessment techniques giving different results under the same measurement conditions, other techniques such as half-cell potential (HCP) measurement have been reported to give varied results depending on the measurement conditions. With respect to HCP, studies have shown that there is no general correlation between i_{corr} and HCP [28]. Furthermore, the HCP values can only be interpreted to give the likelihood or expected severity of corrosion in the structure. The use of such a measurement technique as the only source of data for model development (for example as done by Katwan *et al*. [201]), may therefore not be ideal.

In general, i_{corr} results from different corrosion assessment techniques should be carefully interpreted and/or compared bearing in mind the technique employed.

2.14.4 *Reinforced concrete versus reinforced mortar specimens*

Prediction models developed using data obtained from corrosion tests carried out using reinforced mortar (RM) specimens [e.g. 175, 195, 211] may not be representative of in-service RC structures, mainly because the properties of mortar are different from those of concrete and can neither be used nor claimed to simulate the latter. For example, use of mortar minimises the effect of aggregate on crack propagation [211], influences chloride ingress [62] and may also result in different mechanical or interfacial properties. Further, previous studies have shown that the presence of aggregates influences chloride ingress [212]. It is therefore recommended that RC specimens are used as opposed to RM ones, in a bid to close the gap between in-service and laboratory specimens. Tuutti [76] stated that corrosion studies of steel embedded in concrete should be carried out in concrete, and that experiments in which a different 'environment' (such as mortar or simulated pore solutions) is used entail a further variable whose effect can be misinterpreted. In fact conflicting research results which have previously been reported on this subject may be due to the use of non-concrete environments.

2.14.5 *Accelerated laboratory tests*

The use of accelerated galvanostatic or potentiostatic corrosion tests in the laboratory has become a common technique to simulate corrosion-induced damage in RC structures, mainly because results can be obtained within a short period of time. However, this technique has been criticised for not being

representative of the natural corrosion process and hence the results obtained from such tests may not be reliably extended to real structures [158, 159]. Furthermore, previous studies [e.g. 158] have shown that the use of Faraday's law to obtain corrosion rates from such tests may not be valid and leads to over- or under-estimation of mass losses. In most studies, 100% current efficiency is assumed i.e. all the applied or resulting current is assumed to be consumed in the dissolution of steel [158]. However, this may not be the case because (i) acidification (to a pH of approximately 3) developed by the progressive corrosion may induce a simultaneous additional corrosion [158], (ii) there are parts of the metal that may not dissolve electrolytically but that spall from the metal surface when the surrounding material is oxidised [158], (iii) heat generation may cause losses in current [159], and (iv) some of the current may be lost to corrosion of metallic support pedestals (if present) [160]. For example, results by Ballim and Reid [160] in an accelerated corrosion study to investigate the effect of corrosion on beam deflection, showed that Faraday's law over-estimated mass loss and that the current efficiency was less than 100%; some of the results are presented in Table 2.7. Ballim and Reid [160] further suggest that the difference between the extent of corrosion determined by the two methods also confirms that, while the anodic reaction may be the dominant reaction, it may not be the only reaction taking place at the corrosion sites.

Table 2.7: Comparison of gravimetric and Faraday's law to quantify corrosion rate [data from 156, 160]

Current efficiency (%)	Mass loss (%)		Difference between mass loss obtained by gravimetric method and Faraday's law (%)
	Gravimetric	Faraday's law	
69.6	5.61	8.06	44
63.6	5.88	9.24	57
69.5	6.38	9.18	44
71.1	6.56	9.23	41
72.0	7.98	11.08	39
75.0	8.47	11.30	33

Further, El Maaddawy and Soudki [156] found that the degree of variation between predicted (based on Faraday's law) and measured mass loss is also dependent on the amount of impressed current density applied (see Figure 2.33). Similar results were also obtained by Malumbela [174]. It is therefore important that results from accelerated tests are used with care to validate numerical and analytical models e.g. by using acceleration factors to obtain equivalent natural corrosion rates [205, 213].

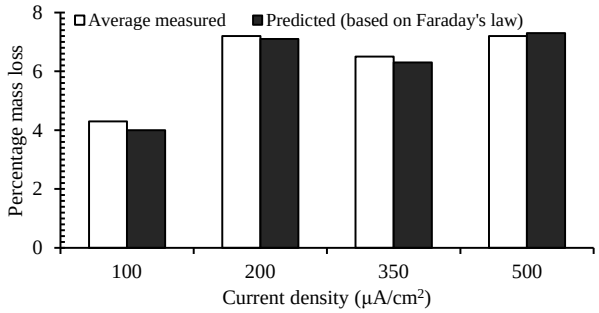

Figure 2.33: Comparison of predicted vs. measured mass losses for different current densities [156]

It is also important to note that there is no standard acceleration test method for steel corrosion in concrete. In most cases, specimen geometry and test parameters are selected to suit the investigation at hand. In the case of chloride-induced corrosion, the accelerated ASTM G-109 [171] test method, which was originally developed for testing the performance of corrosion inhibitors in concrete, is usually modified and used to carry out experiments on steel corrosion in concrete [214-216]. However, despite being an accelerated test, it has been criticized for its long testing periods especially when good quality concrete is used, for example, due to low w/b ratio or use of supplementary cementitious materials such as FA and GGBS [217].

2.14.6 *Model input parameters*

One of the major drawbacks of existing corrosion rate prediction models is the difficulty in obtaining accurate and easily quantifiable input parameters. Most of the existing models have input parameters (e.g. temperature, oxygen content and chloride concentration) which, due to the inability to easily obtain actual values, are usually estimated based on laboratory tests. Take for example the DuraCrete model, Eqn. (2.56), where corrosion rate is presented as a parameter depending on a number of input variables such as chloride content, galvanic effects, continuous formation and ageing of oxides, and availability of oxygen, but no mention is made with respect to their quantification i.e. no guidelines are given on how to obtain or predict the values. Further, a critical examination of some corrosion rate prediction models [e.g. 10, 218, 219, 220] indicated that they are not universally applicable and that, for accurate results to be obtained, it is necessary that the models are validated and/or calibrated using long-term results. However, the universal applicability of a prediction model, especially an empirical one, should not be taken as a model weakness so long as, at least, it is reasonably accurate and practically applicable to RC structures in exposure conditions similar to those used to obtain date used in its development.

2.14.7 *Size of test specimens and sample size*

It is common that (accelerated) laboratory tests, and even field tests, are carried out using small-sized as opposed to real-sized RC specimens mainly due to cost, space and testing equipment constraints [10, 159]. Specifically, accelerated corrosion damage tests carried out using such specimens may not be representative of the real RC structure with respect to its response to applied loads and corrosion-induced damage. These models are usually developed based on isolated RC specimens [159, 221], which in most cases are beams. It is important to appreciate that the response of an isolated RC member may not be the same as that of the same member when considered as a part of the RC structure as a whole. However, due to the complications that may be associated with carrying out tests on real structures, the use of isolated elements may be justified. The interpretation of the isolated member behaviour should therefore be clearly distinguished from that of the structure.

The sample size used to obtain data, especially for the purposes of model validation, is also an important aspect to consider. The need for a statistically sufficient number of test specimens, even though costly, is paramount if the data collected are to be considered reliable [222]. A good factorial experimental design can limit the number of test specimens while still achieving the requirements for a statistically representative sample size.

2.14.8 *Validation of models*

Performing accelerated corrosion experiments is a common technique to simulate corrosion-induced damage in RC structures. Consequently, most of the existing i_{corr} prediction models (see Section 2.13) have been developed using results from accelerated experiments. Such models should be validated using natural i_{corr} data. This is an important stage in ensuring that the model is representative of the actual performance of in-service RC structures.

2.14.9 *Accounting for variability*

Variability of model input parameters is important and should be modelled in such a way that realistic results, and hence decisions, can be derived from the model. In order to adequately account for the variability in i_{corr}, it is important that the variability of the i_{corr}-influencing factors such as cover depth, cracking and concrete quality are taken into consideration. The outcome of such an approach should be ranges of expected i_{corr} and not single point ones.

However, accounting for variability should not only be taken to mean a statistical analysis of i_{corr} data, regardless of how rigorous the process may be. It requires availability of not only a representative sample but also accurate data. None of the available models that were reviewed in Section 2.13 is based on probabilistic analysis. The development of a probabilistic model has been hindered mainly by lack of adequate data to determine relevant statistical distributions for the various factors affecting i_{corr} [203]. Further, it is important to ensure that if a data-set comprising results from different sources is used, the sub-sets must be compatible especially with respect to, for example, the measurement techniques.

Taking into consideration the critique on the use of accelerated corrosion experiments discussed earlier, it may be debatable as to whether a stochastic model developed using data from an accelerated corrosion testing regime is valid or not for application to real structures. The use of natural i_{corr} data would be ideal but in its absence, using data from accelerated tests appears acceptable subject to the model being validated in future as natural i_{corr} data become available.

2.15 *Closure - review of corrosion rate prediction models and the need for further research*

This part of the literature review covered various existing corrosion rate prediction models, and it was shown that there are still significant challenges that need to be addressed. Notwithstanding this, tremendous strides have been made in the recent decades with respect to understanding the corrosion propagation process, its effects on RC structural performance and prediction. Furthermore, the improvements have enabled the advancement of steps towards the development of pro-active maintenance strategies for the management of corrosion-affected RC structures even though more work still needs to be done to make the process both optimal and sustainable. The review presented demonstrated that:

(i) The inherent variability of both the corrosion process and its governing factors should be accounted for in the prediction models. Attempts to achieve this have been made although more work is still required.

(ii) Service load-induced cracking, crack properties (width, density, orientation, self-healing potential and activity or dormancy) and the mechanical damage at the steel-concrete interface have been

acknowledged to have an effect on corrosion propagation. This study focuses on the influence of crack width on corrosion rate even though the other crack characteristics can be equally important.

(iii) Much research on model development and/or validation is carried out using data from laboratory accelerated corrosion tests as opposed to data from in-service RC structures. Furthermore, there is a need to find a correlation between accelerated and natural corrosion rate. This will enable the use of accelerated corrosion rate results in a more confident way than is now the case. In this study, both accelerated and natural corrosion experiments were carried out in parallel in an attempt to overcome this shortcoming.

In summary, even though the existing corrosion rate prediction models have been critiqued in the review presented in this chapter, it is important to acknowledge that effort has been made by various researchers to predict corrosion rate in order to facilitate the quantification of the propagation phase. These are summarized in the following three points:

1. It is difficult to obtain a universally applicable corrosion rate prediction model. This is because corrosion rate of steel in concrete depends on a variety of inter-related factors some of which are additive, synergistic, or opposing. In any given situation, of importance is to identify the corrosion rate governing parameters depending on the exposure environment and other factors such as whether the cover concrete is cracked or not, concrete resistivity, concrete quality, and so on. Specifically, in the case of empirical models which rely on experimental data, it is only possible to consider a limited combination of factors affecting corrosion rate at a time. This makes such models have limited application with respect to the experimental set-up used in their development. However, because of their simplicity in form and ease of quantification of the input data in in-service RC structures, they are very common.
2. Even though corrosion rate is affected by many inter-related factors, the empirical prediction models reviewed showed some similarity with respect to input parameters. These are summarized in Table 2.8. From this summary, it is clear that most of the input parameters such as concrete resistivity, cover depth, concrete quality (binder type, w/b ratio and ageing) and chloride concentration at the steel level can be easily measured in in-service RC structures. Even though some input parameters such as oxygen concentration and temperature are also used in some models, they are not easily quantifiable in in-service RC structures. However, the ease of quantification should not be explicitly used to determine which parameters to incorporate in a prediction model - but it can serve as a rough guide especially for experimental design purposes. It is important that other factors such as type of corrosion (carbonation-induced or chloride-induced), exposure conditions and the presence of cover cracking are also taken into account if necessary. It is also important to note that with respect to the development of empirical models, which is the approach used in this study, easily quantifiable parameters are usually selected. This may be the reason why some parameters such as concrete resistivity, quality and cover, in addition to being important corrosion rate-governing parameters, are also the most common input parameters in the prediction models.
3. Following on (2), is it also important to note that even though empirical corrosion rate prediction models may be limited to the experimental set-up used in their development, useful insights can be drawn from these models in respect of the input parameters used in the models and the general

relationship between corrosion rate and these parameters. This can in turn help in the selection of design parameters such as cover depth, concrete quality (binder type and w/b ratio) and limiting cover crack widths for new structures. For example, it can be seen from the review carried out in this chapter that corrosion rate is, in general, inversely proportional to concrete resistivity, concrete quality and cover depth. Therefore, even though these models may be limited in their scope of application, they can still provide useful information for the selection of suitable combinations of corrosion-influencing parameters.

Table 2.8: Summary of common input parameters for empirical corrosion rate prediction models

Reference	Concrete resistivity	Concrete quality			Temperature	Cover depth	Chloride concentration	Oxygen concentration	RH [c] (moisture content)	Time after corrosion initiation
		w/b ratio	Binder type	Ageing						
Alonso *et al*. (1988)[a]	✓	–	–	–	–	–	–	–	–	–
Morinaga (1990)[b]	✓	✓	–	–	✓	✓	✓	✓	–	–
Morinaga (1996)[b]	–	–	–	–	✓	–	–	–	✓	✓
Liu and Weyers' (1998)[b]	✓	–	–	–	✓	–	✓	–	–	✓
Duracrete (1998)[b]	✓	–	–	✓	✓	–	✓	✓	–	–
Vu and Stewart (2000)[b]	–	✓	–	–	–	✓	–	–	–	✓
Scott (2004)[b]	–	✓	✓	–	–	✓	–	–	–	–

[a]: Carbonation-induced corrosion rate prediction model
[b]: Chloride-induced corrosion rate prediction model
[c]: Relative humidity

2.16 *References*

[1] Pleith, W. (2008) *Electrochemistry for Materials Science*, Elsevier, Amsterdam, The Netherlands.

[2] Heckroodt, R. O. (2002) *Guide to deterioration and failure of building materials*, Thomas Telford Ltd, 1 Heron Quay, London E14 4JD.

[3] Prasad, K. K., Ray, H. S. & Abraham, K. P. (2007) *Chemical and Meturllugical Thermodynamics*, New Age International (P) Ltd., New Delhi.

[4] Revie, R. W. & Uhlig, H. H. (2008) *Corrosion and Corrosion Control: An introduction to corrosion science and engineering, 4th Edition*, John Wiley & Sons Inc., New Jersey, USA.

[5] Cox, J. D. (1982) Notation for states and processes, significance of the word 'standard' in chemical thermodynamics, and remarks on commonly tabulated forms of thermodynamic functions. *Pure and Applied Chemistry*, Vol. 54(6)**,** pp. 1239-1250.

[6] Scully, J. C. (1990) *The Fundamentals of Corrosion, 3rd Edition*, Pergamon Press, United Kingdom, 226 pp.

[7] Stansbury, E. E. & Buchanan, R. A. (2000) *Fundamentals of Electrochemical Corrosion*, ASM International, Ohio.

[8] Pourbaix, M. (1974) Atlas of electrochemical equilibria in aqueous solutions. Pergamon Press, New York.

[9] Shreir, L. L. (1976) Corrosion - Metal/Environment reactions in Corrosion. Newnes-Butterworth, London, England.

[10] Scott, A. N. (2004) The influence of binder type and cracking on reinforcing steel corrosion in concrete. *PhD Thesis*, Department of civil engineering, University of Cape Town.

[11] Stern, M. & Geary, A. L. (1957) Electrochemical polarization - I: theoretical analysis of shape of polarization curves. *Journal of Electrochemical Society*, Vol. 104(1)**,** pp. 56-63.

[12] Bohni, H. (2005) *Corrosion in reinforced concrete structures*, Woodhead Publishing Ltd., Cambridge, England.

[13] Isgor, O. B. (2001) A durability model for chloride and carbonation induced steel corrosion in reinforced concrete members, *PhD Thesis*, Cartelon University, Ottawa, Ontario, Canada.

[14] Isgor, O., B. & Razaqpur, A. G. (2006) Modelling steel corrosion in concrete structures. *Materials and Structures*, Vol. 39(3)**,** pp. 291-302.

[15] Stommen, R. D. (1992) Computer modelling of offshore cathodic protection systems: method and experience in computer modelling in corrosion. *ASTM STP 1154*, Philadelphia**,** pp. 229-247.

[16] Scott, A. N. & Alexander, M. G. (2007) The influence of binder type, cracking and cover on corrosion rates of steel in chloride-contaminated concrete. *Magazine of Concrete Research,* Vol. 59(7)**,** pp. 495-505.
[17] Pour-Ghaz, M., Isgor, O. B. & Ghods, P. (2009) The effect of temperature on the corrosion of steel in concrete - Part 1: Simulated resistance tests and model development. *Corrosion Science,* Vol. 51(2)**,** pp. 415-425.
[18] Dao, L. T. N., Dao, V. T. N. & Ann, K. Y. (2010) Modeling steel corrosion in concrete structures - Part 1: A new inverse relation between current density and potential for the cathodic reaction. *International Journal of Electrochemical Science,* Vol. 5(3)**,** pp. 302-313.
[19] Gulikers, J. (2005) *Numerical modelling of reinforcement corrosion in concrete, Chapter 3, In: Corrosion in reinforced concrete structures, Edited by Bohni, H.*, Woodhead Publishing Ltd., Cambridge, England.
[20] Bockris, J. O'M., Reddy, A. K. N. & Gamboa-Aldeco, M. E. (2000) Modern electrochemistry 2A: Fundamentals of electrodics (2nd Edition). Kluwer Academic/Plenum Publishers.
[21] Richardson, M. G. (2002) *Fundamentals of durable concrete*, Modern Concrete Technology, Spon Press, London.
[22] Schwertmann, U. & Cornell, R. M. (2000) *Iron oxides in the laboratory: preparation and characterisation (2nd Edition)*, WILEY-VCH Verlag GmbH, D-69469 Weinheim (Federal Republic of Germany).
[23] Hausmann, D. A. (1967) Steel corrosion in concrete. How does it occur? *Journal of Materials Protection,* November Issue**,** pp. 19-23.
[24] Andrade, C., Merino, P., Nóvoa, X. R., Pérez, M. C. & Soler, L. (1995) Passivation of reinforcing steel in concrete. *Materials Science Forum,* Vol. (192-194)**,** pp. 891-898.
[25] Singh, J. K. & Singh, D. D. N. (2012) The nature of rusts and corrosion characteristics of low alloy and plain carbon steels in three kinds of concrete pore solution with salinity and different pH. *Corrosion Science,* Vol. 56**,** pp. 129-142.
[26] Szklarska-Smialowska, Z. (2002) Mechanism of pit nucleation by electrical breakdown of the passive film. *Corrosion Science,* Vol. 44(5)**,** pp. 1143-1149.
[27] Bockris, J., Conway, B., Yeager, E. & White, R. Ed. (1981) *Comprehensive treatise of electrochemistry, Electrochemical Materials Science,* Vol. 4. Plenum Press, New York.
[28] Broomfield, J. P. (2007) *Corrosion of steel in concrete - understanding, investigation and repair (2nd Edition)*, Taylor & Francis, Oxford, United Kingdom.
[29] Cornell, R. & Schwerttmann, U. (1996) *The iron oxides: structure, properties, reactions, occurrence and uses*, VCH, Weinheim.
[30] Mackechnie, J. R. (2001) Predictions of reinforced concrete durability in the marine environment. *Research Monograph No. 1***,** Department of civil engineering, University of Cape Town and the University of Witwatersrand.
[31] Liu, Y. (1996) Modelling the time-to-corrosion cracking of the cover concrete in chloride-contaminated reinforced concrete structures. *PhD Thesis*, Department of civil engineering, Virginia Polytechnic Institute and State University.
[32] Care, S., Nguyen, Q. T., L'Hostis, V. & Berthaud, Y. (2008) Mechanical properties if the rust layer induced by impressed current method in reinforced mortar. *Cement and Concrete Research,* Vol. 38(8-9)**,** pp. 1079-1091.
[33] Otieno, M. B., Alexander, M. G. & Beushausen, H.-D. (2010) Corrosion in cracked and uncracked concrete - influence of crack width, concrete quality and crack re-opening. *Magazine of Concrete Research,* Vol. 62(6)**,** pp. 393-404.
[34] Alexander, M. G. & Mindess, S. (2005) *Aggregates in Concrete*, Taylor and Francis Group, London.
[35] Poulsen, E. & Mejlbro (2006) *Diffusion of chloride in concrete - Theory and application*, Taylor & Francis, Oxford, UK.
[36] Stanish, K. & Thomas, M. (2003) The use of bulk diffusion tests to establish time-dependent concrete chloride diffusion coefficients. *Cement and Concrete Research,* Vol. 33(1)**,** pp. 55-62.
[37] Mohamed, B., Sakai, K., Banthia, N. & Yoshida, H. (2003) Prediction of chloride ions ingress in uncracked and cracked concrete. *ACI Materials Journal,* Vol. 100(1)**,** pp. 38-48.
[38] Breysse, D. & Gerard, B. (1997) *Transport of fluids in cracked Media, RILEM report 16 - Barriers to organic and contaminating liquids*, Edited by Reinhardt, H. W., E & FN SPON, London, pp. 123-153.
[39] Nilsson, L. O., Poulsen, E., Sandberg, P., Sorensen, H. E. & Klinghoffer, O. (1996) Chloride penetration into concrete, state-of-the-art, transport processes, corrosion initiation, test methods and prediction models. HETEK Report No. 53.
[40] Angst, U., Elsener, B., Larsen, C. K. & Vennesland, Ø. (2009) Critical chloride content in reinforced concrete - a review. *Cement and Concrete Research,* Vol. 39(12)**,** pp. 1122-1138.

[41] Fontana, M. G. (1987) *Corrosion engineering - Materials science and engineering*, McGraw Hill Inc., 3rd Edition, New York, ISBN 0071003606.
[42] Ritter, J. J. & Rodriguez, M. J. (1982) Corrosion phenomena for iron covered with cellulose nitrate coating. *Corrosion, NACE*, Vol. 38(4)**,** pp. 223-226.
[43] ASTM-C876-91 (1999) *Standard test method for half-cell potentials of uncoated reinforcing steel in concrete*, ASTM International, West Conshohocken, PA 19428-2959, USA.
[44] Foley, R. (1970) Role of the chloride ions in iron corrosion. *Corrosion,* Vol. 26(2)**,** pp. 58-70.
[45] Leek, D. & Poole, A. (1990) The breakdown of the passive film on high yield mild steel by chloride ions, corrosion of reinforcement in concrete. *Society of Chemical Industry, London*.
[46] Sheir, L. Editor. (1979) *Corrosion (Volume 1), Metal-Environment Reactions*, Newnes-Butterworths, London.
[47] Alonso, C., Castellote, M. & Andrade, C. (2002) Chloride threshold dependence of pitting potential of reinforcements. *Electrochimica Acta*, Vol. 47(21)**,** pp. 3469-3481.
[48] Schießl, P. & Raupach, M. (1997) Laboratory studies and calculations on the influence of crack width on chloride-induced corrosion of steel in concrete. *ACI Materials Journal,* Vol. 94(1)**,** pp. 56-62.
[49] Boulfiza, M., Sakai, K., Banthia, N. & Yoshida, H. (2003) Prediction of chloride ions ingress in uncracked and cracked concrete. *ACI Materials Journal,* Vol. 100(1)**,** pp. 38-48.
[50] Ishida, T., Iqbal, P. O. & Anh, H. T. L. (2009) Modelling of chloride diffusivity coupled with non-linear binding capacity in sound and cracked concrete. *Cement and Concrete Research,* Vol. 39(10)**,** pp. 913-923.
[51] Win, P. P., Watanabe, M. & Machida, A. (2004) Penetration profile of chloride ion in cracked reinforced concrete. *Cement and Concrete Research,* Vol. 34(7)**,** pp. 1073-1079.
[52] Tang, L. & Nilsson, L. O. (1992) Rapid determination of the chloride diffusivity in concrete by applying an electric field. *ACI Materials Journal,* Vol. 89(1)**,** pp. 49-53.
[53] Locoge, P., Massat, M., Olliver, J. P. & Richet, C. (1992) Ion diffusion in micro-cracked concrete. *Cement and Concrete Research,* Vol. 22(2-3)**,** pp. 431-438.
[54] Samaha, H. R. & Hover, K. C. (1992) Influence of microcracking on the mass transport properties of concrete. *ACI Materials Journal,* Vol. 89(4)**,** pp. 416-424.
[55] Marsavina, L., Audenaert, K., De Schutter, G., Faura, N. & Marsavina, D. (2009) Experimental and numerical determination of the chloride penetration in cracked concrete. *Construction and Building Materials,* Vol. 23(1)**,** pp. 264-274.
[56] Alahmad, S., Toumi, A., Verdier, J. & Francois, R. (2009) Effect of crack opening in carbon dioxide penetration in cracked mortar. *Materials and Structures,* Vol. 42(5)**,** pp. 559-566.
[57] Ge´rard, B., Breysse, D., Ammouche, A., Houdusse, O. & Didry, O. (1996) Cracking and permeability of concrete under tension. *Materials and Structures,* Vol. 29(187)**,** pp. 141-151.
[58] Rodriguez, J. & Hooton, R. D. (2003) Influence of cracks on chloride ingress into concrete. *ACI Materials Journal,* Vol. 100(2)**,** pp. 120-126.
[59] Nawy, E. G. (2000) Fundamentals of high-performance concrete (2nd Edition). Wiley**,** ISBN-10: 0471385557.
[60] Ge´rard, B. & Marchand, J. (2000) Influence of cracking on the diffusion properties of cement-based materials, Part I: Influence of continuous cracks on the steady-sate regime. *Cement and Concrete Research,* Vol. 30(1)**,** pp. 37-43.
[61] Lim, C. C., Gowripalan, N. & Sirivivatnanon, V. (2000) Microcracking and chloride permeability of concrete under uniaxial compression. *Cement and Concrete Composites,* Vol. 22(5)**,** pp. 353-360.
[62] Wang, L., Soda, M. & Ueda, T. (2008) Simulation of chloride diffusivity for cracked concrete based on RBSM and Truss network model. *Journal of Advanced Concrete Technology,* Vol. 6(1)**,** pp. 143-155.
[63] Wang, K., Jansen, D. C. & Shah, S. P. (1997) Permeability study of cracked concrete. *Cement and Concrete Research,* Vol. 27(3)**,** pp. 181-193.
[64] Ismail, M., Toumi, A., Francis, R. & Gagné, R. (2008) Effect of crack opening on the local diffusion of chloride in cracked mortar samples. *Cement and Concrete Research,* Vol. 38(8-9)**,** pp. 1106-1111.
[65] Gowripalan, N., Sirivivatnanon, V. & Lim, C. C. (2000) Chloride diffusivity of concrete cracked in flexure. *Cement and Concrete Research,* Vol. 30(3)**,** pp. 725-730.
[66] Xing, F., Leng, F. G. & Feng, N. Q. (2005) Chloride diffusivity of plain concrete subjected to sustained flexural loading. *Proceedings of the International Workshop on Durability of Reinforced Concrete under Combined Mechanical and Climate Loads (CMCL)*. October, Qingdao, China. pp. 133-137.
[67] Otieno, M. B. (2008) Corrosion propagation in cracked and uncracked concrete. *Masters Dissertation,* Department of civil engineering, University of Cape Town.
[68] Djerbi, A., Bonnet, S., Khelidj, A. & Baroghel-bouny, V. (2008) Influence of traversing crack on chloride diffusion into concrete. *Cement and Concrete Research,* Vol. 38(6)**,** pp. 877–883.

[69] Fu, C., Jin, X. & Jin, N. (2010) Modeling of chloride ions diffusion in cracked concrete. *Proceedings of the ASCE 12th International conference on Engineering, Science, Construction, and Operations in Challenging Environments (Earth and Space 2010)*. March 2, 2010, Hawaii, USA.
[70] Iqbal, P. O. & Ishida, T. (2009) Modeling of chloride transport coupled with enhanced moisture conductivity in concrete exposed to marine environment. *Cement and Concrete Research,* Vol. 39(4)**,** pp. 329-339.
[71] Ismail, M., Toumi, A., Francis, R. & Gagné, R. (2004) Effect of crack opening on the local diffusion of chloride in inert materials. *Cement and Concrete Research,* Vol. 34(4)**,** pp. 711-716.
[72] Jacobsen, S., Marchand, J. & Boisvert, L. (1996) Effect of cracking and healing on chloride transport in OPC concrete. *Cement and Concrete Research,* Vol. 26(6)**,** pp. 869-881.
[73] De Schutter, G. (1999) Quantification of the influence of cracks in concrete structures on carbonation and chloride penetration. *Magazine of Concrete Research,* Vol. 51(6)**,** pp. 427-435.
[74] Gonzalez, J. A., Andrade, C., Alonso, C. & Feliu, S. (1995) Comparison of rates of general corrosion and maximum pitting penetration on concrete embedded steel reinforcements. *Cement and Concrete Research,* Vol. 25(2)**,** pp. 257-264.
[75] Andrade, C., Martinez, I., Rebolledo, N. & Castilli, A. (2007) Development of an engineering approach for modelling corrosion attack. *RILEM International Workshop on Integral Service Life Modelling of Concrete Structures (PRO 56),* 5-6 November, Guimaraes, Portogal.
[76] Tuutti, K. (1982) Corrosion of steel in concrete. *Swedish Cement and Concrete Research Institute, S-100 44 Stockholm*. Report No. CBI Research 4:82, ISSN 0346-6906, Stockholm, pp. 468.
[77] DuraCrete (1999) Statistical quantification of the variables in the limit state functions: summary. *Brite/EuRam Project BE95-1347,* Report No. BE95-1347-R9.
[78] Harnisch, J. & Raupach, M. (2011) Time dependent surface morphology of corroding reinforcing steel subjected to concrete with high chloride and water contents. *Proceedings of the EUROCOR Conference - Developing Solutions for the Global Challange,* 4-8 September 2011, Stockholm, Sweden**,** 15 pp.
[79] Neff, D., Harnisch, J., Beck, M., L'hostis, V. & Goebbels, J. (2011) Morphology of corrosion products of steel in concrete under macro-cell and self-corrosion conditions. *Materials and Corrosion,* Vol. 62(9)**,** pp. 861-871.
[80] Richens, D. T. (1997) The chemistry of aqua ions: synthesis, structure and reactivity: a tour through the Periodic Table of the elements. Wiley, New York.
[81] Andrade, C., Alonso, C. & Arteaga, A. (1997) Models for predicting corrosion rates. *Brussel: Brite-Euram Project,* No. BE95-1347 (Version1/97, Report 2.2.2).
[82] Harnisch, J. (2012) The time-dependent behaviour of electrochemical and morphological parameters for chloride-induced corrosion of steel in concrete. *PhD Thesis,* Institute of Building Materials Research (ibac), RWTH Aachen University (in German).
[83] Bentur, A., Diamond, S. & Berke, N. (1997) *Steel corrosion in concrete, Fundamentals and Civil Engineering Practice*, E & FN Spon, London. pp. 41-43.
[84] Alexander, M. G. & Magee, B. J. (1999) Durability performance of concrete containing condensed silica fume. *Cement and Concrete Research,* Vol. 29(6)**,** pp. 917-922.
[85] Bijen, J. (1996) Benefits of slag and fly ash. *Construction and Building Materials,* Vol. 10(5)**,** pp. 309-314.
[86] Yuan, Q., Shi, C. & De Schutter, G. (2009) Chloride binding of cement-based materials subjected to external chloride environment - a review. *Construction and Building Materials,* Vol. 23**,** pp. 1-13.
[87] Beushausen, H., Alexander, M. & Ballim, Y. (2012) Early-age properties, strength development and heat of hydration of concrete containing various South African slags at different replacement ratios. *Construction and Building Materials,* Vol. 29(4)**,** pp. 533-540.
[88] Yildirim, H, Ilica, T. & Sengul, O. (2011) Effect of cement type on the resistance of concrete against chloride penetration. *Construction and Building Materials,* Vol. 25(3)**,** pp. 1282-1288.
[89] Mangat, P. S., El-Khatib, J. M. & Molloy, B. T. (1994) Microstructure, chloride diffusion and reinforcement corrosion in blended cement paste and concrete. *Cement and Concrete Composites,* Vol. 16(2)**,** pp. 73-81.
[90] Song, H. W. & Saraswathy, V. (2006) Studies on the corrosion resistance of reinforced steel in concrete with ground granulated blast-furnace slag - an overview. *Journal of Hazardous Materials,* Vol. 138(2)**,** pp. 226-233.
[91] Malhotra, V. M. (1987) Properties of fresh and hardened concrete incorporating ground granulated blast furnace slag, in: Malhotra, V. M. (Ed.), Supplementary cementing materials for concrete. *Minister of Supply and Services, Canada***,** pp. 291-336.
[92] Tromans, D. (1980) Anodic polarization behaviour of mild steel in hot alkaline sulfide solutions. *Journal of Electrochemical Society,* Vol. 127(6)**,** pp. 1253–1256.

[93] Valentini, C., Berardo, L. & Alanis, I. (1990) Influence of blast furnace slags on the corrosion of steel in concrete. *Corrosion of Steel in Concrete, ASTM STP 1065, American Society for Testing and Materials, Philadelphia*, pp. 17–28.
[94] Arya, C. & Xu, Y. (1995) Effect of cement type on chloride binding and corrosion of steel in concrete. *Cemenrt and Concrete Research*, Vol. 25(4), pp. 893-902.
[95] Polder, R. & de-Rooij (2005) Durability of marine concrete structures - field investigations and modeling. *Heron*, Vol. 50(3), pp.133.
[96] Detwiler, R. J., Fapohunda, C. A. & Natale, J. (1994) Use of supplementary cementing materials to increase the resistance to chloride ion penetration of concretes cured at elevated temperatures. *ACI Materials Journal*, Vol. 91(1), pp. 63-66.
[97] Li, S. & Roy, D. M. (1986) Investigation of relations between porosity, pore structure and chloride diffusion of fly ash blended cement pastes. *Cement and Concrete Research*, Vol. 16(5), pp. 749-759.
[98] Saraswathy, V. & Song, H. W. (2006) Corrosion performance of fly ash blended cement concrete: a state-of-art review. *Corrosion Review*, Vol. 24(1-2), pp. 87-122.
[99] Dhir, R. K., El-Mohr, M. A. K. & Dyer, T. D. (1997) Developing chloride resisting concrete using PFA. *Cement and Concrete Research*, Vol. 27(11), pp. 1633-1639.
[100] Arya, C., Buenfeld, N. R. & Newman, J. B. (1990) Factors influencing chloride binding in concrete. *Cement and Concrete Research*, Vol. 20(2), pp. 291-300.
[101] Shi, X., Xie, N., Fortune, K. & Gong, J. (2012) Durability of steel reinforced concrete in chloride environments: An overview. *Construction and Building Materials*, Vol. 30, pp. 125-138.
[102] Nagataki, S., Otsuki, N., Wee, T. H. & Nakashita, K. (1993) Condensation of chloride ion in hardened cement matrix materials and on embedded steel bars. *ACI Materials Journal*, Vol. 90(4), pp. 323-333.
[103] Pettersson, K. (1995) Chloride threshold value and the corrosion rate in reinforced concrete. *Proceedings of Nordic Seminar on corrosion of reinforcement: field and laboratory studies for modelling and service life*, 1-2 February, 1995, Lund.
[104] Polder, R., Andrade, C., Elsener, B., Vennesland, O., Gulikers, J., Weidert, R. & Raupach, M. (2000) Test methods for onsite measurement of resistivity of concrete. *Materials and Structures*, Vol. 33(10), pp. 603-611.
[105] Marta, K-K. & Jezierski, W. (2005) Evaluation of concrete resistance to chloride ion penetration by means of electrical resistivity monitoring. *Journal of Engineering Management*, Vol. 11(2), pp. 109-114.
[106] Gjorv, O. E., Vennesland, O. & E1-Busaidy, A. H. S. (1977) Electrical resistivity of concrete in the oceans. *9th Annual Offshore Technology Conference*, . Houston. paper No. 2803.
[107] Hornbostel, K., Larsen, C. K. & Geiker, M. R. (2013) Relationship between concrete resistivity and corrosion rate - a literature review. *Cement & Concrete Composites*, Vol. 39(5), pp. 60-72.
[108] Raupach, M. (1997) Effect of temperature on chloride-induced steel corrosion in concrete. *Proceedings of the European corrosion congress*, Event No. 208, European Federation of Corrosion, September, 22nd-25th September, Trondheim, Norway.
[109] Hope, B. B., Ip, A. K. & Manning, D. G. (1985) Corrosion and electrical impedance in concrete. *Cement and Concrete Research*, Vol. 15(3), pp. 525-534.
[110] Hunkeler, F. (2005) *Corrosion in reinforced concrete structures*, Woodhead publishing limited, Abington Hall, Abington Cambridge CBI 6AH, England. pp. 1-45.
[111] Rodriguez, J., Ramírez, E. & Gonzalez, J. A. (1994) Methods for studying corrosion in reinforced concrete. *Magazine of Concrete Research*, Vol. 47(167), pp. 81-90.
[112] Otieno, M. B., Alexander, M. G. & Beushausen, H.-D. (2010) Suitability of various measurement techniques for assessing corrosion in cracked concrete. *ACI Materials Journal*, Vol. 107(5), pp. 481-489.
[113] Zivica, V. (2003) Influence of w/c ratio on rate of chloride induced corrosion of steel reinforcement and its dependence on ambient temperature. *Bulletin of Materials Science*, Vol. 26(5), pp. 471-475.
[114] Garcia, A. M., Andrade, C. & Alonso, C. (2002) Oxygen availability at the rebar surface and its relation with corrosion rate. Proceedings of the 15th International Corrosion Congress: Frontiers in Corrosion Science and Technologies, 22-27 September, Granada, Spain, 9 pp.
[115] Raupach, M. (1996) Investigations on the influence of oxygen on corrosion of steel in concrete - Part I. *Materials and Structures*, Vol. 29(3), pp. 174-184.
[116] Lawrence, C. D. (1984) Transport of oxygen through concrete: the chemistry and chemically related properties of cement. *Proceedings of the British Ceramic Society*, Edited by Glasser, F.P., Vol. 35, pp. 277-293.
[117] Gjørv, O. E. (1986) Diffusion of dissolved oxygen through concrete. *Materials Performance*, Vol. 25(12), pp. 39-44.
[118] Andrade, C., Alonso, C. & Garcia, A. M. (1990) Oxygen availability in the corrosion of reinforcements. *Advances in Cement Research*, Vol. 3(11), pp. 127-132.

[119] Wilkins, N. J. M. & Lawrence, P. F. (1980) Fundamental research mechanisms of corrosion of steel reinforcements in concrete immersed in sea-water. *Concrete in the Oceans,* Technical Report No. 6, Cement and Concrete Association, BCA, Wexham Springs**,** cited by: Raupach, M. (1996) Investigations on the influence of oxygen on corrosion of steel in concrete - Part I. *Materials and Structures,* Vol. 29(3), pp. 174-184.
[120] Hope, B. B. & Poland, J. S. (1990) Cathodic protection and hydrogen generation. *ACI Materials Journal,* Vol. 87(5)**,** pp. 469-472.
[121] Galvele, J. R. (1976) Transport processes and the mechanism of pitting of metals. *Journal of the Electrochemical Society,* Vol. 123(4)**,** pp. 464-474.
[122] Iverson, W. P. (1966) Direct evidence for the cathodic depolarization theory of bacterial corrosion. *Science,* Vol. 151**,** pp. 986-988.
[123] King, R. A. & Miller, J. D. A. (1971) Corrosion by sulphate-reducing bacteria. *Nature,* Vol. 233**,** pp. 491-492.
[124] Kuang, F., Wang, J., Yan, L. & Zhang, D. (2007) Effects of sulphate-reducing bacteria on the corrosion behaviour of carbon steel. *Electrochimica Acta,* Vol. 52(20)**,** pp. 6084-6088.
[125] Beech, I. B. & Cheung, C. W. S. (1995) Interactions of exopolymers produced by sulphate-reducing bacteria with metal ions. *International journal of Biodeterioration and Biodegradation,* Vol. 35(1-3)**,** pp. 59-72.
[126] Kuhr, C.A.H. (1923) Sulfate reduction as cause of corrosion of iron pipeline. . *Water en Gas* VII 26**,** pp. 277. Cited by Iverson, W. P. & Olson, G. S. (1984) Anaerobic corrosion of steel: a novel mechanism. Proceedings of the 3rd Internatinal Symposium on Current Prospectives on Microbial Ecology, American Society for Microbiology, 7-12 August, 1983, Michigan State University, USA, pp. 623-627.
[127] Melchers, R. E. & Wells, T. (2006) Models for the anaerobic phases of marine immersion corrosion. *Corrosion Science,* Vol. 48(7)**,** pp. 1791-1811.
[128] Duan, J., Wu, S., Zhang, X., Huang, G., Du, M. & Hou, B. (2008) Corrosion of carbon steel influenced by anaerobic biofilm in natural seawater. *Electrochimica Acta,* Vol. 54(1)**,** pp. 22-28.
[129] meLittle, B. J., Ray, R. I. & Pope, R. K. (2000) Relationship between corrosion and the biological sulphur cycle: a review. *Corrosion (NACE),* Vol. 56(4)**,** pp. 433-443.
[130] Hardy, J. A. (1983) Utilization of cathodic hydrogen by sulphate-reducing bacteria. *Corrosion Journal,* Vol. 18(4)**,** pp. 190-193.
[131] Booth, G. H. & Tiller, A. K. (1968) Cathodic characteristics of mild steel in suspensions of sulphate-reducing bacteria *Corrosion Science,* Vol. 8(8)**,** pp. 583-600.
[132] Cragnolino, G. & Tuovinen, O. H. (1984) The role of sulphate-reducing and sulphur-oxidizing bacteria in the localized corrosion of iron-based alloys - a review. *International Biodeterioration,* Vol. 20(1)**,** pp. 9-26.
[133] Angell, P., Luo, J. S. & White, D. C. (1995) Microbially sustained pittinf corrosion of 304 stainless steel in anaerobic seawater. *Corrosion Science,* Vol. 37(7)**,** pp. 1085-1096.
[134] Melchers, R. E. & Jeffrey, R. (2008) The critical involvement of anaerobic bacterial activity in modelling the corrosion behaviour of mild steel in marine environments. *Electrochimica Acta,* Vol. 54(1)**,** pp. 80-85.
[135] Miller, J. & King, R. A. (1971) Microbial aspects of the deterioration of materials (Ed. Lovelock, D. W. and Gilbert, R. J.). Academic Press, London.
[136] Iverson, W. P. & Olson, G. S. (1984) Anaerobic corrosion of steel: a novel mechanism. Proceedings of the 3rd Internatinal Symposium on Current Prospectives on Microbiology, Col. Klug-Reday. American Society for Microbiology.**,** pp. 623-627.
[137] Crolet, J. L., Dauumas, S. & Magot, M. (1995) pH regulation by sulfate-reducing bacteria. *Corrosion 93,* National Association of Corrosion Engineers, Houston, Texas, USA.
[138] Alvarez, A. & Galvele, J. (1984) Mechanism of pitting of high purity iron in NaCl solutions. *Corrosion Science,* Vol. 24(1)**,** pp. 27-48.
[139] Bamforth, P. B. (1994) Specification and design of concrete for the protection of reinforcement in chloride contaminated environments. UK Corrosion and Eurocorr 94, Bournemouth, Vol. III**,** pp 249-258.
[140] Arya, C. & Wood, L. (1995) The relevance of cracking in concrete to corrosion of reinforcement. *Concrete Society*. Technical report No. 44.
[141] Beeby, A. (1983) Cracking, cover and corrosion of reinforcement. *Concrete International,* Vol. 5(2)**,** pp. 35-40.
[142] Pettersson, K. & Jorgensen, O. (1996) The effect of cracks on reinforcement corrosion in high-performance concrete in a marine environment. *Third ACI/CANMET Int. conference on the Performance of Concrete in Marine Environment*. St. Andrews, Canada. pp. 185-200.
[143] Suzuki, K., Ohno, Y., Praparntanatorn, S. & Tamura, H. (1990) *Mechanism of steel corrosion in cracked concrete*. Page, C., Treadaway, K. & Bramforth, P. Corrosion of reinforcement in concrete. London: Society of Chemical Industry**,** pp. 19-28.

[144] Raupach, M. (1996) Chloride-induced macrocell corrosion of steel in concrete - theoretical background and practical consequences. *Construction and Building Materials,* Vol. 10(5)**,** pp. 329-338.
[145] Miyagawa, T. (1985) Early chloride corrosion of reinforcing steel in concrete. *PhD Thesis,* Department of civil engineering, University of Kyoto.
[146] Mackechnie, J. R., Alexander, M. G. & Jaufeerally, H. (2003) Structural and durability properties of concrete made with Corex slag. *Research monograph No. 6,* University of Cape Town and the University of Witwatersrand.
[147] Arya, C. & Ofori-Darko, F. K. (1996) Influence of crack frequency on reinforcement corrosion in concrete. *Cement and Concrete Research,* Vol. 26(3)**,** pp. 333-353.
[148] Li, M. & Li, V. C. (2011) Cracking and healing of engineered cementitious composites under chloride environment. *ACI Materials Journal,* Vol. 108(3)**,** pp. 333-340.
[149] Neville, A. M. (2002) Autogenous healing - a concrete miracle? *Concrete International,* Vol. 24(11)**,** pp. 76-82.
[150] Gagné, R., Francois, R. & Masse, P. (2001) Chloride penetration testing of cracked mortar samples. *Proceedings of the 3rd International conference on Concrete Under Severe Conditions (CONSEC)*. 18-20 June, University of British Columbia, Vancouver, Canada.
[151] Schießl, P. & Edvardsen, C. (1993) Autogenous healing of cracks in concrete structures subjected to water pressure. *Report No. F361***,** Institute of Building Materials Research, RWTH Aachen University.
[152] Edvardsen, C. (1999) Water permeability and autogenous healing of cracks in concrete. *ACI Materials Journal,* Vol. 96(4)**,** pp. 448-454.
[153] Akhavan, A., Shafaatian, S. M. H. & Rajabipour, F. (2012) Quantifying the effects of crack width, tortuosity, and roughness on water permeability. *Cement and Concrete Research,* Vol.42(2)**,** pp. 313-320.
[154] De Schutter, G. (2000) Durability of marine concrete structures damaged by early age thermal cracking. Proceedings of the International RILEM Workshop on Life prediction and aging management of concrete structures, Naus, D. (Ed.), PRO 16, 16-17 October**,** pp. 177-186.
[155] Azar, J. H., Janaherian, A., Pishvaie, M. R. & Bidhendi, M. N. (2008) An approach to defining tortuosity and cementation factor in carbonate reservoir rocks. *Journal of Petroleum Science and Engineering,* Vol. 60(2)**,** pp. 125-313.
[156] El Maaddawy, T. A. & Soudki, K. A. (2003) Effectiveness of impressed current technique to simulate corrosion of steel reinforcement in concrete. *ASCE Journal of Materials in Civil Engineering,* Vol. 15(1)**,** pp. 41-47.
[157] Jaffer, S. J. & Hansson, C. M. (2009) Chloride-induced corrosion products of steel in cracked-concrete subjected to different loading conditions. *Cement and Concrete Research,* Vol. 39(2)**,** pp. 116-25.
[158] Alonso, C., Andrade, C., Rodriguez, J. & Diez, J. M. (1998) Factors controlling cracking of concrete affected by reinforcement corrosion. *Materials and Structures,* Vol. 31(7)**,** pp. 435-441.
[159] Andrade, C., Alonso, C. & Molina, F. J. (1993) Cover cracking as a function of bar corrosion: Part I-Experimental test. *Materials and Structures,* Vol. 26(8)**,** pp. 453-464.
[160] Ballim, Y. & Reid, J. C. (2003) Reinforcement corrosion and the deflection of RC beams - an experimental critique of current test methods. *Cement and Concrete Composites,* Vol. 25(6)**,** pp. 625-632.
[161] Care, S. & Raharinaivo, A. (2007) Influence of impressed current on the initiation of damage in reinforced mortar due to corrosion of embedded steel. *Cement and Concrete Research,* Vol. 37(12)**,** pp. 1598-1612.
[162] Austin, S. A., Lyons, R. & Ing, M. J. (2004) Electrochemical behavior of steel-reinforced concrete during accelerated corrosion testing. *Corrosion,* Vol. 60(2)**,** pp. 203-212.
[163] Andrade, C. (1993) Calculation of chloride diffusion coefficients in concrete from ionic migration measurements. *Cement and Concrete Research,* Vol. 23(3)**,** pp. 724-742.
[164] Mangat, P. S. & Elgarf, M. S. (1999) Flexural strength of concrete beams with corroding reinforcement. *ACI Structural Journal,* Vol. 96(1)**,** pp. 149-158.
[165] Mohamed, T. U., Otsuki, N. & Hamada, H. (2003) Corrosion of steel bars in cracked concrete under marine environment. *ASCE Journal of Materials in Civil Engineering,* Vol. 15(5)**,** pp. 460-469.
[166] Vidal, T., Castel, A. & François, R. (2007) Corrosion process and structural performance of a 17 year old reinforced concrete beam stored in chloride environment. *Cement and Concrete Research,* Vol. 37(11)**,** pp. 1551-1561.
[167] Cairns, J., Dut, Y. & Law, D. (2008) Structural performance of corrosion-damaged concrete beams. *Magazine of Concrete Research,* Vol. 60(5)**,** pp. 359-70.
[168] Cabrera, J. G. (1996) Deterioration of concrete due to reinforcement steel corrosion. *Cement and Concrete Composites,* Vol. 18(1)**,** pp. 47-59.
[169] Chang, Y. T., Cherry, B. & Marosszeky, M. (2008) Polarisation behaviour of steel bar samples in concrete in seawater - Part I: Experimental measurement of polarisation curves of steel in concrete. *Corrosion Science,* Vol. 50(2)**,** pp. 357-364.

[170] Yuan, Y., Ji, Y. & Jiang, J. (2009) Effect of corrosion layer of steel bar in concrete on time-variant corrosion rate. *Materials and Structures,* Vol. 42(10)**,** pp. 1443-1450.
[171] ASTM-G109 (2007) Standard test method for determining effects of chemical admixtures on corrosion of embedded steel reinforcement in concrete exposed to chloride environments. *ASTM International***,** West Conshohocken, PA 19428-2959, USA, 6 pp.
[172] Yuan, Y., Ji, Y. & Shah, S. P. (2007) Comparison of two accelerated corrosion techniques for concrete structures. *ACI Structural Journal,* Vol. 104(3)**,** pp. 344-347.
[173] Collier, N. C., Sharp, J. H., Milestone, N. B., Hill, J. & Godfrey, I. H. (2008) The influence of water removal techniques on the composition and microstructure of hardened cement pastes. *Cement and Concrete Research,* Vol. 38(6)**,** pp. 737-744.
[174] Malumbela, G. (2010) Measurable parameters for performance of corroded and repaired RC beams under load. *PhD Thesis*, Department of civil engineering, University of Cape Town.
[175] Jaggi, S., Bohni, H. & Elsener, B. (2001) Macrocell corrosion of steel in concrete - experiments and numerical modelling. *Eurocorr 2001*. 1st - 4th Octpber, Milan, Italy. 11 pp.
[176] Joiret, S., Keddam, M., Novoa, X. R., Perez, M. C., Tangel, C. & Takenouti, H. (2002) Use of EIS, ring-disk electrode, EQCM and Raman spectroscopy to study the film of oxides formed on iron in 1M NaOH. *Cement and Concrete Composites,* Vol. 24(1)**,** pp. 7-15.
[177] Yu, H., Chiang, K-T. K. & Yang, L. (2012) Threshold chloride level and characteristics of reinforcement corrosion initiation in simulated concrete pore solutions. *Construction and Building Materials,* Vol. 26(1)**,** pp. 723-729.
[178] Raupach, M. (2006) Models for the propagation phase of reinforcement corrosion - an overview. *Materials and Corrosion,* Vol. 57(8)**,** pp. 605-612.
[179] Redaelli, E., Bertolini, L., W., Peelen & Polder, R. (2006) FEM-models for the corrosion propagation period of chloride-induced reinforcement corrosion. *Materials and Corrosion,* Vol. 57(8)**,** pp. 628-634.
[180] Warkus, J., Brem, M. & Raupach, M. (2006) BEM-models for the corrosion propagation period of chloride-induced reinforcement corrosion. *Materials and Corrosion,* Vol. 57(8)**,** pp. 636-641.
[181] Li, C. Q., Melchers, R. E. & Zheng, J. J. (2006) An analytical model for corrosion-induced crack width in reinforced concrete structures. *ACI Structural Journal,* Vol. 103(4)**,** pp. 479-487.
[182] Cox, D. R. (1958) *Planning of experiments*, John Wiley and Sons, Inc., New York.
[183] Liu, T. & Weyers, R. W. (1998) Modelling the dynamic corrosion process in chloride contaminated concrete structures. *Cement and Concrete Research,* Vol. 28(3)**,** pp. 365-379.
[184] Song, X. & Liu, X. (2000) Experiment research on corrosion of reinforcement in concrete through cathode-to-anode area ratio. *ACI Materials Journal,* Vol. 97(2)**,** pp. 148-155.
[185] Bjegovic, D., Krstic, V. & Mikulic, D. (2006) Design for durability including initiation and propagation period based on the fuzzy set theory. *Materials and Corrosion,* Vol. 57(8)**,** pp. 642-647.
[186] Gottwald, S. (2008) Foundations of a set theory for fuzzy sets - 40 years of development. *International Journal of General Systems,* Vol. 37(1)**,** pp. 69-81.
[187] Sobhani, J. & Ramezaninpour, A. A. (2009) Modelling the corrosion of reinforced concrete structures based on the fuzzy systems. *3rd International Conference on Concrete and development*. 27-29 April, 2009, Tehran, Iran. pp. 730-741.
[188] Gao, X., Gao, Q. S., Hu, Y. & Li, L. (2006) A Probability-like new fuzzy set theory. *International Journal of Pattern Recognition and Artificial Intelligence,* Vol. 20(3)**,** pp. 441-462.
[189] Andrade, C., Alonso, C., Arteaga, A. & Tanner, P. (2000) Methodology based on the electrical resistivity for the calculation of reinforcement service life. *Proceedings of the 5th Canmet/ACI International Conference on Durability of concrete – Supplementary papers volume*. Barcelona, Spain. pp. 899-915.
[190] Gulikers, J. & Raupach, M. (2006) Numerical models for the propagation period of reinforcement corrosion. *Materials and Corrosion,* Vol. 57(8)**,** pp. 618-627.
[191] Zienkiewicz, O. C., Taylor, R. L. & Zhu, J. Z. (2005) *The Finite Element Method: Its Basis and Fundamentals, 6th Edition*, Elsevier Butterworth-Heinemann, Linacre House, Jordan Hill, Oxford OX2 8DP.
[192] Francois, R., Castel, A. & Vidal, T. (2006) A finite macro-element for corroded reinforced concrete. *Materials and Structures,* Vol. 39(5)**,** pp. 571-584.
[193] Jia, J. X., Song, G. & Atrens, A. (2006) Influence of geometry on galvanic corrosion of AZ91D coupled to steel. *Corrosion Science,* Vol. 48(8)**,** pp. 2133-2153.
[194] Pour-Ghaz, M. (2007) A novel approach for practical modelling of steel corrosion in concrete. *Master of Applied Science Thesis*, Department of civil and environmental Engineering, Carleton University, Ottawa, Ontario, Canada.
[195] Alonso, C., Andrade, C. & Gonzalez, J. A. (1988) Relation between resistivity and corrosion rate of reinforcements in carbonated mortar made with several cement types. *Cement and Concrete Research,* Vol. 18(5)**,** pp. 687-698.

[196] Azad, A. K., Ahmad, S. & Al-Gohi, B. H. A. (2010) Flexural strength of corroded reinforced concrete beams. *Magazine of Concrete Research,* Vol. 62(6)**,** pp. 405-414.
[197] Otieno, M. B., Beushausen, H.-D. & Alexander, M G. (2010) Corrosion propagation in reinforced concrete structures - state of the art review and way forward. *Proceedings of the 6th international conference on Concrete under severe conditions - Environment and loading, CONSEC'10 (Volume I)*. June 7th -9th 2010, Merida, Yucatan, Mexico. pp. 461-469.
[198] Andrade, C. (2009) Types of models of service life of reinforcement: the case of the resistivity. *Proceedings of the 7th Asia Pacific Structural Engineering and Construction Conference & 2nd European Asian Civil Engineering Forum (APSEC / EACEF 2009)*. 4th - 6th August 2009, Langkawi, Malaysia, Kedah, Malaysia pp. 30-35.
[199] Morinaga, S. (1990) Prediction of service lives of reinforced concrete buildings based on rate of corrosion of reinforcing steel. *Proceedings of the 5th International conference on durability of building materials and components*. 7-9 November, Brighton, UK.
[200] Morinaga, S. (1996) Remaining life of reinforced concrete structures after corrosion cracking. *Proceedings of the 7th International conference on the Durability of Building Materials,* 19-23 May, 1996, Stockholm, Sweden (Vol. 1)**,** pp. 127-136.
[201] Katwan, M. J., Hodgkiess, T. & Arthur, P. D. (1996) Electrochemical noise technique for the prediction of corrosion rate of steel in concrete. *Materials and Structures,* Vol. 29(5)**,** pp. 286-294.
[202] Page, C. L. & Lambert, P. (1986) Analytical and electrochemical investigations of reinforcement corrosion. *Contractor Report 30,* Transport and Road Research Laboratory (TRRL)**,** Crowthorne.
[203] DuraCrete (1998) Probabilistic performance-based durability design: modelling of degradation. Document No. BE95-1347/R4-5**,** The Netherlands.
[204] Vu, K. & Stewart, M. G. (2000) Structural reliability of concrete bridges including improved chloride-induced corrosion models. *Structural Safety,* Vol. 22(4)**,** pp. 313-333.
[205] Vu, K., Stewart, M. G. & Mullard, J. (2005) Corrosion-induced cracking: experimental data and predictive models. *ACI Structural Journal,* Vol. 102(5)**,** pp. 719-726.
[206] Streicher, P. E. & Alexander, M. G. (1995) A chloride conduction test for concrete. *Cement and Concrete Research,* Vol. 25(6)**,** pp. 1284–1294.
[207] Melchers, R. E. & Li, C. Q. (2006) Phenomenological modeling of reinforcement corrosion in marine environments. *ACI Materials Journal,* Vol. 103(1)**,** pp. 25-32.
[208] Yuan, Y., Jiang, J. & Peng, T. (2010) Corrosion process of steel bar in concrete in full lifetime. *ACI Materials Journal,* Vol. 107(6)**,** pp. 562-567.
[209] Breysse, D., Klysz, G., Derobert, X., Sirieix, C. & Lataste, J. F. (2008) How to combine several non-destructive techniques for a better assessment of concrete structures. *Cement and Concrete Research,* Vol. 38(6)**,** pp. 783-793.
[210] Nygaard, P. V. & Geiker, M. R. (2012) Measuring the corrosion rate of steel in concrete - effect of measurement technique, polarisation time and current. *Materials and Corrosion,* Vol. 63(3)**,** pp. 200-214.
[211] Care, S., Nguyen, Q. T., Beddiar, K. & Berthaud, Y. (2010) Times to cracking in reinforced mortar beams subjected to accelerated corrosion tests. *Materials and Structures,* Vol. 43(1-2)**,** pp. 107-124.
[212] Delagrave, A., Bigs, J. P., Ollivier, J. P., Marchand, J. & Pigeon, M. (1997) Influence of the interfacial transition zone on the chloride diffusivity of mortars. *Advanced Cement Based Materials,* Vol. 5(3-4)**,** pp. 86-91.
[213] Yuzer, N., Akoz, F. & Kabay, N. (2008) Prediction of time to crack initiation in reinforced concrete exposed to chloride *Construction and Building Materials,* Vol. 22(6)**,** pp. 1100-1107.
[214] Dry, C. M. & Corsaw, M. J. T. (1998) A time-release technique for corrosion prevention. *Cement and Concrete Research,* Vol. 28(8)**,** pp. 1133-1140.
[215] Hansson, C. M., Poursaee, A. & Laurent, A. (2006) Macrocell and microcell corrosion of steel in ordinary Portland cement and high performance concretes. *Cement and Concrete Research,* Vol. 36(11)**,** pp. 2098-2102.
[216] Poursaee, A. & Hansson, C. M. (2008) The influence of longitudinal cracks on the corrosion protection afforded to reinforcing steel in high performance concrete. *Cement and Concrete Research,* Vol. 38(8-9)**,** pp. 1098-1105.
[217] Halmen, C. & Trejo, D. (2012) Accelerating standard test method for assessing corrosion of steel in concrete. *ACI Materials Journal,* Vol. 109(4)**,** pp. 421-430.
[218] Yalcyn, H. & Ergun, M. (1996) The prediction of corrosion rates of reinforcing steels in concrete. *Cement and Concrete Research,* Vol. 26(10)**,** pp. 1593-1599.
[219] Li, C. Q., Yang, Y. & Melchers, R. E. (2008) Prediction of reinforcement corrosion in concrete and its effects on concrete cracking and strength reduction. *ACI Materials Journal,* Vol. 105(1)**,** pp. 3-10.

[220] Bastidas-Arteaga, E., Bressolette, P., Chateauneuf, A. & Sánchez-Silva, M. (2009) Probabilistic lifetime assessment of RC structures under coupled corrosion - fatigue deterioration processes. *Structural Safety,* Vol. 31(1)**,** pp. 84-96.
[221] Molina, F. J., Alonso, C. & Andrade, C. (1993) Cover cracking as a function of rebar corrosion: Part II-Numerical model. *Materials and Structures,* Vol. 26(9)**,** pp. 532-548.
[222] Quinn, G. P. & Keough, M. J. (2002) *Experimental Design and Data Analysis for Biologists*, Cambridge University Press, The Edinburg Building, Cambridge CB2 2RU, UK.

Chapter 3

Laboratory and field investigations

3.1 *Introduction*

This chapter presents details of the laboratory-based and field-based corrosion experiments, and the related tests carried out in this study. The underlying objective is to establish empirical correlations between cracking, crack width, concrete quality, cover depth and concrete resistivity on chloride-induced corrosion rate. In Chapter 2, it was shown that corrosion rate (i_{corr}) is affected by several inter-related factors whose quantification still presents a challenge in the development of corrosion rate prediction models (see Equation (2.48), Chapter 2). The different possible combinations of the factors affecting corrosion rate is evidence of how challenging it is to model corrosion rate. However, under natural conditions, only some of these factors may prevail with only a few being dominant (i.e. corrosion rate-governing). Therefore, the main problem is the selection and replication of the salient corrosion rate-governing factors (or isolation of the 'less influential' ones) in either laboratory-based tests or mathematical models. There is still no clear guidance in the literature on how it should be handled. In this study, the main corrosion-affecting factors investigated are concrete quality (binder type and w/b ratio), concrete resistivity, cover depth and surface crack width. The criteria used to select these parameters are covered in this chapter.

The literature review in Chapter 2 not only pointed out positive developments in the modelling of steel corrosion in RC structures, but also highlighted some of the challenges associated with the development and application of corrosion rate prediction models. However, as was mentioned in Chapter 2, it is not within the scope of this study to provide redress to all those issues. Attempt was made to address only those that are in line with the objectives, and within the scope of this study.

3.2 *Selection of the experimental corrosion rate-affecting factors*

As stated in the previous section, corrosion rate of steel in concrete is a multi-factor dependent phenomenon. Further, and more importantly, it is an electrochemical process in which three mechanisms may be used to limit it: anodic control, cathodic control and resistivity control (these were covered in Chapter 2). A combination of these can also be used. These forms of corrosion control played an important role in selecting the concrete parameters to include in the experimental set-up.

Cathodic control is mainly concerned with oxygen availability at the cathode and hence becomes dominant when the concrete is highly saturated (e.g. in submerged conditions or in saturated soil) or when the concrete cover is sufficiently thick to ensure that oxygen concentration at the steel level is very low [1]. Anodic control occurs when the steel is still in the passive state i.e. when the passive protective film on the steel surface is still present. This passive film limits further dissolution of iron resulting in very low reaction rates despite the availability of oxygen to sustain higher reaction rates. In chloride-induced corrosion, the dissolution of the passive film occurs when the chloride content at

the steel reaches a threshold concentration. As stated in Chapter 2, the chloride threshold is not a universal value for all concretes; it is affected by, among other factors, cover thickness and quality, and chemistry of the binder [2]. Finally, resistivity control is the main corrosion rate-controlling factor in non-saturated or semi-saturated concrete conditions. It limits the corrosion rate by hindering the mobility of hydroxyl ions (OH^-) between the anode and cathode. Concrete resistivity, as was discussed in Part I Chapter 2, is affected by a variety of factors including level of moisture saturation, presence of chlorides in the pore solution and binder type. The inclusion of supplementary cementitious materials, which greatly affect the concrete pore structure and solution and its chloride binding capacity [3], also has a major influence on concrete resistivity. Therefore, both the pore solution chemistry and physical properties of the cover may have an influence on the corrosion rate of steel in concrete.

In summary, based on these fundamental corrosion rate control mechanisms, the following factors were considered relevant and hence included directly or indirectly in the experimental set-up: concrete resistivity (by varying both binder type and w/b ratio), concrete penetrability (by varying both binder type and w/b ratio), cover depth, and condition of the cover (by incorporating flexural cracks). It is important to mention that in addition to these fundamental corrosion rate-controlling factors, other factors such as temperature [4], chloride content at steel level, degree of concrete saturation, oxygen availability and loading level [5] are also important. However, in this study, these were not incorporated in the experimental programme but can be inferred from literature. For example the influence of temperature on corrosion rate (and even concrete resistivity [6]) can be taken into account using the Arrhenius law (see Chapter 2 Part I).

The following sections present both the experimental variables and set-up used for both the laboratory-based and field-based experiments. Before proceeding it is important to mention that both the laboratory-based and field-based experiments were carried out in parallel.

3.3 *Experimental variables*

3.3.1 *Binder types*

Three binder types, PC (CEM I 42.5N), GGBS and FA, were used. Except for concrete used to make reference specimens using 100% PC, PC was blended with either GGBS or FA based on commonly used replacement ratios in the (South African) construction industry for marine concrete. These are summarized below:

(i) 50/50 PC/GGBS blend: Blast furnace slag is a non-metallic material consisting essentially of silicates and alumina-silicates of calcium. It is a latent hydraulic binder and is typically used to replace between 35 and 65% of PC in concrete. However, previous studies have shown that a 50/50 replacement ratio provides optimum results with respect to resistance to chloride penetration in concrete [7].

(ii) 70/30 PC/FA blend: Fly ash, a by-product from the combustion of pulverized coal, is a pozzolanic material. Its pozzolanicity is more related to its fineness, mineralogy and glassy nature than its chemical nature. Common replacement levels of FA range between 15 and 35% by mass of total cementitious material [8]; with 30% being the most commonly used in South Africa. It improves workability, lowers the water demand but adversely affects early-age strength [9].

100% PC, which is not recommended for marine concrete due to its relatively high chloride penetrability [10], was used to make reference (i.e. control) specimens. The use of PC can also be justified considering that it was the most common binder used to make concrete for construction of old/deteriorated (age > 30 years) RC structures and that the development and application of maintenance and repair strategies for these structures relies on knowledge of its expected long-term durability performance.

The compressive strength development (7, 14, 21, 28, 56 and 90 day) and tensile strengths (28 and 90 day) for the various concretes used in this study are presented in Appendix A. The measured oxide composition and mineralogical analyses of the binders used are presented in Table 3.1.

Table 3.1: Measured oxide composition and mineralogical analyses of binders used (%)

Oxide	PC	GGBS	FA	Mineralogy* (PC)	%
CaO	64.12	36.42	4.14	C_3S	64.2
SiO_2	20.75	37.06	54.87	C_2S	11.1
Al_2O_3	4.17	12.83	31.34	C_3A	5.6
Fe_2O_3	3.21	0.72	3.70	C_4AF	9.8
SO_3	2.30	2.24	0.19	* By Bogue formulae	
MgO	0.74	8.13	1.00	C_3S: $3CaO \cdot SiO_2$	
K_2O	0.73	1.07	0.71	C_2S: $2CaO \cdot SiO_2$	
TiO_2	0.28	0.59	1.67	C_3A: $3CaO \cdot Al_2O_3$	
Mn_2O_3	0.05	0.98	0.06	C_4AF: $4CaO \cdot Al_2O_3 \cdot Fe_2O_3$	
Na_2O	0.04	0.50	0.36		
P_2O_5	0.08	0.00	0.49		

Note: Oxide composition by x-ray difraction method.
Data provided by supplier (PPC Cement Ltd)

3.3.2 *Water-binder ratio*

Eurocode EN206-1 [11] specifies a maximum w/b ratio of 0.45 for marine exposure Class XS (subclass XS3a, see Table 1.1, Chapter 1). In this study, two w/b ratios, 0.40 and 0.55, were used for each of the binders mentioned in Section 3.3.1. The 0.40 w/b ratio meets the requirements for marine concrete but a higher w/b ratio of 0.55 was also used to simulate comparatively low quality concrete which, even though not recommended for marine structures, can be achieved due to poor construction practices such as addition of water to concrete during placement, poor or lack of curing, etc. However, 0.55 w/b ratio was not used with plain PC concrete because it is seldom used for marine structures owing to its poor durability performance i.e. high chloride penetrability. Blended cement concretes are usually preferred. If PC is used, a w/b ratio as high as 0.55 is unacceptable. This type of concrete (i.e. PC with w/b ratio of 0.55) was therefore omitted from the study.

3.3.3 *Concrete cover to steel*

Both Eurocode EN 1992 1-1[12] and the South African concrete design code [13] specify a minimum cover of 40 mm for normal density concrete (2200 to 2500 kg/m^3) exposed to severe environmental conditions such as tidal marine conditions. In this study, two concrete covers, 40 and 20 mm were used to simulate, respectively, normal and adverse practical cover depths for marine RC structures.

3.3.4 *Crack widths*

This study focused on pre-corrosion load-induced cracks that are present before the onset of corrosion. Crack widths investigated in this study were limited to zero mm (uncracked), incipient crack, 0.4 mm and 0.7 mm. The uncracked specimens served as a reference for the respective combinations of binder type, w/b ratio, cover depth, crack width and exposure environment. An incipient crack refers to a crack just induced by 3-point loading of beam specimens and thereafter unloading (details are given in Sections 3.4 and 3.7). A 0.4 mm crack width has, in the past, been taken as the threshold crack width, below which corrosion may proceed similar to uncracked concrete [14]. However, results by Otieno *et al*. [15] have showed that adopting a universal crack width threshold for all concrete types and qualities is not valid - other factors such as concrete quality and cover depth also need to be considered. Consequently, 0.4 mm crack width was investigated. The 0.7 mm crack width was used to simulate adverse crack widths which are rarely encountered but may pose corrosion threat to RC structures. Even though previous research has shown that crack widths $\leq$ 0.3 mm are prone to self-healing [16-18], it was neither possible to ascertain nor quantify crack self-healing in the incipient-cracked specimens due to lack of test equipment. Further, for deep cover depths (say 40 mm) coupled with susceptibility to crack healing, it can be expected that incipient cracks will have negligible effect on corrosion rate. The incipient-cracked specimens were therefore made only for the laboratory and field specimens with 20 mm cover. However, future studies should look into quantifying the effect of these types of cracks on corrosion rate taking into account their self-healing potential.

3.4 *Concrete mix proportions, specimen type and sample size*

A modified version of the ACI volumetric concrete mix design method [19] was used to determine the various mix proportions. The modifications in the ACI method [20] are carried out to suit South African practice [21]. A summary of the concrete mix proportions and selected properties is given in Table 3.2.

Table 3.2: Summary of concrete mix proportions and selected properties

Binder composition	100 % PC	50/50 PC/GGBS		70/30 PC/FA	
w/b ratio	0.40	0.40	0.55	0.40	0.55
Material (kg/m^3) Mix label	**PC-40**	**SL-40**	**SL-55**	**FA-40**	**FA-55**
PC (CEM I 42.5N)[a]	500	231	168	324	236
GGBS[b]	-	231	168	-	-
FA[c]	-	-	-	139	101
Fine aggregate: Klipheuwel sand (2 mm max.)	529	749	855	749	855
Coarse aggregate: Granite (13 mm max.)	960	1040	1040	1040	1040
Water	200	185	185	185	185
Superplasticizer (SP) (litres/m^3)[d]	2.1[g] (0.4)	1.8 (0.4)	0.3 (0.1)	0.4 (0.1)	-
Slump (mm)	120	105	150	85	200
28-day compressive[e] strength (MPa)	58.2 (3.0)[h]	48.1 (2.0)	35.3 (0.9)	50.7 (0.9)	28.6 (1.9)
28-day tensile[f] strength (MPa)	3.7 (0.3)	2.8 (0.2)	2.3 (0.3)	3.4 (0.4)	2.3 (0.1)

[a]: Supplied by PPC Ltd (Riebeek West)
[b]: Supplied by AfriSam, South Africa
[c]: Supplied by Ash Resources (Pty) Ltd
[d]: See Appendix F for product details
[e]: Tests performed on 100 mm cubes
[f]: 100 mm cube splitting tensile strength
[g]: Percentage of SP by mass of total binder
[h]: Standard deviation

Crushed granite stone (13 mm max., consolidated bulk density: 1760 kg/m^3 and relative density: 2.65) was used as coarse aggregate. Granite rocks are composed of crystalline igneous and metamorphic minerals of differing grain sizes, consisting essentially of quartz and feldspar together with differing amounts of silicates (mica and amphibole) and iron oxides. The 13 mm granite stone was used because of its availability, and should not be taken to represent the use of mortar specimens that was discussed in Chapter 2, Section 2.14.4. The high cement content of the concrete mixes used (> 300 kg/m^3) posed a threat of alkali aggregate reaction (AAR) and hence granite was preferred to other readily available coarse aggregates such as greywacke which are prone to AAR attack [22]. Specifically, it is important to note the high binder content that was used for PC-40 concrete; even though it was not explored in this study, the use of an increased dosage of the superplasticizer would have decreased the binder content. Siliceous Klipheuwel pit sand (2 mm max., fineness modulus: 2.5 and relative density: 2.7) was used as fine aggregate. These sands have a very high percentage of fines - up to 20% minus-150-µm and 15% minus-75-µm [22]. The grading curves for the fine and coarse aggregates used, and detailed compressive and tensile strength results for the various concrete mixes are given in Appendix A.

Three corrosion beams were cast per binder, per specimen type (w/b ratio, cover depth, crack width, and exposure environment). A total of 210 beams (120 x 130 x 375 mm, see Figure 3.1) were cast. It is important to note that even though the extent to which specimen size influences the results and progress of the corrosion process is seldom discussed, it is generally considered to be of minor importance from an electrochemical point of view for localized corrosion, provided that adequate cathode area is available [23]. However, for specimens with highly active anodes and a comparatively small cathode area, cathodic control may be dominant and limit the corrosion rate. In this study, it was assumed that the latter case did not apply.

For each concrete mix, companion 100 mm cube specimens were cast for strength and chloride conductivity tests (covered later in Sections 3.12 and 3.13). Although it has already been mentioned in Section 3.3.2, it is necessary to reiterate that the 0.55 w/b ratio was not used for PC specimens.

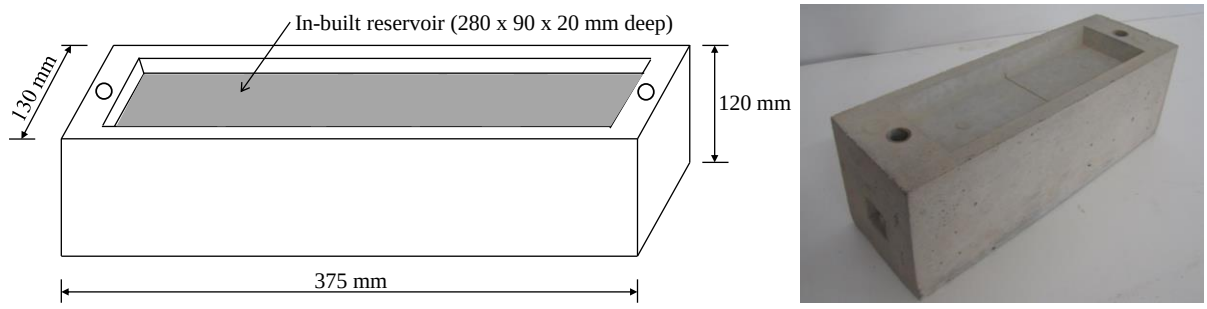

Figure 3.1: Sketch and photograph of a typical 120 x 130 x 375 mm beam specimen

3.5 *Casting and curing of specimens*

High yield strength ribbed deformed steel reinforcement bars (nominal diameter: 10 mm, average yield strength (f_y): 520 MPa (std. dev.= 3 MPa)) complying to SANS 920 [24] were used for all the beam specimens. It is the most common type of reinforcing steel used in South Africa and is therefore preferable for investigating corrosion. A single bar was embedded in each beam. Prior to casting, the

reinforcing bars were wire-brushed to remove mill scale and thoroughly cleaned with acetone. A wire was attached to one end of each steel bar for the purposes of (i) inducing active corrosion using impressed anodic current (covered in Section 3.6) and, (ii) monitoring both corrosion rate and half-cell potential (covered in Section 3.12). Both ends of the bars were covered with electroplating tape and epoxy-coated to provide an effective exposed surface area of approximately 86 cm^2 (approx. 27.5 cm long circumferencial steel surface). Just before casting, the bars were again cleaned and de-greased with acetone. A 10 mm diameter x 150 mm long stainless steel bar was placed in each beam during casting (see Figure 3.2 in Section 3.6) to act as a counter electrode for corrosion rate measurements.

A pan mixer was used for concrete mixing. Both the beams and companion cube specimens were compacted on a vibrating table immediately after placing the concrete in the moulds (in three successive layers), and thereafter covered with polythene sheets for 24 hours in the laboratory at ambient conditions (approximately 25 ± 2 °C), after which they were de-moulded and placed in a tap-water bath at approximately 23 ± 2 °C for curing. The beam specimens were cured for 28 days while the cube companion specimens were cured to their respective testing ages (for strength and chloride conductivity tests).

3.6 *Acceleration of corrosion initiation and propagation*

After 28-days curing and 10 days air-drying in the laboratory, and prior to cracking the beam specimens, anodic impressed current (IC) was used to eliminate the corrosion initiation phase (i.e. t_i = 0) for both the laboratory-based and field-based specimens. Cyclic wetting and drying was thereafter used to accelerate corrosion in the laboratory-based specimens while the field-based specimens were exposed to a natural environment (described in Section 3.9). The initiation phase was eliminated because this study focused on the corrosion propagation phase. The set-up used to initiate active corrosion in the specimens using IC is shown in Figure 3.2.

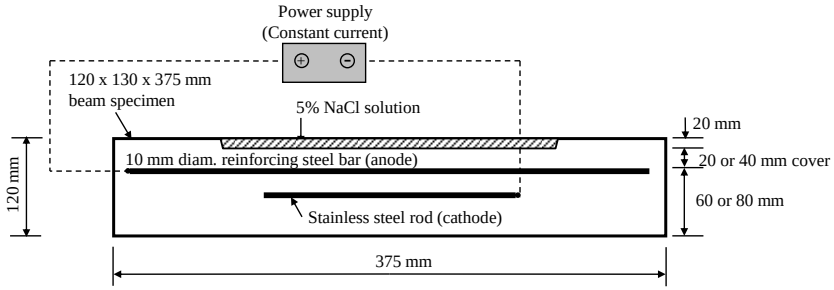

Figure 3.2: Schematic of set-up to induce active corrosion in the specimens

The theoretical time ($t_{steel\ level}$) and amount of IC required to drive the chlorides through the cover depth to the steel level was estimated using the Nernst-Planck Equation that was presented in Chapter 2 (see Eqn. (2.47)) in the following form, Eqn. (3.1):

$$t_{steel\ level} = c\left(-D\left(\frac{zF}{RT}\right)\left(\frac{\partial E}{\partial x}\right)\right)^{-1} \tag{3.1}$$

where *c* is the cover depth (20 or 40 mm), and *D* is the diffusion coefficient obtained from the measured 28-day chloride conductivity index (CCI, obtained from the chloride conductivity test) [25, 26] for each of the concrete mixes summarized in Table 3.2. The diffusion coefficients presented in Table 3.3 were determined based on an empirical relationship between CCI and diffusion coefficient [27] – see Appendix D.

Table 3.3: 28-day Chloride conductivity index (CCI) and corresponding diffusion coefficients

Mix label	28-day CCI (mS/cm)	Corresponding diffusion coefficient, D* (cm^2/s) x 10^{-7}
PC-40	1.24	25.7
FA-40	0.37	1.9
FA-55	0.89	3.2
SL-40	0.26	1.4
SL-55	0.59	1.9

* Determined based on an empirical correlation between CCI and *D* - see Appendix D

In order to determine the anodic IC required to induce active corrosion rate in the specimens of a given cover depth for each of the five concrete mixes, and after a series of iterations (of time and IC), the time to apply the IC was fixed at 1.5 hours to limit the effective applied current to less than 2.0 Amperes. The term 'effective applied current' is used here to refer to the actual applied current taking into account the corresponding 28-day measured resistance of the (water-saturated) concrete. The current was limited to less than 2.0 Amperes to ensure chlorides reach the steel and to minimize the steel mass loss, if any. The effective currents applied to the various concretes are presented in Table 3.4. It is important to note that the effective applied currents were theoretically not expected to cause any steel mass loss; these currents were only meant to drive the chlorides to the steel level within approximately 1.5 hours (taking into account cover depth and concrete quality). Beam specimens of the same binder type, w/b ratio and cover depth were connected in series, and the appropriate anodic IC (Table 3.4) applied continuously for 1.5 hours after which all the 72 beams were connected in series and an effective current of 8.6 µA applied for a further 2 hours – this was expected to result in a corrosion rate of approximately 0.1 $\mu A/cm^2$ in all the specimens (assuming the whole exposed steel surface of 86 cm^2 was polarized). A corrosion rate of 0.1 $\mu A/cm^2$ is conventionally taken to denote the transition from passive (initiation) to active (propagation) corrosion [28, 29].

Table 3.4: Summary of anodic impressed currents applied to the specimens for 1.5 hours

Mix label	Cover depth (mm)	Effective applied current (A)
PC-40	20	0.03
	40	0.13
FA-40	20	0.44
	40	1.67
FA-55	20	0.25
	40	1.01
SL-40	20	0.57
	40	1.70
SL-55	20	0.44
	40	1.67

It is important to note that the estimation of the anodic IC required to induce active corrosion was based on the assumption that the polarized steel surface area is equal to the uncoated steel surface area of approximately 86 cm^2. In reality, the polarized steel surface area may be less, leading to a higher corrosion current density than the active corrosion rate threshold of 0.1 $\mu A/cm^2$. Current commercial instruments such as Gecor 8® employ the use of an annular guard ring to confine the polarized steel surface area (Figure 3.3). Even though the objective of this approach is to limit gross errors in the estimation of the polarized area of steel by ensuring that a measurement is taken from a defined area of steel, its accuracy cannot be ascertained. This issue will be discussed further in Chapter 4.

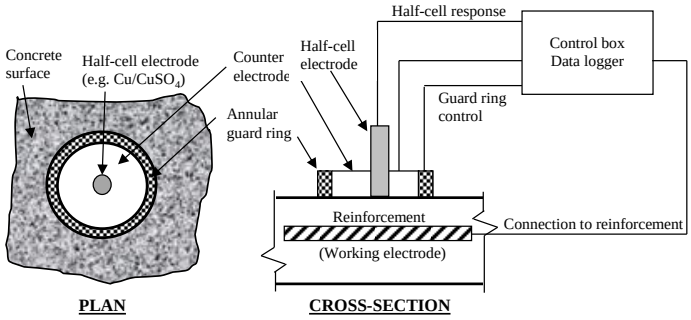

Figure 3.3: Schematic of corrosion rate measurement with a guard-ring incorporated [30]

3.7 *Crack inducement, measurement and loading criteria*

To facilitate the formation of a transverse (flexural) crack at approximately the longitudinal centre of the beam specimens during machine loading, a 1.0 mm thick x 4 mm deep PVC sheet was placed at the centre of each beam (transversely) during casting as shown in Figure 3.4. The PVC sheet was embedded in the beam mould, and did not remain in the beam specimen at de-moulding 24 hours after casting.

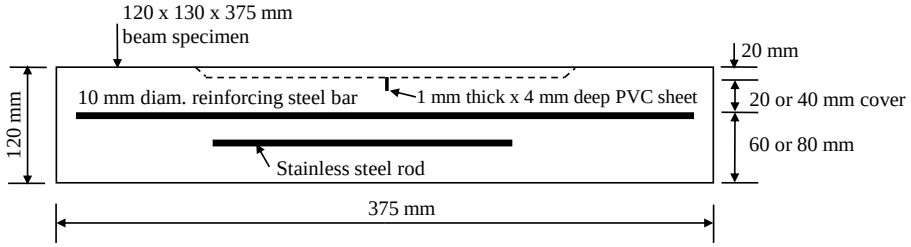

Figure 3.4: Schematic of a beam specimen with 1.0 mm thick PVC sheet

The PVC sheet acted as a notch to increase the probability of obtaining a more or less centrally placed flexural crack under 3-point loading. After inducing active corrosion (see Section 3.6), the beams were pre-cracked under 3-point flexural machine loading. It is important to note that even though the cover depth at the crack in the cracked specimens was effectively either 16 or 36 mm (due to the 4 mm deep cast-in PVC sheet), and not, respectively, 20 or 40 mm as in the uncracked ones, this difference was considered negligible with respect to the corrosion process. In cracked concrete, the cathodes will in most cases be located away from the crack (where the cover depth was not altered) as opposed to the anodes which are located at the crack region. The travel path for O_2 ingress, which controls the

cathodic reaction process, can therefore be assumed to be the same in both the cracked and uncracked specimens.

During the loading process, crack width was measured using a crack width detection microscope with a magnification of X40 and accuracy of ±0.02 mm. The incipient cracks were produced by load application until a crack was visually detected using a hand-held lens (magnification X40) and then unloading after which the crack was no longer visible. Before releasing the load, the load required to attain a given crack width for each specimen was recorded; these are given in Appendix A.

All the cracks closed when the load was removed. Thereafter, the respective crack widths (except the incipient crack) were re-opened and maintained using the 3-point manual loading rig shown in Figure 3.5 and Figure 3.6. All the 0.4 and 0.7 mm cracked specimens remained in individual loading rigs for the duration of the experimental programme.

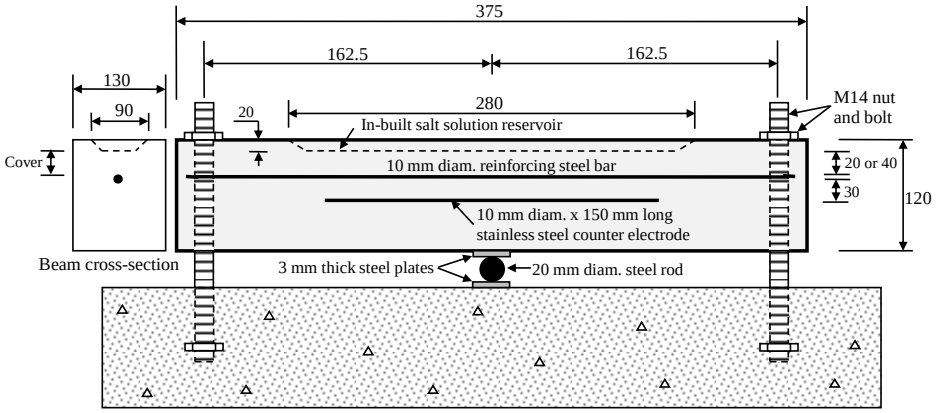

Figure 3.5: Beam loading set-up for 0.4 and 0.7 mm cracked specimens (dimensions in mm)

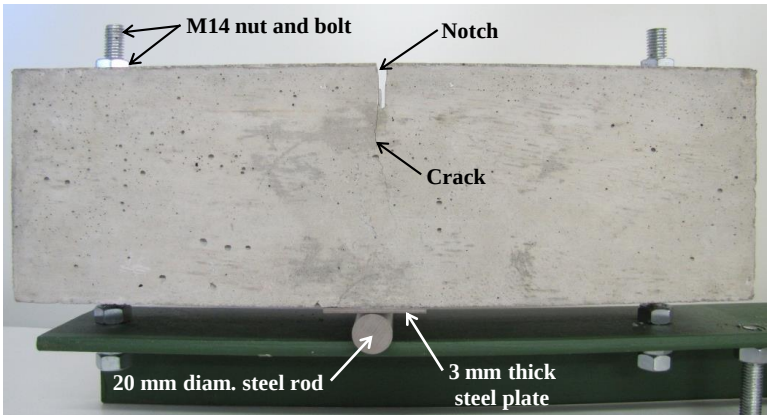

Figure 3.6: Photograph of a typical cracked beam loading rig set-up

Even though previous studies have shown that the loading (or stress) level plays an important role in corrosion propagation [5, 31], it was not a variable in this study but future studies may need to incorporate it and if possible, extend the corrosion rate prediction models proposed in Chapter 5; high stress levels (in the concrete) lead to increased number, size and interconnectivity of cracks and hence

increased penetrability of the concrete. Furthermore, these studies also reported that high steel stresses result in higher corrosion rates.

3.7.1 *Crack width monitoring*

To ensure that the 0.4 and 0.7 mm crack widths remained more or less constant, demountable mechanical (demec) studs were placed on the concrete surface across the crack and the distance between the studs monitored bi-weekly using a 100 mm demec gauge (see Figure 3.7 and Figure 3.8). The loading rig shown in Figure 3.5 was then used to adjust the crack widths as required (via the bolts and nuts).

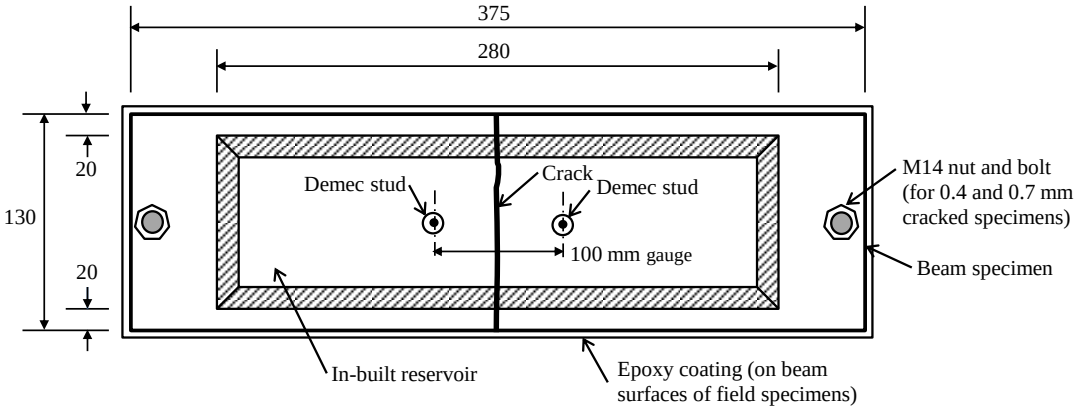

Figure 3.7: Location of demec studs for monitoring crack width in cracked specimens

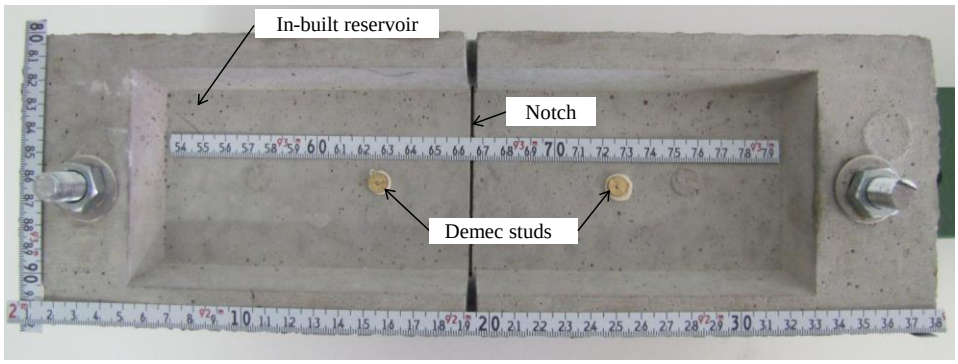

(a) Position of demec studs

(b) Measurement using demec gauge

Figure 3.8: Photographs showing position of demec studs and measurement using demec gauge

3.8 *Epoxy-coating of the field specimens*

Prior to field exposure, all the faces of the field-exposed beams, except that with the specified cover depth, were coated with epoxy (Sikafloor®-261 ZA, see Appendix F for product details) to prevent ingress of corrosion agents (Cl^-, O_2 and H_2O), and drying from those surfaces (see Figure 3.9). In essence, this ensured that chlorides penetrate the concrete only from the face with the specified cover depth. A similar treatment has been used by previous researchers [32, 33].

It is important to note that even though the intention of the epoxy-coating of the field-based specimens was to simulate chloride ingress in the laboratory-based specimens, an unintended secondary effect is that it prevented drying through the sealed surfaces. This was not the case in the laboratory-based specimens, and because the moisture content of the concrete was not monitored in this study, its effect on the corrosion process was not quantified. More discussion on this will be presented in Chapter 4 with the experimental results.

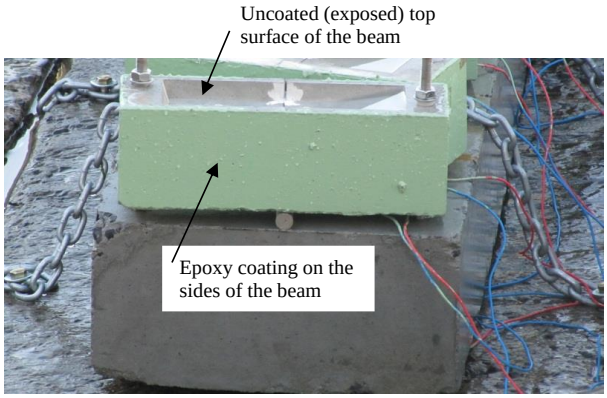

Figure 3.9: Photo showing a typical field-exposed specimen with epoxy-coated sides

3.9 *Exposure conditions*

3.9.1 *Field exposure*

The classification of marine environments, for example in EN 206-1 [11], as tidal, splash, spray (atmospheric), splash/spray and submerged is usually based on the aggressiveness of chloride-induced corrosion i.e. in terms of the corrosion-induced damage over a given period of time. As was mentioned in Chapter 1, RC structures in the tidal, splash and spray zones are considered the most affected by corrosion i.e. exposure class XS3. The field-based specimens were therefore exposed to tidal marine zone in Cape Town (Table Bay); see Figure 3.10 (also see Figure 1.3, Chapter 1 for details of the exposure site location).

The salinity (chloride content) of the sea-water at the exposure site is approximately 2% (average of 10 samples, standard deviation = 0.02%). This was determined from samples taken at random time intervals during the experimental period. The temperature and relative humidity of the exposure site ranged between 1 and 37 °C, and 65 and 83% respectively. The monthly variation of temperature and relative humidity is given in Appendix C.

It is important to note that all the specimens in this exposure condition were located within an approximately 5 m long zone between the seaward and inland specimens, and between the high and low water tide-marks (see Figure 3.10). They were therefore assumed to be exposed to similar tidal conditions.

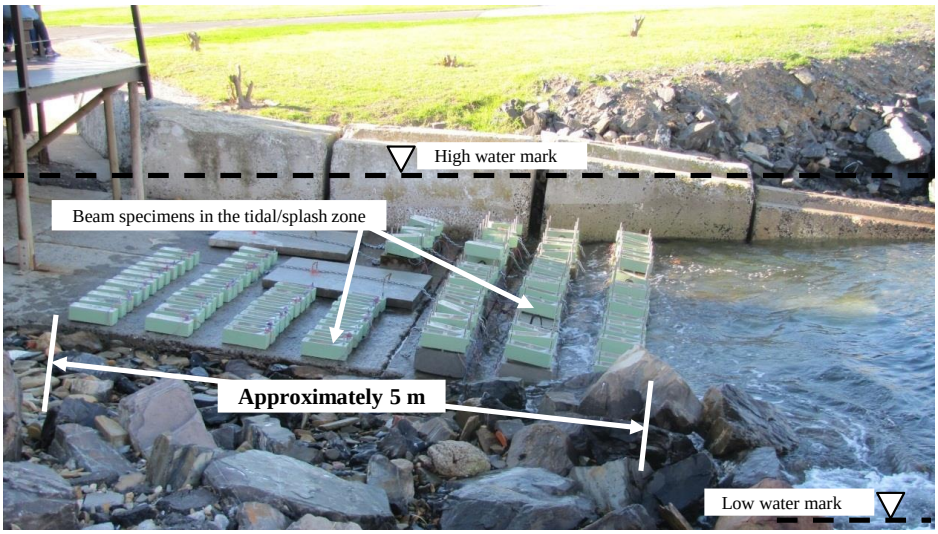

Figure 3.10: Photograph showing the field-based specimens in the tidal zone

3.9.2 *Laboratory exposure*

The laboratory-based specimens (see Figure 3.11) were subjected to cycles of 3-day wetting with 5% NaCl solution followed by 4-day drying (temperature: 25 ± 2 °C and relative humidity: 50 ± 5%) throughout the experimental period. A 5% NaCl solution was used, based on the consideration of previous studies [e.g. 33, 34]. The equivalent chloride content in the 5% NaCl solution is 3%; this is 50% higher than the measured chloride content of the sea-water at the exposure site i.e. 2%.

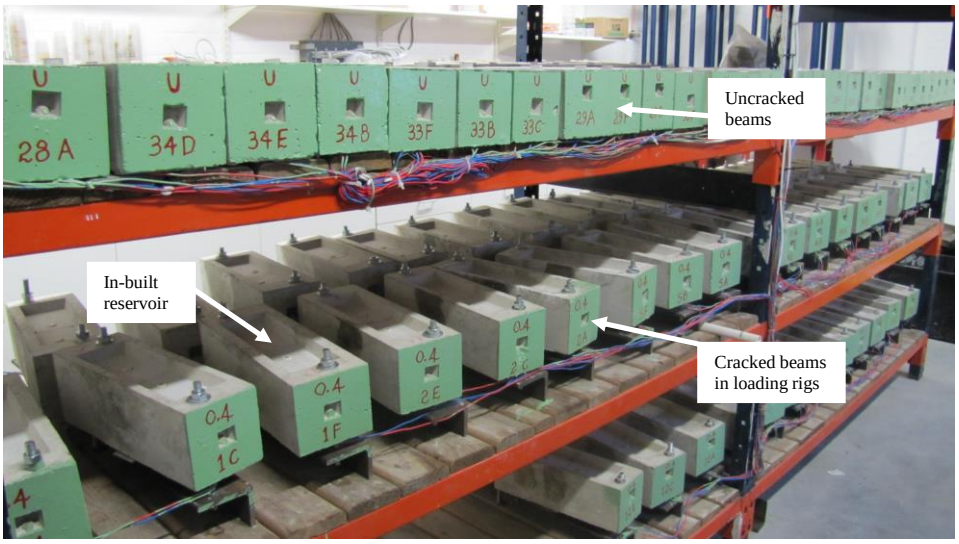

Figure 3.11: Photograph showing some of the laboratory-based specimens

The process of setting-up the beam specimens in the field and laboratory exposure environments was completed 15 days after inducing active corrosion rates in the specimens, and cracking (if required).

3.10 *Corrosion assessment and monitoring*

Corrosion rate, half-cell potential, concrete resistivity and crack width were monitored. These are detailed in the sub-sections following.

3.10.1 *Corrosion rate measurement*

Corrosion rate was measured using the coulostatic technique (a linear polarisation resistance method) whereby a small charge is applied to the steel and the relaxation of potential monitored over a short period of time, to determine the polarization resistance (R_P). A typical potential transient monitored over 25 seconds is shown in Figure 3.12. The theoretical development and principles of the coulostatic method is available in the literature [35, 36]. A brief summary is presented here.

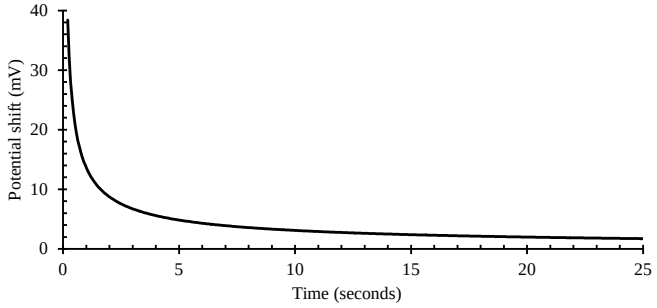

Figure 3.12: Typical potential transient of steel after application of a small perturbation charge

Theoretically, corrosion rates are related to the time constant (τ_c) describing the corrosion potential decay induced by a small current perturbation as the time constant is related to R_p through the double layer capacitance (C) [35, 37]. The potential transient is described by the equation [36]:

$$n_t = n_o \exp\left(\frac{-t}{\tau_c}\right) \tag{3.2}$$

where n_t is the potential shift at time t and n_o is the initial potential shift. The polarization resistance, R_p, is then obtained:

$$R_p = \frac{\tau_c}{C} \tag{3.3}$$

$$C = \frac{q_s}{n_o} \tag{3.4}$$

$$q_s = \frac{t_{pulse} \times I_{applied}}{A} \tag{3.5}$$

where q_s is the applied charge density, t_{pulse} (ms) is the pulse duration, $I_{applied}$ (mA) is the applied current and A is the (polarized) steel surface area. As already mentioned in Section 3.6, the polarized steel surface area, A, was assumed to be equal to the exposed steel surface area of approximately

86 cm^2 due to the difficulty in determining the actual polarized steel surface area. The consequences of this assumption will be discussed in Chapter 4.

Experimentally, R_p values are obtained by fitting Equation (3.2) to the results for a curve such as that shown in Figure 3.12. The value of n_o is obtained from the fitted equation. Potential measurements are taken 0.1 seconds after the cessation of the charge which allows many of the very earlier to dissipate. The potential readings were taken for at least 30 seconds. The length of the charge (i.e. pulse period) effects the shape of the relaxation transient but marginal differences have been reported for relaxation curves for perturbations of approximately 35 ms and 4.65 ms [37]. The charge was delivered by means of a pulse generator capable of supplying from 1 to 30 mA and from 1 to > 100 ms. Most of the pulses used in this study were less than approximately 35 ms.

Measurements were taken at a rate of ten readings per second both before and after the application of the charge. The pre-perturbation potential was monitored until reasonable stability was achieved at which point a known charge was sent to the working electrode (embedded reinforcing steel) by means of an embedded stainless steel counter electrode (see Figure 3.13). Any underlying potential trend determined prior to the application of the charge was removed from subsequent value after the perturbation thus ensuring only the true change in potential was used for curve fitting Equation (3.2). Potential data was collected using a HP 34970A data acquisition unit and analysed using a MATLAB® program. A schematic of the set-up is shown in Figure 3.13.

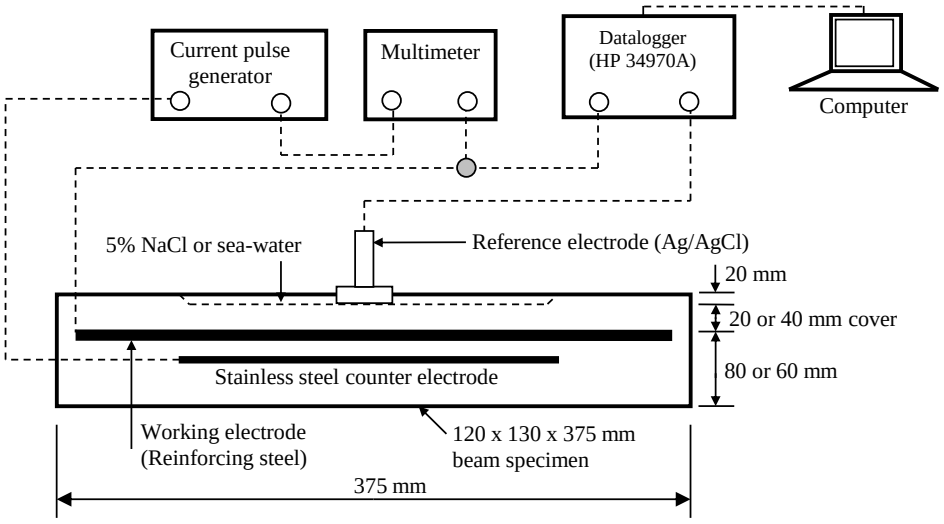

Figure 3.13: Schematic diagram of the coulostatic corrosion rate measurement set-up

The polarization resistance is related to the corrosion current density (i_{corr}) by means of the Stern-Geary coefficient B as shown in Equation (3.6) [38, 39].

$$i_{corr} = \frac{B}{R_p} \tag{3.6}$$

where B is the Stern-Geary coefficient varying between 13 and 52 mV depending on the corrosion state of the steel (i.e. passive or active). A value of 26 mV for corroding (active) steel and of 52 mV

for passive steel in the case of concrete has been established and used by a number of researchers [40-42]. In this study, therefore, a value of 26 mV was used.

The specimens were monitored bi-weekly for corrosion rate.

3.10.2 *Half-cell potential measurement*

This is one of the most widely used electrochemical methods for the assessment of corrosion in RC structures. It was introduced in the early 1970s to locate corroding steel bars in concrete structures [43, 44]. It is based on the measurement of the potential difference between the embedded reinforcement and a reference electrode (also called *half-cell*) such as $Cu/CuSO_4$ and Ag/AgCl as shown in Figure 3.14 [45, 46].

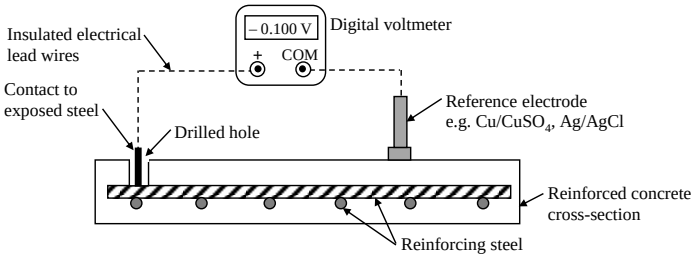

Figure 3.14: Schematic of half-cell potential measurement circuitry [47]

The technique is used to evaluate the probability of corrosion before damage is evident at the concrete surface. Half-cell potential (HCP) measurements only give an indication of corrosion risk and are linked empirically to the probability of corrosion. The numerical value of the potential between the embedded steel and the reference electrode depends on the type of reference electrode used and the corrosion condition of the steel in the concrete [47]. It is therefore important to report the reference electrode used for HCP measurements. The ASTM C876-91 [48] criterion for interpreting HCP readings is presented in Table 3.5.

Table 3.5: Criteria for interpretation of half-cell potential measurements [48]

$Cu/CuSO_4$ electrode	Ag/AgCl electrode	Likely corrosion condition
> -200 mV	> -106 mV	Low (10% risk of corrosion)
-200 to -350 mV	-106 to -256 mV	Intermediate corrosion risk
< -350 mV	< -256 mV	High (>90% risk of corrosion)
< - 500 mV	< - 406 mV	Severe corrosion

It is important to note that there is no general correlation between corrosion rate and half-cell corrosion potential, because both parameters respond differently to the same variables, particularly moisture content (or oxygen availability), temperature and concrete resistivity [49]. Consequently, it is recommended that HCP measurements be complemented with other corrosion assessment methods, because although reliable relationships between potential and corrosion rate can be found in the laboratory for well-conditioned experiments, such relationships may not be generalised, since wide variations in the corrosion rate are possible in a narrow range of potentials [50].

HCP readings were taken simultaneously during corrosion rate measurements using Ag/AgCl reference electrodes (see Figure 3.13). The specimens were monitored bi-weekly for HCP.

3.10.3 *Concrete resistivity measurement*

A four-point Wenner probe was used to measure surface concrete resistivity. The apparatus consists of four probes equally spaced (Figure 3.15). A small alternating current of low frequency is applied between the outer probes and potential drop measured between the inner probes [51]. This approach, to some extent, eliminates any effects due to surface contact resistances.

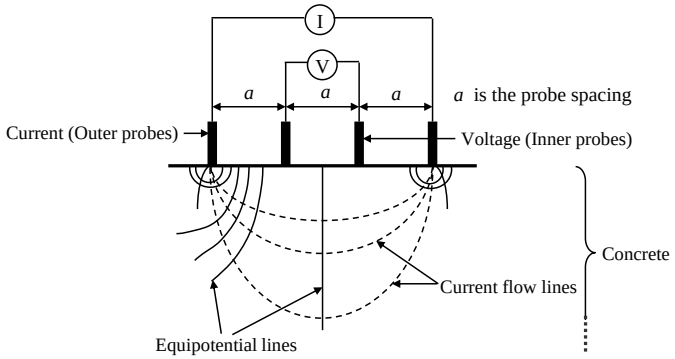

(a) Schematic drawing of resistivity measurement

(b) Photograph of the 4-point Wenner probe used (www.proceq.com)

Figure 3.15: Resistivity measurement using 4-point Wenner probe [52]

Using this technique, the apparent resistivity of concrete, ρ, in Ω-cm is expressed as:

$$\rho = 2\pi\left(\frac{V}{I}\right)a \tag{3.7}$$

where V is the voltage drop (volts), I is the applied current (amperes) and a is the probe spacing (cm). In this study, a probe spacing of 50 mm was used based on the recommendations by Gowers and Millard [52] whose experimental results showed that in order to limit measurement errors, the probe spacing should either be ≥ 1.5 x maximum aggregate size or > 40 mm, whichever is greater. In this study, maximum aggregate size = 13 mm, hence $a \geq 19.5$ mm. Therefore, the lower limit (a > 40 mm) was adopted. The Resipod® 4-point Wenner probe resistivity meter supplied by Proceq® was used (see Figure 3.15 (b)). This device has a fixed probe spacing of 50 mm, operates within the range of 0 to 1000 kΩ-cm at a frequency of 40 Hz, and has a resolution of up to ± 2 kΩ-cm [details from 53].

Similar to corrosion rate and HCP, concrete resistivity was monitored bi-weekly. No surface pre-wetting was required for the laboratory-based specimens as it was carried out at the end of the 3-day wetting period (see Section 3.9.2). For the field-based specimens, surface pre-wetting was done, if necessary, by spraying tap-water prior to taking the resistivity measurements.

3.11 *Chloride content measurements*

After 73 weeks of exposure in the respective environments (laboratory and field), 20 ± 2 mm cores were taken from specimens to facilitate chloride content measurements (at the steel level). The age at

chloride content measurement (after 73 weeks) was informed by the measured corrosion rates in the field-based specimens which, despite the inducement of active corrosion (see Section 3.6), showed significantly low (< 0.2 μA/cm^2) corrosion rates after 73 weeks of exposure. Chloride content measurement was therefore more of an exploratory exercise to establish the reasons for the corrosion state in the field-based specimens than a planned one. The cores were taken on one side of the crack at two locations: 30 mm and 90 mm from the crack (see Figure 3.16). After extraction of the core samples, the holes in the beam specimens were sealed using epoxy. The chloride content was detemined by potentiometric titration using a 0.1M $AgNO_3$ solution. The chloride content determined by this method reflects the total chlorides in the concrete i.e. acid-soluble chlorides [54].

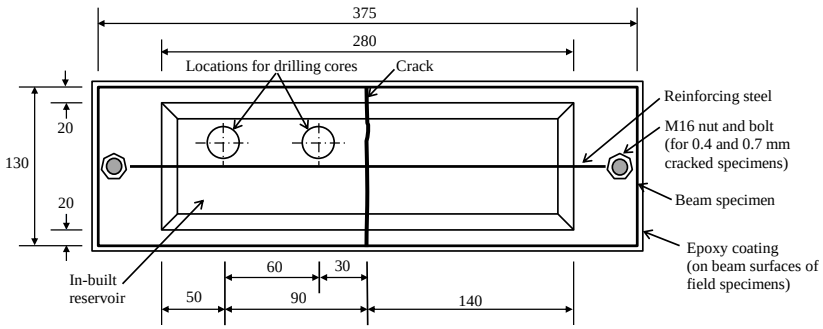

Figure 3.16: Locations for core extraction for chloride content measurements (dimensions in mm)

The test procedure, in summary, involves using the following reagents: 0.1M $AgNO_3$ (silver nitrate), 1.0M HNO_3 (nitric acid) and sodium acetate solution (abbreviated NaOAc). First, the concrete sample mechanically ground to fine powder. The powdered concrete sample is sealed in a Ziploc© bag. Approximately 2.1-2.5 g of the powdered concrete is then measured (to the nearest milligram) and placed in a 100 mL plastic titration beaker and dispersed with a little distilled water just to cover the sample. 2.0 mL of 1.0M HNO_3 acid is then slowly added to the sample as the beaker is slowly swirled to bring the concrete powder into suspension. The solution is then left to stand in the laboratory (temperature: 25 ± 2 °C, relative humidity: 50 ± 5%) for at least 30 minutes after which 2.5 mL of NaOAc is added. The beaker is then filled up to the 60 mL mark with distilled water and titrated using 0.1M $AgNO_3$. The equivalence point is determined by measuring the electrical potential between a silver ion-specific electrode (silver ring in a 1.0M KNO_3 electrolyte) and a reference electrode (Ag/AgCl) as the titration progresses. A commercially available system (Mettler Toledo® DMi141-SC) in which both the silver ion-specific and reference electrodes are conjoined in a glass shaft was used. The titration was performed using a commercial Mettler Toledo® DL50 automatic titration machine. The total chloride content expressed as a percentage relative to the mass of cement (%Cl) is calculated using the following expression:

$$\%\mathrm{Cl} = \left(\frac{M \times Q_{Ag} \times P_{Ag}}{m \times Eq} \right) \times \left(\frac{B_c}{D_c} \right) \times 100 \tag{3.8}$$

where M is the molar mass of chlorine (35.453 g/mole), Q_{Ag} is the volume of $AgNO_3$ added (L), P_{Ag} is the molarity of the $AgNO_3$ solution (i.e. 0.1 M), m is the mass of the concrete sample portion (g), Eq is

the equivalence number of chloride ion (Eq = 1), B_c is the binder content in the concrete (kg/m^3) and D_c is the density of concrete (kg/m^3).

3.12 *Chloride conductivity index test*

The chloride conductivity index (CCI) test is one of three (South African) durability index (DI) tests used to characterize concrete cover quality with respect to penetration of corrosion species (O_2, CO_2, Cl^- and H_2O); the other tests are oxygen permeability and water sorptivity index tests [55]. Each of the DI tests is linked to a transport mechanism relevant to a particular deterioration process. Even though the DI tests were developed, and are carried out on uncracked concrete, their applicability to cracked concrete is questionable and the results will be critically examined in Chapter 4. Furthermore, even though it will be discussed in detail in Chapter 4, it is important to mention that the CCI was used to obtain the chloride diffusion coefficients of the concretes used (see Section 3.4). The diffusion coefficients were used to characterize the relative penetrabilities of the different concretes to corrosion-sustaining agents and not to quantify a specific transport parameter as is usually the case in Fickian-based corrosion initiation prediction models.

The CCI test procedure and its empirical relationship with chloride diffusion coefficient is given in Appendix D but in summary [55], nominally 70 ± 2 mm diameter, 30 ± 2 mm thick concrete discs are prepared (usually at 28 days), four specimens for the test. The specimens are then conditioned in a 50 ± 5 °C oven for 7 days prior to testing. The specimens were obtained by coring from 100 mm companion concrete cubes prepared during casting of the beams. The concrete specimens are vacuum-saturated with a 5M NaCl solution. The saturated specimen is then placed in a test rig with a cell filled with the same salt solution on either side. Applying a voltage across the specimen and measuring the current that results allows the conductivity to be calculated. The actual voltage across the specimen is measured by the use of probes within the solutions contained in the test chambers, rather than taking the voltage applied by the power supply [26].

3.13 *Other tests*

In addition to the corrosion rate, half-cell potential, resistivity measurements and tests mentioned in the previous sections, compressive strength [56] and tensile strength [57] tests were also carried out on companion 100 mm concrete cube specimens.

3.14 *Summary of experimental set-up and corrosion assessment timeline*

The experimental programme used in this study was presented in this chapter. A summary of the experimental variables is summarized in Table 3.6. The sequence of events prior to commencement of corrosion measurements is summarized in Table 3.7.

Table 3.6: Summary of experimental variables

Mix label	Exposure	w/b ratio	Cover (mm)	Uncracked	Incipient cracked	0.4 mm cracked	0.7 mm cracked
PC-40	Lab[a] and Field[b]	0.40	40	✓	x	✓	✓
			20	✓	✓	✓	✓
SL-40	Lab and Field	0.40	40	✓	x	✓	✓
			20	✓	✓	✓	✓
SL-55	Lab and Field	0.55	40	✓	x	✓	✓
			20	✓	✓	✓	✓
FA-40	Lab and Field	0.40	40	✓	x	✓	✓
			20	✓	✓	✓	✓
FA-55	Lab and Field	0.55	40	✓	x	✓	✓
			20	✓	✓	✓	✓

PC: Plain Portland cement concrete - 100 % CEM I 42.5N (PC)

SL: Slag concrete - 50/50 PC/GGBS

FA: Fly ash concrete - 70/30 PC/FA

[a]: Laboratory accelerated corrosion by cyclic 3-days wetting (with 5% NaCl) and 4-days air-drying (25 °C, 50% RH)

[b]: Field natural corrosion in marine tidal/splash zone

Table 3.7: Summary of sequence of events prior to commencement of corrosion assessment

Event	Duration (days)	
	For each event	Cumulative
Specimen in mould after casting	1	1
Curing under water (23 ± 2 °C)	27	28
Air-drying (25 ± 2 °C, 50 ± 5 % relative humidity)	10	38
Active corrosion inducement (using anodic impressed current)	10	48
3-point load-induced cracking of cracked specimens	2	50
Set-up in laboratory (25 ± 2 °C, 50 ± 5 % RH) and field (tidal/splash marine exposure)	15	65
Time before first corrosion measurements - i_{corr} [a], HCP[b] and resistivity (after set-up)[c]	14	79

[a]: Corrosion rate

[b]: Half-cell potential

[c]: 80 days after casting of the specimens

3.15 *References*

[1] Alonso, C., Andrade, C. & Gonzalez, J. A. (1988) Relation between resistivity and corrosion rate of reinforcements in carbonated mortar made with several cement types. *Cement and Concrete Research,* Vol. 18(5)**,** pp. 687-698.

[2] Nilsson, L. O., Poulsen, E., Sandberg, P., Sorensen, H. E. & Klinghoffer, O. (1996) Chloride penetration into concrete, state-of-the-art, transport processes, corrosion initiation, test methods and prediction models. HETEK Report No. 53.

[3] Glass, G., Hassanein, N. & Buenfeld, N. (1997) Neural network modelling of chloride binding. *Magazine of Concrete Research,* Vol. 49(181)**,** pp. 323-335.

[4] Zivica, V. (2003) Influence of w/c ratio on rate of chloride induced corrosion of steel reinforcement and its dependence on ambient temperature. *Bulletin of Materials Science,* Vol. 26(5)**,** pp. 471-475.

[5] Yoon, S., Wang, K., Weis, W. J. & Shah, S. P. (2000) Interaction between loading, corrosion, and serviceability of reinforced concrete. *ACI Materials Journal,* Vol. 97(6)**,** pp. 637-644.

[6] Hope, B. & Ip, A. (1987) Chloride corrosion threshold levels for corrosion induced deterioration of steel in concrete. *ACI Materials Journal,* Vol. 84(4)**,** pp. 306-313.

[7] Mackechnie, J. R., Alexander, M. G. & Jaufeerally, H. (2003) Structural and durability properties of concrete made with Corex slag. *Research monograph No. 6,* University of Cape Town and the University of Witwatersrand.

[8] ACI-Committee-232.2R-03 (2003) Use of fly ash in concrete. *American Concrete Institute*.
[9] Ramezanianpour, A. A. & Malhotra, V. M. (1995) Effect of curing on the compressive strength, resistance to chloride ion penetration and porosity of concretes incorporating slag. *Cement & Concrete Composites*, Vol. 17(2)**,** pp. 125-133.
[10] Song, H. W. & Saraswathy, V. (2006) Studies on the corrosion resistance of reinforced steel in concrete with ground granulated blast-furnace slag - an overview. *Journal of Hazardous Materials*, Vol. 138(2)**,** pp. 226-233.
[11] BS-EN-206-1 (2000) *Concrete - Part 1: Specification, performance, production and conformity*, European Standard.
[12] BS-EN-1992-1-1 (2004) Eurocode 2: Design of concrete structures - Part 1-1: General rules and rules for buildings. European Standard.
[13] SANS-10100-2 (1994) *The structural use of concrete, Part 2: Materials and execution of work (as amended, 1994)*, South African Standard Code of practice.
[14] fib-Model-Code (2010) 3rd FIP/CEB Model Code for concrete structures. *Comite Euro-International du Beton and Federation International de Precontrainte*.
[15] Otieno, M. B., Alexander, M. G. & Beushausen, H.-D. (2010) Corrosion in cracked and uncracked concrete - influence of crack width, concrete quality and crack re-opening. *Magazine of Concrete Research*, Vol. 62(6)**,** pp. 393-404.
[16] Clear, C. A. (1985) *Cement and Concrete Association*, Technical Report No. 559**,** England.
[17] Neville, A. M. (2002) Autogenous healing - a concrete miracle? *Concrete International*, Vol. 24(11)**,** pp. 76-82.
[18] Hearn, N. (1991) A recording permeameter for measuring time-sensitive permeability of concrete. *Advances in Cementitious Materials (Ceramic Transactions)*, Editor: Mindess, S., Vol. 16**,** Published by the American Ceramic Society (July, 1991), ISBN-13: 978-0944904336, pp. 463-475.
[19] ACI-Committee-211 (2001) Guide for use of normal weight and heavy weight aggregates in Concrete, ACI 211R-96 (Re-approved 2001), American Concrete Institute manual for concrete practice. *Farmington Hills, MI: American Concrete Institute, American Concrete Institute*.
[20] ACI (1991) Standard practice for selecting proportions for normal, heavyweight and mass concrete. *American Concrete Institute***,** (ACI 211.1-91).
[21] Addis, B. & Goodman, J. (2009) *Concrete mix design*. Fulton's Concrete technology, 9th Edition (Chapter 11). Midrand, South Africa, Erstwhile Cement and Concrete Institute**,** pp. 219-228.
[22] Grieve, G. (2009) *Aggregates for concrete*. Fulton's Concrete technology, 9th Edition (Chapter 3). Midrand, South Africa, Erstwhile Cement and Concrete Institute**,** pp. 25-61.
[23] Angst, U., Elsener, B., Larsen, C. K. & Vennesland, Ø. (2010) Considerations on the effect of sample size for the critical chloride content in concrete. *Proceedings of the 2nd International Symposium on Service Life Design for Infrastructure***,** 4th - 6th October, 2010, Delft, The Netherlands.
[24] SANS-920 (2011) Steel bars for concrete reinforcement (Edition 2.3). South African Standard Code of practice, ISBN 978-0-626-25730-9.
[25] Mackechnie, J. R. (1996) Predictions of reinforced concrete durability in the marine environment. *PhD Thesis*, Department of civil engineering, University of Cape Town.
[26] Streicher, P. E. & Alexander, M. G. (1995) A chloride conduction test for concrete. *Cement and Concrete Research*, Vol. 25(6)**,** pp. 1284–1294.
[27] Mackechnie, J. R. (2001) Predictions of reinforced concrete durability in the marine environment. *Research Monograph No. 1***,** Department of civil engineering, University of Cape Town and the University of Witwatersrand.
[28] Alonso, C., Castellote, M. & Andrade, C. (2002) Chloride threshold dependence of pitting potential of reinforcements. *Electrochimica Acta*, Vol. 47(21)**,** pp. 3469-3481.
[29] Stansbury, E. E. & Buchanan, R. A. (2000) *Fundamentals of Electrochemical Corrosion*, ASM International, Ohio.
[30] Richardson, M. G. (2002) *Fundamentals of durable concrete*, Modern Concrete Technology, Spon Press, London.
[31] Ababneh, A. & Sheban, M. (2011) Impact of mechanical loading on the corrosion of steel reinforcement in concrete structures. *Materials and Structures*, Vol. 44(6)**,** pp. 1123-1137.
[32] Maruya, T., Takeda, H., Horiguchi, K., Koyama, S. & Hsu, K. (2007) Simulation of steel corrosion in concrete based on the model of macro-cell corrosion circuit. *Journal of Advanced Concrete Technology*, Vol. 5(3)**,** pp. 343-362.
[33] Li, G., Hu, F. & Wu, Y. (2011) Chloride ion penetration in stressed concrete. *ASCE Journal of Materials in Civil Engineering*, Vol. 23(8)**,** pp. 1145-1153.
[34] Otieno, M. B. (2008) Corrosion propagation in cracked and uncracked concrete. *Masters Dissertation*, Department of civil engineering, University of Cape Town.

[35] Glass, G., Page, C., Short, N. & Yu, S. (1993) An investigation of galvanostatic transient methods used to monitor the corrosion rate of steel in concrete. *Corrosion Science,* Vol. 35(5-8)**,** pp. 1585-1592.
[36] Hassanien, A., Glass, G. & Buenfeld, N. (1998) The use of small electrochemical perturbations to assess the corrosion of steel in concrete *NDT & E International,* Vol. 31(4)**,** pp. 265-272.
[37] Glass, G. (1995) An assessment of the coulostatic method applied to the corrosion of steel in concrete. *Corrosion Science,* Vol 37(4)**,** pp. 597-605.
[38] Rodriguez, P. & Gonzalez, J. (1994) Use of the coulostatic method for measuring corrosion rates of embedded metal in concrete. *Magazine of Concrete Research,* Vol. 45(167)**,** pp. 91-97.
[39] Stern, M. & Geary, A. L. (1957) Electrochemical polarization - I: theoretical analysis of shape of polarization curves. *Journal of Electrochemical Society,* Vol. 104(1)**,** pp. 56-63.
[40] Feliu, V., Gonzalez, J. A. & Feliu, S. (2007) Corrosion estimates from transient response to a potential step. *Corrosion Science,* Vol. 49(8)**,** pp. 3241-3255.
[41] Andrade, C. & Alonso, C. (1996) Corrosion rate monitoring in the laboratory and on-site. *Construction and Building Materials,* Vol. 10(5)**,** pp. 315-328.
[42] Gonzalez, J. A., Miranda, J. M. & Feliu, S. (2004) Consideration on the reproducibility of potential and corrosion rate measurements in reinforced concrete. *Corrosion Science,* Vol. 46(10)**,** pp. 2467-2485.
[43] Stratfull, R. F. (1973) Half-cell potential and the corrosion of steel in concrete. *Highway Research Record No. 433***,** pp. 12-21.
[44] Elsener, B. & Bohni, H. (1990) Potential mapping and corrosion of steel in concrete. *Corrosion rates of steel in concrete, ASTM STP 1065,* Berke, N. S., Chaker, V., Whiting, D., Eds., American Society for Testing and Materials, Philadephia**,** pp. 143-156.
[45] Rodriguez, J., Ramírez, E. & Gonzalez, J. A. (1994) Methods for studying corrosion in reinforced concrete. *Magazine of Concrete Research,* Vol. 47(167)**,** pp. 81-90.
[46] Szab´o, S. & Bakos, I. (2011) Reference electrodes in metal corrosion - review. *International Journal of Corrosion,* Volume 2010 (doi:10.1155/2010/756950)**,** 20 pp.
[47] Broomfield, J. P. (2007) *Corrosion of steel in concrete - understanding, investigation and repair (2nd Edition),* Taylor & Francis, Oxford, United Kingdom.
[48] ASTM-C876-91 (1999) *Standard test method for half-cell potentials of uncoated reinforcing steel in concrete,* ASTM International, West Conshohocken, PA 19428-2959, USA.
[49] Broomfield, J. P., Rodriguez, J., Ortega, L. M. & Garcia, A. M. (1993) Corrosion rate measurements in reinforced concrete structures by a linear polarization device. *Proceedings of the International symposium on condition assessment, protection, repair, and rehabilitation of concrete bridges exposed to aggressive environments, ACI Fall Convention*. 9th –10th November, Minneapolis, MN. pp. 644-651.
[50] Otieno, M. B., Alexander, M. G. & Beushausen, H.-D. (2010) Suitability of various measurement techniques for assessing corrosion in cracked concrete. *ACI Materials Journal,* Vol. 107(5)**,** pp. 481-489.
[51] Millard, S. G., Ghassemi, M. H., Bugey, J. & Jafar, M. I. (1990) *Assessing the electrical resistivity of concrete structures for corrosion durability studies, corrosion of reinforcement in concrete* (Eds.: Page, Treadaway, Bamforth), Elsevier, London, pp. 303-313.
[52] Gowers, K. R. & Millard, S. G. (1999) Measurement of concrete resistivity for assessment of corrosion severity of steel using Wenner technique. *ACI Materials Journal,* Vol. 96(5)**,** pp. 536-541.
[53] www.proceq.com**,** www.proceq.com/fileadmin/documents/proceq/products/Concrete/Resipod, accessed on 02 December, 2011.
[54] RILEM_TC-178-TMC (2002) Analysis of total chloride content in concrete (recommendation). *Materials and Structures,* Vol. 35**,** pp. 583-585.
[55] Stanish, K., Alexander, M. & Ballim, Y. (2006) Assessing the repeatability and reproducibility values of South African durability index tests. *Journal of the South African Institution of Civil Engineering* Vol. 48(2)**,** pp. 10-17.
[56] SANS-5863 (1994) *Concrete tests - compressive strength of hardened concrete*, South African Standard Code of practice, First revision.
[57] SANS-6253 (2006) *Concrete tests - Tensile splitting strength of concrete (Edition 1.01)*, South African Standard Code of practice.

Chapter 4

Experimental results, analyses and discussion

Influence of crack width, cover depth and concrete quality on corrosion rate

4.1 *Introduction*

This chapter presents the results and analyses of the laboratory-based and field-based corrosion assessments carried out in this study. It explores in detail the influence of the various experimental variables on corrosion rate of steel in 120 x 130 x 375 mm beam specimens made using different binders, w/b ratios, concrete cover depths and surface cover crack widths as was presented in the previous chapter. Analysis and discussion of the field-based and laboratory-based corrosion results is presented. In addition, correlations between corrosion rate (i_{corr}) and the various experimental variables are explored.

Note the following:

1. The corrosion rate, half-cell potential and resistivity results presented in this chapter refer to those collected during exposure of the beam specimens in their respective environments for up to 122 weeks (approximately 2¼ years).
2. The specimen notation used in the presentation of the experimental results in this chapter (and in other parts of this thesis) is given in Figure 4.1.

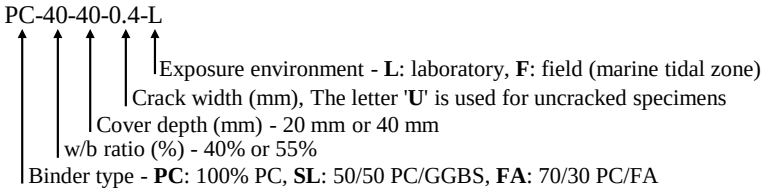

Figure 4.1: Specimen notation used in the presentation of experimental results

3. For any corrosion rate vs. time, half-cell potential vs. time or resistivity vs. time plots presented, '*week zero*' corresponds to the time when the specimens were placed in their respective exposure environments (laboratory or field); the first measurement was taken 14 days after exposure to the respective environments.
4. For a given exposure and test parameter, three specimens were monitored bi-weekly for corrosion rate and half-cell potential, and concrete resistivity. For each combination of binder type, cover depth and crack width, three individual specimen readings were taken and then averaged to obtain one result. Before averaging the three readings, outliers were detected and consequently rejected based on Grubb's outlier test. This test is summarized in Appendix E.
5. '*Average corrosion rate*', '*average half-cell potential*' and '*average resistivity*' as used in this chapter refer, respectively, to the arithmetic mean of the measured corrosion rates, half-cell potentials and concrete resistivities between weeks 104 and 120. This duration was selected because the time-development trends of the respective parameters (especially the (laboratory-

based) corrosion rate and half-cell potential) showed a relatively more or less plateau phase. It should be noted that even though the average corrosion rates for the field-based specimens were also determined between weeks 104 and 120, these are not taken as the long-term stable corrosion rates similar to those for the laboratory-based specimens. The time development trends for corrosion rate in these specimens showed negligible increases but this was mainly attributed to the seasonal weather changes, in this case, from summer (with maximum temperatures of approximately 27 °C) to winter (with maximum temperatures of approximately 15 °C) – see Figure C.1, Appendix C. The term *pseudo-plateau* is used in the chapter to refer to this phase in the field-based specimens.

6. A '2-*point moving average'* was used to represent all the corrosion rate, half-cell potential and resistivity vs. time plots in order to minimize sharp kinks and make the trends distinct, but without changing the actual trends. A moving average smoothes data by replacing each data point with the average of the neighbouring data points. The procedure for calculation of moving average is presented in Appendix E. A '2-point' moving average was used to avoid averaging the measured results over a long period of time (> 2 weeks), taking into account that the measurements were taken bi-weekly.
7. The term *concrete quality* is used to refer the ease of ingress of corrosion-sustaining agents (chlorides, oxygen and moisture). It was varied by using different binder types and w/b ratios, and quantified using the chloride diffusion coefficient obtained empirically from the conductivity index (see Appendix D). Therefore, the diffusion coefficients of the concretes will be used to solely *depict the relative penetrabilities of the different concretes to corrosion-sustaining agents* and not to quantify a specific transport parameter of concrete as is usually the case in Fickian-based corrosion initiation prediction models. *Concrete quality* will be used interchangeably with the term *concrete penetrability*.

4.2 *Objective of the chapter*

The main objective of this chapter is to analyse and synthesize the laboratory and field corrosion assessment results in order to understand the relationship between corrosion rate and the different test variables namely crack width, binder type, w/b ratio, cover depth, concrete resistivity, half-cell potential and chloride content at the steel level. Empirical correlations between corrosion rate and these parameters are derived from the results. These will be used in Chapter 5 to develop chloride-induced corrosion rate prediction models. A general outlook of the results summarizing the main findings is given at the end of the chapter. Detailed results relating to corrosion rate, half-cell potential, resistivity chloride concentration and durability indices are presented in the Appendices.

4.3 *Corrosion rate results*

4.3.1 *General overview of corrosion rate results*

Typical time-development trends for corrosion rate obtained during the experimental period (approximately 2¼ years) are shown in Figure 4.2(a) to (f) - see Appendix B for a complete set of time-development results. A general overview of the average corrosion rates (week 104-120) is given in Figure 4.3 to Figure 4.6. These figures depict the influence of exposure environment (i.e. accelerated laboratory vs. natural field corrosion), crack width, cover depth and concrete quality (binder type and w/b ratio). These will be discussed in detail later in this chapter. The corrosion rate of

0.1 μA/cm^2 is highlighted in Figure 4.3 to Figure 4.6 because it is conventionally taken to depict the transition from passive to active corrosion.

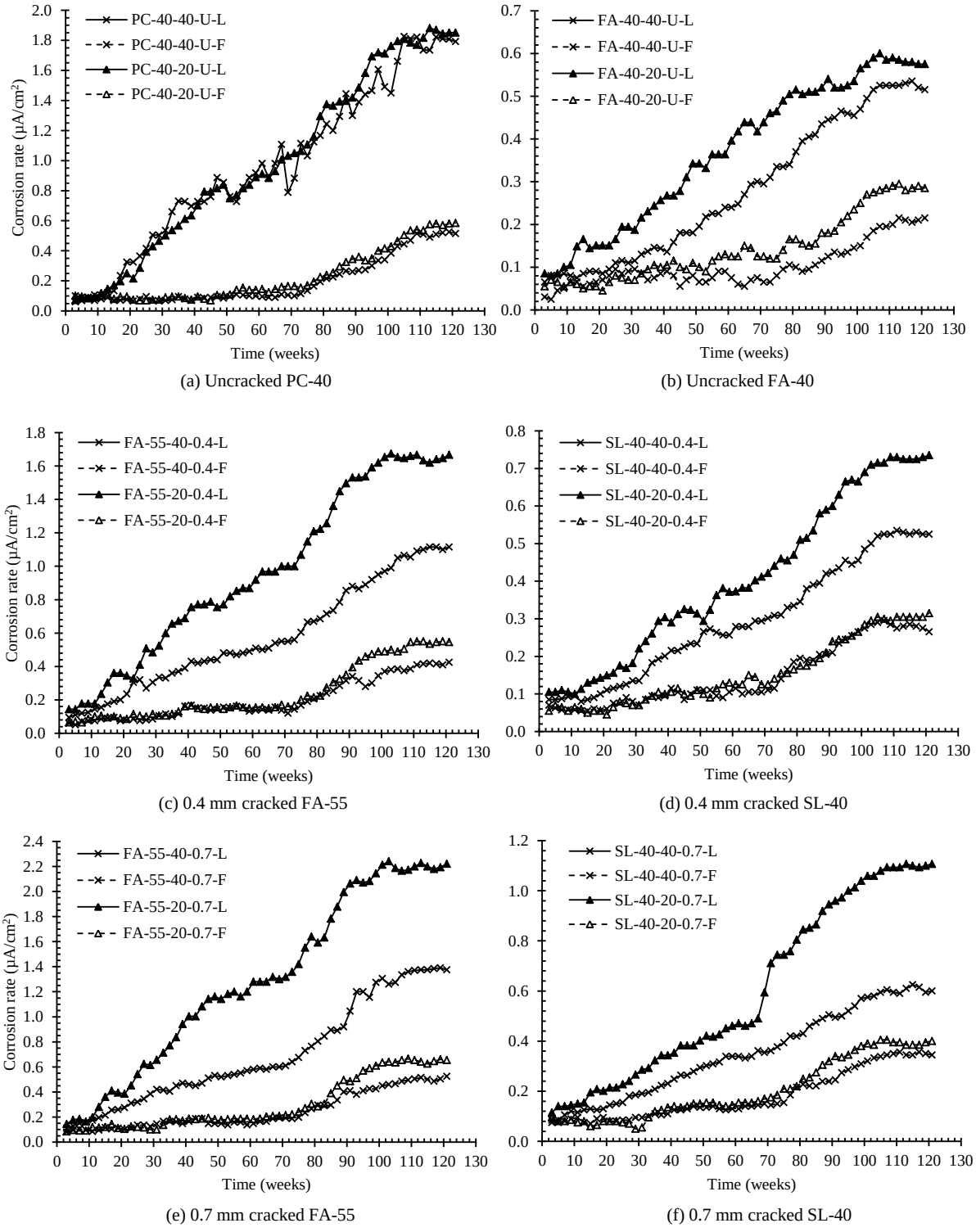

(a) Uncracked PC-40

(b) Uncracked FA-40

(c) 0.4 mm cracked FA-55

(d) 0.4 mm cracked SL-40

(e) 0.7 mm cracked FA-55

(f) 0.7 mm cracked SL-40

Figure 4.2: Typical corrosion rate time-development graphs

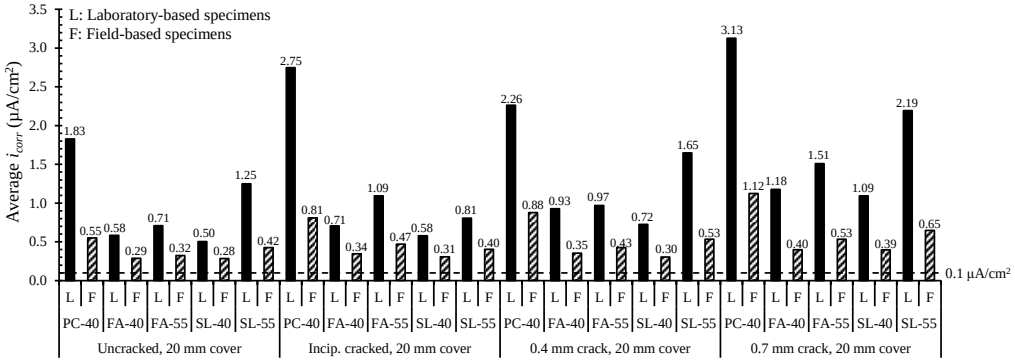

Figure 4.3: Average corrosion rates (week 104-120) for lab and field specimens with 20 mm cover (Note: Full size figure is provided in Appendix B)

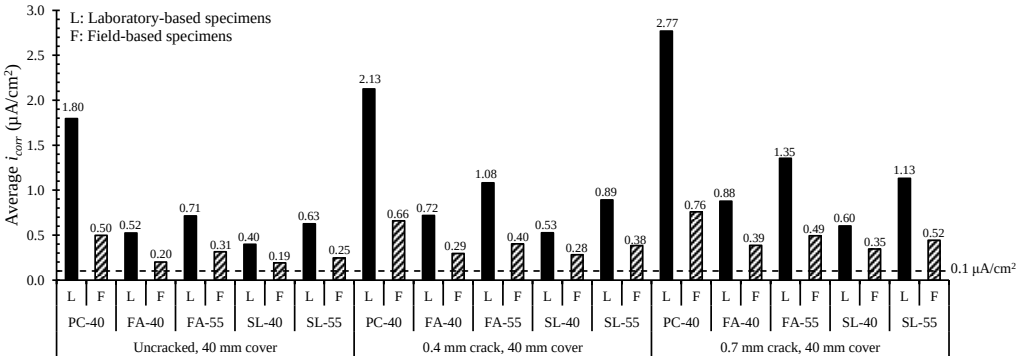

Figure 4.4: Average corrosion rates (week 104-120) for lab and field specimens with 40 mm cover (Note: Full size figure is provided in Appendix B)

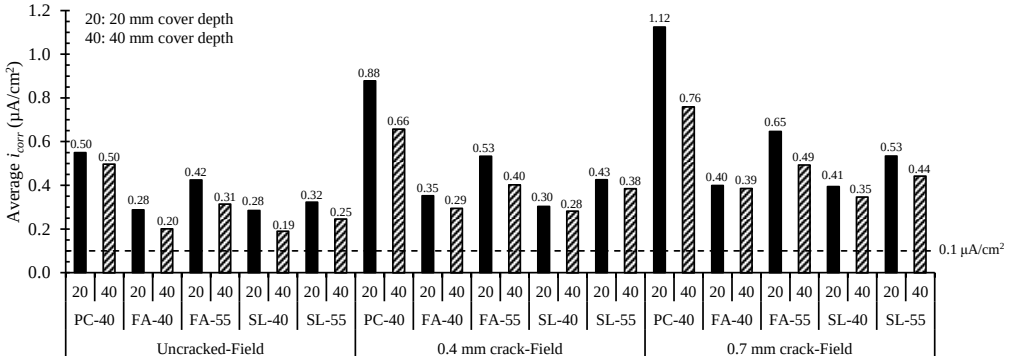

Figure 4.5: Average corrosion rates (week 104-120) for field specimens with 20 and 40 mm cover (Note: Full size figure is provided in Appendix B)

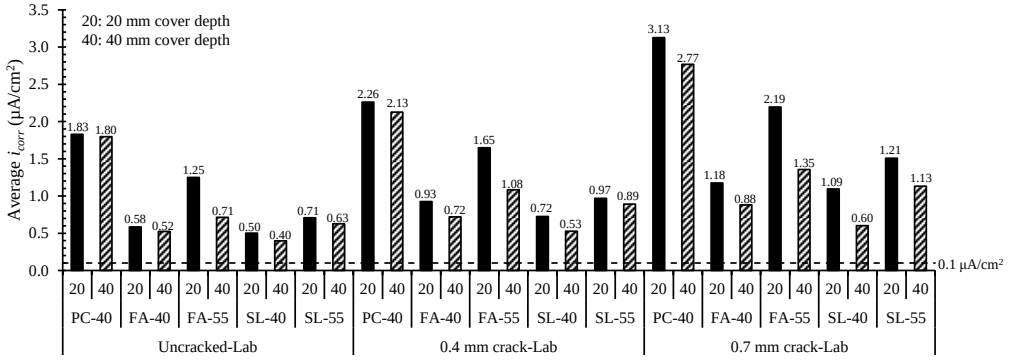

Figure 4.6: Average corrosion rates (week 104-120) for lab specimens with 20 and 40 mm cover (Note: Full size figure is provided in Appendix B)

In summary the following general trends were noted in the corrosion rate results obtained during the experimental period:

(i) In some specimens (both field-based and laboratory-based), after exposure to the respective environments, corrosion rates reverted to passive state (i_{corr} < 0.1 μA/cm^2) but later regained active state; the field-based specimens took a longer time to regain active corrosion state than the laboratory-based ones. At the end of the experimental period, all the specimens were actively corroding with the lowest average corrosion rates of 0.4 and 0.2 μA/cm^2 being in, respectively, the laboratory-based and field-based uncracked SL-40 specimens (40 mm cover).

(ii) Regardless of the exposure environment, corrosion rates increased with time but at a much slower rate in the field-based specimens than in the laboratory-based specimens (see Figure 4.2(a) to (f), and Appendix B for complete time-development results). The same trend was observed with the half-cell potential results where the field-based specimens became more negative with time but at a much slower rate than the laboratory-based ones.

(iii) Regardless of the exposure environment (laboratory or field), for a given cover depth and concrete quality, corrosion rate increased with increase in crack width. However, the corrosion rates for the field-based specimens were significantly lower than the corresponding laboratory-based ones. Furthermore, the effect of cover cracking on corrosion rate was, in most cases, higher in the laboratory-based specimens than in the field-based ones.

(iv) Regardless of the exposure environment, for a given crack width and concrete quality, corrosion rate increased with decrease in cover depth from 40 to 20 mm (see Figure 4.5 and Figure 4.6).

(v) Regardless of the exposure environment, for a given crack width and cover depth, corrosion rate increased with decrease in concrete quality. Specimens made using plain PC concrete (PC-40) had the highest corrosion rates compared to those for blended cement concretes (SL-40, SL-55, FA-40 and FA-55).

(vi) Up to approximately week 74, corrosion rates in the uncracked and cracked field-based specimens did not show a good correlation with half-cell potential as opposed to the laboratory-based ones where a good correlation was observed. During this period, corrosion rates in the field-based specimens were unstable (high fluctuation with time) as opposed to the laboratory-based ones which were stable. After this period (week 75-124), the field-based corrosion rates gradually increased and became more or less stable, and showed a relatively good correlation with half-cell potential.

(vii) At the end of the experimental period, no corrosion-induced cover cracking was observed in both the uncracked and cracked specimens.

4.3.2 *Induction and sustenance of active corrosion, and early-age corrosion rate trends*

The term *early-age* is used here to refer to corrosion rate trends *up to week 32*. Figure 4.7 to Figure 4.11 present corrosion rate results measured 5 hours after withdrawal of the anodic impressed current (IC) used to induce active corrosion in the specimens, and a measurable corrosion rate in the specimens after 2 weeks exposure in the respective environments. These results show that the specimens displayed corrosion rates in the range $0.10 \leq i_{corr} \leq 0.13$ μA/cm^2; an indication that active corrosion was successfully induced in the specimens. However, there were no general trends between corrosion rate and either cover depth (20 or 40 mm), w/b ratio (0.40 or 0.55) or binder type (PC, GGBS, FA).

The results also show that two weeks after exposure to the respective environments, corrosion rates in all the specimens dropped relative to those measured after withdrawal of the anodic IC (Figure 4.7 to Figure 4.11). Therefore, despite corrosion rates in all the field-based (tidal) and laboratory-based specimens being active (> 0.1 μA/cm^2) 5 hours after withdrawal of the anodic IC, after exposure in either the laboratory or tidal zone for two weeks, they all dropped, with some specimens reverting to passive corrosion state. No general trend was evident in the drop in corrosion rate in the specimens; the drop varied from specimen to specimen regardless of initial corrosion rate measured 5 hours after withdrawal of the anodic IC, concrete quality (binder type and w/b ratio) or cover depth. However, significant decreases were noted in the blended cement concrete specimens with 40 mm cover where the corrosion rates decreased to a passive state (by up to 60% in SL-40 uncracked field specimens with 40 mm cover i.e. SL-40-40-F) and in those with 20 mm cover (up to 50% in FA-40 uncracked field specimens with 20 mm cover i.e. FA-40-20-F). The effect of supplementary cementitious materials (SCMs) will be discussed in detail in Section 4.5.

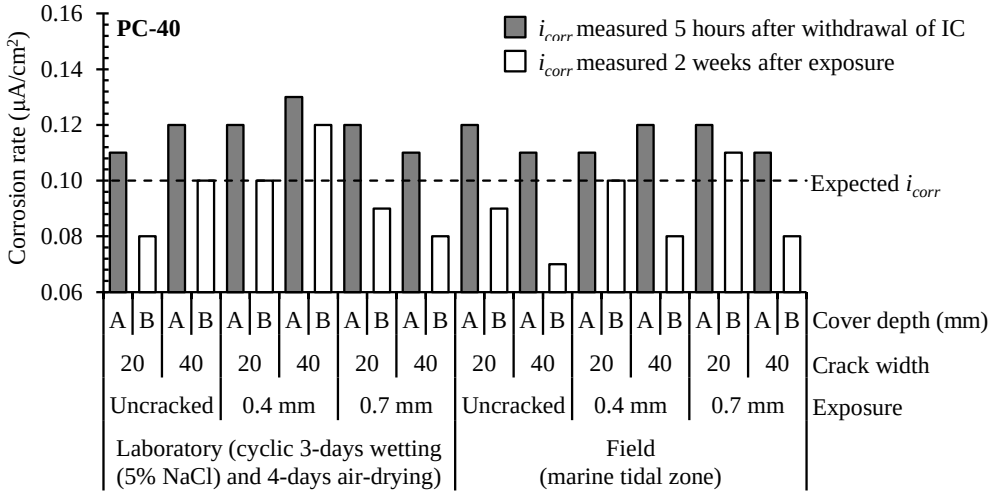

Figure 4.7: Corrosion rates measured 5 hours after withdrawal of impressed current – PC-40

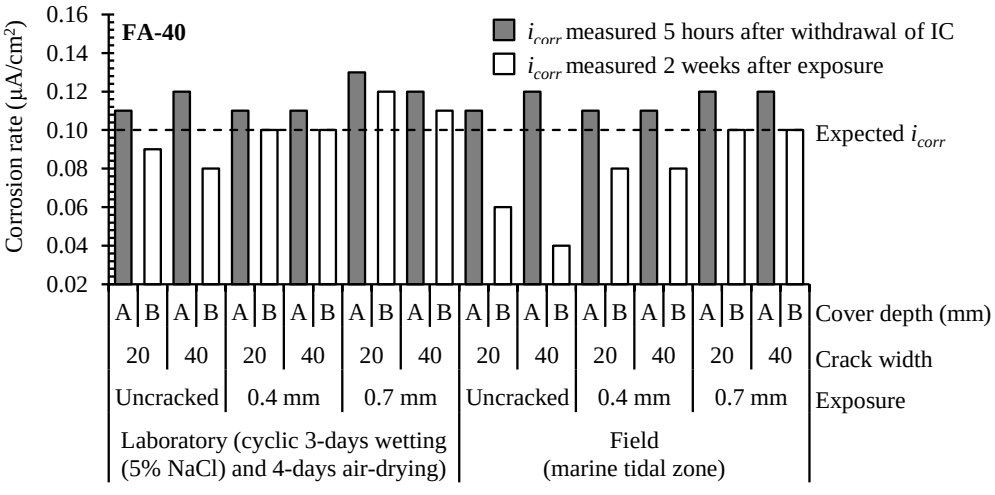

Figure 4.8: Corrosion rates measured 5 hours after withdrawal of impressed current – FA-40

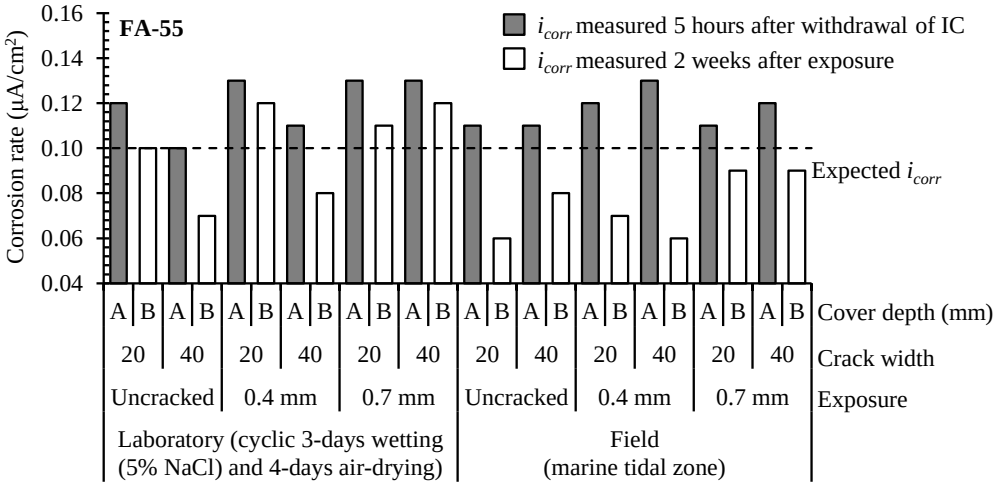

Figure 4.9: Corrosion rates measured 5 hours after withdrawal of impressed current – FA-55

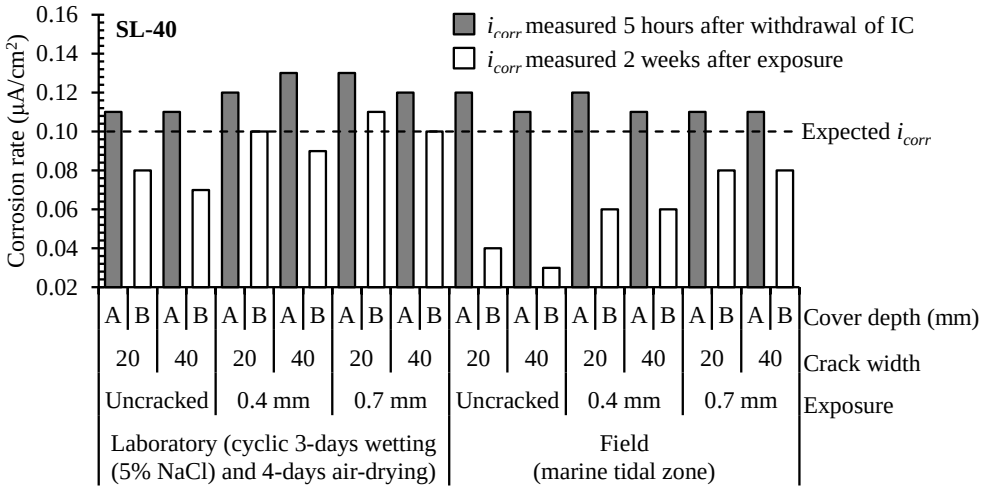

Figure 4.10: Corrosion rates measured 5 hours after withdrawal of impressed current – SL-40

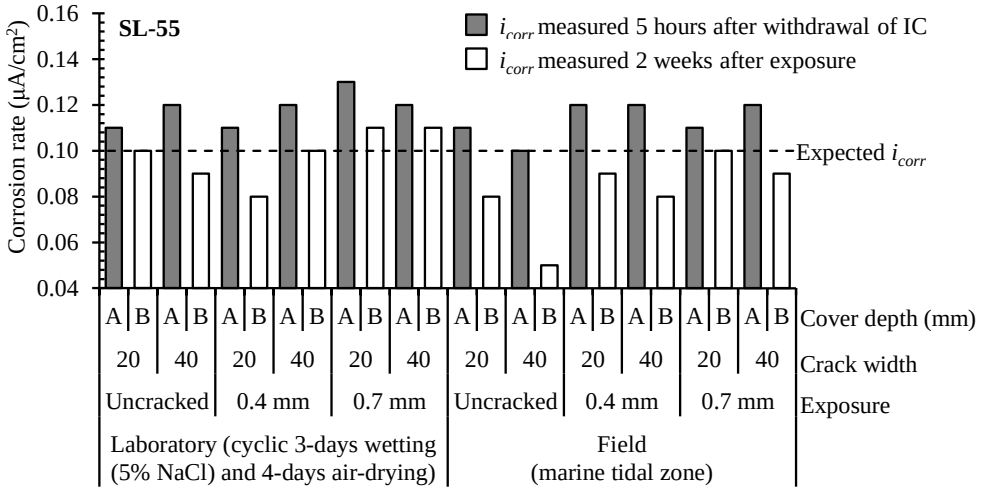

Figure 4.11: Corrosion rates measured 5 hours after withdrawal of impressed current – SL-55

The drop in corrosion rates in the field-based and laboratory-based specimens after withdrawal of the IC and exposure to the respective environments can be attributed to one or a combination of the following phenomena:

(i) Decrease in the availability of corrosion agents such as dissolved oxygen (especially in the uncracked specimens) to sustain the cathodic reaction. In the laboratory-based specimens, oxygen supply (if deficient) was enhanced during the drying period, and also due to a constant temperature (25 ± 2 °C) and relative humidity (RH, 50 ± 5%).

(ii) Tendency of the steel to revert to a passive corrosion state if the chloride content at the steel level is less than the chloride threshold. Even though the chloride concentration at the steel level was not measured after withdrawal of the IC due to the destructive nature of the test, it is plausible that after the 3.5 hours application of anodic IC, the chloride contents in some concretes may have not reached the threshold level.

(iii) Tendency of the corrosion rate (and potential) to decay and revert to equilibrium conditions (not necessarily passive corrosion state) after withdrawal of the IC. It would have been beneficial to continuously record the decay phase of the corrosion current in the specimens after the withdrawal of the anodic IC to see how long it took before reverting back to equilibrium. However, this was not possible due to unavailability of data-capture equipment, and should be explored in future studies.

Before proceeding, it is important to note that similar results depicting reduction in corrosion rate of steel with time (but in saturated concrete i.e. oxygen-deprived conditions) have been reported in the past by Raupach [1]. Similar trends were observed in the laboratory-based half-cell potential (HCP) measurements (i.e. decrease to less negative values) where temperature and relative humidity were controlled (see Appendix B for HCP vs. time trends). The field-based HCP measurements, as expected, were quite unstable and no general trend could be deduced from the early-age results. This unstable nature of HCP and its lack of a clear correlation with corrosion rate in the field-based specimens is due to the fact that both parameters respond differently to the same variables, particularly moisture (or oxygen availability), temperature and concrete resistivity. It must also be noted that past studies have shown that there is no general correlation between corrosion rate and half-cell potentials [2], and that although reliable relationships between corrosion rate and HCP can be obtained in the laboratory for well-conditioned experiments, such relationships cannot be generalized because wide variations in corrosion rate are possible in a narrow range of potentials. Typical HCP vs. time trends will be presented in Section 4.8.

After exposure in the respective environments for 20 weeks, some specimens that had displayed a passive corrosion state regained an active state with time. In general, after 20 weeks exposure:

(i) all the uncracked field-specimens except FA-55 (20 mm cover) remained in passive state (i.e. $i_{corr} < 0.1$ μA/cm^2).

(ii) all the laboratory-based specimens that reverted back to a passive state after withdrawal of IC were actively corroding after 20 weeks, with the exception of uncracked SL-40 and FA-40 specimens with 40 mm cover. These concretes had the lowest chloride conductivity values (presented later in Section 4.6) depicting low penetrability to chlorides and, in general, corrosion

species (O_2, H_2O). This, together with the high cover depth (40 mm) and uncracked state of these specimens, probably also contributed to the prolonged passive corrosion state in these specimens.

At the end of the experimental period (2¼ years), all the specimens exhibited an active corrosion state (see Figures B.1 to B.17 in Appendix B for i_{corr} vs. time trends).

4.3.3 *Temporal stabilization of corrosion rates*

Over the experimental period (122 weeks), nearly all the field-based specimens did not show significant increases in corrosion rate until around week 80 when notable steady increases were recorded (see Figure 4.2). Even though it was expected that corrosion rates in these specimens would significantly increase due to increase in temperature [3] during the first summer period between weeks 12 and 30 (see Figure C.1, Appendix C) when the maximum and minimum environmental temperatures increased from, respectively, 21 and 11 °C in week 12 to 26 and 16 °C in week 30, this was not the case. Most of the specimens continued to show passive corrosion states (i_{corr} < 0.1 μA/cm^2) which later became active but at varied times - corrosion rates in the uncracked and incipient cracked specimens took longer (up to 86 weeks after field exposure in the uncracked SL-40 specimens with 40 mm cover) to become active than in the 0.4 and 0.7 mm cracked ones (up to 16 weeks in the 0.7 mm cracked FA-55 specimens with 20 mm cover). The results showed that the time to re-gaining an active corrosion state was partly dependent on the cover depth, concrete quality (binder type and w/b ratio) and crack width - these will be discussed in detail later in this chapter. After gaining an active corrosion state, corrosion rates in the field-based specimens showed negligible increases up to around week 80 (end of a summer season, see Figure C.1 in Appendix C) when steady increases were experienced up to approximately week 100 (during a winter season, see Figure C.1 in Appendix C) when most specimens showed a pseudo-plateau phase. This phase was experienced in most of the specimens until the end of the experimental period (just after the commencement of a summer season, see Figure C.1, Appendix C). A typical plot of the seasonal variation of corrosion rate in the field-based specimens is shown in Figure 4.12.

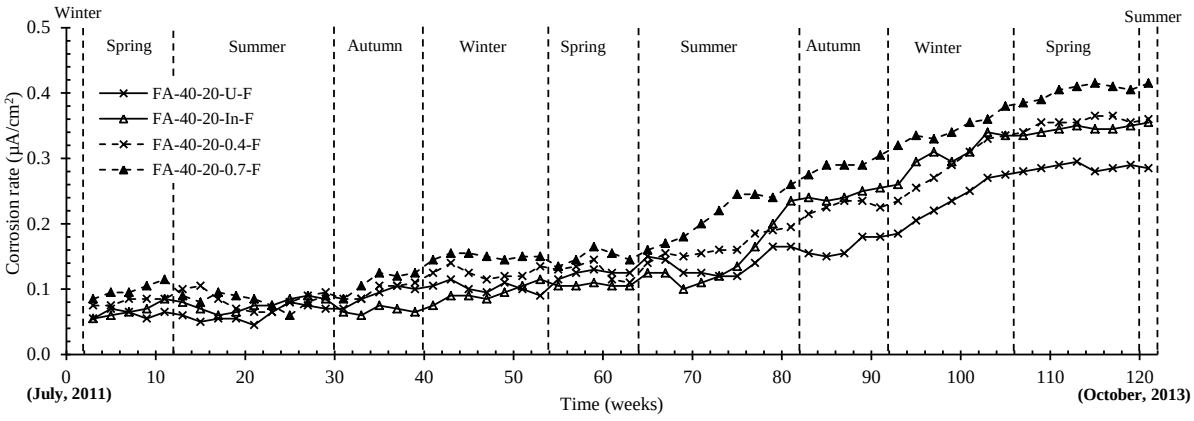

Figure 4.12: Typical trend of corrosion rates with time and seasonal changes in the field specimens

In the laboratory-based specimens, corrosion rates generally increased with time up to between weeks 100 and 122 when they gradually stabilized - see typical plots of corrosion rate vs. time in Figure 4.2. Corrosion rates in the uncracked specimens stabilized earlier than those in the cracked ones.

In summary, the following can be inferred from the temporal variation of corrosion rates in the field-based and laboratory-based specimens:

(i) Corrosion rates in the field-based specimens did not show a close correlation with the seasonal variations up to around week 70 when most specimens started to actively corrode. However, after week 70 when most field-based specimens were actively corroding, corrosion rates in these specimens showed a slight correlation with the seasonal variations, especially temperature changes.

(ii) The stabilization of corrosion rates in the laboratory-based specimens between weeks 100 and 122 can be attributed to the accumulation of corrosion products around the steel hence limiting its access to oxygen from the concrete surface. This also explains why the corrosion rates in the cracked specimens took a slightly longer time to stabilize compared to those in the uncracked ones. In the cracked specimens, corrosion products (at the anode) are exuded through the cracks hence exposing (to some extent) the non-corroded steel to corrosion agents leading to continued corrosion. In the laboratory-based specimens, rust stains were seen in the crack area in the cracked specimens (except the incipient-cracked). Rust stains were not observed in the uncracked specimens.

Temporal variations were also experienced in the resistivity and half-cell potential results. These will be discussed in, respectively, Sections 4.7 and 4.8.

4.4 *Effect of crack width on corrosion rate*

The literature reviewed in Chapter 2 showed that crack width (w_{cr}) affects corrosion rate - with increasing w_{cr} leading to increased corrosion rates but to an extent dependent on concrete cover, quality and resistivity. The latter mainly affects corrosion rate in blended cement concretes, which will be covered in subsequent sections. Both the laboratory and field corrosion rates followed this trend. Detailed results showing the variation of corrosion rate with time are given in Appendix B. Typical plots are shown in Figure 4.13 - note that Figure 4.13(a) does not have data for incipient-cracked specimens because these were only made for 20 mm cover.

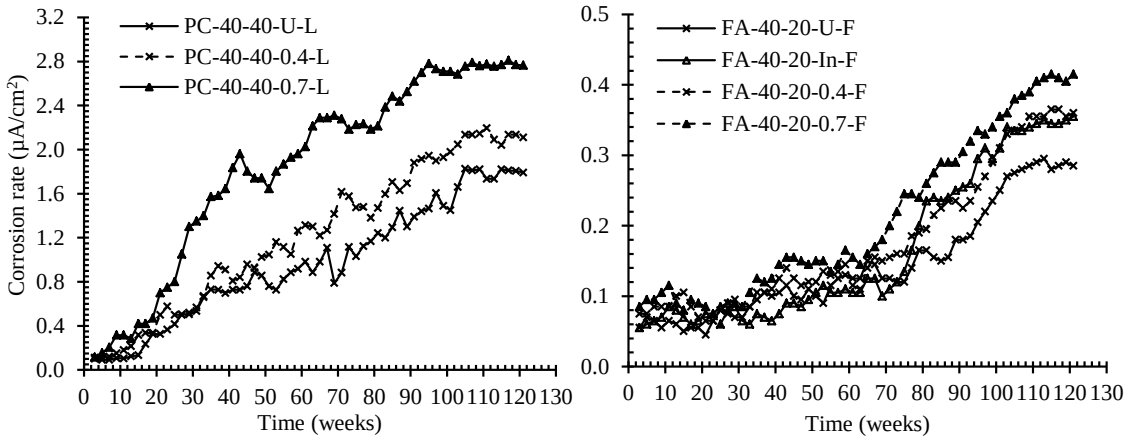

(a) PC-40 lab specimens (40 mm cover) (b) FA-40 field specimens (20 mm cover)

Figure 4.13: Typical plot – effect of crack width on corrosion rate

It is important to note that the results discussed here should be viewed taking into consideration that other crack characteristics such as frequency/density, self-healing potential and whether the crack is active or dormant may also influence corrosion rate. These crack characteristics were not considered as they were outside the scope of this study.

A comparison of the average corrosion rates (week 104-120) for specimens of the same exposure environment (laboratory or field), cover depth and concrete quality (binder type and w/b ratio) but different crack widths are presented in Figure 4.14 to Figure 4.18. The maximum and minimum i_{corr} presented in these figures were obtained from a statistical analysis of the measured results ($i_{corr,max} = i_{corr,average} + 1.96\sigma$, and $i_{corr,min} = i_{corr,average} - 1.96\sigma$ where σ is the standard deviation - the value 1.96 is obtained from a standard *t*-distribution table at a 95% confidence interval). These results are discussed in conjunction with the detailed ones presented in Appendix B.

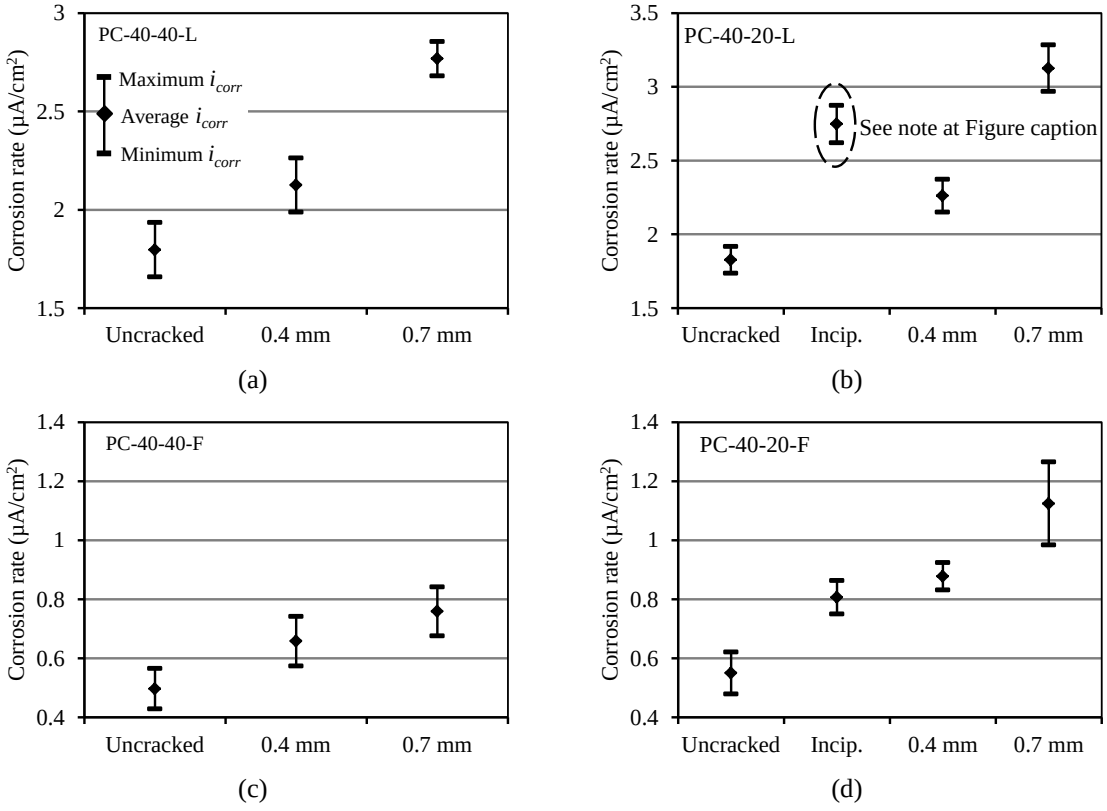

Figure 4.14: Average corrosion rates in uncracked vs. cracked - PC-40 specimens (L: lab, F: field)

Note on Figure 4.14(b): Corrosion rate for incipient-cracked PC-40 specimen with 20 mm cover was unexpectedly higher than for 0.4 mm cracked specimens. This was inexplicable and hence not used in the analyses.

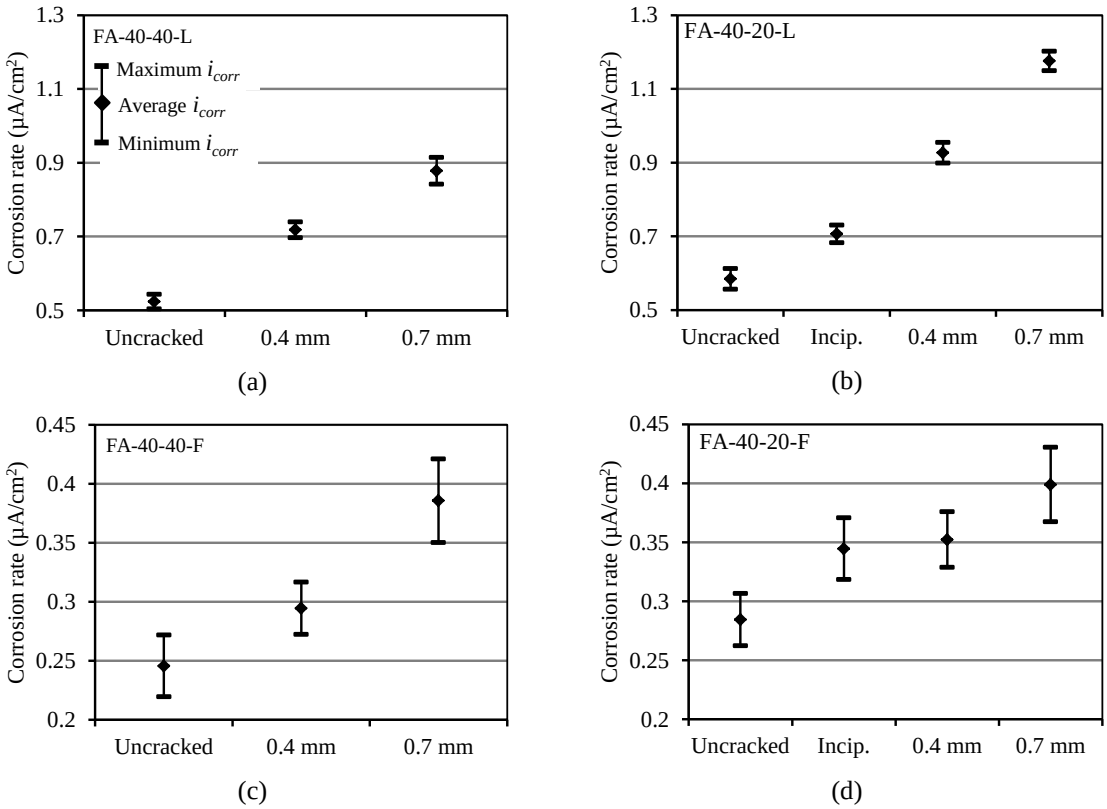

Figure 4.15: Average corrosion rates in uncracked vs. cracked - FA-40 specimens (L: lab, F: field)

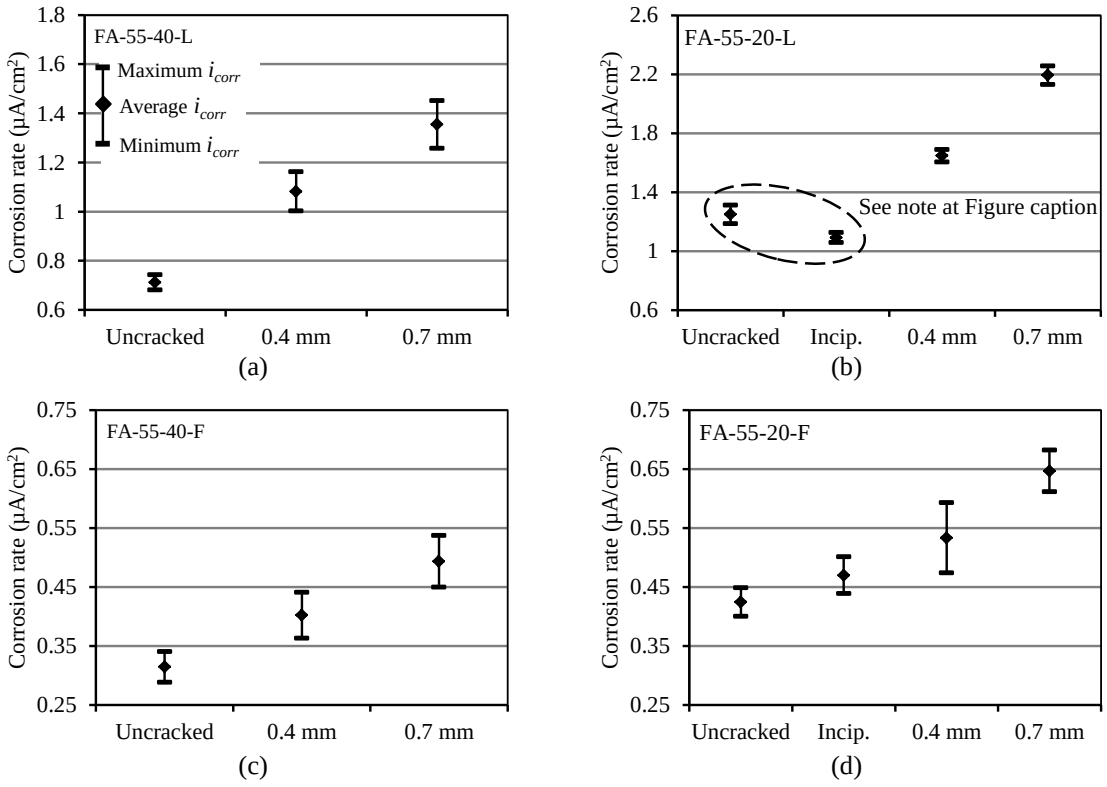

Figure 4.16: Average corrosion rates in uncracked vs. cracked - FA-55 specimens (L: lab, F: field)

Note on Figure 4.16(b): The trend between the average corrosion rate for incipient-cracked and uncracked FA-55 specimen with 20 mm cover was inexplicable, and ascribed to experimental anomalies.

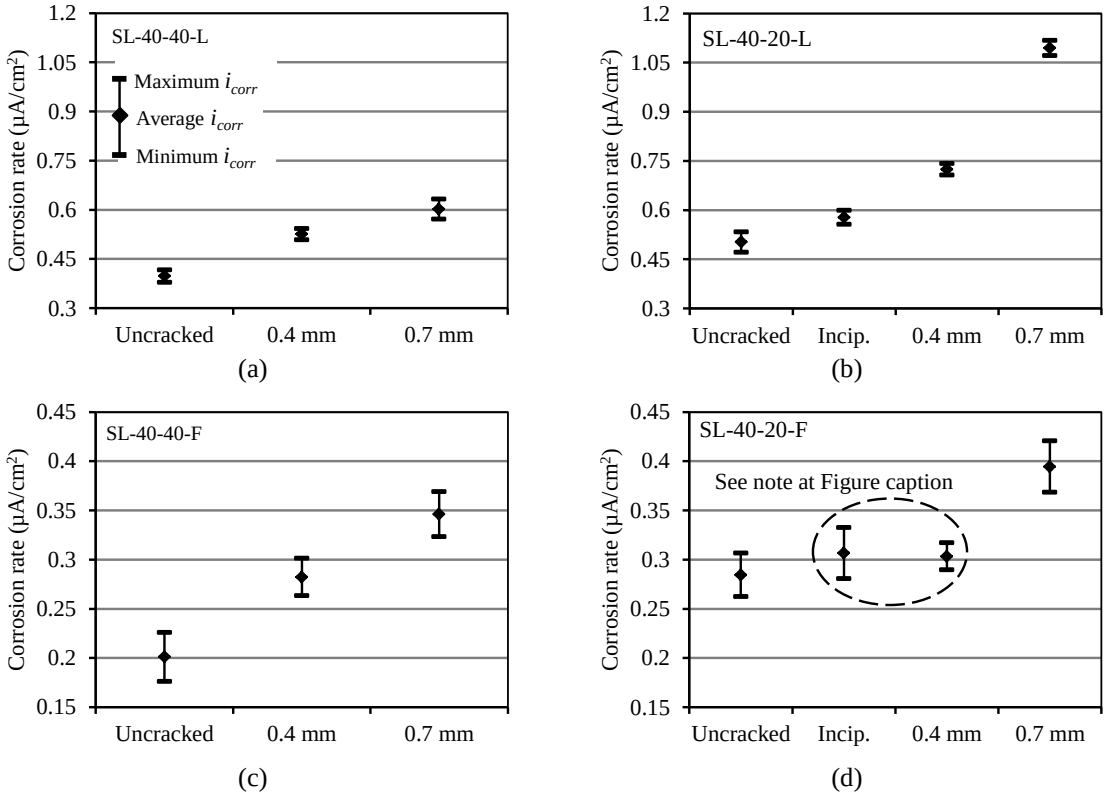

Figure 4.17: Average corrosion rates in uncracked vs. cracked - SL-40 specimens (L: lab, F: field)

Note on Figure 4.17(d): The statistical analysis shows that the average corrosion rates for incipient-cracked and 0.4 mm cracked SL-40 specimens with 20 mm cover were equal. This was unexpected taking into account the trends obtained in other specimens.

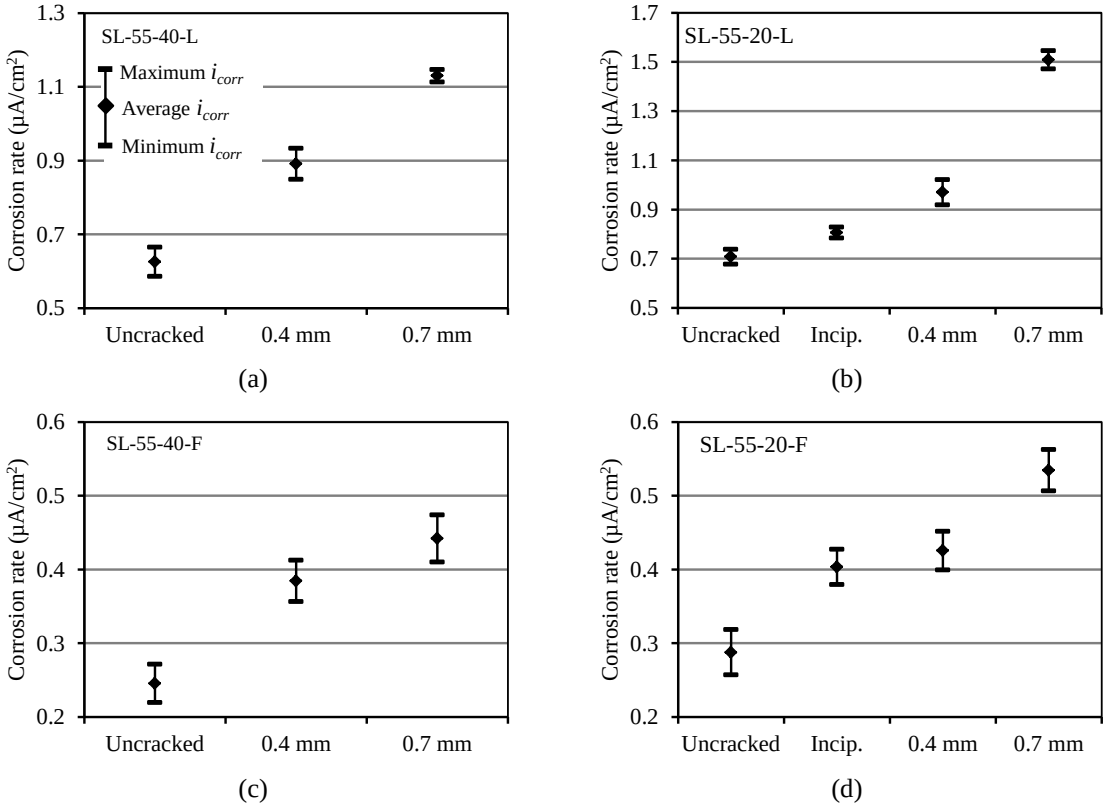

Figure 4.18: Average corrosion rates in uncracked vs. cracked - SL-55 specimens (L: lab, F: field)

The results show that regardless of the exposure environment (laboratory or field), for a given binder type, w/b ratio and cover depth, corrosion rates generally increased with increase in crack width (w_{cr}) in the order uncracked → incipient-cracked → 0.4 mm cracked → 0.7 mm cracked. However, for a given exposure environment, corrosion rate at a given crack width varied depending on the cover depth, binder type and w/b ratio - these are covered in the subsequent sections. In the presence of cover cracking, the impact of increasing cover depth may be substantially reduced. This was the case especially in the field-based specimens with 0.4 and 0.7 mm crack widths where, for a given concrete, corrosion rates in the specimens were similar regardless of the cover depth (the influence of cover depth on corrosion rate is discussed in detail in the next section). This observation motivates the need to consider both cover depth and crack width simultaneously at the design stage of a RC structure, as will be seen in Section 4.10. It also suggests that in in-service RC structures, for a given binder type, w/b ratio and cover depth, variations in crack width within a given range (not quantified in this study), for example 0.4 to 0.5 mm, may increase corrosion rate to similar extents relative to uncracked concrete; this will be explored further in Chapter 5 when a sensitivity analysis is carried out on the proposed corrosion rate prediction model. Further studies are required to verify this observation but the design implication of this finding is that depending on the concrete quality and cover depth, a given range of crack widths may have similar corrosion risks.

A summary of the effect of crack width on corrosion rate is presented in Table 4.1. The summary shows that in general, the presence of incipient cracks as opposed to uncracked specimens had a similar effect on corrosion rate in both the laboratory-based and field-based specimens. This was also the case for laboratory-based and field-based specimens where crack width increased from 0.4 to 0.7 mm. However, the results show that generally, increase in crack width from incipient-cracked to 0.4 mm had a relatively lesser effect on corrosion rate in the field-based specimens than in the corresponding laboratory-based ones. Even though not quantified in this study, it can be expected that, to a given degree, crack healing occurred in the incipient-cracked specimens. However, the results presented in Table 4.1 indicate that generally, this phenomenon may have occurred to a higher degree in the field-based specimens than in the laboratory-based ones. This can be attributed to the sealing of the cracks with debris in the sea-water. This was believed, to some extent, to have sealed the incipient cracks and limited the penetration of corrosion agents (mainly O_2 and H_2O) to the steel level hence leading to a reduction in corrosion rate in these specimens compared to the corresponding uncracked ones. However, further studies are necessary to ascertain and quantify the assumption of crack healing and its effect on decreasing corrosion rate. The 18%, 13% and 1% reductions in corrosion rates in, respectively, the laboratory-based PC-40 specimens with 20 mm cover, field-based FA-55 specimens with 20 mm cover and field-based SL-40 specimens with 20 mm cover due to the presence of 0.4 mm cracks are inexplicable. They were therefore not included in the general trends and conclusions drawn relating to the effect of cracking on corrosion rate. Based on this comparison (Table 4.1), no general trend on the effect of crack width on corrosion rate could be drawn between the laboratory-based and field-based specimens; in some cases, the percentage change was higher in the laboratory-based specimens while in other cases, the reverse was true.

Table 4.1: Summary of the effect of cracking and crack width on corrosion rate

Mix label	Cover (mm)	Percentage change in corrosion rate due to increase in w_{cr} (%)					
		Uncrack.→Incip. crack		Incip. crack→0.4 mm		0.4 mm→0.7 mm	
		Lab	Field	Lab	Field	Lab	Field
PC-40	20	+50	+47	**[b]	+9	+38	+28
	40	–*	–	–	–	+30	+15
SL-40	20	+15	+8	+25	**[c]	+51	+30
	40	–	–	–	–	+15	+23
SL-55	20	+14	+25	+20	+6	+56	+26
	40	–	–	–	–	+27	+15
FA-40	20	+21	+20	+31	+2	+27	+13
	40	–	–	–	–	+22	+31
FA-55	20	**[a]	+11	+51	+13	+33	+21
	40	–	–	–	–	+25	+23

* Note: Incipient-cracked specimens only made for 20 mm cover

** % change in i_{corr} not included because a reduction in i_{corr} due to increase in w_{cr} was obtained

[a]: -13%, [b]: -18%, [c]: -1%

From a practical point of view, it was necessary to investigate whether the corrosion rates in both the laboratory and field specimens were sensitive to the crack widths that were used. To achieve this, a statistical analysis at a 95% confidence interval was carried out based on the average corrosion rates (presented in Figure 4.3 and Figure 4.4). The results have already been presented in Figure 4.14 to Figure 4.18. These results show that in general, regardless of the exposure environment, for a given binder type, w/b ratio and cover depth, differences in average corrosion rates in specimens with different crack widths were not negligible. In a previous study by Scott and Alexander [4], corrosion rates for specimens of the same binder type, w/b ratio and cover depth but different crack widths (0.2 and 0.7 mm) were averaged even though a statistical analysis on their results clearly showed the averaging was not valid. The analyses presented here disapprove of averaging corrosion rates for the specimens with 0.4 and 0.7 mm crack widths (with a 75% difference). Even in the field-based specimens where corrosion rates were highly unstable, the 0.7 mm cracked specimens still had higher corrosion rates than the corresponding 0.4 mm cracked specimens. Based on this, these crack widths were dealt with separately. Furthermore, even from a practical or service life prediction point of view, taking into account that corrosion rate is an important input paramater in corrosion-induced damage prediction models, the decision on whether the corrosion rates in 0.4 and 0.7 mm cracked concrete should be averaged or not should be based on whether the limit state adopted (e.g. loss in steel cross section) is sensitive to change in corrosion rate due to slight change in crack width (e.g. from 0.4 to 0.7 mm), or not. The subject of quantification of the propagation phase will be covered in detail in Chapter 5 after a corrosion rate prediction model taking into account the influence of cover depth, crack width and concrete quality, and using the results presented in this chapter, is presented.

In order to compare the relative sensitivity of the different concretes (binder type and w/b ratio) with respect to the effect of increasing crack width on corrosion rate, the percentage increases in corrosion rates (due to increase in crack width) presented in Table 4.1 were plotted as shown in Figure 4.19 to Figure 4.22. In these figures, average i_{corr} in PC-40 specimens was used as a reference except in the

case of change in crack width from incipient-cracked to 0.4 mm cracked where PC-40 could not be used as a reference because of the inexplicable negative changes in i_{corr} due to increase in w_{cr} in some specimens (see Table 4.1). From these figures, it is evident that the increase in corrosion rate due to increase in crack width, regardless of the binder type, w/b ratio and cover depth, was higher in the PC concrete specimens than in the blended cement concrete specimens. In 71% and 64% of, respectively, the laboratory and field specimens, PC-40 showed a higher increase in corrosion rate due to increase in crack width than in the blended cement concrete specimens. However, considering the field-based specimens with 40 mm cover (Figure 4.22), it is evident that the effect of increasing crack width was higher in the blended cement concrete specimens than in the PC specimens. This trend was not observed in the field-based specimens with 20 mm cover (Figure 4.19). Even though a direct comparison cannot be made due to the variations in w/b ratios because PC concrete was only made using 0.40 w/b ratio, it can be inferred that, for high cover depths, the increase in increase in crack width had a higher effect on corrosion rate in the blended cement concretes than in the PC concrete ones. In the PC specimens, the relatively high penetrability of the concrete even in the absence of cracks seems to diminish the effect of increased crack width. On the contrary, in the blended cement concretes, their relatively low penetrability in the uncracked state is significantly increased in the presence of cracks, and further, due to increase in crack width. Concrete quality (binder type and w/b ratio) will be discussed in detail in Section 4.6. From Figure 4.19 to Figure 4.22, no specific trend on the effect of increase in crack width on corrosion rate is evident in the blended cement concretes.

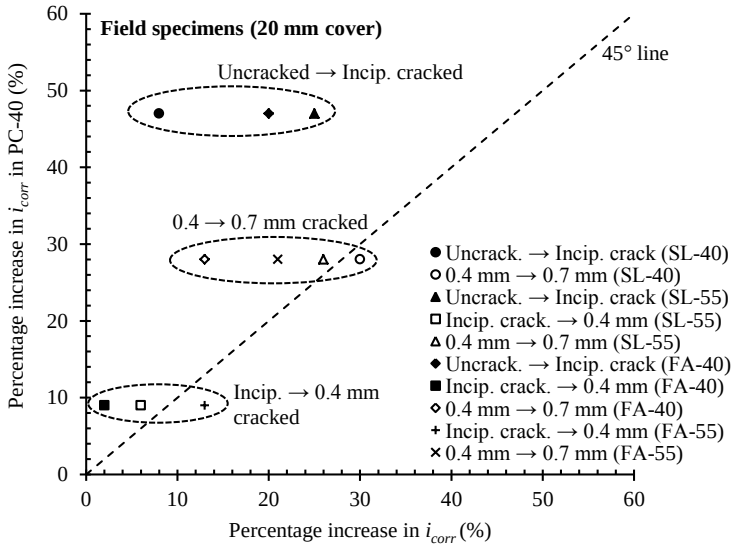

Figure 4.19: Effect of increase in crack width on i_{corr} in different concretes (Field, 20 mm cover)
(Note: average i_{corr} for PC-40 used as a reference)

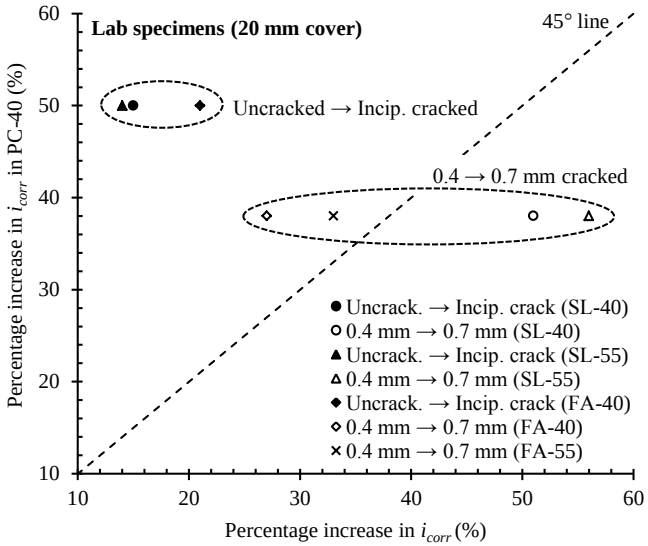

Note: A comparison due to change in crack width from incip. cracked to 0.4 mm, with PC-40 as a reference, is not made here because because the change in i_{corr} in the PC-40 lab specimens (20 mm cover) due to increase in crack width from incip.-crack. to 0.4 mm was negative. The comparison is made in the next figure.

Figure 4.20: Effect of increase in crack width on i_{corr} in different concretes (Lab, 20 mm cover) (Note: average i_{corr} for PC-40 used as a reference)

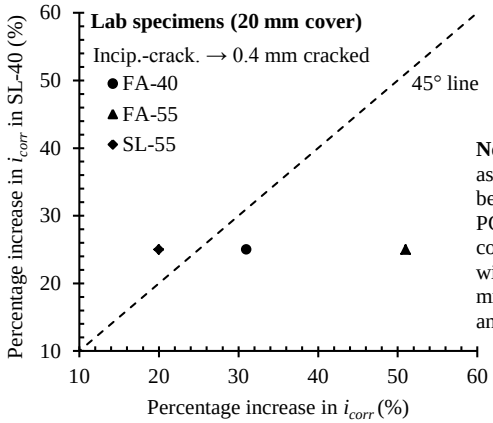

Note: SL-40 is arbitrarily chosen as a reference (*y-axis*) in this case because the change in i_{corr} in the PC-40 lab specimens (20 mm cover) due to increase in crack width from incip.-crack. to 0.4 mm was inexplicably negative, and could not used.

Figure 4.21: Effect of increase in crack width on i_{corr} in different concretes (Lab, 20 mm cover) (Note: average i_{corr} for SL-40 used as a reference)

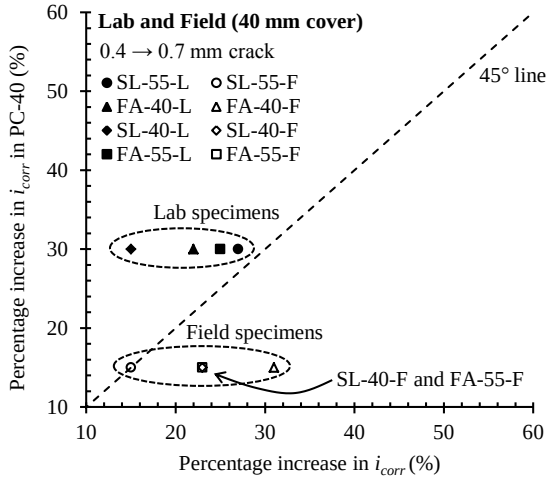

Note: The incip. cracked specimens were only made with 20 mm cover. Therefore, in the case of 40 mm cover, no comparison could be made for either change in crack width from uncracked to incip. cracked or incip. cracked to 0.4 mm.

Figure 4.22: Effect of increase in crack width on i_{corr} in different concretes (Lab and field, 40 mm cover) (Note: average i_{corr} for PC-40 used as a reference)

4.5 *Effect of cover depth on corrosion rate*

Cover depths of 20 and 40 mm were used in this study. The incipient-cracked specimens were made using only 20 mm cover. A comparison of the average corrosion rates for laboratory-based and field-based specimens with 20 and 40 mm cover depths is presented in Figure 4.23 to Figure 4.25. Even though these figures also depict the influence of binder type and w/b ratio, these will be discussed in Section 4.6.

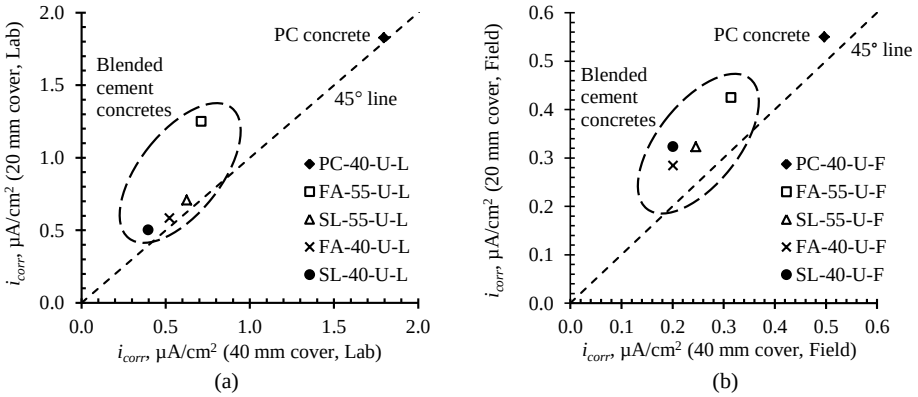

Figure 4.23: Comparison of i_{corr} for 20 and 40 mm cover – uncracked lab and field specimens

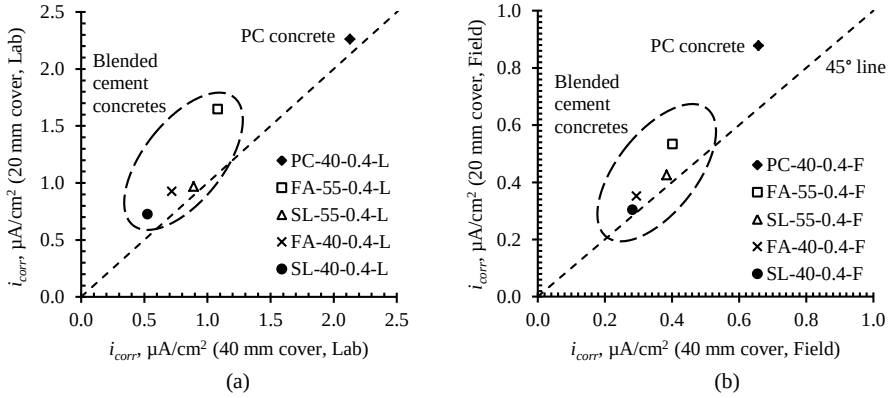

Figure 4.24: Comparison of i_{corr} for 20 and 40 mm cover – 0.4 mm cracked lab and field specimens

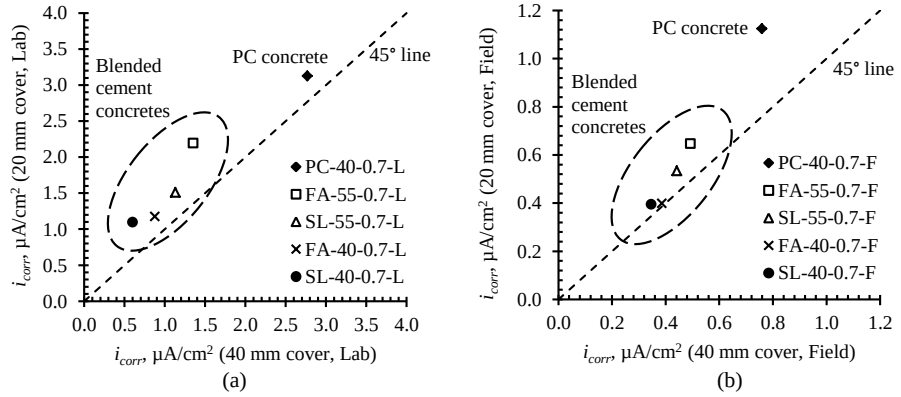

Figure 4.25: Comparison of i_{corr} for 20 and 40 mm cover – 0.7 mm cracked lab and field specimens

The results show that for a given combination of binder type, w/b ratio and crack width, corrosion rates in both the laboratory-based and field-based specimens increased with decrease in cover depth

(from 40 to 20 mm). Similar results have been obtained by Akatsuka *et al*. [5] and Scott and Alexander [4]. This trend is attributed mainly to the limited oxygen availability (as cover depth increases) to support the cathodic reaction during corrosion by increasing its travel path from the concrete surface to the steel level. This phenomenon is applicable to both the uncracked and cracked specimens because even in cracked concrete, the cathodes are mainly located in the uncracked concrete regions [6]. This was covered in detail in Chapter 2. The results also show that for a given combination of crack width, binder type and w/b ratio, even though increasing cover depth was expected to have a significant impact in the uncracked specimens, this was not the case.

Table 4.2 summarizes the impact of increasing cover depth on corrosion rate. These results are similar to those obtained by Scott and Alexander [4]; the results of Scott and Alexander [4] were presented and discussed in detail in Chapter 2. In general, in the laboratory-based specimens, the highest reductions in corrosion rates as a result of increased cover depth were recorded in the blended cement concrete specimens. This contradicts previous findings in the study by Scott and Alexander [4] where the highest reductions in corrosion rates as a result of increased cover depth were recorded in the plain Portland cement concretes (see Table 4.2). It is not clear why this trend was reversed in this study. However, this trend was not observed in the field-based specimens where no specific trend was evident. The 17% increase in corrosion rate due to increase in cover depth from 20 to 40 mm in the uncracked field-based FA-55 specimens was inexplicable. Comparing the effect of increasing cover depth in the laboratory-based and field-based specimens, Table 4.2, shows that in both the 0.4 and 0.7 mm cracked specimens, there was no consistent trend. However, in the uncracked specimens, the field-based specimens exhibited higher reductions in corrosion rate than the corresponding laboratory-based ones. Remember that previously in Section 4.4, we saw that in the field-based specimens with 20 mm cover, increase in crack width from 0 (uncracked) to incipient-cracked showed the highest percentage increase in corrosion rate compared to either an increase from incipient-cracked to 0.4 mm or 0.4 to 0.7 mm (see Figure 4.19). These results show a dominating influence of cover depth in these specimens and that even incipient-cracks can significantly increase corrosion rate.

Table 4.2: Effect of increasing cover depth on corrosion rate

Crack width	Mix label	% reduction in i_{corr} due to change in cover from 20 to 40 mm (at constant w_{cr})	
		Lab specimens	Field specimens
Uncracked	PC-40	2	10
	SL-40	21	33
	SL-55	12	24
	FA-40	10	30
	FA-55	43	-17
0.4 mm	PC-40	6	25
	SL-40	27	7
	SL-55	8	10
	FA-40	23	16
	FA-55	34	25
0.7 mm	PC-40	11	33
	SL-40	45	12
	SL-55	25	17
	FA-40	25	3
	FA-55	38	24

4.6 *Effect of binder type and w/b ratio on corrosion rate*

Concrete quality (binder type and w/b ratio) was quantified using the chloride diffusion coefficients determined from the rapid chloride conductivity index (CCI). CCI is used as a measure of the resistance of concrete to chloride ingress by diffusion, with an increase in the CCI value depicting a decrease in chloride penetration resistance. It is an indirect measure of concrete resistivity and can therefore be correlated to corrosion rate. It is empirically correlated to the chloride diffusion coefficient (see Appendix D for details of the empirical model) taking into account the effect of marine exposure environment, concrete ageing and binder type [7, 8] i.e. the empirical model has a capability of estimating the time- and exposure-dependent apparent chloride diffusion coefficient for commonly used binder types and marine exposure environments in South Africa.

The empirical model is currently used for service life prediction defined based on the time to corrosion initiation [9, 10] but recent studies have also shown that it exhibits a good correlation with corrosion rate [11, 12]. The good correlation between CCI and corrosion rate can be attributed to the fact that, (i) it is theoretically the inverse of concrete resistivity which is inversely proportional to corrosion rate [13], and (ii) through the chloride diffusion coefficient, it can fundamentally be used to depict relative penetrabilities of concretes made using different binder types and w/b ratios. Concrete penetrability determines the ease of ingress of corrosion-sustaining agents (mainly oxygen and moisture) through non-saturated concrete during the propagation period.

Concretes made using different supplementary cementitious materials (e.g. FA, GGBS) can exhibit the same CCI but different diffusion coefficients mainly due to differences in chloride binding capacities [7, 14]. This poses a major challenge if the CCI is to be used as an input parameter in a corrosion initiation or propagation prediction model. In this study, the objective was to characterize concrete quality so that it can be incorporated in the corrosion rate prediction model which will be presented in Chapter 5. Therefore, in order to differentiate between the different binders, the equivalent diffusion coefficients of the CCI values of different binders were determined using the empirical relationship (in Appendix D) between the two parameters. It is important to underscore that *the diffusion coefficients of the concretes, even when correlated to corrosion rate (later in Section 4.6.1), was be used to solely depict the relative penetrabilities of the different concretes to corrosion-sustaining agents* and not to quantify a specific transport parameter as is usually the case in Fickian-based corrosion initiation prediction models.

Both the 28-day and 90-day CCI values were measured for all the concretes. The results obtained (Figure 4.26) show that both binder type and w/b ratio affect the CCI value and hence the penetrability of the concrete. The trend in diffusion coefficient values (D_{90}) presented in Table 4.3 (obtained from the 90-day CCI values) for the various concrete mixes, in increasing order i.e. decreasing concrete quality, was as follows: SL-40 → SL-55 → FA-40 → FA-55 → PC-40. The diffusion coefficients obtained from the 28-day CCI were presented in Chapter 3, and follow the same trend. The diffusion coefficients obtained from the 90-day CCI were used here to account for the slow rate of maturity of the FA and GGBS concretes. In general, for a given binder, diffusion coefficient values decreased with decreasing w/b ratio (from 0.55 to 0.40) and with increasing age (from 28 to 90 days). Furthermore, the blended cement concretes had lower diffusion coefficients than PC concrete. This trend is

attributed to the refined microstructure and higher chloride binding capacity in the blended cement concretes than in plain PC concrete [15, 16]. These results depict the effectiveness of the different SCMs used i.e. fly ash (FA) and GGBS. The diffusion coefficient values for GGBS concretes (SL-40 and SL-55) were lower than those for fly ash concretes (FA-40 and FA-55). This means that for the replacement levels used, GGBS concrete can be expected to have better durability performance than FA concrete with respect to ingress of chlorides and other corrosion agents (moisture and oxygen).

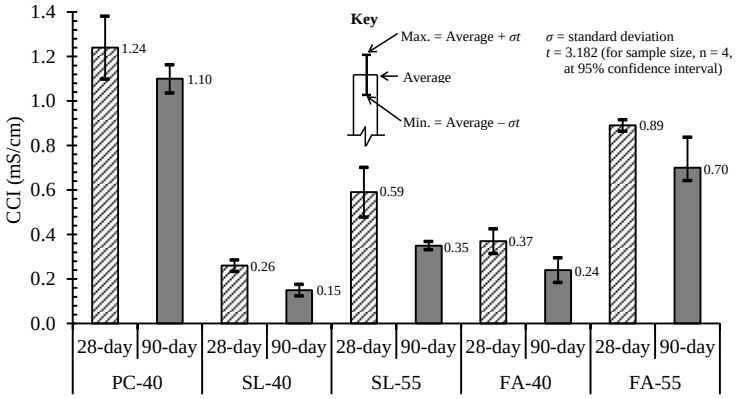

Figure 4.26: 28 and 90-day chloride conductivity index results

Table 4.3: Chloride diffusion coefficients for the concretes used

Mix label	Diffusion coefficient (cm^2/s) x 10^{-10} (determined from 90-day chloride conductivity index)
PC-40	47.4
FA-40	9.6
FA-55	14.8
SL-40	7.0
SL-55	8.4

For a given cover depth and crack width, corrosion rate generally increased with decrease in concrete quality in the order SL-40 → FA-40 → SL-55 → FA-55 → PC-40. This trend is similar to that obtained for the diffusion coefficients already presented. However, these results show that in cracked RC, quality alone cannot be used to predict durability performance with respect to reinforcement corrosion. A similar conclusion was arrived at in a similar experimental study by Otieno [11, 17]. In cracked concrete, corrosion of steel depends on the availability of oxygen, not in the crack region (which mainly hosts the anodes [18-20]), but in the surrounding concrete away from the crack (which hosts mainly the cathodes) and hence, on the rate at which oxygen can diffuse through the cover concrete. Furthermore, the influence of concrete resistivity, covered in Section 4.7, is also important.

For both cracked and uncracked specimens, the results show that concrete quality influences corrosion rate and can be used to control its propagation. Specifically, the use of blended cement concretes is more effective in controlling steel corrosion than plain PC concretes as was mentioned previously - see Figure 4.27 to Figure 4.30. These figures also show that there was a significant difference between the corrosion rates for specimens made with plain PC concrete (PC-40) and those made with blended cement concrete (SL-40 and FA-40) in comparison to those for blended cement concretes.

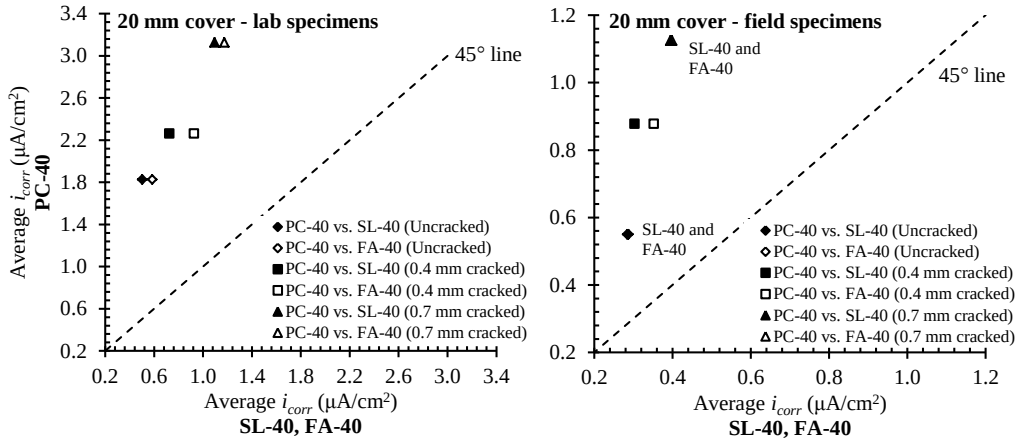

Figure 4.27: Comparison of average i_{corr} for PC-40, and SL-40 and FA-40 specimens (20 mm cover) (Note: average i_{corr} for PC-40 used as reference)

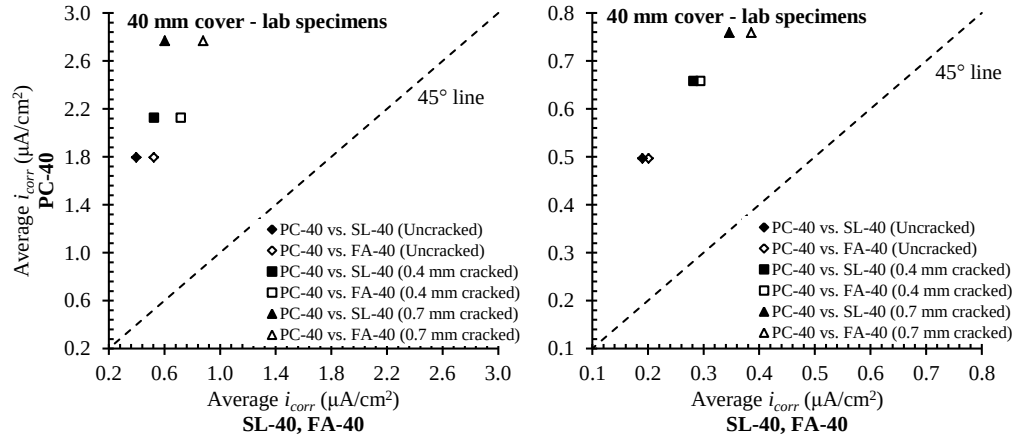

Figure 4.28: Comparison of average i_{corr} for PC-40, and SL-40 and FA-40 specimens (40 mm cover) (Note: average i_{corr} for PC-40 used as reference)

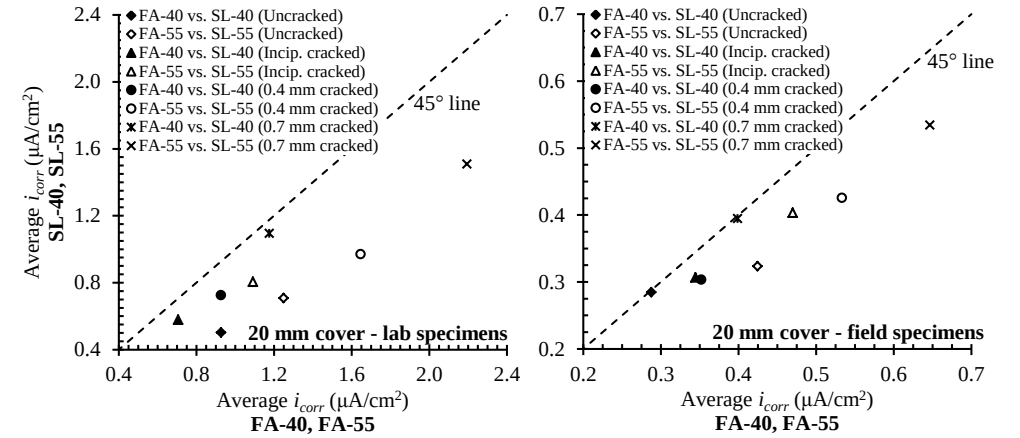

Figure 4.29: Comparison of average i_{corr} for blended cement concrete specimens (20 mm cover) (Note: average i_{corr} for PC-40 used as reference)

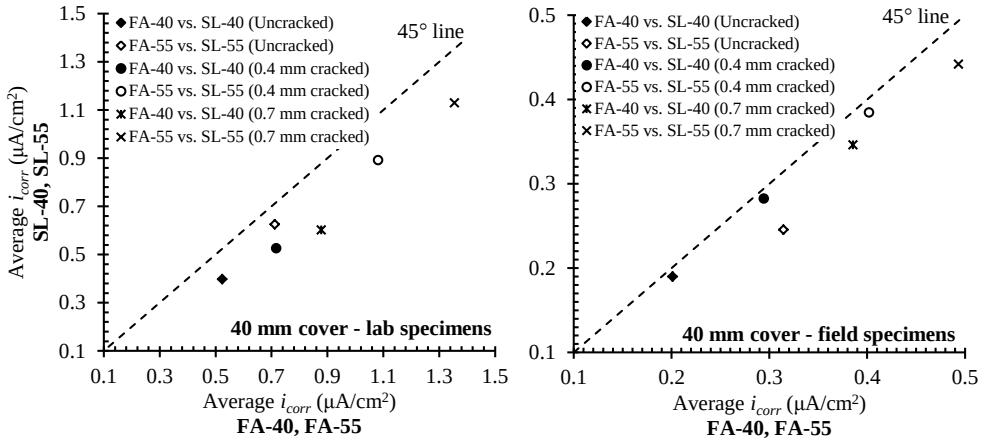

Figure 4.30: Comparison of average i_{corr} for blended cement concrete specimens (40 mm cover)
(Note: average i_{corr} for PC-40 used as reference)

In addition, Figure 4.23 to Figure 4.25 presented previously in Section 4.5 showed a distinct trend in corrosion rates for both the laboratory-based and field-based specimens made with blended cement concretes regardless of the w/b ratio. In both cases, corrosion rates for the blended cement concretes were in most cases clustered together and isolated from those of PC concretes. These results also show that for a given supplementary cementitious material (SCM), even though reducing the w/b ratio further increases the concrete's quality and hence decreases corrosion rate, the effect is small compared to that of the presence of the SCM itself. This suggests that the high concrete resistivity in blended cement concretes has a major influence on corrosion rate than concrete quality due to change in w/b ratio (resistivity results will be presented in Section 4.7).

A summary of the influence of concrete quality on corrosion rate is presented in Table 4.4 and Table 4.5. The effect of concrete quality on corrosion rate is compared by considering both the change in binder type for a given w/b ratio, crack width and cover depth (Table 4.4), and the change in w/b ratio for a given binder type, crack width and cover depth (Table 4.5). The latter comparison is only carried out for the fly ash and slag specimens because PC concrete was only made using 0.40 w/b ratio.

Table 4.4: Effect of change in binder type on corrosion rate

Crack width and exposure		Percentage reduction in i_{corr} due to change in binder type (at a constant w/b ratio and cover)			
		PC-40 → FA-40		PC-40 → SL-40	
		20 mm	40 mm	20 mm	40 mm
Uncracked	Lab	68	71	73	78
	Field	48	60	48	62
Incipient crack	Lab	74	–*	79	–
	Field	57	–	62	–
0.4 mm	Lab	59	66	68	75
	Field	60	55	65	57
0.7 mm	Lab	62	68	65	78
	Field	65	49	65	54

* Incipient-cracked specimens were only made with 20 mm cover

Table 4.5: Effect of change in w/b ratio on corrosion rate

Crack width and exposure		Percentage reduction in i_{corr} due to change in w/b ratio (for a given binder type and cover)			
		FA-55 → FA-40		SL-55 → SL-40	
		20 mm	40 mm	20 mm	40 mm
Uncracked	Lab	53	27	29	36
	Field	32	60	12	23
Incipient crack	Lab	35	–*	28	–
	Field	27	–	24	–
0.4 mm	Lab	44	27	25	41
	Field	34	35	29	27
0.7 mm	Lab	46	22	27	47
	Field	38	22	26	22

* Incipient-cracked specimens were only made with 20 mm cover

Table 4.4 shows that regardless of the exposure environment, for a given w/b ratio, cover depth and crack width, partial replacement of PC with either FA (30%) or GGBS (50%) led to significant reductions in corrosion rate. The results also show that there was no marked difference in the changes in corrosion rate between the field-based and laboratory-based specimens due to partial replacement of PC with either FA (30%) or GGBS (50%). These results show that accelerated corrosion by cyclic wetting (with a chloride-based salt solution) and drying that was used in this study is sensitive to change in concrete quality due to replacement of plain PC with blended cements (or change in w/b ratio as will be seen later) - this may not be the case with other accelerated corrosion techniques such as the use of anodic impressed current (see Chapter 2, Part II where accelerated corrosion techniques were reviewed).

With respect to effect of change in concrete quality due to change in w/b ratio on corrosion rate, the analysis presented in Table 4.5 shows that both the blended cement concretes generally respond to changes in w/b ratio in a similar manner. Similar results have been reported in previous studies by Otieno *et al*. [11] and Somma *et al*. [21].

These results also suggest that for a given cover depth, there can be a number of possible combinations of corrosion-influencing parameters (e.g. crack width and concrete quality) that can be used to control corrosion rate hence the need to simultaneously consider their influence. This aspect is covered in Section 4.10. The effect of crack width is also evident in the analyses presented in Table 4.4 and Table 4.5, especially for the 0.4 and 0.7 mm cracked specimens, but these were discussed in detail in Section 4.4.

4.6.1 *Correlation between concrete quality and corrosion rate*

Even though both 28-day and 90-day chloride conductivity tests were carried out, only the 90-day CCI values, C_{90}, (and consequently the chloride diffusion coefficients determined from the 90-day CCI, D_{90}) were used in the correlation analyses between corrosion rate and concrete quality. This was done to account for the slow rate of maturity of the FA and GGBS concretes; a study by Mackechnie [8] also found out that the CCI of these concretes are reasonably stable at this age. Concrete quality was therefore represented using D_{90}. Correlations of average corrosion rate and concrete quality (D_{90}) are

presented in Figure 4.31 to Figure 4.34. The trendlines shown in these figures were obtained by regression analysis (least squares method) to find the line of best fit (see Appendix E for details).

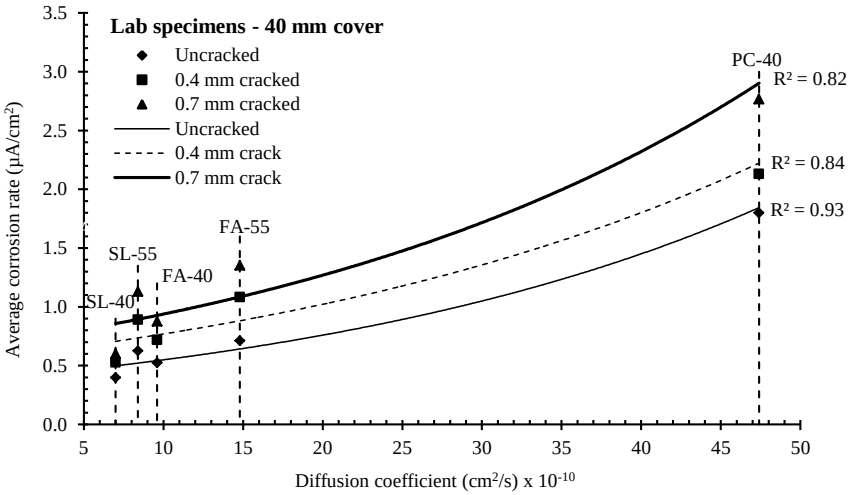

Figure 4.31: Average corrosion rate vs. diffusion coefficient (lab specimens, 40 mm cover)

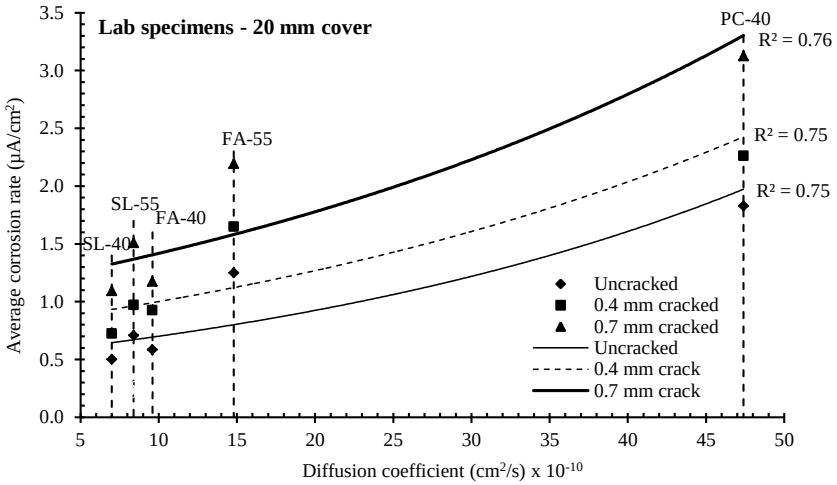

Figure 4.32: Average corrosion rate vs. diffusion coefficient (lab specimens, 20 mm cover)

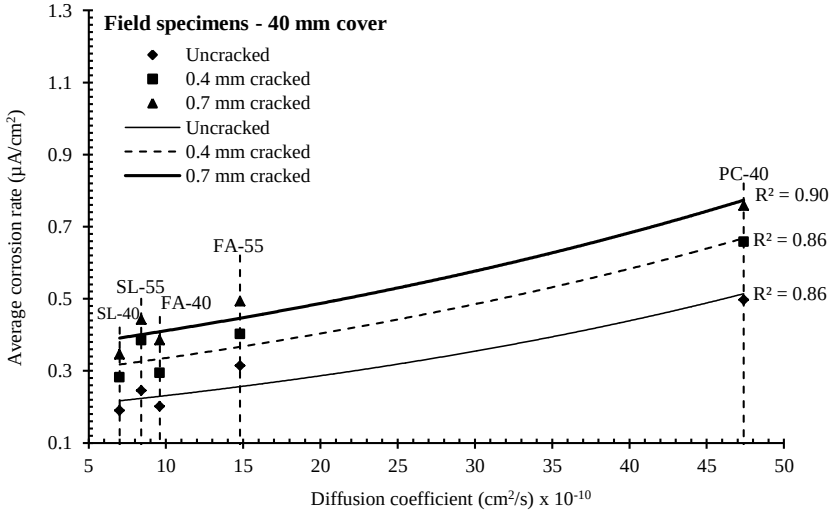

Figure 4.33: Average corrosion rate vs. diffusion coefficient (field specimens, 40 mm cover)

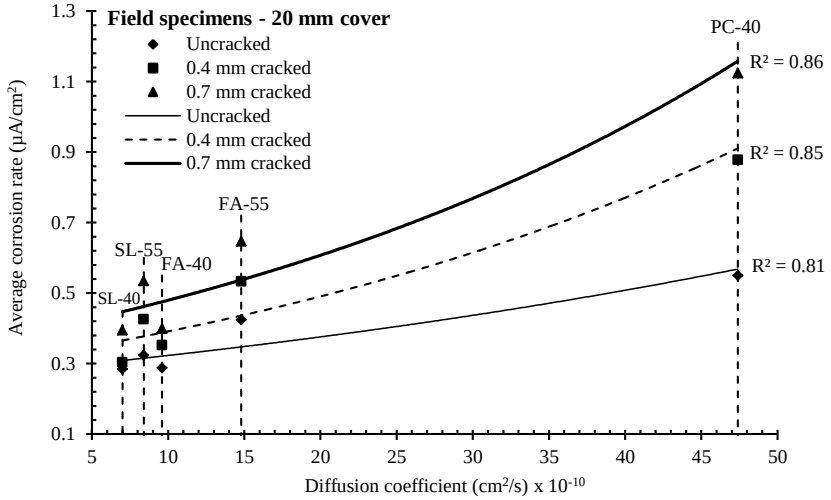

Figure 4.34: Average corrosion rate vs. diffusion coefficient (field specimens, 20 mm cover)

The analyses show that in both the field-based and laboratory-based specimens, irrespective of binder type, there exists a reasonably good correlation (R^2 generally > 0.7)[4] between the D_{90} and corrosion rate for a given crack width and cover depth. For a given binder type and the corresponding D_{90} value, corrosion rate increases with increasing crack width. However, even though there is a high correlation between corrosion rate and D_{90}, the latter cannot be used in isolation to predict durability performance especially in cracked concrete. Other factors affecting corrosion rate such as cover depth and crack width must also be taken into account. The trends shown in Figure 4.31 to Figure 4.34 between corrosion rate and D_{90} (concrete quality) can be expressed as follows:

$$i_{corr} = k_1 e^{A_1\left(D_{90}\times 10^{10}\right)} \ [\mu A/cm^2] \tag{4.1}$$

where k_1 ($\mu A/cm^2$) and A_1 (s/cm^2) are coefficients whose values are dependent on cover depth (20 or 40 mm), crack width (0.4 or 0.7 mm) and exposure environment (laboratory and field). As mentioned previously, the chloride conductivity value used to determine the diffusion coefficient, D_{90}, is obtained using uncracked concrete specimens, and even though high correlation factors can be obtained between corrosion rate and D_{90} even in the cracked specimens, the influence of cracking (and cover depth) should be taken into account to predict a realistic durability performance. Therefore, even though these results show that D_{90} can be used as an input parameter in corrosion rate prediction model (to depict concrete quality), the effect of cracking and cover depth should also be incorporated. This will be discussed further in Section 4.10 and in Chapter 5.

4.7 *Concrete resistivity results*

Concrete resistivity is also an important factor that influences corrosion rate of steel in RC structures. Previous studies have shown that high concrete resistivity can stifle the cathodic reaction process by limiting the flow of OH^- ions in the concrete pore solution [4, 16, 22, 23]. Concrete resistivity is

[4] R^2 gives a measure of the goodness of the fit. In a sense, it is a measure of how much of the variability in the y-axis values can be accounted for by changes in the x-axis values.

mainly influenced by the moisture content, binder type (especially the presence of SCMs) and w/b ratio but other factors such as temperature and chloride content are also important [24].

The 2-point moving average laboratory and field resistivity results obtained for the different concretes used in this study are presented in Figure 4.35 and Figure 4.36 (see Appendix E for calculation of moving average). The resistivities for the cracked and uncracked concretes were found to have negligible differences in both the laboratory-based and field-based specimens. This is because the resistivity measurements (using the 4-point Wenner probe) in the cracked specimens were taken only in the uncracked concrete portions; no measurements were taken across the cracks. The results were therefore averaged and analysed in terms of binder type and w/b ratio. Average resistivities (week 104-120) of the various concretes (both field-based and laboratory-based) are presented in Figure 4.37. Detailed results are presented in Appendix B. The error bars shown in Figure 4.37 are calculated in the same way as those that were presented in Figure 4.26 for chloride conductivity results. A comparison of the concrete resistivity values for laboratory-based and field-based specimens is presented in Figure 4.38(a) and (b).

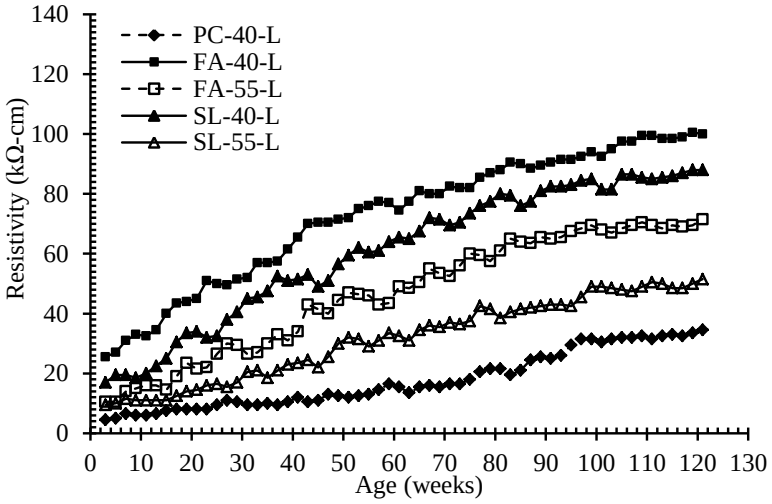

Figure 4.35: 2-point moving average resistivity for laboratory-based specimens

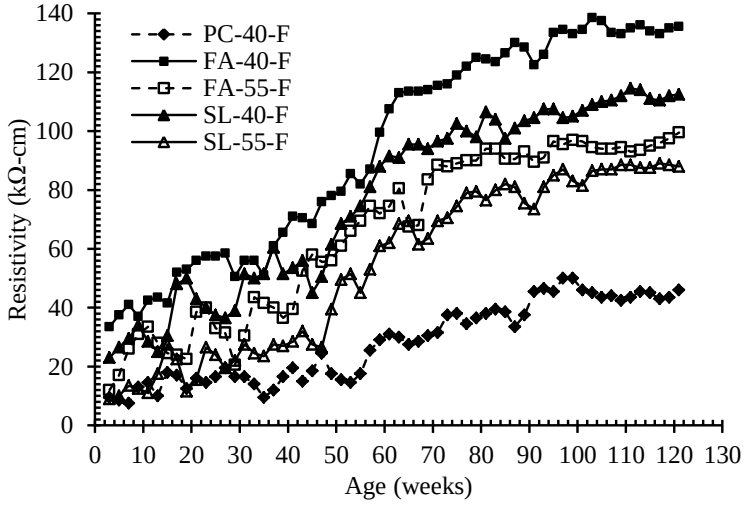

Figure 4.36: 2-point moving average resistivity for field-based specimens

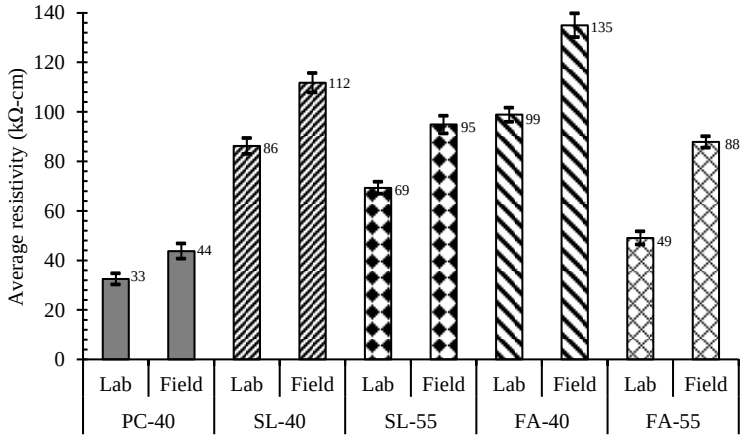

Figure 4.37: Average resistivity (week 104-120) for both field-based and laboratory-based specimens

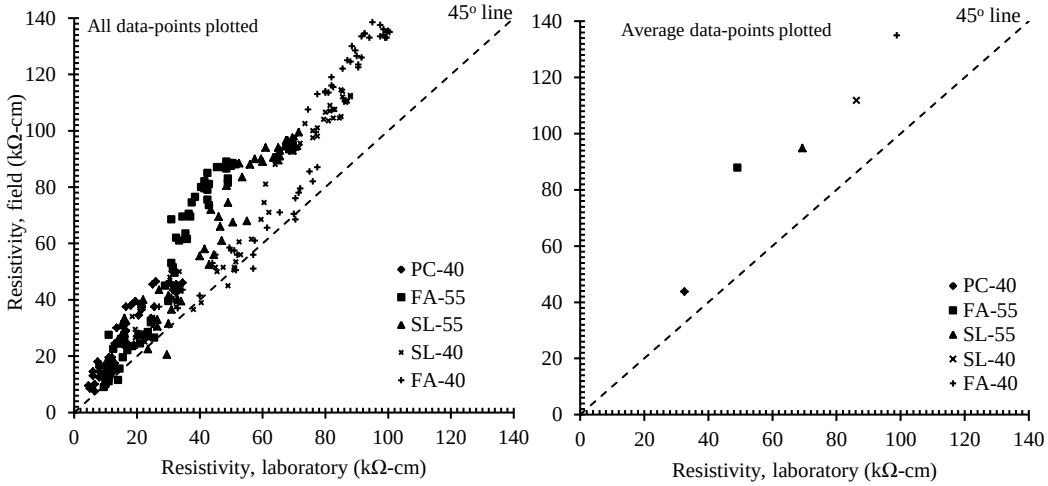

(a) Plot of all bi-weekly data-points

(b) Plot of average resistivities (week 104-120)

Figure 4.38: Comparison of resistivities for field-based and laboratory-based specimens

From these results, it is evident that resistivity increased with time irrespective of the binder type and w/b ratio. This phenomenon is attributed to continued hydration of the binder with time which leads to refinement of the concrete microstructure [25] and a lower ionic concentration [24] even though the latter may not be the case for concretes exposed to chlorides as was the case in this study. The results also show that the presence of SCMs (FA and GGBS) in concrete increases concrete resistivity. The PC concrete had the lowest resistivity while FA concrete had higher resistivity than GGBS concrete.

It is also important to note the unstable nature (i.e. random fluctuation with time) of the field-based concrete resistivities in comparison to the laboratory-based ones. This unstable nature is mainly attributable to, even though not measured, the relatively high variations in the moisture content and temperature (especially in the upper 10 - 20 mm concrete surface layer [26-28]) as opposed to the laboratory-based specimens where exposure conditions (relative humidity and temperature) were controlled throughout the experiment duration. The comparison of the concrete resistivity values for laboratory-based and field-based specimens (Figure 4.38(a) and (b)) shows that the field resistivities were higher than the corresponding laboratory ones. This trend can possibly be attributed to one or a combination of the following two factors:

(i) Lower moisture contents in the field-based concretes (especially in the upper 10 - 20 mm concrete surface layer) in comparison to those in the laboratory. Resistivity measurements in the laboratory-based specimens were taken at the end of the 3-day wetting (with 5% NaCl solution), which probably resulted in saturation of the specimens. The issue of low and highly variable moisture content is one of the major challenges to using in-situ surface resistivity measurements to assess the corrosion risk in RC structures.

(ii) Formation of a dense insoluble layer of $Mg(OH)_2$ (i.e. brucite) on the concrete surface [29]. This should not be misinterpreted to mean high resistivity concrete [27, 28]. Brucite crystallizes on the exposed concrete surface as small compact crystals that clog concrete pores and can retard the diffusion of oxygen to the steel surface. The reaction involves reaction of $Ca(OH)_2$ in the concrete pore solution with Mg^{2+} ions in the sea water [29]. However, the presence of brucite on the concrete surfaces of the field-based specimens could not be ascertained because it was not assessed. Further work will be needed to ascertain this assumption.

Overall, despite the differences between field-based and laboratory-based concrete resistivities, the resistivities of both the field-based and laboratory-based specimens increased in the following order: PC-40 → FA-55 → SL-55 → SL-40 → FA-40. This trend is closely the reverse to that for diffusion coefficients (obtained from chloride conductivities) presented earlier in Section 4.6 except for SL-40 and FA-40 (which are reversed). The similarity in the trends for concrete resistivity and diffusion coefficient is attributed to the fact that conductivity which was used to determine diffusion coefficient is theoretically the inverse of resistivity, or vice versa.

In the cracked specimens made using blended cement concretes (with high resistivities), relatively high corrosion rates were still recorded. This shows that in the presence of cracks, the high resistivity of blended cement concretes cannot solely be relied on to inhibit corrosion, and brings to question the validity of interpreting resistivity measurements using guidelines such as the one proposed by Polder *et al*. [30] (see Chapter 2, Table 2.5). The results clearly show that, if the influence of cover cracking on corrosion rate is to be appreciated, such guidelines have to be used carefully, or revised to allow for the influence of cover cracking. Other factors such as crack width, concrete quality and cover depth should be taken into account - these have already been discussed in previous sections. Furthermore, even for the field-based specimens (both uncracked and cracked), the relatively high concrete resistivities could not be relied on to quantify the corrosion risk. This is because despite the high resistivity measured on the concrete surface (using the 4-point Wenner probe), as already mentioned, due to either the drying effect of the outer concrete layer or presence of brucite layer on the concrete surface [29], the interior regions closer to the steel surface may still have relatively adequate moisture contents to sustain corrosion rate, especially for specimens with low cover depths i.e. 20 mm [31-33]. A study by Chrisp *et al*. [34] showed that the effect of drying or wetting on concrete conductivity (the inverse of resistivity) decreases with depth up to about 50 mm where drying and wetting will have little or no effect.

4.7.1 *Relationship between concrete resistivity and corrosion rate*

The correlations between average corrosion rate and average resistivity (week 104-120) for both the laboratory-based and field-based specimens are given in Figure 4.39 to Figure 4.42. The trendlines

shown in these figures were obtained by regression analysis (least squares method) to find the line of best fit (see Appendix E for details).

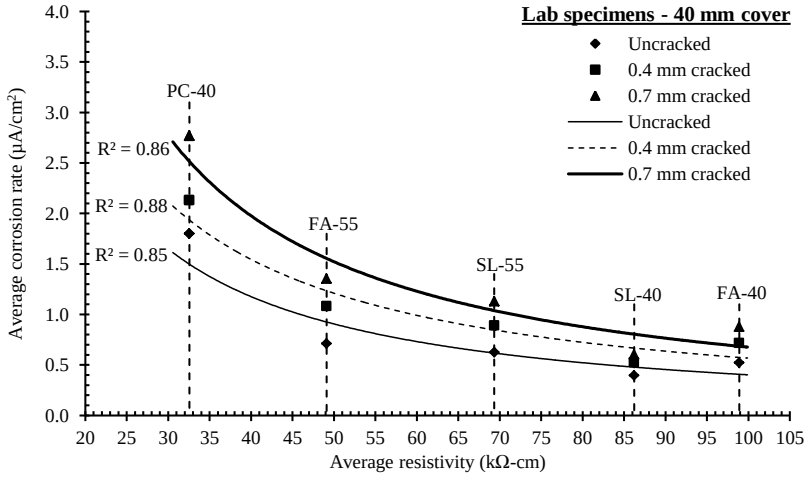

Figure 4.39: Average corrosion rate vs. average resistivity (lab specimens, 40 mm cover)

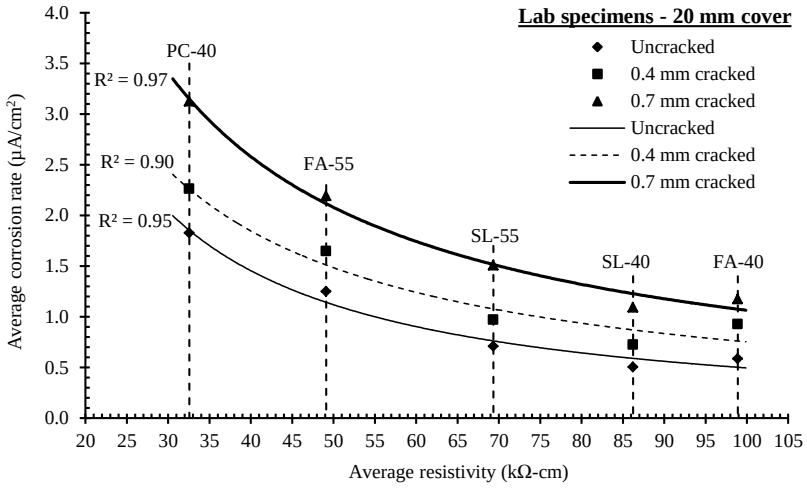

Figure 4.40: Average corrosion rate vs. average resistivity (lab specimens, 20 mm cover)

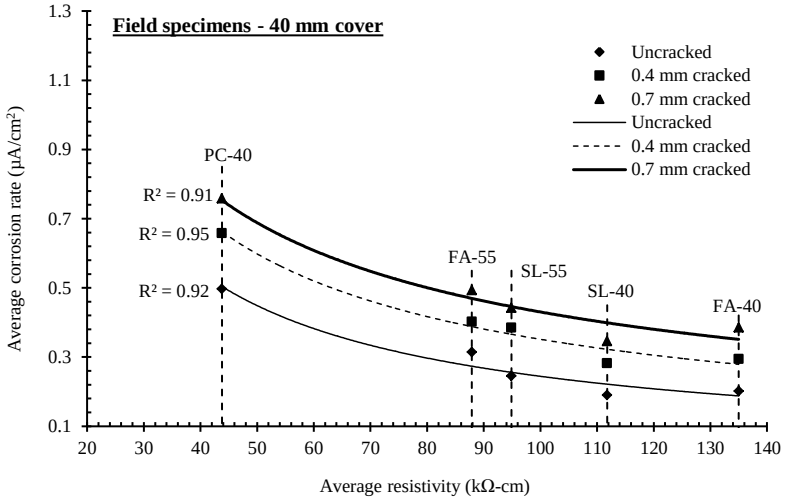

Figure 4.41: Average corrosion rate vs. average resistivity (field specimens, 40 mm cover)

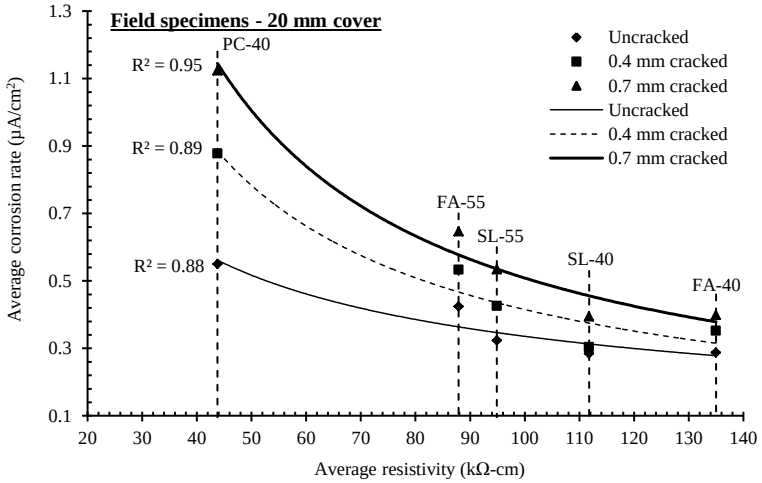

Figure 4.42: Average corrosion rate vs. average resistivity (field specimens, 20 mm cover)

From the results, the general trend is an inverse relationship between concrete resistivity and corrosion rate:

$$i_{corr} = k_2\left(\frac{1}{\rho^{A_2}}\right) \text{ [µA/cm}^2\text{]} \tag{4.2}$$

where k_2 ((µA/cm^2)/kΩ-cm) and A_2 (–) are coefficients whose values are dependent on cover depth (20 or 40 mm), crack width (0.4 or 0.7 mm) and exposure environment (laboratory and field).

The inverse relationship between concrete resistivity and corrosion rate conforms to findings from previous studies such as that of Alonso *et al*. [35] (see Chapter 2 on literature review). The difference between Alonso *et al*.'s model and the one presented here lies in the coefficient k_2; in Alonso *et al*.'s model, the coefficient k_2 has a constant value while in the relationship presented in this study, for a given exposure environment, it varies depending on cover depth and crack width. Equation (4.2) is therefore an improvement to Alonso *et al*.'s model. The results show that generally, for all specimens, higher corrosion rates were observed in those with lower resistivities and vice versa. The trend for cracked specimens showed that for a given concrete resistivity, corrosion rate increased with increasing crack width. This was the case for both the field and laboratory specimens. Previous studies by Scott and Alexander [4] and Otieno *et al*. [11] have shown that corrosion rate is not a function of resistivity alone, but also depends on the limiting availability of oxygen at the cathode, particularly when resistivity is fairly low, and availability of moisture [36, 37]. These results motivate the need for provision of adequate cover in low-resistivity concretes, and underscore the previous statement that resistivity alone, even though important, cannot be used alone to control corrosion in RC structures. However, the provision of adequate cover depth alone may not suffice to control corrosion. In Section 4.5, we saw that increase in cover depth in the PC concrete specimens (with relatively low resistivities) did not necessarily result in low corrosion rates. A holistic approach taking into consideration the factors influencing corrosion rate is therefore needed. This will be discussed further in Section 4.10.

Finally, these results illustrate the limitation of using resistivity (measured using 4-point Wenner probe) as a tool to assess the susceptibility of cracked RC structures to steel corrosion. Even though the dominating effect of high resistivity (in the blended cement concretes) on corrosion rate is still evident, the performance of the different concretes with respect to corrosion can still be distinguished by the different crack widths. This was the case in both the field-based and laboratory-based specimens. It can therefore be concluded that resistivity measurements (using the 4-point Wenner probe) cannot be reliably used to assess the susceptibility of cracked RC to steel corrosion. Nevertheless, resistivity can still serve as a good first indicator for corrosion activity in cracked RC structures but further complementary assessments such as corrosion rate and half-cell potential measurements are necessary. As stated by Otieno *et al*. [38], what is required is a means of also allowing for the effects of cracking. With sufficient data from long-term studies, a relationship between corrosion rate and resistivity for both uncracked and cracked concrete can be established.

However, based on the results of this study, a hypothetical approach is proposed (see Figure 4.43) where the influence of cover cracking is taken into consideration when interpreting resistivity measurements. In the proposed framework, corrosion risk of the RC structure is assessed taking into account the influence of both the concrete resistivity and pre-corrosion cover cracking on corrosion rate. However, for such an approach to be used, it is necessary to determine, for a given range of resistivity values (say 10-50, >50-100 and >100 kΩ-cm), the corresponding values of the crack widths or crack width ranges that define the boundaries between the different corrosion risk levels. These resistivity ranges are based on the current ones used to interpret resistivity measurements [30] - see Table 2.5, Chapter 2. At present, the crack widths ranges shown in the proposed framework (Figure 4.43) are based on the experimental results of this study and those of Otieno *et al*. [11] and Scott and Alexander [4], and should therefore be taken as rough empirical guidelines (see Figure 2.23 and Figure 2.24 in Chapter 2). The results of Otieno *et al*. and Scott and Alexander were presented in Chapter 2. Further work is still required in this area. The reasons for adopting the proposed crack width (w_{cr}) ranges are as follows:

(i) $0 < w_{cr} \leq 0.2$ mm: the experimental results showed that the presence of incipient cracks resulted in relatively higher corrosion rates than in uncracked concrete. A measurement of the incipient-crack widths in some specimens after unloading showed that the surface cracks widths ranged between 0.03 mm to 0.15 mm. However, the corrosion rates in specimens of the same cover depth, binder type and w/b ratio, and with crack widths within this range did not show significant differences (max. standard deviation: 0.03 μA/cm^2). An upper limit of 0.2 mm was therefore adopted in the framework.

(ii) 0.2 mm $< w_{cr} \leq 0.4$ mm: the upper limit of 0.4 mm was adopted because the corrosion rates in the 0.4 mm and 0.7 mm cracked specimens of the same binder type, w/b ratio and cover depth showed stark differences (see Figure 2.24 in Chapter 2).

(iii) $w_{cr} > 0.4$ mm: even though the maximum crack width used in the experimental studies reported in this paper was limited to 0.7 mm, it was not adopted as the upper limit because it is deemed that for crack widths > 0.4 mm, the influence of resistivity on corrosion rate, even though still evident, will be decreased (especially for resistivities < 50 kΩ-cm).

It is important to acknowledge that even though the proposed framework presented here is limited to single transverse (flexural) cracks based on the experimental data used, and in addition to crack width, the influence of other crack characteristics such as density (or frequency), activity or dormancy, orientation with respect to reinforcing steel, geometry (tortuosity, depth and surface roughness) and self-healing capacity on corrosion rate should, in future, also be quantified and taken into account.

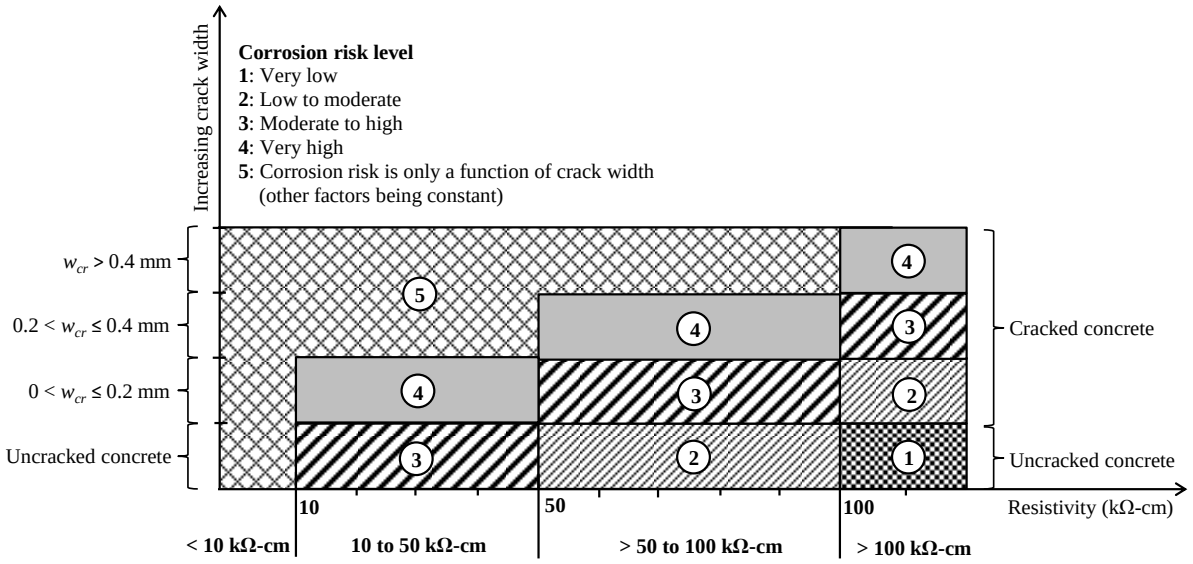

Figure 4.43: Hypothetical schematic for interpretation of resistivity measurements in cracked concrete

At the moment, considering that in-service RC structures are usually in a cracked state, and in addition to its sensitivity to moisture content variations in concrete, surface resistivity measurements using the 4-point Wenner probe should not be relied on as the sole basis to make decisions with respect to their susceptibility to steel corrosion. Nevertheless, it can still serve as a good first indicator for corrosion activity in cracked RC structures but further complementary assessments such as chloride content at steel level, corrosion rate and half-cell potential measurements are necessary.

4.8 *Half-cell potential results*

4.8.1 *General trends in half-cell potential results*

Typical time-development trends for HCP obtained during the experimental period are shown in Figure 4.44(a) to (f). A general overview of the average HCP (week 104-120) is given in Figure 4.45 and Figure 4.46. Detailed results are given in Appendix B. In Figure 4.45 and Figure 4.46, the -256 mV (Ag/AgCl) HCP mark is highlighted because according to ASTM C876-91 [39] guidelines (see Table 3.5, Chapter 3), values equal to or more negative than -256 mV (Ag/AgCl) are interpreted to mean a high (> 90%) probability of active corrosion, which is conventionally depicted by $i_{corr} \geq 0.1$ μA/cm^2 [40, 41], while those less negative than -256 mV (Ag/AgCl) are generally interpreted as intermediate corrosion risk.

Fundamentally, a HCP value depicts the corrosion condition of the embedded steel in concrete [42] and should therefore, for specimens with the same binder type, w/b ratio, cover depth, crack width and

exposure environment, have similar trends to those for corrosion rates already presented in previous sections. The results presented in Figure 4.44 to Figure 4.46 show the following trends:

(i) for a given exposure environment (laboratory or field), cover depth and crack width, average HCP became less negative in the following order: PC-40 → FA-55 → SL-55 → FA-40 → SL-40. This trend is similar to the correlation between corrosion rate and concrete quality that was discussed in Section 4.6.

(ii) HCP values for the field-based specimens were lower (less negative) than the laboratory-based ones (Figure 4.45 and Figure 4.46). This trend corresponds to that for the corrosion rate results already discussed Section 4.4.

(iii) the HCP trends with respect to time over the entire experimental period show that the HCP values for both laboratory-based and field-based specimens became more negative with time (as expected) but at a relatively slower rate in comparison to that for corrosion rate as should have been the case. Notably, the corrosion rate trends for laboratory-based specimens showed remarkable increases (more negative) in HCP with time in comparison to corresponding field specimens. This difference in trends is partly attributed to the corrosion rate measurement technique used in this study i.e. coulostatic linear polarization resistance technique, as was mentioned in Chapter 3. In applying this technique to obtain corrosion rate, the polarized steel surface area was assumed to be equal to the exposed surface area of approximately 86 cm^2 (steel diameter of 10 mm, length approximately 27.5 cm - see Chapter 3 for details). This value was used to calculate the corrosion current density, i_{corr}. However, it is important to acknowledge that, even though the temporal evolution of surface morphology of corroded steel was not assessed, it can be expected that the anodic steel area was not constant throughout the test duration as assumed, and that it increased with time. Consequently, as the corrosion current (and hence cumulative steel mass loss) increases with time, there is also a corresponding increase in the anodic surface area (or formation of new anodes on the steel surface). Depending on the level of increase in the anodic steel area, the corrosion current density (i_{corr}) can be expected to remain more or less constant, or have significant changes only after long periods of time. This trend was not evident in the results reported in this study due to the use of a constant polarized steel surface area to calculate the corrosion current density.

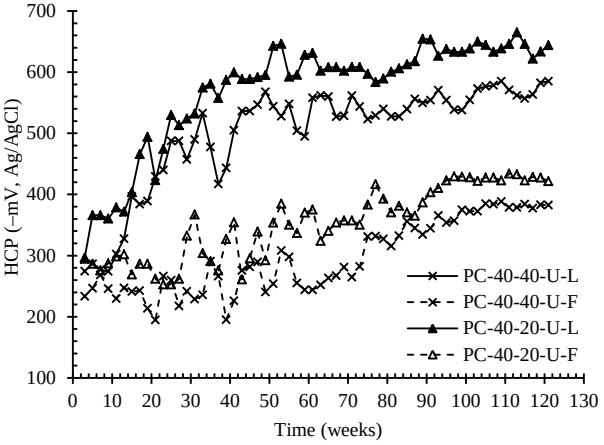

(a) Uncracked PC-40

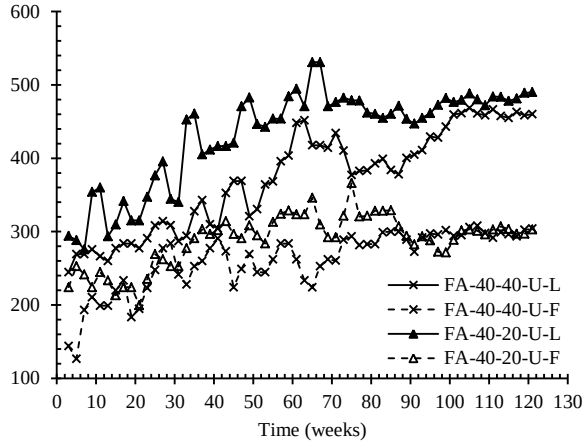

(b) Uncracked FA-40

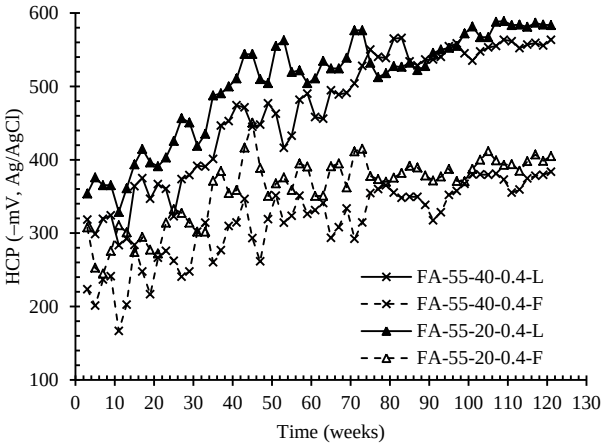

(c) 0.4 mm cracked FA-55

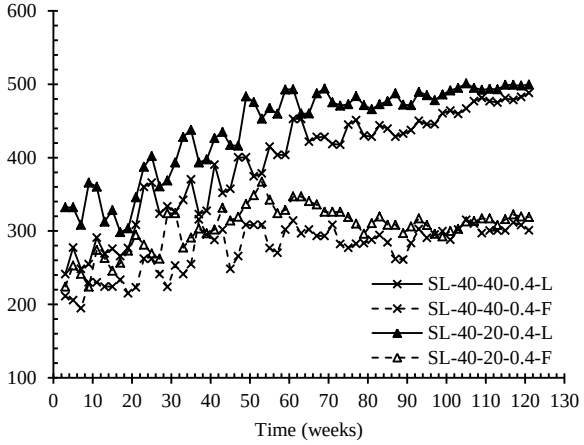

(d) 0.4 mm cracked SL-40

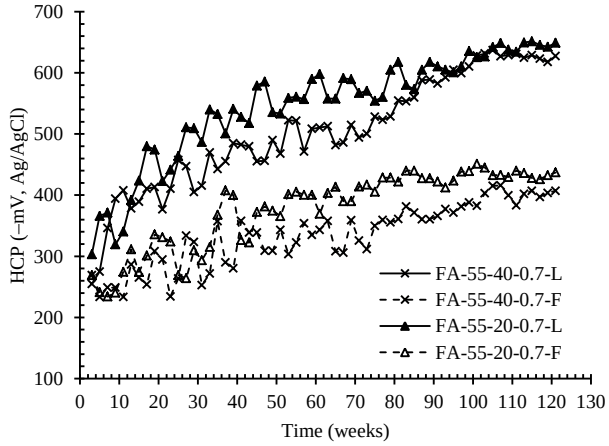

(e) 0.7 mm cracked FA-55

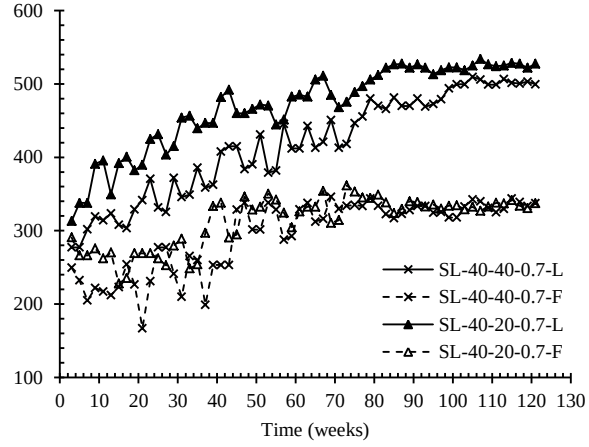

(f) 0.7 mm cracked SL-40

Figure 4.44: Typical half-cell potential time-development trends
(Note: see Appendix B for full results)

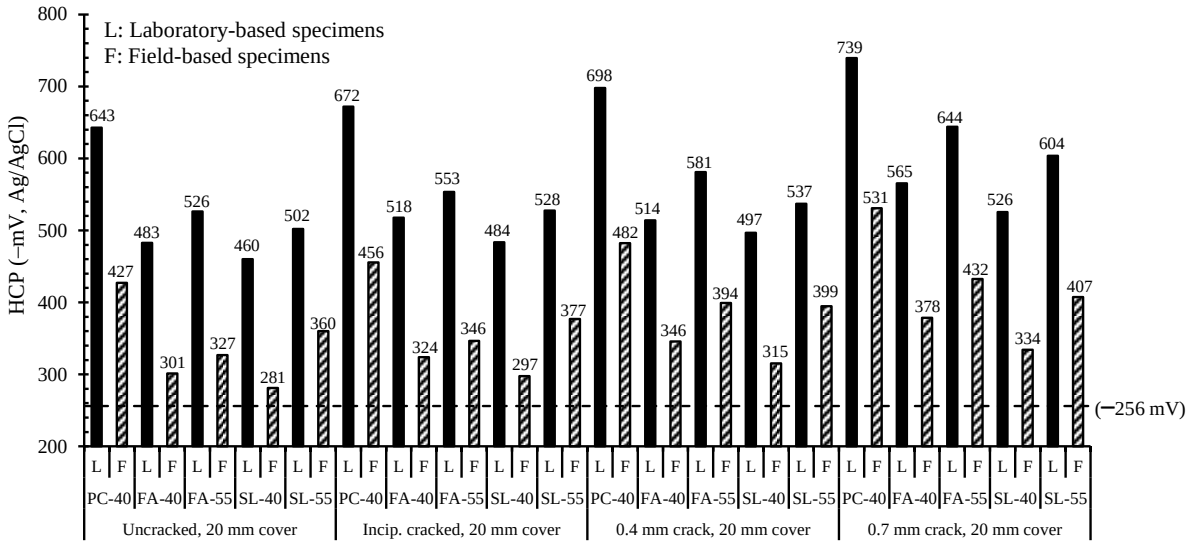

Figure 4.45: Average half-cell potentials for lab and field specimens with 20 mm cover
(Note: Full size figure is provided in Appendix B)

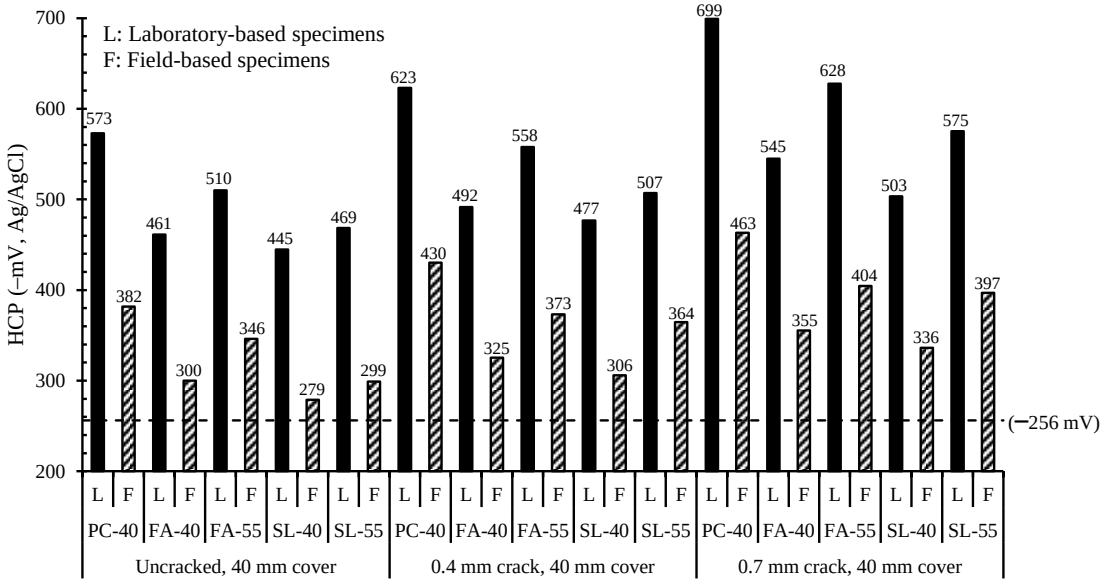

Figure 4.46: Average half-cell potentials for lab and field specimens with 40 mm cover
(Note: Full size figure is provided in Appendix B)

(iv) week 0 to 74: during this period, HCP results for the field-based specimens were quite unstable (i.e. random fluctuation with time) compared to the corresponding laboratory-based ones but later became relatively stable (see Figures B.18 to B.34 in Appendix B). In this period, no distinct trends in HCP were observed in the field-based specimens for different cover depths, binder types, w/b ratios or crack widths. This trend of fluctuating HCP values bearing no correlation with corrosion rate that was observed in the field-based specimens during this period was not experienced in the laboratory-based specimens where HCP values showed a good relationship (more negative HCP values for higher corrosion rates, and vice versa) with corrosion rate throughout the experimental period, and was attributed to the controlled exposure conditions (temperature and relative humidity) in the laboratory. These results imply that the use of HCP measurement as a corrosion assessment technique can be quite unreliable for field applications

especially for RC structures that have just started to corrode actively (say 0.1-0.2 μA/cm^2) when corrosion rates are, in most cases, unstable. In such cases, once-off instanteneous HCP point-measurements, which is the common procedure in practice, can be misleading unless they are complimented with other corrosion assessment techniques such as corrosion rate measurement. This problem can also, to some extent, be overcome by taking consecutive HCP measurements over an extended period of time.

(v) week 75 to 122: after week 74, the differences in HCP values for specimens with different cover depth, crack width and concrete quality were visible and correponded to trends of more negative values with (a) increase in crack width (Figure 4.47 to Figure 4.51) - the maximum and minimum HCP presented in these figures were obtained from a statistical analysis ($HCP_{max} = HCP_{average} + 1.96\sigma$, and $HCP_{min} = HCP_{average} - 1.96\sigma$ where σ is the standard deviation - the value 1.96 is obtained from a standard *t*-distribution table at a 95% confidence interval) of the measured results, (b) decrease in cover depth, and (c) decrease in concrete quality. The HCP trends obtained during week 75 to 122 were similar to those for corrosion rate already presented in Sections 4.4, 4.5 and 4.6 i.e. the HCP values became more negative as the corrosion rates increased with time.

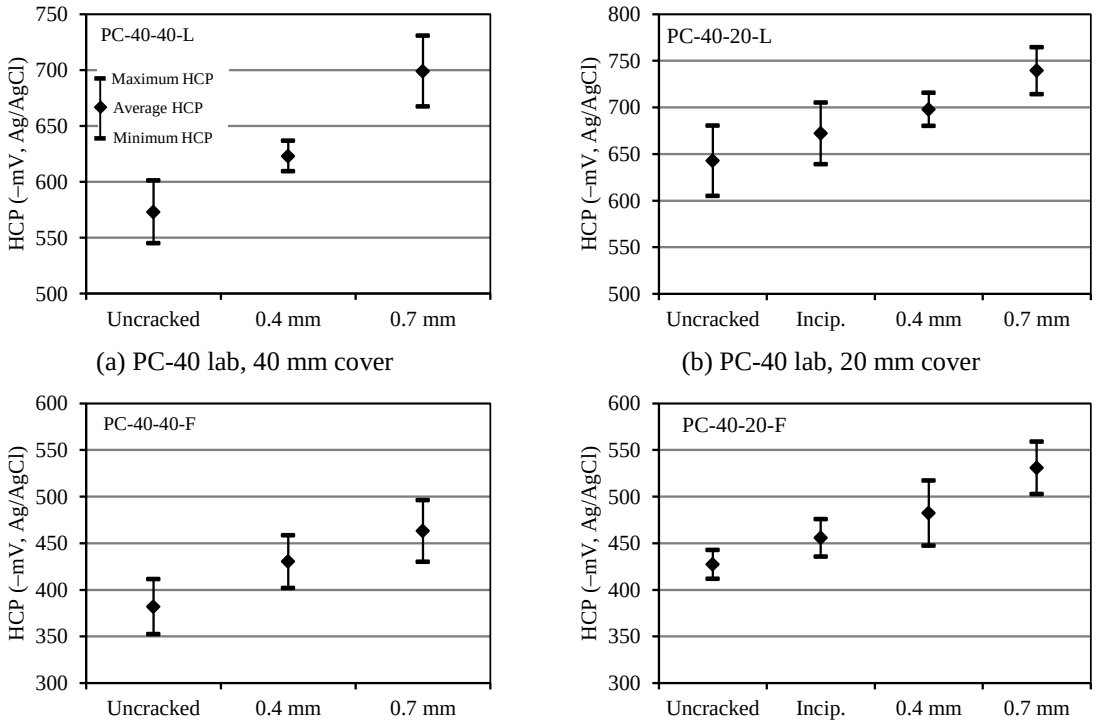

(a) PC-40 lab, 40 mm cover

(b) PC-40 lab, 20 mm cover

(c) PC-40 field, 40 mm cover

(d) PC-40 field, 20 mm cover

Figure 4.47: Comparison of average HCP for uncracked and cracked PC-40 specimens (L: lab, F: field)

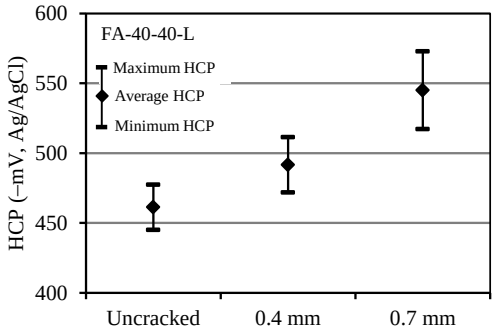

(a) FA-40 lab, 40 mm cover

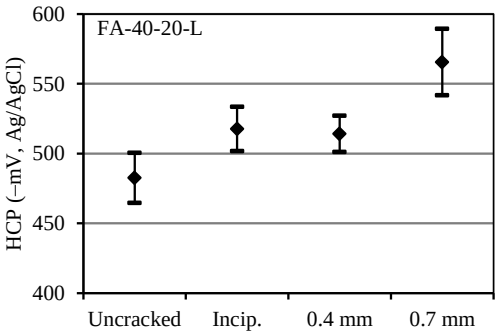

(b) FA-40 lab, 20 mm cover

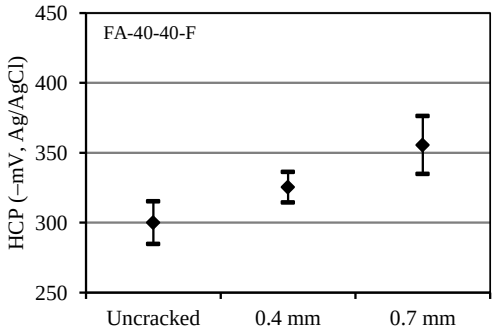

(c) FA-40 field, 40 mm cover

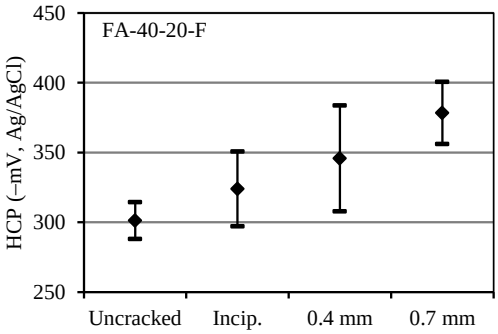

(d) FA-40 field, 40 mm cover

Figure 4.48: Comparison of average HCP for uncracked and cracked FA-40 specimens (L: lab, F: field)

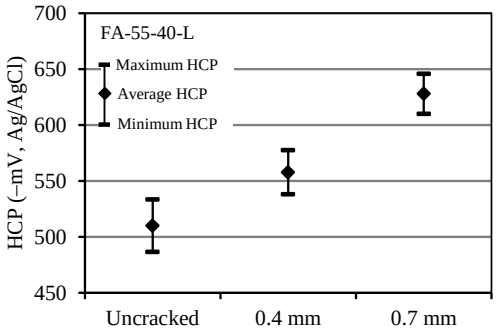

(a) FA-55 lab, 40 mm cover

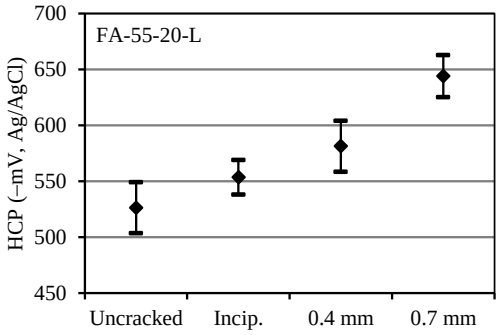

(b) FA-55 lab, 20 mm cover

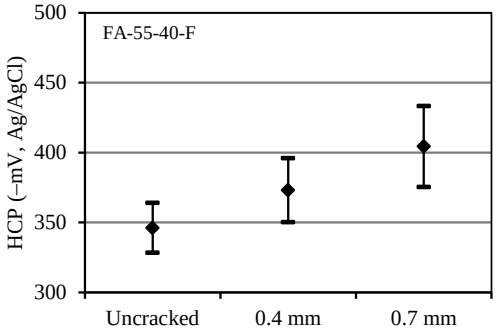

(c) FA-55 field, 40 mm cover

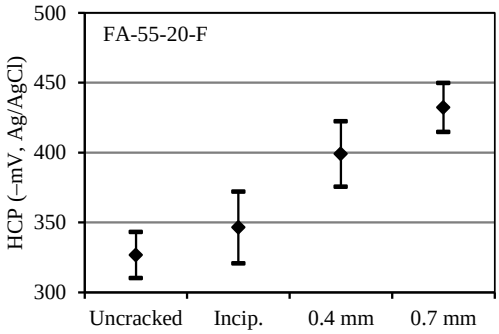

(d) FA-55 field, 20 mm cover

Figure 4.49: Comparison of average HCP for uncracked and cracked FA-55 specimens (L: lab, F: field)

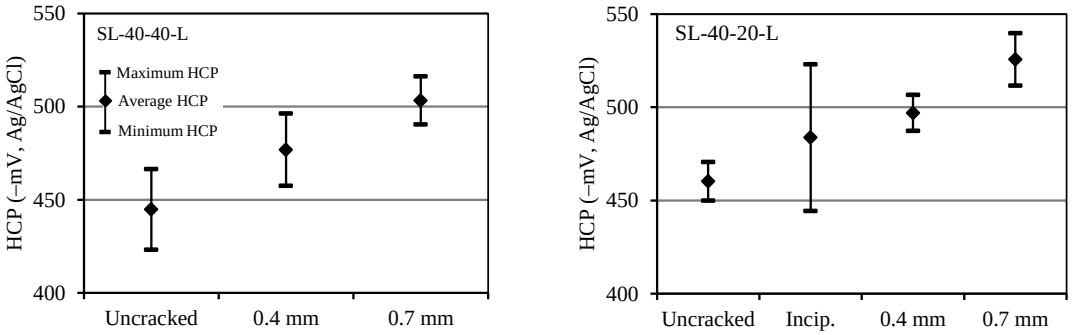

(a) SL-40 lab, 40 mm cover

(b) SL-40 lab, 20 mm cover

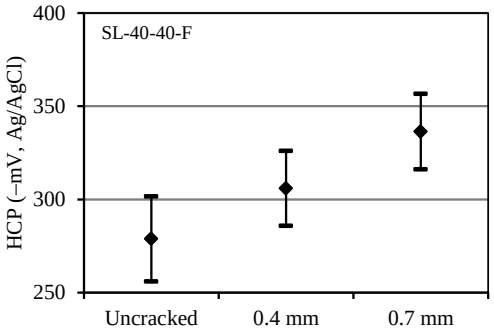

(c) SL-40 field, 40 mm cover

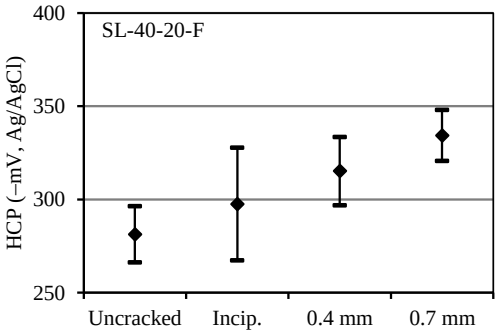

(d) SL-40 field, 20 mm cover

Figure 4.50: Comparison of average HCP for uncracked and cracked SL-40 specimens (L: lab, F: field)

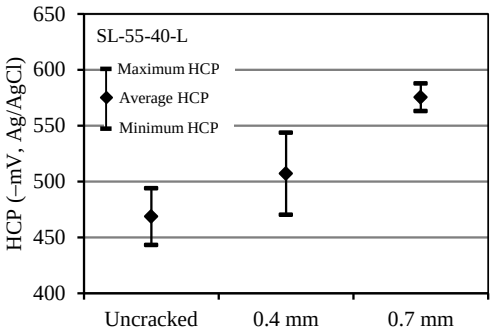

(a) SL-55 lab, 40 mm cover

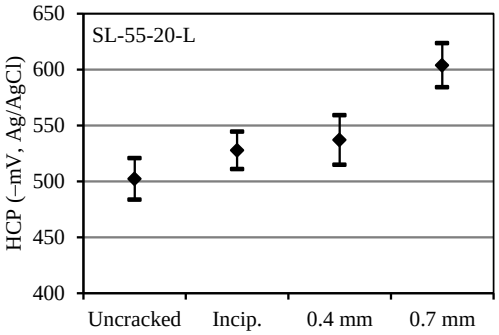

(b) SL-55 lab, 20 mm cover

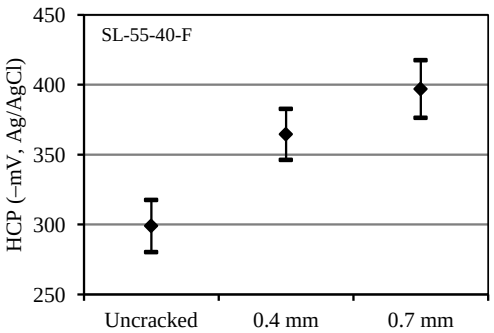

(c) SL-55 field, 40 mm cover

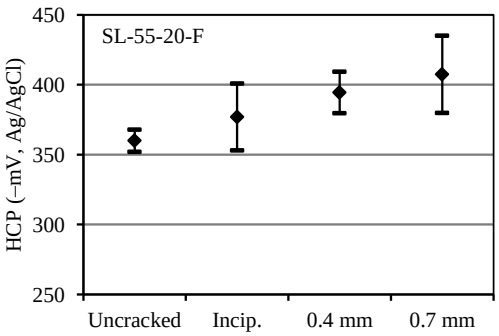

(d) SL-55 field, 240 mm cover

Figure 4.51: Comparison of average HCP for uncracked and cracked SL-55 specimens (L: lab, F: field)

Finally, for a given exposure environment, cover depth, crack width and w/b ratio, a comparison of the average HCP results (Figure 4.52 to Figure 4.53) showed a similar trend to that for concrete quality and resistivity that were presented in previous sections - the HCP values of blended cement concrete

specimens were less negative than those of plain PC concrete (PC-40) specimens. However, even though specimens made with fly ash concretes (FA-40 and FA-55) showed more negative HCP values than those made with GGBS concretes (SL-40 and SL-55), the differences were not as high as those between PC-40 and SL-40 specimens. These differences are attributed to the reasons already given in Sections 4.6 and 4.7 where, respectively, concrete quality and resistivity were discussed.

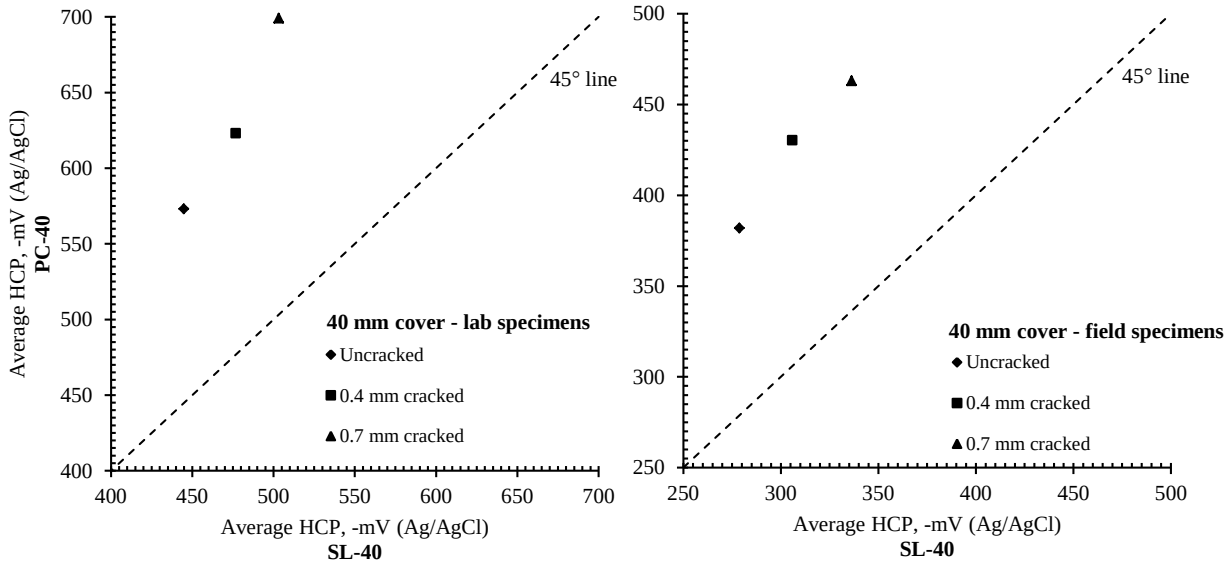

Figure 4.52: Comparison of average HCP for PC-40 and SL-40 specimens (40 mm cover)

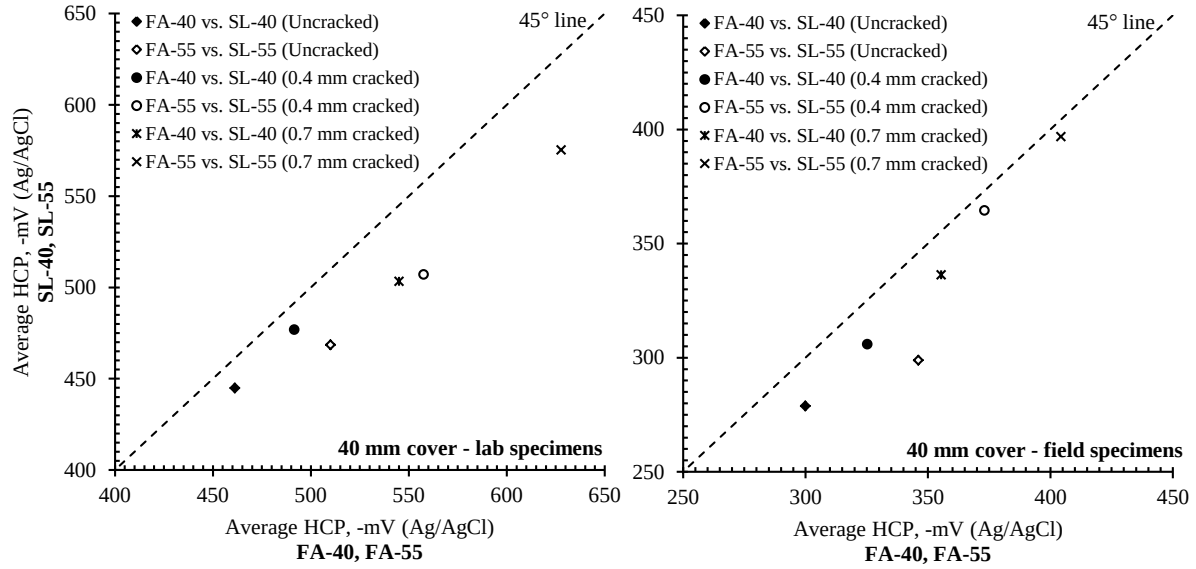

Figure 4.53: Comparison of average HCP for blended cement concrete specimens (40 mm cover)

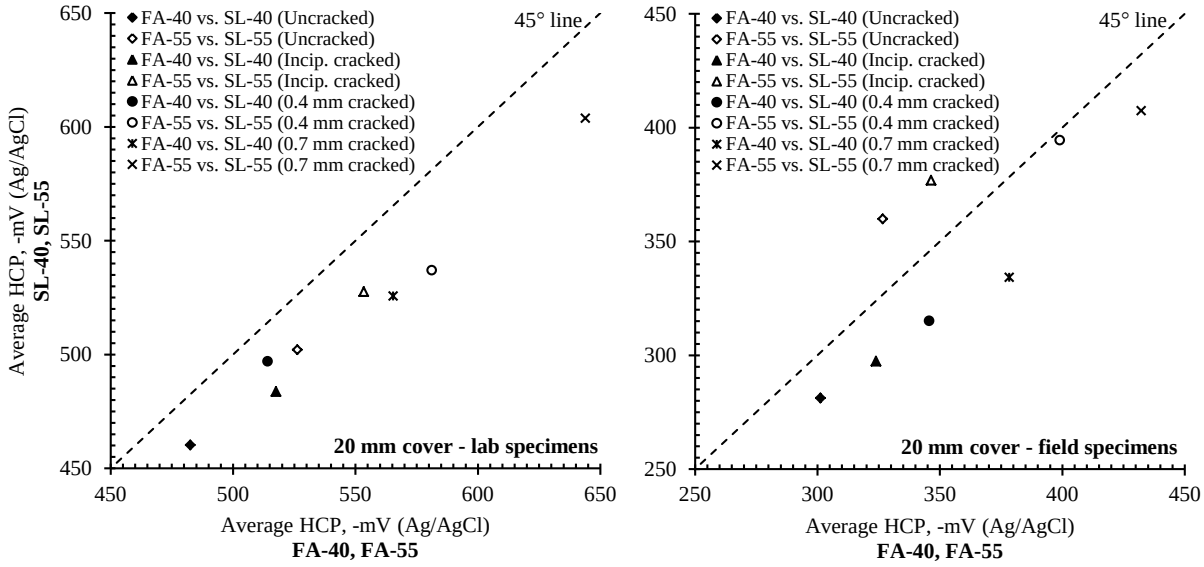

Figure 4.54: Comparison of average HCP for blended cement concrete specimens (20 mm cover)

4.8.2 *Correlation between half-cell potential and corrosion rate*

The relationships between average corrosion rate and average HCP (week 104-120) for the laboratory-based and field-based specimens are given in Figure 4.55 and Figure 4.56. The trendlines shown in these figures were obtained by regression analysis (least squares method) to find the line of best fit (see Appendix E for details). These results show that HCP values for both the field-based and laboratory-based specimens showed a good correlation ($R^2 > 0.9$) with corrosion rate i.e. higher corrosion rates corresponded to more negative HCP values. The good correlation between HCP and corrosion rate in the laboratory-based specimens is not surprising because the specimens were in a well-controlled environment, and similar results have been obtained in past studies [4, 38]. However, for the field-based specimens, even though it was expected that, compared to the laboratory-based specimens, the HCP measurements would show a poor correlation with corrosion rate due to in-situ variations in temperature and relative humidity, as has been reported in the literature [43], this was not the case. As already mentioned, HCP in these specimens only showed a poor correlation with corrosion rate up to about week 74 when high temporal fluctuations in HCP and corrosion rates were observed. The good correlation between HCP and corrosion rate in the field-based specimens can be attributed to the stabilization of corrosion rate (after week 74), and means that temperature and relative humidity did not (to a large extent) affect HCP values. This is inferred from the laboratory where these parameters were controlled, and similar results were obtained i.e. good correlation between HCP and corrosion rate. As already mentioned, these results show that HCP measurements were only reliable (i.e. showed good correlation with corrosion rate) after stabilization of corrosion rate.

Finally, these results also show that HCP measurements are more reliable than resistivity (4-point Wenner probe) measurements when used to assess corrosion of steel in cracked concrete. This is because the value of HCP measured reflects the corrosion state of the anode-cathode system of the steel in concrete [39].

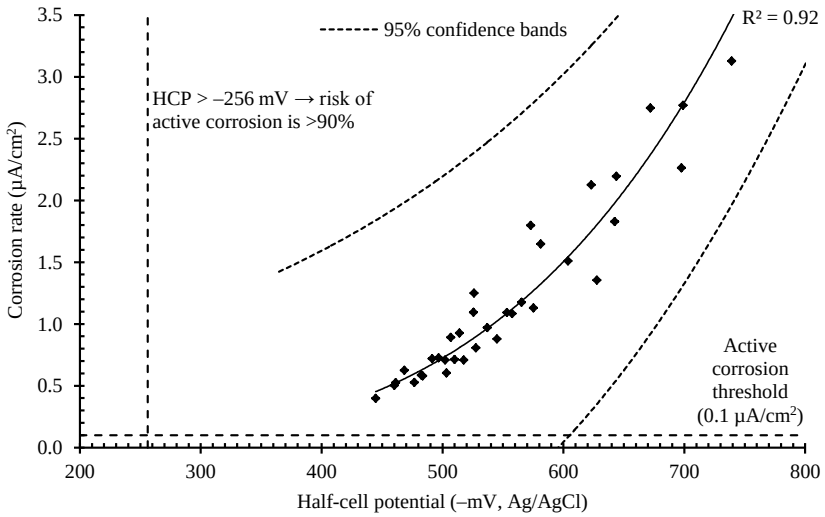

Figure 4.55: Average i_{corr} vs. half-cell potentials for all laboratory-based specimens (week 104-120)

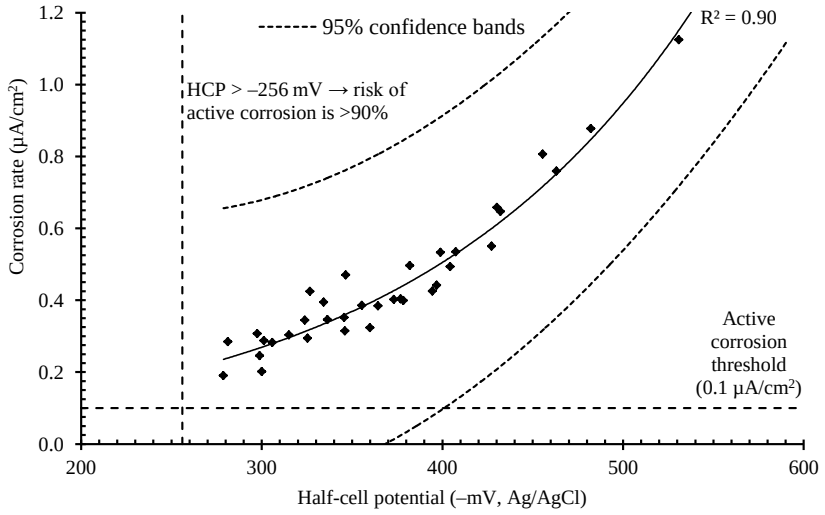

Figure 4.56: Average i_{corr} vs. half-cell potentials for all field-based specimens (week 104-120)

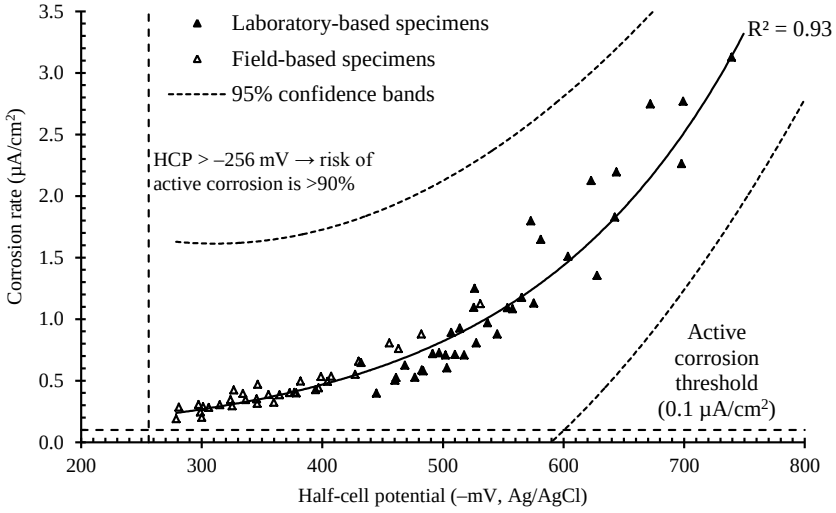

Figure 4.57: Average i_{corr} vs. half-cell potentials for all field and laboratory specimens (week 104-120)

4.9 *Chloride content measurements at steel level*

After 73 weeks of exposure in the respective environments, chloride content measurements at the steel level were made by taking 20 ± 2 mm cores from the laboratory-based and field-based specimens at two locations, on one side of the crack i.e. 30 mm along the steel and 90 mm along the steel from the crack, see Figure 3.16 in Chapter 3. This action was taken to ascertain whether the chloride concentration at the steel level, especially in the majority of field-based specimens which were passively corroding (i_{corr} < 0.1 μA/cm^2), was high enough to induce active corrosion. The results are presented in Figure 4.58 to Figure 4.61 (see Appendix B for detailed results). The chloride contents referred to here are total (acid-soluble) chlorides determined by acid potentiometric titration.

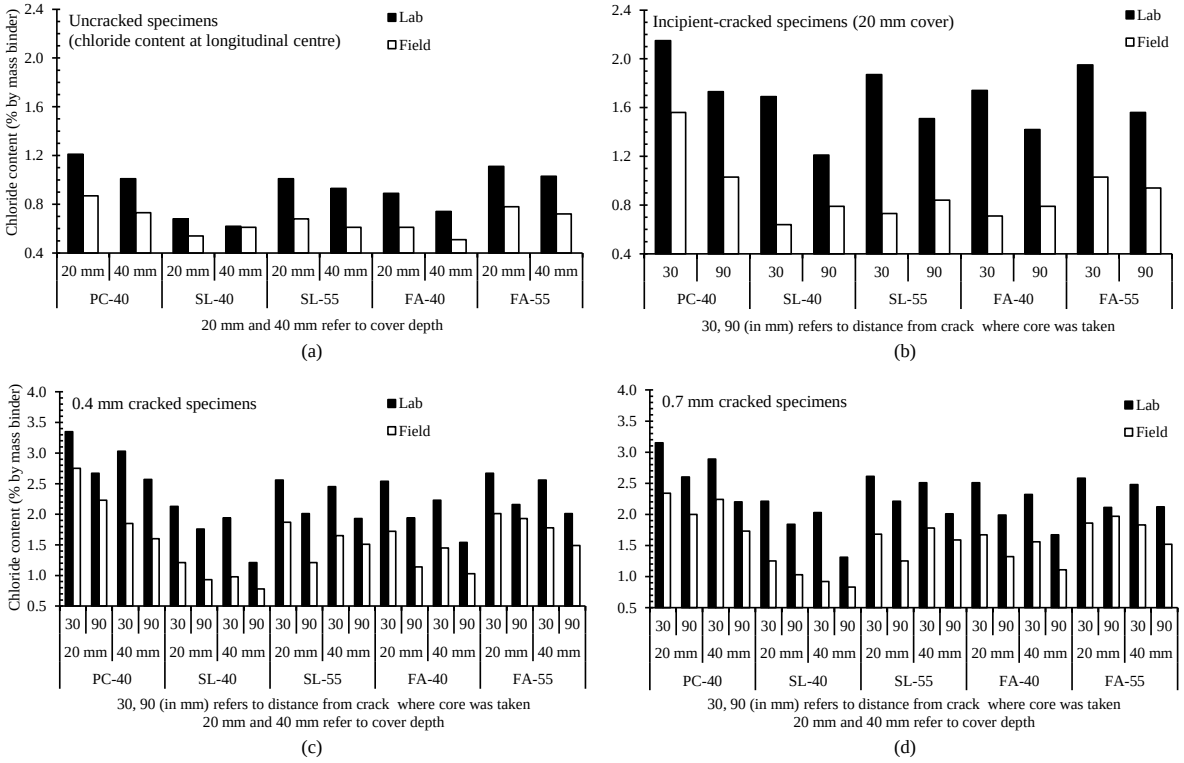

Figure 4.58: Comparison of total chloride content (at steel level) for different concretes and cover depths

From the results, the following observations can be made:

(i) In both the field and laboratory exposure environments, for a given crack width and cover depth, the chloride contents in the plain PC concrete (PC-40) specimens were higher than those in the blended cement concrete (SL-40, SL-55, FA-40 and FA-55) specimens. This trend is attributed to the high penetrability of the PC-40 concretes in comparison to the blended cement concretes as was discussed earlier in Section 4.6.

(ii) In both the field and laboratory exposure environments, for a given concrete quality and crack width, chloride concentrations in the specimens with 20 mm cover were higher than that in the corresponding specimens with 40 mm cover (Figure 4.58). For a given concrete type (binder type and w/b ratio) and crack width, this trend was attributable to the shorter travel (diffusion) path in the specimens with 20 mm cover relative to those with 40 mm cover. However, for different concrete types (e.g. SL-40 and SL-55) and crack widths in a given exposure environment, this trend was not evident mainly because of the differences in concrete

penetrability. It is also important to note that, even though not investigated in this study, the trend of decreased chloride content at the steel level with increased cover depth may not be the case if the crack intersects the steel (i.e. the crack depth is greater that the cover depth). In such a case, the cover depth may effectively be considered to be zero, and the chloride concentration at the steel level will depend on, if present, the virtual resistance of the uncracked concrete ligaments [44] in the crack profile. This is especially important in blended cement concretes which have high resistivities.

(iii) The chloride contents in the laboratory-based specimens were higher than those for the field-based specimens (see Figure 4.59 - this figure is plotted using the chloride contents at both 30 mm and 90 mm from the crack). This was the trend for chloride contents at 30 mm and 90 mm from the crack. Up to 164% difference was recorded for corresponding chloride contents between the field-based and laboratory-based incipient-cracked SL-40 specimens with 20 mm cover. This trend was not surprising mainly because the chloride content in the 5% NaCl solution (i.e. 3%) was 50% higher than that of sea-water (i.e. 2%).

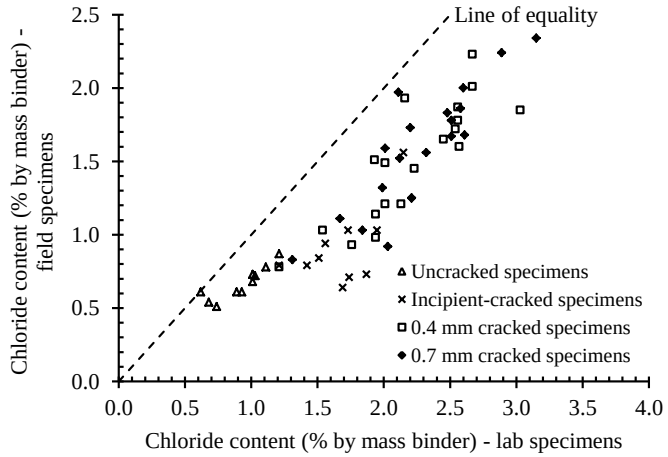

Figure 4.59: Comparison of total chloride content at steel level in field and laboratory specimens (Note: Figure plotted using the chloride contents at both 30 mm and 90 mm from the crack)

(iv) In the cracked specimens, the chloride contents at 30 mm from crack were higher than those at 90 mm from crack; up to a maximum of 144% difference was recorded in the laboratory-based 0.4 mm cracked PC-40 specimens with 40 mm cover, see Figure 4.58. This trend is not surprising because contrary to uncracked concrete (i.e. 90 mm from crack) where chloride ingress is mainly a diffusion process and is governed by the penetrability of the cover concrete, close to the crack (i.e. 30 mm from crack), chlorides penetrate the concrete not only from the exposed concrete surface but also from the crack surfaces. Similar trends have been reported by Scott [12] and Audenaert *et al*. [45]. Exceptions to this trend of decreasing chloride concentration with distance from the crack were incipient-cracked SL-40 and SL-55 field-based specimens with 20 mm cover and 0.7 mm cracked FA-55 field-based specimens with 20 mm cover. No specific trend can be seen in these specimens but this observation can be attributed to either:

a) ease of chloride penetration along the steel-concrete interface especially if there was damage of the steel-concrete bond e.g. due to slip during the initial 3-point loading to crack the beams and (especially in the case of the 0.7 mm cracked specimens which required higher crack width opening loads) subsequent tightening and/or loosening of the rigs to maintain the

required surface crack width; the penetration of chloride along the steel in cracked concrete has been reported in past studies such as the one by Win *et al*. [46], or

b) the presence of microcracks other than the 'single crack' that was intended at the longitudinal centre of the beam specimen due to 3-point loading. However, a visual inspection of these specimens using a hand-held lens (magnification X40) showed that this was not the case.

(v) In comparison to the difference in chloride contents between uncracked and incipient-cracked specimens, there was little difference between the chloride contents in the laboratory-based and field-based 0.4 mm and 0.7 mm cracked specimens (see Figure 4.60(a) to (f) - these figures are plotted using the chloride contents at 30 mm from the crack). This observation can also be attributed to the reasons already given in (iv)(a) and (b). Maximum percentage differences in chloride contents of up to 49% and 114% in, respectively, the field-based and laboratory-based specimens were recorded between the uncracked and incipient-cracked specimens while differences of only up to 15% and 10% were recorded in, respectively, the field-based and laboratory-based specimens between the 0.4 mm and 0.7 mm cracked specimens.

(vi) The general trend in the laboratory-based specimens is that higher chloride contents correspond to higher corrosion rates – see Figure 4.61(a) to (d) which are plotted using average corrosion rates between weeks 52 and 72 (given in Appendix B, to correspond to the time when the chloride contents were measured i.e. week 73) and average chloride concentration i.e. average of chloride concentration at 30 mm and 90 mm away from the crack.

This trend is, to some extent, as expected. However, it is interesting to note that in the case of 0.4 and 0.7 mm cracked field-based and laboratory-based specimens, despite having similar chloride contents (see Figure 4.61(c) and (d)), the 0.7 mm cracked specimens showed higher corrosion rates than the corresponding 0.4 mm cracked ones. This trend shows that in addition to chloride content in these specimens, other factors including crack width affected corrosion rate. The literature reviewed in Chapter 2 showed that as the chloride ion concentration increases, the corrosion rate should also be expected to increase due to decrease in pitting (transpassive) potential and increase in electrolyte conductivity. At the same time, the oxygen solubility progressively decreases and hence its limited availability at the cathode stifles the cathodic reaction. In the laboratory-based specimens, oxygen deficiency was reduced by virtue of not epoxy-coating the specimen faces as was the case in the field-based specimens. This facilitated a relatively faster drying (during the 4 days air-drying period) and consequently easy ingress of oxygen to sustain cathodic reaction. In the field-based specimens, the high chloride concentrations measured at the steel level did not correspond to high corrosion rates, and is attributed to the oxygen deficiency to support the cathodic reaction. Low oxygen concentration can be attributed to two possible causes; (i) its decreased solubility in salt solution [47], and (ii) the high moisture content of the field-exposed specimens due to the epoxy coating which prevented drying from the specimen sides (during low tides). Even though oxygen solubility was also expected to have decreased due to presence of chloride salts in the concrete pore solution, the 4-days air-drying of the laboratory specimens counteracted this by allowing oxygen ingress during this period.

In this study, as already discussed, no valid trend was not obtained between corrosion rate and chloride concentration in the field-based specimens. An attempt to fit lines-of-best fit to the data presented in Figure 4.61(a) to (d) resulted in trend-lines for the field-based data having high R^2 values but small positive slopes (maximum of 33% for the field-based incipient-cracked specimens with 20 mm cover).

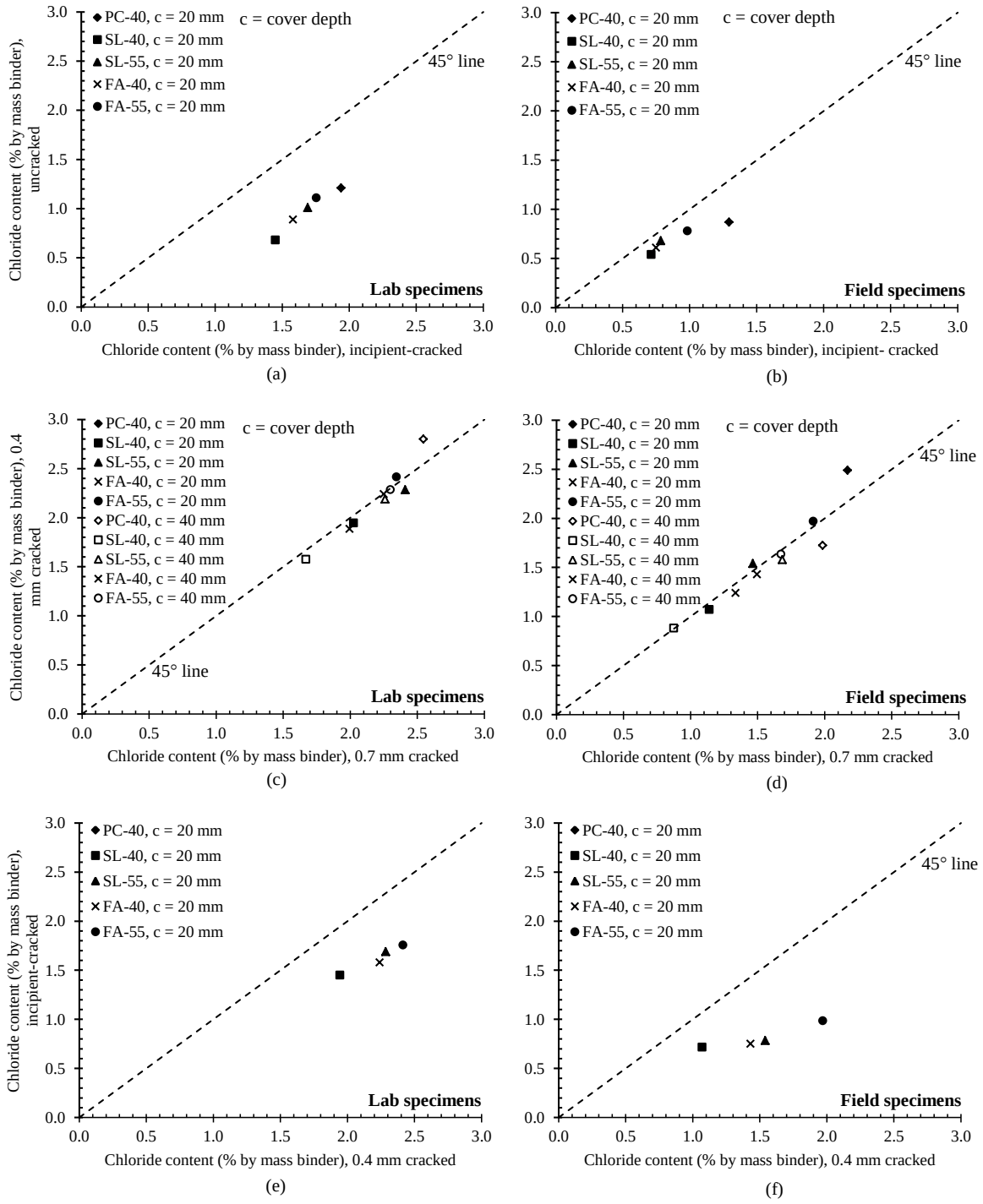

Figure 4.60: Comparison of total chloride content at steel level for different crack widths

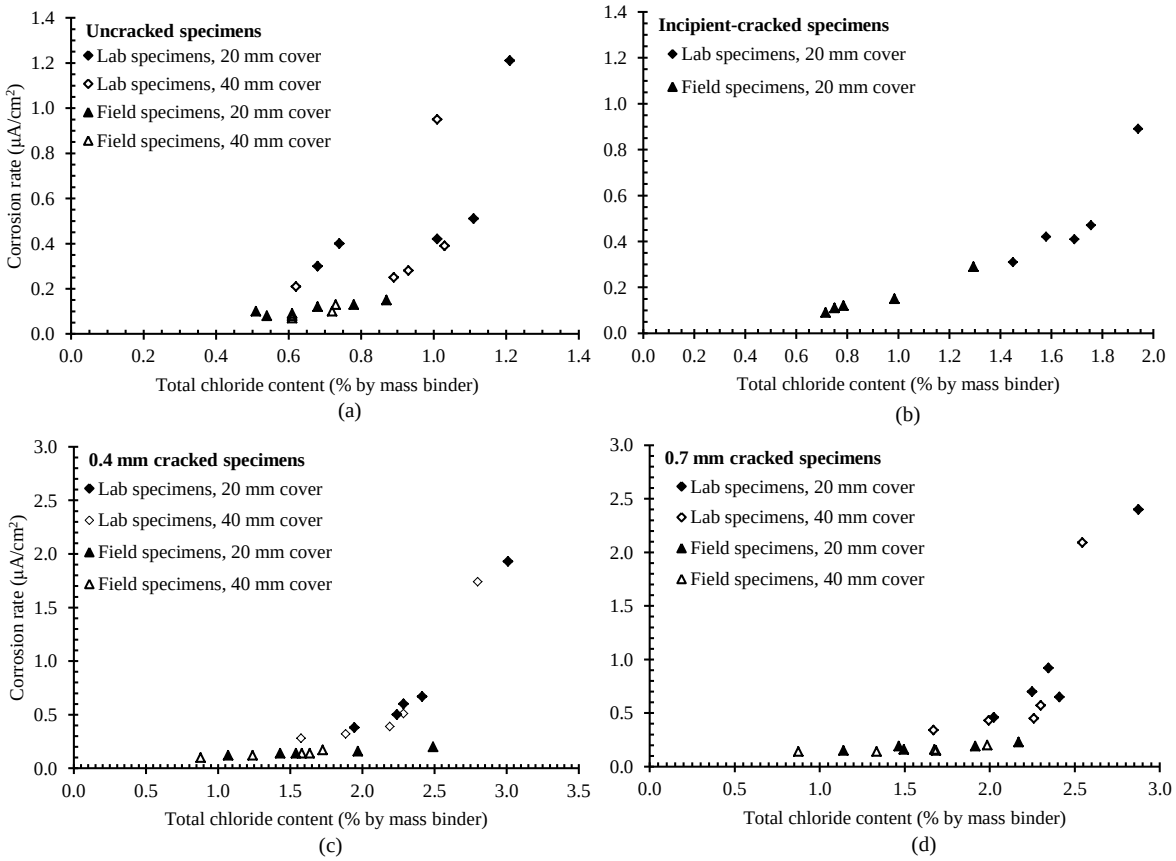

Figure 4.61: Corrosion rate vs. total chloride content at steel level (lab and field specimens)

4.10 *The concept of c/w_{cr} ratio vs. concrete quality and corrosion rate*

The results obtained in this study underscore those of previous studies [e.g. 4, 11, 48] showing that crack width (w_{cr}), cover thickness (c) and concrete quality affect corrosion rate. This motivates the need to shift from the conventional approach of considering each of these parameters in isolation, to one where the combined effect of these parameters is considered in order to obtain a suitable combination during design to meet the desired durability performance.

A study by Gowripalan *et al*. [49] showed that if concrete quality is kept constant, the probabilities of corrosion initiation and corrosion rate are increased as the as c/w_{cr} ratio decreases and vice versa. They suggested that it is desirable to maximize c/w_{cr} ratio as opposed to only limiting the crack width. However, their study did not incorporate the influence of concrete quality on corrosion rate in the presence of cracking. If this is taken into account, as was the case in this study, a general trend similar to the one proposed by Gowripalan *et al*. may not be applicable. In addition to considering the c/w_{cr} ratio, concrete quality should also be taken into account. The objective should also shift from maximizing the c/w_{cr} ratio, to determination of a suitable combination of c/w_{cr} ratio and concrete quality to meet the desired durability performance. To facilitate the application of such a criterion in the durability design of cracked RC structures, it is necessary to develop a framework to objectively select a suitable combination of c/w_{cr} ratio and concrete quality. This is covered later in this section.

In this study, the quantified crack widths were limited to 0, 0.4 and 0.7 mm while two cover depths, 20 and 40 mm, were used. The respective c/w_{cr} ratios for the crack widths and cover depths used are summarised in Table 4.6. The incipient-cracked specimens (see Chapter 3) are not used here because it was not possible to quantify the crack widths. The c/w_{cr} ratio is also not applicable to uncracked concrete where cover depth and concrete quality are the only variables to be considered with respect to corrosion. A comparison of the different c/w_{cr} ratios and their respective average corrosion rates is presented in Figure 4.62(a) to (h).

Table 4.6: Cover depth/crack width (c/w_{cr}) ratios

Cover depth	c/w_{cr} ratio			
	Uncracked	Incipient crack	0.4 mm crack	0.7 mm crack
20 mm	–	–	50	29
40 mm	–	–	100	57

The results show that using c/w_{cr} ratio as opposed to only w_{cr} provides a more objective way to compare corrosion rates for specimens with similar concrete qualities (binder type and w/b ratio) but different cover depths and crack widths e.g. comparison of i_{corr} for a specimen with 40 mm cover and 0.4 mm crack width with that for a specimen with 20 mm cover and 0.7 mm crack width (see Figure 4.62(e) and (f)). This is very useful from a design point of view. However, a general conclusion similar to that reported by Gowripalan *et al*. [49] that corrosion rate increases as the c/w_{cr} ratio decreases cannot be made based on the results of this study; some of the comparisons (see Figure 4.62(g) and (h)) do not follow such a trend. This can be attributed to the incorporation of concrete quality in the analyses; a factor that Gowripalan *et al*. did not consider in their work. The relationship between corrosion rate and c/w_{cr} ratio is presented in Figure 4.63 and Figure 4.64. The trendlines shown in these figures were obtained by regression analysis (least squares method) to find the line of best fit (see Appendix E for details).

The results show a similar trend between corrosion rate and c/w_{cr} ratio for both the laboratory-based and field-based specimens. For a given c/w_{cr} ratio, a range of corrosion rates are possible depending on the concrete quality. These graphs also underscore the superior performance of blended cement concretes in comparison to PC concretes discussed earlier. The results show that it is possible to objectively use the c/w_{cr} ratio in the selection of cover depth, crack width and concrete quality to control corrosion rate.

The trends shown in Figure 4.63 and Figure 4.64 between corrosion rate and c/w_{cr} ratio can be expressed as follows:

$$i_{corr} = k_3\left(\frac{c}{w_{cr}}\right)^{-A_3} \quad [\mu A/cm^2] \tag{4.3}$$

where k_3 ($\mu A/cm^2$) and A_3 (–) are coefficients whose values are dependent on binder type and w/b ratio (PC-40, FA-40, FA-55, SL-40 and SL-55), and exposure environment (laboratory and field).

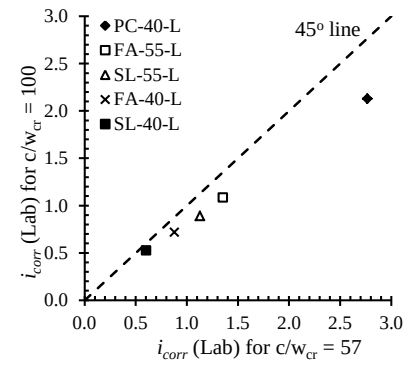

(a)

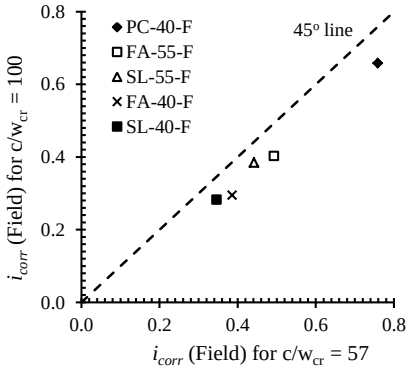

(b)

(a), (b): Comparison of i_{corr} for 0.4 and 0.7 mm cracked specimens (40 mm cover)

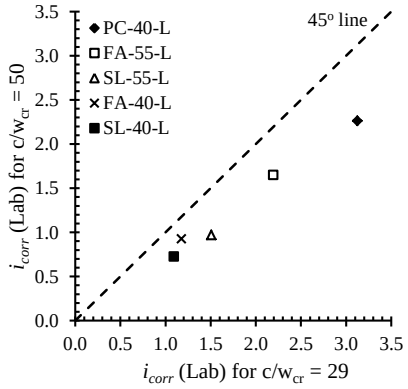

(c)

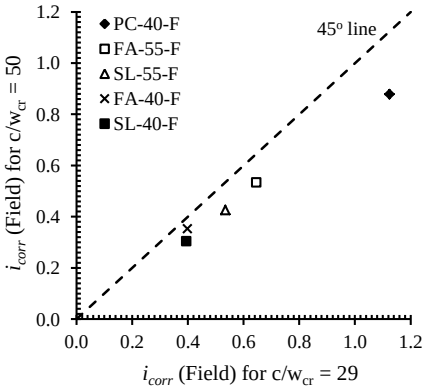

(d)

(c), (d): Comparison of i_{corr} for 0.4 and 0.7 mm cracked specimens (20 mm cover)

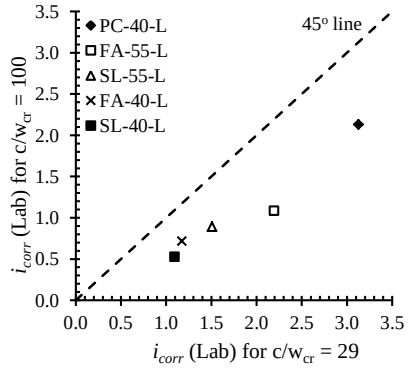

(e)

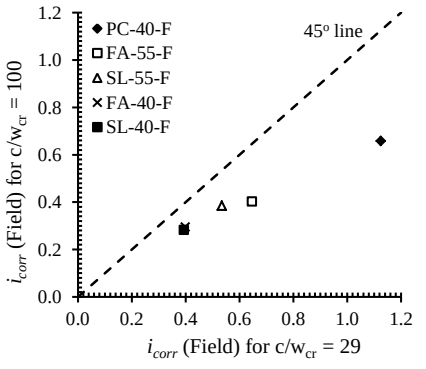

(f)

(e), (f): Comparison of i_{corr} for 0.4 mm crack (40 mm cover) and 0.7 mm crack (20 mm cover)

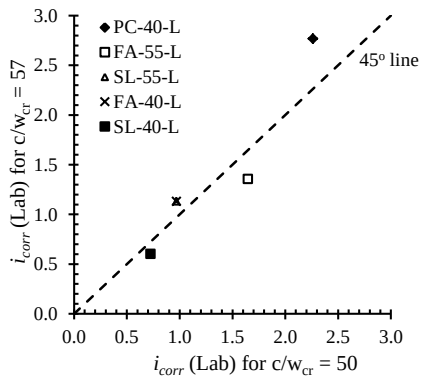

(g)

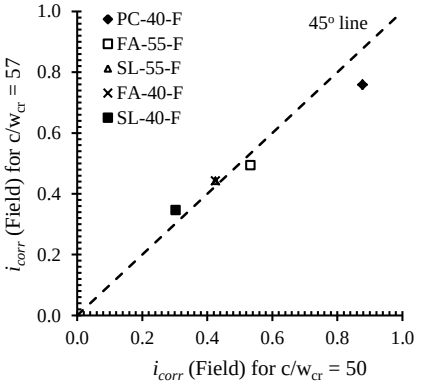

(h)

(g), (h): Comparison of i_{corr} for 0.7 mm crack (40 mm cover) and 0.4 mm crack (20 mm cover)

Figure 4.62: Comparison of i_{corr} for 0.4 and 0.7 mm cracked specimens (20 and 40 mm cover)

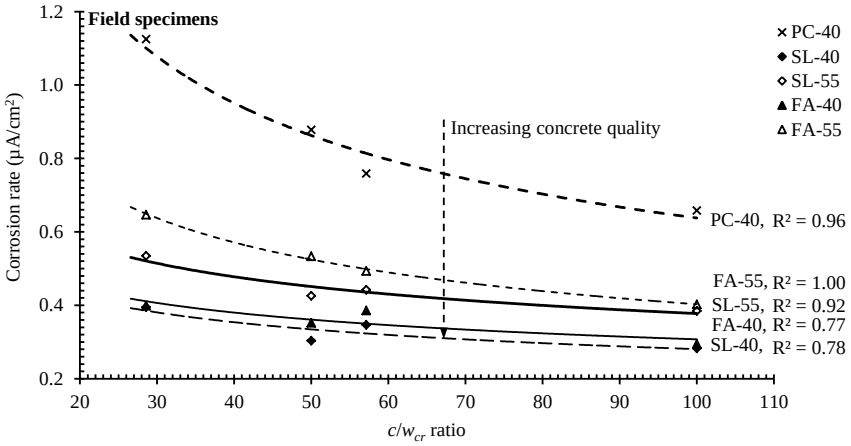

Figure 4.63: Relationship between corrosion rate, c/w_{cr} ratio and concrete quality - field specimens

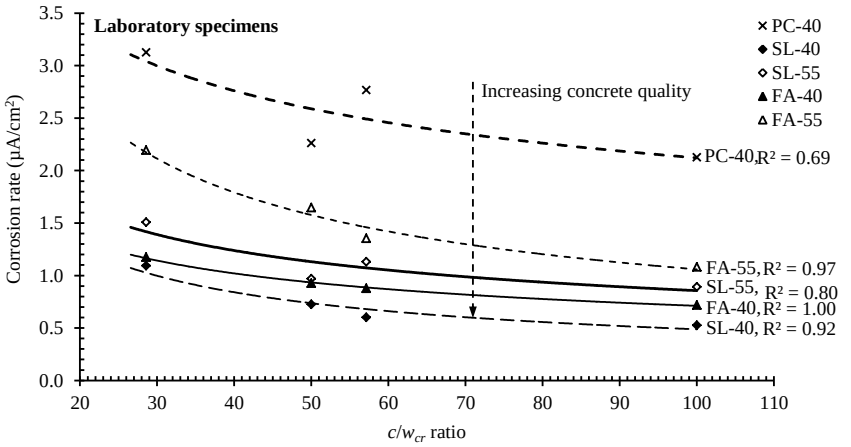

Figure 4.64: Relationship between corrosion rate, c/w_{cr} ratio and concrete quality - lab specimens

The trends presented in Figure 4.63 and Figure 4.64 are similar to a proposed relationship between corrosion rate, oxygen availability and resistivity by Scott and Alexander [4], Figure 4.65. However, their proposal did not incorporate the influence of cover cracking on corrosion rate even though it was investigated.

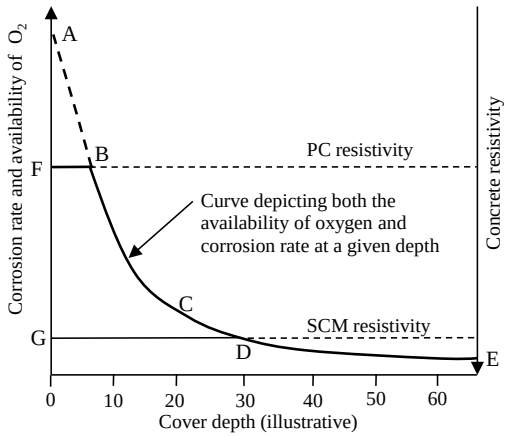

Figure 4.65: Schematic relationship between corrosion rate, oxygen availability and resistivity [4] (PC: plain Portland cement, SCM: supplementary cementitious materials)

In Figure 4.65, the availability of oxygen at a given cover depth is defined by curve ACE. The same curve is also used as a representation of the corrosion rate since oxygen is required for the cathodic reaction. Concrete resistivity however also controls the maximum possible corrosion rate even if there is sufficient oxygen and moisture to support a higher reaction rate. The resistivity controls are shown as horizontal lines '*PC resistivity*' and '*SCM resistivity*', where PC would be representative of plain PC concretes, and SCM of concretes produced with blended cements. The horizontal lines (for 'PC resistivity' and 'SCM resistivity') should be thought of as conductivity lines, where conductivity is the inverse of resistivity; also, the lines would likely be sloped somewhat to account for the variation in resistivity with cover depth. As noted by Scott and Alexander [4], more research is required to define the slopes of these lines. For a concrete resistivity given by 'PC', the possible corrosion rate curve is given by the composite line FBCE. The expected corrosion rate (on the left hand vertical axis of Figure 4.65) is very sensitive to cover depth, particularly for low cover. These rates are oxygen-availability dependent. Conversely, for a slag concrete (resistivity 'SCM'), the corrosion rate curve is given by the line GDE. In this case, corrosion rate is relatively insensitive to cover depth, and will be mainly resistivity-controlled (although cover depth will exercise a secondary influence). Before proceeding, it is important to note that in their work, Scott and Alexander [4] did not make direct measurements of oxygen at the depth of the steel; their proposal of the limiting effect of oxygen was based on a synthesis of the measured corrosion rates, resistivity values, the assumption that the cathodic process is dependent on the availability of oxygen, and available literature.

An extended framework of this model incorporating the influence of cover cracking on corrosion rate was later proposed by Otieno *et al*. [11] as shown in Figure 4.66. In their study, Otieno *et al*. investigated the influence of cover cracking and concrete quality (binder type and w/b ratio) but cover depth was not varied. Its influence was therefore not objectively incorporated in the improved model. In their framework, they proposed that; (i) the maximum crack width (represented by line HK in Figure 4.66 (b)) should be set to a crack width that is tolerable with respect to corrosion, taking into consideration both the cover depth and concrete quality, (ii) other factors such as crack self-healing can also be considered depending on whether they increase or decrease corrosion rate, and that (iii) corrosion rates for crack widths between zero (uncracked, line HJ) and the maximum crack width (line HK) can be obtained by interpolation using sound engineering judgment.

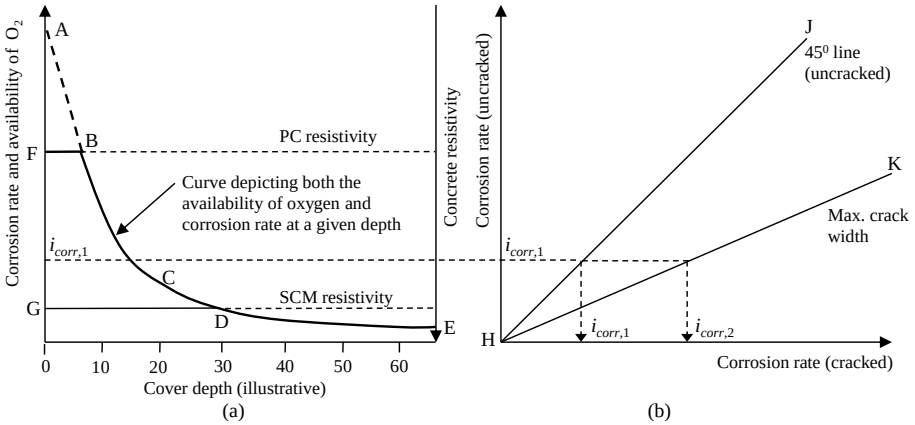

Figure 4.66: Revised schematic relationship between corrosion rate, oxygen availability, resistivity and crack width [11]

The proposals by Scott and Alexander [4] and Otieno *et al*. [11] pose major challenges to the designer, and an objective way to select a suitable combination of the parameters (concrete quality, cover depth and crack width) in cracked concrete is required. To overcome these challenges, this study proposes a framework that takes into account the inter-relationship between cover cracking, concrete quality (binder type, w/b ratio), resistivity and cover depth on corrosion rate. A schematic presentation of the framework is shown in Figure 4.67.

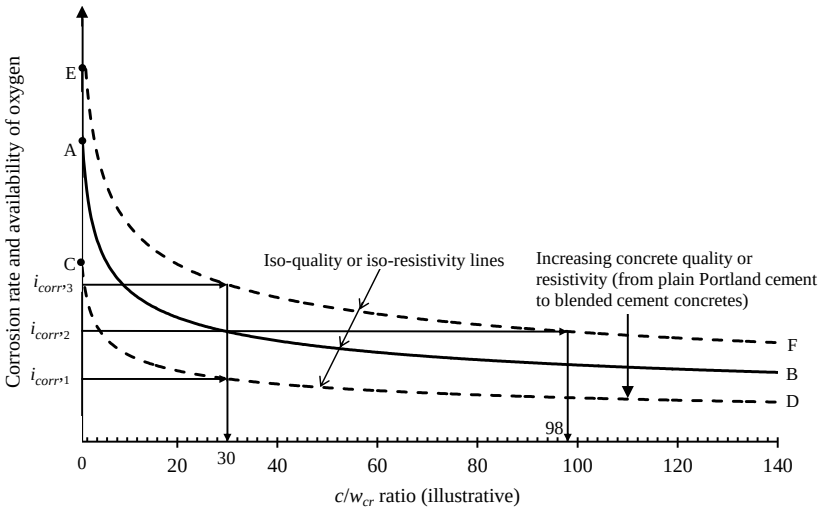

Figure 4.67: Proposed schematic relationship between corrosion rate, crack width, cover depth, concrete quality and resistivity

The shapes of the curves A-B, C-D and E-F are based on the trends obtained between i_{corr} and c/w_{cr} ratio from the experimental results of this study (see Figure 4.63 and Figure 4.64). In Figure 4.67, for a given c/w_{cr} ratio, corrosion rate varies depending on the concrete quality and resistivity. For example, at a c/w_{cr} = 30, it is possible to obtain $i_{corr,1} < i_{corr,2} < i_{corr,3}$. These corrosion rates correspond to the respective iso-quality (or iso-resistivity) curves as shown in Figure 4.67. If a nomogram of iso-quality and iso-resistivity curves is developed, it can be useful in the selection of a suitable combination of concrete quality, cover depth and crack width. In service life design, such a nomogram can be applied by first establishing the required time to a pre-defined corrosion-induced damage such as loss in steel cross section area. The corrosion-induced damage is then expressed in terms of an equivalent corrosion rate based on the selected time to maintenance or repair. Once the design corrosion rate is known, a suitable combination of c/w_{cr} ratio and concrete quality can be obtained from the nomogram. For example, in Figure 4.67, for corrosion rate $i_{corr,2}$, it is possible to select either a c/w_{cr} ratio of 98 (e.g. c = 39 mm, w_{cr} = 0.4 mm) or 30 (e.g. c = 21 mm, w_{cr} = 0.7 mm) - both lie on different iso-quality curves. However, the shift from c/w_{cr} ratio of 98 to 30 requires an improvement of concrete quality e.g. by using blended cements. At present, the main challenge in the development of such a nomogram is the construction of the iso-quality curves. This requires long-term data for different combinations of corrosion rate, cover depth, crack width and concrete quality or resistivity. Even though the cover depths (20 and 40 mm) and crack widths (0.4 and 0.7 mm) used in this study were limited to c/w_{cr} ratios ranging between 30 and 100, in the proposed schematic framework (Figure 4.67) it has been assumed to be applicable beyond these boundaries. This assumption needs to be investigated in further studies to check its validity.

Finally, even though this study proposes the use of c/w_{cr} ratio in conjunction with concrete quality (or resistivity) as durability design parameters for cracked concrete, it is important to acknowledge that this proposal is based on the crack width measured on the concrete surface. This is the most common approach for in-service RC structures. However, cracks may have different profiles (depth and shape). In the case of wedge-shaped cracks which are most common for flexural cracks, it is expected that the crack width at the steel level will be smaller than that measured on the concrete surface. At present, it is not clear how the crack profile (in combination with depth) may affect the application of the c/w_{cr} ratio but taking into account that in this study, all crack widths were measured on the concrete surface as has been done in most past studies [4, 11, 48, 50-52], it can be expected that this factor should not have an effect on the trends obtained in this study, and on which the proposed schematic nomogram (Figure 4.67) is based. Nevertheless, further studies are required to (i) ascertain if crack profile has a significant effect on corrosion rate (if any) and hence on the c/w_{cr} ratio, and (ii) understand the effect of steel-concrete interface damage on corrosion rate in cracked flexural RC members.

4.11 *Summary of experimental results*

Experimental results were presented and discussed in detail in this chapter. In this section, a summary of these findings is presented, and a number of trends and conclusions are generalized to draw useful insights. In addition, areas that need further research are highlighted.

The (laboratory and field) results obtained in this study, and in previous studies, have shown that cover depth, concrete quality, resistivity, cracking and crack width all affect corrosion rate. In summary, the following general conclusions can be made with respect to the results obtained in this study:

1. Crack width
   (a) For a given binder type, w/b ratio and cover depth, corrosion rate increased with increase in crack width. The extent of increase depended on the concrete cover, quality and resistivity. However, it is also logical to acknowledge that even though corrosion rate increases with an increase in crack width, this trend cannot be infinite. Other factors being constant, there will be a maximum crack width beyond which corrosion rate is no longer dependent on the increase in crack width. This could not be established in this study due to the limited number of crack widths used.
   (b) No general trend on the effect of crack width on corrosion rate could be drawn between the laboratory-based and field-based specimens; in some cases, the increase was higher in the laboratory-based specimens while in other cases, the reverse was true.
2. Cover depth:
   (a) For a given w/b ratio, corrosion rate increased with decrease in cover depth. This trend was observed in both the cracked and uncracked specimens.
   (b) In the presence of cover cracking, the impact of increasing cover depth can be substantially reduced, as was the case especially in the field-based specimens with 0.4 and 0.7 mm crack widths where, for a given concrete, corrosion rates in the specimens were similar for both 20 and 40 mm cover depths.
   (c) The impact of increasing cover on corrosion rate was relatively less in the field-based specimens than in the laboratory-based specimens.

3. w/b ratio:
   (a) For a given binder type, crack width and cover depth, corrosion rate increased with increase in w/b ratio. However, for a given cover depth, the corrosion rates in the blended cement concrete specimens were less affected than in PC concrete specimens by the change in w/b ratio from 0.55 to 0.40.
   (b) The effect of change in w/b ratio generally had a similar effect (i.e. decrease) on corrosion rate in both the field-based and laboratory-based specimens.
   (c) Concrete resistivity for a given binder type also decreased with increase in w/b ratio.
4. Binder type:
   (a) For a given w/b ratio, cover depth and crack width, partial replacement of PC with a supplementary cementitious material, SCM, (30% FA or 50% GGBS) resulted in decrease in corrosion rate.
   (b) There was no marked difference in the decreases in corrosion rate between the field-based and laboratory-based specimens due to partial replacement of plain PC with SCM.
   (c) For a given SCM, even though reducing the w/b ratio further increased the concrete's resistance to chloride ingress and hence corrosion rate, the effect was small compared to that of the presence of the SCM itself. This suggests that the high concrete resistivity in blended cement concretes had a major influence on corrosion rate than concrete quality due to change in w/b ratio
   (d) Concrete resistivity for a given w/b ratio increased with the partial replacement of PC with SCM. However, even though the dominating effect of high resistivity (in the blended cement concretes) on corrosion rate was still evident, the performance of the different concretes, both in the laboratory and in the field, with respect to corrosion could still be distinguished by the different crack widths.

At the design stage, it is usually difficult to establish a suitable combination of cover depth, crack width and quality. In this chapter a framework that can be used to achieve this was proposed, and will be exemplified in Chapter 5. Furthermore, such a framework can help in the selection of a suitable combination of these parameters to meet desired durability requirements. The use of c/w_{cr} ratio in conjunction with concrete quality was proposed but this still needs to be refined for design purposes. In general, corrosion rate was found to decrease with increasing c/w_{cr} ratio. From a practical viewpoint, it is usually convenient to deal with crack width ranges as opposed to specific crack widths. This means that for a given crack width range, a corresponding range of corrosion rates can be expected. However, it was not possible to achieve this in this study considering the limited number of crack widths used i.e. 0.4 and 0.7 mm crack widths for which the statistical analyses showed that for a given w/b ratio, cover depth and exposure environment, the corrosion rates in specimens with these crack widths were different and could not be averaged.

Concrete quality can be improved by, in addition to good construction practices (e.g. adequate compaction and proper curing), reduction in w/b ratio or the replacement of plain Portland cement (PC) with supplementary cementitious materials (SCMs) such as FA and GGBS. The results from both the field-based and laboratory-based corrosion investigations indicate that the partial replacement of PC with SCMs resulted in significant reductions in corrosion rate - up to 78% and 65% in,

respectively, slag (laboratory 0.7 mm cracked, 40 mm cover), and slag and fly ash (field 0.4 and 0.7 mm cracked, 20 mm cover). However, for a given w/b ratio, the blended cement concrete specimens had similar corrosion rates i.e. the corrosion performance of the blended cement concretes were less affected than PC concrete by the reduction in w/b ratio from 0.55 to 0.40. Even though only one w/b ratio (0.40) was used for the PC concrete, a previous study by Otieno *et al*. [11] showed similar results for blended cement concretes and higher changes in quality of PC concretes due to change in w/b ratio from 0.55 to 0.40 than in the blended cement concretes.

The results also showed that the accumulation of chlorides at the steel level was higher in cracked concrete (in the vicinity of the crack) than in uncracked concrete. However, even though high chloride contents were synonymous with high corrosion rates in the laboratory-based specimens, this was not the case in the field-based specimens. In the latter, corrosion rates remained low despite high chloride contents. This was attributed to the epoxy coating of their surfaces (except the top face) which prevented adequate drying out to facilitate ingress of oxygen to sustain cathodic reaction process. This was similar to the condition in the submerged zone in marine structures.

Finally, it is important to comment on the pitting effect of chloride-induced corrosion especially in cracked concrete. Even though the corrosion rates reported in this chapter were averaged over the whole steel surface, it must be acknowledged that this assumption leads to under-estimation of chloride-induced corrosion rates and consequently, the penetration depths obtained using such corrosion rates are also under-estimated. This is important especially for cracked RC where high local pitting occurs in the crack region. To account for this, pitting factors are usually introduced. This was covered in detail in Chapter 2. It is therefore recommended that gravimetric mass loss measurements be carried out at a later stage and compared with those calculated using the corrosion rate results reported here to quantify, if any, the error in the coulostatic linear polarization resistance measurements.

The next chapter deals with the development of the empirical chloride-induced corrosion rate prediction model based on the results and analyses presented in this chapter.

4.12 *References*

[1] Raupach, M. (1996) Investigations on the influence of oxygen on corrosion of steel in concrete - Part I. *Materials and Structures,* Vol. 29(3)**,** pp. 174-184.

[2] Andrade, C., Gulikers, J., Polder, R. & Raupach, M. (2003) Half-cell potential measurements- potential mapping on reinforced concrete structures *Materials and Structures,* Vol. 36(7)**,** pp 461-471.

[3] Zivica, V. (2003) Influence of w/c ratio on rate of chloride induced corrosion of steel reinforcement and its dependence on ambient temperature. *Bulletin of Materials Science,* Vol. 26(5)**,** pp. 471-475.

[4] Scott, A. N. & Alexander, M. G. (2007) The influence of binder type, cracking and cover on corrosion rates of steel in chloride-contaminated concrete. *Magazine of Concrete Research,* Vol. 59(7)**,** pp. 495-505.

[5] Akatsuka, Y., Seki, H. & Asaoka, K. (1966) Crack width and reinforcement corrosion in reinforced concrete attacked by sea-water. *Cement and Concrete Association,* No. 266 (January)**,** pp. 38-43.

[6] Schießl, P. & Raupach, M. (1997) Laboratory studies and calculations on the influence of crack width on chloride-induced corrosion of steel in concrete. *ACI Materials Journal,* Vol. 94(1)**,** pp. 56-62.

[7] Mackechnie, J. R. (2001) Predictions of reinforced concrete durability in the marine environment. *Research Monograph No. 1***,** Department of civil engineering, University of Cape Town and the University of Witwatersrand.

[8] Mackechnie, J. R. (1996) Predictions of reinforced concrete durability in the marine environment. *PhD Thesis*, Department of civil engineering, University of Cape Town.
[9] Alexander, M. G., Ballim, Y. & Stanish, K. (2008) A framework for use of durability indexes in performance-based design and specifications for reinforced concrete structures. *Materials and Structures*, Vol. 41(5)**,** pp. 921-936.
[10] Muigai, R., Moyo, P. & Alexander, M. (2012) Durability design of reinforced concrete structures: a comparison of the use of durability indexes in the deemed-to-satisfy approach and the full-probabilistic approach. *Materials and Structures*, Vol. 45(8)**,** pp. 1233-1244.
[11] Otieno, M. B., Alexander, M. G. & Beushausen, H.-D. (2010) Corrosion in cracked and uncracked concrete - influence of crack width, concrete quality and crack re-opening. *Magazine of Concrete Research*, Vol. 62(6)**,** pp. 393-404.
[12] Scott, A. N. (2004) The influence of binder type and cracking on reinforcing steel corrosion in concrete. *PhD Thesis*, Department of civil engineering, University of Cape Town.
[13] Hunkeler, F. (2005) *Corrosion in reinforced concrete structures*, Woodhead publishing limited, Abington Hall, Abington Cambridge CBI 6AH, England. pp. 1-45.
[14] Arya, C., Buenfeld, N. R. & Newman, J. B. (1990) Factors influencing chloride binding in concrete. *Cement and Concrete Research*, Vol. 20(2)**,** pp. 291-300.
[15] Rose, J. H. (1987) Effect of cementitious blastfurnace slag on chloride permeability of concrete. *ACI Special Publication*, Vol. 102(September)**,** pp. 107-126.
[16] Malhotra, V. M. (1987) Properties of fresh and hardened concrete incorporating ground granulated blast furnace slag, in: Malhotra, V. M. (Ed.), Supplementary cementing materials for concrete. *Minister of Supply and Services, Canada***,** pp. 291-336.
[17] Otieno, M. B. (2008) Corrosion propagation in cracked and uncracked concrete. *Masters Dissertation*, Department of civil engineering, University of Cape Town.
[18] Lewis, D. A. & Copenhagen, W. J. (1959) Corrosion of reinforcing steel in concrete in marine atmospheres. *Corrosion*, Vol. 15 (7)**,** pp. 382-388.
[19] Alvarez, A. & Galvele, J. (1984) Mechanism of pitting of high purity iron in NaCl solutions. *Corrosion Science*, Vol. 24(1)**,** pp. 27-48.
[20] Bamforth, P. B. (1994) Specification and design of concrete for the protection of reinforcement in chloride contaminated environments. UK Corrosion and Eurocorr 94, Bournemouth, Vol. III**,** pp 249-258.
[21] Somma, R., Jaturapitakkul, C., Chalee, W. & Rattanachu, P. (2012) Effect of the water-to-binder ratio and ground fly ash on properties of recycled aggregate concrete *Journal of Materials in Civil Engineering*, Vol. 24(1)**,** pp. 16-22.
[22] Shi, C. (2004) Effect of mixing proportions of concrete on its electrical conductivity and the rapid chloride permeability test (ASTM C1202 or ASSHTO T277) results. *Cement and Concrete Research*, Vol. 34(3)**,** pp. 537-545.
[23] Baweja, D., Roper, H. & Sirivivatnanon, V. (1996) Corrosion of steel in marine concrete: long-term half-cell potential and resistivity data. *Proceedings of the 3rd CANMET/ACI International conference on concrete in marine environment*, SP-163, American Concrete Institute**,** St. Andrews-by-the-Sea, New Brunswick, Canada, 4th -9th August, pp. 89-110.
[24] Whiting, D. A. & Nagi, M. A. (2003) Electrical resistivity of concrete - a literature review. *Portland Cement Association***,** Illinois, 56 pp.
[25] Hope, B. B., Ip, A. K. & Manning, D. G. (1985) Corrosion and electrical impedance in concrete. *Cement and Concrete Research*, Vol. 15(3)**,** pp. 525-534.
[26] Weydert, R. & Gehlen, C. (1999) Electrolytic resistivity of cover concrete: relevance, measurement and interpretation. *Proceedings of CIB W078 Workshop on information technology in construction, 31 May - 3 June, 1999***,** 11 pp.
[27] Cohen, M. D. & Bentur, A. (1988) Durability of Portland cement-silica fume pastes in magnesium sulphate and sodium sulphate solutions. *ACI Materials Journal*, Vol. 85(3)**,** pp. 148-157.
[28] Buenfeld, N. R., Newman, J. B. & Page, C. L. (1986) The resistivity of mortars immersed in sea-water. *Cement and Concrete Research*, Vol. 16(4)**,** pp. 511-524.
[29] Buenfeld, N. R. & Newman, J. B. (1986) The development and stability of surface layers on concrete exposed to sea-water. *Cement and Concrete Research*, Vol. 16(5)**,** pp. 721-732.
[30] Polder, R., Andrade, C., Elsener, B., Vennesland, O., Gulikers, J., Weidert, R. & Raupach, M. (2000) Test methods for onsite measurement of resistivity of concrete. *Materials and Structures*, Vol. 33(10)**,** pp. 603-611.
[31] Bisschop, J. & Mier, J. G. M. (2008) Effect of aggregates and microcracks on the drying rate of cementitious composites. *Cement and Concrete Research*, Vol. 38(10)**,** pp. 1190-1196.
[32] Bažant, Z. P. & Najjar, L. J. (1971) Drying of concrete as a nonlinear diffusion problem. *Cement and Concrete Research*, Vol. 1(5)**,** pp. 461-473.

[33] Akita, H., Fujiwara, T. & Ozaka, Y. (1997) A practical procedure for the analysis of moisture transfer within concrete due to drying. *Magazine of Concrete Research,* Vol. 49(179)**,** pp. 129-137.
[34] Chrisp, T. M., McCarter, W. J., Starrs, G., Basheer, P. A. M. & Blewett, J. (2002) Depth-related variation in conductivity to study cover-zone concrete during wetting and drying. *Cement and Concrete Composites,* Vol. 24(5)**,** pp. 415-426.
[35] Alonso, C., Andrade, C. & Gonzalez, J. A. (1988) Relation between resistivity and corrosion rate of reinforcements in carbonated mortar made with several cement types. *Cement and Concrete Research,* Vol. 18(5)**,** pp. 687-698.
[36] Andrade, C., Alonso, C. & Garcia, A. M. (1990) Oxygen availability in the corrosion of reinforcements. *Advances in Cement Research,* Vol. 3(11)**,** pp. 127-132.
[37] Gjørv, O. E. (1986) Diffusion of dissolved oxygen through concrete. *Materials Performance,* Vol. 25(12)**,** pp. 39-44.
[38] Otieno, M. B., Alexander, M. G. & Beushausen, H.-D. (2010) Suitability of various measurement techniques for assessing corrosion in cracked concrete. *ACI Materials Journal,* Vol. 107(5)**,** pp. 481-489.
[39] ASTM-C876-91 (1999) *Standard test method for half-cell potentials of uncoated reinforcing steel in concrete*, ASTM International, West Conshohocken, PA 19428-2959, USA.
[40] Alonso, C., Castellote, M. & Andrade, C. (2002) Chloride threshold dependence of pitting potential of reinforcements. *Electrochimica Acta,* Vol. 47(21)**,** pp. 3469-3481.
[41] Stansbury, E. E. & Buchanan, R. A. (2000) *Fundamentals of Electrochemical Corrosion*, ASM International, Ohio.
[42] Broomfield, J. P. (2007) *Corrosion of steel in concrete - understanding, investigation and repair (2nd Edition)*, Taylor & Francis, Oxford, United Kingdom.
[43] Broomfield, J. P., Rodriguez, J., Ortega, L. M. & Garcia, A. M. (1993) Corrosion rate measurements in reinforced concrete structures by a linear polarization device. *Proceedings of the International symposium on condition assessment, protection, repair, and rehabilitation of concrete bridges exposed to aggressive environments, ACI Fall Convention*. 9th –10th November, Minneapolis, MN. pp. 644-651.
[44] Bažant, Z. P. (1987) Snapback instability at crack ligament tearing and its implication for fracture micro-mechanics. *Cement and Concrete Research,* Vol. 17(6)**,** pp. 951-967.
[45] Audenaert, K., Marsavina, L. & De Schutter, G. (2009) Influence of cracks on the service life of concrete structures in a marine environment *Key Engineering Materials,* Vol. 399**,** pp. 153-160.
[46] Win, P. P., Watanabe, M. & Machida, A. (2004) Penetration profile of chloride ion in cracked reinforced concrete. *Cement and Concrete Research,* Vol. 34(7)**,** pp. 1073-1079.
[47] Foley, R. (1970) Role of the chloride ions in iron corrosion. *Corrosion,* Vol. 26(2)**,** pp. 58-70.
[48] Beeby, A. (1983) Cracking, cover and corrosion of reinforcement. *Concrete International,* Vol. 5(2)**,** pp. 35-40.
[49] Gowripalan, N., Sirivivatnanon, V. & Lim, C. C. (2000) Chloride diffusivity of concrete cracked in flexure. *Cement and Concrete Research,* Vol. 30(3)**,** pp. 725-730.
[50] Suzuki, K., Ohno, Y., Praparntanatorn, S. & Tamura, H. (1990) *Mechanism of steel corrosion in cracked concrete*. Page, C., Treadaway, K. & Bramforth, P. Corrosion of reinforcement in concrete. London: Society of Chemical Industry**,** pp. 19-28.
[51] Tuutti, K. (1982) Corrosion of steel in concrete. *Swedish Cement and Concrete Research Institute, S-100 44 Stockholm*. Report No. CBI Research 4:82, ISSN 0346-6906, Stockholm, pp. 468.
[52] Rooij, M. R., Yoon, I. & Schlagen, E. (2007) Chloride ingress and critical crack width. *Proceedings of the International Conference on Integral Service Life Modelling of Concrete Structures,* 5-6 November, 2007, Guimaraes, Portugal**,** pp. 79-86.

Chapter 5

Corrosion rate prediction models

5.1 *Introduction*

This chapter presents the framework of empirical chloride-induced corrosion rate prediction models developed based on the experimental results that were presented in Chapter 4. A model is proposed each for the laboratory-based and field-based specimens; each model comprises two parts, one for cracked and the other for uncracked concrete. This chapter focuses mainly on the cracked corrosion rate prediction models although those for uncracked concrete are also discussed. The phrase '*corrosion rate prediction*' is used in this chapter to refer to the process of using the proposed model to predict a corrosion rate value at approximately 2¼ years after corrosion initiation in the laboratory or field exposure environments. The time 2¼ years was the experimental duration. Note that the phrase "approximately 2¼ years" is used because the time taken for 0.4 and 0.7 mm cracked specimens, which reverted to passive state after exposure to either laboratory or field environments, to regain active corrosion state was up to 16 and 36 weeks for, respectively, laboratory and field specimens. It is important to note that the average corrosion rates used to determine the prediction models for field corrosion rates were not necessarily stable as was the case with the laboratory-based specimens. The pseudo-plateau phase shown in the field-based specimens was attributed to seasonal weather changes (from summer to winter); this was discussed in Chapter 4. This is a limitation to the application of the field-based corrosion rate prediction models. Long-term field corrosion rates will need to be collected in order to update the models. The results of the experimental investigations led to general conclusions being made with regard to specific parameters influencing chloride-induced corrosion rate of steel in concrete. These can be summarized as: (i) corrosion rate (i_{corr}) increases as the surface crack width (w_{cr}) increases but to an extent dependent on concrete quality (binder type and w/b ratio), (ii) i_{corr} decreases with increasing cover depth (c), and that (iii) concrete resistivity affects i_{corr} mainly in blended cement concretes.

The empirical laboratory-based and field-based models proposed in this chapter are limited to three main parameters namely cover depth, crack width and concrete quality (quantified using the chloride diffusion coefficient, D_{90}, obtained from 90-day chloride conductivity index – see Appendix D). However, it is important to acknowledge that corrosion rate is affected by many other inter-related parameters; further work will be needed to incorporate the relevant ones in the model depending on the prevailing exposure conditions. Furthermore, other aspects such as its temporal variation can be incorporated in the model if the constantly-changing environment around the steel is monitored and its corrosion-sustaining potential and effects quantified; however, contrary to laboratory experiments and numerical modelling where the conditions around the steel can, to some extent, be quantified, this is seldom the case for in-service RC structures. In this study, the conditions around the steel such as temperature, relative humidity and pH were not monitored. The temporal aspect of corrosion rate was therefore not incorporated in the models.

Only active corrosion rate data (i.e. $i_{corr} \geq 0.1$ μA/cm^2) were used in the development of the models. Passive corrosion rates were not used as they depict the corrosion initiation phase which can be predicted using available well-established Fickian-based models such as DuraCrete [1], LIFE365 [2], and the South African model [3]. It is also important to note that even though incipient-cracked specimens were investigated (for specimens with 20 mm cover depth), and shown in Chapter 4 to influence both the chloride ingress, and corrosion rate depending on the binder type, w/b ratio and exposure environment (laboratory and field), it was not possible to objectively quantify their effect on corrosion rate; corrosion rates for incipient-cracked specimens were therefore not included in the development of the models.

Finally, this chapter also deals with the quantification of variability in the laboratory and field corrosion rate results based on the proposed model. First, a summary of the empirical correlations between corrosion rate and the various experimental variables is presented.

5.2 *Corrosion rate prediction models*

In Chapter 4, empirical relationships between average corrosion rate (i_{corr}), crack width (w_{cr}), concrete quality (represented by the diffusion coefficient obtained from the 90-day chloride conductivity index, D_{90}), cover depth (c) and resistivity (ρ) were obtained from the regression analyses of both the field-based and laboratory-based results - see Sections 4.6.1, 4.7.1 and 4.10 in Chapter 4. The general relationships between corrosion rate and these parameters were expressed as follows:

i_{corr} vs. diffusion coefficient (D_{90}): $$i_{corr} = k_1 e^{A_1\left(D_{90}\times 10^{10}\right)} \text{ [μA/cm}^2\text{]} \quad (5.1)$$

i_{corr} vs. resistivity (ρ): $$i_{corr} = k_2\left(\frac{1}{\rho^{A_2}}\right) \text{ [μA/cm}^2\text{]} \quad (5.2)$$

i_{corr} vs. c/w_{cr} ratio: $$i_{corr} = k_3\left(\frac{c}{w_{cr}}\right)^{-A_3} \text{ [μA/cm}^2\text{]} \quad (5.3)$$

The values of the coefficients k_1, k_2, k_3 and A_1, A_2, A_3, based on the experimental results presented in Chapter 4, are summarised in Table 5.1. The experimental results also showed that the values for coefficients k_1 (μA/cm^2), k_2 ((μA/cm^2)/kΩ-cm), A_1 (s/cm^2) and A_2 (–) are dependent on cover depth, crack width and exposure environment while the values for k_3 (μA/cm^2) and A_3 (–) are dependent on binder type and w/b ratio, and exposure environment. It is important to note that even though only cover depth, concrete quality, resistivity and crack width are represented in these equations, other factors such as temperature and crack density also affect corrosion rate but were not investigated in this study. The justification for focusing on cover depth, concrete quality, resistivity and crack width was discussed in Chapter 3.

Table 5.1: Coefficients for Equations (5.1), (5.2) and (5.3) based on experimental results

Reference equation	Crack width	Cover (mm)	Laboratory specimens		Field specimens	
Eqn. (5.1) $i_{corr} = k_1 e^{A_1 (D_{90} \times 10^{10})}$			k_1*	A_1	k_1	A_1
	Uncracked	20	0.44	0.05	0.25	0.02
		40	0.33	0.05	0.16	0.03
	0.4 mm	20	0.67	0.04	0.27	0.04
		40	0.49	0.05	0.25	0.03
	0.7 mm	20	0.97	0.04	0.33	0.04
		40	0.58	0.05	0.31	0.03
Eqn. (5.2) $i_{corr} = k_2 \left(\frac{1}{\rho^{A_2}} \right)$			k_2	A_2	k_2	A_2
	Uncracked	20	112.06	1.18	5.91	0.62
		40	88.71	1.17	13.88	0.88
	0.4 mm	20	68.87	0.98	28.16	0.92
		40	87.20	1.09	12.08	0.77
	0.7 mm	20	91.69	0.97	46.93	0.98
		40	148.21	1.17	9.75	0.68
Eqn. (5.3) $i_{corr} = k_3 \left(\frac{c}{w_{cr}} \right)^{-A_3}$	Mix label		k_3	A_3	k_3	A_3
	PC-40		7.60	0.29	4.74	0.44
	SL-40		5.58	0.59	0.90	0.25
	SL-55		5.41	0.40	1.23	0.26
	FA-40		6.20	0.39	0.89	0.23
	FA-55		6.05	0.57	2.33	0.38

* : Units for coefficients

k_1 : μA/cm^2 k_2 : (μA/cm^2) / kΩ-cm k_3 : μA/cm^2

A_1 : s/cm^2 A_2 : [–] A_3 : [–]

The empirical relationships in Equations (5.1), (5.2) and (4.3) are based on average corrosion rates (between week 104 and 120); the models can therefore be considered to be true reflections of the actual corrosion rates in the respective environments at approximately 2¼ years after corrosion initiation t_i i.e. t_i + 2¼ years. Even though resistivity results showed high correlation ($R^2 > 0.8$) with corrosion rate, the diffusion coefficient (D_{90}) was used in the model development. The decision to use D_{90} obtained from the 90-day chloride conductivity index instead of concrete resistivity was motivated by the current challenges associated with using the 4-point Wenner probe for in-situ surface resistivity measurement where high variations in concrete moisture content are usually experienced. This problem is not experienced in the chloride conductivity test due to the sample pre-conditioning carried out prior to the test (see Appendix D). The reasons for using the diffusion coefficient obtained from the 90-day chloride conductivity index and not the 28-day chloride conductivity index was discussed in Chapter 4 and mainly relate to the slow rate of maturity in the blended cement concretes (especially fly ash concrete). It is also important to note that Eqn. (5.3) is based on the corrosion rate data for only the 0.4 and 0.7 mm cracked specimens (for both 20 and 40 mm cover depths) because, as already mentioned, the incipient-crack widths were not quantified. Furthermore, only one cover depth (20 mm) was used for these specimens. This was discussed in detail in Chapter 4.

To obtain empirical equations for corrosion rate prediction models incorporating D_{90}, c and w_{cr} for the cracked specimens and D_{90} and c for uncracked specimens, Equations (5.1) and (5.3) were logically combined as follows:

(i) Cracked specimens (laboratory and field): the coefficients A_3 and k_3, both of which incorporate the effect of binder type and w/b ratio on corrosion rate, were plotted against D_{90} values for the corresponding concretes to establish their variation with change in concrete quality, D_{90}.

(ii) Uncracked specimens (laboratory and field): only Eqn. (5.1) was used. The arithmetic mean value of A_1 was obtained while k_1 was plotted against cover depth to establish how it varies with change in cover depth. Both A_1 and k_1 incorporate the effect of crack width (zero in this case) and cover depth on corrosion rate. It is important to note that the regression trends obtained between k_1 and c, Eqn. (5.7), were based on limited data and will need to be updated in future if more data becomes available.

The resulting equations are as follows:

$$k_3 \text{ vs. } D_{90} \begin{cases} k_{3,lab,cracked} = 5.18\mathrm{e}^{0.01\left(D_{90}\times 10^{10}\right)},\ R^2 = 0.9 \\ k_{3,\,field\,,cracked} = 0.64\mathrm{e}^{0.06\left(D_{90}\times 10^{10}\right)},\ R^2 = 0.9 \end{cases} \tag{5.4}$$

$$\mathrm{A}_3 \text{ vs. } D_{90} \begin{cases} \mathrm{A}_{3,lab,cracked} = 0.96\left(D_{90}\times 10^{10}\right)^{-0.35},\ R^2 = 0.7 \\ \mathrm{A}_{3,\,field\,,cracked} = 0.21\mathrm{e}^{0.02\left(D_{90}\times 10^{10}\right)},\ R^2 = 0.8 \end{cases} \tag{5.5}$$

$$\text{Arithmetic mean of } \mathrm{A}_{1,uncracked} \begin{cases} \text{Laboratory specimens} = 0.05 \\ \text{Field specimens} = 0.03 \end{cases} \tag{5.6}$$

$$k_1 \text{ vs. } c \ \left(\text{uncracked}\right) \begin{cases} k_{1,\,field} = 1.19c^{-0.34},\ R^2 = 0.8 \\ k_{1,lab} = 1.72c^{-0.64},\ R^2 = 0.9 \end{cases} \tag{5.7}$$

In the case of cracked specimens, the coefficients k_3 and A_3 in Eqn. (5.3) were then replaced with those in Equations (5.4) and (5.5) while in the case of uncracked specimens, the coefficients A_1 and k_1 in Eqn. (5.1) were replaced with those in Equations (5.6) and (5.7). The resulting empirical corrosion rate prediction models are given in Equations (5.8) and (5.9) for, respectively, laboratory and field corrosion rates:

$$i_{corr,lab\ (t_i+2.25\text{ years})} = \begin{cases} \left(5.18\mathrm{e}^{0.01\left(D_{90}\times 10^{10}\right)}\right)\left(\dfrac{c}{w_{cr}}\right)^{-a} & \text{for cracked RC} \\ \left(\dfrac{1.19}{c^{0.34}}\right)\mathrm{e}^{0.05\left(D_{90}\times 10^{10}\right)} & \text{for uncracked RC} \end{cases} \quad [\mu\text{A/cm}^2] \tag{5.8}$$

$$i_{corr,\,field\ (t_i+2.25\ \text{years})} = \begin{cases} \left(0.64\mathrm{e}^{0.06\left(D_{90}\times 10^{10}\right)}\right)\left(\dfrac{c}{w_{cr}}\right)^{-b} & \text{for cracked RC} \\ \left(\dfrac{1.72}{c^{0.64}}\right)\mathrm{e}^{0.03\left(D_{90}\times 10^{10}\right)} & \text{for uncracked RC} \end{cases} \quad [\mu\text{A/cm}^2] \tag{5.9}$$

where $a = 0.96\left(D_{90}\times 10^{10}\right)^{-0.35}$ and $b = 0.21\mathrm{e}^{0.02\left(D_{90}\times 10^{10}\right)}$. Note that the term 'cracked RC' as used here refers to the 0.4 and 0.7 mm cracked specimens.

Before proceeding, an assessment of the error introduced in the empirical correlations after combining the separate empirical equations for laboratory and field corrosion rates (i.e. Eqns. (5.1) and (5.3)) to give Equations (5.8) and (5.9) was carried out. This was achieved by comparing the predicted corrosion rates (using Eqns. (5.8) and (5.9)) with the corresponding average measured (week 104-120) laboratory and field corrosion rates (see Figure 5.1).

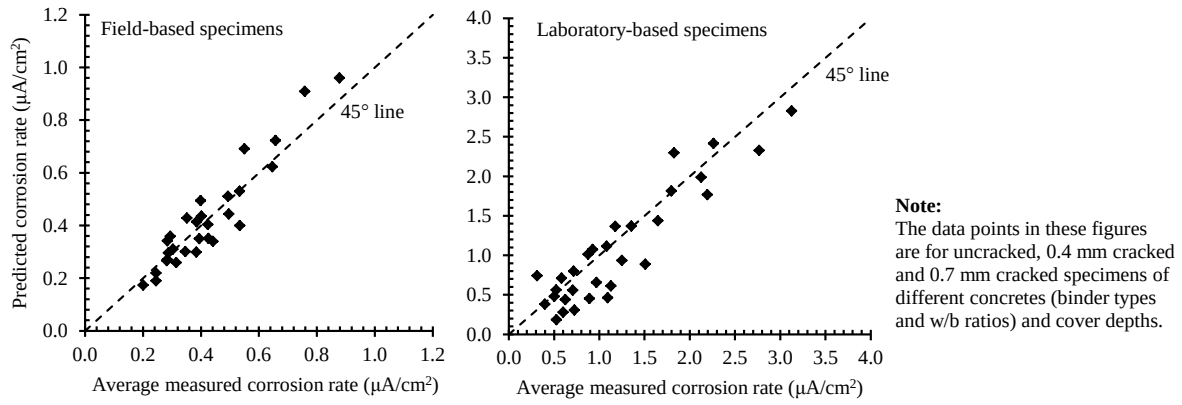

Figure 5.1: Summary of predicted vs. actual field and laboratory corrosion rates (data from current study)

Figure 5.1 shows that the predicted field-based and laboratory-based corrosion rates are generally in good agreement with the corresponding actual measured corrosion rates. However, the model accuracy cannot be inferred from this comparison. An analysis will need to be carried out in the future to assess the accuracy of the proposed models in predicting corrosion rates measured in studies similar to this one. Due to unavailability of data obtained from independent sources for both accelerated and natural corrosion rate from other studies the model accuracy could not be ascertained. It is important to note that in the case of the corrosion rate model for accelerated corrosion rate ($i_{corr,lab}$), corrosion rate results from similar studies by Scott and Alexander [4] and Otieno [5] would have been used to check its accuracy but the data were limited to shorter time periods (less than 2 years). In addition to checking the accuracy of the proposed models ($i_{corr,field}$ and $i_{corr,lab}$), they will still need to be calibrated and modified to improve on their accuracy as long-term results become available.

Equations (5.8) and (5.9) incorporate the influence of concrete quality (binder type and w/b ratio), cover depth (c, mm) and crack width (w_{cr}, mm) on corrosion rate. For illustration purposes, graphical representations of Equations (5.8) and (5.9) for various combinations of crack width, cover depth and concrete quality (Table 5.2 and Table 5.3) are given in Figure 5.2 to Figure 5.5. The combinations of

crack width, cover depth and concrete quality were arbitrarily selected to show the potential of using the empirical models to objectively compare the potential durability performance (with respect to steel corrosion) of concretes with different cover depths, crack widths and qualities (penetrability).

Table 5.2: Input parameters used for Equations (5.8) and (5.9) - (Figure 5.2 to Figure 5.5)

		Cover depth (mm)	Crack width (mm)	D_{90} (cm^2/s) x 10^{-10}
Case I	Scenario A	Variable (5 - 100)	0 (uncracked)	Constant (7.5)
	Scenario B		0.4	
	Scenario C		0.7	
	Scenario D		1.0	
Case II	Scenario A	Variable (5 - 100)	0 (uncracked)	6.9
	Scenario B		0.4	9.4
	Scenario C		0.4	13.5
	Scenario D		0.4	6.9
Case III	Scenario A	Variable (5 - 100)	0 (uncracked)	7.5
	Scenario B		1.0	7.2
	Scenario C		0.3	7.5
	Scenario D		0.7	13.5
Case IV	Scenario A	Constant (40)	Variable (0 - 1)	6.9
	Scenario B			7.5
	Scenario C			13.5

Note: Combinations of crack width, cover depth and concrete quality were arbitrarily selected

Table 5.3: Equivalent chloride conductivity values for D_{90} values given in Table 5.2

Diffusion coefficient D_{90} x 10^{-10} (cm^2/s)	Equivalent 90-day chloride conductivity, C_{90} (mS/cm)[a]	
	50/50 PC/GGBS	70/30 PC/FA
6.9	0.13	–[b]
7.2	0.17	–
7.5	0.22	–
9.4	0.47	0.22
13.5	0.87	0.60

[a] See Appendix D for empirical relationship between CCI and diffusion coefficient

[b] Such low diffusion coefficients are not realistic for fly ash concretes

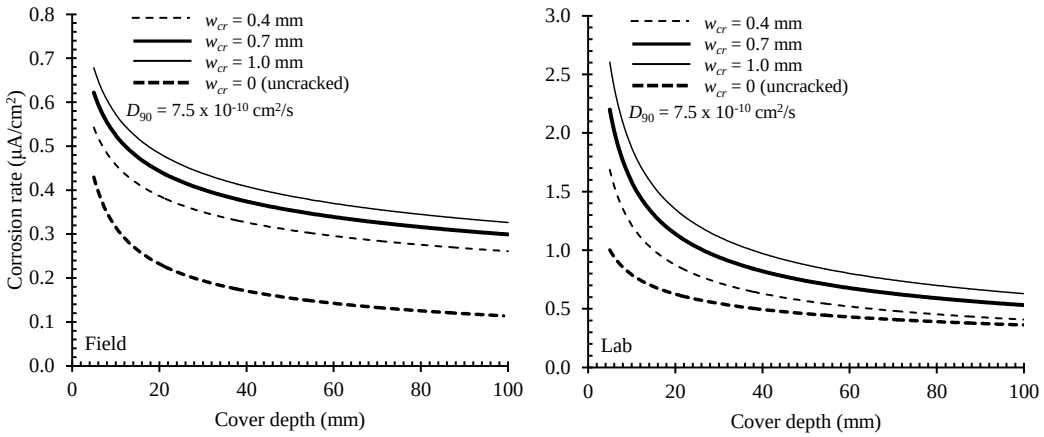

Figure 5.2: Variation of corrosion rate with cover and crack width - Case I

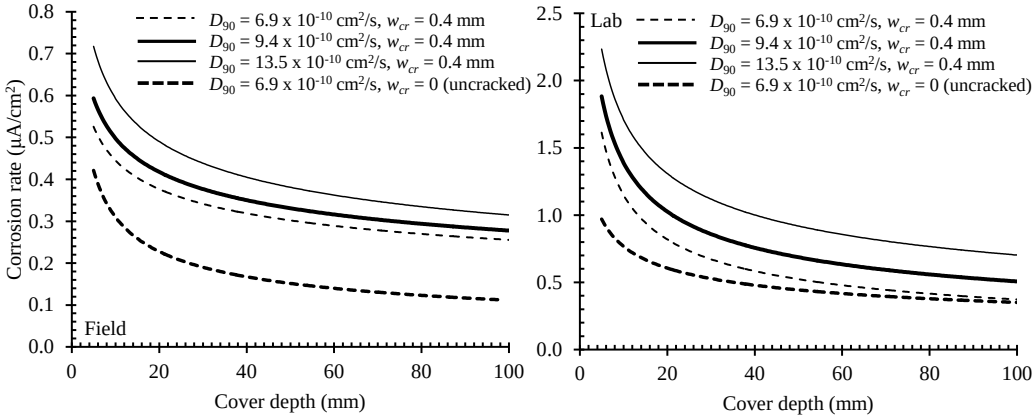

Figure 5.3: Variation of corrosion rate with cover and concrete quality - Case II

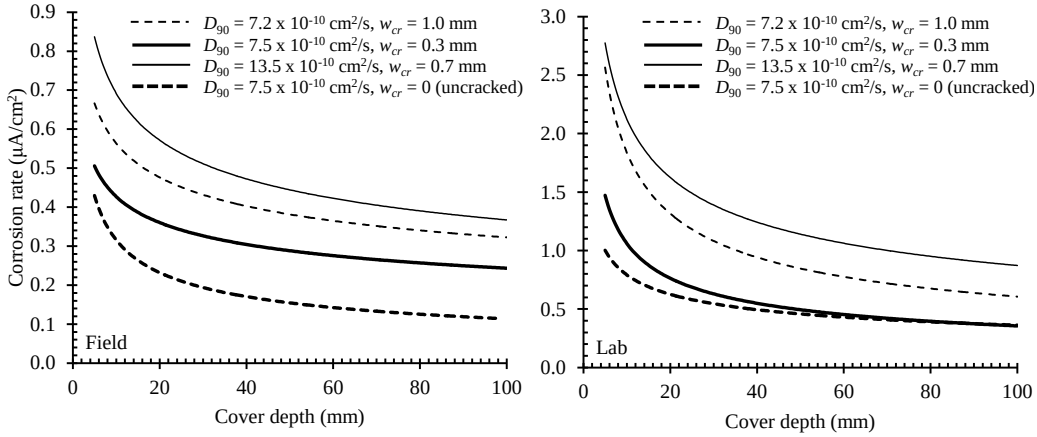

Figure 5.4: Variation of corrosion rate with cover, crack width and concrete quality - Case III

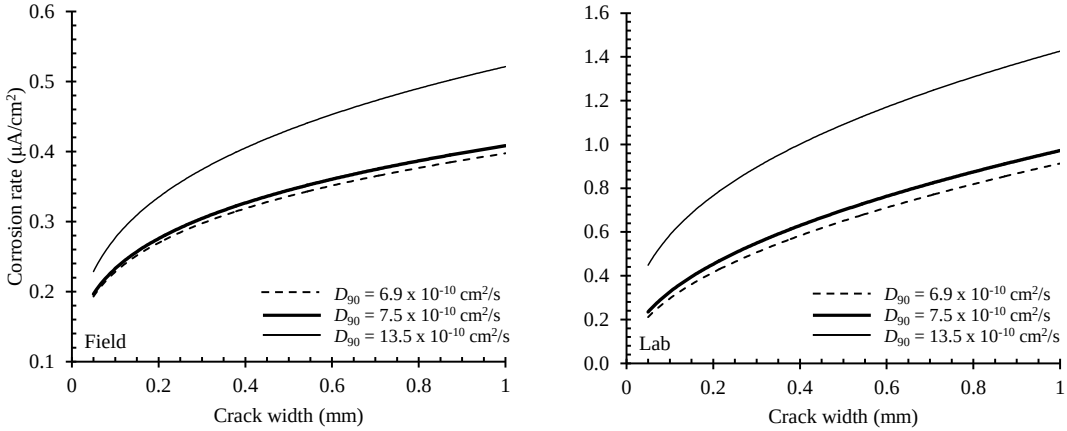

Figure 5.5: Variation of corrosion rate with crack width and concrete quality - Case IV

The following general observations can be made from Figure 5.2 to Figure 5.5:

(i) For a given cover depth, corrosion rate is sensitive to both concrete quality and crack width. Analyses will be carried out in Section 5.5 to establish the relative sensitivity of corrosion rate to these parameters.

(ii) In the laboratory-based concretes, as the cover depth increases, the effect of cover cracking on corrosion rate becomes less dominant (especially for w_{cr} < 0.3 mm, see Figure 5.4) than in the

field-based ones. This observation, as was mentioned in Chapter 4, can probably be attributed to the effect of crack self-healing for w_{cr} < 0.3 mm [6-8]. For the field-based concretes, the proposed $i_{corr,field}$ model (cracked and uncracked) show that there is still a stark difference in corrosion rates between uncracked and cracked concretes even as the cover depth increases. It is not clear why the proposed $i_{corr,field}$ models do not follow the trend shown by the laboratory-based concretes even though crack self-healing is expected to have also occurred in the field-based specimens as a result of (i) continued cement hydration, and (ii) deposition of debris from the sea water in the crack. This observation affirms the need for further work to investigate and quantify the effect of crack self-healing, if any, on corrosion rate in both laboratory-based and field-based specimens.

5.3 *Correlation between laboratory and field corrosion rates*

In the experimental programme (see Chapter 3), after inducement of active corrosion in all the specimens using an anodic impressed current, accelerated corrosion in the laboratory was achieved by 3-days wetting (with 5% NaCl solution) and 4-days air-drying (25 °C and 50% RH) while the field-based specimens were exposed to a tidal marine exposure to undergo natural corrosion.

In an attempt to establish a correlation between laboratory and field corrosion rates, the ratio between laboratory and corresponding field corrosion rates was determined (i.e. λ^{-1}-ratio, Eqn. (5.10)) but only for cases where both laboratory and field corrosion rates were active i.e. ≥ 0.1 μA/cm^2.

$$i_{corr,\,field\,(t_i+2,25)} = \lambda\left(i_{corr,lab(t_i+2.25)}\right) \tag{5.10}$$

This analysis showed that determining a constant λ^{-1}-ratio between laboratory and field corrosion rates was not possible due to the high variability in the λ^{-1}-ratios ranging from 0.8 to 15.3 (see box and whisker plot, Figure 5.6), and corresponds to the high temporal variability in the laboratory and field corrosion rates. The distribution of the λ^{-1}-ratios was such that 93% of values for λ^{-1} were ≤ 6 while 7% were > 6.

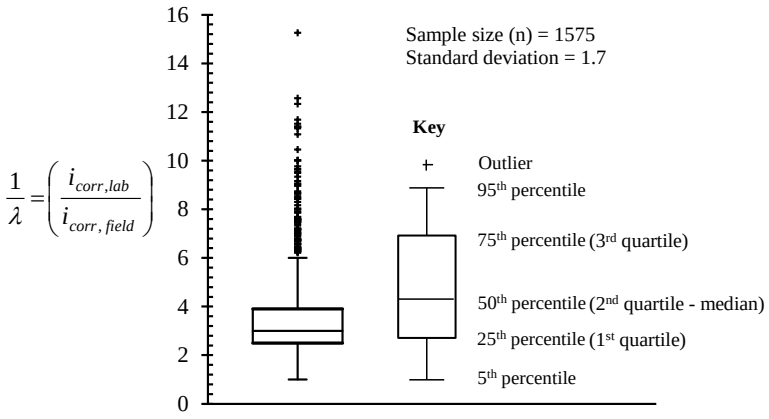

Figure 5.6: Box and whisker plot showing variability in the λ^{-1}ratios

Therefore, a parameter-dependent ratio (λ) of the laboratory (accelerated) and field (natural) corrosion rates (i.e. Equations (5.11) and (5.12)) was determined.

For cracked specimens:

$$\lambda_{cracked} = \frac{\left(0.64e^{0.06\left(D_{90}\times10^{10}\right)}\right)\left(\frac{c}{w_{cr}}\right)^{-b}}{\left(5.18e^{0.01\left(D_{90}\times10^{10}\right)}\right)\left(\frac{c}{w_{cr}}\right)^{-a}} = \left(\frac{0.64}{5.18}\right)\times\left(e^{0.05\left(D_{90}\times10^{10}\right)}\right)\times\left(\frac{c}{w_{cr}}\right)^{k} \quad (5.11)$$

$$= \left(0.124e^{0.05\left(D_{90}\times10^{10}\right)}\right)\left(\frac{c}{w_{cr}}\right)^{k}$$

$$\text{where } k = a - b = \left(0.96\left(D_{90}\times10^{10}\right)^{-0.35}\right) - \left(0.21e^{0.02\left(D_{90}\times10^{10}\right)}\right)$$

$$= 0.96\left(D_{90}\times10^{10}\right)^{-0.35} - 0.214^{\left(D_{90}\times10^{10}\right)}$$

and for uncracked specimens:

$$\lambda_{uncracked} = \frac{\left(\frac{1.72}{c^{0.64}}\right)e^{0.03\left(D_{90}\times10^{10}\right)}}{\left(\frac{1.19}{c^{0.34}}\right)e^{0.05\left(D_{90}\times10^{10}\right)}} = \left(\frac{1.72}{1.19}\right)c^{-0.3}\,e^{-0.02\left(D_{90}\times10^{10}\right)} \quad (5.12)$$

$$= \left(\frac{1.445}{c^{0.3}}\right)0.98^{\left(D_{90}\times10^{10}\right)}$$

where $i_{corr,field}$ and $i_{corr,lab}$ are, respectively, the field-based and laboratory-based corrosion rates ($\mu A/cm^2$), D_{90} is the diffusion coefficient (cm^2/s), c is the cover depth (mm) and w_{cr} is the surface crack width (mm). The relationships between laboratory and field corrosion rates in cracked and uncracked concrete in Eqn. (5.11) and (5.12) are illustrated, using randomly selected values for D_{90}, c and w_{cr}, in Figure 5.7.

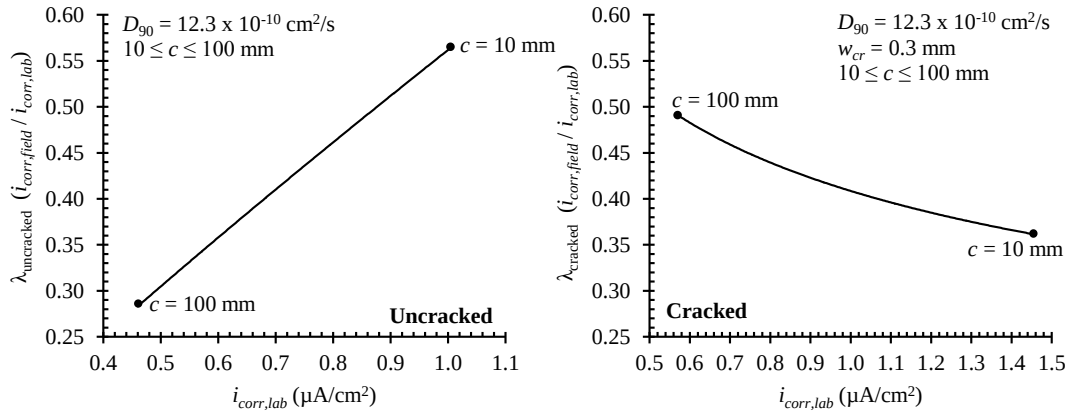

Note: The values for D_{90}, c and w_{cr} are randomly selected for illustration

Figure 5.7: Graphical illustration of the correlation between laboratory and field corrosion rates (based on Equations (5.11) and (5.12))

These empirical relationships provide a means of using accelerated corrosion in the laboratory by cyclic wetting and drying to predict field performance under similar exposure conditions. Equation

(5.12) shows that the 'scaling factor' λ is a function of concrete quality, crack width and cover depth. However, similar to the corrosion rate models (Eqns. (5.8) and (5.9)), this empirical correlation between laboratory and field corrosion rates is valid at approximately t_i + 2¼ years, and long-term (field) data is required to validate it. Furthermore, the correlation should also incorporate other factors such as temperature and relative humidity which affect corrosion but were not explicitly included in the experimental programme as variables, and hence not included in the proposed models.

5.4 *Comparison of proposed model with selected previous models*

In Chapter 2, a number of empirical corrosion rate prediction models were reviewed and their strengths and shortcomings highlighted. In this section the proposed $i_{corr,lab}$ model (Eqn. (5.8)) is compared with those of Scott [9] and Vu *et al*. [10]; only $i_{corr,lab}$ model is used for consistency with the these models which were developed using data from accelerated corrosion experiments. The models are selected because the input parameters are available from this study. The models are summarized in Table 5.4. More specific details on Scott's and Vu *et al*.'s models can be found in Chapter 2. Only the proposed model incorporates crack width as an input parameter.

Table 5.4: Corrosion rate prediction models for Scott (2004), Vu et al. (2005) and current study

Reference	Model	Input parameters
Vu *et al*. (2005)	$i_{corr} = \left(\frac{37.8(1-w/b)^{-1.64}}{c}\right)\alpha\, t_p^{\beta}$	Cover depth, c (cm) w/b ratio Time after corrosion initiation, t_p (yrs)
Scott (2004)	$i_{corr} = \left(1.43\frac{CCI_{90}}{f} + 0.02\right)\exp\left[\left(\frac{40-c}{20}\right)\times 1.2\left(\frac{CCI_{90}}{f}\right)^3\right]$	Cover depth, c (mm) Concrete quality, CCI_{90} (mS/cm)[a] $f = 10^{(\lvert 0.5-S\rvert -0.5+S)}$
This study ($i_{corr.lab}$)	$i_{corr,lab\ (t_i+2.25\ years)} = \begin{cases} \left(5.18e^{0.01\left(D_{90}\times 10^{10}\right)}\right)\left(\frac{c}{w_{cr}}\right)^{-a} & \text{Cracked} \\ \left(\frac{1.19}{c^{0.34}}\right)e^{0.05\left(D_{90}\times 10^{10}\right)} & \text{Uncracked} \end{cases}$ $a = 0.96\left(D_{90}\times 10^{10}\right)^{-0.35}$	Cover depth, c (mm) Crack width, w_{cr} (mm) Concrete quality, D_{90} (cm^2/s)[b]

[a] Concrete quality characterized by 90-day chloride conductivity index, CCI_{90}

[b] Concrete quality characterized by diffusion coefficient, D_{90} (determined using 90-day chloride condictivity index)

S, in Scott's model, is the amount of supplementary cementitious material expressed as a decimal e.g. 0.25 for 25%

In Table 5.4, α and β are, respectively, 1.0 and 0 (for time invariant corrosion rate) and f is a correction factor. The arbitrarily selected input variables used to compare the corrosion rates predicted by the three models are summarized in Table 5.5 - two Cases I and II which essentially differ in concrete quality and crack width are used. The predicted corrosion rates for the three models (Table 5.4) using the input parameters in Table 5.5 are presented in Figure 5.8(a), (b) and (c).

Table 5.5: Input variables used to compare proposed model with Scott's [9] and Vu *et al.*'s [10] models

Model input parameter	Case I		Case II	
	Uncracked	Cracked	Uncracked	Cracked
Binder	50/50 PC/GGBS	50/50 PC/GGBS	70/30 PC/FA	70/30 PC/FA
w/b ratio	0.40	0.40	0.40	0.40
90-day chloride conductivity index (CCI_{90}), mS/cm	0.12	0.12	0.48	0.48
Diffusion coefficient (D_{90}), x 10^{-10} cm^2/s	6.87[a]	6.87[a]	11.99[b]	11.99[b]
Crack width (w_{cr}), mm	0	0.70	0	0.40
Cover depth (c), (mm)	$5 \leq c \leq 100$	$5 \leq c \leq 100$	$5 \leq c \leq 100$	$5 \leq c \leq 100$

[a] Diffusion coefficient corresponding to the CCI_{90} of 0.12 mS/cm

[b] Diffusion coefficient corresponding to the CCI_{90} of 0.48 mS/cm

Note: (a) See Appendix D for empirical relationship between chloride conductivity and diffusion coefficient

(b) Parameters arbitrarily selected

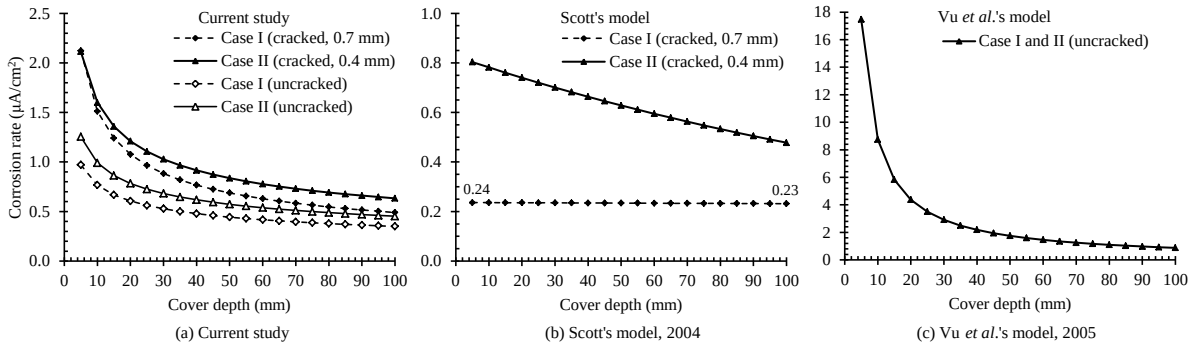

Figure 5.8: Comparison of Vu *et al.*'s model, Scott's model and the proposed $i_{corr,lab}$ models

The results show that Vu *et al.*'s model, in addition to not taking into account the effect of cracking on corrosion rate, cannot distinguish between uncracked Case I and II. Even though concrete quality is an indirect input parameter in the model through the w/b ratio, it cannot also distinguish between different binders having the same w/b ratio as is the case in this example. Scott's model is not sensitive to the influence of change in cover depth on corrosion rate when the concrete quality is high (i.e. Case I (cracked)), giving the impression that cover depth is insignificant when concrete quality is high (i.e. blended cement concretes). It is important to note that even though Scott's model was developed using data from 0.2 and 0.7 mm cracked specimens, it does not explicitly incorporate crack width as an input parameter. This was discussed in detail in Chapter 2. The difference between corrosion rates for the two cases using Scott's model is also high compared to that in the current model e.g. 168% and 10% for, respectively, Scott's model and the proposed $i_{corr,lab}$ model at 50 mm cover. This is mainly because Scott's model does not explicitly account for the effect of cracking on corrosion rate. Even though corrosion rate in blended cement concretes is primarily resistivity-controlled, the analysis of the experimental results in Chapter 4 showed that the presence of cracks leads to increase in corrosion rate but to an extent dependent on the concrete quality. In summary, the proposed model is sensitive to variations in concrete quality, cover depth and crack width while Scott's and Vu *et al.*'s models are not.

5.5 *Sensitivity analysis of the model input variables*

The objective of a sensitivity analysis is to examine the impact of varying the input parameters on the model output, and which input parameters have the highest influence on the model output. It evaluates how the variations in the model output can be apportioned to variations in model parameters [11, 12]. In addition, a sensitivity analysis is useful in exploring and quantifying the impact of possible errors in input data on model output, and understanding the relationships between input and output variables.

Sensitivity analysis techniques are classified into two categories, namely local methods and global (range) methods. In local sensitivity analysis, the response of the model output is examined by varying one input parameter while keeping others constant. It is easy to implement but the result is dependent on the base-case (initial) values chosen for the other input parameters. In global sensitivity analysis, more than one or all the input parameters are varied within a selected range and the response of the model output examined. Both local and global sensitivity analyses were used in the sensitivity analyses presented here. Global sensitivity analysis can be performed using different techniques such as, among others, Monte-Carlo based techniques and Fourier amplitude sensitivity test [13]. The former technique was used because of its simplicity and wide application.

In this study, a two tier sensitivity analysis was devised and then carried out using standard sensitivity analysis procedures in the literature in order to determine (i) which combination of two variables (out of the possible three i.e. concrete quality, D_{90}, cover depth, c, and crack width, w_{cr}) corrosion rate is most sensitive to, and (ii) which individual parameter corrosion rate is most sensitive to. For the first case, the three possible two-variable combinations are (i) varying both c and D_{90} simultaneously while keeping w_{cr} constant, (ii) varying both w_{cr} and D_{90} simultaneously while keeping c constant, and (iii) varying both c and w_{cr} simultaneously while keeping D_{90} constant. The two tier approach was adopted because even though it is necessary to establish the sensitivity of corrosion rate to each input parameter in the model, at the design stage, any two variables may need to be changed to obtain a suitable combination of cover depth, concrete quality and crack width. Furthermore, it also allows us, to some extent, to gauge the interaction between the variables. Two variables are said to interact when the effect of one factor on corrosion rate depends on the value at which the other variable is set.

The model input variables c, D_{90} and w_{cr} were varied as follows $10 \leq c \leq 100$ mm, $0.4 \leq w_{cr} \leq 0.7$ mm and $7.2 \leq D_{90} \times 10^{-10} \leq 23.1$ cm^2/s (equivalent to $0.2 \leq CCI_{90} \leq 1.5$ mS/cm for 50/50 PC/GGBS concrete). The variation was done by changing (increasing or decreasing) the parameters by 30% to ensure that a change in each parameter would lead to a reduction in corrosion rate e.g. increasing cover by 30% and decreasing D_{90} by 30%. The combinations of D_{90}, c and w_{cr} (within the aforementioned ranges) used in the sensitivity analyses are presented in Table 5.6. The proposed $i_{corr,field\ (cracked)}$ model was used to carry out the sensitivity analyses due to its output being natural corrosion rate; the sensitivity analyses results obtained using the other models would result in the similar trends obtained using the $i_{corr,field\ (cracked)}$ model. The sensitivity analysis results are presented in Figure 5.11 to Figure 5.13. In order to clearly show the trends obtained from the sensitivity analyses results, a 2-D axis system (y-x and y-z planes) was used instead of a 3-D x-y-z axis system. Figure 5.9 and Figure 5.10 illustrate, respectively, the notation used to present the sensitivity analyses results and interpretation of the results presented in Figure 5.11 to Figure 5.13.

Table 5.6: Combinations of D_{90}, c and w_{cr} used in the sensitivity analyses

D_{90} and w_{cr} varied, c constant			D_{90} and c varied, w_{cr} constant			c and w_{cr} varied, D_{90} constant		
D_{90} x 10^{-10} (cm^2/s)	w_{cr} (mm)	c (mm)	D_{90} x 10^{-10} (cm^2/s)	c (mm)	w_{cr} (mm)	c (mm)	w_{cr} (mm)	D_{90} x 10^{-10} (cm^2/s)
7.2	0.40	10	7.2	10	0.40	10	0.40	7.2
7.9	0.42	17	7.9	17	0.42	17	0.42	7.9
8.6	0.45	24	8.6	24	0.45	24	0.45	8.6
9.4	0.47	31	9.4	31	0.47	31	0.47	9.4
10.3	0.49	38	10.3	38	0.49	38	0.49	10.3
11.3	0.52	45	11.3	45	0.52	45	0.52	11.3
12.3	0.54	52	12.3	52	0.54	52	0.54	12.3
13.5	0.56	59	13.5	59	0.56	59	0.56	13.5
14.8	0.58	66	14.8	66	0.58	66	0.58	14.8
16.1	0.61	73	16.1	73	0.61	73	0.61	16.1
17.7	0.63	80	17.7	80	0.63	80	0.63	17.7
19.3	0.65	87	19.3	87	0.65	87	0.65	19.3
21.1	0.68	94	21.1	94	0.68	94	0.68	21.1
23.1	0.70	100	23.1	100	0.70	100	0.70	23.1

Base case values i.e. values before D_{90}, c and w_{cr} are, respectively, decreased, increased and decreased by 30%.

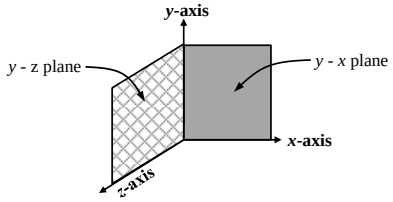

Figure 5.9: Notation used in Figure 5.11 to Figure 5.13

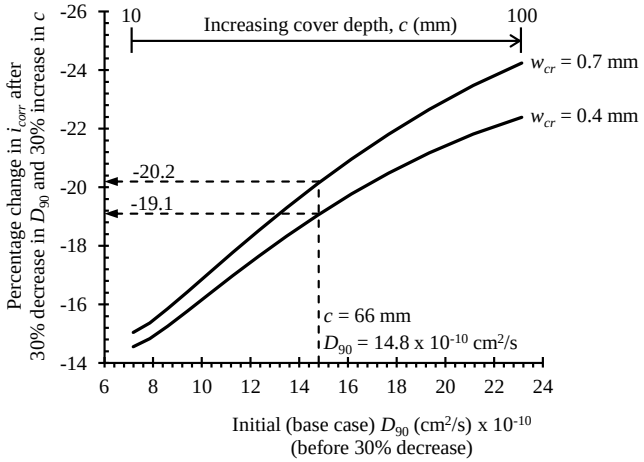

If the initial (base case) values for D_{90} (14.8 x 10^{-10} cm^2/s) and c (66 mm) are, respectively, decreased and increased by 30%, the sensitivity analyses results show that the percentage decrease in corrosion rate is dependent on the crack width. In this case, corrosion rate decreases by 19.1% and 20.2% if the crack width is, respectively, 0.4 and 0.7 mm. (The cover depth of 66 mm is read directly from Table 5.6.)

Figure 5.10: Illustrative example: interpretation of sensitivity results in Figure 5.11 to Figure 5.13

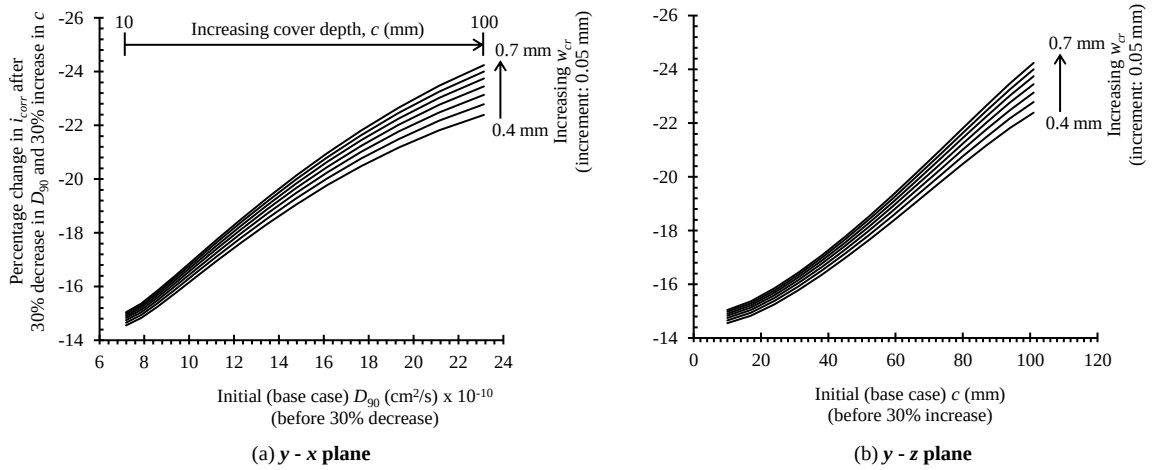

Figure 5.11: Sensitivity of corrosion rate to change in both concrete quality and cover depth for different w_{cr}

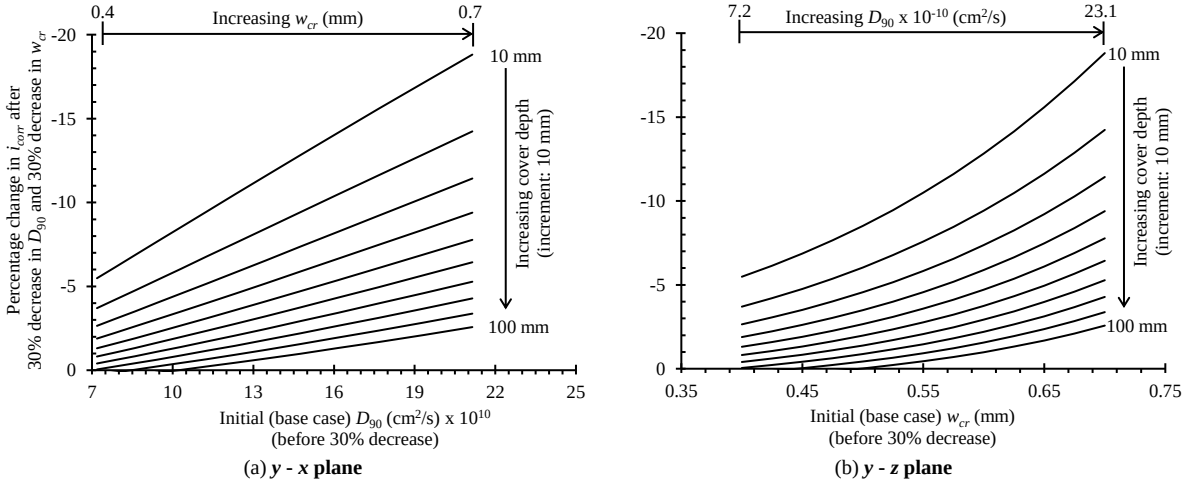

Figure 5.12: Sensitivity of corrosion rate to change in both concrete quality and crack width for different *c*

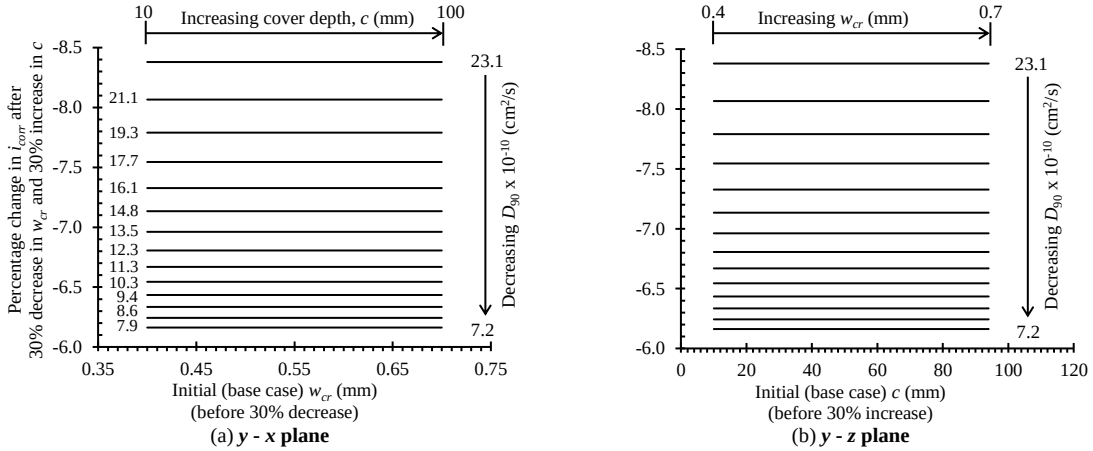

Figure 5.13: Sensitivity of corrosion rate to change in both cover depth and crack width for different D_{90}

From the sensitivity analysis results presented in Figure 5.11 to Figure 5.13, the following can be observed:

(i) The extent to which a combined change in both D_{90} and c affects corrosion rate is dependent on the crack width; the higher the crack width, the greater the change in corrosion rate due to a combined variation in D_{90} and c (Figure 5.11). However, for two different crack widths that do not vary by a large margin (e.g. 0.4 and 0.5 mm), the effect of changing both D_{90} and c on corrosion rate appears to be negligible.

(ii) The extent to which a combined change in both D_{90} and w_{cr} affects corrosion rate is dependent on the cover depth; the lower the cover depth, the greater the change in corrosion rate due to a combined variation in D_{90} and w_{cr} (Figure 5.12). Figure 5.12 also shows that as the cover depth increases, there is a point (approximately $c > 70$ mm) where change in either concrete quality (D_{90}) or crack width does not affect corrosion rate.

(iii) The extent to which a combined change in c and w_{cr} affects corrosion rate is dependent on D_{90}; the higher the D_{90} (i.e. lower concrete quality), the greater the change in corrosion rate due to a combined variation in c and w_{cr} (Figure 5.13). However, for a given concrete quality, the extent to which a combined change in w_{cr} and c affects corrosion rate is independent of the crack width and cover depth. This, to some extent, depicts the dominating effect of concrete quality on corrosion rate.

The second step in the sensitivity analysis was to determine if there is an individual parameter (D_{90}, c or w_{cr}) to which corrosion rate is most sensitive. To establish this, the model input variables c, D_{90} and w_{cr} were varied as follows: $10 \leq c \leq 100$ mm, $0.1 \leq w_{cr} \leq 0.7$ mm and $7.2 \leq D_{90}$ x 10^{-10} cm^2/s ≤ 23.1. Figure 5.14 to Figure 5.16 show the results of the percentage increases in corrosion rate as a result of the 30% increase in cover depth, 30% reduction in crack width or 30% reduction in D_{90}. Cover depth was increased, crack width decreased and concrete quality increased to ensure that the variation of each parameter resulted in a reduction in corrosion rate. It is important to mention that the 30% change in the three input variables was arbitrarily chosen for illustration purposes; using a different value (e.g. ± 40%) will result in different changes in corrosion rate but will not change the trends obtained here.

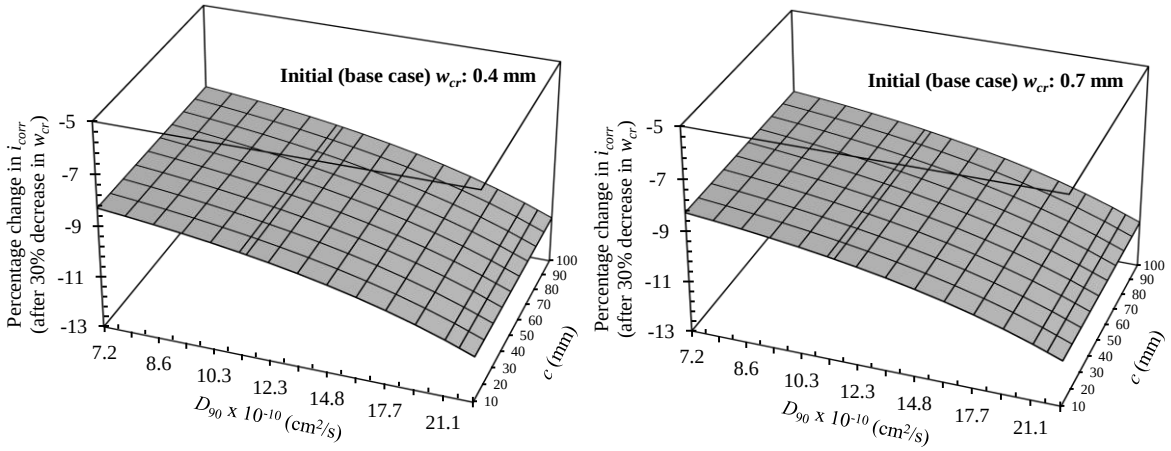

Figure 5.14: Sensitivity of corrosion rate to change in crack width

Note: Despite being identical, the trends in Figure 5.14 have been presented here to show that the extent to which change in crack width affects corrosion rate is independent of the initial crack width – in this case, 0.4 and 0.7 mm.

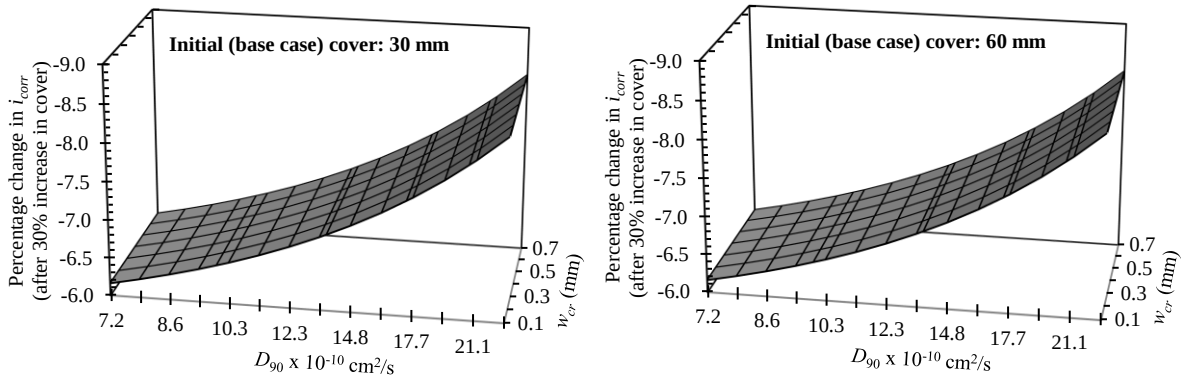

Figure 5.15: Sensitivity of corrosion rate to change in cover depth

Note: Despite being identical, the trends in Figure 5.15 have been presented here to show that the extent to which change in cover depth affects corrosion rate is independent of the initial cover depth – in this case, 30 and 60 mm.

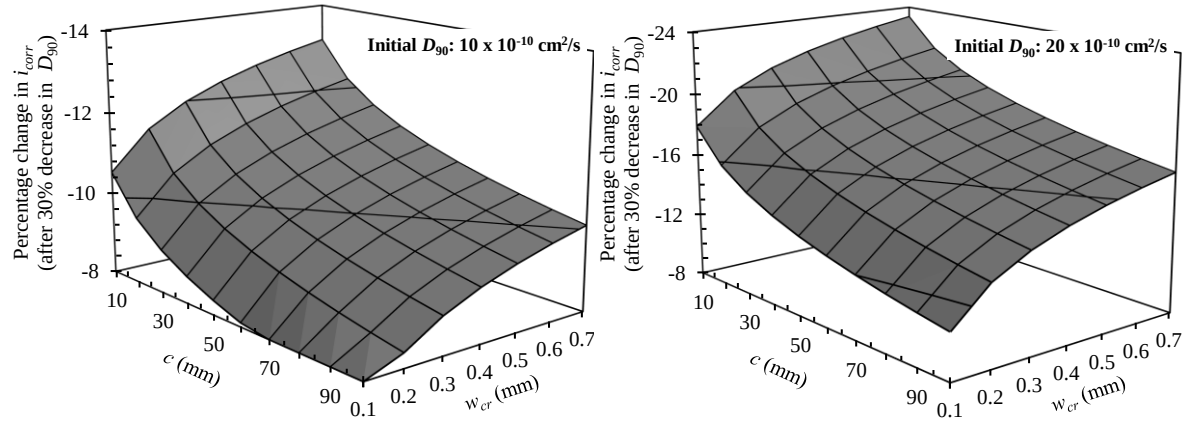

Figure 5.16: Sensitivity of corrosion rate to change in concrete quality

The sensitivity of corrosion rate to cover depth, concrete quality or crack width, as presented in Figure 5.14 to Figure 5.16, can be summarized as follows:

(i) The extent to which a change in crack width affects corrosion rate is dependent on the concrete quality (Figure 5.14). The lower the concrete quality (higher D_{90}), the higher the extent to which a change in crack width affects corrosion rate. The initial crack width does not affect the extent to which a change in crack width affects corrosion rate.

(ii) The extent to which a change in cover depth affects corrosion rate is dependent on the concrete quality (Figure 5.15). The lower the concrete quality (higher D_{90}), the higher the extent to which a change in cover depth affects corrosion rate. The initial cover depth does not affect the extent to which a change in cover depth affects corrosion rate.

(iii) The extent to which a change in concrete quality affects corrosion rate is dependent on both cover depth and crack width (Figure 5.16). A combination of low cover depth and high crack width results in the highest effect on corrosion rate due to change in concrete quality.

Table 5.7 gives a summary of the sensitivity analyses results for the various parameters (c, w_{cr} and D_{90}) and parameter combinations (w_{cr} and D_{90}, c and D_{90}, and w_{cr} and c). The results are in agreement to those reported in some previous studies where concrete quality was expressly mentioned to have a higher effect (or more important) on corrosion rate than crack width [4, 14]. The results here show that the change in corrosion rate is greater if concrete quality is varied than if either crack width or cover

depth are varied. In short, concrete quality has a dominating role on the effect of either crack width or cover depth on corrosion rate. The practical implication of these findings is that even though cracking increases corrosion rate, and that it should be minimized, corrosion protection cannot be achieved solely by limitation of crack width; a holistic approach, in this case, considering cover depth, concrete quality and crack width should be adopted.

Table 5.7: Summary of sensitivity analyses results of the model input parameters

Parameter(s) varied	Percentage decrease in corrosion rate (%)			
	Minimum	Maximum	Range* (%)	
w_{cr} and D_{90}	0.2	18.8	98.8	
c and D_{90}	14.6	24.3	40.0	
w_{cr} and c	6.2	8.4	25.5	Decreasing sensitivity of corrosion rate
D_{90}	10.9	23.3	53.3	
c	6.1	8.4	27.3	
w_{cr}	8.2	11.2	27.0	

$$* \text{Range} = \left(\frac{\text{Max. decrease} - \text{Min. decrease}}{\text{Max. decrease}} \right) \times 100$$

5.6 *Statistical characterization of model output*

Variability in data is usually accommodated by specifying the average value of a quantity, and/or the maximum and minimum values i.e. range. In the latter case, variability is characterized by the range between the extreme values and a measure of central tendency (e.g. mean, mode and median). However, for a parameter such as corrosion rate, the quantification of variability and uncertainty should include other aspects such as the distribution type, standard deviation, its fluctuation pattern in time (i.e. temporal variability) and its fluctuation pattern at different locations of the structure (i.e. spatial variability); the last two types of variability were outside the scope of this study. Furthermore, long-term corrosion data would be required for their quantification.

Statistical distributions are used to represent and quantify the variability of a parameter. A suitable statistical distribution to represent a parameter can be determined using one of the following methods: (i) using the observed data to define an empirical statistical distribution, and (ii) fitting a theoretical statistical distribution to the histogram of the observed data. The latter is preferred to the former as it allows analyzing the system for situations outside the norm; this is essential when carrying out an experimental data analysis. The principle behind fitting distributions to data is to find the type of statistical distribution (e.g. normal, lognormal, gamma, Poisson) and the values of the parameters of the selected distribution (e.g. mean, standard deviation and variance) that give the highest probability of producing the observed data. Taking into account that there are many statistical distributions which could fit a set of observed data, it is essential to ensure that the selected distribution to model the observed data truly reflects the properties of the data. This is ensured by carrying out goodness-of-fit (GOF) tests.

One of the methods to check the GOF of a statistical distribution to observed data is by visual assessment where a statistical distribution plot (i.e. probability density function, *pdf*) is superimposed

on the histogram plot of the observed data. In the visual assessment of the GOF, the shape of each statistical distribution is compared with that of the histogram of observed data. The *pdf* that has the closest matching shape with the histogram is selected and used to represent the data. However, visual assessment is subjective and susceptible to potential human error, and is seldom used. To overcome this, and to improve confidence in the selection of a statistical distribution to model the observed data, standard statistical tests are used to quantify the GOF of a selected distribution. Statistical GOF tests measure the compatibility of a random sample with a theoretical statistical distribution. They provide a probability, depending on the confidence interval or significance level chosen, that random data generated from the fitted distribution would have produced a GOF statistic value as low as that calculated for the observed data. The three main GOF tests are the Karl-Pearson's Chi-squared (χ^2) test, Kolmogorov-Smirnov test and Anderson-Darling test [15]. These tests are well established and can be found in the literature. However, regardless of the GOF test used, it is important to note that: (i) a larger data set improves the confidence of fitting a statistical distribution to observed data, and (ii) considering field data with experimental data is also desirable in selection of a statistical distribution [16].

In order to confidently fit a statistical distribution to the observed data, a sufficiently large and representative data-set is needed. Such data was not available. However, previous published studies and reports have reported statistical distributions that can be adopted for various corrosion-influencing parameters; this study adopted the distributions presented in Table 5.8.

Table 5.8: Summary of statistical characterization of model input variables

Input variable	Statistical distribution selected	Coefficient of variation ($\sigma / \overline{x}$)
c (mm)	Lognormal[a]	30%
w_{cr} (mm)	Lognormal[b]	50%
D_{90} (mS/cm)	Normal[a]	28.5%

References: [a]: [17], [b]: [18, 19]

The next step is to establish the statistical distribution of the predicted corrosion rate ($i_{corr,field}$ and $i_{corr,lab}$) based on the statistical distributions for the input parameters presented in Table 5.8. In order to achieve this, Monte Carlo analysis (simulations) of the proposed model was carried out using randomly generated values of the input parameters (c, w_{cr} and D_{90}) based on their respective statistical distributions (Table 5.8). A Monte Carlo analysis aims at performing a sufficiently large sequence of simulations, n, each with different values for each input parameter, to quantify the statistical distributions of the targeted outcomes. It requires selecting n samples out of each of the statistical distributions of the input parameters [20]. A total of 39 000 random values (mainly based on computational limitations) of the input parameters were generated based on the respective statistical distributions to meet the following criteria: $5 \leq c \leq 40$ mm, $0.1 \leq w_{cr} \leq 0.7$ mm and $6 \leq D_{90} \times 10^{-10} \leq 25$ cm^2/s. These limits were chosen such that the maximum experimental values used or obtained in this study were not exceeded. In the case of uncracked concrete, the crack width limits were omitted. Consequently, 39 000 model simulations were carried out to generate simulated $i_{corr,field}$ and $i_{corr,lab}$ values. Statistical distributions were then fitted to the simulated corrosion rates. The selection of the best fitting statistical distribution was carried out using the Chi-squared (χ^2) goodness-

of-fit test at a 95% confidence interval (see Appendix E). This procedure was implemented in MATLAB®. The results are presented in Figure 5.17 to Figure 5.20. A summary of the selected statistical distributions and the corresponding relevant parameters are summarized in Table 5.9.

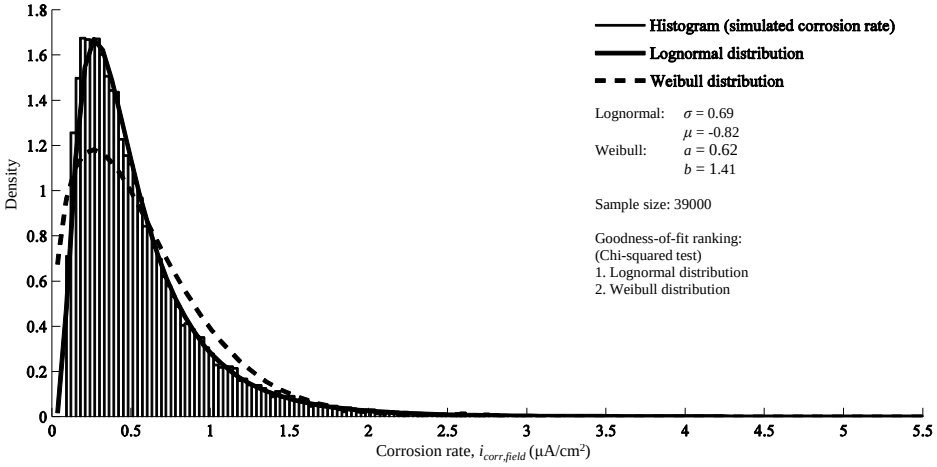

Figure 5.17: Histogram and distribution fit of simulated corrosion rate based on $i_{corr,field}$ (cracked) model

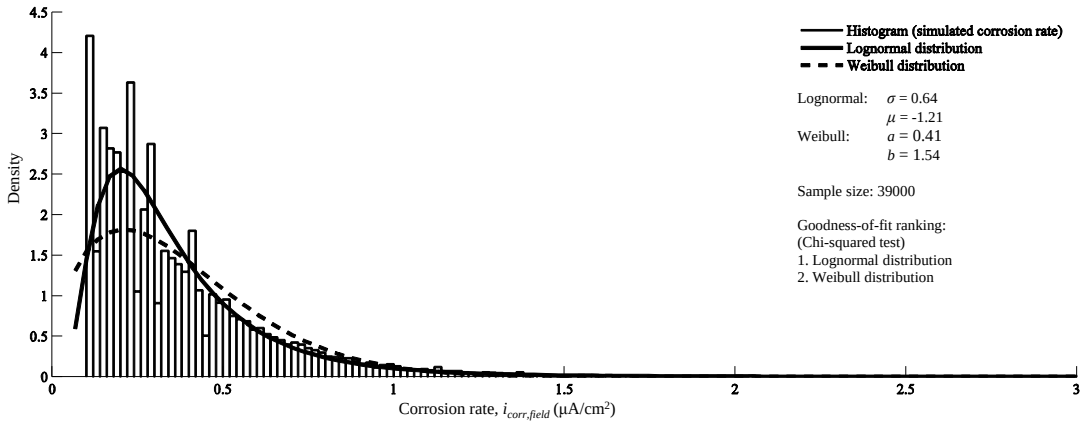

Figure 5.18: Histogram and distribution fit of simulated corrosion rate based on $i_{corr,field}$ (uncracked) model

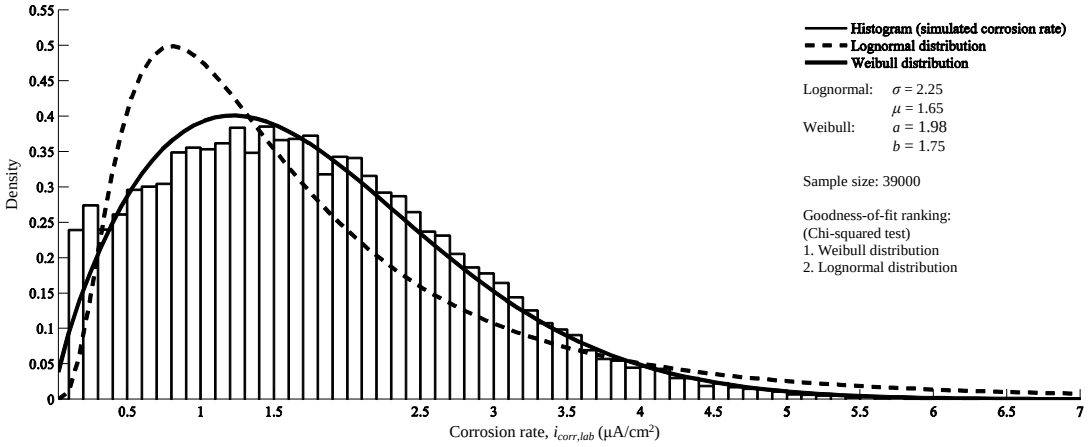

Figure 5.19: Histogram and distribution fit of simulated corrosion rate based on $i_{corr,lab}$ (cracked) model

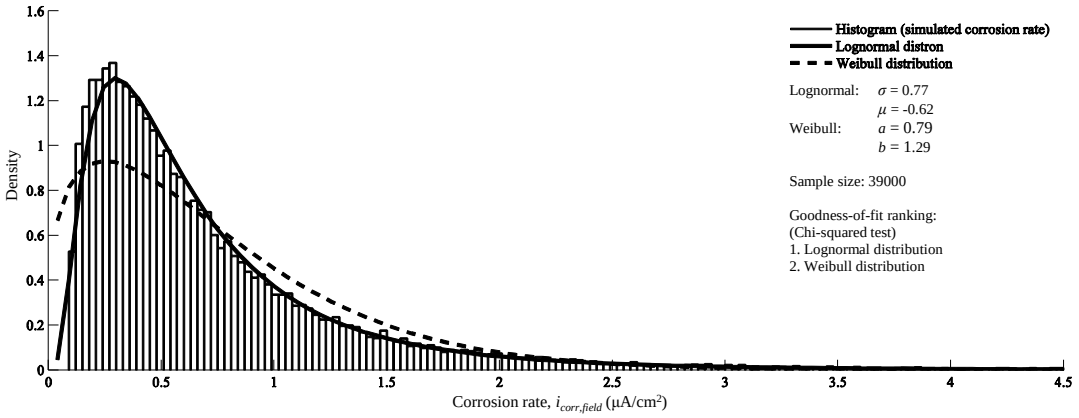

Figure 5.20: Histogram and distribution fit of simulated corrosion rate based on $i_{corr,lab}$ (uncracked) model

Table 5.9: Summary of selected statistical distributions for corrosion rate

Corrosion rate prediction model		Type of distribution	Statistical parameters			
			a	b	σ	μ
$i_{corr,field}$ (t_i + 2¼ yrs)	Cracked	Lognormal	–	–	0.69	-0.82
	Uncracked	Lognormal	–	–	0.64	-1.21
$i_{corr,lab}$ (t_i + 2¼ yrs)	Cracked	Weibull	1.98	1.75	–	–
	Uncracked	Lognormal	–	–	0.77	-0.62

It is clear that except for corrosion rate values obtained from the prediction model of laboratory cracked specimens which exhibited a Weibull distribution, all the other laboratory and field corrosion rates (cracked and uncracked) exhibited lognormal distribution. The probability distribution functions for lognormal and Weibull distributions of a variable x are given in Equations (5.13) and (5.14):

$$\text{Lognormal distribution: } f(x) = \frac{1}{\sigma\sqrt{2\pi x}} \exp\left[-\frac{1}{2}\left(\frac{\ln(x)-\mu}{\sigma}\right)^2\right] \tag{5.13}$$

$$\text{Weibull distribution: } f(x) = \left(\frac{b}{a^b}\right) x^{b-1} \exp\left(-\left(\frac{x}{a}\right)^b\right) \tag{5.14}$$

where μ and σ are, respectively, the mean and standard deviation of the variable's natural logarithm, ln(x), and $a > 0$ and $b > 0$ are, respectively, the scale and shape parameters. More literature on these distributions can be found in Appendix E.

The lognormal and Weibull distributions have been used in the past to describe corrosion rate data. Knowledge of the corrosion rate statistical distribution is critical for developing reliability and risk-based models for inspection and maintenance planning of corroded RC structures [21]. The statistical distributions can also assist in estimating the variability associated with the prediction models. However, in order to adequately account for the high variability and uncertainty associated with corrosion rate and the factors affecting it, a probabilistic approach should be adopted. This was not pursued because it was outside the scope of this study, but should be considered in future work.

5.7 *Model limitations and recommendations for further work*

In addition to the limitations of the proposed models that have already been mentioned in this chapter, the following should be noted:

1. A single reinforcing bar was embedded in the beam specimens used in the experimental investigations. This is not representative of in-service RC structures where, for example, reinforcing steel mats are used. Therefore, the model should be validated, adjusted and calibrated using long-term corrosion rate data from in-service RC structures or appropriate larger scale field specimens.
2. Even though the field-based specimens were exposed to a marine tidal zone, environmental parameters (temperature and relative humidity) were not incorporated in the proposed models. These parameters affect corrosion rate and should, in future, be directly or indirectly incorporated in the model. For example the effect of temperature on corrosion rate can be incorporated using the Arrhenius law [1, 22] – see Eqn. (2.40) in Chapter 2.
3. Cracking and crack width was one of the main experimental variables in this study. However, only single flexural cracks were dealt with. In in-service RC structures, this is seldom the case; there are usually numerous flexural cracks of varied widths due to applied loads. Other crack characteristics such as self-healing, frequency/density and activity or dormancy were also not incorporated in the models. The applicability of this model therefore needs to be checked and calibrated to account for the effect of these crack characteristics on corrosion rate.
4. The laboratory-based specimens were exposed to a cycle of 3-days wetting (with 5% NaCl solution) and 4-days air-drying (at a temperature and relative humidity of 25 ± 2 ^{o}C and 50 ± 5% respectively); it is necessary to investigate the applicability of the model to other cyclic wetting and drying regimes e.g. using other concentrations of NaCl, different wetting and drying durations, etc. With respect to the field exposure environment, it is necessary to investigate the applicability of the model to other tidal marine conditions in future studies.

5.8 *Framework for practical application of the proposed models*

5.8.1 *Selection of suitable design combinations of concrete cover, quality and crack width*

To date, only Fickian-based corrosion initiation models have been used in the selection of concrete quality and cover depth; it is assumed that concrete is uncracked, a scenario which is seldom the case in in-service RC structures. Therefore, even though the concrete quality and cover depth selected may satisfy durability requirements with respect to the initiation phase, the same may not be the case in the presence of cracking where the initiation phase may either be significantly shortened or completely eliminated due to the increased penetrability of the concrete. The proposed models overcome this problem by incorporating the influence of crack width on corrosion rate especially for the propagation phase.

In addition to predicting corrosion rate, the models can also be used to select a suitable combination of concrete quality, cover and crack width to meet target durability requirements with respect to chloride-induced corrosion. With the proposed models, the designer can objectively perform a number of permutations to determine the most suitable combination of concrete quality, crack width and cover depth to meet the desired durability performance (with respect to steel corrosion) of a given RC structure in the marine environment.

5.8.1.1 *Example I – selection of a suitable combination of cover depth, quality and crack width (new structures)*

The objective of this example is to show how the proposed model can be used to select a suitable combination of concrete cover, quality and crack width to achieve a desired limit state for the propagation phase. The analyses will involve using the proposed field-based corrosion rate prediction model ($i_{corr,field}$) to determine not only the concrete quality and cover depth but also the limiting crack width to achieve a propagation phase of at least 20 years. Note that even though the $i_{corr,field}$ model is used here, the laboratory-based one can equally be used. The limit state used in this example for the propagation phase is attainment of a 15% loss of steel cross section area 20 years after corrosion initiation. The task is therefore to select concrete parameters (cover depth, quality and crack width) to achieve the 20 year propagation phase.

The justification for selection of a 15% loss of steel cross section area as a limit state for the propagation phase is as follows: The end of the service life of the RC structure is usually associated with a loss of cross sectional area between 5% and 25% [23]; this is mainly due to the partial factors of safety incorporated in the calculations during design to account for variations in material properties, construction and loading. These safety factors can accommodate a certain loss in cross-section area. A loss of cross-section between 5% and 25% therefore provides a reasonable estimate for the end of a structure's service life i.e. limit state. Even though a reduction in cross sectional area is chosen as a limit state in this example, other limit states such as time to cover cracking can be used. However, their adoption is not straight forward because the prediction models associated with them e.g. time to cover cracking models by Liu and Weyers [24] and El Maaddawy and Soudki [25] were developed considering uncracked concrete.

The corrosion initiation phase is not included in this example because, in addition to the focus being on the propagation phase, past studies which were reviewed in Chapter 2 showed that in cracked RC structures, the initiation phase may be significantly shortened or completely eliminated. Furthermore, it is still not possible, with the current state of knowledge, to quantify chloride ingress in cracked concrete in order to estimate the time to corrosion initiation, if any. Table 5.10 presents a summary of the parameters used in this example. Note that in this example, crack width is limited to 0.5 mm and that the pitting factor in Table 5.10 is incorporated in the analysis to account for localized loss in cross-sectional area in the crack region (see Chapter 2 for literature on pitting and pitting factor).

Table 5.10: Summary of parameters used in Example I

Limit state (end of propagation phase, t_p)	15% loss of steel cross-section
Desired time to attainment of limit state	20 years after corrosion initiation (t_i)
Initial bar diameter (mm)	20
Pitting factor (α_{pit}) for cracked concrete*	10
Exposure environment	Marine tidal zone
Crack width (w_{cr})	0.5 mm

*: Pitting factor is incorporated to account for localized loss in steel cross-sectional area in the crack region [23] - see Chapter 2 for literature on pitting and pitting factor.

Even though crack width (w_{cr}) is kept constant at 0.5 mm in this example, either of the other two parameters (D_{90} or c) can also be kept constant and a suitable combination of the other remaining parameters required to achieve the desired limit state (i.e. 15% loss of steel cross section area) determined.

The next step is to determine, for a crack width of 0.5 mm, the corresponding concrete quality (in this case the diffusion coefficient, D_{90}) and cover depth required to meet the specified 20-year propagation phase. Faraday's law (Eqn. (2.34)) is used to determine the corrosion rate required to result in a 15% cumulative loss in steel cross section area due to corrosion, 20 years after corrosion initiation. The results are presented in Figure 5.21.

$$m = \frac{MIt}{zF} = 0.0116\ it\alpha_{\text{pit}} \tag{2.34}$$

where m is the mass loss, M is the atomic mass of steel (56 g), I is the corrosion current, i is the corrosion current density (μA/cm^2), t is the time of electrolysis (s), z is the ionic charge of steel (2), F is Faraday's constant (96500 C/mol) and α_{pit} is the pitting factor.

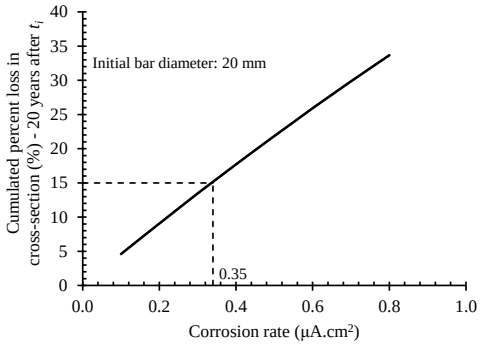

Figure 5.21: Stable corrosion rate required to cause a 15% cumulated loss in cross section after 20 years

Figure 5.21 shows that a maximum stable corrosion rate (also referred to as *threshold corrosion rate*) of 0.35 μA/cm^2 will result in achieving the pre-defined limit state for the propagation phase (15% loss in steel cross section) 20 years after corrosion initiation. Even though the effects of corrosion-induced damage (e.g. cover cracking) on corrosion rate are not accounted for in this example, this should be done in a real-life scenario. The determination of the possible combinations of concrete quality (D_{90}) and cover depth (c) is now carried out using the proposed model (Eqn. (5.9), reproduced here for easy reference):

$$i_{corr,\,field\ (t_i+2.25\ \text{years})} = \left(0.64\text{e}^{0.06\left(D_{90}\times 10^{-10}\right)}\right)\left(\frac{c}{w_{cr}}\right)^{-b} \quad [\mu\text{A/cm}^2] \tag{5.9}$$

$$\text{where } b = 0.21\text{e}^{0.02\left(D_{90}\times 10^{-10}\right)}$$

It is important to note that it is assumed that the stable corrosion rate obtained after approximately 2¼ years (as predicted using Eqn. (5.9)), will be valid 20 years after corrosion initiation. Figure 5.22 is

obtained by trying various combinations of cover depth and concrete quality for a crack width of 0.5 mm. It shows that there are a number of possible combinations of cover depth and concrete quality that can be selected to achieve the (maximum) required corrosion rate of 0.35 μA/cm^2. Therefore, if a cover of 50 mm is selected, a maximum diffusion coefficient of 11.5 x 10^{-10} cm^2/s is required (Figure 5.22). The results of concrete quality and cover depth (for the propagation phase) are summarized in Table 5.11.

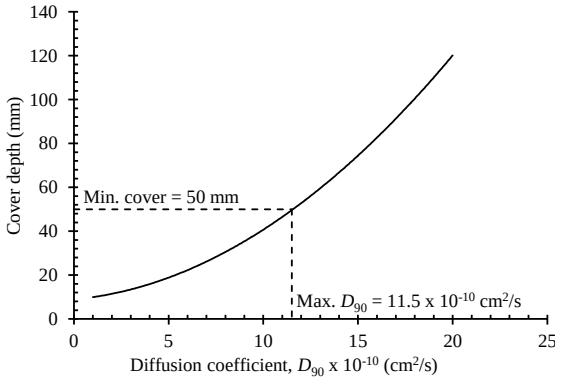

Figure 5.22: Cover and concrete quality required to achieve a corrosion rate of 0.35 μA/cm^2

Table 5.11: Summary of possible design options for concrete quality and cover depth

Minimum cover depth (mm)	50
Diffusion coefficient, D_{90} (cm^2/s) x 10^{-10}	11.5
90-day chloride conductivity index corresponding to D_{90}	
100% PC concrete	Not feasible[a]
70/30 PC/FA concrete	0.43 mS/cm
50/50 PC/GGBS concrete	0.69 mS/cm

[a] A corresponding chloride conductivity value is not feasible in PC concrete for such a low diffusion coefficient (11.5 x 10^{-10} cm^2/s)

5.8.2 *Quantification of the propagation phase*

A *limit state* was defined in Chapter 1 as a state beyond which the structure no longer satisfies the relevant design performance requirements [26]. Contrary to the corrosion initiation phase where the initiation limit state is defined by either attainment of a chloride concentration threshold or a corrosion rate of 0.1 μA/cm^2, different limit states can be adopted for the propagation phase. Limit states for the propagation phase refer to the various progressive corrosion-induced damages on the RC structure such as appearance of visible surface corrosion-induced cracks, surface corrosion crack widths [e.g. 0.3-1.0 mm, 27], spalling of the cover concrete, loss of steel-concrete interface bond, loss of steel cross-section area, loss of flexural stiffness, longitudinal deflections (of flexural members) and loss of a member's ultimate load-carrying capacity.

Regardless of the limit state selected for the propagation phase, of importance to the engineer, client and asset manager is the ability to reasonably estimate the residual life of the structure or time to maintenance; this process is in turn significantly dependent on the corrosion rate used in the appropriate damage prediction model. It is common practice to adopt a representative corrosion rate as

an input parameter in damage prediction models to quantify the corrosion propagation phase. The term 'representative corrosion rate' ($i_{corr,REP}$) is conventionally used to refer to a corrosion rate value adopted for the entire propagation phase for the estimation of corrosion-induced damage using appropriate damage prediction models [26]. To date, there are still major challenges in the determination of $i_{corr,REP}$ mainly because of lack of confidence in predicting corrosion rate. In order to confidently predict corrosion rate, it is necessary to accurately quantify the future corrosion regime with regard to the relevant corrosion-sustaining species e.g. dissolved oxygen concentration, moisture content, chloride content, concrete resistivity (or its inverse conductivity) and temperature. These were discussed in detail in Chapter 2. Three approaches have been proposed in the past to estimate $i_{corr,REP}$.

The first and most commonly used conservative approach is the assumption of a constant corrosion rate for the propagation phase. This approach was first adopted by researchers such as Tuutti [28], Andrade *et al*. [29] and Clear [30] who assumed a linear progression of corrosion-induced damage depicting an assumed constant corrosion rate during the propagation phase. Later, the approach was adopted in DuraCrete [31] where constant corrosion rates are proposed for the various EN 206-1 [32] marine exposure Classes (see Table 5.12). Even though the suggested corrosion rate values take into account the different concrete grades specified in the Code for the corresponding exposure classes, other salient factors such as cover cracking, cover depth, binder type, moisture content, contamination with deleterious species (Cl^-, CO_2) and oxygen availability are not accounted for. Further, even though the proposed corrosion rate values are rather too high and cannot be used immediately after corrosion initiation, it is not clear how long it takes (after corrosion initiation) for the proposed corrosion rates to be attained; this should depend on several inter-related factors affecting corrosion rate. The main assumption made in this approach (of adopting a constant corrosion rate) is that the corrosion-regime remains more or less unchanged throughout the propagation phase. Specifically, in the case of DuraCrete, a further assumption is that under any given combination of corrosion-sustaining conditions and exposure environment, the corrosion rates given in Table 5.12 will be achieved. In short, this approach ignores the fact that the variation of corrosion rate with time depends on the prevailing corrosion regime and that after a given period of continued corrosion, factors such as the accumulation of corrosion products and cover cracking may, respectively, eventually stagnate or accelerate the process. However, despite all these shortcomings, it is the most commonly used conservative approach to quantify the propagation phase, with the main challenge being the determination of a corrosion rate value to adopt for the propagation phase.

Table 5.12: Proposed average corrosion rates for EN 206-1 exposure classes [31]

Exposure class (chloride-induced corrosion)		$i_{corr,REP}$ ($\mu A/cm^2$)
XS1	Exposed to airborne salt but not in direct contact with sea water	2.6 (0.17)
XS2	Permanently submerged	– *
XS3	Tidal, splash and spray zones	6.0 (3.4)

( ): standard deviation, *: Corrosion not expected except for poor quality concrete or low cover

The second approach involves the use of an empirical model proposed by Yancyn and Ergun [33] to forecast corrosion rate; the model is an exponential relationship between the corrosion rate and time, and was developed using results obtained in an accelerated corrosion study (using admixed chlorides:

6 kg Cl^-/m^3 concrete) using 150 mm diameter x 150 mm height specimens made with 90/10 PC/Pozzolanic cement concrete (w/b ratio: 0.60). Corrosion was evaluated by measuring half-cell potential and linear polarization resistance. Corrosion rate measurements were taken for a period of up to 90 days (i.e. at 1, 7, 28, 60 and 90 days). The model is given in Eqn. (5.15):

$$i_{corr}(t) = i_o e^{-Ct} \tag{5.15}$$

where $i_{corr}(t)$ is the corrosion rate ($\mu A/cm^2$) at time t (days), i_o is the initial (measured instantaneous) corrosion rate and C is a corrosion constant that depends on the degree of concrete pore saturation, pH, permeability and the cover depth; Yalcyn and Ergun proposed a value of C (evaluated from i_{corr} vs. time curves) as 1.1 x 10^{-3} day^{-1}. Important points to note about the empirical model are as follows: (i) the model was developed using i_{corr} from uncracked concrete and is therefore not applicable to cracked concrete, (ii) it is not realistic for corrosion rate to increase at a constant rate throughout the propagation phase, (iii) factors which affect corrosion rate such as cover depth and cracking, temperature, concrete quality and resistivity are not incorporated in the model; the model assumes that the corrosion regime does not change, and that future corrosion rate is only dependent on time. However, these factors may vary from time to time and consequently affect corrosion rate, and (iv) the empirical constant C cannot be assumed to be applicable to other concretes (binder types and w/b ratios). The approach can therefore not be confidently applied to determine $i_{corr,REP}$.

The third approach was proposed recently by Martinez and Andrade [34]. Their approach involves a series of steps to determine an annual-averaged corrosion rate from actual corrosion rate (and resistivity) measurements. The approach involved three main steps as follows: (i) single isolated instantaneous in-situ corrosion rate measurements ($i_{corr,single}$) are taken, (ii) in-situ concrete cores are then taken close to the corrosion rate measurement points and conditioned to 85% RH (for structures sheltered from rain) or vacuum water-saturated (for non-sheltered or submerged ones) for resistivity measurements, and (iii) using an empirical corrosion rate vs. resistivity nomogram, the corrosion rate corresponding to concrete resistivity is determined ($i_{corr,max}$). The $i_{corr,REP}$ is defined as follows:

$$i_{corr,REP} = \frac{i_{corr,\text{single}} + i_{corr,\text{max}}}{2} \tag{5.16}$$

This approach assumes that all corrosion processes are resistivity-controlled, a phenomenon that may only be the case in high resistivity concretes e.g. in blended cement concretes [4]. Furthermore, even in situations where the corrosion process is resistivity-controlled, differences may still arise depending on, for example, concrete quality and presence of cracks [4, 35].

Considering that the temporal (time-dependent) aspect of corrosion rate was not incorporated in the models proposed in this study, and for purposes of practical applicability, it is conservative to assume that only the corrosion rates predicted by the proposed $i_{corr,lab}$ model after approximately 2¼ years of exposure in the laboratory environment can be used to quantify the propagation phase depending on the pre-defined limit state; the proposed field-based corrosion rate prediction model, $i_{corr,field}$, cannot, at this moment, be objectively used because of the pseudo-stable nature of the field corrosion rate data

used in its development. As stated previously (and also in Chapter 4), long-term stable field corrosion rate data will be needed to update the $i_{corr,field}$ model. Similarly, it is important to note that the main limitation of the proposed laboratory-based corrosion rate prediction model, $i_{corr,lab}$, is that it was developed using accelerated corrosion rate data. Therefore, in this chapter, $i_{corr,field}$ model, is used, is only for illustration purposes.

The approach of using a single corrosion rate value for the propagation phase is similar to the one used in DuraCrete [31] already discussed. However, it does not support the adoption of universal corrosion rate values in DuraCrete for a given EN 206-1 exposure Class and for all concretes (see Table 5.12). The results indicate that the corrosion rate value adopted for the propagation phase ($i_{corr,prop}$) should be dependent on not only the exposure Class but also other corrosion rate-influencing factors such as, among others, concrete quality, cover depth and crack width. To achieve this, the proposed corrosion rate prediction models can be used. The proposed models are used to predict corrosion rate for a given combination of concrete quality, cover depth and crack width. This corrosion rate, $i_{corr,prop}$, should be considered stable and used to quantify the propagation phase using an appropriate corrosion-induced damage model depending on the pre-defined limit state. The method improves on the DuraCrete approach of adopting constant corrosion rates regardless of concrete quality, cover depth and cracking. However, as already mentioned, long-term stable field corrosion rate results are needed to update the $i_{corr,field}$ prediction model before it can be used in corrosion-induced damage prediction models to quantify the propagation phase. This approach can be applied to both new and existing corrosion-affected RC structures.

For new structures, in addition to being used to select suitable combinations of concrete quality, cover depth and crack width (see Section 5.8.1), it can also be used to develop pro-active maintenance strategies. In the case of existing corrosion-affected RC structures, the approach can be used to estimate the residual life. In this case, the procedure presented in Figure 5.23 can be used to quantify the propagation phase.

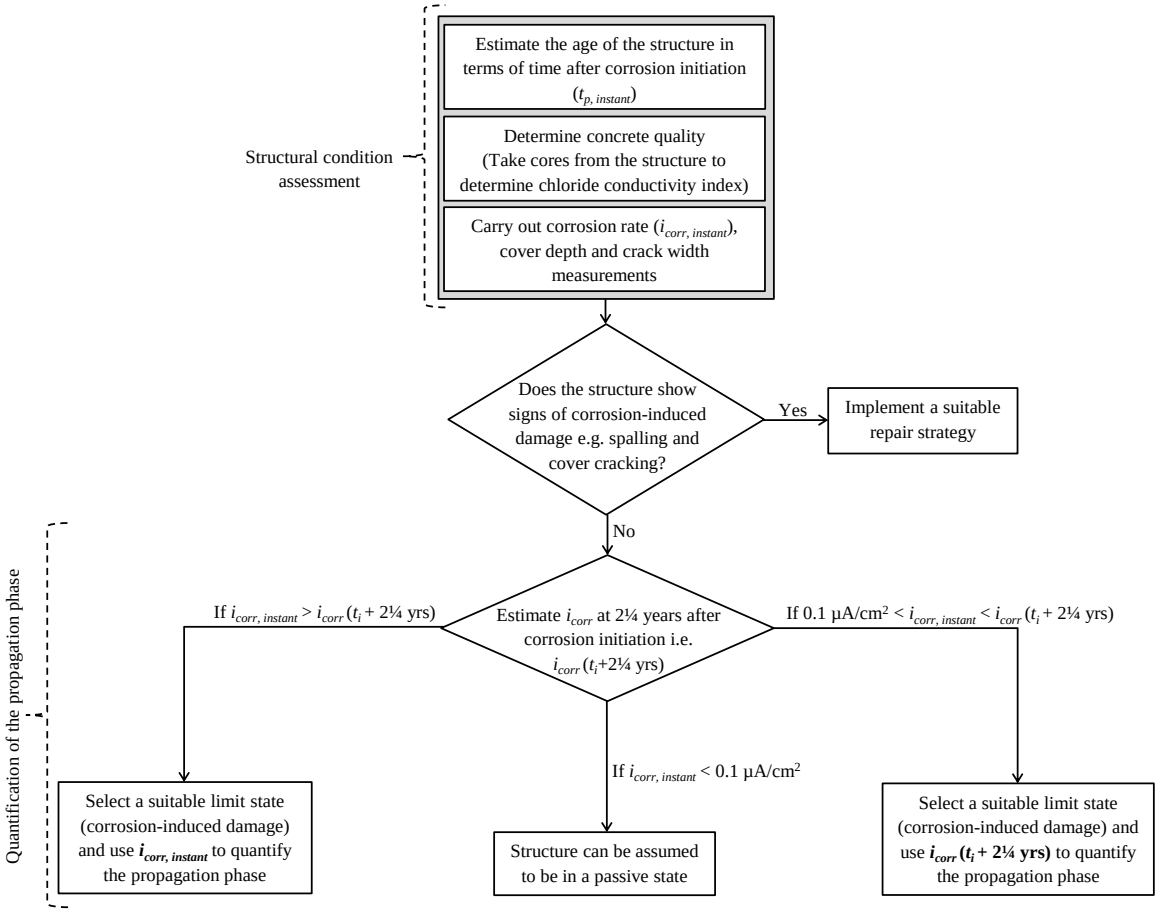

Figure 5.23: Schematic of quantification of propagation phase for existing corrosion-affected structures

5.8.2.1 *Example II - application of the proposed model to new structures*

The objective of this example is to illustrate how the proposed models can be used to predict the time to attainment of a given limit state in the propagation phase. The proposed $i_{corr,field}$ model will be used in this example. For this example, consider three RC structures in a tidal marine exposure. The maximum allowable reduction in steel cross-sectional area is 15% i.e. a 15% reduction in cross sectional area is the limit state (see Section 5.8.1.1 for the reasons for adopting 15% loss in steel cross-sectional area as a limit state). The service life prediction calculations begin at the end of the initiation period i.e. i_{corr} = 0.1 µA/cm^2. Parameters used in this example are summarized in Table 5.13. The parameters were selected in order to depict the following scenarios:

(i) Case I: depicts the effect of high quality concrete on corrosion rate in situations where cover depth is low and crack width is high.

(ii) Case II: depicts the effect of high cover depth on corrosion rate in situations where both concrete quality and crack width are relatively low (compared to case I).

(iii) Case III: depicts the effect of very high cover depth on corrosion rate in situations where concrete quality is lower than that in Case II, and crack width is also higher than that in Case II.

Table 5.13: Parameters used in Example II

Parameter	Value		
Variables (model input parameters)	Case I	Case II	Case III
Diffusion coefficient (50/50 PC/slag concrete), $cm^2/s \times 10^{-10}$	7.5	8.6	12.9
Cover depth (c), mm	20	40	60
Crack width (w_{cr}), mm	1.0	0.4	0.7
Constants	For Case I, II and III		
Initial bar diameter (d_o), mm	20		
Pitting factor (α_{pit}) for cracked concrete[a]	10		
Limit state for propagation phase, as a reduction in steel cross-section	15%		

[a]: Pitting factor is incorporated to account for localized loss in cross-sectional area in the crack region (see Chapter 2 for literature on pitting and pitting factor)

Using the proposed $i_{corr,field}$ model, Eqn. (5.9), the expected corrosion rates for the respective combinations of the parameters in the three cases at approximately t_i + 2¼ years are 0.32, 0.49 and 0.41 μA/cm^2 for Case I, Case II and Case III respectively (see Figure 5.24). These corrosion rates are assumed to be constant during the propagation phase and hence used for its quantification. Faraday's law is used to facilitate the calculation of loss in cross-sectional area. The results for the reduction in cross sectional area are presented in Figure 5.25.

It can be seen in Figure 5.25 that the duration of the propagation phase for Case I, Case II and Case II are, respectively, 21, 14 and 17 years. The service life for the three structures, incorporating the propagation phase, are thus t_i + 21, t_i + 14 and t_i + 17 years for, respectively, Case I, Case II and Case III. These years (t_i + 21, t_i + 14 and t_i + 17 years) may be further extended by the initial 2¼ years leading to the attainment of the predicted stable corrosion rates. However, t_i is incorporated here on the assumption that it exists; previous studies have shown that in the presence of cracking, active corrosion may commence instantaneously when corrosion-sustaining species are present [4, 35]. In such cases, it is only the propagation phase to be considered as the service life of the structure.

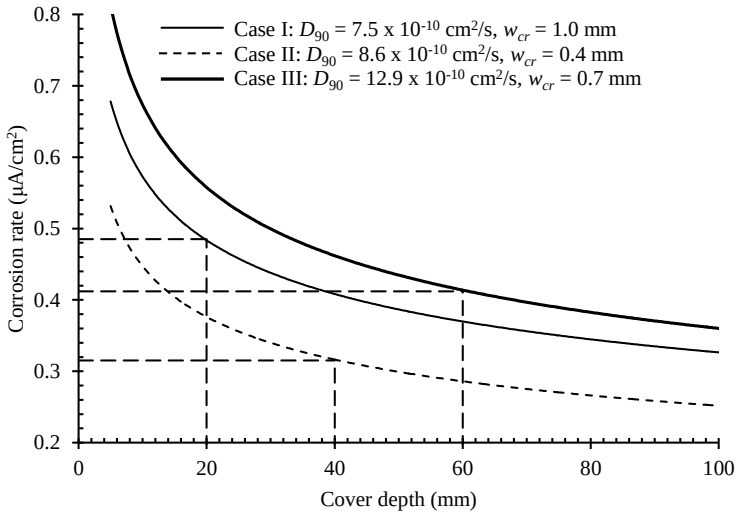

Figure 5.24: Expected corrosion rates at approx. 2¼ years after corrosion initiation based on Eqn. (5.9)

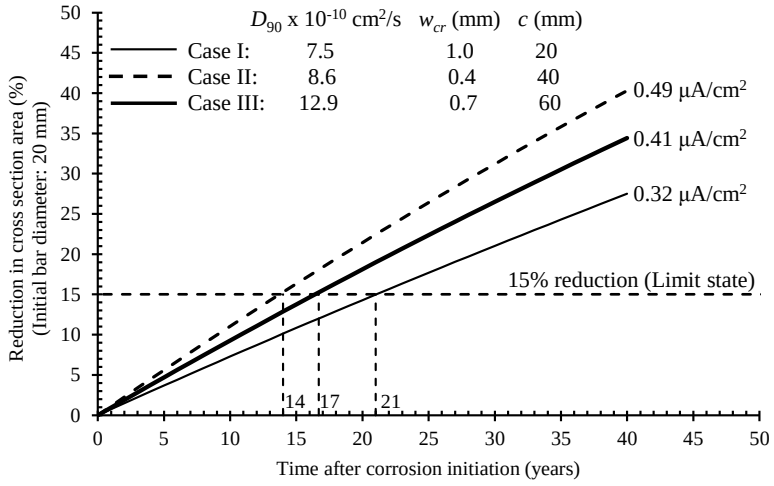

Figure 5.25: Percentage reduction in cross section area due to corrosion with time

5.9 *Concluding remarks on the proposed corrosion rate prediction model*

Empirical chloride-induced corrosion rate prediction models ($i_{corr,field}$ and $i_{corr,field}$) for cracked and uncracked RC were proposed and discussed in detail in this chapter. However, the $i_{corr,field}$ model still needs long-term stable corrosion rate data to update it. In summary, the following can be stated:

1. The models are applicable to marine RC structures in the marine tidal zone. Based on the laboratory and field data used to develop the models, the predicted corrosion rates correspond to approximately 2¼ years after corrosion initiation. However, contrary to DuraCrete's approach, it does not support the adoption of a universal value for a given exposure class regardless of other corrosion rate-influencing factors such as cover depth, cover cracking and concrete quality. The proposed models can be used to estimate different corrosion rate values depending on cover depth, concrete quality and crack width.
2. Even though the proposed models may not be applicable to exposure conditions other than those similar to the ones used in this study (i.e. tidal marine zone), the models can still be used as a valuable tool to select suitable combinations of concrete quality, cover depth and crack width to achieve desirable durability of a RC structure prone to chloride-induced corrosion. The models take into account the fact that a universal crack width is not applicable to all structures regardless of the concrete quality and cover depth. This is contrary to previous approaches that adopt 0.4 mm as a universal crack width regardless of concrete quality and cover depth (see Chapter 2).
3. Even though the models incorporate three input parameters (concrete quality, cover depth and crack width), the sensitivity analysis carried out showed that corrosion rate is more sensitive to simultaneous variation of concrete quality and crack width than it is to simultaneous variation of either cover depth and concrete quality or cover depth and crack width. Further, the analysis showed that contrary to the view in some previous studies where concrete quality is expressly mentioned to have a higher effect on corrosion rate than crack width [4, 36], concrete quality, cover and crack width all affect corrosion rate but the extent of the impact of each parameter depends on the initial values of the other parameters. The practical implication of this is that even though cracking increases corrosion rate, and that it should be minimized, corrosion protection cannot be achieved solely by limitation of crack width only; a holistic approach considering the combined

influence of cover depth, concrete quality and crack width on corrosion rate should be adopted to determine a suitable combination of these parameters. This can be achieved using the proposed model.

4. In addition to the model input parameters considered (i.e. cover depth, concrete quality and crack width), corrosion rate is affected by other factors which have synergistic, opposing or additive effects e.g. temperature, moisture content of the concrete and crack self-healing. These parameters were not incorporated in the proposed models, but may be equally important in the prediction of corrosion rate. Further studies are required to either directly or indirectly incorporate these parameters to improve on the prediction accuracy (with respect to the actual corrosion rates) of the models. This should be done using long-term field (natural) corrosion data.
5. The applicability of the proposed models will need to be validated for values of the cover depth and crack width outside the limits of those used in the development of the model i.e. 20 and 40 mm, and 0.4 and 0.7 mm respectively.
6. The proposed models are valuable tools for the development of pro-active maintenance strategies for corrosion-affected RC structure in tidal marine exposure conditions.

5.10 *References*

[1] DuraCrete (1998) Probabilistic performance-based durability design: modelling of degradation. Document No. BE95-1347/R4-5**,** The Netherlands.

[2] LIFE-365 (2005) Computer program for predicting the service life and life-cycle costs of reinforced concrete exposed to chlorides. *ACI Committee 365*.

[3] Mackechnie, J. R. (1996) Predictions of reinforced concrete durability in the marine environment. *PhD Thesis*, Department of civil engineering, University of Cape Town.

[4] Scott, A. N. & Alexander, M. G. (2007) The influence of binder type, cracking and cover on corrosion rates of steel in chloride-contaminated concrete. *Magazine of Concrete Research,* Vol. 59(7)**,** pp. 495-505.

[5] Otieno, M. B. (2008) Corrosion propagation in cracked and uncracked concrete. *Masters Dissertation*, Department of civil engineering, University of Cape Town.

[6] Clear, C. A. (1985) *Cement and Concrete Association,* Technical Report No. 559**,** England.

[7] Neville, A. M. (2002) Autogenous healing - a concrete miracle? *Concrete International,* Vol. 24(11)**,** pp. 76-82.

[8] Hearn, N. (1991) A recording permeameter for measuring time-sensitive permeability of concrete. *Advances in Cementitious Materials (Ceramic Transactions),* Editor: Mindess, S., Vol. 16**,** Published by the American Ceramic Society (July, 1991), ISBN-13: 978-0944904336, pp. 463-475.

[9] Scott, A. N. (2004) The influence of binder type and cracking on reinforcing steel corrosion in concrete. *PhD Thesis*, Department of civil engineering, University of Cape Town.

[10] Vu, K., Stewart, M. G. & Mullard, J. (2005) Corrosion-induced cracking: experimental data and predictive models. *ACI Structural Journal,* Vol. 102(5)**,** pp. 719-726.

[11] Crosetto, M. & Tarantola, S. (2001) Uncertainty and sensitivity analysis: tools for GIS-based model implementation. *International Journal of Geographic Information Science,* Vol. 15(5)**,** pp. 415-437.

[12] Everitt, B. S. & Skrondal, A. (2010) *The Cambridge Dictionary of Statistics*, Cambridge University Press, The Edinburgh Building, Cambridge CB2 8RU, UK.

[13] Helton, J. C. (1993) Uncertainty and sensitivity analysis techniques for use in performance assessment for radioactive waste disposal. *Reliability Engineering & System Safety,* Vol. 42(2-3)**,** pp. 327-367.

[14] Raupach, M. (1996) Chloride-induced macrocell corrosion of steel in concrete - theoretical background and practical consequences. *Construction and Building Materials,* Vol. 10(5)**,** pp. 329-338.

[15] Walpole, R. E., Myers, R. H., Myers, S. L. & Ye, K. (2007) Probability and statistics for engineers and scientists, 8th Edition. Prentice Hall.

[16] Marita, L. A. (1995) Probability of corrosion-induced cracking of reinforced concrete. *Cement and Concrete Research,* Vol. 25(6)**,** pp. 1179-1190.

[17] DuraCrete (1999) Statistical quantification of the variables in the limit state functions: summary. *Brite/EuRam Project BE95-1347,* Report No. BE95-1347-R9.

[18] Boulfiza, M., Sakai, K., Banthia, N. & Yoshida, H. (2003) Prediction of chloride ions ingress in uncracked and cracked concrete. *ACI Materials Journal,* Vol. 100(1)**,** pp. 38-48.
[19] Gale, J. E. (1987) Comparison of coupled fracture deformation and fluid flow models with direct measurements of fracture pore structure and stress-flow properties. *Proceedings of the 28th US Symposium on Rock Mechanics,* 28th June - 1st July, 1987, Tucson, Arizona, U.S.**,** pp. 1213-1222.
[20] Rubinstein, R. Y. (1981) Simulation and the Monte Carlo method. John Wiley & Sons, New York.
[21] Caleyo, F., Velázquez, J. C., Valor, A. & Hallen, J. M. (2009) Probability distribution of pitting corrosion depth and rate in underground pipelines: a Monte Carlo study. *Corrosion Science,* Vol. 51(9)**,** pp. 1925-1934.
[22] Hunkeler, F. (2005) *Corrosion in reinforced concrete structures*, Woodhead publishing limited, Abington Hall, Abington Cambridge CBI 6AH, England. pp. 1-45.
[23] Andrade, C., Alonso, C. & Arteaga, A. (1997) Models for predicting corrosion rates. *Brussel: Brite-Euram Project,* No. BE95-1347 (Version1/97, Report 2.2.2).
[24] Liu, Y. & Weyers, R. E. (1998) Modelling the time-to-corrosion cracking in chloride contaminated reinforced concrete structures. *ACI Materials Journal,* Vol. 95(6)**,** pp. 675-681.
[25] El Maaddawy, T. & Soudki, K. (2007) A model for prediction of time from corrosion initiation to corrosion cracking. *Cement & Concrete Composites,* Vol. 29(3)**,** pp. 168-175.
[26] ISO-2394 (1998) General principles on reliability for structures. *International Organization for Standardization, Geneva*.
[27] DuraCrete (2000) Probabilistic performance-based durability design of concrete structy - Final Technical Report. Report No. BE95-1347/R17.
[28] Tuutti, K. (1982) Corrosion of steel in concrete. *Swedish Cement and Concrete Research Institute, S-100 44 Stockholm*. Report No. CBI Research 4:82, ISSN 0346-6906, Stockholm, pp. 468.
[29] Andrade, C., Alonso, C., Gonzalez, J. A. & Rodriguez, J. (1989) Remaining service life of corroding structures. *IABSE Report 57/1 on Durability of Structures***,** pp. 359-364.
[30] Clear, K. C. (1989) Measuring rate of corrosion of steel in field concrete structures. *68th Annual Transportation Research Meeting,* Paper No. 88-0324**,** pp. 28-37.
[31] DuraCrete (1998) Modelling of degradation. The European Union - Brite Euram III Project BE95-1347, Document BE95-1347/R4-5.
[32] BS-EN-206-1 (2000) *Concrete - Part 1: Specification, performance, production and conformity*, European Standard.
[33] Yalcyn, H. & Ergun, M. (1996) The prediction of corrosion rates of reinforcing steels in concrete. *Cement and Concrete Research,* Vol. 26(10)**,** pp. 1593-1599.
[34] Martínez, I. & Andrade, C. (2009) Examples of reinforcement corrosion monitoring by embedded sensors in concrete structures. *Cement & Concrete Composites,* Vol. 31(8)**,** pp. 545-554.
[35] Otieno, M. B., Alexander, M. G. & Beushausen, H.-D. (2010) Corrosion in cracked and uncracked concrete - influence of crack width, concrete quality and crack re-opening. *Magazine of Concrete Research,* Vol. 62(6)**,** pp. 393-404.
[36] Schießl, P. & Raupach, M. (1997) Laboratory studies and calculations on the influence of crack width on chloride-induced corrosion of steel in concrete. *ACI Materials Journal,* Vol. 94(1)**,** pp. 56-62.

Chapter 6

Conclusions and recommendations

6.1 *Introduction*

The main objective of this work was to develop empirical chloride-induced corrosion rate prediction models for cracked and uncracked steel RC structures in the marine tidal environment. The study was motivated by the need to quantify, in addition to the initiation phase, the propagation phase as part of the service life of corrosion-affected RC structures, and consequently the need to understand the corrosion propagation process and predict corrosion-induced damage. However, inasmuch as it is acknowledged that in the past much research effort has been put towards the achievement of these goals, most of it has focused on the prediction of corrosion-induced damage such as, among others, loss of steel cross-section area, loss of steel-concrete interface bond, cover cracking and loss of load carrying capacity. Limited research has focused on the prediction of corrosion rate which is one of the main input parameters in corrosion-induced damage prediction models. This, to some extent, poses a major challenge in the quantification and incorporation of the propagation phase in the service life of corrosion-affected RC structures. This study contributes towards overcoming this challenge.

Parallel corrosion experiments were carried out in the laboratory (accelerated corrosion) and field (natural corrosion) to investigate and quantify the combined influence of pre-corrosion load-induced crack width, cover depth and concrete quality (binder type and w/b ratio) on corrosion rate. A correlation between natural corrosion in a marine tidal zone and accelerated corrosion by cyclic wetting (with a chloride-based solution) and drying was also sought. Details of the experimental programme and the results were presented in, respectively, Chapters 3 and 4. Based on the analysis of the results and the inferences made thereof, empirical chloride-induced corrosion rate prediction models were proposed in Chapter 5. Detailed conclusions of Chapters 4 and 5 were given at the end of the respective chapters. This final chapter presents a summary of the study findings while drawing specific, general and practical conclusions in light of the study objectives and highlights areas that need further work.

The conclusions presented in this chapter are divided into three broad sections namely, (a) *Experimental results*, (b) *Corrosion rate prediction models*, and (c) *General conclusions – a practical outlook*. A final part of this chapter, *Recommendations*, summarizes the various aspects emanating from this research which require further work.

6.2 *Conclusions - Experimental results*

The conclusions drawn from the experimental results mainly revolve around the corrosion rate results for the different combinations of experimental variables i.e. cover depth, binder type, w/b ratio, crack width and exposure environment. Corrosion rate was measured using the coulostatic technique. This is a linear polarization resistance method; the details were given in Chapter 3.

6.2.1 *Effect of crack width on corrosion rate*

The pre-corrosion cover cracking investigated in this study was mechanically (load) induced, and measured on the concrete surface. The general trend for a given concrete quality (binder type and w/b ratio), cover depth and exposure environment was that of increasing corrosion rate with increasing crack width as follows: uncracked → incipient-cracked → 0.4 mm cracked → 0.7 mm cracked.

The trend of increasing corrosion rate with increasing crack width was observed in both the laboratory-based and field-based specimens. However, the field-based corrosion rates were lower than the corresponding laboratory-based ones, a trend that was mainly attributed to the diminishing oxygen availability at the steel level due to slow drying out of the concrete caused by the epoxy-coating on all the faces (except that with the specified cover) of the field-based specimens. Further, even though not significant, the difference between corrosion rates in the 0.4 mm and 0.7 mm cracked field-based specimens was less pronounced than in the laboratory-based specimens. This was mainly attributed to the well-controlled exposure conditions (temperature and relative humidity) in the laboratory in comparison to that for the field-based specimens. Even though it could not be confirmed from the results of this study due to a limited number of crack widths that were investigated, the field-based results suggest that as the crack width increases, the influence of further increase in crack width on corrosion rate seems to diminish.

Contrary to a previous study by Scott [1] where corrosion rates on 0.2 and 0.7 mm cracked RC beam specimens were averaged, a statistical analysis of the results of this study showed that the averaging was not valid for the 0.4 and 0.7 mm cracked specimens in this study. A similar conclusion was reached after a statistical analysis of Scott's [1] results. It was therefore concluded that, from a practical or service life prediction point of view, and taking into account that corrosion rate is an important input paramater in corrosion-induced damage prediction models, the decision on whether corrosion rates of different crack widths should be averaged or not should be based on whether the propagation limit state adopted (e.g. corrosion-induced cover cracking) is sensitive to change in corrosion rate due to change in crack widths within a given range, or not.

The results of this study also confirmed a previous assertion by Otieno *et al*. [2] that adopting 0.4 mm, which is conventionally considered a universal corrosion threshold crack width for all concretes below which corrosion rate is similar to that in uncracked concrete regardless of quality and cover depth as proposed by the fib Model Code 2010 [3] is, inasmuch as being conservative, prescriptive and not valid. The results of this study underscore those of Otieno *et al*. [2] and Scott and Alexander [4] that the extent to which crack width increases corrosion rate depends on both concrete quality and cover depth, and that limiting crack widths should consider these factors. This study proposes the adoption of performance-based crack width limits that take into account the combined influence of relevant factors affecting corrosion rate, in this case, cover depth, crack width and concrete quality. It is on this understanding that the proposed corrosion rate prediction models (summarized later in Section 6.3) incorporating concrete quality, cover depth and crack width as input parameters were developed.

6.2.2 *Effect of cover depth on corrosion rate*

Two cover depths, 20 and 40 mm, were used in the experimental work of this study. The incipient-cracked specimens were made using only 20 mm cover. The following general conclusions can be made regarding the influence of cover depth on corrosion rate:

(i) Regardless of the exposure environment, for a given crack width and concrete quality, corrosion rate increases with decreasing cover depth. However, the impact of increasing cover on corrosion rate was relatively lesser in the field-based specimens than in the laboratory-based specimens.

(ii) The highest reductions in corrosion rates as a result of increased cover depth were recorded in the laboratory-based blended cement specimens (70/30 PC/FA and 50/50 PC/GGBS). These results contradict those of Scott and Alexander [4] where the highest reductions in corrosion rates as a result of increased cover depth were recorded in the plain Portland cement concretes. It was not clear why this trend was reversed in this study. This trend was not observed in the field-based specimens where no specific trend was evident, and highlights, to some extent, the limitations of relying solely on laboratory-based accelerated corrosion experiments to predict the performance of in-service RC structures. It clearly shows that in in-service RC structures, other inter-related factors such as the existence of corrosion micro-climates (i.e. spatial variability), even though not usually considered in laboratory experiments and numerical simulations, should be taken into account. The effect of spatial variability on corrosion rate was not considered in this study, but should be taken into account in future work.

Although the impact of increasing cover depth was expected to have a significant impact on the uncracked specimens, this was not the case, and underscored the fact that corrosion rate is not only controlled by cover depth but by a complex interaction of other influencing parameters such as, among others, concrete quality, temperature and moisture content of the concrete. In general, it can be concluded that cover depth is an important parameter in the control of corrosion. In addition, the condition of the cover concrete (e.g. cracking and quality) is equally important and should also be taken into account.

6.2.3 *Effect of concrete quality on corrosion rate*

Concrete quality was varied in this study by using three binder types (100% PC, 70/30 PC/FA and 50/50 PC/GGBS) and two w/b ratios (0.40 and 0.55), and quantified using the chloride diffusion coefficient (D_{90}) obtained from the 90-day chloride conductivity index (CCI) test - see Appendix D for the empirical relationship between CCI and diffusion coefficient. The trend in the D_{90} values for the various concretes, in increasing order i.e. decreasing concrete quality, was 50/50 PC/GGBS (0.40 w/b) → 50/50 PC/GGBS (0.55 w/b) → 70/30 PC/FA (0.40 w/b) → 70/30 PC/FA (0.55 w/b) → 100% PC (0.40 w/b). In general, for a given binder, diffusion coefficient values decreased with decreasing w/b ratio. Furthermore, the blended cement concretes had lower diffusion coefficients than PC concrete. The D_{90} values were used in this study to depict the penetrability of the concrete cover with respect to the ease of ingress of corrosion-sustaining agents (oxygen and moisture).

For a given crack width, cover depth and exposure environment (laboratory or field), corrosion rate increased with decreasing concrete quality (or increase in penetrability). The following conclusions

can be made with respect to the effect of change in concrete quality due to change in either binder type or w/b ratio on corrosion rate:

(i) The change in concrete quality due to change in binder type has a relatively lesser effect on corrosion rate than change in concrete quality due to change in w/b ratio. Furthermore, this effect was less in the field-based specimens than in the laboratory-based ones. It can therefore be concluded that even though differences in concrete quality may be found between blended cements in the laboratory, these differences cannot be easily extended to field applications unless valid correlations are established between accelerated laboratory and natural field corrosion performance of different concretes.

(ii) Blended cement concretes respond to changes in w/b ratio in a similar manner i.e. they are not highly sensitive to the change in w/b ratio. Similar to the effect of change in concrete quality due to change in binder type, the effect of change in w/b ratio had a relatively lesser effect in the field-based specimens than in the laboratory-based specimens.

(iii) For blended cement concretes, even though reducing the w/b ratio further increases the concrete's resistance to chloride ingress and hence corrosion rate, the effect is small compared to that of the partial replacement of PC with a supplementary cementitious material. This suggests that the high concrete resistivity and decreased penetrability due to microstructure densification and chloride binding in blended cement concretes has a major influence on corrosion rate than concrete quality. However, this trend, unless confirmed in future studies, may only be applicable for small changes in w/b ratio such as the one used in this study.

In both the field-based and laboratory-based specimens, irrespective of binder type, there existed a good correlation ($R^2 > 0.7$) between D_{90} and corrosion rate for a given crack width and cover depth. For a given binder type and the corresponding D_{90} value, corrosion rate increased with increasing crack width. The general trend between corrosion rate and D_{90} based on the results is given in Equation (6.1):

$$i_{corr} = k_1 e^{A_1\left(D_{90}\times 10^{10}\right)} \ [\mu A/cm^2] \tag{6.1}$$

where k_1 ($\mu A/cm^2$) and A_1 (s/cm^2) are empirical coefficients whose values are dependent on cover depth, crack width and exposure environment (laboratory or field). The actual values of these coefficients were given in Chapter 5.

6.2.4 *Relationship between corrosion rate and concrete resistivity*

Concrete resistivity was measured on the concrete surface using a 4-point Wenner probe. The resistivities for the cracked and uncracked concretes were found to have negligible differences in both the laboratory-based and field-based specimens because the measurements in the cracked specimens were taken only in the uncracked concrete portions; no measurements were taken across the cracks. In both the field-based and laboratory-based specimens, resistivity in all the concretes increased with time. The concrete resistivities of both the field-based and laboratory-based specimens increased in the following order: 100% PC (0.40 w/b) → 50/50 PC/GGBS (0.55 w/b) → 70/30 PC/FA (0.55 w/b) → 50/50 PC/GGBS (0.40 w/b) → 70/30 PC/FA (0.40 w/b). This trend depicts an increase in concrete

resistivity with both the presence of supplementary cementitious materials (FA and GGBS) and decrease in w/b ratio (for a given binder), as expected.

The resistivity values for the field-based specimens were relatively higher than the corresponding laboratory-based ones. This trend was attributed to either one or a combination of the following two possible reasons:

(i) Lower moisture contents in the field-based concretes (especially in the upper 10 - 20 mm concrete surface layer) in comparison to those in the laboratory where resistivity measurements were taken at the end of the 3-day wetting with 5% NaCl solution which probably resulted in saturation of the specimens.

(ii) Formation of a dense insoluble layer of magnesium hydroxide, $Mg(OH)_2$, (i.e. brucite) on the concrete surface [5].

It was not possible to identify which of these two possible phenomena had a major effect on concrete resistivity because they were not measured. Further work is required to do this.

The results showed an inverse relationship between corrosion rate and concrete resistivity. This is expressed in Equation (6.2):

$$i_{corr} = k_2\left(\frac{1}{\rho^{A_2}}\right) \text{ [}\mu\text{A/cm}^2\text{]} \tag{6.2}$$

where k_2 ((μA/cm^2)/kΩ-cm) and A_2 (–) are empirical coefficients whose values are dependent on cover depth, crack width and exposure environment (laboratory or field). The actual values of these coefficients were given in Chapter 5.

In both the field-based and laboratory-based specimens, for a given concrete resistivity, cover depth, exposure environment and concrete quality (binder type and w/b ratio), higher corrosion rates were recorded in the cracked specimens than in the uncracked ones. The results showed that in the presence of cracks, the high resistivity of blended cement concretes cannot solely be relied on to inhibit corrosion. Other factors such as crack width, concrete quality and cover depth should be taken into account. In general, the dominating effect of the inherent high resistivity on corrosion rate in blended cement concretes is still evident even in cracked concrete. This is a limitation to the use of concrete resistivity (measured using 4-point Wenner probe) as a tool to assess the susceptibility of cracked RC structures to steel corrosion. It also brings to question the validity of the conventional guidelines used to interpret resistivity results (in terms of corrosion risk) in RC concrete structures (see Table 2.5, Chapter 2). The results clearly showed that, if the influence of cover cracking on corrosion rate is to be appreciated, such guidelines have to be used carefully, or revised to allow for the influence of cover cracking on corrosion rate. A hypothetical approach in which the influence of cover cracking is taken into consideration when interpreting resistivity measurements in cracked concrete was therefore proposed in this study (see Chapter 4). Finally, the results of this study also support the proposal by Otieno *et al*. [6] that resistivity measurements should be complemented with other corrosion assessment techniques such as half-cell potential and corrosion rate measurement.

6.2.5 *Relationship between corrosion rate and half-cell potential*

Half-cell potential (HCP) measurements were carried out with reference to a Ag/AgCl electrode, and interpreted according to the ASTM C876-91 [7] guidelines. Generally, the HCP results for the field-based specimens were lower (less negative) than the corresponding laboratory-based ones. The general trend in HCP values for the laboratory-based and field-based specimens was the same as that for corrosion rate where the latter increased with (a) increase in crack width, (b) decrease in cover depth, and (c) decrease in concrete quality. For a given exposure environment (laboratory or field), cover depth and crack width, average HCP became less negative in the following order: 100% PC (0.40 w/b) → 70/30 PC/FA (0.55 w/b) → 50/50 PC/GGBS (0.55 w/b) → 70/30 PC/FA (0.40 w/b) → 50/50 PC/GGBS (0.40 w/b).

Contrary to resistivity measurements, HCP measurements could be used to assess the influence of cracks; the value of HCP measured reflected the actual corrosion state of the steel in concrete.

6.2.6 *Relationship between corrosion rate and chloride content*

Total chloride content measurements at the steel level were carried out after 73 weeks of exposure of the specimens in the laboratory and field. Chloride content was detemined by potentiometric titration using 0.1M $AgNO_3$ solution. The cores used for chloride content measurements were taken at 30 and 90 mm from the crack (on one side of the crack). The general trend in the laboratory-based specimens showed that higher chloride contents corresponded to higher corrosion rates. However, in the field-based specimens, the high chloride concentrations measured at the steel level did not correspond to high corrosion rates, and was attributed to the oxygen deficiency to support the cathodic reaction. Low oxygen concentration was attributed to two possible causes; (i) its decreased solubility in salt solution, and (ii) the high moisture content of the field-exposed specimens due to the epoxy coating which prevented drying from the specimen sides (during low tides). The moisture content of the concrete was not monitored in this study but this should be carried out in future work. Even though oxygen solubility was also expected to have decreased due to presence of chloride salts in the concrete pore solution, the 4-days air-drying of the laboratory specimens counteracted this by allowing oxygen ingress during this period.

In addition, the following general conclusions can be made:

(i) for a given crack width, cover depth, exposure environment and exposure time, the use of supplementary cementitious materials such as FA and GGBS leads to decreased concentration of chlorides at the steel level in comparison to plain PC concretes. This trend is mainly attributable to the effects of increased chloride binding capacity and concrete microstructure densification.

(ii) for a given concrete quality (influenced by binder type and w/b ratio), crack width, exposure environment and exposure time, increasing the cover depth leads to decreased chloride concentration at the steel level mainly due to increased travel path. However, even though not investigated in this study, this may not be the case if the crack intersects the steel (i.e. the crack depth is much greater that the cover depth). In such a case, the cover depth may effectively be considered to be zero, and the chloride concentration at the steel level will depend on, if present, the virtual resistance of the uncracked concrete ligaments in the crack profile [8]. This is especially important in blended cement concretes with high concrete resistivities.

(iii) the presence of cover cracking increases the chloride concentration at the steel level, even in regions away from the crack mainly due to either one or a combination of the following phenomena:
   a) ease of chloride penetration along the steel-concrete interface due to damage of the steel-concrete bond during loading, or
   b) the presence of microcracks on the concrete cover in addition to wider cracks.

There was little difference between the chloride content at the steel level in the labopratory-based and field-based 0.4 and 0.7 mm cracked specimens. Maximum percentage differences in chloride contents of up to 49% and 114% in, respectively, the field-based and laboratory-based specimens were recorded between the uncracked and incipient-cracked specimens while differences of only up to 15% and 10% were recorded in, respectively, the field-based and laboratory-based specimens between the 0.4 mm and 0.7 mm cracked specimens. This observation was attributed to the reasons already given in (iii) above. The trend is similar to that for corrosion rate in the field-based specimens with these crack widths which showed less stark differences, and underscores the hypothesis stated in Section 6.2.1 that as the crack width increases, the influence of cracking on corrosion rate seems to diminish.

6.2.7 *Comment on the aggressiveness of the marine tidal zone*

The tidal zone in marine exposure environments is usually considered the most aggressive with respect to chloride-induced corrosion initiation and corrosion-induced damage. It is on this basis that it was selected as an exposure environment for the field-based specimens in this study. However, considering that the initiation phase in the specimens was eliminated before exposure using impressed anodic current, the levels of corrosion rates obtained in the field-based specimens after approximately 2¼ years of exposure did not conform to the expected aggressiveness of the tidal zone, and motivate for a review of its aggressiveness in comparison to other zones such as splash and spray zones. Even though the field-based specimens were epoxy-coated on all the faces except that with the specified cover depth, and that this affected their degree of drying during low tides, it is clear that the relative duration of low and high tides also plays a major role in the drying process, and that this aspect should be taken into account in specifying the aggressiveness of the tidal zone relative to other zones. It is therefore important that classifications such as those in EN 206-1 [9] are used only as guidelines and should be carefully reviewed and modified to account for variations in marine exposure conditions from one geographical location to another. Furthermore, factors such as concrete quality and cover depth also need to be taken into consideration.

6.2.8 *The concept of c/w_{cr} ratio vs. concrete quality and corrosion rate*

The results obtained in this study motivated the development of a framework that incorporates the combined effect of crack width (w_{cr}), cover depth (c) and concrete quality (binder type and w/b ratio) on corrosion rate in order to obtain a suitable combination of these parameters during design to meet desired durability requirements. This framework laid the background for the development of the corrosion rate prediction models summarized later in Section 6.3. The results showed a similar trend between corrosion rate and c/w_{cr} ratio for both the laboratory-based and field-based specimens. For a given c/w_{cr} ratio, a range of corrosion rates are possible depending on the concrete quality (see Figure 4.67). The general trend between corrosion rate and c/w_{cr} ratio was as given in Equation (4.3):

$$i_{corr} = k_3\left(\frac{c}{w_{cr}}\right)^{-A_3} \quad [\mu A/cm^2] \tag{6.3}$$

where k_3 ($\mu A/cm^2$) and A_3 (–) are empirical coefficients whose values are dependent on concrete quality and exposure environment (laboratory or field). The actual values of these coefficients were given in Chapter 5.

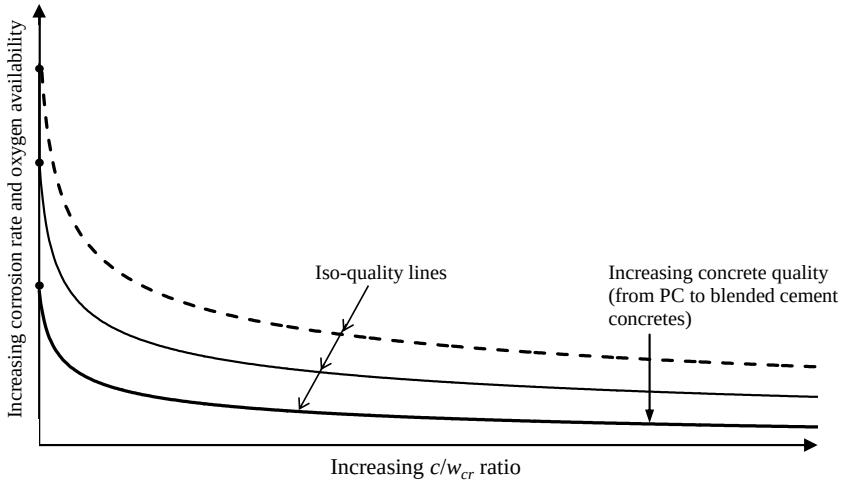

Figure 6.1: Schematic relationship between corrosion rate, crack width, cover depth and concrete quality

The use of c/w_{cr} ratio in conjunction with concrete quality, as opposed to only w_{cr} provides an objective way to compare corrosion rates for specimens with similar concrete qualities (binder type and w/b ratio) but different cover depths and crack widths. However, even though this study proposes the use of c/w_{cr} ratio in conjunction with concrete quality as durability design parameters for cracked concrete, it is acknowledged that this proposal is based on the crack width measured on the concrete surface. This is the most common approach for in-service RC structures. Further studies are required to (i) ascertain if crack profile and tortuosity have a significant effect on corrosion rate and hence on the c/w_{cr} ratio, and (ii) understand the effect of steel-concrete interface damage on corrosion rate in cracked flexural RC members.

6.3 *Conclusions - Corrosion rate prediction models*

Based on the experimental results, empirical chloride-induced corrosion rate prediction models were proposed for both the laboratory-based and field-based (marine tidal zone) specimens; each model comprised two parts, one for cracked and the other for uncracked concrete. The general forms of the proposed models are as follows:

$$i_{corr,lab\ (t_i+2.25\ \text{years})} = \begin{cases} \left(5.18e^{0.01\left(D_{90\times10^{10}}\right)}\right)\left(\frac{c}{w_{cr}}\right)^{-a} & \text{for cracked RC} \\ \left(\frac{1.19}{c^{0.34}}\right)e^{0.05\left(D_{90\times10^{10}}\right)} & \text{for uncracked RC} \end{cases} \quad [\mu A/cm^2] \tag{6.4}$$

$$i_{corr,\,field\ (t_i+2.25\ \text{years})} = \begin{cases} \left(0.64\mathrm{e}^{0.06\left(D_{90}\times 10^{10}\right)}\right)\left(\dfrac{c}{w_{cr}}\right)^{-b} & \text{for cracked RC} \\ \left(\dfrac{1.72}{c^{0.64}}\right)\mathrm{e}^{0.03\left(D_{90}\times 10^{10}\right)} & \text{for uncracked RC} \end{cases} \quad [\mu\text{A/cm}^2] \tag{6.5}$$

where $a = 0.96\left(D_{90}\times 10^{10}\right)^{-0.35}$ and $b = 0.21\mathrm{e}^{0.02\left(D_{90}\times 10^{10}\right)}$.

The proposed models can aid in the:

(i) selection of suitable design combinations of concrete cover, quality and crack width,

(ii) quantification of the propagation phase with respect to a given performance limit for the propagation phase, e.g. loss of steel cross-section area. This can be achieved using relevant corrosion-induced damage prediction models.

To date, only Fickian-based corrosion initiation models have been used in the selection of concrete durability design parameters (mainly concrete quality and cover depth); it is assumed that concrete is uncracked, a scenario which is seldom the case in in-service RC structures. Therefore, even though the concrete quality and cover depth selected may satisfy durability requirements with respect to the initiation phase, the same may not be the case in the presence of cracking where the initiation phase may either be significantly shortened or completely eliminated due to the increased penetrability of the concrete. The proposed models overcome this problem by incorporating the influence of crack width on corrosion rate especially for the propagation phase. With the proposed models, the designer can objectively perform a number of permutations to determine the most suitable combination of concrete quality, crack width and cover depth to meet the desired durability performance (with respect to steel corrosion) of a given RC structure in the marine environment. These were exemplified in Chapter 5.

6.3.1 *Sensitivity of corrosion rate to crack width, cover depth and concrete quality*

The sensitivity analyses carried out on the proposed models to establish the sensitivity of corrosion rate to (i) the individual input parameters (concrete quality (D_{90}), cover depth (c) and crack width (w_{cr})), and (ii) a combination of the input parameters revealed in the following trends:

(i) The extent to which a change in either crack width or cover depth affects corrosion rate is dependent on the concrete quality. The lower the concrete quality (higher D_{90}), the higher the extent to which a change in either crack width or cover depth affects corrosion rate. It was also established that the initial cover depth does not affect the extent to which a change in cover depth affects corrosion rate while the initial crack width does not affect the extent to which a change in crack width affects corrosion rate.

(ii) The extent to which a change in concrete quality affects corrosion rate is dependent on the values of both cover depth and crack width. A combination of low cover depth and large crack width results in the highest effect on corrosion rate due to change in concrete quality.

(iii) The extent to which a combined change in both D_{90} and c affects corrosion rate is dependent on the value of crack width; the higher the crack width, the greater the change in corrosion rate due

to a combined variation in D_{90} and c. However, for two different crack widths that do not vary by a large margin (e.g. 0.4 and 0.5 mm), the effect of changing both D_{90} and c is negligible.

(iv) The extent to which a combined change in both D_{90} and w_{cr} affects corrosion rate is dependent on the value of cover depth; the lower the cover depth, the greater the change in corrosion rate due to a combined variation in D_{90} and w_{cr}. As the cover depth increases, there may a point where change in either concrete quality (D_{90}) or crack width does not affect corrosion rate. However, this point could not be established in this study due to the limited scope of the experiments.

(v) The extent to which a combined change in c and w_{cr} affects corrosion rate is dependent on the value of D_{90}; the higher the D_{90} (i.e. low concrete quality), the greater the change in corrosion rate due to a combined variation in c and w_{cr}. However, for a given concrete quality, the extent to which a combined change in w_{cr} and c affects corrosion rate is independent of the crack width and cover depth. This, to some extent, depicts the dominating effect of concrete quality on corrosion rate.

The findings of this study are in agreement with those of some previous studies where corrosion rate is reported to be more sensitive to change in concrete quality than crack width [4, 10]. In conclusion, concrete quality was found to have a dominating role on the effect of either crack width or cover depth on corrosion rate. The practical implication of these findings is that even though pre-corrosion cover cracking increases corrosion rate, and that it should be minimized, corrosion protection cannot be achieved solely by limitation of crack width; a holistic approach, in this case, considering cover depth, concrete quality and crack width should be adopted.

6.3.2 *Practical application of the model*

One of the aims of this study was to develop practical chloride-induced corrosion rate prediction models for cracked and uncracked RC that can aid the engineer at both the design stage in the selection of suitable design variables and after construction or repair to develop pro-active maintenance strategies for corrosion-affected RC structures. These were exemplified in Chapter 5. Even though (i) long-term data is still needed to calibrate the proposed models for field application, and (ii) it is acknowledged that other relevant input parameters such as temperature and relative humidity will still need to be incorporated into the models, the model structure is not expected to change significantly with respect to the relationship between the input parameters (cover depth, concrete quality and crack width) and corrosion rate. These parameters can easily be quantified, and therefore make the models easily applicable. This is in contrast to some previous models that were presented in Chapter 2 in which the input parameters are not easily quantifiable, e.g. availability of oxygen at the steel level. A typical example is the DuraCrete model [11] that was presented in Chapter 2.

The proposed models also provide a practical framework in which suitable combinations of cover depth, concrete quality and crack width can be selected and even optimized with respect to a pre-defined criterion e.g. economic implications. This is important because the experimental results of this study and the sensitivity analyses carried out on the proposed models showed that a holistic approach taking into account the interaction between the relevant factors affecting corrosion should be adopted. However, it is important to acknowledge the limitations of the proposed models that were presented in

Chapter 4 – the limitations are associated mainly with the experimental set-up and scope used in this study.

6.4 *General conclusions – a practical outlook*

This study and previous ones have shown that cover cracking is an important factor affecting corrosion rate of steel in RC structures. Therefore, taking a step further, and from a practical viewpoint, what is now required is a design framework to incorporate the effect of cracking in design codes; this is an onerous task and requires researchers and practicing design engineers to recognize and appreciate that:

(i) durability and sustainability requirements are key pillars in the design of today's RC structures; an optimal selection of design parameters and materials taking the two requirements into account should be sought.

(ii) a multi-disciplinary and integrated approach is inevitable; this calls for structural and material engineers/scientists to work together to obtain an optimal design framework for cracked corrosion-affected RC structures.

(iii) with respect to implementing performance based limiting crack widths, more accurate measurement and prediction models for both crack width and the resulting corrosion rate are required. Currently, there are a number of corrosion rate prediction models (see Chapter 2), and several studies are focusing on the development of more accurate and practical ones; this study has contributed towards achieving this goal.

To effectively incorporate the effect of cover cracking on steel corrosion in performance-based design codes for RC structures, it is essential to quantify its effect on both corrosion initiation and its propagation. This should be similar to the approach used in the performance-based design for service life of RC structures considering only the initiation period where well established test methods are used to quantify concrete cover quality. For example, in South Africa, the durability index (DI) tests, comprising of the chloride conductivity and oxygen permeability tests [12], are used to quantify concrete cover quality and hence specify as-built concrete quality targets. However, it is important to note that such tests are essentially applicable only to uncracked concrete. Their applicability to cracked concrete is not straightforward and needs to be explored. They can therefore not be objectively used to directly quantify limiting cover crack widths for RC structures. A suitable approach is needed to quantify the effect of cover cracking on corrosion rate to enable its incorporation in a performance-based durability design. In this study, the diffusion coefficient obtained from the chloride conductivity index (CCI) test was only used to characterize concrete quality – the CCI test cannot be used on its own to predict the durability performance in cracked concrete.

In summary, to incorporate the effect of cover cracking on corrosion rate in design codes, the following issues need to be addressed:

(i) Development of accurate models to quantify transport properties in cracked concrete; the transport properties of cracked concrete are fundamentally different from those of uncracked ones.

(ii) Development of corrosion rate prediction models. The following factors should be considered in the development of corrosion rate prediction models: (a) the model should be (as far as possible) representative of the actual corrosion rate characteristics in the RC structure in its service environment, (b) it should account for variability and uncertainty of both the input parameters and corrosion rate (model output), and (c) it should be capable of being adjusted to suit different exposure conditions, and

(iii) Establishment of standard corrosion rate assessment techniques and the interpretation of results

This study was an effort towards achieving the above challenges but further work is inevitably still needed.

6.5 *Recommendations for further work*

This work achieved its objectives as outlined in Chapter 1. However, from the research findings already presented, and in addition to the limited scope of the study and the model limitations, the following areas need further research work:

1. The quantification of the combined influence of other crack characteristics such as crack self-healing or sealing, crack density and crack activity or dormancy on corrosion rate needs to be investigated further, and used to update the proposed models. In addition, the characterization of the damage at the concrete-steel interface due to cracking should be carried out and its effect on chloride ingress and corrosion rate quantified.
2. Even though it could not be confirmed from the results of this study due to a limited number of crack widths that were investigated, the field-based results suggest that, other factors being constant, as the crack width increases, the influence of cracking on corrosion rate seems to diminish. Further work is needed to ascertain this trend.
3. The influence of spatial variability on corrosion rate was not considered in this study, and should be investigated and quantified.

   Corrosion rate in this study was measured using a linear polarization technique (LPR). The main shortcoming of this technique is the difficulty to determine the actual surface area of steel that is actively corroding or polarized during corrosion rate measurements. In most cases, as was the case in this study, the steel surface area is assumed. It is therefore important that the corrosion rate results reported in this study are, in future, compared with those from gravimetric measurements on the corroded steel bars. This process will aid in quantifying the error between the measured and actual corrosion rate. This should be taken into account in the proposed corrosion rate prediction models e.g. by determining the ratio between the gravimetric and LPR corrosion rates, $\beta = (i_{corr,\,\text{gravimetric}}) \times (i_{corr,\,\text{LPR}})^{-1}$, and incorporating this in the proposed models.
4. Corrosion rate and the factors affecting it are known to be highly variable and uncertain. To account for this, a probabilistic approach should be adopted. Even though the variability of the different parameters used in the model was acknowledged, this was not taken into account during the model development, and should be considered in future work.
5. Further work is needed to revise the guidelines that are currently being used in the interpretation of concrete resistivity measurements (in terms of corrosion risk). The results clearly show that the

guidelines are not applicable in the presence of cover cracking. A hypothetical framework was proposed but this needs further work before it can be implemented.

6. Even though the empirical model used to obtain the chloride diffusion coefficients of the concretes from their respective chloride conductivity indices was developed using data obtained from plain and blended CEM I 42.5N (PC) concretes, and was applicable to this study, its applicability needs to be investigated and/or validated for a wide variety of (new) binder types. Deviations, if any, from the current empirical relationship between the chloride conductivity index and diffusion coefficient should be reconciled and taken into account when using the proposed corrosion rate prediction models.
7. In the corrosion beam specimens used in this study, only one horizontal steel bar acting as tensile reinforcement was used. However, in reality, other layers of horizontal bars could exist and hence have an effect on macro-cell corrosion. Furthermore, if stirrups are present, they can create weak points in the concrete members leading to bending cracks at stirrup locations. This can lead to a complex interaction between transverse and longitudinal cracks. This can result in a complex distribution of anodic and cathodic sites, which can, as a result, protect the tensile bar(s) from corrosion due to the presence of anodic sites on the stirrups. The reverse could also occur. In addition, the presence of many layers of reinforcement could modify the anode-to-cathode ratio. These scenarios should be investigated further.

6.6 *References*

[1] Scott, A. N. (2004) The influence of binder type and cracking on reinforcing steel corrosion in concrete. *PhD Thesis*, Department of civil engineering, University of Cape Town.

[2] Otieno, M. B., Alexander, M. G. & Beushausen, H.-D. (2010) Corrosion in cracked and uncracked concrete - influence of crack width, concrete quality and crack re-opening. *Magazine of Concrete Research,* Vol. 62(6)**,** pp. 393-404.

[3] fib-Model-Code (2010) 3rd FIP/CEB Model Code for concrete structures. *Comite Euro-International du Beton and Federation International de Precontrainte*.

[4] Scott, A. N. & Alexander, M. G. (2007) The influence of binder type, cracking and cover on corrosion rates of steel in chloride-contaminated concrete. *Magazine of Concrete Research,* Vol. 59(7)**,** pp. 495-505.

[5] Buenfeld, N. R. (1986) The development of surface layers on concrete exposed to sea-water. *Cement and Concrete Research,* Vol. 16(5)**,** pp. 721-732.

[6] Otieno, M. B., Alexander, M. G. & Beushausen, H.-D. (2010) Suitability of various measurement techniques for assessing corrosion in cracked concrete. *ACI Materials Journal,* Vol. 107(5)**,** pp. 481-489.

[7] ASTM-C876-91 (1999) *Standard test method for half-cell potentials of uncoated reinforcing steel in concrete*, ASTM International, West Conshohocken, PA 19428-2959, USA.

[8] Bažant, Z. P. (1987) Snapback instability at crack ligament tearing and its implication for fracture micro-mechanics. *Cement and Concrete Research,* Vol. 17(6)**,** pp. 951-967.

[9] BS-EN-206-1 (2000) *Concrete - Part 1: Specification, performance, production and conformity*, European Standard.

[10] Raupach, M. (1996) Chloride-induced macrocell corrosion of steel in concrete - theoretical background and practical consequences. *Construction and Building Materials,* Vol. 10(5)**,** pp. 329-338.

[11] DuraCrete (1998) Probabilistic performance-based durability design: modelling of degradation. Document No. BE95-1347/R4-5**,** The Netherlands.

[12] Alexander, M. G., Ballim, Y. & Mackechnie, J. R. (2001) Use of durability indexes to achieve durable cover concrete in reinforced concrete structures. *Materials Science of Concrete,* VI**,** pp. 483-511.

Appendix A

Experimental data and detailed results

A.1 *Compressive and tensile strength results*

Table A.1: Compressive strength results

Mix label	Age (days)	Average*		Standard deviation (for strength, MPa)
		Density (kg/m^3)	Strength (MPa)	
PC-40	7	2373	43.8	1.6
	14	2377	54.3	1.4
	21	2395	56.2	1.3
	28	2397	58.2	3.0
	56	2395	62.6	1.4
	90	2403	67.0	1.7
SL-40	7	2407	28.8	0.6
	14	2405	40.6	0.1
	21	2397	46.2	0.6
	28	2417	48.1	2.0
	56	2423	54.5	2.2
	90	2408	62.1	0.8
SL-55	7	2397	19.7	0.6
	14	2388	28.0	0.1
	21	2377	32.3	1.2
	28	2387	35.3	0.9
	56	2382	44.5	0.6
	90	2408	47.9	2.9
FA-40	7	2388	30.9	0.6
	14	2373	44.0	0.4
	21	2377	47.7	0.5
	28	2367	50.7	0.9
	56	2363	61.0	2.2
	90	2393	73.6	0.9
FA-55	7	2365	17.7	0.6
	14	2368	20.5	2.6
	21	2372	24.7	0.6
	28	2377	28.6	1.9
	56	2400	35.5	1.1
	90	2372	41.1	2.4

* Average of 3 readings

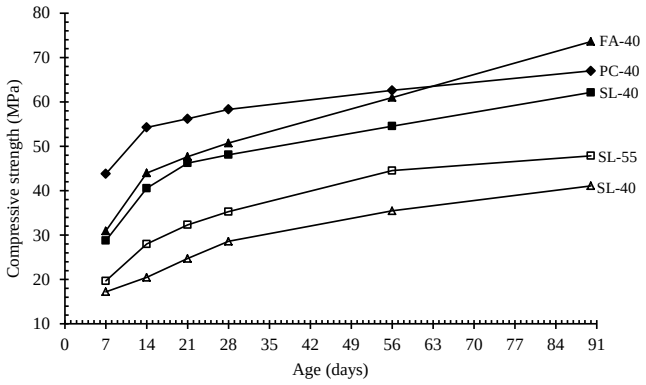

Figure A.1: Compressive strength development trends for the different concretes

Table A.2: Tensile strength results

Mix label	Age (days)	Average* (MPa)	Standard deviation (MPa)
PC-40	28	3.69	0.25
	90	4.01	0.06
SL-40	28	2.82	0.16
	90	3.37	0.06
SL-55	28	2.33	0.27
	90	2.65	0.10
FA-40	28	3.42	0.37
	90	3.90	0.04
FA-55	28	2.25	0.10
	90	3.04	0.02

* Average of 3 readings

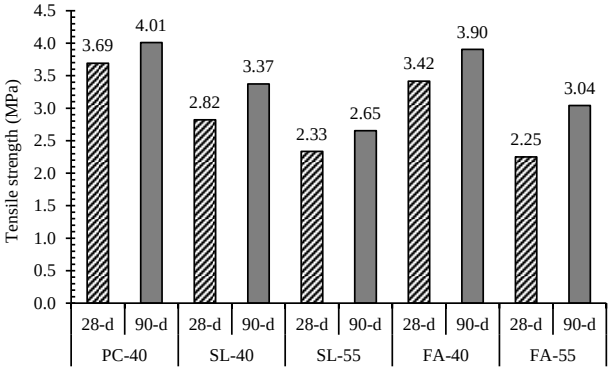

Figure A.2: 28 and 90-day tensile strengths

A.2 *Aggregate sieve analyses*

Table A.3: Fine and coarse aggregate sieve analysis results

Aggregate	Sieve size	Mass retained (g)	% mass retained	Cumulative % mass retained	Cumulative % mass passing
Fine aggregate	2360 µm	8.0	0.8	0.8	99.2
(Klipheuwel)	1180 µm	89.5	9.0	9.8	90.3
Sample size: 1.0 kg	600 µm	215.8	21.6	31.3	68.7
	300 µm	250.0	25.0	56.3	43.7
	150 µm	373.7	37.4	93.7	6.3
	75 µm	52.4	5.2	98.9	1.1
	<75 µm	10.6	1.1	100.0	0.0
Coarse aggregate	16 mm	7.9	0.8	0.8	99.2
(Granite)	13.2 mm	89.3	8.9	9.7	90.3
Sample size: 1.0 kg	9.5 mm	842.8	84.3	94.0	6.0
	6.7 mm	58.4	5.8	99.9	0.1
	4.75 mm	1.6	0.2	100.0	0.0

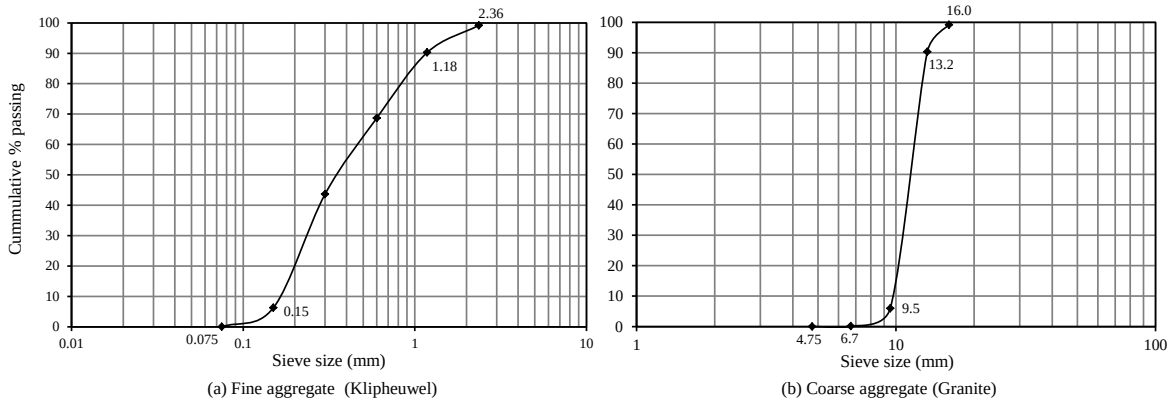

(a) Fine aggregate (Klipheuwel) (b) Coarse aggregate (Granite)

Figure A.3: Grading curves for fine and coarse aggregate

A.3 *Chloride conductivity index test results*

Table A.4: Chloride conductivity index test results

		28-day					90-day				
		PC-40	SL-40	SL-55	FA-40	FA-55	PC-40	SL-40	SL-55	FA-40	FA-55
Average*		**1.24**	**0.26**	**0.59**	**0.37**	**0.89**	**1.10**	**0.15**	**0.35**	**0.24**	**0.70**
Standard deviation (σ)		0.04	0.01	0.04	0.02	0.01	0.02	0.01	0.01	0.02	0.03
Coeff. of variation (%)		4.64	3.14	9.62	2.94	0.92	2.35	5.44	2.44	5.02	4.36
σt		0.14	0.03	0.11	0.06	0.03	0.06	0.03	0.02	0.06	0.10
Range	Min.	1.10	0.23	0.48	0.31	0.86	1.04	0.12	0.33	0.18	0.60
	Max.	1.38	0.29	0.70	0.43	0.92	1.16	0.18	0.37	0.30	0.80

* Average of 4 readings, Range = Average ± σt where t = 3.182 for 95% confidence level

Table A.5: *t* distribution

Dgrees of freedom (v)	Probability α (level of significance)			
	0.10	0.05	0.01	0.001
	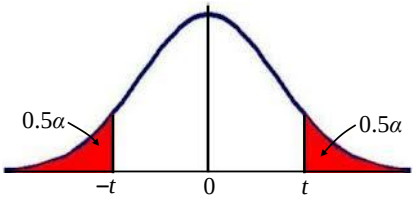			
1	6.314	12.706	63.657	636.619
2	2.920	4.303	9.925	31.598
3	2.353	3.182	5.841	12.941
4	2.132	2.776	4.604	8.610
5	2.015	2.571	4.032	6.859
6	1.943	2.447	3.707	5.959
7	1.895	2.365	3.499	5.405
8	1.860	2.306	3.355	5.041
9	1.833	2.262	3.250	4.781
10	1.812	2.228	3.169	4.587
11	1.796	2.201	3.106	4.437
12	1.782	2.179	3.055	4.318
13	1.771	2.160	3.012	4.221
14	1.761	2.145	2.977	4.140
15	1.753	2.131	2.947	4.073
16	1.746	2.120	2.921	4.015
17	1.740	2.110	2.898	3.965
18	1.734	2.101	2.878	3.922
19	1.729	2.093	2.861	3.883
20	1.725	2.086	2.845	3.850

A.4 *Flexural cracking loads*

Table A.6: Average flexural cracking loads (3-point bending) for the cracked beam specimens

Mix label	Load (kN)				
	Incipient crack	0.4 mm crack		0.7 mm crack	
	20 mm cover	20 mm cover	40 mm cover	20 mm cover	40 mm cover
PC-40	26.0* (1.7)**	28.0 (1.7)	20.3 (2.8)	30.4 (1.5)	24.3 (2.2)
SL-40	28.6 (2.4)	26.7 (1.8)	17.1 (1.2)	31.2 (2.2)	19.9 (1.5)
SL-55	24.1 (1.3)	23.9 (1.4)	15.2 (1.0)	26.4 (1.1)	18.5 (2.0)
FA-40	26.3 (1.3)	28.1 (1.6)	20.2 (2.2)	25.6 (0.5)	16.5 (1.3)
FA-55	21.6 (2.2)	23.9 (1.2)	14.4 (0.5)	23.0 (1.3)	15.2 (0.6)

* Average of 6 readings, ** Standard deviation

Appendix B

Corrosion rate, half-cell potential, resistivity and chloride concentration results

Note:

(i) '*Week zero*' in the figures for results presented here corresponds to the time when the specimens were placed in their respective exposure environments (laboratory or field); the first measurement was taken 14 days after exposure to the respective environments.

(ii) The procedure for calculation of 2-point moving average is presented later in Appendix F.

B.1 *2-point moving average corrosion rate vs. time trends*

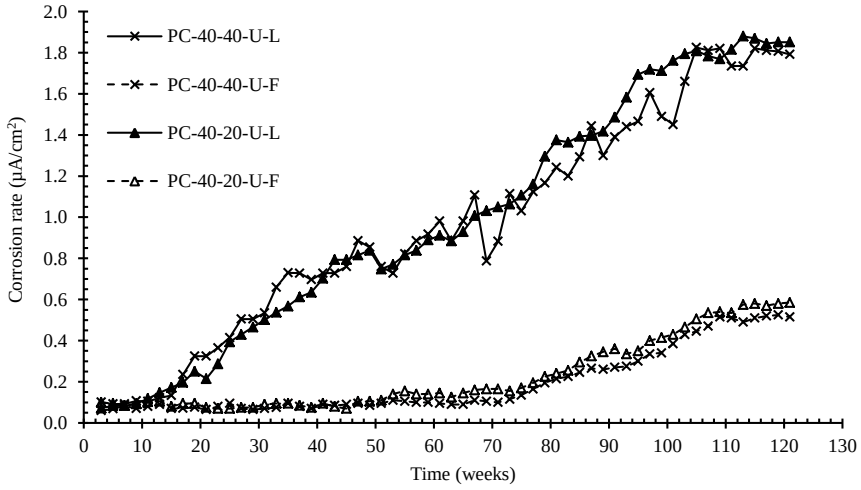

Figure B.1: Moving average i_{corr} for uncracked lab and field PC-40 specimens (20 and 40 mm cover)

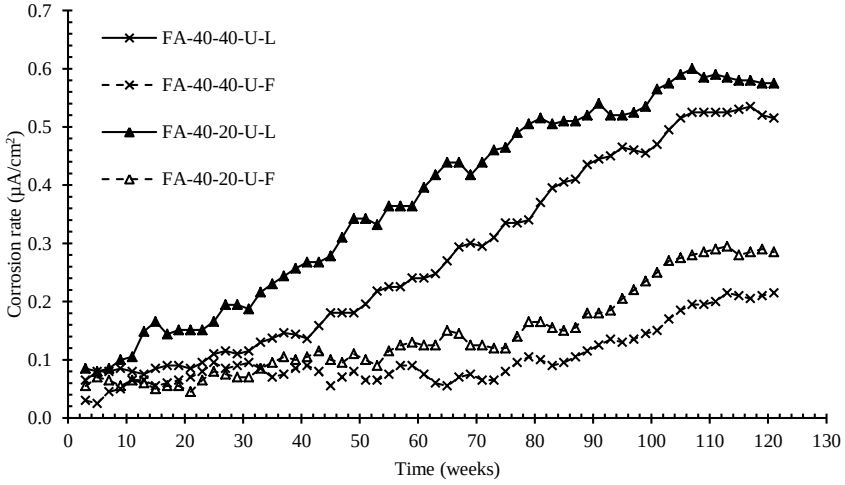

Figure B.2: Moving average i_{corr} for uncracked lab and field FA-40 specimens (20 and 40 mm cover)

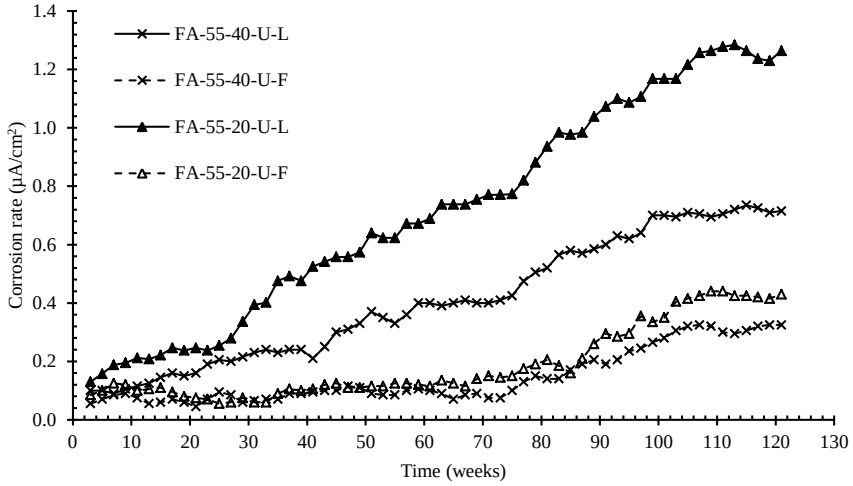

Figure B.3: Moving average i_{corr} for uncracked lab and field FA-55 specimens (20 and 40 mm cover)

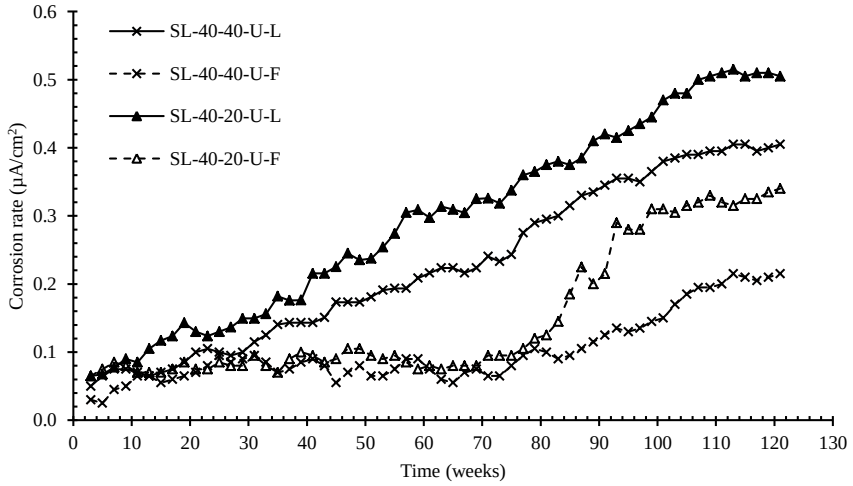

Figure B.4: Moving average i_{corr} for uncracked lab and field SL-40 specimens (20 and 40 mm cover)

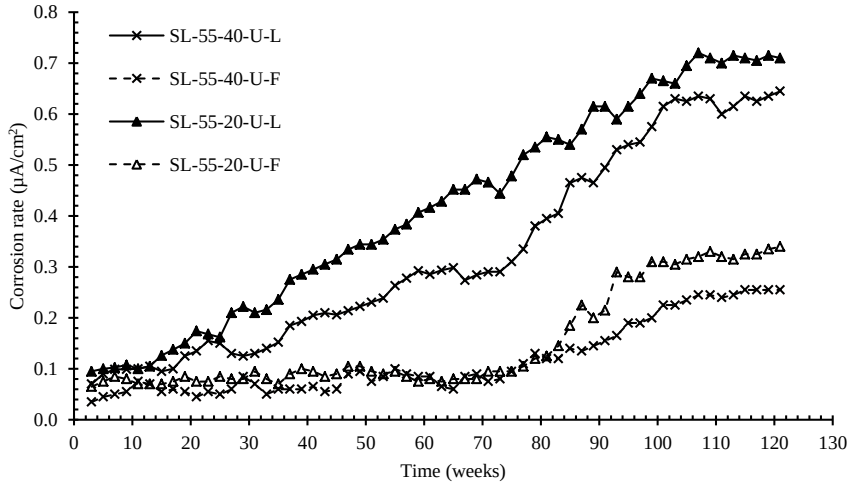

Figure B.5: Moving average i_{corr} for uncracked lab and field SL-55 specimens (20 and 40 mm cover)

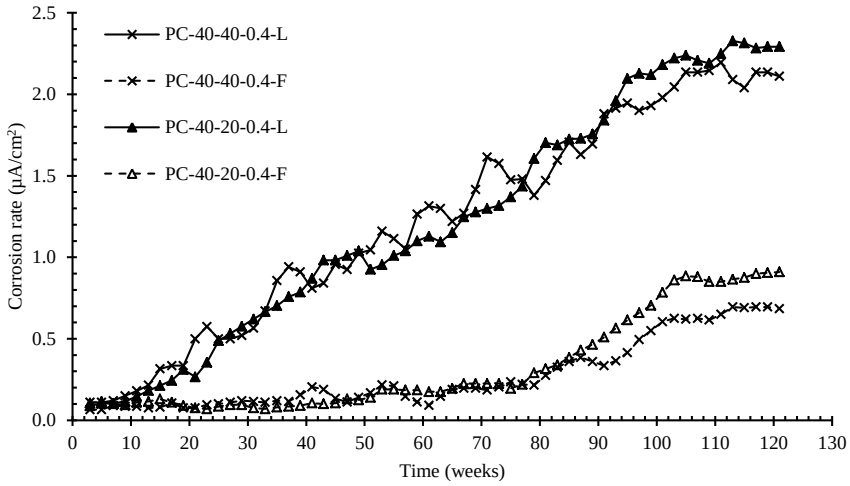

Figure B.6: Moving average i_{corr} for 0.4 mm cracked lab and field PC-40 specimens (20 and 40 mm cover)

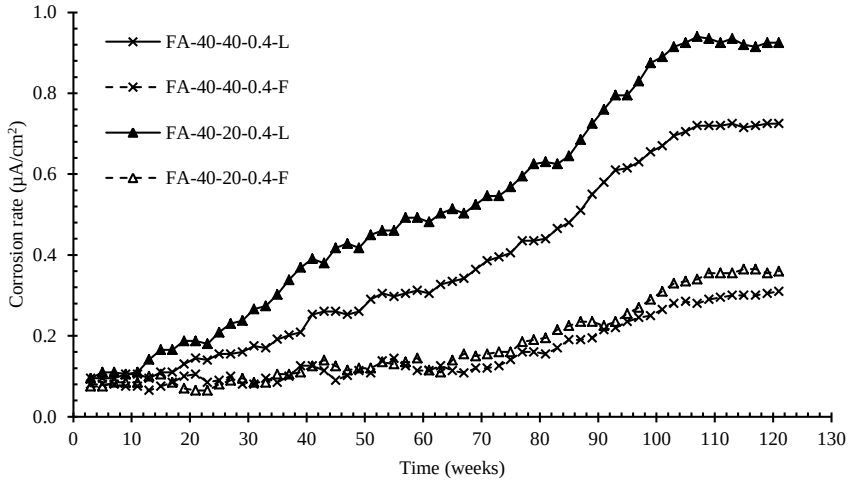

Figure B.7: Moving average i_{corr} for 0.4 mm cracked lab and field FA-40 specimens (20 and 40 mm cover)

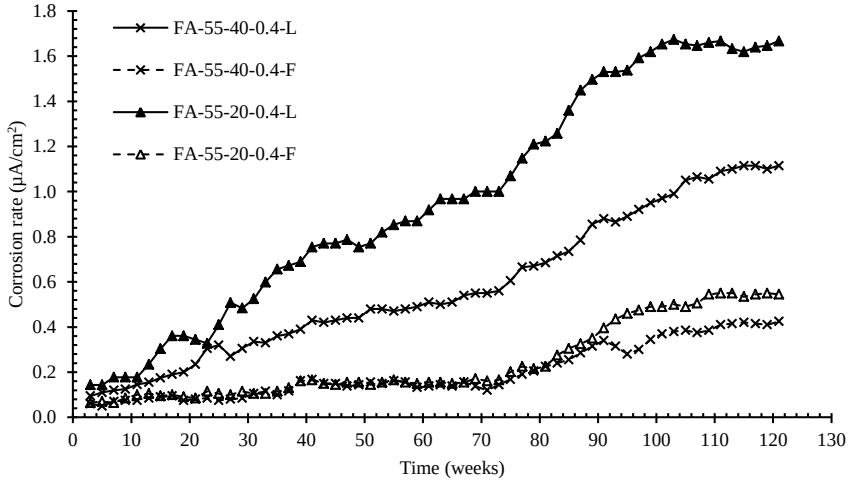

Figure B.8: Moving average i_{corr} for 0.4 mm cracked lab and field FA-55 specimens (20 and 40 mm cover)

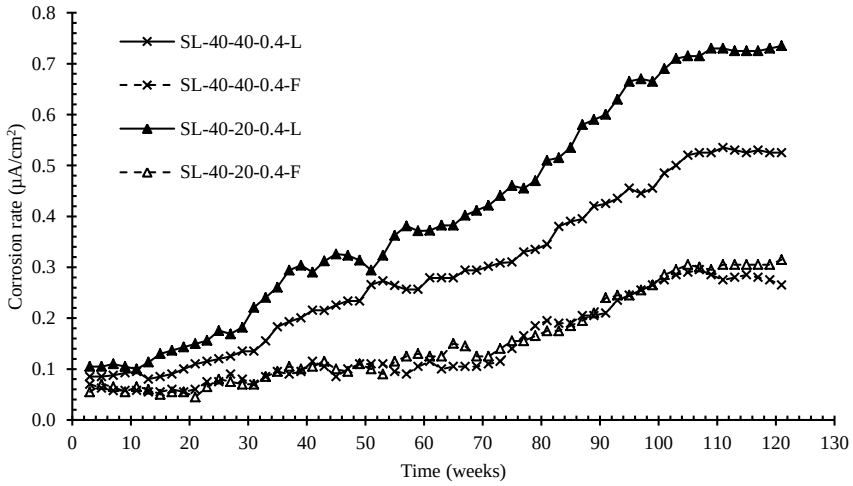

Figure B.9: Moving average i_{corr} for 0.4 mm cracked lab and field SL-40 specimens (20 and 40 mm cover)

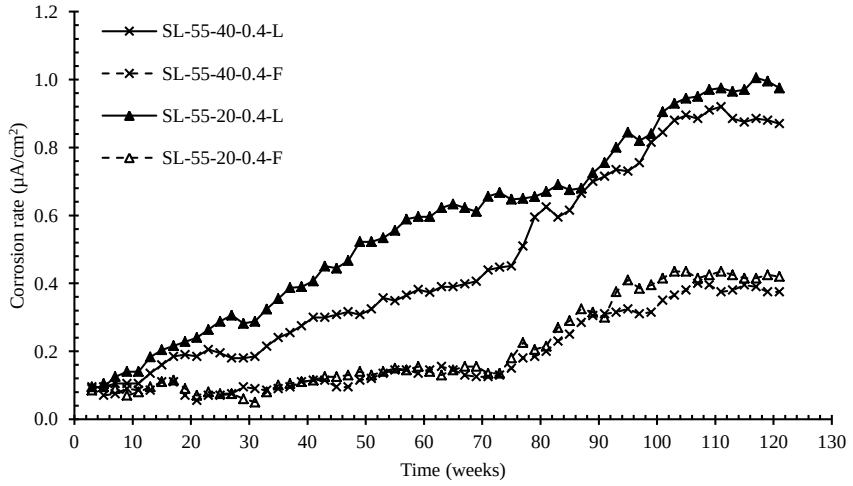

Figure B.10: Moving average i_{corr} for 0.4 mm cracked lab and field SL-55 specimens (20 and 40 mm cover)

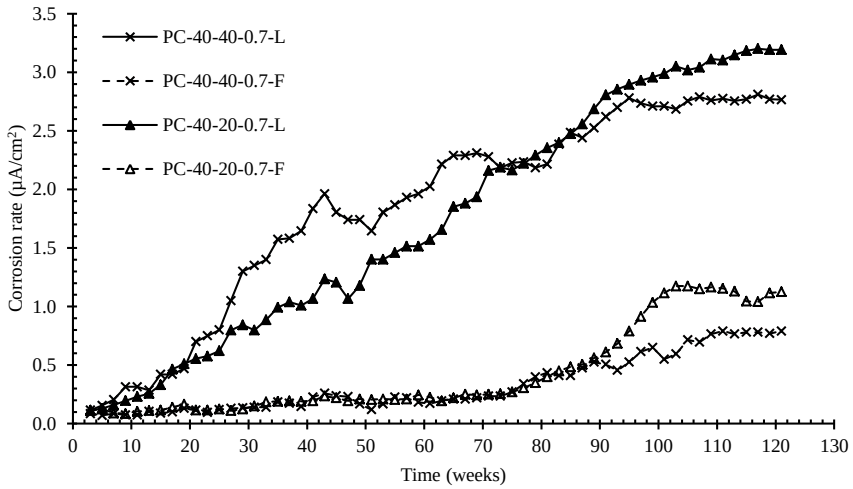

Figure B.11: Moving average i_{corr} for 0.7 mm cracked lab and field PC-40 specimens (20 and 40 mm cover)

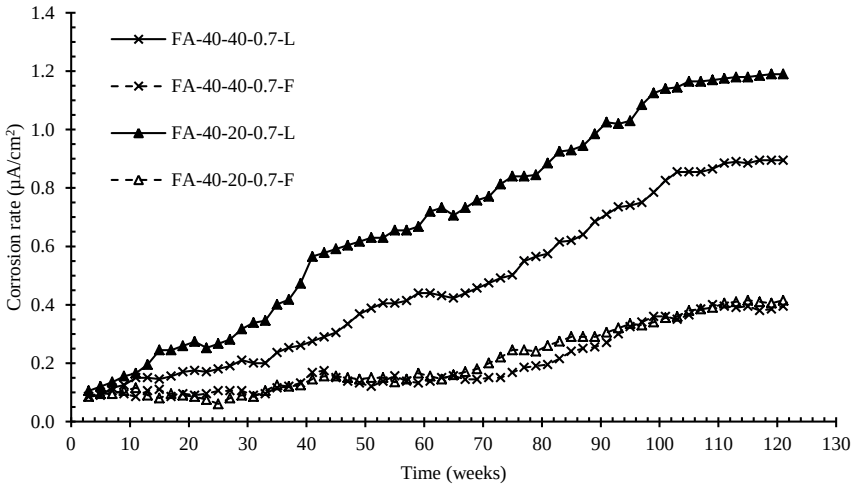

Figure B.12: Moving average i_{corr} for 0.7 mm cracked lab and field FA-40 specimens (20 and 40 mm cover)

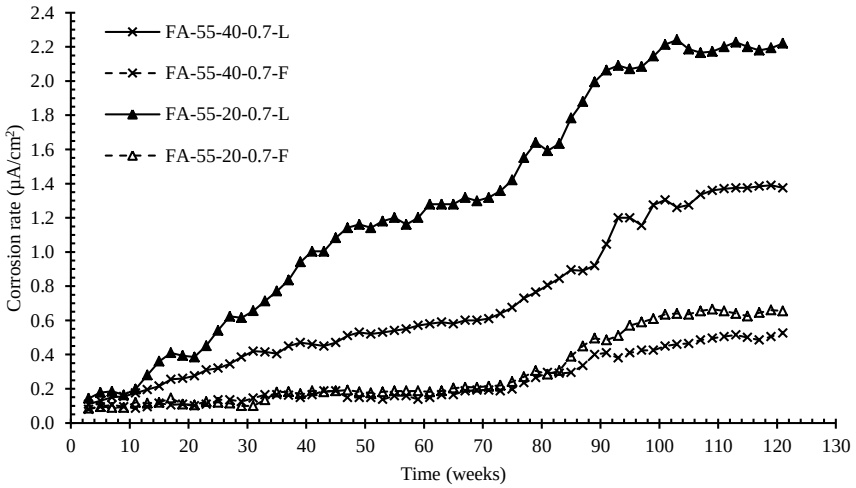

Figure B.13: Moving average i_{corr} for 0.7 mm cracked lab and field FA-55 specimens (20 and 40 mm cover)

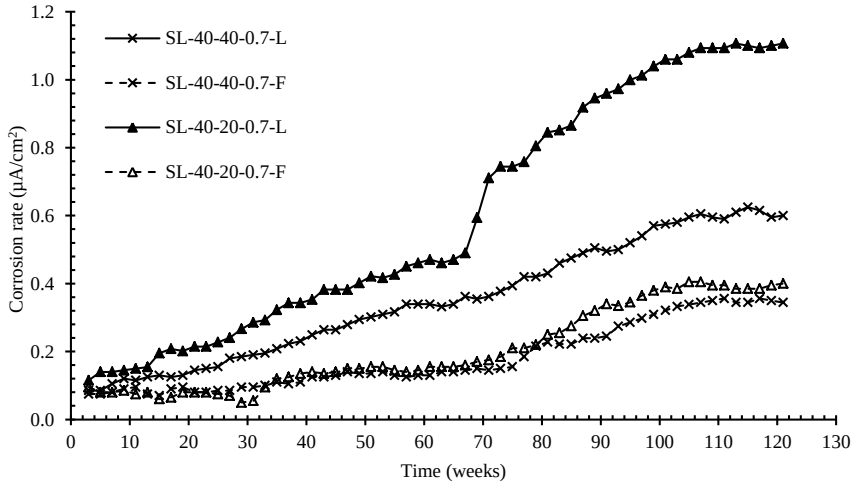

Figure B.14: Moving average i_{corr} for 0.7 mm cracked lab and field SL-40 specimens (20 and 40 mm cover)

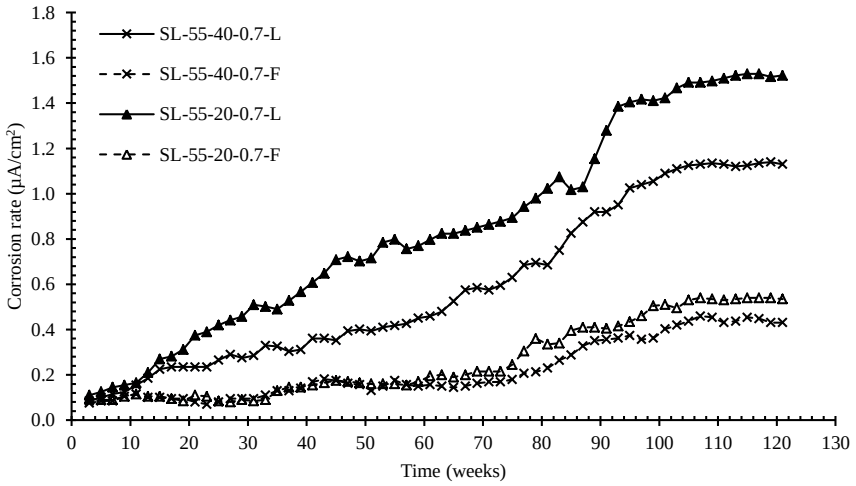

Figure B.15: Moving average i_{corr} for 0.7 mm cracked lab and field SL-55 specimens (20 and 40 mm cover)

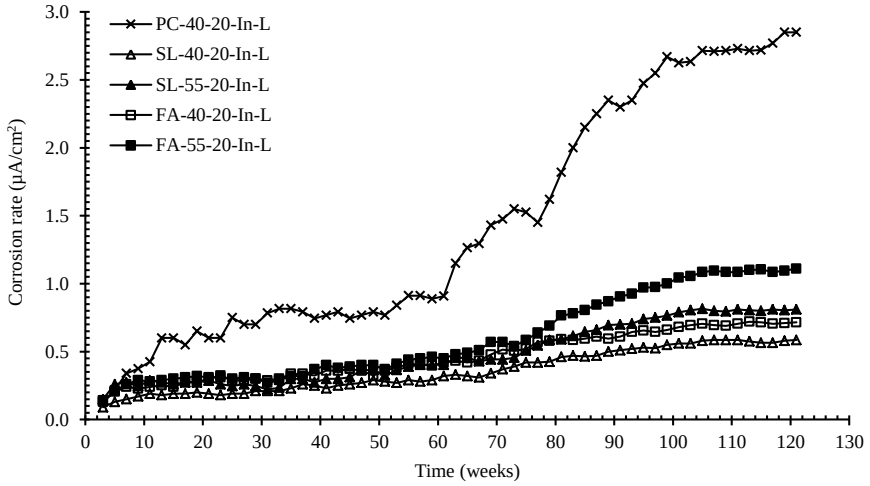

Figure B.16: Moving average i_{corr} for incipient-cracked lab specimens (20 mm cover)

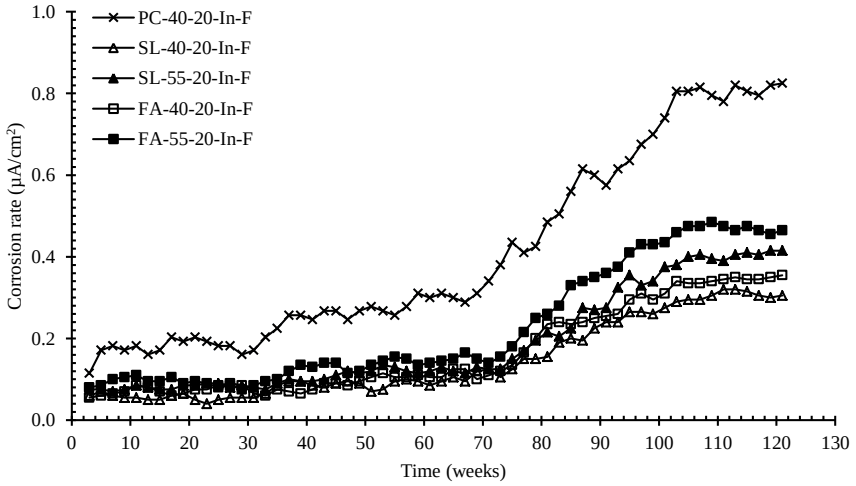

Figure B.17: Moving average i_{corr} for incipient-cracked field specimens (20 mm cover)

B.2 *2-point moving average half-cell potential vs. time trends*

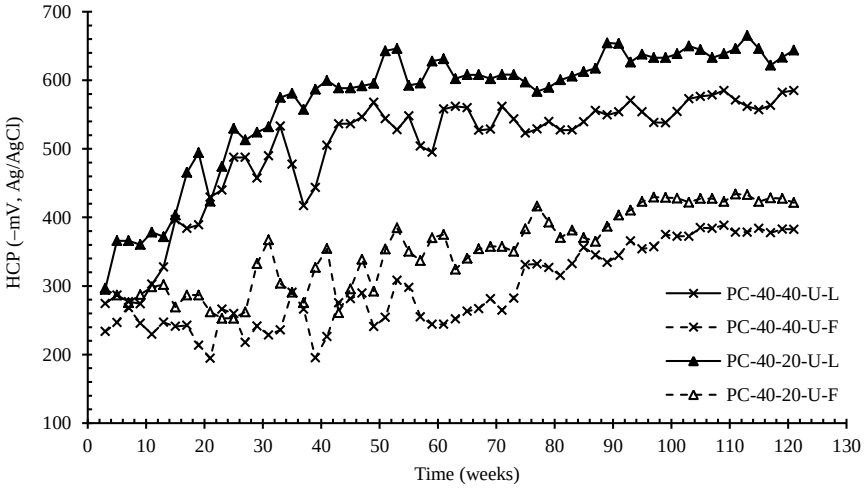

Figure B.18: Moving average HCP for uncracked lab and field PC-40 specimens (20 and 40 mm cover)

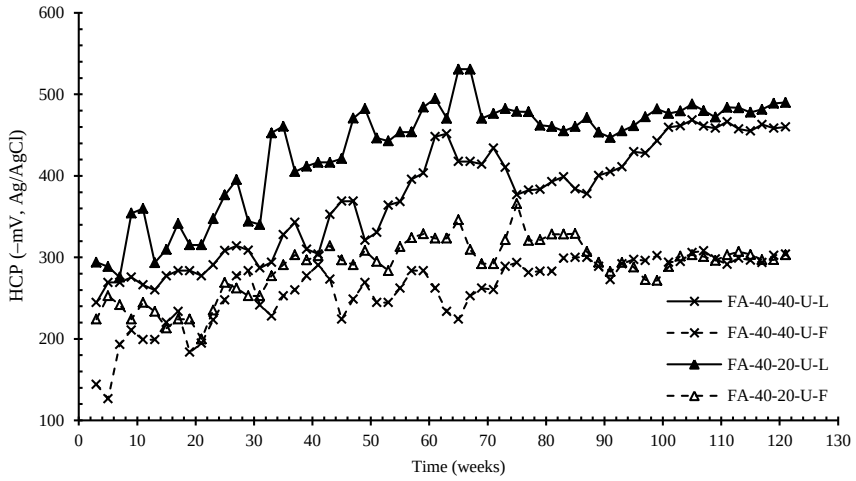

Figure B.19: Moving average HCP for uncracked lab and field FA-40 specimens (20 and 40 mm cover)

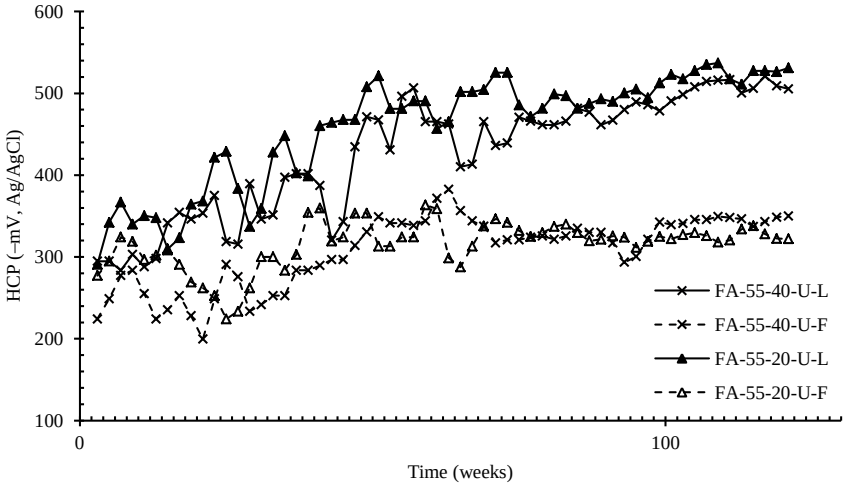

Figure B.20: Moving average HCP for uncracked lab and field FA-55 specimens (20 and 40 mm cover)

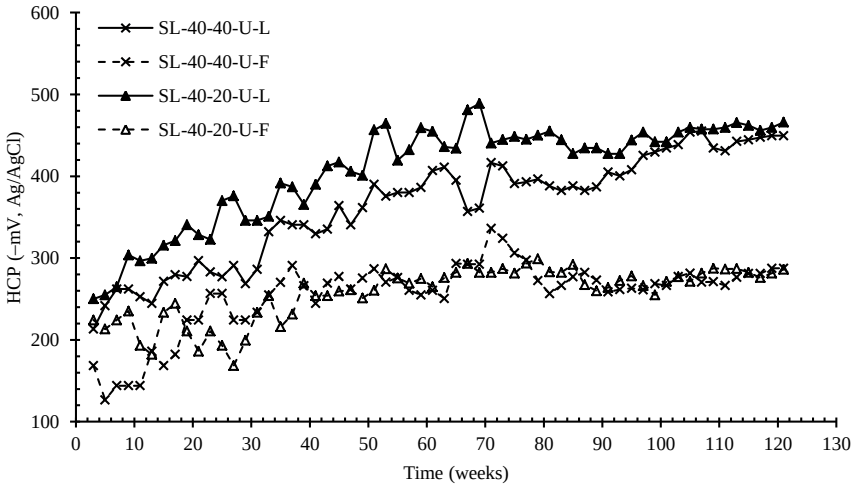

Figure B.21: Moving average HCP for uncracked lab and field SL-40 specimens (20 and 40 mm cover)

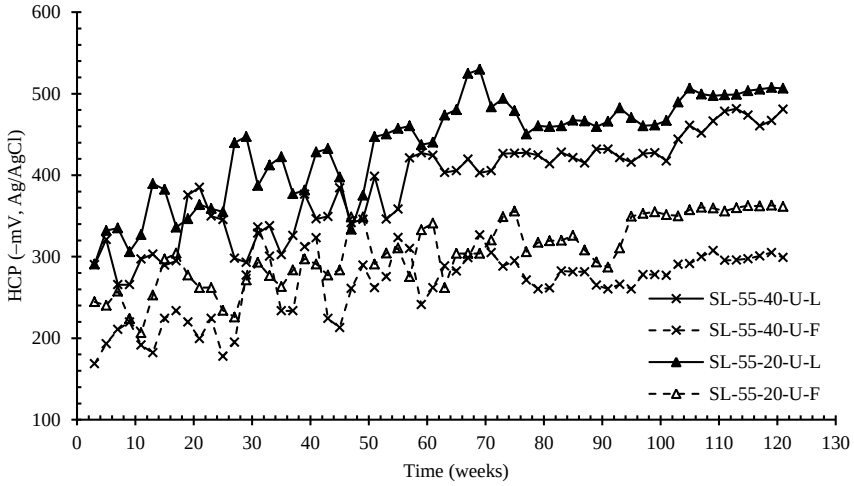

Figure B.22: Moving average HCP for uncracked lab and field SL-55 specimens (20 and 40 mm cover)

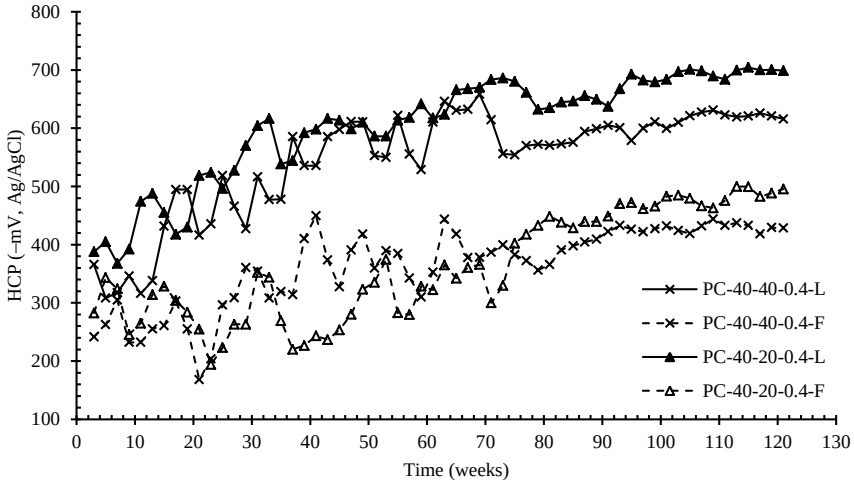

Figure B.23: Moving average HCP for 0.4 mm cracked lab and field PC-40 specimens (20 and 40 mm cover)

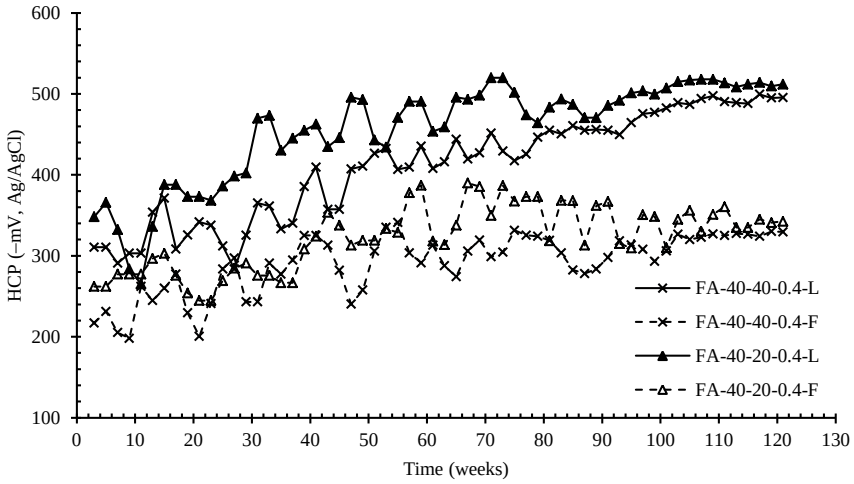

Figure B.24: Moving average HCP for 0.4 mm cracked lab and field FA-40 specimens (20 and 40 mm cover)

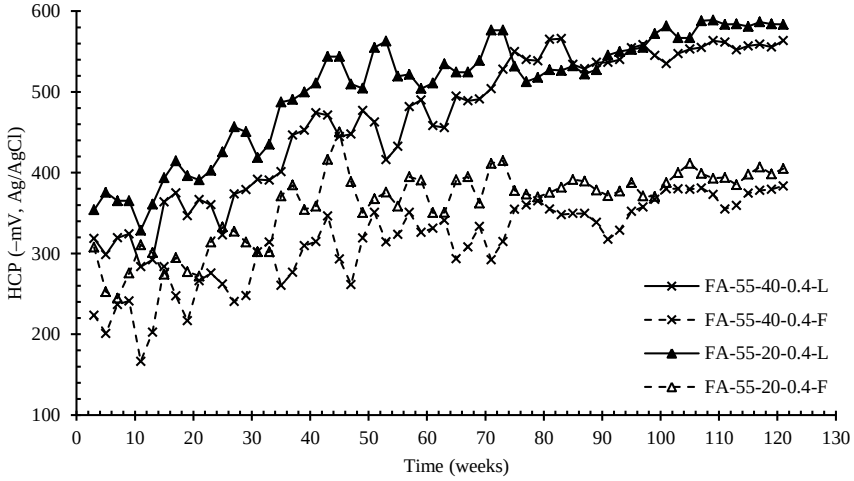

Figure B.25: Moving average HCP for 0.4 mm cracked lab and field FA-55 specimens (20 and 40 mm cover)

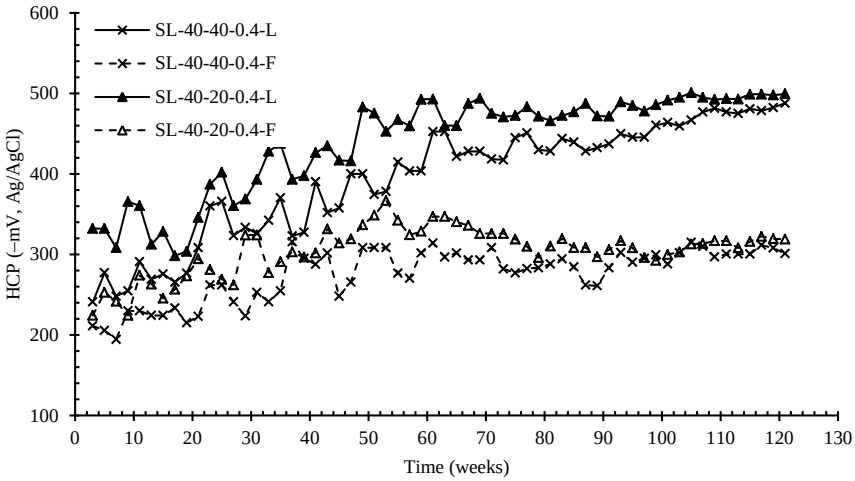

Figure B.26: Moving average HCP for 0.4 mm cracked lab and field SL-40 specimens (20 and 40 mm cover)

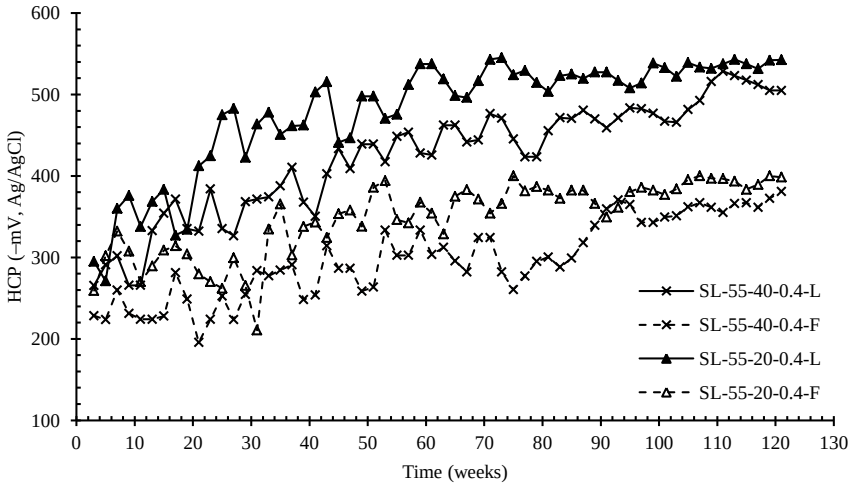

Figure B.27: Moving average HCP for 0.4 mm cracked lab and field SL-55 specimens (20 and 40 mm cover)

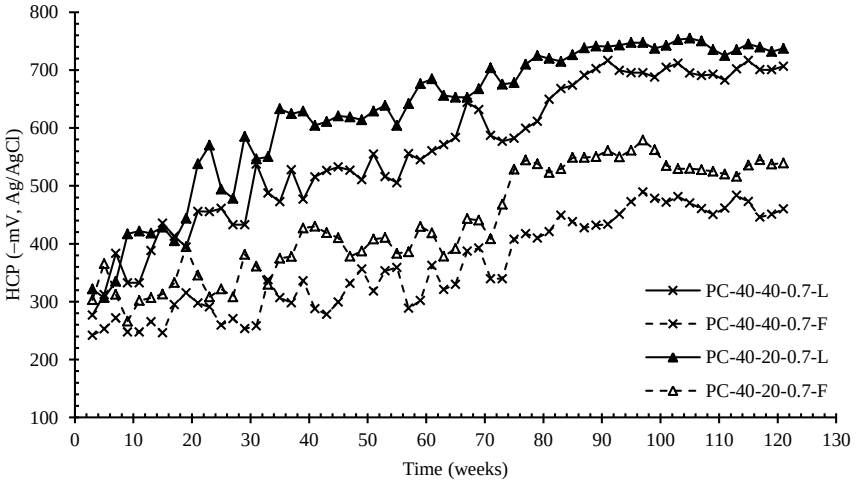

Figure B.28: Moving average HCP for 0.7 mm cracked lab and field PC-40 specimens (20 and 40 mm cover)

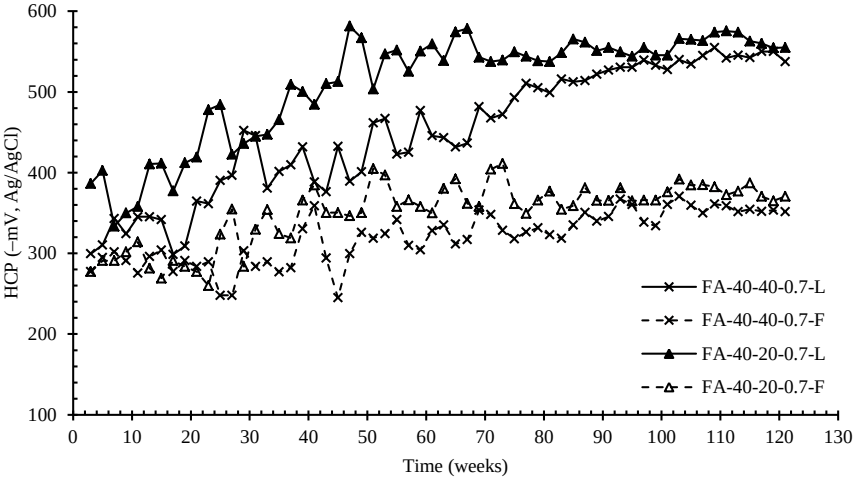

Figure B.29: Moving average HCP for 0.7 mm cracked lab and field FA-40 specimens (20 and 40 mm cover)

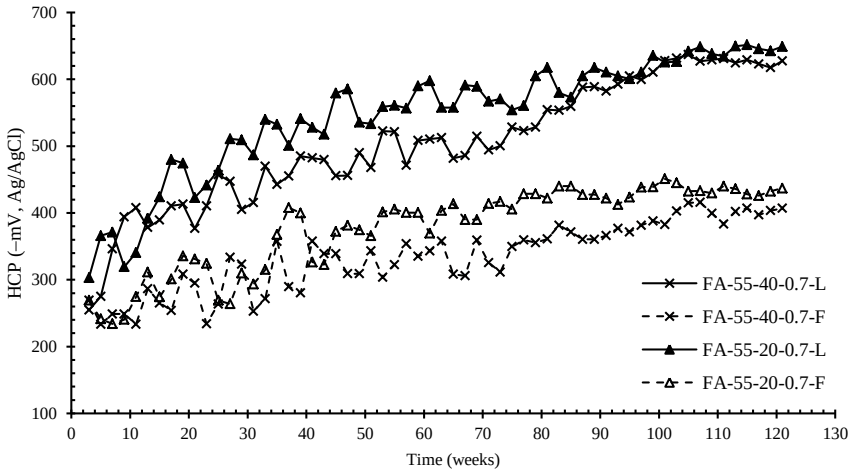

Figure B.30: Moving average HCP for 0.7 mm cracked lab and field FA-55 specimens (20 and 40 mm cover)

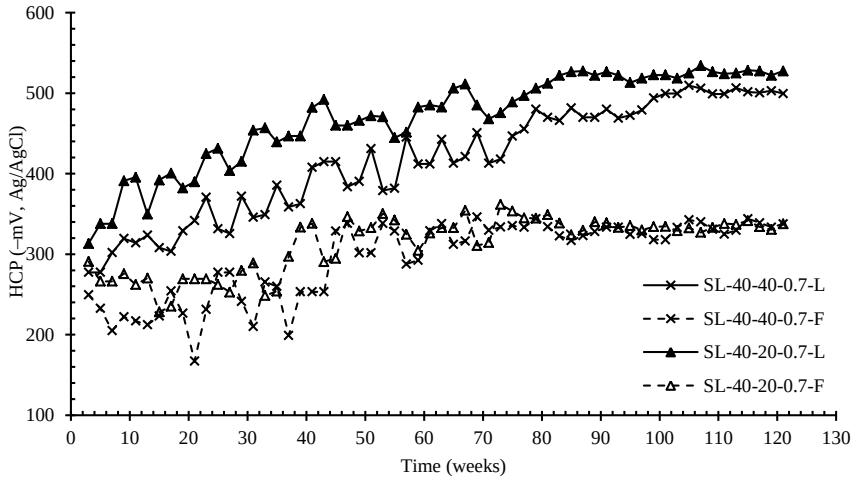

Figure B.31: Moving average HCP for 0.7 mm cracked lab and field SL-40 specimens (20 and 40 mm cover)

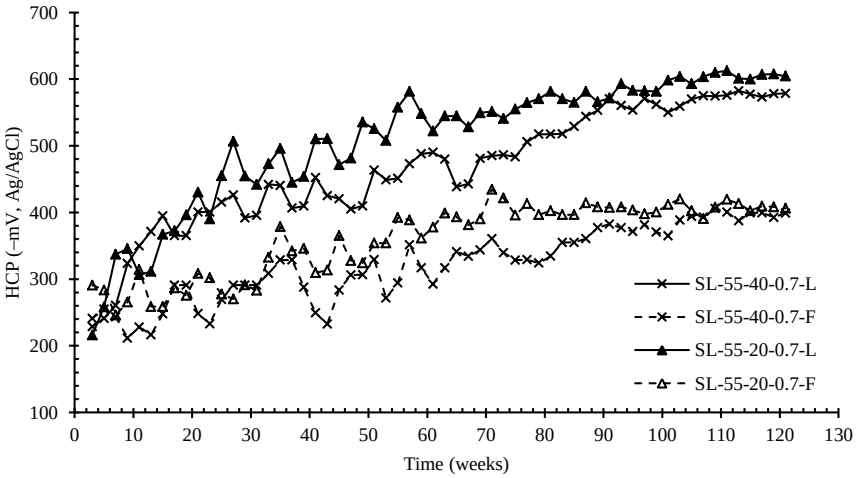

Figure B.32: Moving average HCP for 0.7 mm cracked lab and field SL-55 specimens (20 and 40 mm cover)

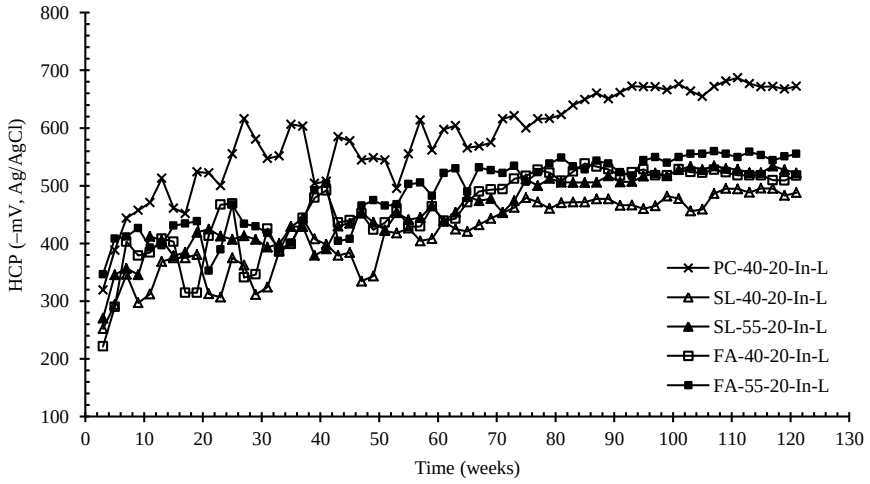

Figure B.33: Moving average HCP for incipient-cracked lab specimens (20 mm cover)

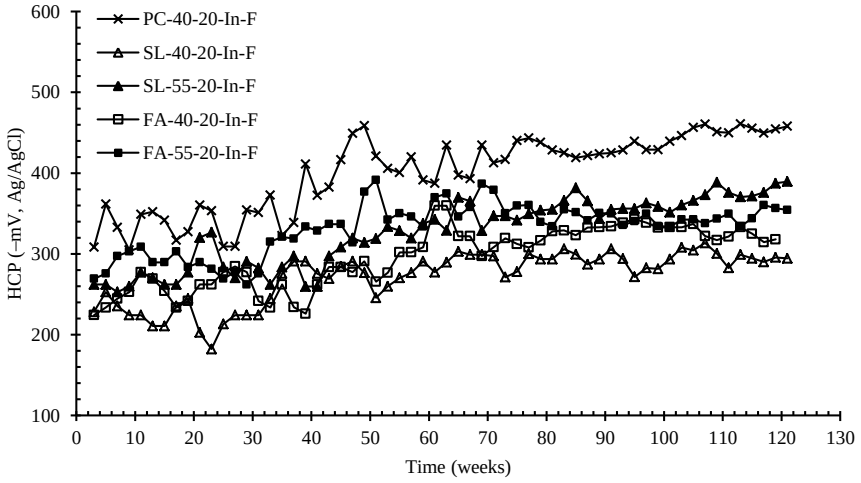

Figure B.34: Moving average HCP for incipient-cracked field specimens (20 mm cover)

B.3 *Average corrosion rate and half-cell potential results*

Table B.1: Average corrosion rates for field and laboratory specimens (week 52-72)

Mix label	Cover (mm)	Average corrosion rates (week 52-72), µA/cm^2							
		Uncracked		Incipient		0.4 mm		0.7 mm	
		Lab	Field	Lab	Field	Lab	Field	Lab	Field
PC-40	20	1.21 (0.08)	0.15 (0.02)	0.91 (0.0.8)	0.31 (0.02)	1.93 (0.31)	0.20 (0.03)	2.40 (0.15)	0.23 (0.03)
	40	0.95 (0.15)	0.13 (0.01)	-	-	1.74 (0.28)	0.17 (0.05)	2.09 (0.16)	0.20 (0.03)
SL-40	20	0.30 (0.02)	0.08 (0.01)	0.32 (0.03)	0.10 (0.01)	0.38 (0.02)	0.12 (0.02)	0.46 (0.02)	0.15 (0.01)
	40	0.21 (0.01)	0.07 (0.01)	-	-	0.28 (0.28)	0.12 (0.01)	0.34 (0.02)	0.14 (0.01)
SL-55	20	0.42 (0.03)	0.12 (0.01)	0.41 (0.03)	0.12 (0.01)	0.60 (0.03)	0.14 (0.02)	0.65 (0.03)	0.19 (0.02)
	40	0.28 (0.02)	0.09 (0.01)	-	-	0.39 (0.03)	0.14 (0.01)	0.45 (0.02)	0.15 (0.01)
FA-40	20	0.40 (0.04)	0.10 (0.02)	0.42 (0.03)	0.11 (0.02)	0.50 (0.03)	0.14 (0.02)	0.70 (0.05)	0.16 (0.01)
	40	0.25 (0.02)	0.08 (0.02)	-	-	0.32 (0.02)	0.12 (0.01)	0.43 (0.03)	0.14 (0.01)
FA-55	20	0.51 (0.03)	0.13 (0.02)	0.49 (0.04)	0.15 (0.01)	0.67 (0.04)	0.16 (0.01)	0.92 (0.05)	0.19 (0.02)
	40	0.39 (0.02)	0.10 (0.02)	-	-	0.51 (0.03)	0.14 (0..02)	0.57 (0.03)	0.16 (0.03)

( ) Standard deviation

Table B.2: Average corrosion rates for field and laboratory specimens (week 104-120)

Mix label	Cover (mm)	Average corrosion rate (week 104-120), µA/cm^2							
		Uncracked		Incipient		0.4 mm		0.7 mm	
		Lab	Field	Lab	Field	Lab	Field	Lab	Field
PC-40	20	1.83 (0.05)*	0.55 (0.04)	2.75 (0.06)	0.81 (0.03)	2.26 (0.06)	0.88 (0.02)	3.13 (0.08)	1.12 (0.07)
	40	1.80 (0.01)	0.50 (0.04)	– –	– –	2.13 (0.02)	0.66 (0.04)	2.77 (0.04)	0.76 (0.04)
SL-40	20	0.50 (0.02)	0.28 (0.01)	0.58 (0.01)	0.31 (0.01)	0.72 (0.01)	0.30 (0.01)	1.09 (0.01)	0.39 (0.01)
	40	0.40 (0.01)	0.19 (0.01)	– –	– –	0.53 (0.01)	0.28 (0.01)	0.60 (0.02)	0.35 (0.01)
SL-55	20	0.71 (0.02)	0.32 (0.01)	0.81 (0.01)	0.40 (0.01)	0.97 (0.03)	0.43 (0.01)	1.51 (0.02)	0.53 (0.01)
	40	0.63 (0.02)	0.25 (0.01)	– –	– –	0.89 (0.02)	0.38 (0.01)	1.13 (0.01)	0.44 (0.02)
FA-40	20	0.58 (0.01)	0.29 (0.02)	0.71 (0.01)	0.34 (0.01)	0.93 (0.01)	0.35 (0.01)	1.18 (0.01)	0.40 (0.02)
	40	0.52 (0.01)	0.20 (0.01)	– –	– –	0.72 (0.01)	0.29 (0.01)	0.88 (0.02)	0.39 (0.02)
FA-55	20	1.25 (0.03)	0.42 (0.01)	1.09 (0.02)	0.47 (0.02)	1.65 (0.02)	0.53 (0.03)	2.19 (0.03)	0.65 (0.02)
	40	0.71 (0.02)	0.50 (0.04)	– –	– –	1.08 (0.04)	0.40 (0.02)	1.35 (0.05)	0.49 (0.02)

*( ) Standard deviation

Table B.3: Average half-cell potentials for field and laboratory specimens (week 104-120)

Mix label	Cover (mm)	Average half-cell potential (week 104-120), –mV, Ag/AgCl							
		Uncracked		Incipient		0.4 mm		0.7 mm	
		Lab	Field	Lab	Field	Lab	Field	Lab	Field
PC-40	20	643 (19)*	427 (8)	672 (17)	456 (10)	698 (9)	482 (18)	739 (13)	531 (14)
	40	573 (14)	382 (15)	–	–	623 (7)	430 (14)	699 (16)	463 (17)
SL-40	20	502 (9)	281 (8)	484 (20)	297 (15)	497 (5)	315 (9)	526 (7)	334 (7)
	40	445 (11)	279 (12)	–	–	477 (10)	306 (10)	503 (7)	336 (10)
SL-55	20	502 (9)	360 (4)	528 (9)	377 (12)	537 (11)	394 (8)	604 (10)	407 (14)
	40	469 (13)	299 (10)	–	–	477 (10)	364 (9)	575 (6)	397 (11)
FA-40	20	483 (9)	301 (7)	518 (8)	324 (14)	514 (7)	346 (19)	514 (7)	378 (11)
	40	461 (8)	300 (8)	–	–	492 (10)	325 (6)	545 (14)	355 (11)
FA-55	20	526 (12)	327 (8)	553 (8)	346 (13)	581 (12)	399 (12)	644 (10)	432 (9)
	40	510 (12)	346 (9)	–	–	558 (10)	373 (12)	628 (9)	404 (15)

*( ) Standard deviation

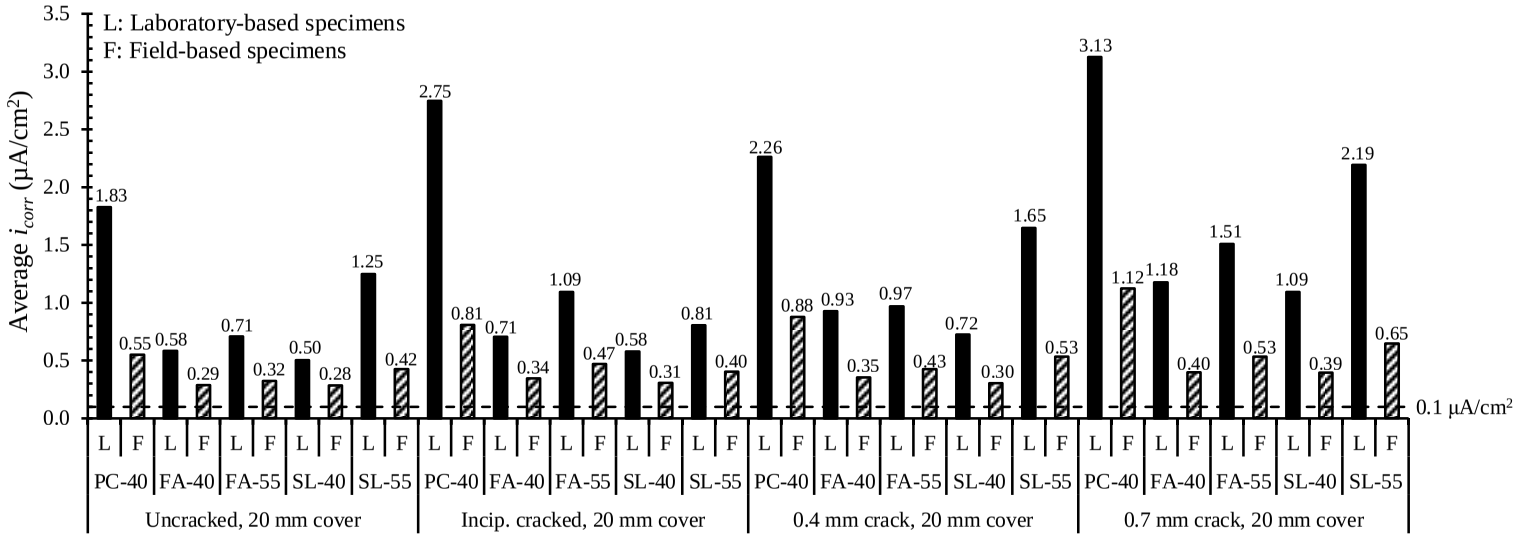

Figure B.35: Average corrosion rates (week 104-120) for lab and field specimens with 20 mm cover

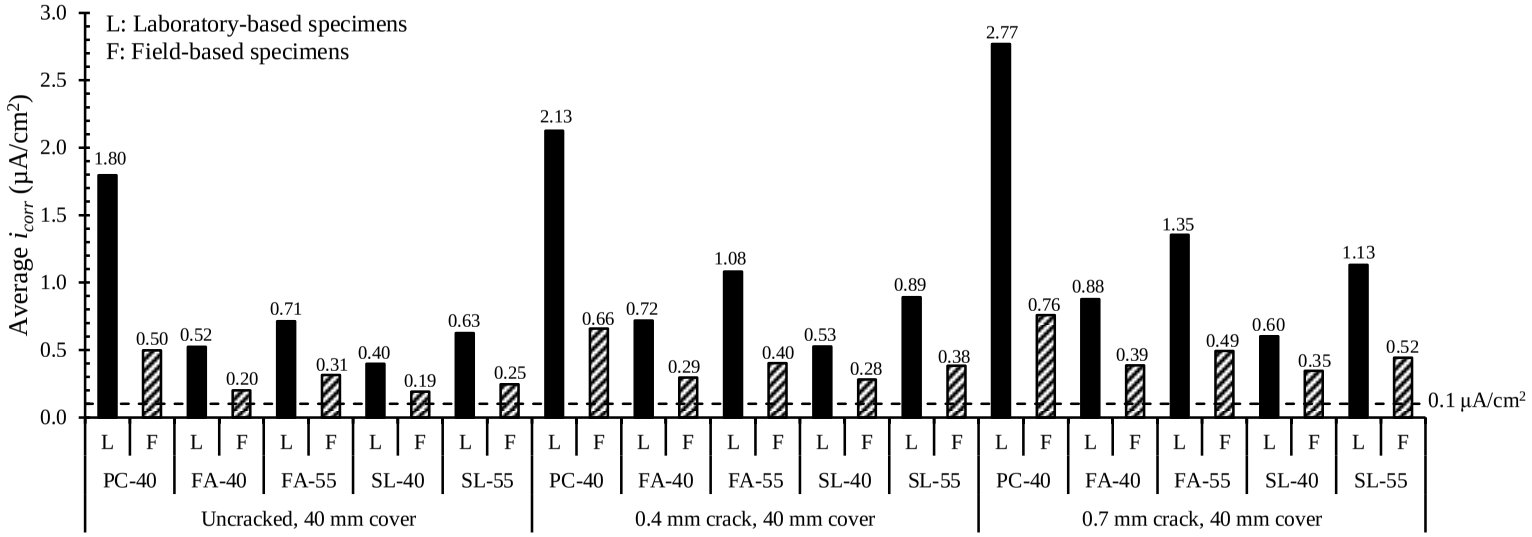

Figure B.36: Average corrosion rates (week 104-120) for lab and field specimens with 40 mm cover

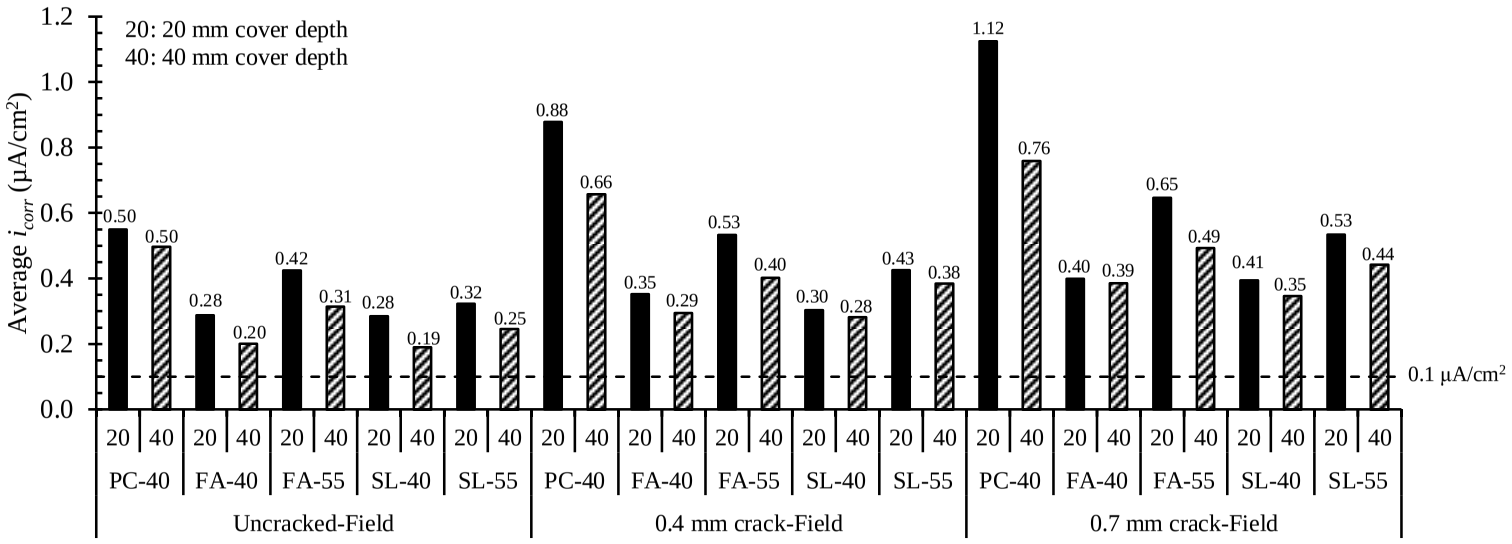

Figure B.37: Average corrosion rates (week 104-120) for field specimens with 20 and 40 mm cover

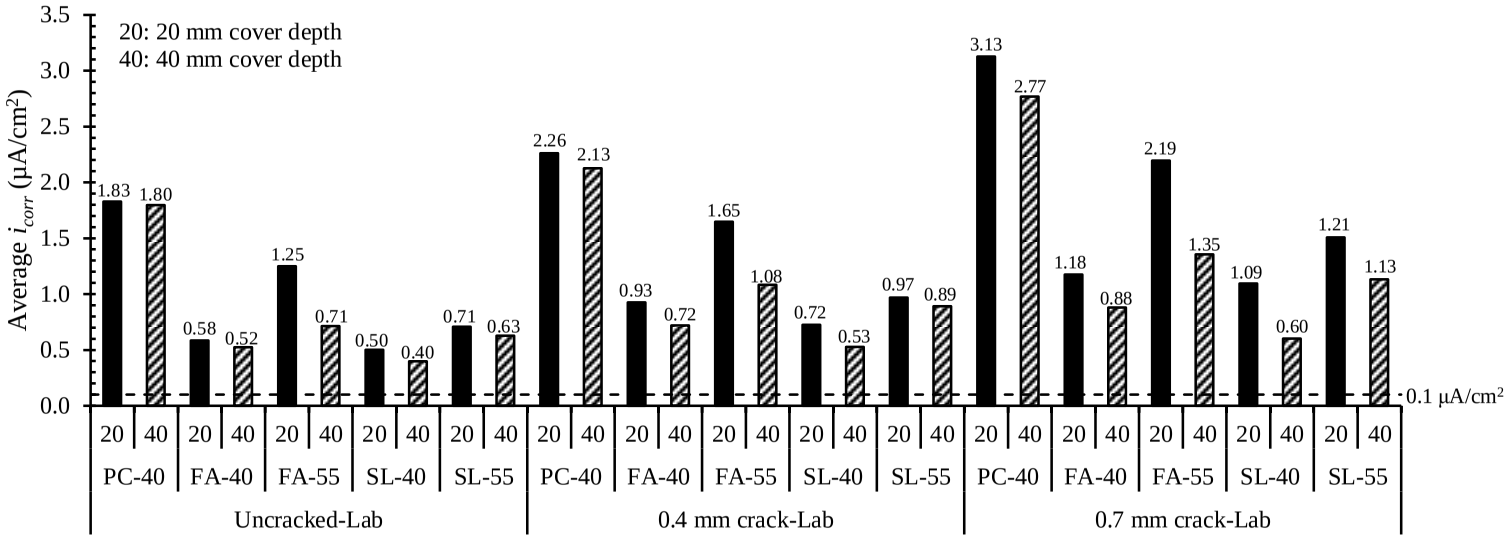

Figure B.38: Average corrosion rates (week 104-120) for lab specimens with 20 and 40 mm cover

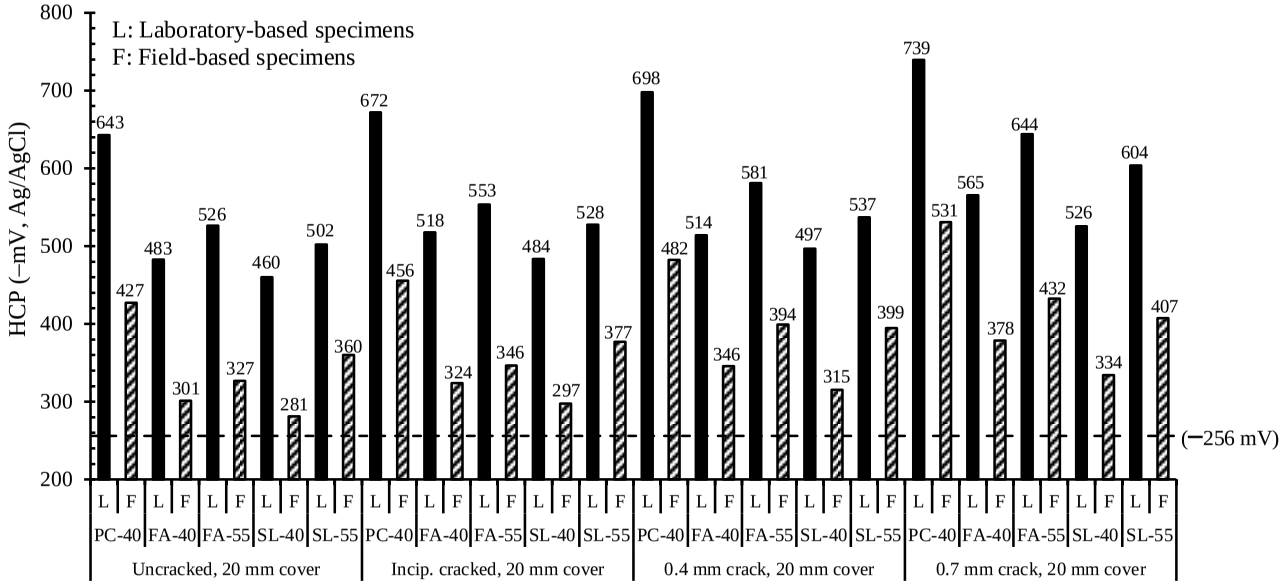

Figure B.39: Average half-cell potentials for lab and field specimens with 20 mm cover

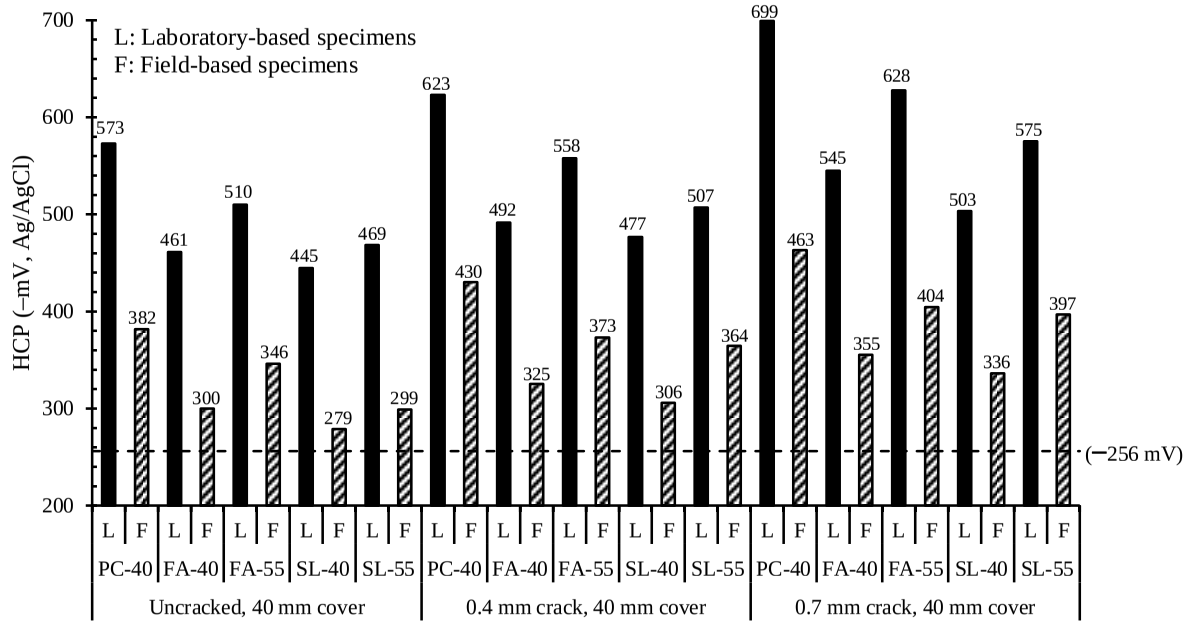

Figure B.40: Average half-cell potentials for lab and field specimens with 40 mm cover

B.4 *Chloride concentration measurement results*

Table B.4: Chloride content at steel level after 73 weeks exposure (% by mass of binder)

Concrete mix label	Cover depth (mm)	Core sampling location (distance from crack, mm)*	Total chloride concentration at steel level (% mass of binder) after 73 weeks							
			Uncracked*		Incipient cracked		0.4 mm cracked		0.7 mm cracked	
			Lab	Field	Lab	Field	Lab	Field	Lab	Field
PC-40	20	30	1.21	0.87	2.15	1.56	3.35	2.23	3.15	2.34
		90			1.73	1.03	2.14	1.54	2.23	2.00
	40	30	1.01	0.73	–	–	3.03	2.13	2.89	2.24
		90			–	–	1.24	1.03	1.50	1.23
SL-40	20	30	0.68	0.54	1.69	0.64	2.13	1.21	2.21	1.25
		90			1.21	0.79	1.76	0.93	1.84	1.03
	40	30	0.62	0.61	–	–	1.94	0.98	2.03	0.92
		90			–	–	1.21	0.78	1.31	0.83
SL-55	20	30	1.01	0.68	1.87	0.73	2.56	1.87	2.61	1.68
		90			1.51	0.84	2.01	1.21	2.21	1.25
	40	30	0.93	0.61	–	–	2.45	1.65	2.51	1.78
		90			–	–	1.93	1.51	2.01	1.59
FA-40	20	30	0.74	0.51	1.74	0.71	2.54	1.72	2.51	1.67
		90			1.42	0.79	1.94	1.14	1.99	1.32
	40	30	0.89	0.61	–	–	2.23	1.45	2.32	1.56
		90			–	–	1.54	1.03	1.67	1.11
FA-55	20	30	1.11	0.78	1.95	1.03	2.67	2.01	2.58	1.86
		90			1.56	0.94	2.16	1.93	2.11	1.97
	40	30	1.03	0.72	–	–	2.56	1.78	2.48	1.83
		90			–	–	2.01	1.49	2.12	1.52

*In the uncracked specimens, cores were taken at the longitudinal centre

B.5 *Average resistivity results*

Table B.5: Average resistivity (kΩ-cm) results and the corresponding statistics (week 104-120)

		PC-40		SL-40		SL-55		FA-40		FA-55	
		Lab	Field	Lab	Field	Lab	Field	Lab	Field	Lab	Field
Average		33	44	86	112	69	95	99	135	49	88
Standard deviation (σ)		1.1	1.6	1.6	2.0	1.2	1.8	1.5	2.4	1.4	1.2
Coefficient of variation (%)		3.5	3.6	1.9	1.8	1.8	1.9	1.5	1.8	2.8	1.3
σt		2.2	3.1	3.2	3.9	2.4	3.6	2.8	4.8	2.7	2.3
Range	Min.	30	41	83	108	67	91	96	130	46	86
	Max.	35	47	89	116	72	98	102	140	52	90

Range = Average ± σt where t = 1.96 for 95% confidence level

Appendix C

Temperature and relative humidity trends in the marine exposure region

C.1 *Typical average monthly temperature and relative humidity trends during study period*

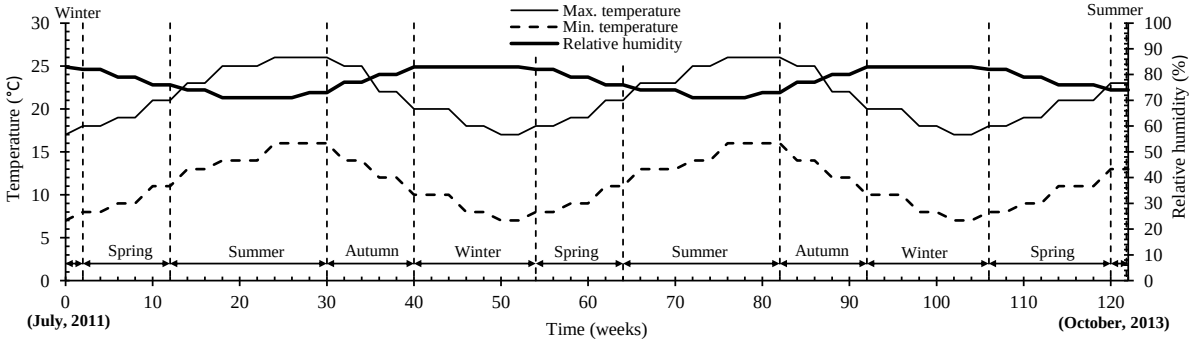

Figure C.1: Typical seasonal changes (temperature and RH) during the study period [1]

C.2 *Reference*

[1] Weather_SA (2013) http:// www.weathersa.co.za, accessed on 10th October, 2013.

Appendix D

Chloride conductivity index test

The chloride conductivity is used as an index to characterize the intrinsic potential of a given concrete to resist chloride penetration [1-3]. It is important to mention that the test was developed using, and is performed on uncracked concrete specimens.

D.1 *Test procedure*

The test involves measuring the ionic flux (current) across a concrete disc specimen (70 ± 2 mm diameter and 30 ± 2 mm thickness) due to a 10 V potential difference as shown in Figure D.1. The 10 V potential difference was obtained using a commercial power supply (CIC® PS1830) with output ranges of 0 ~ 30 V and 0 ~ 5A for, respectively, voltage and current. The voltage and current were measured using commercial digital multimeters (Brymen® TBM805) with measurement ranges of 0 ~ 10A and 0 ~ 600V. The specimens are pre-conditioned before testing by placing in an oven at 50 ± 2 °C for 7 days ± 4 hours (to ensure uniform moisture content) followed by vacuum saturation (-75 to -80 kPa) in a 5M NaCl solution for 1 hour ± 15 min after which it is allowed to soak in the salt solution for a further 18 hours ± 15 min before testing. The selection of this set of pre-conditioning conditions was based on an extensive experimental study using different concretes [1].

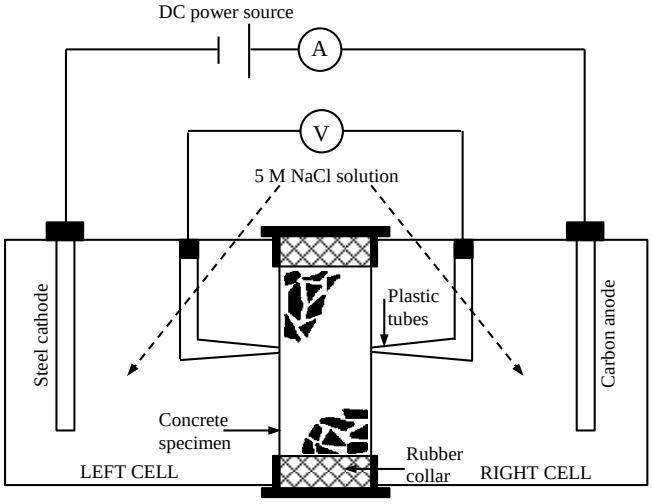

Figure D.1: Schematic of chloride conductivity test [2]

The test allows for a very rapid determination of the chloride conductivity value defined as follows [2]:

$$\sigma = \frac{it}{VA} \tag{D.1}$$

where σ is the conductivity of the specimen (mS/cm), *i* is the electric current (mA), V is the voltage difference (Volts), *t* is the average thickness of specimen (cm) and A is the cross-sectional area of the

specimen (cm^2). The chloride conductivity is fundamentally related to steady state diffusivity (D_s) by the Nernst–Einstein equation which relates the conductivity of a bulk material to the diffusion coefficient as follows [4]:

$$Q = \frac{D_s}{D_o} = \frac{\sigma}{\sigma_o} \tag{D.2}$$

where Q is the diffusivity ratio, σ is the conductivity of concrete (S/m), σ_o is the conductivity of the pore solution (S/m), D_s is the steady state diffusivity of chloride ions through concrete (m^2/s) and D_o is the diffusivity of chloride ions in the equivalent pore solution (m^2/s).

D.2 *Empirical relationship between chloride conductivity and diffusion coefficient*

The empirical relationship between CCI and apparent diffusion coefficient is based on experiments by Mackechnie and Alexander [5] in which the objective was to establish a correlation between long-term (time-dependent) apparent chloride diffusion coefficient and the CCI. They used an approach to establish:

(i) Laboratory-based experimental correlations between CCI values and apparent chloride diffusion coefficients. The specimens used covered a range of binder types, w/b ratios and curing regimes.

(ii) Correlation between the CCI values and chloride ingress in in-service RC structures in the Western Cape Province of South Africa.

From the correlations, they developed empirical relationships between the CCI value and short-term apparent diffusion coefficient (D_i) for commonly used binder types (100% CEM I 42.5N (PC), 50/50 PC/GGBS and 70/30 PC/FA) and marine exposure environments in South Africa. The classification of marine exposure environment in the empirical model is as follows:

(i) Extreme: marine tidal and splash zone; structure exposed to wave action

(ii) Very severe: marine tidal and splash zone; structure exposed to little wave action

(iii) Severe: marine spray zone

Option (ii), 'very severe' exposure, was selected for this study as it closely described the marine exposure conditions for the field-based specimens. In the case of this study, the empirical relationships between CCI and the D_i corresponding to the age of concrete used to determine CCI for 100% CEM I 42.5N (PC), 50/50 PC/GGBS and 70/30 PC/FA concretes exposed to 'very severe' marine conditions are expressed as follows:

For CEM I 42.5N (PC) concrete: $$D_i = \left(6.5803\times10^{-7}\right)e^{1.0999CCI}\ \text{cm}^2/\text{s} \tag{D.3}$$

For 50/50 PC/GGBS concrete: $$D_i = \left(1.1072\times10^{-3}\right)e^{0.8999CCI}\ \text{cm}^2/\text{s} \tag{D.4}$$

For 70/30 PC/FA concrete: $$D_i = \left(1.3689\times10^{-3}\right)e^{0.9499CCI}\ \text{cm}^2/\text{s} \tag{D.5}$$

To account for the time-dependent reduction in the diffusion coefficient due to effects such as continued chloride binding and cementitious reactions, particularly for FA and GGBS blended concretes, the short-term diffusion coefficient is then forecast into a long-term apparent diffusion

coefficient (D_{age}), taking into account the marine exposure environment. The empirical relationship between the short-term apparent diffusion coefficient (D_i) and the long-term one (D_{age}) is expressed as follows:

$$D_{age} = \frac{D_i}{\left(t_{age}\right)^{\alpha}} \tag{D.6}$$

where D_i is the apparent diffusion coefficient corresponding to the age of concrete used to determine CCI, D_{age} is the apparent diffusion coefficient at a given age t_{age} and α is a binder-dependent diffusion coefficient reduction factor (α = 0.29 for PC concrete and 0.68 for 70/30 PC/FA and 50/50 PC/GGBS concrete). Taking into account that this study focused on the corrosion propagation phase, a 50-year ageing/exposure period (t_{age}), a commonly used (corrosion initiation) service life for most RC structures [6] was used in the empirical model.

D.3 ***References***

[1] Streicher, P. E. (1997) The development of a rapid chloride test for concrete and its use in engineering practice. *PhD Thesis***,** Department of Civil Engineering, University of Cape Town.

[2] Streicher, P. E. & Alexander, M. G. (1995) A chloride conduction test for concrete. *Cement and Concrete Research,* Vol. 25(6)**,** pp. 1284–1294.

[3] Alexander, M. G., Ballim, Y. & Mackechnie, J. R. (2009) Durability Index Testing Procedure Manual (Ver 1.0, 25 Feb 2009) - Revised Research Monograph No. 4 (1999), Department of civil engineering, University of Cape Town. *Concrete Materials and Structural Integrity Research Unit - University of Cape Town***,** 30 pp.

[4] Garboczi, E. J. & Bentz, D. P. Computer simulation of the diffusivity of cement-based materials. *Journal of Materials Science,* Vol. 27(8)**,** pp. 2083-2092.

[5] Mackechnie, J. & Alexander, M. G. (1996) Marine exposure of concrete under selected South African conditions. *Third ACI/CANMET Int. Conference on the Performance of Concrete in Marine Environment*. St. Andrews, Canada. pp. 205-216.

[6] BS-EN-1990 (2002) Eurocode - Basis of structural design. European Standard.

Appendix E

Literature on selected statistical measures and distributions

E.1 *Method of least squares and regression*

Note: The literature presented here is adapted from [1].

If a linear relation $y = a + bx$ is postulated, two pairs of values (x_1, y_1) and (x_2, y_2) determine the constants in the equation. This is satisfactory provided that the observed quantities are free from error. However, in practice, observations are seldom free of error, and if a further observation is taken, say (x_3, y_3), we may obtain a point which does not fit exactly on the straight line through the original two points. This also applies to curves involving powers of x and y. Statistical methods help to fit the 'best' line to a given set of data, instead of simply drawing a line 'by eye'.

The principle underlying the fitting of the 'best' line is that of least squares; this states that if y is a linear function of an independent variable x, the most probable position of a line $y = x + bx$ is such that the sum of squares of deviations of all points (x_i, y_i) from the line is a minimum; the deviations are measured *in the direction of the y-axis*. It should be stressed that the underlying assumption is that x is either free from error (being assigned) or subject to negligible error only, while y is the observed or measured quantity, subject to errors which have to be 'eliminated' by the method of least squares. The observed y is thus a random value from the population of values of y corresponding to a given x. Such a situation exists in controlled experiments, where we are interested in finding the mean value of $\overline{y_i}$ bar for each value of x_i.

Suppose our observations consist of n pairs of values:

$$\begin{cases} x_1, x_2, \ldots, x_n \\ y_1, y_2, \ldots, y_n \end{cases} \tag{E.1}$$

and imagine that the various pairs plot as points shown in Figure E.1. Assume further that from the physical nature of the relation between y and x we know that the relation is linear, or alternatively expect it to be linear. We postulate therefore the relation as:

$$y = a + bx \tag{E.2}$$

Our problem is to find the values of a and b for the line of 'best fit'. For a point i on this line:

$$y_i - (a + bx_i) = 0 \tag{E.3}$$

but if there is error in the measurement, there will be a residual ϵ_i such that:

$$y_i - (a + bx_i) = \epsilon_i \tag{E.4}$$

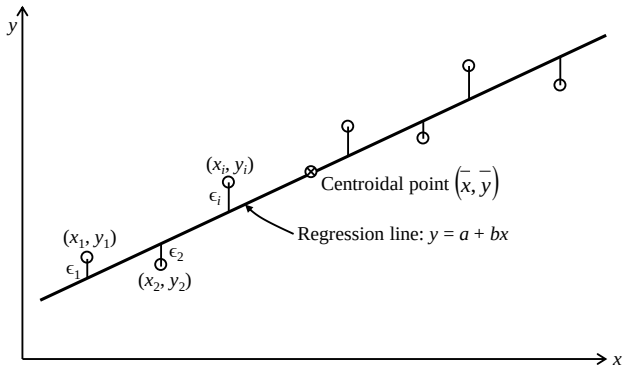

Figure E.1: Regression line (method of least squares)

With *n* observations we have *n* equations:

$$\begin{aligned} y_i - (a + bx_1) &= \in_1 \\ y_i - (a + bx_2) &= \in_2 \\ \cdot \quad & \quad \cdot \quad \cdot \\ \cdot \quad & \quad \cdot \quad \cdot \\ \cdot \quad & \quad \cdot \quad \cdot \\ y_i - (a + bx_n) &= \in_n \end{aligned} \tag{E.5}$$

Using the summation notation, we can write the sum of squares of residuals as:

$$P = \sum \in_i^2 \tag{E.6}$$

or

$$P = \sum_{i=1}^{n} \left[y_i - (a + bx_i) \right]^2 \tag{E.7}$$

As stated earlier, we have to satisfy the condition that the sum of squares of residuals is a minimum, i.e. *P* is a minimum. This occurs when:

$$\frac{\partial P}{\partial a} = 0 \text{ and } \frac{\partial P}{\partial b} = 0 \tag{E.8}$$

or

$$\sum \left[y_i - (a + bx_i) \right] = 0 \tag{E.9}$$

and

$$\sum x_i \left[y_i - (a + bx_i) \right] = 0 \tag{E.10}$$

Omitting the subscripts we can write Eqn. (E.9) as:

$$\sum y - \sum a - b \sum x = 0 \tag{E.11}$$

Since *a* is a constant, we have:

$$\sum y = na + b\sum x \tag{E.12}$$

or

$$\frac{\sum y}{n} = a + b\frac{\sum x}{n} \tag{E.13}$$

Thus:

$$\bar{y} = a + b\bar{x} \tag{E.14}$$

Eqn. (E.14) states that the line passes through the point ($\bar{x}$, $\bar{y}$), i.e. through the point whose co-ordinates are the appropriate means of all observations; we can call this point the centroidal point of all observations. From the fact that the point ($\bar{x}$, $\bar{y}$) lies on the line, it follows that Eqn. (E.2) can be written also as:

$$y - \bar{y} = b(x - \bar{x}) \tag{E.15}$$

Returning now to Eqn. (E.10) we have:

$$\sum xy = a\sum x + b\sum x^2 \tag{E.16}$$

Equations (E.12) and (E.16) are called the *normal equations*.

Solving the normal equations:

$$\sum y = na + b\sum x \tag{E.12}$$

$$y - \bar{y} = b(x - \bar{x}) \tag{E.16}$$

we obtain:

$$a = \frac{\sum x^2 \sum y - \sum x \sum xy}{n\sum x^2 - \left(\sum x\right)^2} \tag{E.17}$$

and

$$b = \frac{n\sum xy - \sum x \sum y}{n\sum x^2 - \left(\sum x\right)^2} \tag{E.18}$$

Hence the equation to the line of best fit can be written as:

$$y = \frac{\sum x^2 \sum y - \sum x \sum xy}{n\sum x^2 - \left(\sum x\right)^2} + \left(\frac{n\sum xy - \sum x \sum y}{n\sum x^2 - \left(\sum x\right)^2}\right)x \tag{E.19}$$

The line given by Eqn. (E.19) is called the line of *regression* of *y* on *x*.

E.2 ***Correlation***

Note: The literature presented here is adapted from [1].

The operation of fitting the best line must be followed by a test of the goodness of fit. Referring to Eqn. (E.19), we can observe that, if there is no correlation between *y* and *x*, i.e. if *y* is independent of *x*, the coefficient of *x* (i.e. the slope *b*) is zero and the line plots as a horizontal line i.e.:

$$\frac{n\sum xy - \sum x \sum y}{n\sum x^2 - \left(\sum x\right)^2} = 0 \tag{E.20}$$

Considering now the regression of *x* on *y*, there is no correlation if *x* is independent of *y*, i.e. if the line is described by Eqn. (E.21) is vertical.

$$x = \frac{\sum y^2 \sum x - \sum y \sum xy}{n\sum y^2 - \left(\sum y\right)^2} + \left(\frac{n\sum xy - \sum x \sum y}{n\sum y^2 - \left(\sum y\right)^2}\right) y \tag{E.21}$$

Thus, referring the slope to a vertical axis:

$$\frac{n\sum xy - \sum x \sum y}{n\sum y^2 - \left(\sum y\right)^2} = 0 \tag{E.22}$$

and expressing slope in the usual way (*y* vertical and *x* horizontal):

$$\frac{n\sum y^2 - \left(\sum y\right)^2}{n\sum xy - \sum x \sum y} = \infty \tag{E.23}$$

If there is no correlation between the two variables being studied, the product of the slopes given by Eqn. (E.20) and (E.22) is zero, i.e.:

$$\left(\frac{n\sum xy - \sum x \sum y}{n\sum x^2 - \left(\sum x\right)^2}\right) \times \left(\frac{n\sum xy - \sum x \sum y}{n\sum y^2 - \left(\sum y\right)^2}\right) = 0 \tag{E.24}$$

Conversely, when there is a perfect correlation, i.e. all the points lie exactly on each of the two regression lines, the lines coincide; their slopes are therefore equal, namely:

$$\frac{n\sum xy - \sum x \sum y}{n\sum x^2 - \left(\sum x\right)^2} = \frac{n\sum y^2 - \left(\sum y\right)^2}{n\sum xy - \sum x \sum y} \tag{E.25}$$

or

$$\left(\frac{n\sum xy-\sum x\sum y}{n\sum x^2-\left(\sum x\right)^2}\right)\times\left(\frac{n\sum xy-\sum x\sum y}{n\sum y^2-\left(\sum y\right)^2}\right)=1 \qquad \text{(E.26)}$$

Thus we find that the value of the product on the left-hand side of (E.26) gives a measure of correlation: when the value is zero, there is no correlation; when it is unity, the correlation is perfect. We call the square root of this product the *correlation coefficient* and denote it by *r*:

$$r=\frac{n\sum xy-\sum x\sum y}{\left(\left(n\sum x^2-\left(\sum x\right)^2\right)\left(n\sum y^2-\left(\sum y\right)^2\right)\right)^{0.5}} \qquad \text{(E.27)}$$

We can note that *r* is symmetrical with respect to *y* so that the correlation coefficient of a line of regression of *y* on *x* is the same as that of regression of *x* on *y*. Correlation is, in fact, concerned only with the association between the variables and not with their dependence or independence.

The correlation coefficient *r* must lie in the range $0 \leq |r| \leq 1$ but in practice, because of random errors, $0 < |r| < 1$.

E.3 *Calculation of moving average*

An *n*-point moving average (also referred to as *running mean*) represents the average of the respective sample and the *n*-1 number of preceding samples [2]. A moving average smoothes data by replacing each data point with the average of the neighbouring data points defined within the range of data points. The following expression is used [3]:

$$y_s(i)=\frac{1}{2N+1}\left[y(i+N)+y(i+N-1)+....+y(i-N)\right] \qquad \text{(E.28)}$$

where $y_s(i)$ is the moving averaged value for the i^{th} data point and *N* is the number of neighbouring data points on either side of $y_s(i)$.

In this study, a 2-point moving average was used for the analysis of corrosion rate, resistivity and half-cell potential results. Take, for example, corrosion rate (i_{corr}) averaged values for the first three consecutive bi-weekly measurements i.e. $i_{corr,1}$, $i_{corr,2}$ and $i_{corr,3}$. According to Eqn. (E.28):

The 1st moving averaged data point is: $\left(\frac{i_{corr,1}+i_{corr,2}}{2}\right)$ and is plotted on the 3rd week;

The 2nd moving averaged data point is: $\left(\frac{i_{corr,2}+i_{corr,3}}{2}\right)$ and is plotted on the 5th week;

and so on.

E.4 ***Grubb's outlier test***

An outlier is defined as an observation or data point which does not appear to fall within the expected distribution of a particular data set [4, 5]. They can affect the results of analyses. Outliers may be rejected outright if they are caused by a known or demonstrated physical reason, such as sample spillage, contamination, mechanical failure, or improper calibration. However, data points which appear to deviate from the expected sample distribution for no known physical reason must be verified as outliers using statistical criteria [6].The rejection of suspect observations must be based on an objective criterion and not on subjective or intuitive grounds. This can be achieved by using statistically sound tests for the detection of outliers. On such test, which was adopted in this study, is the Grubb's test.

Grubb's outlier test is used to determine single-sided outliers when both the population mean (μ) and the population standard deviation (s) are unknown. It was developed by Grubbs [7] and is included in standard methods:

$$T_u = \frac{X_n - \bar{x}}{\sigma} \quad \text{(for high-sided outliers)} \tag{E.29}$$

$$T_l = \frac{\bar{x} - X_l}{\sigma} \quad \text{(for low-sided outliers)} \tag{E.30}$$

where X_n and X_l are the data points in question (suspected outlier), $\bar{x}$ is the sample mean and σ is the sample standard deviation. The value T_u or T_l is then compared against critical values depending on the number of replicates and significance (or confidence) level. If T_u or T_l is greater than the critical value for the appropriate number of replicates at the appropriate significance level, the questionable data point is an outlier, and may be rejected. The critical values for various numbers of replicates at the 5% significance level, which was used in this study, is given in Table E.1.

Table E.1: Critical values for Grubb's outlier test [4]

No. of observations	Critical value
3	1.15
4	1.46
5	1.67
6	1.82
7	1.94
8	2.03
9	2.11

E.5 ***Normal distribution***

A continuous random variable x is said to have a normal (or Gaussian) distribution if the probability density function (pdf) of x is given by Eqn. (E.31). The normal distribution is specified by giving the mean (μ) and the standard deviation (σ); where $-\infty < \mu < \infty$ and $\sigma > 0$.

$$f(x)=\left(\frac{1}{\sigma\sqrt{2\pi}}\right)e^{-\frac{1}{2}\left(\frac{x-\mu}{\sigma}\right)^2} \tag{E.31}$$

E.6 *Lognormal distribution*

A random variable x is said to be lognormally distributed if $\log(x)$ is normally distributed. The distribution is skewed to the left. Skewed distributions are particularly common when mean values are low and variances are high. In addition, values cannot be negative. The lognormal distribution of a random variable x is defined by:

$$f(x)=\frac{1}{\sigma\sqrt{2\pi}x}\exp\left[-\frac{1}{2}\left(\frac{\ln(x)-\mu}{\sigma}\right)^2\right] \tag{E.32}$$

where μ and σ are, respectively, the mean and standard deviation of the variable's natural logarithm, $\ln(x)$.

E.7 *Weibull distribution*

The Weibull variate is commonly used as a lifetime distribution in reliability applications. Weibull distribution can represent decreasing, constant, or increasing failure rates. The probability distribution function is given as:

$$f(x)=\left(\frac{b}{a^b}\right)x^{b-1}e^{-\left(\frac{x}{a}\right)^b} \tag{E.33}$$

where $a > 0$ and $b > 0$ are, respectively, the scale and shape parameters of the distribution.

E.8 *Karl Pearson's Chi-squared (χ2) test*

The χ^2 statistic measures how well the expected frequency of the fitted distribution compares with the observed frequency of a histogram of the observed data. The test makes assumptions that (i) the observed data consists of a random sample of n independent data points, (ii) the measurement scale can be nominal (i.e. non-numeric) or numerical, and (iii) the n data points can be arranged into histogram form with N contiguous (adjacent) classes that cover the entire possible range of the variable. Critical values for the χ^2 test are found directly from the χ^2 distribution (an asymmetric distribution that has a minimum value of 0, but no maximum value, Figure E.2) depending on the confidence level chosen (Table E.2).

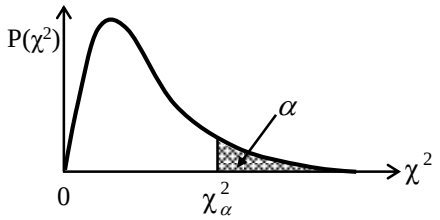

Figure E.2: The Chi-squared (χ^2) distribution

The shape and range of the χ^2 distribution are defined by the degrees of freedom v, where $\nu = N - k - 1$ where N is the number of histogram bars or classes and k is the number of parameters that are estimated to determine the best-fitting distribution.

Table E.2: Critical values for Chi-squared distribution

Degrees of freedom (v)	Confidence level (%)										
	0.5	**2.5**	**80**	**90**	**95**	**97.5**	**98**	**99**	**99.5**	**99.8**	**99.9**
	p-value										
1	3.93E-05	9.82E-04	1.642	2.706	3.841	5.024	5.412	6.635	7.879	9.550	10.828
2	0.010	0.051	3.219	4.605	5.991	7.378	7.824	9.210	10.597	12.429	13.816
3	0.072	0.216	4.642	6.251	7.815	9.348	9.837	11.345	12.838	14.796	16.266
4	0.207	0.484	5.989	7.779	9.488	11.143	11.668	13.277	14.860	16.924	18.467
5	0.412	0.831	7.289	9.236	11.070	12.833	13.388	15.086	16.750	18.907	20.515
6	0.676	1.237	8.558	10.645	12.592	14.449	15.033	16.812	18.548	20.791	22.458
7	0.989	1.690	9.803	12.017	14.067	16.013	16.622	18.475	20.278	22.601	24.322
8	1.344	2.180	11.030	13.362	15.507	17.535	18.168	20.090	21.955	24.352	26.124
9	1.735	2.700	12.242	14.684	16.919	19.023	19.679	21.666	23.589	26.056	27.877
10	2.156	3.247	13.442	15.987	18.307	20.483	21.161	23.209	25.188	27.722	29.588
100	67.328	74.222	111.667	118.498	124.342	129.561	131.142	135.807	140.169	145.577	149.449
1000	888.564	914.257	1037.431	1057.724	1074.679	1089.531	1093.977	1106.969	1118.948	1133.579	1143.917

Note: The 95% confidence level was used in this study.

For any given level of significance, the critical region (α) begins at a larger χ^2 value, the larger the degree of freedom (see Figure E.2). The χ^2 statistic is calculated as follows:

$$\chi^2 = \sum_{i=1}^{n} \left[\frac{(O_i - E_i)^2}{E_i} \right] \tag{E.34}$$

where O_i is the observed frequency of the i^{th} histogram class or bar and E_i is the expected frequency from the fitted distribution of x-values falling within the x-range of the i^{th} histogram bar. E_i is calculated as follows:

$$E_i = n\left(F_{i_{\max}} - F_{i_{\min}}\right) \tag{E.35}$$

where F_i is the distribution function of the fitted distribution, i_{max} is the x-value upper bound of the i^{th} histogram bar and i_{min} is the x-value lower bound of the i^{th} histogram bar. Since the χ^2 statistic sums the squares of all the errors (O_i - E_i), it can be disproportionately sensitive to any large errors, e.g. if the error of one bar is three times that of another bar, it will contribute nine times more to the statistic (assuming the same E_i for both). χ^2 is very dependent on the number of bars, N, that are used. By changing the value of N, one can quite easily switch ranking between two distribution types. However, there are no rules for selecting the value of N.

By equating the calculation to a χ^2 distribution, it is assumed that (O_i - E_i) follows a normal distribution with zero mean. Since O_i is in fact binomial this approximation only works when there are a large number of data points within each class.

E.9 *References*

[1] Neville, A. M. & Kennedy, J. B. (1964) Basic statistical methods for engineers and scientists. ISBN 0 7002 0075 4, International Texbook Company Inc. Scranton, Pa, USA.

[2] Chambers, J. M., Cleveland, W. S., Tukey, P. A. & Kleiner, B. (1983) Graphical methods for data analysis. Duxbury Press - Statistics/Probability Series.

[3] Cleveland, W. C. (1988) Dynamic graphics for statistics (1st Edition). Springer.

[4] Barnett, V., Lewis, T. & Rothamsted, V. (1994) Outliers in statistical data, Wiley series in probability and mathematical statistics, applied probability and statistics. John Wiley & Sons.

[5] Everitt, B. S. & Skrondal, A. (2010) *The Cambridge Dictionary of Statistics*, Cambridge University Press, The Edinburgh Building, Cambridge CB2 8RU, UK.

[6] Quinn, G. P. & Keough, M. J. (2002) *Experimental Design and Data Analysis for Biologists*, Cambridge University Press, The Edinburg Building, Cambridge CB2 2RU, UK.

[7] Grubbs, F. E. (1979) Procedures for detecting outlying observations. Army Statistics Manual DARCOM-P706-103, U.S. Army Research and Development Center, Aberdeen Proving Ground, MD 21005.

Appendix F

Details of some commercial products used

Note: Details provided here are summarized from [1].

F.1 *Sikament® - NN: High range water reducing admixture*

Product desctiption: Chloride-free liquid superplasticizer
Complies with ASTM C 494-81 Type F
Chemical base: Naphthalene formaldehyde sulphonate
Density: 1.2 kg/litre
pH: Approximately 7.5

F.2 *Sikafloor® - 261 ZA: Epoxy resin*

Product description: 2-part multi-purpose binder based on epoxy resin
Complies with: DIN 51130 (Skid / slip resistance)
Chemical base: Epoxy
Density: Mixed resin approx. 1.4 kg/litre at 23 °C
Compressive strength: Resin: approx. 60 MPa (28 days, 23 °C)
Thermal resistance: Permanent exposure to dry heat: approx. 50 °C

F.3 *Reference*

[1] Sika (2011) Sika Product Manual (Construction) - 2011 Edition, Sika South Africa (Pty) Ltd.

Appendix G

EBE Faculty: Assessment of ethics in research projects

Any person planning to undertake research in the Faculty of Engineering and the Built Environment at the University of Cape Town is required to complete this form before collecting or analysing data. When completed it should be submitted to the supervisor (where applicable) and from there to the Head of Department. If any of the questions below have been answered YES, and the applicant is NOT a fourth year student, the Head should forward this form for approval by the Faculty EIR committee: submit to Ms Zulpha Geyer (Zulpha.Geyer@uct.ac.za; Chemical Engineering Building, Ph 021 650 4791).

NB: A copy of this signed form must be included with the thesis/dissertation/report when it is submitted for examination

This form must only be completed once the most recent revision EBE EiR Handbook has been read.

Name of Principal Researcher/Student: **Mike Benjamin Otieno** Department: **Civil Engineering**

Preferred email address of the applicant: **OTNMIK001@myuct.ac.za** or **mikexbenjamin@gmail.com**

If a student: Degree: **Doctoral** Supervisor: **Assoc./Prof. Hans Beushausen**

If a Research Contract indicate source of funding/sponsorship: **Not applicable**

Research Project Title: The development of empirical chloride-induced corrosion rate prediction models for cracked and uncracked steel reinforced concrete structures in the marine tidal zone

Overview of ethics issues in your research project:

		YES	NO
Question 1:	**Is there a possibility that your research could cause harm to a third party (i.e. a person not involved in your project)?**	☐	☒
Question 2:	**Is your research making use of human subjects as sources of data?** If your answer is YES, please complete Addendum 2.	☐	☒
Question 3:	**Does your research involve the participation of or provision of services to communities?** If your answer is YES, please complete Addendum 3.	☐	☒
Question 4:	**If your research is sponsored, is there any potential for conflicts of interest?** If your answer is YES, please complete Addendum 4.	☐	☒

If you have answered YES to any of the above questions, please append a copy of your research proposal, as well as any interview schedules or questionnaires (Addendum 1) and please complete further addenda as appropriate. Ensure that you refer to the EiR Handbook to assist you in completing the documentation requirements for this form.

I hereby undertake to carry out my research in such a way that

- there is no apparent legal objection to the nature or the method of research; and
- the research will not compromise staff or students or the other responsibilities of the University;
- the stated objective will be achieved, and the findings will have a high degree of validity;
- limitations and alternative interpretations will be considered;
- the findings could be subject to peer review and publicly available; and
- I will comply with the conventions of copyright and avoid any practice that would constitute plagiarism.

Signed by:	Full name and signature	Date
Principal Researcher/Student:	Mike Benjamin Otieno	22-JULY-2013

This application is approved by:

Supervisor (if applicable):	Assoc/Prof. Hans Beushausen	22-7-13
HOD (or delegated nominee): *Final authority for all assessments with NO to all questions and for all undergraduate research.*	Assoc/Prof. Neil Armitage	22-7-13
Chair : Faculty EIR Committee *For applicants other than undergraduate students who have answered YES to any of the above questions.*	*Not applicable*	*Not applicable*